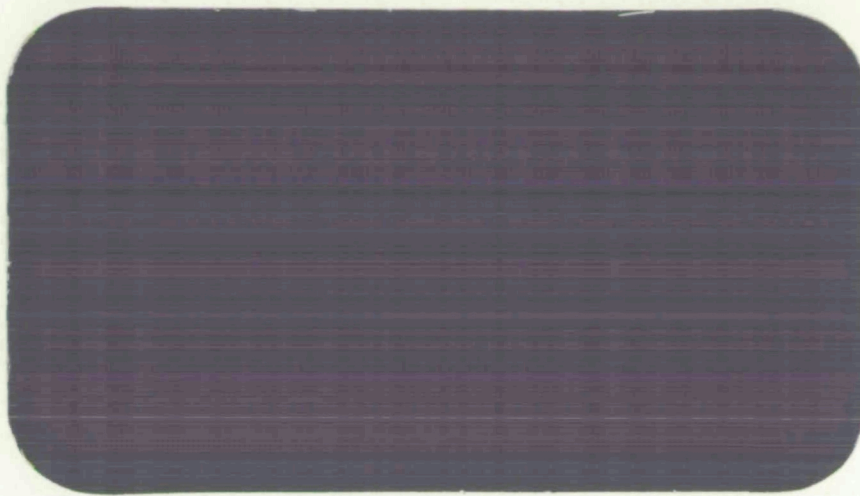


N73-31688



CASE FILE
COPY



Rocketdyne
North American Rockwell

NASA CR-

R-8866

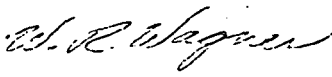
INTERIM REPORT
REGENERATIVELY COOLED ROCKET ENGINE
FOR SPACE STORABLE PROPELLANTS
CONTRACT NAS7-765


March 1973

ROCKETDYNE
A DIVISION OF ROCKWELL INTERNATIONAL CORPORATION
6633 CANOGA AVENUE
CANOGA PARK, CALIFORNIA 91304

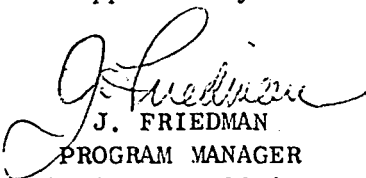
Prepared For
NATIONAL AERONAUTICS AND SPACE ADMINISTRATION
JET PROPULSION LABORATORY
PROGRAM TECHNICAL MONITOR - W. B. POWELL

Prepared By


W. R. WAGNER
PROJECT DEVELOPMENT ENGINEER
ADVANCED PROGRAMS


B. J. WALDMAN
PROJECT DEVELOPMENT ENGINEER
ADVANCED PROGRAMS

Approved By


J. FRIEDMAN
PROGRAM MANAGER
ADVANCED PROGRAMS

ACKNOWLEDGMENTS

The contributions of the following personnel are gratefully acknowledged: Mr. G. Osugi for detailed and difficult heat transfer analyses, Messrs. R. Knight and A. Huebner for a fine test effort, and Mr. R. Kuhn for exacting design support.

Special thanks go to the Yoke and Reno Stand test crews and the large number of supporting fabrication, computing, supervisory personnel, etc., who benefitted the program greatly throughout its entirety.

FOREWORD

The results of the analytical and experimental studies conducted by Rocketdyne, a Division of the Rockwell International Corporation, under Contract NAS7-765, are presented in this report. Technical direction of the program was supplied by W. B. Powell of the NASA Jet Propulsion Laboratory.

The analyses and experiments reported were conducted from May 1970 through December 1971.

ABSTRACT

Analyses and experimental study were performed with the OF_2 (F_2/O_2)/ B_2H_6 propellant combination over a range in operating conditions to determine suitability for a space storable pressure fed engine configuration for an extended flight space vehicle configuration.

The regenerative cooling mode selected for the thrust chamber was explored in detail with the use of both the fuel and oxidizer as coolants in an advanced milled channel construction thrust chamber design operating at 100 psia chamber pressure and a nominal mixture ratio of 3.0 with a 60:1 area ratio nozzle. Benefits of the simultaneous cooling as related to gaseous injection of both fuel and oxidizer propellants were defined.

Heat transfer rates, performance and combustor stability were developed for impinging element triplet injectors in uncooled copper calorimeter hardware with flow, pressure and temperature instrumentation. Study of the capabilities of the B_2H_6 and OF_2 during analytical study and numerous tests with flow through electrically heated blocks provided design criteria for subsequent regenerative chamber design and fabrication.

Two regenerative chambers were constructed and nine tests were provided over a range in mixture ratio at 100 psia with a 20:1 area ratio nozzle in an altitude ejector-diffuser to 45 seconds duration, establishing the validity of the engine concept.

TABLE OF CONTENTS

Acknowledgments	ii
Foreword	iii
Abstract	iv
Introduction	1
Summary	4
Task I - Preliminary Analysis and Experimentation	4
Task II - Determination of Design Criteria and Critical Limitations	4
Task III - Design and Fabrication of the Regenerative Thrust Chamber	6
Task IV - Calorimeter/Regenerative Chamber Testing	7
Conclusions and Recommendations	10
Technical Discussion	
Task I - Preliminary Analysis and Experimentation	12
Thrust Chamber and Cooling Configuration Selection	12
Injector Design Selection	21
Task II - Determination of Design Criteria and Critical Limitations	44
Combustion Chamber Design	45
Triplet No. 1 Injector Fabrication	55
Task II - Calorimeter Test Program	68
Task II - Calorimeter Test Results	71
Coolant Heat Transfer Test Hardware	102
OF ₂ and B ₂ H ₆ Hardware Installation and Test Procedures	107
B ₂ H ₆ Coolant Heat Transfer Test Results	115
OF ₂ Coolant Heat Transfer Results	123
Regenerative Chamber Coolant Channel Geometry Optimization	128
Task III - Regenerative Chamber and Triplet No. 2 Design/Fabrication	149
Thrust Chamber Design Features	149
Regenerative Chamber Hardware Fabrication and Assembly	159
Triplet Injector (No. 2) Fabrication and Assembly	176

Calorimeter Chamber Modification	183
Task IV - Calorimeter/Regenerative Chamber Testing	187
Test Facility Preparation - Yoke Stand (Propulsion Research Area)	187
Diffuser Initial Installation	192
Diffuser Test Operation	196
F ₂ /O ₂ -B ₂ H ₆ Test Program	207
Blowdown Test Series for Calorimeter Operation	207
Calorimeter Test Series	211
Blowdown Testing for Regenerative Operation	218
Regenerative Test Series	220
Task IV - Calorimeter-Regenerative Test Series Data Analysis	236
Calorimeter Series Test Data Analysis	236
Regenerative Series - Test Data Analysis	243
References	259
Nomenclature	261
Appendix A	A-1
JANNAF Thrust Chamber Performance Procedure	A-1
Introduction	A-1
JANNAF Specific Impulse Performance Prediction General Approach	A-2
Thrust Chamber Specific Impulse Performance Method (JANNAF Simplified Procedure)	A-3
Thrust Chamber Characteristic Velocity Performance (JANNAF Simplified Method)	A-5
Appendix B	B-1
Theoretical Performance Curves	B-1
Characteristic Velocity (c*)	B-1
Combustion Temperature (T _c)	B-1
Combustion Enthalpy (H _c)	B-1
Specific Impulse Performance (I _{sp})	B-1
Characteristic Velocity Kinetic Efficiency (η _{c*} ^{vac})	B-9
Specific Impulse Kinetic Efficiency (η _{I_s} ^{kin})	B-9

Characteristic Velocity -- Enthalpy Influence Coefficient	B-9
Specific Impulse -- Enthalpy Influence Coefficients	B-9
Appendix C	C-1
Performance Data Reduction and Injector Calculations	C-1
Calorimeter Series C* Parameters	C-2
Regenerative Series C* Parameters	C-4
Summary of Calculable Losses and Performance Evaluation Factors	C-6
Appendix D	D-1
Two-Dimensional Isotherms of FLOX-B ₂ H ₆ Regeneratively Cooled Chamber	D-1
Appendix E	E-1
PRA Test Facility and Data Acquisition	E-1
FLOX (Oxidizer) System Assembly	E-1
B ₂ H ₆ (Fuel) System	E-1
Propellant Vent Systems	E-3
Coolant Water System	E-3
Purge Systems	E-3
Propellant Sampling	E-3
Altitude Diffuser	E-3
Start Sequence	E-4
Instrumentation	E-4
Data Recording	E-7
Appendix F	F-1
Reno Test Facility and Data Acquisition	F-1
Oxidizer System	F-1
Fuel System	F-3
Altitude Facility	F-3
Instrumentation Systems	F-4
Engine Installation and Measurements	F-4
Data Acquisition	F-7

ILLUSTRATIONS

1. Final Assembly of No. 1 Thrust Chamber With Auxiliary Water Cooling Jacket Installed	3
2. Stanton Number Correlation of IR&D B_2H_6 Heat Transfer Data	13
3. Gaseous Diborane Throat Cooling Capability	16
4. Prototype OF_2/B_2H_6 Cooled Thrust Chamber Assembly (Sketch)	17
5. Throat Wall Isotherms for Typical OF_2/B_2H_6 Water-Jacketed Chamber Design	22
6. Throat Wall Isotherms for Typical OF_2/B_2H_6 Double Panel Design	23
7. Demonstrator Thrust Chamber Assembly (H_2O/B_2H_6 Cooled)	24
8. Injector Assembly of OF_2/B_2H_6	28
9. Injector Zone Mixture Ratio Distribution	29
10. Estimated Diborane Decomposition Rate at High Temperatures	33
11. Steady-State Injector Temperatures for FLOX/ B_2H_6 in Uncooled Thrust Chamber Mode	35
12. Steady-State Injector Temperatures for FLOX/ B_2H_6 in Regenerative Cooling Mode	36
13. Injector Steady-State Temperature Distribution for 0.5 Btu/in ² -sec Heat Input and Heated Diborane	37
14. Potential Acoustic Cavity Orientations	39
15. Candidate BLC Inlet Configurations	40
16. Injector Face Inlet and Inlet Port Temperature and Pressure Instrumentation	42
17. Preliminary Injector/Thrust Chamber Interface Design	43
18. Heat Flux to the Throat as a Function of Diborane Boundary Film	47
19. Heat Flux to the Throat as a Function of Injector to Throat Distance	48
20. Heat Input to Combustion Chamber Wall for OF_2/B_2H_6	49
21. Heat Input to Nozzle Wall From Throat to $\epsilon = 3.45:1$ for OF_2/B_2H_6	50
22. Calorimeter Thrust Chamber Design	52
23. Calorimeter Chamber Viewed from Injector End	53
24. Thermal Response of Calorimeter Chamber Instrumentation	54
25. Combustion Chamber Extension -- 5.0 Inches	56

26.	Calorimeter Chamber Showing Hardware Variations With Basic Injector End and Nozzle Entrance Wall Chamber Pressures	57
27.	Nozzle Extension to 10:1 Area Ratio	58
28.	Nozzle Extension to 20:1 Area Ratio	59
29.	Diffuser for 10:1 Area Ratio Nozzle	60
30.	Two-Piece Cylindrical Diffuser for 20:1 Area Ratio Nozzle . . .	61
31.	Exploded View of Injector Components	62
32.	Injector Oxidizer Dome and Manifold Ring	64
33.	Front View of Injector With Acoustic Cavity Cover in Place . . .	65
34.	Water Flow of Film Coolant Orifices	66
35.	Water Flow of Injector Core Triplet Elements	67
36.	Film Coolant and Mixture Ratio Relationships for Calorimeter Test Program	70
37.	Performance Results for F_2-O_2/B_2H_6 With the 12-Inch Combustion Chamber	76
38.	Injector Efficiency as a Function of Film Coolant Flowrate for 12-Inch Combustion Chamber	77
39.	Injector Performance Comparison With Predictions Based on Injected Mixture Ratio Maldistribution	78
40.	Cross-Section of Combustor Heat Transfer Isolation Segments . .	79
41.	Isolation Segment Normalized Temperature History (Includes Start Transient)	81
42.	Heat Flux Profile for Nominal Test Conditions With 9.5-Inch Combustion Chamber	82
43.	Throat Heat Flux Data for 9.5-Inch Combustion Chamber	83
44.	Throat Heat Flux Data for 12-Inch Combustion Chamber	84
45.	Throat Normalized Film Coefficient Data for 9.5-Inch Combustion Chamber	86
46.	Throat Normalized Film Coefficient Data for 12-Inch Combustion Chamber	87
47.	Throat Normalized Film Coefficient Correlation With Outer Zone Mixture Ratio for 9.5-Inch Combustion Chamber	88
48.	Throat Normalized Film Coefficient Correlation With Outer Zone Mixture Ratio for 12-Inch Combustion Chamber	89
49.	Throat Heat Flux Correlation With Injector Efficiency for 12-Inch Combustion Chamber	90
50.	Injector Temperature Histories for Tests 083 and 084	92
51.	Injector Face Heating Correlation	93

52.	Injector Face Deposits After Tests 070 Through 082	94
53.	Injector Face Deposits After Tests 086 Through 094	96
54.	Cavity Cover Stains After Tests 083 Through 094	99
55.	Acoustic Cavity Temperature History for Tests 083 and 083	100
56.	Test Number Dependence of Acoustic Cavity Temperature	101
57.	Diborane Heat Transfer Flow Schematic	103
58.	Diborane Heat Transfer Liquid Block	104
59.	Diborane Heat Transfer Gas Block	105
60.	Diborane Heat Transfer Curvature Block	106
61.	Photograph of Diborane Heat Transfer Test Hardware	108
62.	Oxygen Difluoride Heat Transfer Flow Schematic	109
63.	Oxygen Difluoride Heat Transfer Liquid Block	110
64.	Oxygen Difluoride Heat Transfer Gas Block	111
65.	Photograph of Oxygen Difluoride Heat Transfer Test Hardware	112
66.	Oxygen Difluoride Heat Transfer Test Setup Before Installation	113
67.	Diborane Heat Transfer Test Setup Before Insulation	114
68.	Diborane Coolant Property Test Range	118
69.	Gaseous Diborane Heat Transfer Data Correlation	120
70.	Experimental Boiling Data for Diborane	122
71.	Diborane Coolant Channel Profile	130
72.	Diborane Coolant Temperature Profile (Predicted)	132
73.	Nozzle Area Ratio vs Length	133
74.	Hot Gas Side Heat Flux Distribution	134
75.	Coolant Heat Load Profile	135
76.	Wall Temperature Predictions for Single Panel Cooling Design	136
77.	Throat Wall Temperature Predictions for Double Panel Cooling Design	138
78.	Ratio of Hot Gas Area to Coolant Area in the Thrust Chamber Nozzle	139
79.	Coolant Heat Flux Distribution for the Nozzle Section Cooled by Liquid Diborane (Based on Two Dimensional Analysis)	140
80.	Experimental Boiling Data for Diborane	141
81.	Nozzle Coolant Heat Flux Distribution for Selected Channel Design	143
82.	Wall Temperature Distribution	145

83.	Throat Isotherms for Non-Boiling Water Heat Transfer and One Blocked Diborane Passage	146
84.	Throat Isotherms for Boiling Water Heat Transfer and a Local Heat Flux Increase	148
85.	Inlet/Distribution Manifold	150
86.	Outlet Manifold	152
87.	Injector - Thrust Chamber Interface	154
88.	Nozzle-End Coolant Channel Access Ports	155
89.	Water Jacket Assembly	157
90.	OFHC Copper Liner Fabrication Sequence	160
91.	Internally and Externally Contoured Nozzle	162
92.	Combustor Region Channel Passage Machining	164
93.	Nozzle Region Channel Passage Machining	164
94.	Typical Electroforming Sequence	165
95.	Machined Liner Prepared With Electroform Shielding Prior to Immersion Into the Nickel Bath for Plating	166
96.	Regenerative Liner No. 1 With Channel Closeout Nickel Plating	168
97.	Machined No. 1 Regeneratively Cooled Thrust Chamber Prior to Manifold Attachment	169
98.	Water Cooled Jacket Assembly Closure Machining Operation	171
99.	Thrust Chamber Assembly End View Illustrating Coolant Passage Discharge Porting	173
100.	Final Assembly of No. 1 Thrust Chamber With Auxiliary Water Cooling Jacket Installed	174
101.	Triplet No. 2 Injector Face Detail of Assembly Post Second Braze Cycle	177
102.	No. 2 Injector Illustrating Braze Void on Oxidizer Dome Closure Prior to Successful Second Braze Effort	179
103.	Water Flow Testing on No. 2 Triplet Injector-Fuel Side	181
104.	Water Flow Testing on No. 2 Triplet Injector-Oxidizer Side	182
105.	$F_2/O_2-B_2H_6$ Copper Calorimeter Chamber With Recessed Temperature Plug Porting	184
106.	20:1 Area Ratio $F_2/O_2-B_2H_6$ Nozzle Extension With Temperature and Pressure Instrumentation Ports	185
107.	20:1 Calorimeter Nozzle Extension Temperature and Pressure Location Summary	186
108.	FLOX System Yoke Stand - PRA	189

109.	B_2H_6 System Yoke Stand - PRA	190
110.	Yoke Stand (Propulsion Research Area) Installation of $F_2/O_2-B_2H_6$ Regenerative Chamber With Altitude Diffuser	193
111.	Diffuser Support and Mounting Detail	195
112.	Altitude Diffuser Section Internal Geometry and Operating Conditions	197
113.	30:1 Exit Nozzle Wall Pressure Tap vs Time (Run 006)	198
114.	Exit Nozzle Wall Pressure vs Modified "T" Section (Runs 007 and 008)	200
115.	Yoke Stand $F_2/O_2-B_2H_6$ Diffuser Pressure Without Engine Operation (Location 1)	201
116.	Upstream Diffuser Pressure vs Time (Test 015)	203
117.	Ejector and Thrust Chamber Thrust vs Time (Test 015)	204
118.	Diffuser Forward End Modified With $180^\circ H_2O$ Coolant Flow Inlets	206
119.	Calorimeter Chamber Test Setup With Steel Inline and Copper Coil Bath Heat Exchangers	210
120.	Triplet Injector Post Test 004-005 Showing Lack of Face Deposits	212
121.	Triplet No. 2 Injector Post Test 006 Showing Oxidizer Ring Erosion Resulting From Acoustic Instability	214
122.	FLOX/ B_2H_6 Injector Temperature History	215
123.	Triplet Injector With Acoustic Cavities - Post Test 007-008	217
124.	$F_2/O_2-B_2H_6$ Thrust Chamber Jacket Inlet Pressure and Discharge Temperature During Fuel Lead Sequence	219
125.	Chamber Pressure vs Time (Test 009)	221
126.	$F_2/O_2-B_2H_6$ Triplet Injector Face Photo Post Test 009 (1/2 Sec Test)	222
127.	No. 1 Regenerative Chamber Viewed From Nozzle End Post Test 009 (1/2 Sec Duration)	223
128.	$F_2/O_2-B_2H_6$ Triplet Injector Face Post Test 010-011 (1.5 and 3.5 Sec Duration)	224
129.	B_2H_6 Regenerative Coolant Discharge Temperature vs Time During Test 013	226
130.	$F_2/O_2-B_2H_6$ Triplet No. 2 Injector Face Post Test 012-013 (2 and 10 Sec Duration)	227
131.	$F_2/O_2-B_2H_6$ Regenerative Chamber Viewed From Injector And Chamber End; and Triplet Injector Face View Post Test 014 and 015 (2 and 25 Sec Duration)	229

132.	Chamber Pressure vs Time (Test 015)	230
133.	Triplet Injector and Regenerative Chamber Post Test 016-017	232
134.	$F_2/O_2-B_2H_6$ Regeneratively Cooled Chamber to Diffuser and Thrust Mount Installation (Tests 016-017)	233
135.	Regenerative Chamber -- Diffuser Installation Illustrating Modified Diffuser Cooling System (Tests 016-017)	234
136.	Chamber Pressure (psig) vs Test Run Duration (Test 017)	235
137.	Heat Flux Profile for Nominal Test Conditions With 9.5-Inch Combustion Chamber (Tests 004, 005, 083)	240
138.	Heat Flux Profile for Nominal Test Conditions With 9.5-Inch Combustion Chamber (Tests 007-008)	241
139.	Calorimeter Test Series No. 2 Triplet Injector Experimental Fuel and Oxidizer Side Pressure Drop vs Flow	242
140.	Comparison of Regenerative Chamber BLC Injection Temperature Transients During Ignition and Early Mainstage (Tests 009-017)	246
141.	Main Fuel Injection Temperature vs Time (Test 017)	247
142.	B_2H_6 Coolant Heat Input vs Time (Tests 015 and 017)	248
143.	$F_2/O_2-B_2H_6$ Regenerative Chamber - H_2O Jacket Heat Load vs Time (Tests 009 to 017)	249
144.	$F_2/O_2-B_2H_6$ Regenerative Nozzle Back Wall Temperature vs Time (Tests 013 and 017)	250
145.	$F_2/O_2-B_2H_6$ Regenerative Nozzle Cold Wall Heat Flux vs Area Ratio	252
146.	Summary of $F_2/O_2-B_2H_6$ Experimental Injector Face Temperatures vs Run Time	253
147.	Coolant Jacket Inlet Pressure vs Time (Test 017)	254
148.	B_2H_6 Coolant Jacket Discharge Pressure vs Time (Test 017)	255
149.	Regenerative Chamber Testing-Injector Pressure Drop vs Flowrate Summary	256
150.	Chamber Pressure Rise vs Elapsed Time (Test 010)	258
B-1.	Effect of Mixture Ratio on Equilibrium Characteristic Velocity for F_2-O_2 (70-30)/ B_2H_6	B-2
B-2.	$F_2/O_2-B_2H_6$ Theoretical c^* vs Mixture Ratio Full Shifting Composition	B-3
B-3.	Equilibrium 70/30 $F_2/O_2-B_2H_6$ Flame Temperature and Enthalpy vs Mixture Ratio (77 F)	B-4
B-4.	Effect of Mixture Ratio on Equilibrium Specific Impulse for F_2-O_2 (70-30)/ B_2H_6	B-5

B-5.	Effect of Area Ratio on Equilibrium Specific Impulse for F_2-O_2 (70-30)/ B_2H_6	B-6
B-6.	Effect of Chamber Pressure on Equilibrium Specific Impulse for F_2-O_2 (70-30)/ B_2H_6	B-7
B-7.	Effect of Chamber Pressure on Equilibrium Specific Impulse for F_2-O_2 (70-30)/ B_2H_6	B-8
B-8.	Effect of Mixture Ratio on Nozzle Reaction Kinetic Efficiency for 15-Degree Long Throat Cone for 100 psia Chamber Pressure (Sudden Freezing Assumed)	B-10
B-9.	Characteristic Velocity Heat Loss Efficiency vs Mixture Ratio for 50 psia Chamber Pressure	B-11
B-10.	Characteristic Velocity Heat Loss Efficiency vs Mixture Ratio for 100 psia Chamber Pressure	B-12
B-11.	Characteristic Velocity Heat Loss Efficiency vs Mixture Ratio for 200 psia Chamber Pressure	B-13
D-1.	Reference Case Throat Isotherms for Boiling Water Heat Transfer	D-2
D-2.	Throat Isotherms for Boiling Water Heat Transfer and One Blocked Diborane Passage	D-3
D-3.	Reference Case Throat Isotherms for Non-Boiling Water Heat Transfer	D-4
D-4.	Throat Isotherms for Non-Boiling Water Heat Transfer and a Local Heat Flux Increase	D-5
D-5.	Throat Isotherms for Non-Boiling Water Heat Transfer and a Local Heat Flux Increase	D-6
D-6.	Comparison of Wall Isotherms for the ₂ Combustion Chamber at a Heat Flux of 1.5 Btu/in ² -sec	D-7
D-7.	Isotherms at $x = -8.0$ Inches for Selected Design	D-8
D-8.	Isotherms at $x = -6.0$ Inches for Selected Design	D-9
D-9.	Isotherms at $x = -4.0$ Inches and $x = -2.5$ Inches for Selected Design	D-10
D-10.	Isotherms at Sonic Point for Selected Design	D-11
D-11.	Isotherms at $\epsilon = 6.0$ for Selected Design	D-12
D-12.	Isotherms at $\epsilon = 10$ for Selected Design	D-13
D-13.	Isotherms at $\epsilon = 15$ for Selected Design	D-14
D-14.	Isotherms at $\epsilon = 19$ for Selected Design	D-15
E-1.	PRA Test Facility Overall Arrangement	E-2
F-1.	Nevada Field Laboratory Small Engines Area	F-2

TABLES

1.	Coolant Mass Velocity Requirements at Nozzle Throat	15
2.	Nominal Injector Flow Distribution Overall Mixture Ratio = 3.0:1	27
3.	Nominal Injector Mass FLUX Distribution	30
4.	Task II Test Description	69
5.	Task II Test Data Summary	72
6.	Vacuum Specific Impulse Test Summary	73
7.	B ₂ H ₆ Heated Block Testing Summary	116
8.	Summary of OF ₂ Heated Block Testing	124
9.	OF ₂ Coolant Heat Transfer Test 024 Summary	126
10.	Channel Geometry Selection	131
11.	Typical Diborane Pressure Budget	156
12.	Summary of Back Wall Thermocouple Measurement Locations for F ₂ /O ₂ -B ₂ H ₆ Regenerative Chamber	175
13.	F ₂ /O ₂ -B ₂ H ₆ Task IV Experimental Test Program Summary	208
14.	Task IV Calorimeter/Regenerative Data Summary (F ₂ /O ₂ -B ₂ H ₆)	237
15.	Comparative Performance Data for Experimental Calorimeter Testing - O ₂ /F ₂ -B ₂ H ₆	238
16.	Regenerative Testing Performance Evaluation	244
E-1.	Instrumentation List for Task IV Tests	E-5

INTRODUCTION

Previous investigations established the performance and regenerative cooling capabilities of B_2H_6 fuel with FLOX and OF_2 mixtures for space propulsion applications involving low chamber pressures (100 psia) and relatively low thrust levels (1000 lb). The present effort was undertaken because of the expanded interest in application of these propellants to establish workable hardware for future application to space propulsion systems. The overall goal of the investigation was to provide analytical data, with experimental verification, to define the regenerative cooling capabilities of B_2H_6 when used with FLOX mixtures or OF_2 .

The program, conducted at Rocketdyne, was directed to provide these data over a range of variables. To obtain valid experimental heat transfer data in the combustion chamber and throat regions, it was necessary to conduct the tests with a high performance injector. Accordingly, a primary goal of this program was also to provide an injector capable of delivering a high characteristic exhaust velocity (c^*) (93-96 percent of the theoretical value) for the conditions tested. A final goal was to provide an injector capable of stable operation at the design point.

The completed project had a duration of 20 months and was initiated on 1 May 1970. The report to follow contains a summary description of the technical effort tasks. The four technical tasks are summarily described as follows:

Task I: Preliminary Analysis and Experimentation

This task consisted of preliminary studies in sufficient depth that the basic cooling concept could be selected and the project plan could be formulated. Backup panel oxidizer cooling with an advanced construction chamber was selected.

Task II: Determination of Design Criteria and Critical Limitations

This task contained experimental and analytical efforts to develop information on both the combustion side and coolant side of the

thermal management problem. The basic triplet injector was also checked out in this task.

Task III: Design and Fabrication of Demonstration Engine

In this task, detailed thermal balance and flow analyses were conducted and two regeneratively cooled thrust chambers were designed and fabricated. A triplet injector modified was also fabricated. The design and thermal analysis details were provided, followed by the fabrication of the injector and chambers.

Task IV: Demonstration Firings

In this task calorimeter and regeneratively cooled thrust chamber assemblies were checked out and fired for successively increasing durations to the final B_2H_6 regenerative testing of 45 seconds duration. Figure 1 illustrates the 20:1 area ratio B_2H_6 regeneratively cooled thrust chamber assembly with the concentric water jacket.

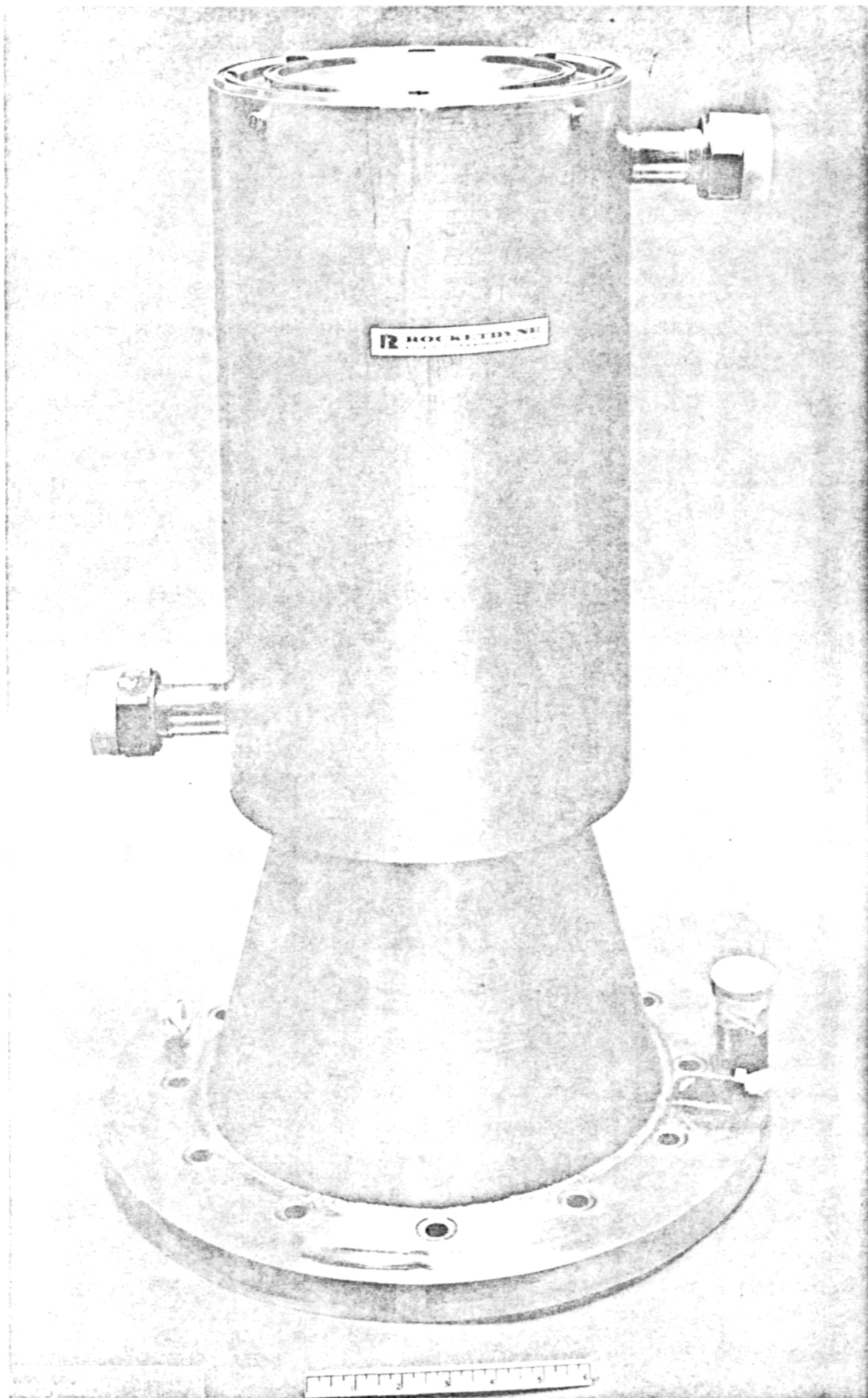


Figure 1. Final Assembly of No. 1 Thrust Chamber with Auxiliary Water Cooling Jacket Installed

SUMMARY

TASK I - PRELIMINARY ANALYSIS AND EXPERIMENTATION

In Task I the engine cooling concept was selected and preliminary analyses were conducted on the thermal management of the thrust chamber. The cooling concept chosen utilized both propellants as coolants with both vaporized within the cooling jackets. The diborane was to be vaporized in the nozzle region and cool the throat and combustion chamber as a gas. The oxidizer was to flow in a cooling panel behind the diborane, cool the throat as a liquid, and be vaporized as the secondary coolant of the combustion chamber. This design was to accommodate a throat peak heat flux of $4-5 \text{ Btu/in}^2\text{-sec}$.

A high performance gas-gas injector was proposed for use in the calorimeter test program and for potential backup use in the regenerative test demonstration during Task IV. The injector had a triplet design with the elements arranged in four rows, with a separately manifolded boundary layer coolant ring.

A heat transfer test program was planned to evaluate the cooling capability over the liquid, two phase and gas range of both propellants. Copper blocks were to be used as constant temperature heat sources for the coolant flowing in a small drilled passage. Instrumentation in the copper mass as well as in the coolant passages were to provide the necessary pressure and temperature data.

TASK II - DETERMINATION OF DESIGN CRITERIA AND CRITICAL LIMITATIONS

The Task II experimental efforts in the areas of coolant property determination and calorimeter thrust chamber tests provided most of the information needed for final design of the demonstration engine. Several critical engine features were demonstrated and the results of Task II, in summary, were a confirmation of the viability of the selected design concept.

Thirteen tests for diborane cooling heat transfer coefficients, both in the gas and liquid phase were conducted. The gas results were in agreement with previous experiments and the liquid data indicated that it would not be difficult to keep the wall temperatures within acceptable limits with nucleate or film boiling conditions. In addition to the normal heat transfer coefficient tests, a single continuous cooling test at extreme conditions was conducted for 1000 seconds, full engine firing duration, without passage deposit problems. In all, 2700 seconds of diborane testing were conducted without servicing the coolant passages in any way.

The OF_2 cooling evaluation was conducted in 29 tests to determine OF_2 capability. During the testing one of the flow bypass lines was inadvertently left open resulting in a questionable test section flowrate. Based on the average pressure level and test section heat flux, however, it is believed that the OF_2 behaved as predicted.

Combustion chamber geometry was examined in a parametric study which led to a nominal design for use in the calorimeter test program. The contraction area ratio selected was 4:1, with a nominal combustion chamber length of 9.5 inches from the injector to the throat. Chamber lengths of 7 and 12 inches were also selected for calorimeter test evaluation. A calorimeter heat sink copper chamber was designed and fabricated.

A gas-gas injector was fabricated and tested in the Task II calorimeter test program at the Rocketdyne Reno facility. The test results showed that the injector with boundary layer bias cooling is capable of controlling heat flux to the chamber wall as expected. The heat flux profile was in good agreement with pre-test predictions. Throat heat flux levels of 3.5 to 4.5 $\text{Btu/in}^2\text{-sec}$ were obtained at performance levels in excess of 96 percent c^* efficiency. Injector face heat flux was somewhat higher than anticipated, at a level of about 1 $\text{Btu/in}^2\text{-sec}$ at nominal conditions. Injector face deposition was satisfactory at nominal conditions but was strongly sensitive to mixture ratio, increasing as mixture ratio decreased. Minor changes to the injector were planned to correct these deficiencies. In all the injector performed well and the next injector differed only in minor details.

Thrust chamber design studies were concentrated on conceptual designs conducted in parallel with coolant passage optimization studies. Coolant passage studies were conducted for the full double panel engine, although a water jacket was used to simulate the OF_2 passages in the demonstrator engine during Task IV study. The planned approach for the Task IV demonstrator engine was to design for a high throat heat flux level and to then maintain the throat heat flux of 3.5 to 4.5 Btu/in²-sec demonstrated in the Task II calorimeter test program.

TASK III - DESIGN AND FABRICATION OF THE REGENERATIVE THRUST CHAMBER

During the Task III period of program activity, effort was spent on the analysis, design and fabrication of the regeneratively cooled demonstration thrust chamber. The engine was designed for primary cooling by diborane and secondary backup cooling by water simulating oxygen difluoride cooling in the actual flight design. In addition, a second modified triplet injector was designed and fabricated.

The heat transfer analysis and design during this study resulted in the selection of a 90 coolant passage geometry with the diborane flowing from the nozzle region upstream toward the injector with the diborane vaporizing as it cooled the nozzle and cooling the throat as a gas. The water was planned to simulate the OF_2 , contributing to the throat and combustion chamber cooling. If OF_2 were actually being used this would allow the OF_2 to vaporize before entering the injector.

Thrust chamber detail design was completed and the design approved for fabrication. Two thrust chambers, one water cooling jacket and the triplet injector were fabricated. Procurement and machining of the No. 1 and No. 2 OFHC copper chamber forgings to the final external and internal chamber contour dimensions were accomplished with excellent dimensional control and tolerances achieved. Completion of the slotting of the coolant channels for the chambers was accomplished preparatory to nickel closeout electroforming. The No. 2 triplet injector copper rings and CRES body were machined and orifice pattern drilled.

Fabrication effort on the No. 1 and 2 regenerative chambers was brought to a successful conclusion through the final phases of slotted liner waxing and surface activation, electroform Ni flash plating and final nickel buildup. Subsequent machining operations of outside surface contouring and manifold braze attachment were also successfully accomplished. The required external water jacket closure and shell were also completed. No fabrication difficulties with the exception of greater than anticipated fabrication flow time and minor upper and lower manifold braze shrinkage cracks and coolant passage plug leakage. Both No. 1 and No. 2 chambers fabricated were excellent, verifying the soundness of the selected fabrication approach.

The No. 2 triplet injector was successfully completed with some early difficulty in ring to land braze bond voids which were remedied by rebrazing a second time at lower temperature. Inspection indicated the No. 2 triplet to be an excellent injector available for the calorimeter and regenerative chamber test series under Task IV.

TASK IV - CALORIMETER/REGENERATIVE CHAMBER TESTING

During Task IV, successful testing of the No. 2 triplet injector in both the uncooled copper calorimeter hardware and the H_2O/B_2H_6 regeneratively cooled copper-nickel chamber was completed. Altitude testing ($\epsilon = 20$) was also successfully accomplished in both the calorimeter chamber hardware and regenerative chamber. Thrust level measurements were taken but not reduced due to diffuser interactions.

Fabrication of the gaseous F_2/O_2 and B_2H_6 flow system and plumbing were completed for the Yoke stand facility at the Santa Susana Propulsion Research Area. The oxidizer side as gas at ambient temperature was provided for calorimeter and regenerative test runs from large gaseous FLOX storage tanks. Liquid B_2H_6 was transferred from dry ice packed portable storage cylinders directly to a 25 gallon run tank. B_2H_6 was gasified by a water to B_2H_6 in-line heat exchanger for the calorimeter testing and fed directly to the chamber inlet for the regenerative series.

Diffuser assembly, water jacketing and mounting were completed with flexible rods for diffuser mounting alignment provided to allow a maximum of diffuser flexibility and correct axial alignment. Modification of the existing GN_2 -ejector-driven altitude diffuser was necessary, after preliminary testing, to provide the altitude pumping capability. With the increased flow capacity GN_2 system completed, tests performed with the modified feed system (60 lb/sec GN_2 flow) permitted an allowable duration of greater than 75 seconds (without excessive tank pressure decay). The diffuser pressure was low (≤ 1.0 psia) to prevent calorimeter and regenerative nozzle ($\epsilon = 20$) flow separation. Modification to the initial H_2O cooling system for the diffuser was also accomplished to provide H_2O flowrates (40 lb/sec) for successful long duration operation when it was determined from initial testing that the water flow supply rate was insufficient (24 lb/sec) for the high performance F_2/O_2 - B_2H_6 propellants. Both the GN_2 and H_2O supply modifications provided successful operation subsequently.

Blowdown testing of both the gaseous F_2/O_2 servo-controlled sonic venturi feed system and the B_2H_6 conditioned fuel system supply for the calorimeter chamber was accomplished in a preparatory test series. Satisfactory calibration, control and passivation of the F_2/O_2 system were accomplished without incident. Three blowdown series for the B_2H_6 supply system were necessary to provide a satisfactory time sequencing and the required B_2H_6 outlet temperature. An initial large volume heat exchange system was also modified to provide a higher response lower volume system. Additional system valving and control were similarly accomplished to develop a satisfactory start and cutoff sequence and to ensure good ignition and a shutdown free of excessive chamber and injector deposits. These modifications were verified by subsequent calorimeter test results. Sonic venturis were provided for the gaseous OF_2 and B_2H_6 . A cavitating venturi was employed for liquid B_2H_6 regenerative testing.

Five calorimeter hot fire tests were conducted to verify injector/chamber stability, performance and integrity, gas side deposit buildup and accumulation effects, and the effects of boundary layer coolant flow on chamber heat transfer and gas side deposits. Test results indicated heat transfer profiles

to be similar to previous Task II calorimeter data on the No. 1 triplet injector. Throat peak heat fluxes were $4.0 \text{ Btu/in}^2\text{-sec}$ with the effects of wall insulating deposits and the boundary layer fuel bias flow. Throughout the Task IV test series there were no heavy deposits on the chamber wall or the injector face, believed due to the better aspirating effects of the triplet No. 2 higher velocity oxidizer injector orifices and test operation at a moderately high o/f ratio (3.0).

High frequency combustion instability was encountered during one high fuel flow bias (43 percent) run (Test 006) with minor injector damage sustained during this test. Acoustic cavities were incorporated into the injector periphery and subsequent tests indicated no instability tendency.

Nominal targeted mixture ratio and chamber pressure were accomplished in a nine-test final series on the regenerative chamber No. 1 employing the No. 2 triplet injector. Satisfactory ignition thrust buildup and mainstage were achieved during successively increasing durations of 0.5 to 45 seconds steady state duration. Stability, performance and injector/chamber deposit conditions appeared good with wall heat load conditions varying to slightly over the originally anticipated target values. Chamber and injector hardware is in original condition.

All phases of the planned $\text{F}_2/\text{O}_2\text{-B}_2\text{H}_6$ program testing were successfully concluded with the final regenerative 45-second demonstration test verifying the regenerative concept.

CONCLUSIONS AND RECOMMENDATIONS

The following specific conclusions and recommendations are based upon the results of the analytical and experimental investigation conducted during the present study.

1. Regenerative cooling with B_2H_6 fuel, and with FLOX or OF_2 as the oxidizer, is feasible over a range of mixture ratios at the 1000-pound thrust level and 100 psia chamber pressure.
2. B_2H_6 cooling appears as predicted with the decomposition aspect controllable.
3. Regenerative cooling with B_2H_6 has been demonstrated at a chamber pressure of 100 psia from $MR = 2.8$ to 3.1 in an advanced construction chamber.
4. The triplet impinging element injectors tested resulted in acceptable heat fluxes in the combustion zone and throat region with augmenting peripheral boundary layer coolant.
5. High injector performance ($\eta_{c*} \geq 95$ percent) and good face heat transfer were demonstrated and are obtainable using a triplet injector pattern with the FLOX/ B_2H_6 propellant combination.
6. Specific impulse values of ≥ 400 seconds can be achieved at a chamber pressure of 100 psia, mixture ratio of 3.0, and nozzle area ratio of 60 with the OF_2/B_2H_6 propellant combination.
7. Fabrication of an OF_2/B_2H_6 copper-nickel thrust chamber with milled channel design is feasible using an electroforming wall closeout.
8. Further component and integration studies leading to development of an OF_2/B_2H_6 engine should be undertaken.
9. Additional regenerative thrust chamber and injector tests should be conducted to further demonstrate:
 - a. Dynamic stability
 - b. Thrust and impulse measurements

- c. Injector modifications to suppress wall deposits
- d. Flightweight hardware fabrication and operating characteristics
- e. Flight required start and cutoff transients
- f. Total heat input reduction techniques
- g. Double jacket $\text{OF}_2/\text{B}_2\text{H}_6$ cooling
- h. A lightweight $\epsilon = 60$ radiation nozzle.

TECHNICAL DISCUSSION

TASK I - PRELIMINARY ANALYSIS AND EXPERIMENTATION

The purposes of Task I study were to develop preliminary studies in sufficient depth and detail to select the basic $\text{OF}_2\text{-B}_2\text{H}_6$ regenerative cooling and thrust chamber concepts, and to provide a design of a compatible, stable, impinging element injector with high performance and good heat transfer characteristics. A description of the thrust chamber and preliminary cooling background, and the injector definition phase are described in the following Task I section.

THRUST CHAMBER AND COOLING CONFIGURATION SELECTION

One of the objectives of Task I preliminary study was to select the choice of propellants to be used as coolant, its phase at injection, approximate wall heat flux levels for design, and candidate regenerative chamber fabrication techniques. Considerations leading to these choices, as well as the selection of the combustion chamber, are described in the following.

Optimum Thrust Cooling Approach

The first critical decision in the thermal management was the means of cooling the nozzle throat. Initially, both oxidizer and fuel in both the liquid and gas state were considered. The necessary diborane heat transfer data were available from a Rocketdyne heat transfer study (summarized in Fig. 2). The results indicated that liquid B_2H_6 under a boiling situation could absorb a heat flux of 1.0 to 1.5 Btu/in²-sec. O_2 and F_2 heat transfer data were examined to compute the cooling capability of gaseous OF_2 . For liquid OF_2 cooling, Gambill's equation for forced convection cooling with nucleate boiling was considered satisfactory (Ref. 1).

Another primary consideration in the selection of the basic coolant condition was the coolant high temperature stability. For exposure times of 1 to 10

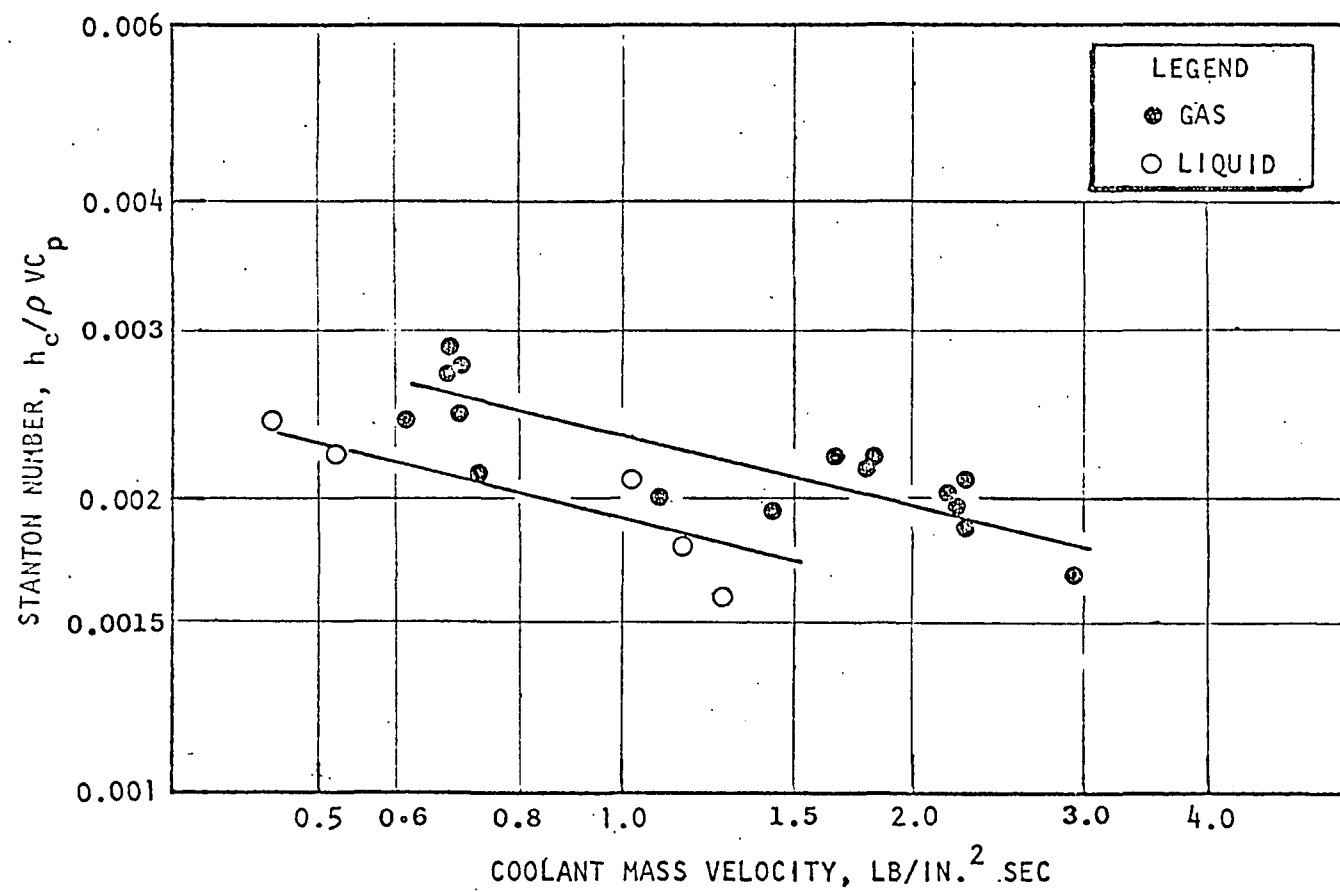


Figure 2 . Stanton Number Correlation of IR&D B₂H₆ Heat Transfer Data

milliseconds (typical thrust chamber stay times) with reasonable jacket temperatures, both OF_2 and B_2H_6 propellants are sufficiently stable to be considered as coolants.

A throat mass velocity requirement comparison was made with the assumptions of a minimum passage size of 0.0016 sq. in., which corresponds to conventional fabrication limits, and a minimum of 80 cooling passages. A throat heat flux value of 3 Btu/in²-sec was developed from analytical and previous experimental study (4-5 Btu/in²-sec design level). The specification of minimum coolant area places a maximum value on coolant mass velocities for the four cooling approaches, and on the actual mass velocity possible with each. The low coolant-side wall temperatures for nucleate boiling (due to the low saturation temperatures of both liquid coolants) lead to considerably higher mass velocity requirements than those available. The calculated mass velocity available for gaseous oxidizer cooling was approximately equal to the mass velocity required to cool the throat. However, this mass velocity can be achieved only at high pressures of 510 psia or more (Mach number ≤ 0.6).

It was evident that neither liquid fuel nor liquid oxidizer was suitable as the primary coolant, and gaseous OF_2 would be marginally capable at lower heat flux levels but intolerable in terms of jacket pressure drop. Table 1 and Fig. 3 indicate gaseous B_2H_6 is a suitable coolant for a 3 Btu/in²-sec throat heat flux with a minimum B_2H_6 pressure of 140 psia (Mach number of 0.6). Heat flux levels moderately above 3 Btu/in²-sec could still be cooled by gaseous B_2H_6 . Available data during Task I study indicated that the throat heat flux was in this range, and gaseous B_2H_6 was capable of regenerative cooling the throat of an $\text{OF}_2/\text{B}_2\text{H}_6$ thrust chamber by itself, even with wall temperatures reduced to avoid the problem of deposition.

Provision of gaseous B_2H_6 , selected as the primary throat coolant, required that liquid B_2H_6 cool some other part of the engine and in doing so be vaporized.

Figure 4 illustrates a cutaway sketch of a prototype configuration.

TABLE 1. COOLANT MASS VELOCITY REQUIREMENTS AT NOZZLE THROAT

GROUND RULES

1. Individual coolant passage area = 0.0016 in^2
2. Minimum of 80 passages
3. Coolant condition near optimum for cooling regime.
4. Throat heat flux = $3 \text{ Btu/in}^2\text{-sec}$

Coolant	Regime	Coolant Side Wall Temperature, (R)	Bulk Temperature, (R)	Required Mass Velocity, $\text{lb/in}^2\text{-sec}$ for $3 \text{ Btu/in}^2\text{-sec}$	Potential Mass Velocity, $\text{lb/in}^2\text{-sec}$	Coolant Pressure,* (psia)
B_2H_6	Nucleate Boiling	450	250	9.0	5.2	---
	Forced Convection Gas Phase	1060	450	2.5	5.2	140
OF_2	Nucleate Boiling	320	190	35	15.9	---
	Forced Convection Gas Phase	1360	350	15	15.9	510

* Minimum pressure for required mass velocity at Mach number less than 0.6

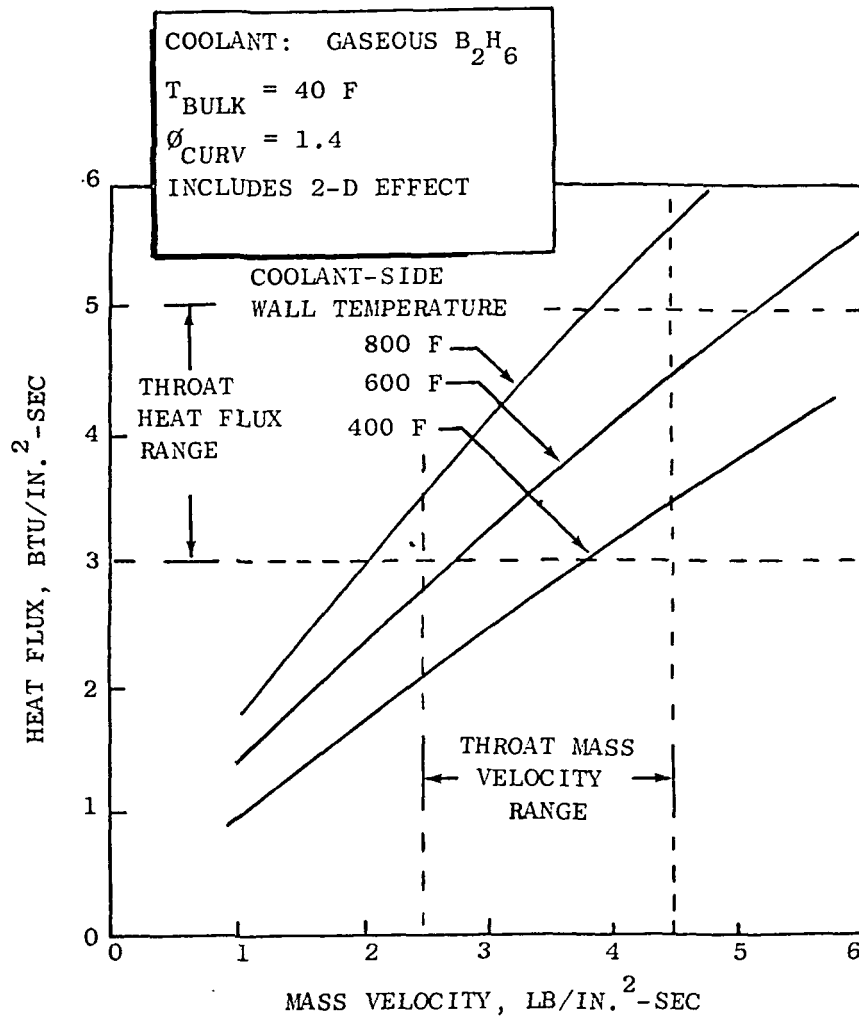


Figure 3 . Gaseous Diborane Throat Cooling Capability

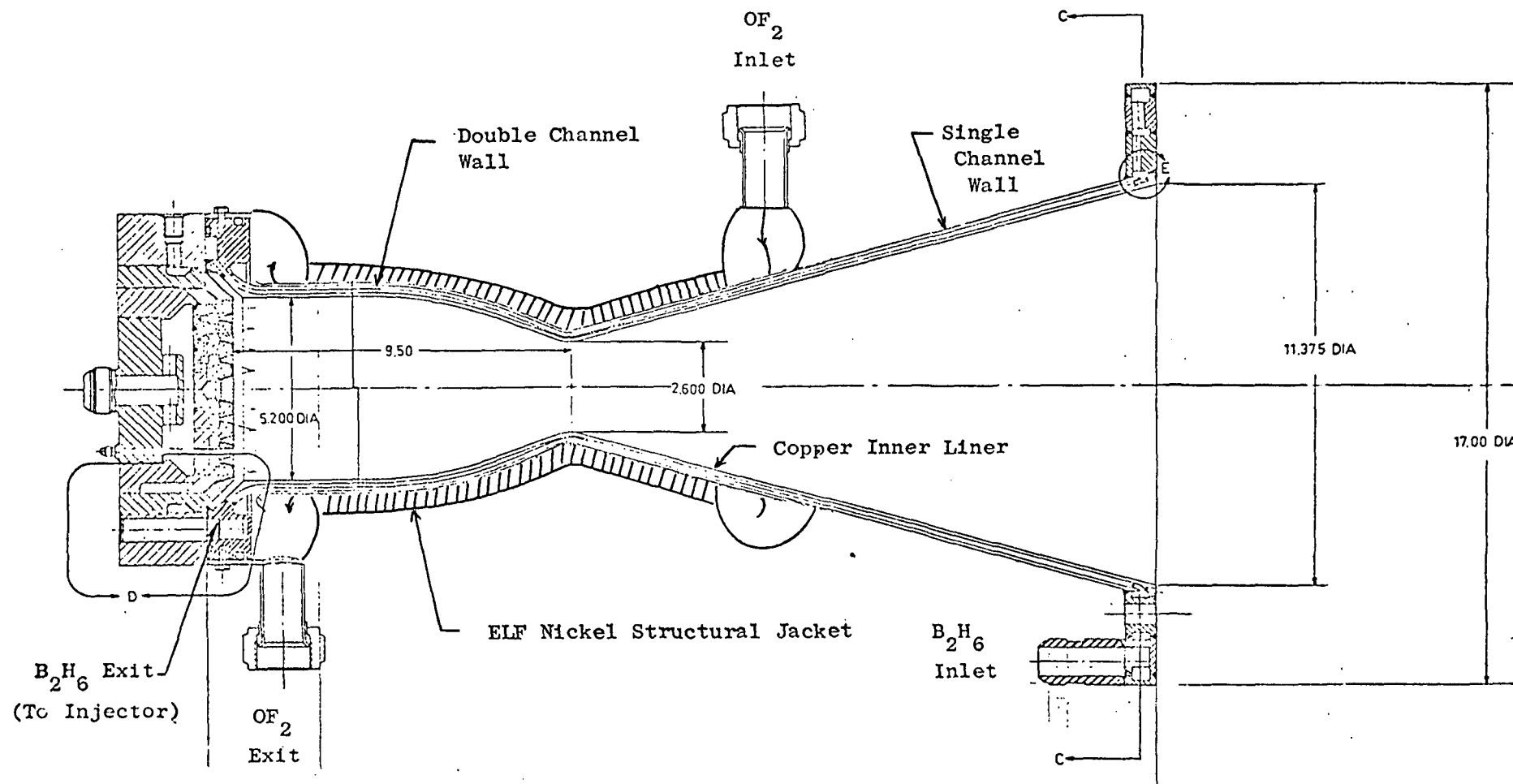


Figure 4. Prototype OF₂/B₂H₆ Cooled Thrust Chamber Assembly (Sketch)

Combustion Chamber and Nozzle Cooling

The two available regions for B_2H_6 liquid cooling and phase transition were the combustion chamber and nozzle. At subcritical pressures, the B_2H_6 film boils and in this condition is a poor coolant. The location in the jacket at which film boiling occurred was dependent on the inlet temperature of the B_2H_6 and is a partially uncontrolled variable. The combustion chamber normally is an area where high local heating may occur for a variety of reasons, and thus was not seen as a desirable location for the primary B_2H_6 coolant to undergo a phase change. The nozzle section operates at a relatively low heat flux, with good uniformity and therefore is the most desirable place for B_2H_6 vaporization. The selected configuration for fuel cooling was a single uppass circuit where the B_2H_6 was vaporized in the low heat flux nozzle before it entered the throat and higher heat flux combustor regions. The highest nozzle area ratio actively B_2H_6 cooled was selected (at 20:1) so that the B_2H_6 could be vaporized with the coldest projected inlet temperature (210 R); this selection was made during Task II.

Although the oxidizer is not adequate as a primary coolant, there are advantages to vaporizing it before injection:

1. The oxidizer can provide backup cooling and increase the throat cooling capability by approximately 1 to 1.5 Btu/in²-sec.
2. Gaseous oxidizer injection assists in achieving high combustion performance and will permit axial injection, which promotes uniformity and aids in thermal control of the combustion chamber and throat.
3. Gaseous injection of both propellants can (at some future date) simplify design of a throttleable version of the basic engine demonstrated in the study.
4. Empirical evidence exists that gaseous injection is favorable from the standpoint of minimizing injector face combustion deposits.
5. Previous Rocketdyne test experience with F_2-O_2 indicated that at the warm end of the nominal OF_2 temperature range (210 to 280 R), it would not be possible to avoid two phasing of the liquid OF_2 in the

injector elements. The potential impact of this phenomenon on mixture ratio control appeared untenable with the only practical solution as gaseous injection.

6. Vaporization of the oxidizer in the jacket permits propellant storage at higher temperatures, because two phasing in the injector would no longer be a problem. This might permit the system benefit of extending the propellant storage range closer to 310 R.
7. Experience gained in Rocketdyne's IR&D heat transfer test program indicated that B_2H_6 exposed to a hot surface (e.g., in a cooling jacket) and partially decomposed in contact with a cold surface causes decaborane deposition, and gaseous oxidizer injection would be required to preclude cryogenic oxidizer entering the injector for repeated testing.

Higher engine costs, weight, and possibly more complex start dynamic conditions are arguments against oxidizer vaporization. Based on the information in favor of gaseous injection, together with gaseous injection data on other oxidizers, it was decided that the oxidizer should be vaporized before injection. The considerations that ruled the oxidizer out as a primary coolant did not affect its use as a secondary coolant with the additional beneficial coolant and heat sink capability provided.

Fabrication Method Selection

The simplest system analyzed for vaporizing the OF_2 was a row of coolant passages behind the fuel passages of the throat and combustion chamber. This approach had been used successfully on a number of previous H_2/O_2 and F_2/H_2 studies. Cooling the nozzle with the oxidizer (and vaporizing the fuel in a second row over the chamber) which was considered has the disadvantages of: (1) the B_2H_6 low heat flux capability as a liquid and its requirement for vaporization, (2) a gas transfer line needed to carry the vaporized OF_2 from the skirt to the injector (start transient fill problem), and (3) a complex manifold joint at approximately 7:1 area ratio.

Two classes of fabrication concept were considered for regenerative cooling. The classical method, used on most regeneratively flight cooled engines to date, is a brazed tube wall construction. Many newer prototype engines however, are of nontubular construction in which coolant channels are provided within a thickness of parent material. Tube wall designs are the lightest designs at a higher cost, however, the corrugated effect on the gas wall contour produces an additional heat load (about 15 percent, Ref. 2). Secondary backup oxidizer coolant circuiting which appeared in an optimum $\text{OF}_2\text{-B}_2\text{H}_6$ configuration was possible with difficulty, since little heat transfer occurs to the back of the thin wall tubes. The channel construction method selected offered the advantage of a flat gas-side surface, with a resultant lower total heat input. A selected variable land width (between channels) design allows control of the quantity of heat flowing to the sides and back of the passages due to fin effect allowing more of the coolant surface available for heat transfer and reducing wall temperature (a critical factor for diborane). Both nickel and copper appeared to have sufficient conductivity for this. The material selection made during Task II was OFHC copper.

Summary of Task I Optimization Study

In summary, the optimum engine configuration determined was as follows:

1. The primary coolant was to be diborane, entering the cooling jacket in the expansion nozzle, vaporizing toward the throat, cooling the throat as a gas, cooling of the combustion chamber as a gas, and injected as a gas.
2. The oxidizer was to enter a secondary backup cooling panel downstream of the throat, contribute to the cooling of the throat as a liquid, flow upstream over the combustion chamber absorbing enough heat to vaporize, and enter the injector as a gas.
3. The injector resulting from the above analysis was a gas-gas injector.

4. Auxiliary cooling (i.e., fuel bias or boundary layer control (BLC)) appeared necessary for combustion chamber heat transfer uniformity and reduced throat heat flux conditions.
5. The thrust chamber design was to be based on the use of a milled channel construction.

Demonstration Configuration

Within the planned scope and budget of the program it did not appear possible to fabricate and test thrust chambers with the double panel optimum design configuration. A less expensive alternate approach was adopted; a single coolant panel built for the diborane and the OF_2 outer cooling panel simulated by a simple water jacket. The feasibility of this approach was examined in a brief study of heat balance to the diborane and water for several cases of interest. Representative results are shown in Fig. 5 and 6, from two-dimensional heat transfer analyses for cases with water and OF_2 as the secondary coolant. The use of water as an OF_2 cooling simulant appeared excellent. A demonstrator shown in Fig. 7 was proposed for testing.

INJECTOR DESIGN SELECTION

In preparation for the Task II uncooled calorimeter test program, the first (Triplet No. 1) injector was designed during Task I. Although primary use for the first injector was for Task II, it was to provide as backup to the Task IV injector (Triplet No. 2). The first injector was designed for suitability with either uncooled calorimeter or regenerative thrust chambers. The following section describes the injector and the analytical studies conducted to support its design.

Injector Requirements

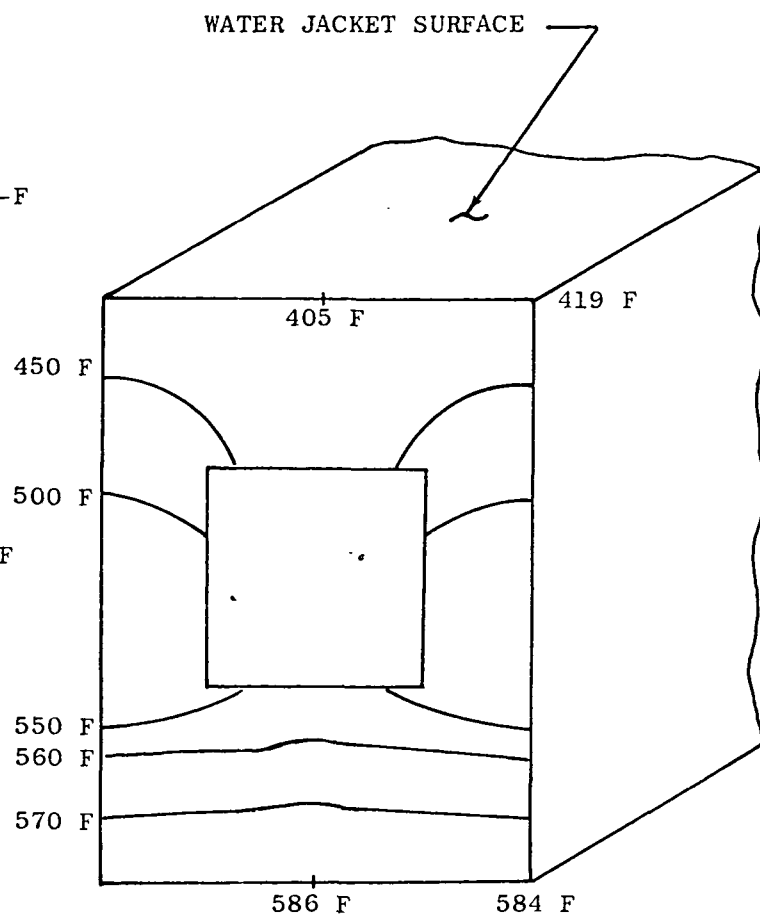
The injector design was controlled by a number of factors, some imposed by the nature of the propellants, others by the thrust chamber cooling concept, by contract requirements, and by program usage. Some of these factors are summarized below.

$$T_B = 70 \text{ F}$$

$$h_c = 0.00342 \text{ BTU/IN.}^2\text{-SEC-F}$$

$$T_{B_2H_6} = 40 \text{ F}$$

$$h_c = 0.0033 \text{ BTU/IN.}^2\text{-SEC-F}$$



$$Q/A = 4.25 \text{ BTU/IN.}^2\text{-SEC}$$

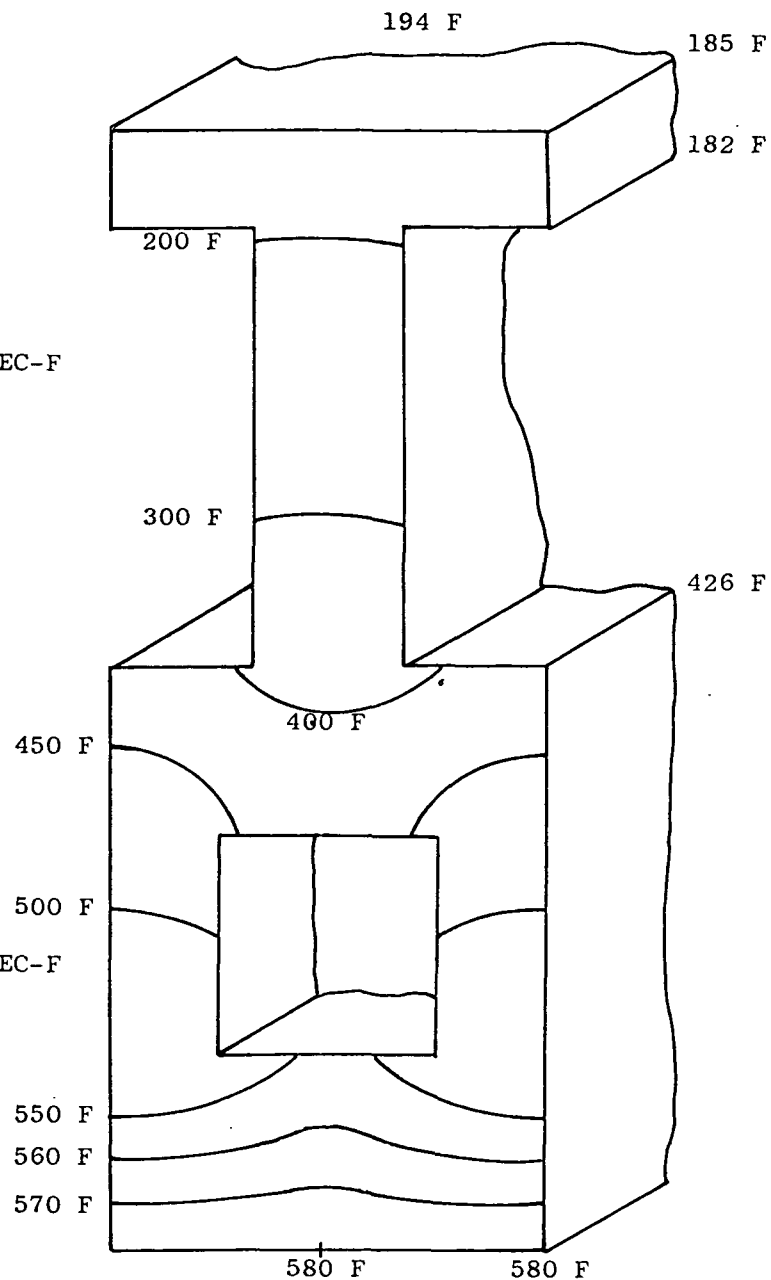
Figure 5 . Throat Wall Isotherms for Typical OF_2/B_2H_6 Water-Jacketed Chamber Design

$$T_{\text{OF}_2} = -175 \text{ F}$$

$$h_c = 0.0008 \text{ BTU/IN}^2\text{-SEC-F}$$

$$T_{\text{B}_2\text{H}_6} = 40 \text{ F}$$

$$h_c = 0.0033 \text{ BTU/IN}^2\text{-SEC-F}$$



$$Q/A = 4.25 \text{ BTU/IN}^2\text{-SEC}$$

Figure 6 . Throat Wall Isotherms for Typical $\text{OF}_2/\text{B}_2\text{H}_6$ Double Panel Design

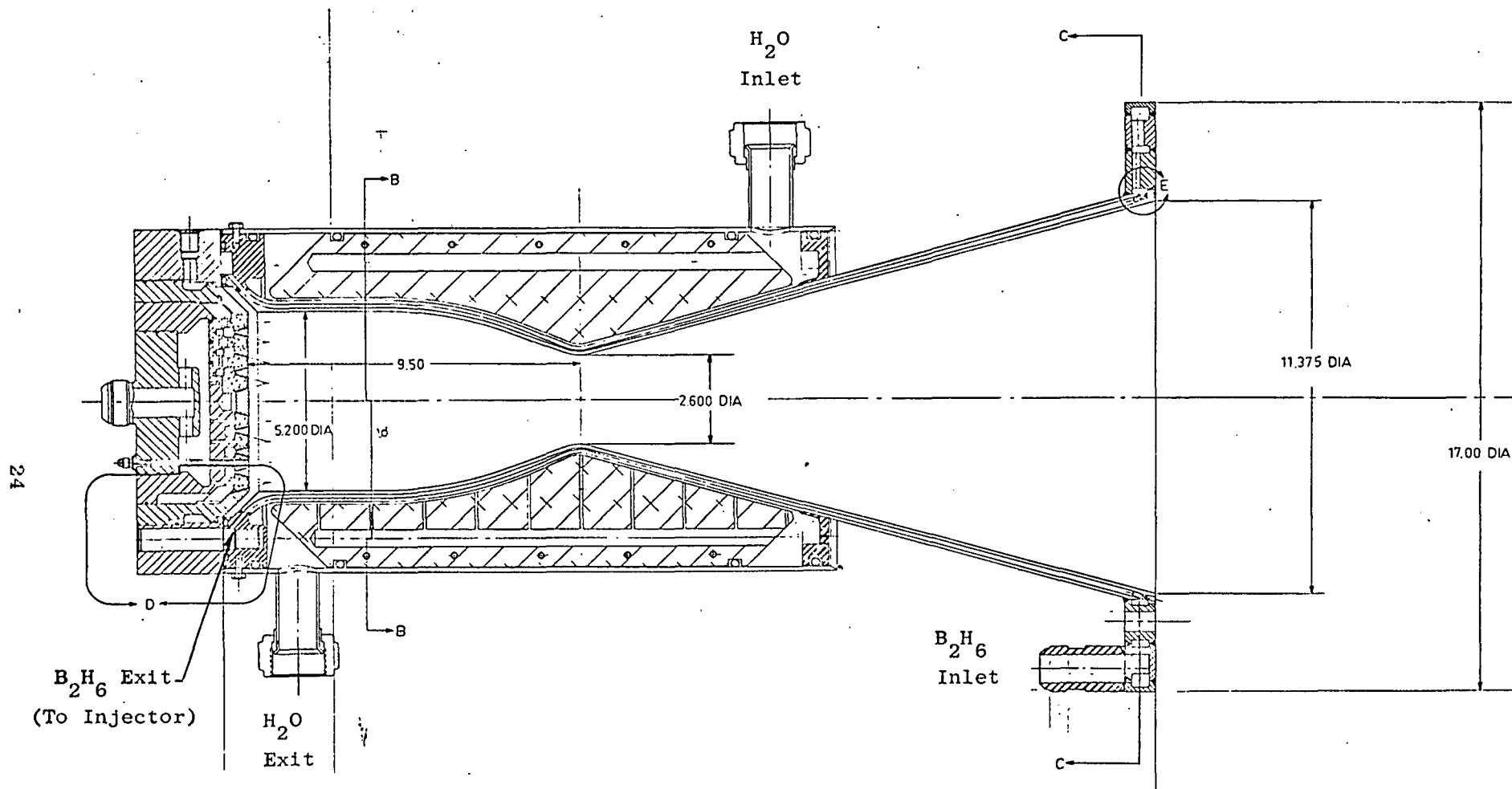


Figure 7 . Demonstrator Thrust Chamber Assembly (H₂O/B₂H₆ Cooled)

1. As a result of the ultimate use of both propellants as thrust chamber coolants, the injector would inject gas (the diborane probably partially decomposed).
2. Because of past experience with diborane in heated metal passages, temperatures of injector surfaces in contact with diborane were to be below 600 F to avoid further decomposition, but above 200 F to prevent deposition of already existing decomposition products ($B_{10}H_{14}$).
3. A conventional impinging (triplet) element pattern was selected. This was specified by the contract and is also in agreement with previous design practice for OF_2/B_2H_6 .
4. Acoustic cavities were to be included in the combustion chamber or injector, as a contract requirement.
5. Separately manifolded and controlled film coolant flow capability was to be provided as a necessity for an economical test program.
6. The injector was to be adaptable as a backup for the regenerative cooling demonstration test program in Task IV.

Injector Design Summary

An injector No. 1 unit was designed which complied with the specifications listed above. The major design features were:

1. The injector pattern contained 96 impinging triplet elements arranged in four concentric rings. The central orifice of each element flows gaseous oxidizer, impinged upon by the two outer gaseous fuel orifices. Both oxidizer and fuel orifices were 10 diameters in length, except the film coolant orifices which were 6 diameters long.
2. The element impingement point was located 0.6 inch from the injector face in an attempt to minimize injector face heating and deposition.
3. The oxidizer entered from behind the injector into a plenum from which the orifices were fed. Both film coolant and core fuel were

radially fed through four inlets each and fed to their respective manifolds for distribution to the injector orifices.

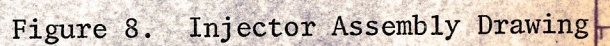
4. At nominal operating conditions, the injector was cooled both by the fuel and oxidizer orifices and secondarily by the fuel manifolds.
5. Nominal injector pressure drop for both propellants was 20 psi at a chamber pressure of 100 psia and an overall mixture ratio of 3.0:1.
6. The injector was a brazed unit, with the portions exposed to high heat flux made of OFHC copper and peripheral parts of 347 stainless steel.
7. The acoustic cavity had one wall in the injector, which also contained the dams, and one wall in the thrust chamber. Orientation was at a 45 degree angle.
8. Instrumentation consisted of injector face pressure measurements, three injector face temperature measurements, two acoustic cavity temperature measurements, and manifold temperature and pressure for each of the three propellant manifolds.
9. Fuel manifold volume was kept as small as possible with required good propellant distribution to minimize B_2H_6 stay time in the injector.

Flowrate Requirements and Flow Distribution

Propellant flowrates were determined for OF_2/B_2H_6 at a vacuum 60:1 area ratio thrust of 1000 lbf with a specific impulse of 405 lbf-sec/lbm. Since, in this program, the oxidizer is a F_2-O_2 mixture instead of OF_2 , the specific impulse was reduced to 398 to account for the difference in propellant base energy level. At a propellant mixture ratio of 3.0:1, the oxidizer and fuel flowrates were estimated.

Oxidizer:	F_2-O_2 (70-30)	1.89 lbm/sec
Fuel:	B_2H_6	0.63 lbm/sec

PAGE MISSING FROM AVAILABLE VERSION

[illegible]

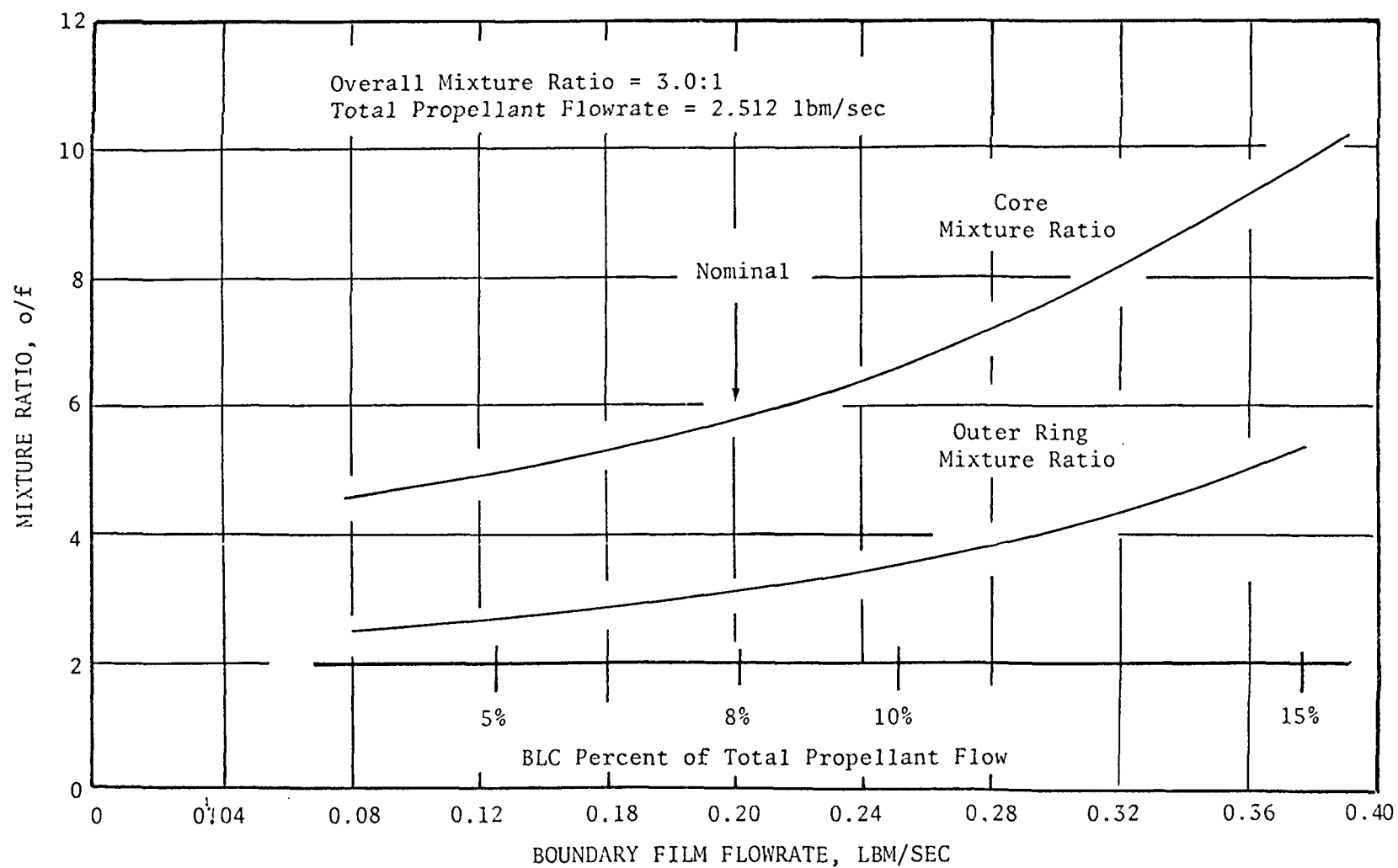


Figure 9. Injector Zone Mixture Ratio Distribution

TABLE 3 . NOMINAL INJECTOR MASS FLUX DISTRIBUTION

Injector Ring (Counting From Inner Ring)	Number of Elements	d_o (in.)	d_f (in.)	Mass Flux $\text{lbm/in}^2\text{-sec}$
1	8	.116	.039	0.090^+
2	18	.116	.039	0.137
3	30	.116	.039	0.118
4	40	.116	.036	0.107^*
Film Coolant	80	--	.0465	

+ For the combined first and second rings, the mass flux is $0.118 \text{ lbm/in}^2\text{-sec}$

* If film coolant is included in the fourth ring, the mass flux is $0.132 \text{ lbm/in}^2\text{-sec}$

Element Design. The triplet element was selected based on study that indicated axially injected oxidizer would minimize both the amount of oxidizer recirculated to the injector face and the likelihood of combustion chamber hot spots resulting from high o/f concentrations. The fuel-oxidizer-fuel (F-O-F) triplet which had an inherently fuel-rich periphery indicated positive mixing of oxidizer and fuel. A showerhead approach was evaluated and eliminated.

A coaxial element injector was eliminated primarily because of the small fuel annulus gap and element plugging appeared more likely with this type of element. An oxidizer annulus would avoid that problem at the expense of an oxidizer-rich periphery, which seemed inadvisable. Moreover, for a coaxial design, the inner propellant flow is unavailable for injector face cooling. Further study with this injector type could be promising but was outside of the scope of the current effort.

Pressure Drop. The injector element pressure drop was selected as 20 psi. Considerations were flow distribution control, Mach number, and chug mode stability (≥ 5 -10 percent pressure drop). Injector face cooling is better at high pressure drop (mass velocity), and pressure-fed propulsion optimization favors low pressure drop. Injector face cooling studies conducted showed that at 20 psi the injector would have a good cooling margin. If the injector face reached its maximum allowable temperature, a heat flux of $1.0 \text{ Btu/in}^2\text{-sec}$ could be tolerated ($0.5 \text{ Btu/in}^2\text{-sec}$ resulted on earlier FLOX/ B_2H_6 testing).

A value of 20 psi was arbitrarily selected to assure that low frequency and chugging were not present. In a further injector-oriented study program, reduction in the pressure drop can be weighed in an overall pressure fed propulsion system balance. A 20-psi pressure drop with the number of fuel orifices produces fuel orifice diameters 0.039 to 0.047 inch (Fig. 8). In previous tests using heated diborane, orifice plugging was never encountered with orifices in this size range. For Task IV use, the fuel pressure drop was expected to increase because of the warmer diborane temperature.

The oxidizer pressure drop was selected as 23 psi with F_2-O_2 (70-30) so that the injector was useful with the more dense OF_2 at a pressure drop of 17 psi.

Manifolding and Feeder Passages

The oxidizer was fed through a dome and then flowed directly from the dome cavity into the injector orifices with volumes and sizes not too critical. For the diborane, two considerations were important. First, the fuel enters from the injector periphery and must be fed radially to the various rings and then circumferentially to the injector elements. Second, the diborane is hot (partially decomposed for Task IV use) when entering the injector. Therefore, stay time must be minimized to prevent further decomposition. To prevent deposition, wall surface temperatures much lower than the freezing point of decaborane (211 F) and stagnation regions were to be avoided.

Figure 10 which extrapolates diborane decomposition data to high temperatures, indicates that at a diborane bulk temperature of 200 F to 300 F, injector volume will not be critical. Stay times will be in the range of 10 milliseconds, compared with a 1-percent decomposition time of 1 second at 300 F. If the diborane reaches 400 F, the diborane stay time will become critical.

In each passage the flow area should be substantially larger than the injector orifice areas that the passage feeds. Following this criterion, the injector pressure drop was distributed such that 98 percent was taken across the element and only 2 percent through the feed passages, to assure that the flow distribution was controlled entirely by the orifice diameter.

Injector Cooling Analysis

A detailed three-dimensional heat transfer study was performed for the selected F-O-F pattern, stratified injector design. A symmetrical section in the vicinity of the first ring which has the highest hot-gas surface area per element was analyzed. Steady-state temperatures were computed considering the cooling of the gaseous diborane flowing in the feed lines and the injector orifices, and the gaseous FLOX flowing through its injector orifices.

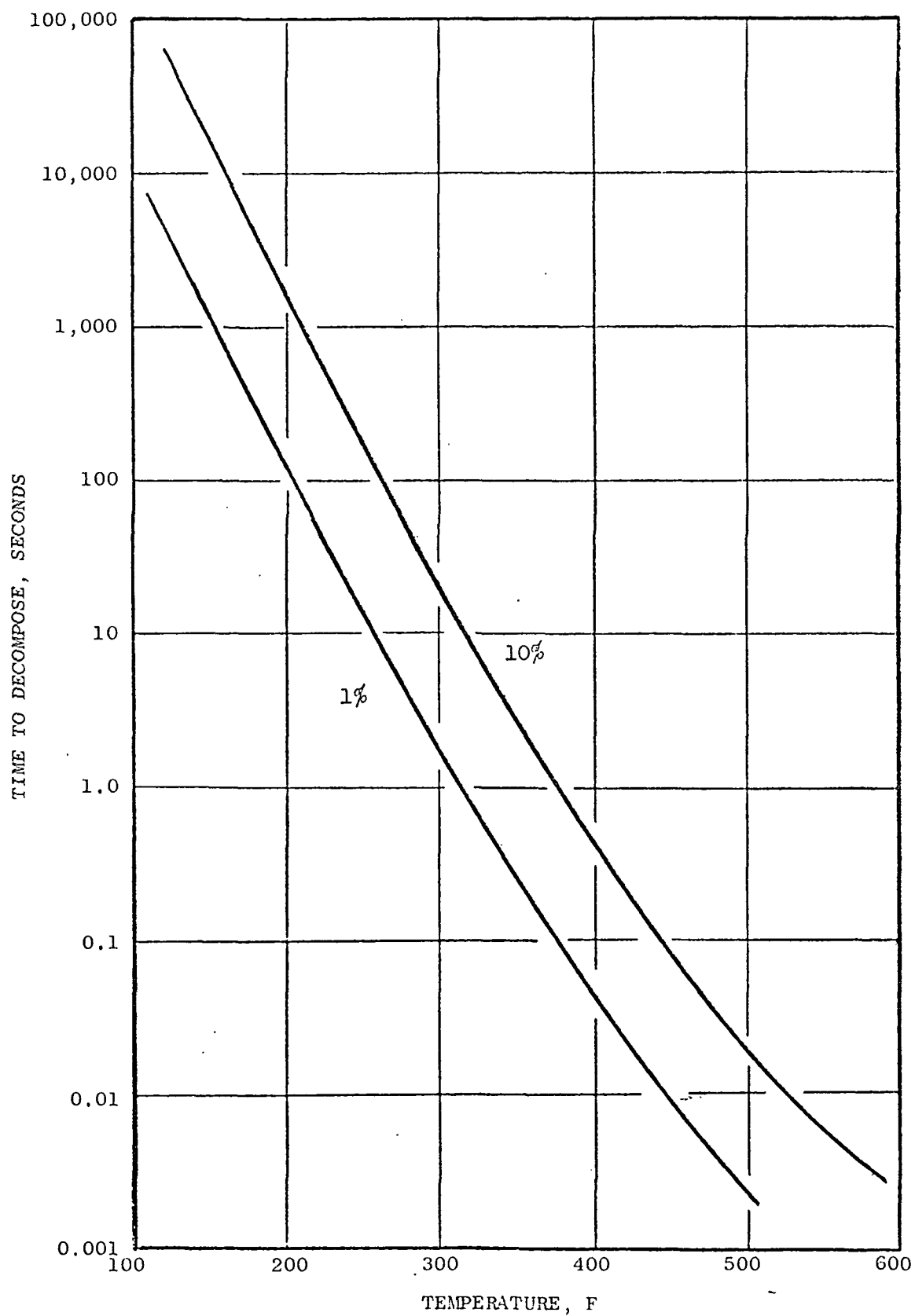


Figure 10. Estimated Diborane Decomposition Rate at High Temperatures

The injector section was analytically simplified to simulate the orifices and diborane feed lines, and wetted surface areas were adjusted to match the actual values. The fuel orifices were considered axial instead of 15 degrees from axial as in the detailed injector design. A 40 F oxidizer and 250 F fuel temperature condition simulated the expected injection temperatures for the uncooled hardware tests under Task II and regeneratively cooled tests under Task IV, respectively. The nominal heat flux was assumed to be $0.5 \text{ Btu/in}^2\text{-sec}$ based on previous Rocketdyne testing with a similar face pattern.

Figures 11 and 12 show representative temperature values for a range of heat fluxes and diborane temperatures of 40 F and 250 F, respectively. Considering the regeneratively cooled hot firings, it was shown that the maximum diborane contact temperature was 325-380 F. If the injector-end heat flux were $1.0 \text{ Btu/in}^2\text{-sec}$, comparative temperatures of 600 F and 510 F would be expected. This means that the injector was capable of absorbing twice the nominal steady state heat load. Comparable temperatures for uncooled operation show that the steady state heat flux margin is 2.5:1.

Injector wall temperature distribution for regenerative cooling operation is shown in Fig. 13 for nominal conditions. Isotherms are located in planes nearly parallel to the hot-gas face. For the nominal heat flux of $0.5 \text{ Btu/in}^2\text{-sec}$, the oxidizer absorbs 71 percent of the total in the regenerative cooling mode, but only 46 percent in the uncooled mode, where the fuel is a more efficient coolant.

Acoustic Cavity

An acoustic damping device was specified for the No. 1 triplet injector. For the purposes of this program, the device was designed to provide the necessary damping and be compatible with the chamber geometry and cooling passages. A quarter-wave acoustic cavity was selected and sized for the first tangential mode of instability. The cavity width was set to provide approximately 10 percent of injector face area based on past experience with acoustic cavities, with the gas temperature in the cavity assumed to be 25 percent of chamber

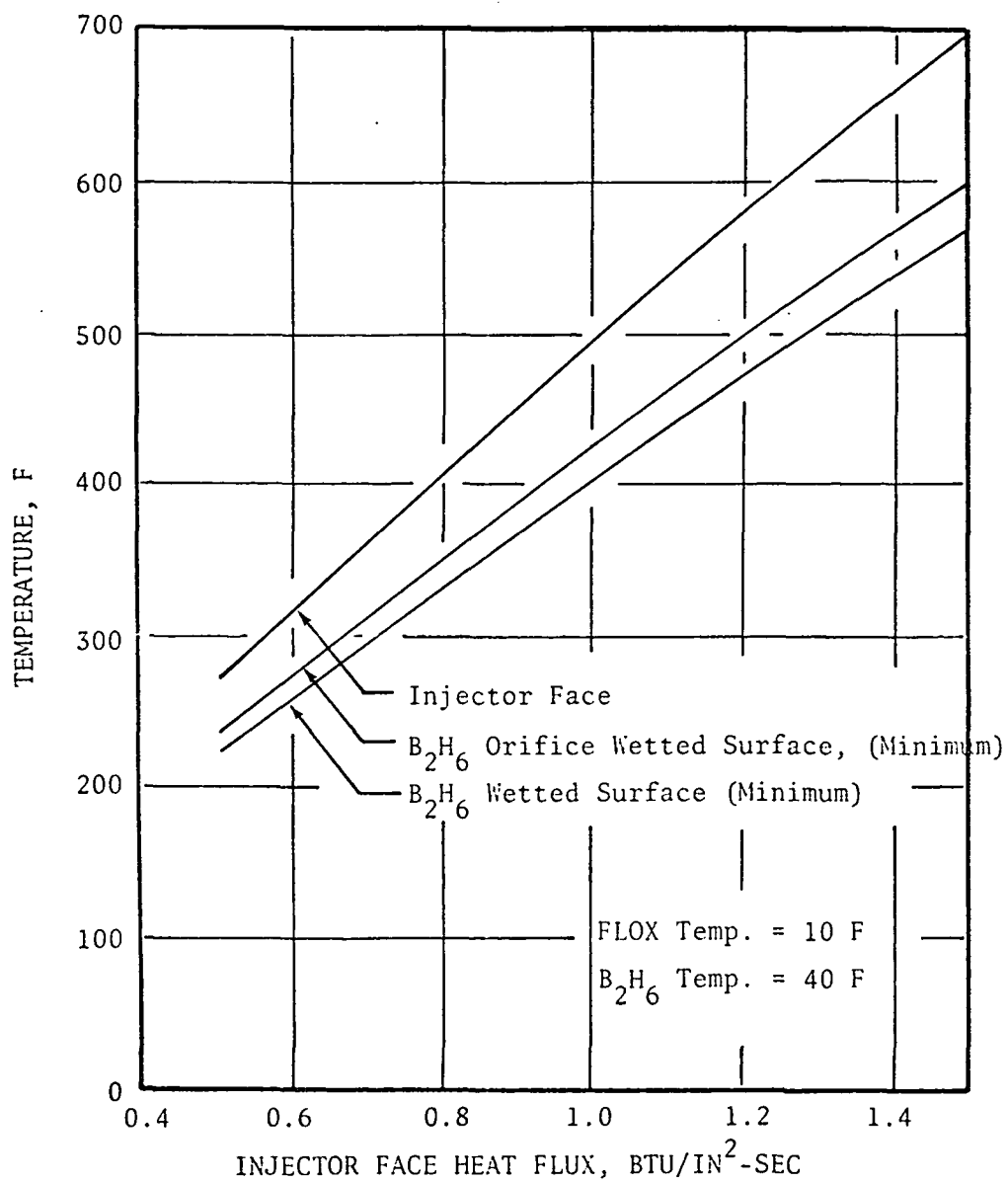


Figure 11 . Steady-State Injector Temperatures for FLOX/ B_2H_6 in Uncooled Thrust Chamber Mode

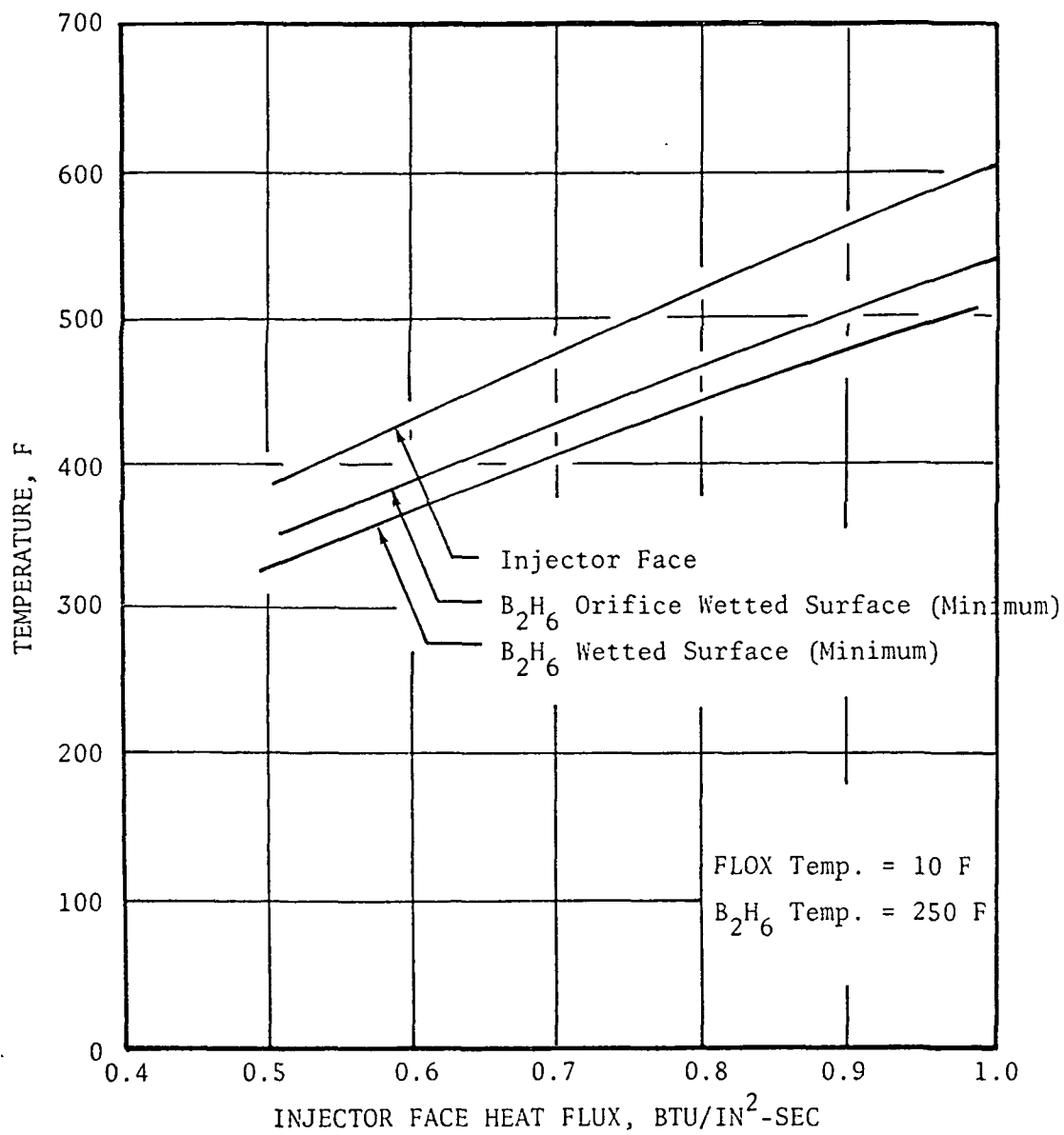


Figure 12 . Steady-State Injector Temperatures for FLOX/ B_2H_6 in Regenerative Cooling Mode

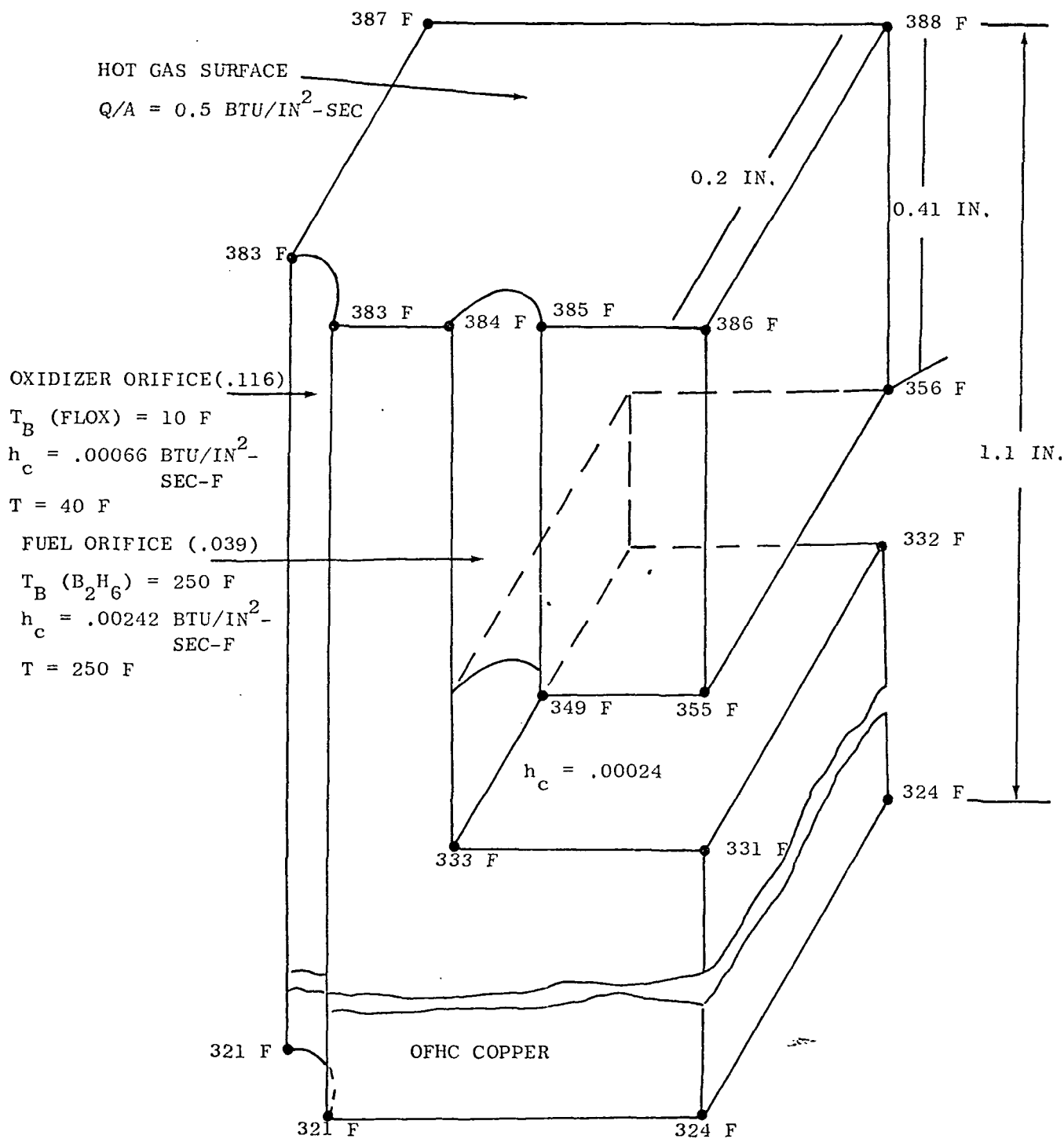


Figure 13. Injector Steady-State Temperature Distribution for $0.5 \text{ Btu/in}^2\text{-sec}$ Heat Input and Heated Diborane

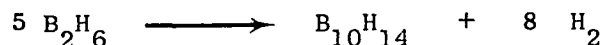
stagnation temperature. The cavity dimensions chosen were 0.13 inch wide and 0.86 inch long.

Three possible cavity orientations were considered (Fig. 14). Axial orientation is shown to interfere with the manifolding and location of both the film coolant and outer row of triplet elements. Angular orientation with the opening in the chamber wall allows film coolant and outer row manifolding to be accommodated and has been shown effective in previous study. This orientation also allows the cavity to be machined and, if necessary, serviced from the side instead of the front as for the axial cavity. The cooling passages can also be terminated in the thrust chamber manifold conveniently without creating a cooling problem. A radial cavity has the same injector manifolding and fabrication advantages, but not the regenerative cooling passage advantage. The angular cavity was the selected cavity concept.

Since two injectors and five combustion chambers (3 calorimeter and 2 regenerative) were built in this program, the dams were located in the injector side of the cavity as a cost savings factor.

The possibility of deposits forming in the cavity and the lack of information about the behavior of a gas film coolant flowing over a cavity opening caused two candidate plans to be considered (Fig. 15). It was judged that the first approach would minimize the likelihood of B_2O_3 deposits accumulating in the cavity and would not seriously affect the film coolant behavior. The second approach would create the best film coolant situation but would be likely to have a deposit problem. The first design was selected.

It was considered likely that the back half of the cavity would contain a noncirculating, but pulsating gas and that the front half would have a fair degree of recirculation. If the deposit is decaborane, the reaction becomes



and this was expected to create a hydrogen environment in the back portion of

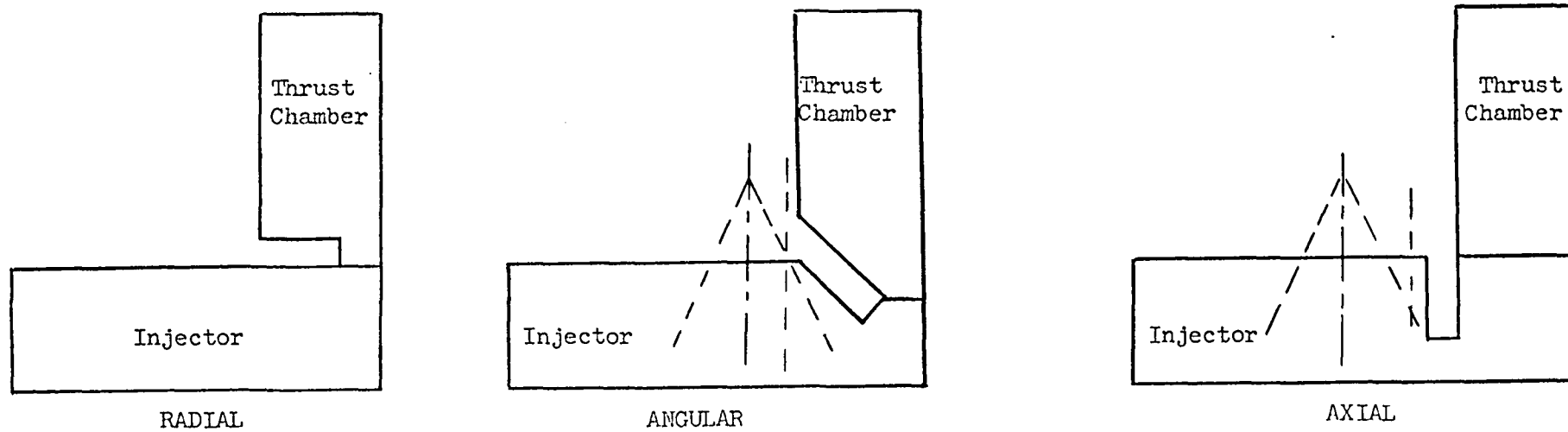
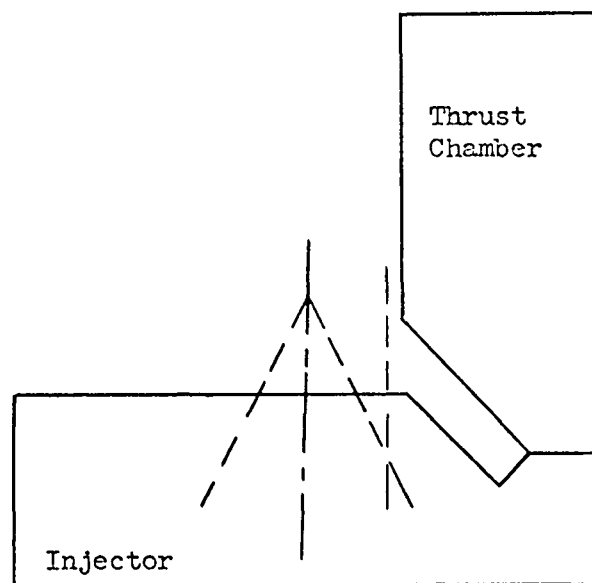
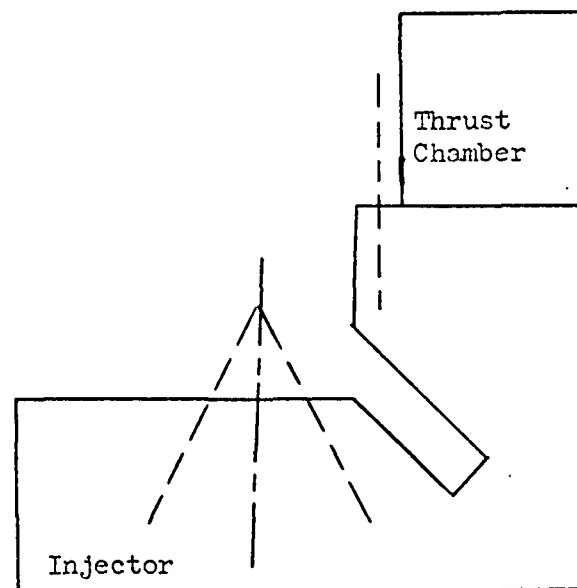


Figure 14. Potential Acoustic Cavity Orientations



FIRST DESIGN



SECOND DESIGN

Figure 15. Candidate BLC Inlet Configurations

the cavity. As described in Task II and IV, the described approach appeared adequate and acceptable deposit conditions were obtained at nominal M.R. situations.

Injector Instrumentation

Instrumentation for Task II and IV use consisted of the following:

Chamber pressure	2
Injector face temperature	2
Acoustic cavity temperature	2
Manifold temperature (1 each)	3
Manifold pressure (1 each)	3

Chamber pressure measurements were located in the third row of elements, between oxidizer orifices, to provide peripheral variances. The third row was selected as a representative location with access. Injector face temperature measurements were taken with closed tip contact thermocouple probes inserted through the oxidizer dome into holes which terminated approximately 0.1 inch from the injector face. Closed tip temperature probes were inserted into the acoustic cavities to measure gas temperatures, and located 180 degrees apart. Injector instrumentation is shown in Fig. 16.

The injector designed was to be made of several components brazed into a single unit. All parts which are exposed to the combustion products were copper for improved heat transfer, while the oxidizer dome and the outer manifold were stainless steel for strength. Final assembly consisted of a single braze operation with no interpropellant braze joints.

Injector/Thrust Chamber Interface

The triplet No. 1 injector was designed for use with the uncooled calorimeter chamber in Task II, and as backup for Task IV. The design was made compatible with the regeneratively cooled chamber. The mechanical interface with the regenerative chamber was examined in a brief study and the preliminary design is shown in Fig. 17.

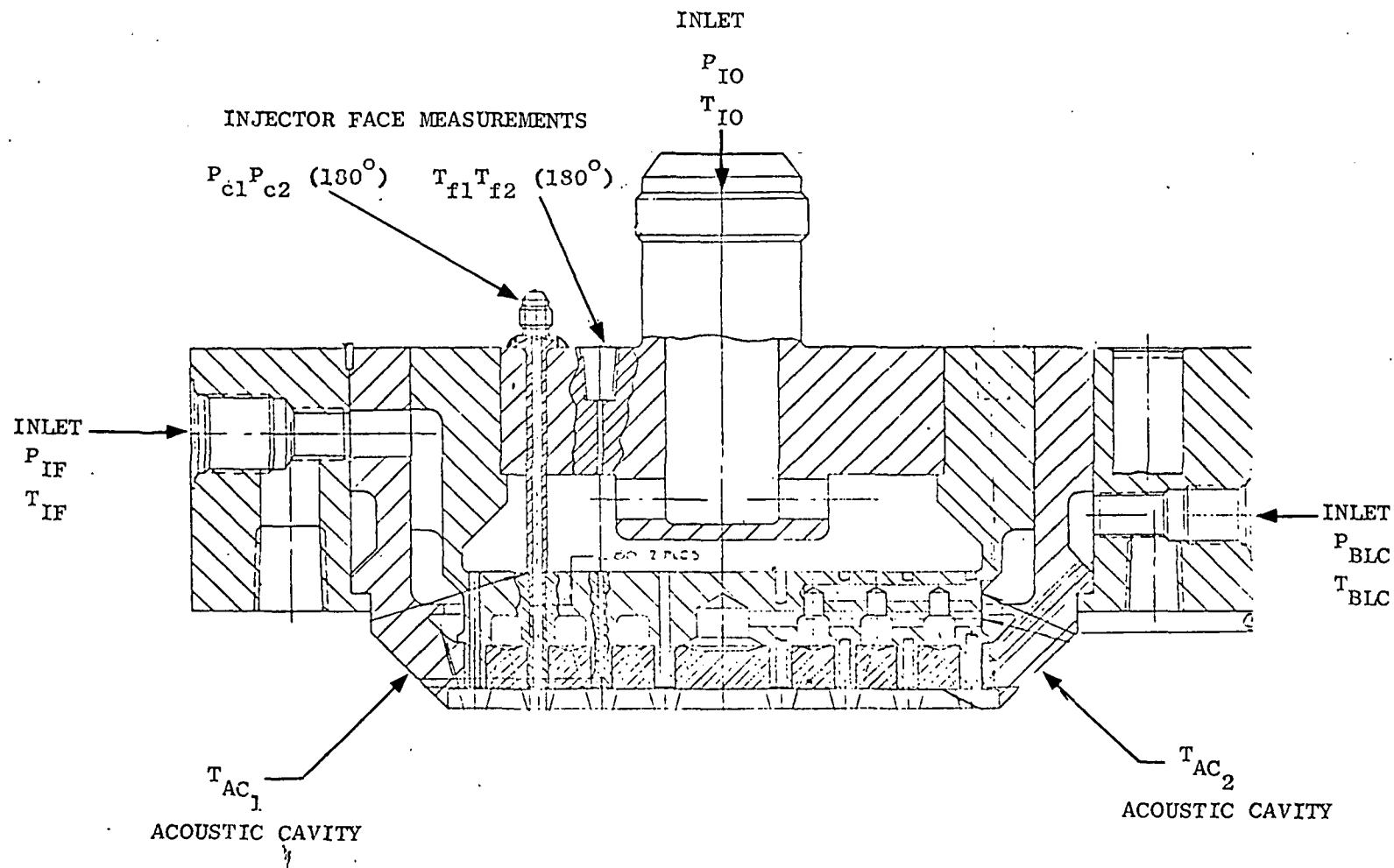


Figure 16. Injector Face Inlet and Inlet Port Temperature & Pressure Instrumentation

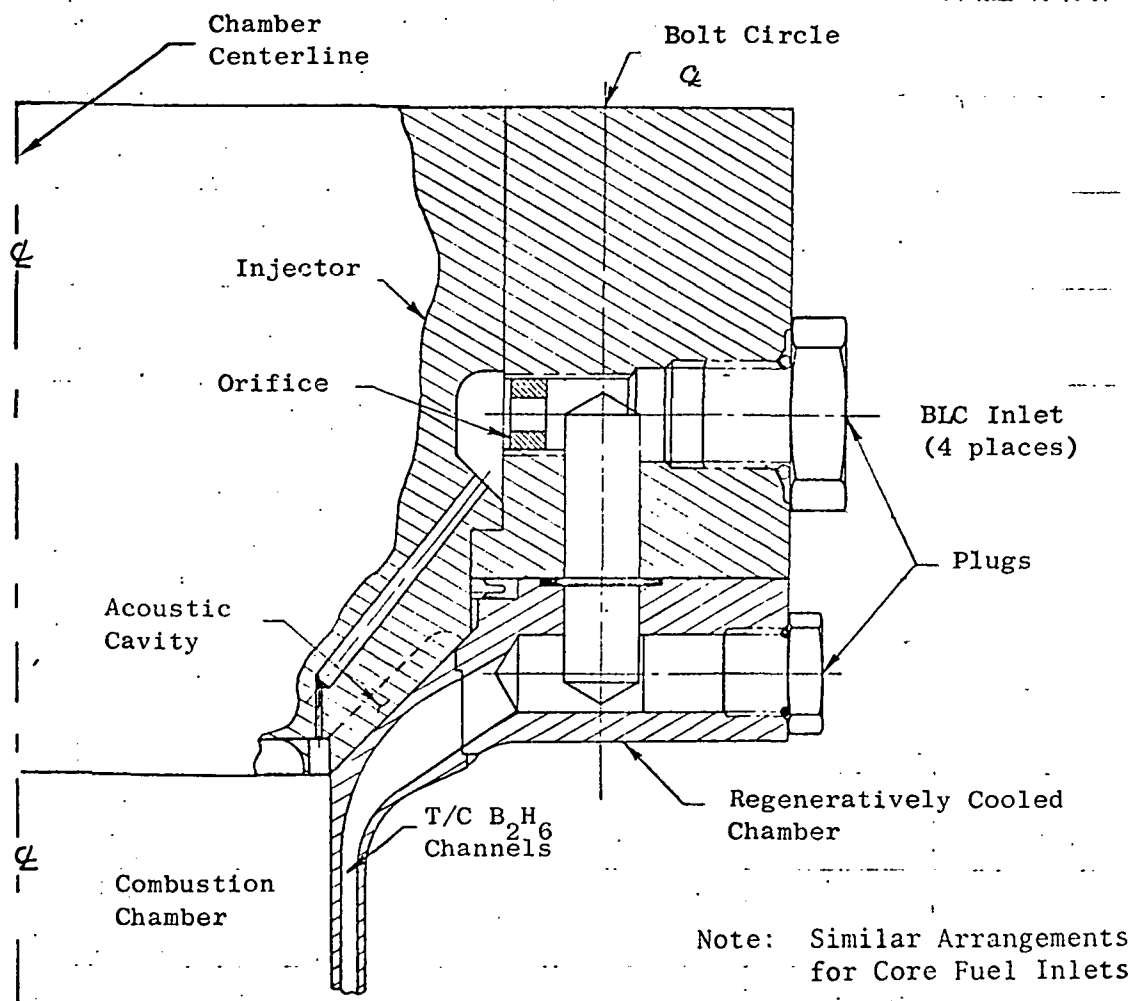


Figure 17. Preliminary Injector/Thrust Chamber Interface Design

TASK II - DETERMINATION OF DESIGN CRITERIA AND CRITICAL LIMITATIONS

Task II provided experimental and analytical efforts to develop information on the combustion chamber geometry and the attendant gas side and coolant side heat transfer rates.

An impinging injector (Triplet No. 1) was optimized, fabricated, and tested during Task II study with uncooled calorimeter hardware designed to provide gas side heat transfer information. The calorimeter hardware was designed to vary combustor length between 6 and 12 inches to determine length effects on integrated heat transfer rate and combustor c^* performance. A series of 27 tests were conducted over a range of mixture ratio from 2.3 to 3.3 at 46 to 103 psia chamber pressure.

Data results showed throat heat flux and integrated heat load conditions to be at acceptable values and in line with previous data from other programs and analytical predictions. Study of combustion deposit effects on both the injector face and chamber wall indicated that $F_2/O_2-B_2H_6$ mixture ratios overall of nearly 3.0 would be necessary in order to prevent heavy boron product deposits from forming and interfering either with the injector flow or film coolant streams or affecting chamber or throat wall geometric dimensions.

A series of 60 OF_2 and B_2H_6 convective cooling tests were also performed during Task II to verify the analytical prediction methods and to determine the suitability of the OF_2 and B_2H_6 fluid phases chosen as coolants in the various locations of the flight thrust chamber. These tests were conducted in instrumented electrically heated "heat sink" blocks with fluid and wall temperature monitored. A satisfactory comparison with predicted conditions was noted.

Based on the combined test and analytical results of this task, a modified injector (Triplet No. 2) and the regenerative chamber geometry were specified.

COMBUSTION CHAMBER DESIGN

The combustion chamber design in terms of the geometrical parameters selected, for a low $\text{OF}_2\text{-B}_2\text{H}_6$ thrust (1,000 lb thrust) configuration of this type, is critical due to the comparatively low prevailing Reynolds number condition. This is as a result of the low chamber pressure (100 psia) together with the small characteristic chamber length dimensions. As a result, the combustion chamber geometry chosen tends toward a minimized length to reduce total integrated heat load (coolant temperature rise and pressure drop). This, however, can only be accomplished at some detriment in performance and increased throat heat flux rate.

Combustion Chamber Geometry

In preparation for the Task II calorimeter thrust chamber tests, combustion chamber geometry was studied in light of the requirements of the selected engine concept. Both throat heat flux and total combustion chamber heat load were to be controlled within limits, and these established the following requirements.

1. Throat heat flux should be $\leq 4.5 \text{ Btu/in}^2\text{-sec}$.
2. Approximately 170 Btu/sec was required to vaporize OF_2 in a cooling jacket and, considering that the OF_2 jacket would be behind the B_2H_6 jacket, about 300 Btu/sec must be transferred into the wall. The excess is absorbed by the B_2H_6 .
3. The OF_2 cooling jacket should begin at a nozzle area ratio of approximately 7:1 and terminate at the injector end.

With these requirements, a parametric study was conducted to evaluate the injector-to-throat length, contraction angle, and film coolant flowrate variables. The ranges considered were:

Injector-to-throat length	6-12 inches
Contraction angle	15, 21, 25 degrees
Film coolant flowrate	5, 10, 15 percent of total flow
Contraction area ratio	2, 4, 6

For the entire study, overall mixture ratio was held at 3.0:1. The core flow distribution was used consistent with values selected in an earlier study.

The results of the throat heat flux studies are summarized in Fig. 18 and 19. Figure 18 depicts predicted throat heat flux as a function of boundary film flowrate for the range of contraction ratios of interest and for a nominal injector-to-throat length. Figure 19 shows similar information as a function of injector-to-throat length for three boundary layer coolant flowrates with a nominal value of contraction ratio. Heat flux levels up to approximately 5 Btu/in²-sec were considered to be tolerable, with a corresponding wide envelope of acceptable contraction ratios, lengths, and boundary layer coolant flowrates. A selected contraction ratio of 4:1 was in the middle of the acceptable range. Because of existing injector and thrust chamber hardware, which could be used as backup, this value was selected.

The total predicted heat load results are shown in Fig. 20 and 21. In Fig. 20, heat load from the injector to the throat is shown as a function of chamber length in parametric values of the other variables. Contraction angle is seen to be of little importance. The nozzle heat load to area ratio of 3.45:1 is shown in Fig. 21 as a function of chamber length, but only for one value of contraction angle. These results, plus the heat flux results shown in the previous progress results, and the mixture ratio information in Fig. 18, led to selection of the nominal conditions indicated. These were:

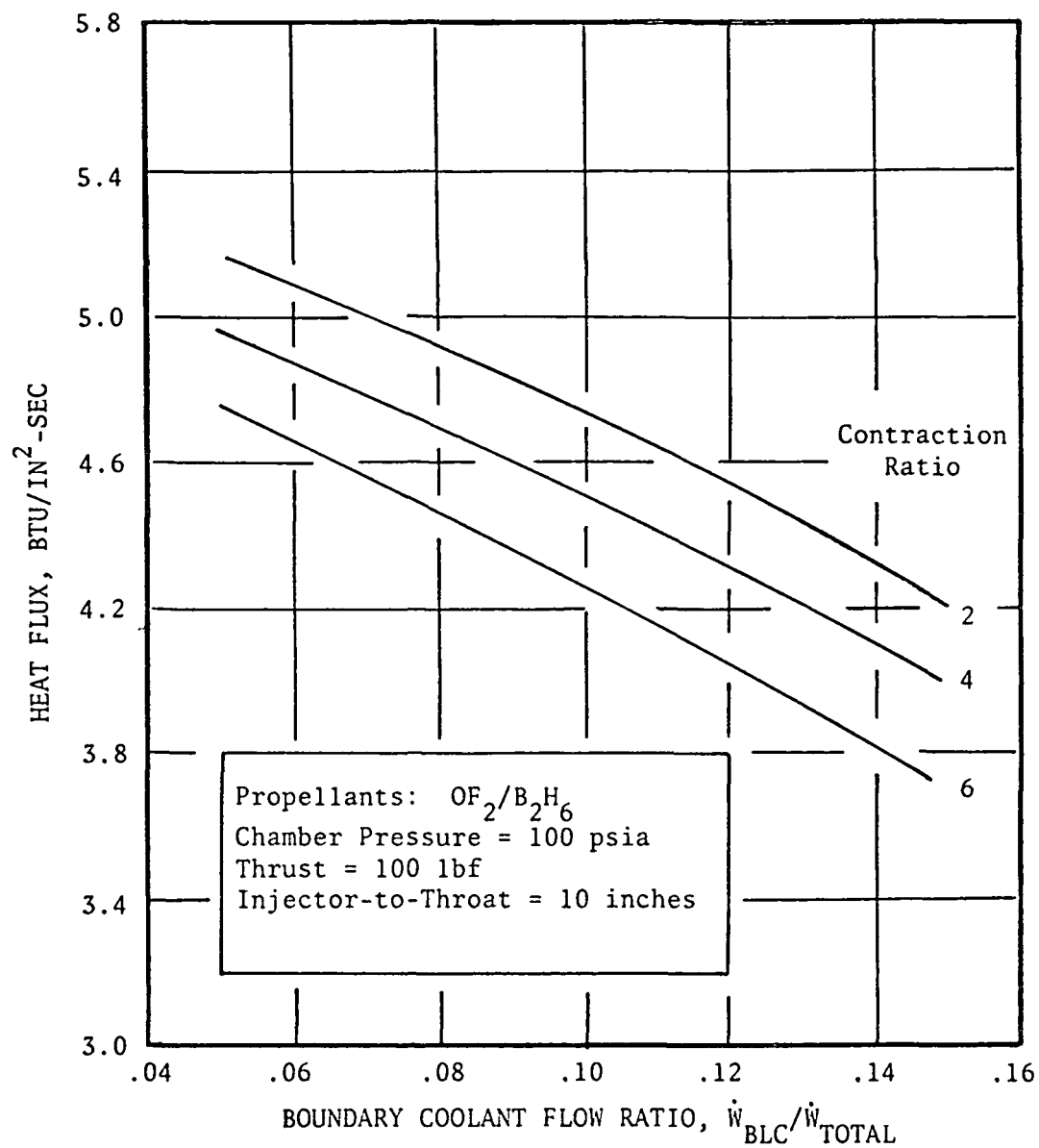


Figure 18. Heat Flux to the Throat as a Function of Diborane Boundary Film

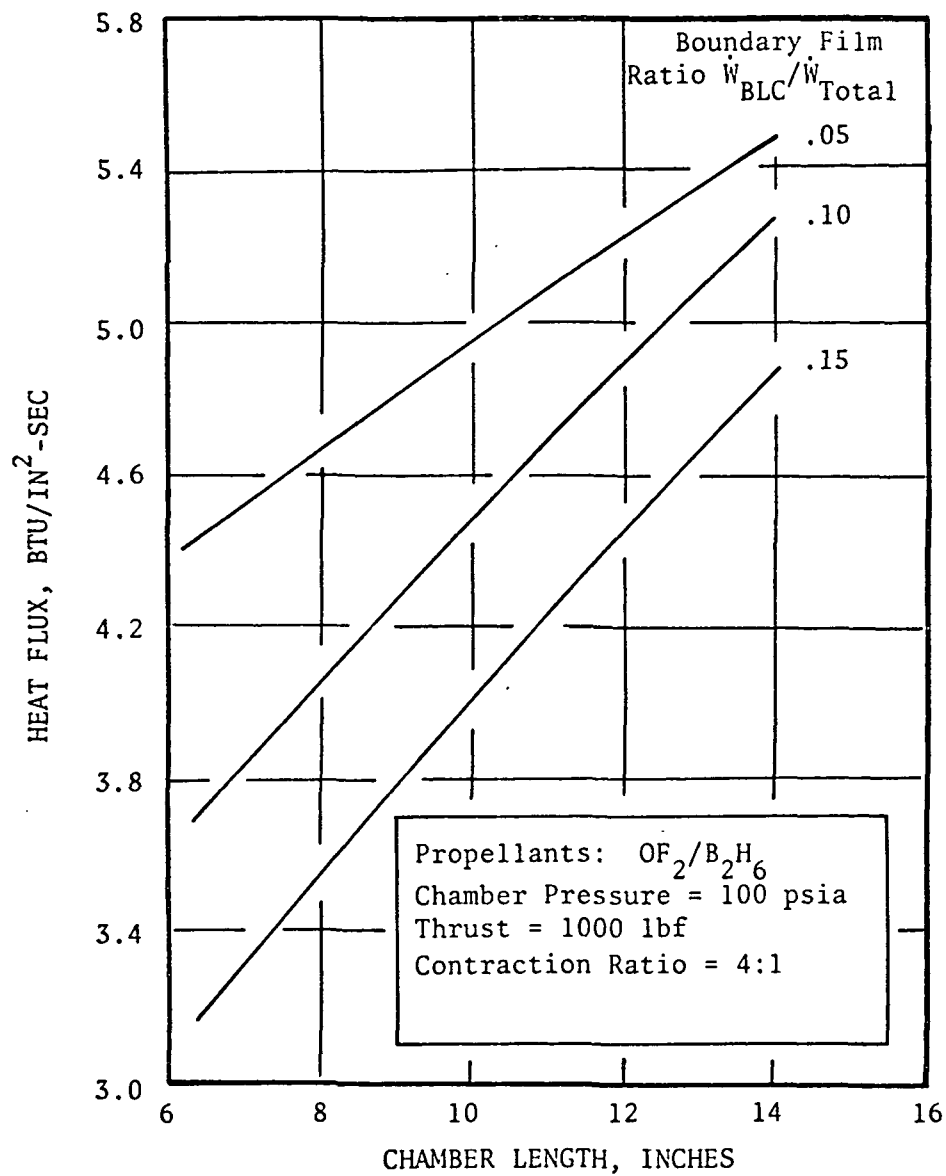


Figure 19 . Heat Flux to the Throat as a Function of Injector to Throat Distance

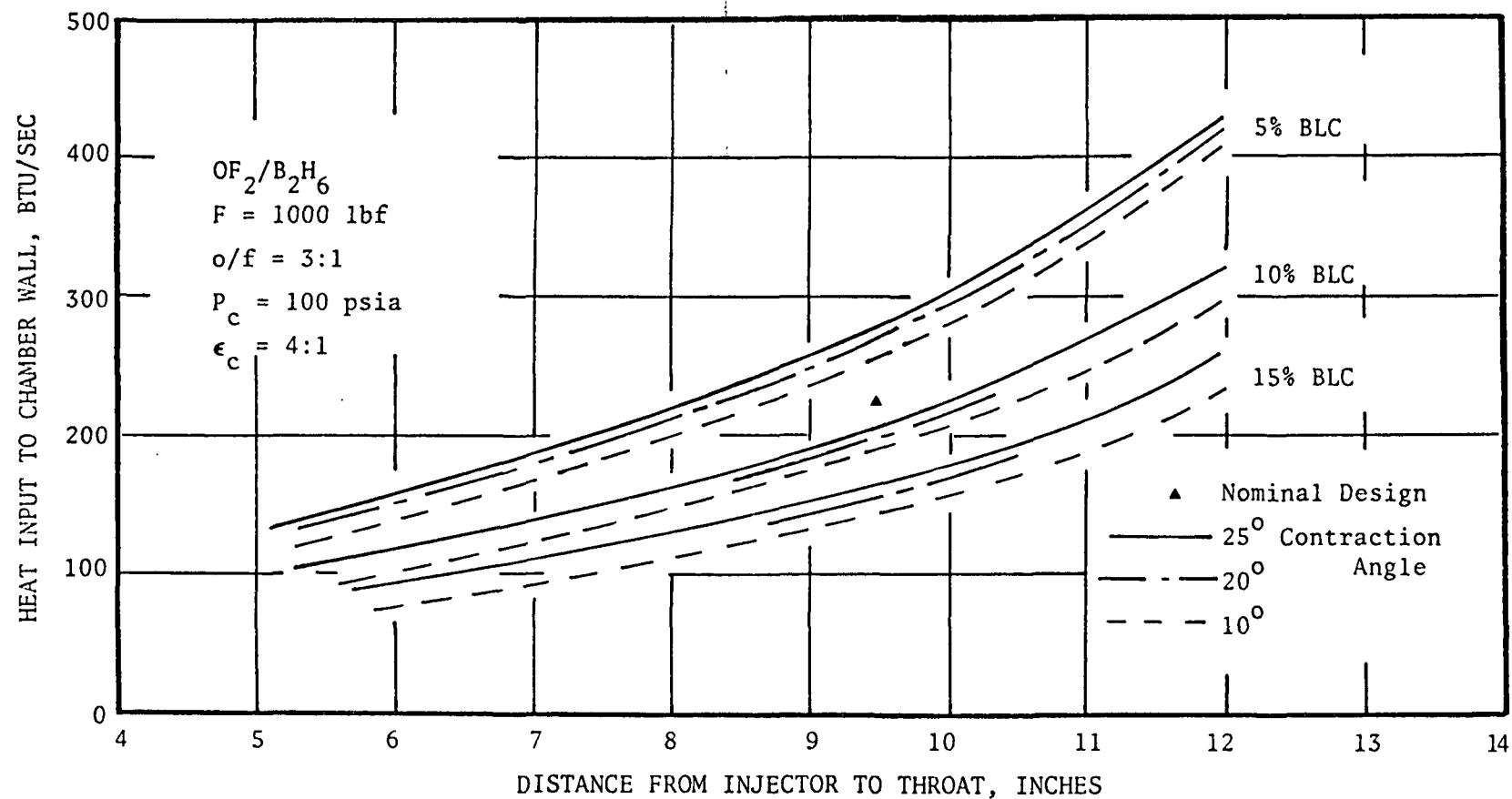


Figure 20. Heat Input to Combustion Chamber Wall for $\text{OF}_2/\text{B}_2\text{H}_6$

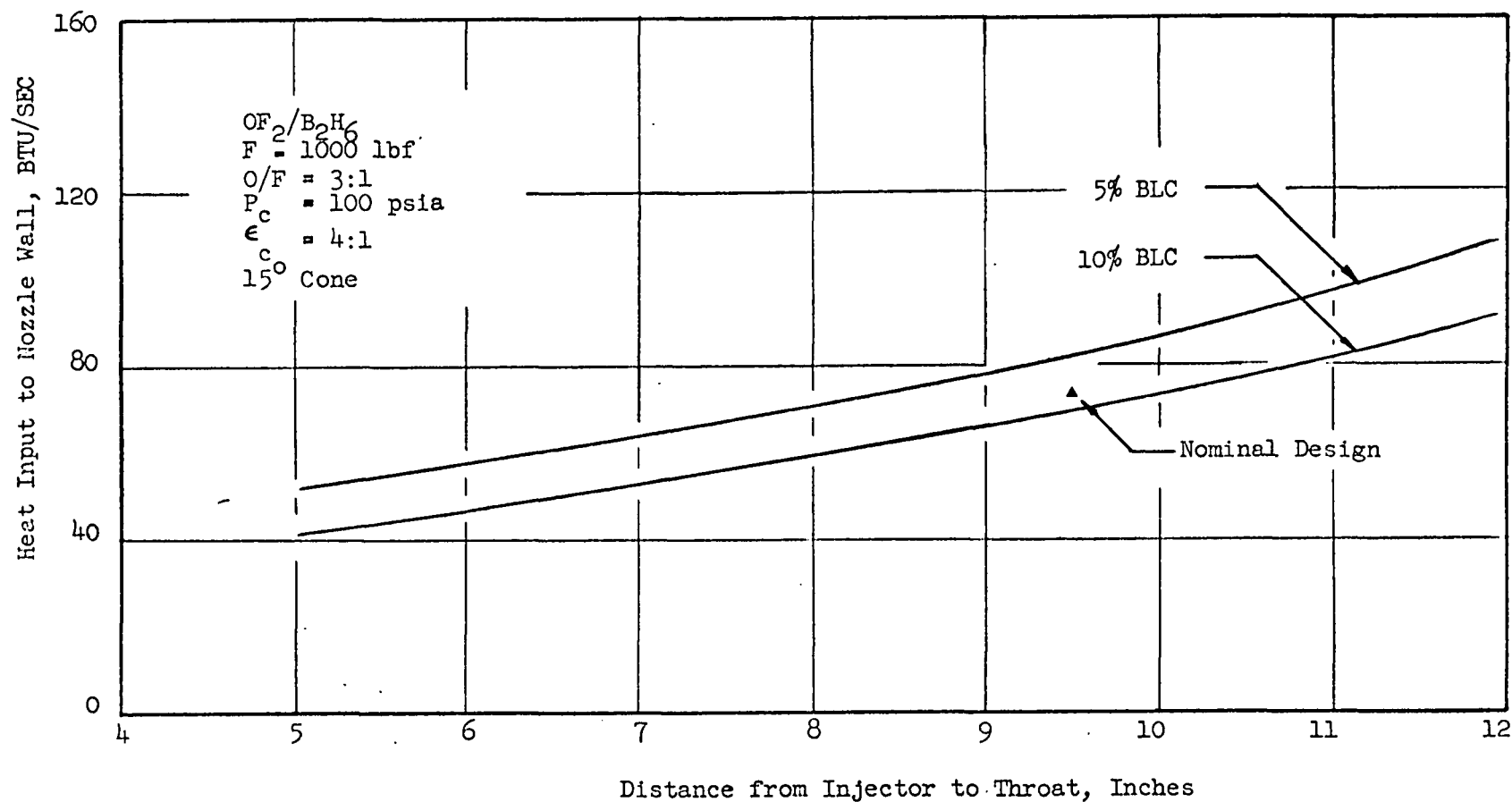


Figure 21. Heat Input to Nozzle Wall from Throat to $\epsilon = 3.45:1$
 for OF₂/B₂H₆

Nominal film coolant flowrate = 8 percent of total flow
Nominal length = 9.5 inches
Nominal contraction angle = 20 degrees

This produces a throat heat flux of $4.6 \text{ Btu/in}^2\text{-sec}$, a total heat load of 300 Btu/sec from the injector to $\epsilon = 3.04:1$ and a configuration which produced high performance in an earlier Rocketdyne sponsored test program.

The other geometry features were selected as tradeoffs between conflicting design considerations. The nozzle expansion radius was selected as 0.5 times the throat radius. A large radius value increases the surface area exposed to the high heat flux levels of the transonic region, but a small radius gives too short a length of curved cooling passage for the full curvature effect to develop by the time the coolant reaches the peak heat flux area.

Similarly the throat upstream radius was selected equal to the throat radius as a compromise between surface area in the high heat flux region and transonic flow distortion. A contraction angle of 20 degrees was chosen to give a gradual contraction with enough cylindrical chamber length to allow a reduced length chamber to be tested in Task II without danger of oxidizer impingement on the wall at the injector end.

Calorimeter Hardware Design

The design of the calorimeter test hardware is shown in Fig. 22. The completed chamber is shown in Fig. 23. A heavy wall copper design was chosen to keep the wall temperatures low during the heat transfer tests. This is important because the regenerative chamber was planned to be designed to achieve wall temperatures of 600 F or less.

Heat transfer test data was to be taken using isolated sections in the chamber wall. Instrumentation locations are indicated in Fig. 22. Typical temperature time response is shown in Fig. 24 as a function of gas-side film coefficient.

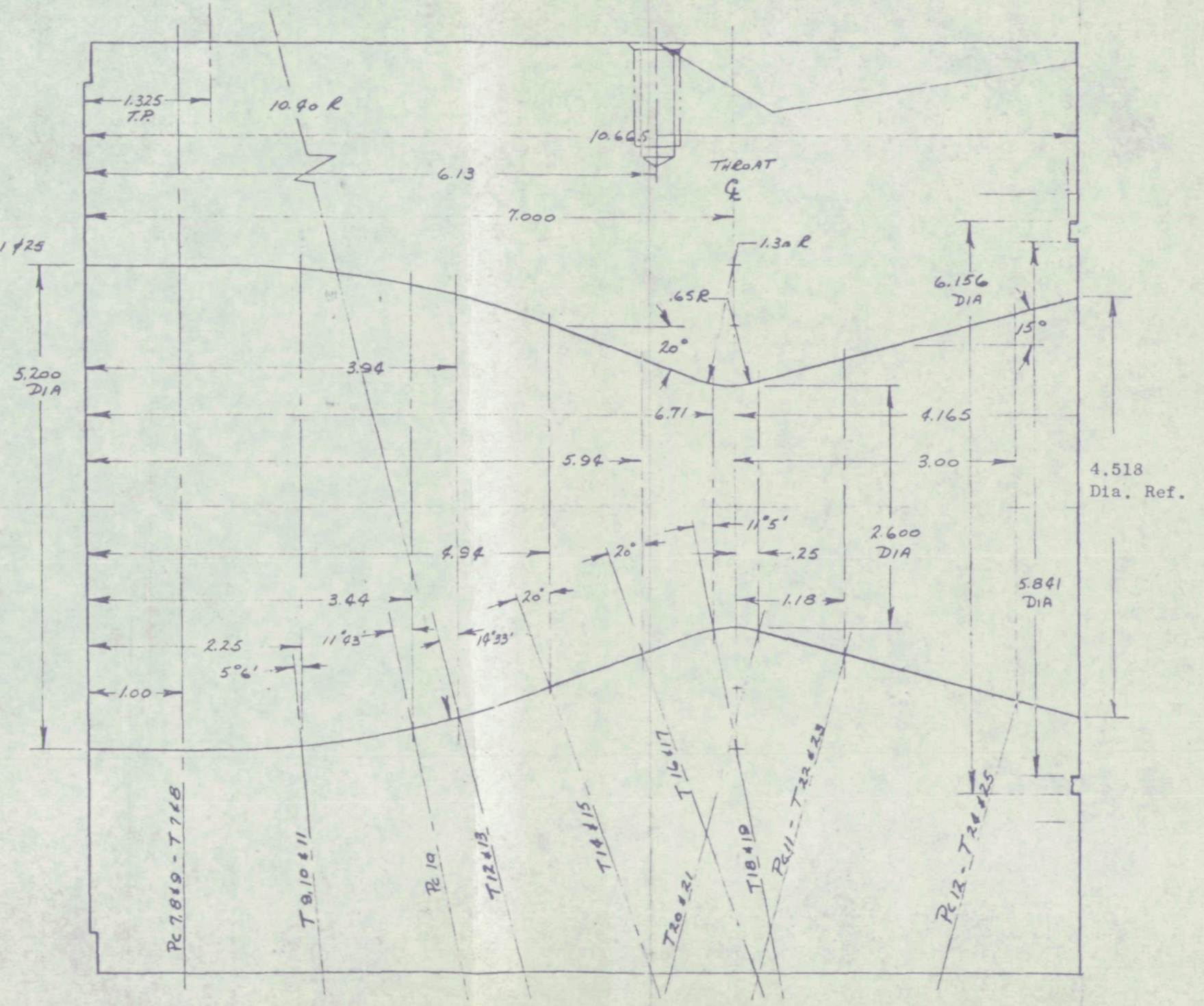
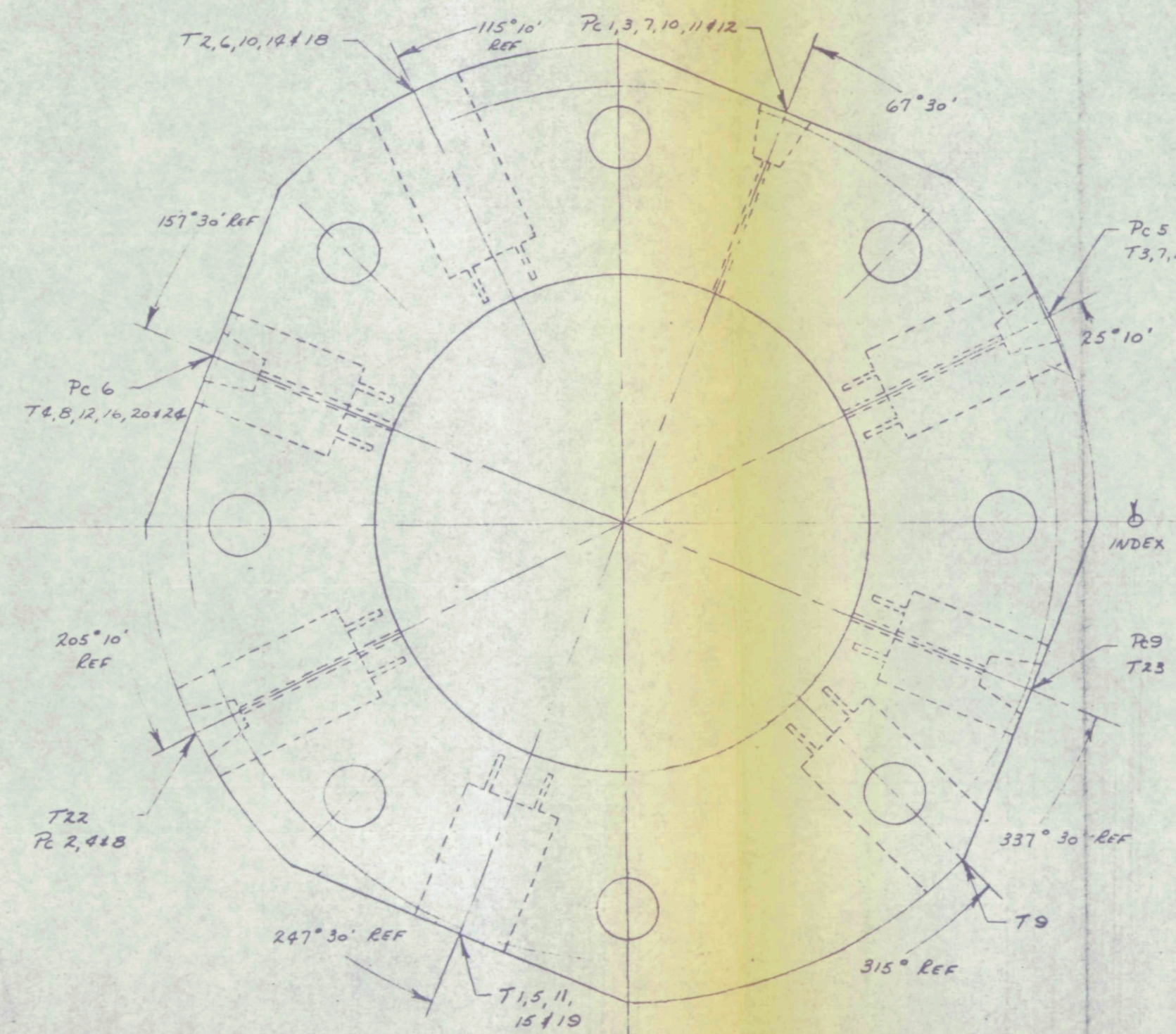


Figure 22. Calorimeter Thrust Chamber Design

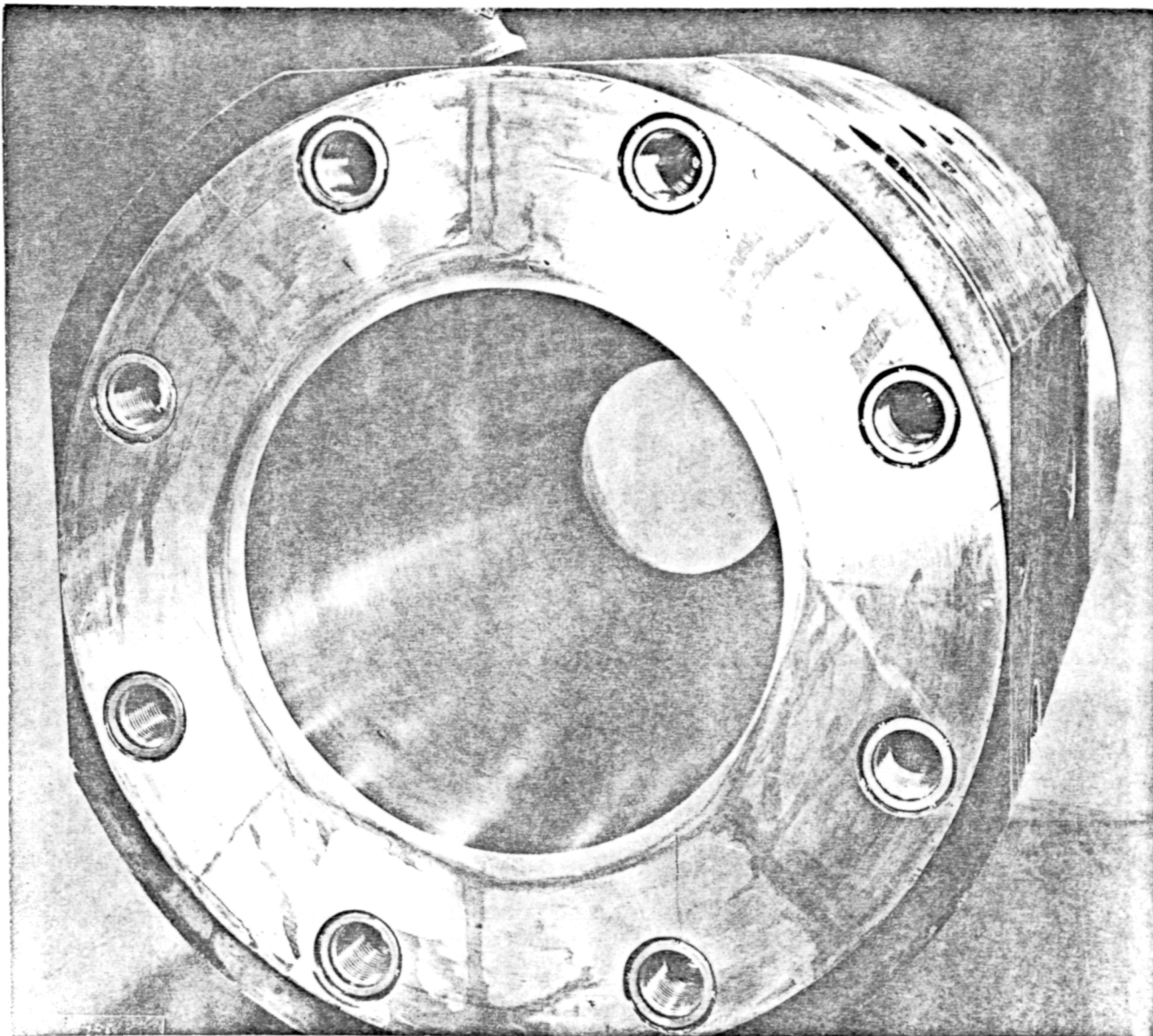


Figure 23. Calorimeter Chamber Viewed from Injector End.

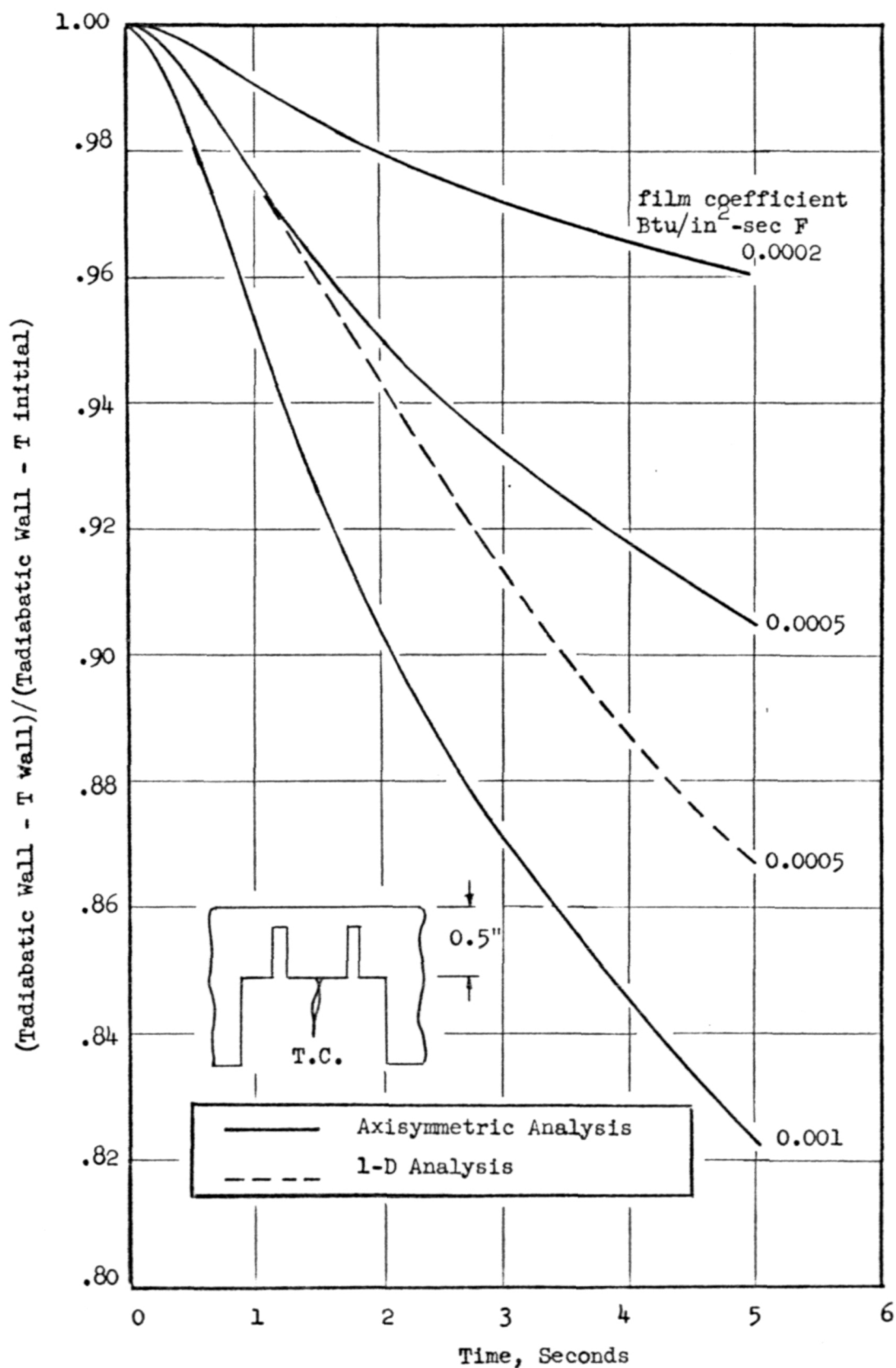


Figure 24. Thermal Response of Calorimeter Chamber Instrumentation

The heat flux data taken were to be used to predict conditions with the regenerative hardware. In the calorimeter chamber, the wall temperature is determined by the heat flux profile, giving highest temperatures near the throat. In the regenerative hardware, the wall temperatures are influenced by the coolant temperature and velocity. The regenerative chamber film coolant was also hotter, 200-350 F, compared with a temperature of 50-100 F which was used in the calorimeter tests.

In addition to the basic 7 inch injector-to-throat length chamber shown (Fig. 23), two copper cylinders of similar design were to be used to extend the length to 9.5 and 12 inches. Figure 25 illustrates the 5 inch extension. Figure 26 shows the assembly cross section variations.

Two nozzle extensions were designed and built during Task II together with diffusers of 10:1 and 20:1 area ratio. The nozzle designs and photographs are shown in Fig. 27 and 28 and the diffusers in Fig. 29 and 30. The 10:1 area ratio nozzle and its diffuser were used in the calorimeter test program. With its diffuser the 10:1 nozzle flowed full at the Nevada test site ambient pressure of 12.1 psia. The 20:1 hardware was used on the calorimeter tests with Triplet No. 2 injector in Task IV.

TRIPLET NO. 1 INJECTOR FABRICATION

The triplet No. 1 injector was fabricated and tested during the Task II effort. The injector concept had previously demonstrated adequacy in ability to control chamber heat flux while delivering high performance. This section contains a description of the first injector fabrication procedure.

Fabrication and Water Flow of First Injector

An exploded view of the No. 1 injector is shown in Fig. 31 . The core body contains most of the core fuel manifolding, the oxidizer cavity and the oxidizer orifices. The drilled fuel rings are brazed into the ring grooves in the core body. The outer zone body contains the film coolant manifold

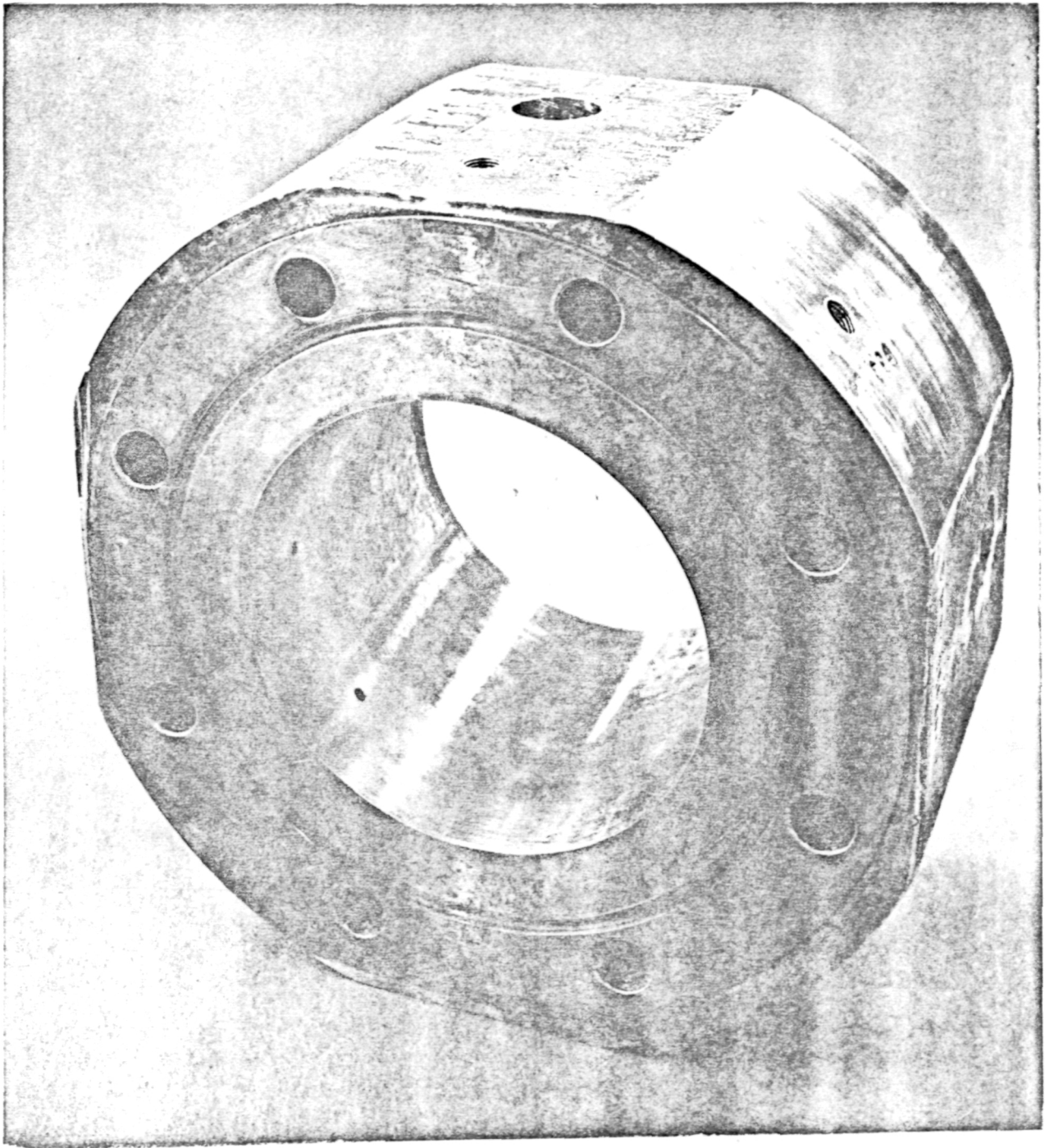


Figure 25. Combustion Chamber Extension -- 5.0 Inches

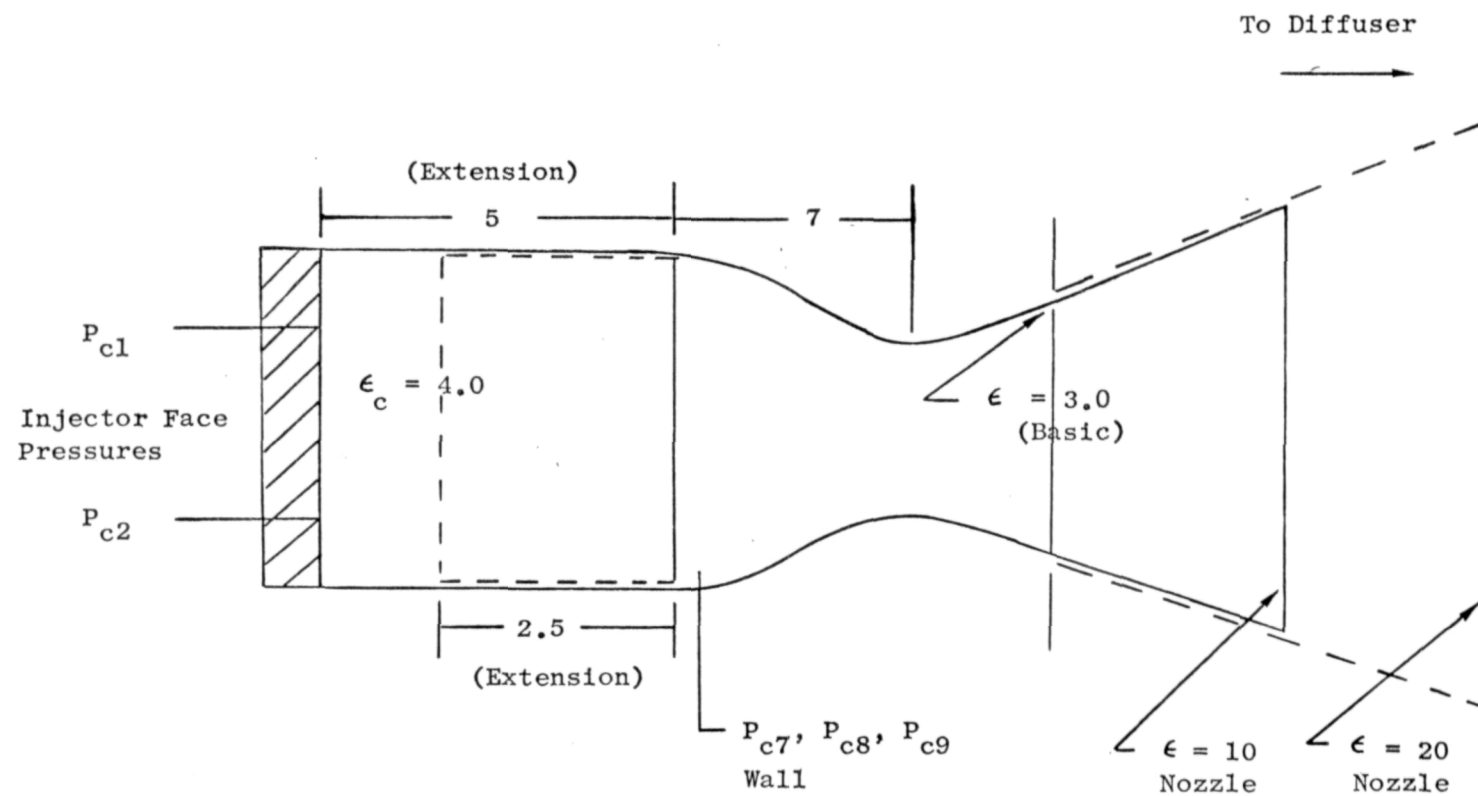


Figure 26. Calorimeter Chamber Showing Hardware Variations With Basic Injector End and Nozzle Entrance Wall Chamber Pressures

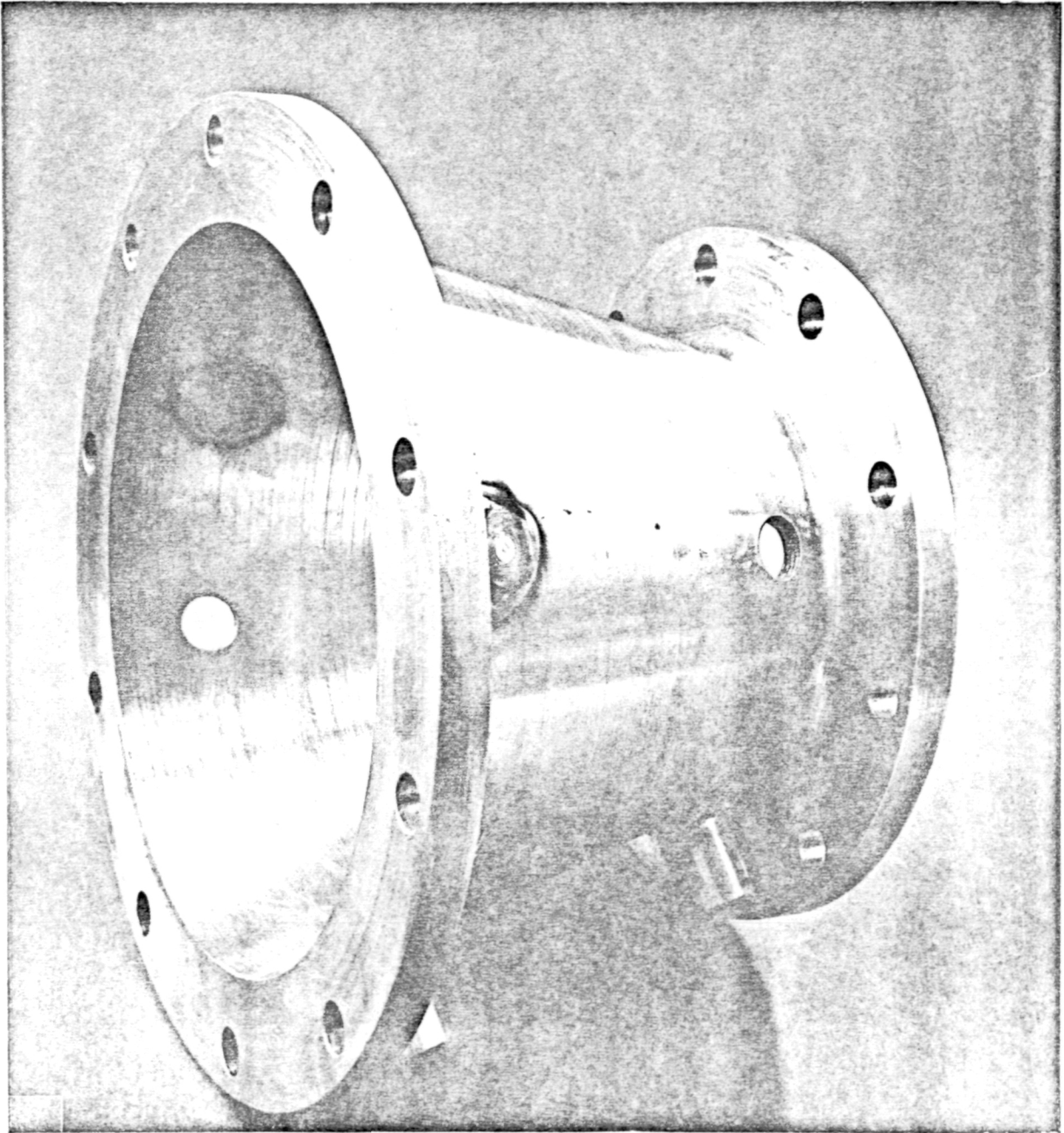


Figure 27. Nozzle Extension to 10:1 Area Ratio

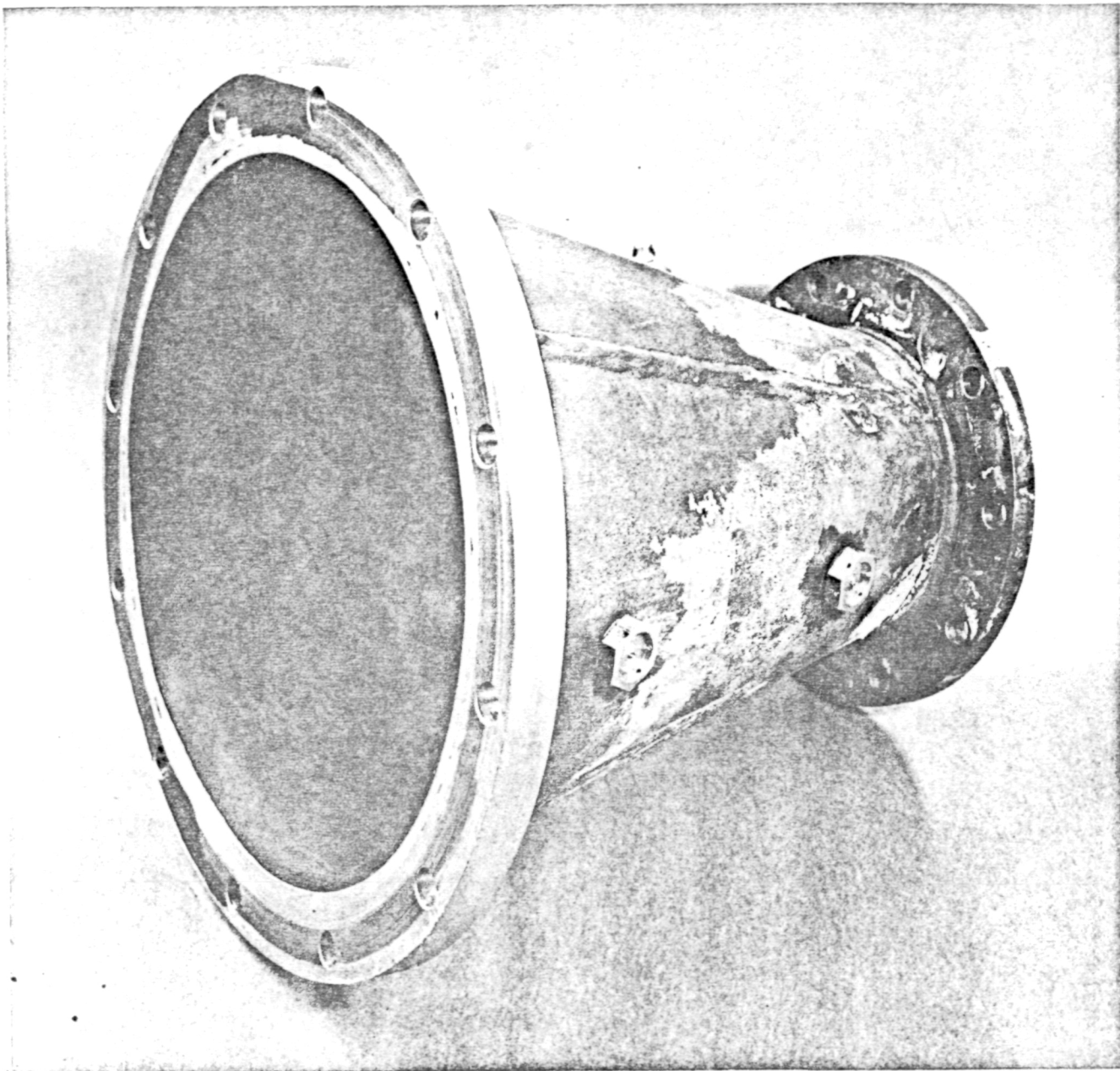


Figure 28. Nozzle Extension to 20:1 Area Ratio

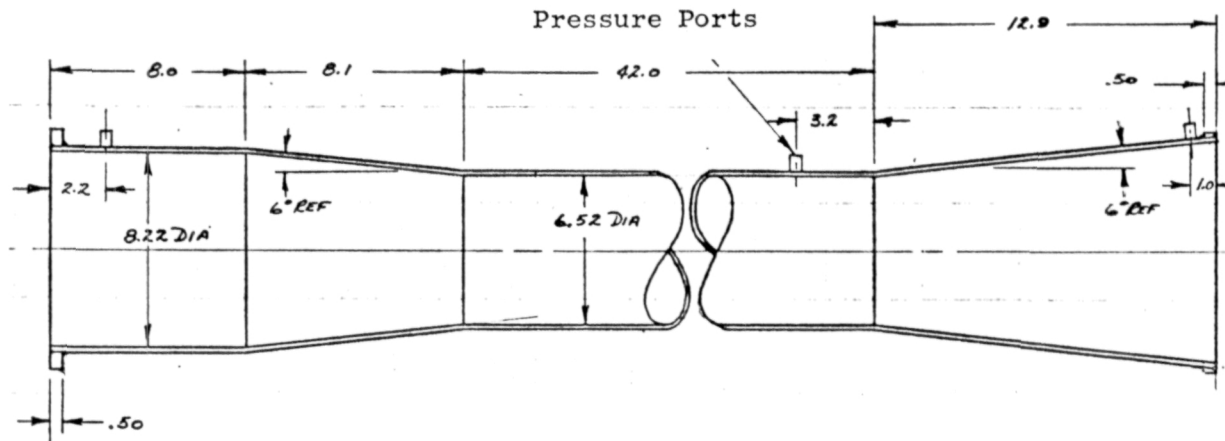


Figure 29 . Diffuser for 10:1 Area Ratio Nozzle

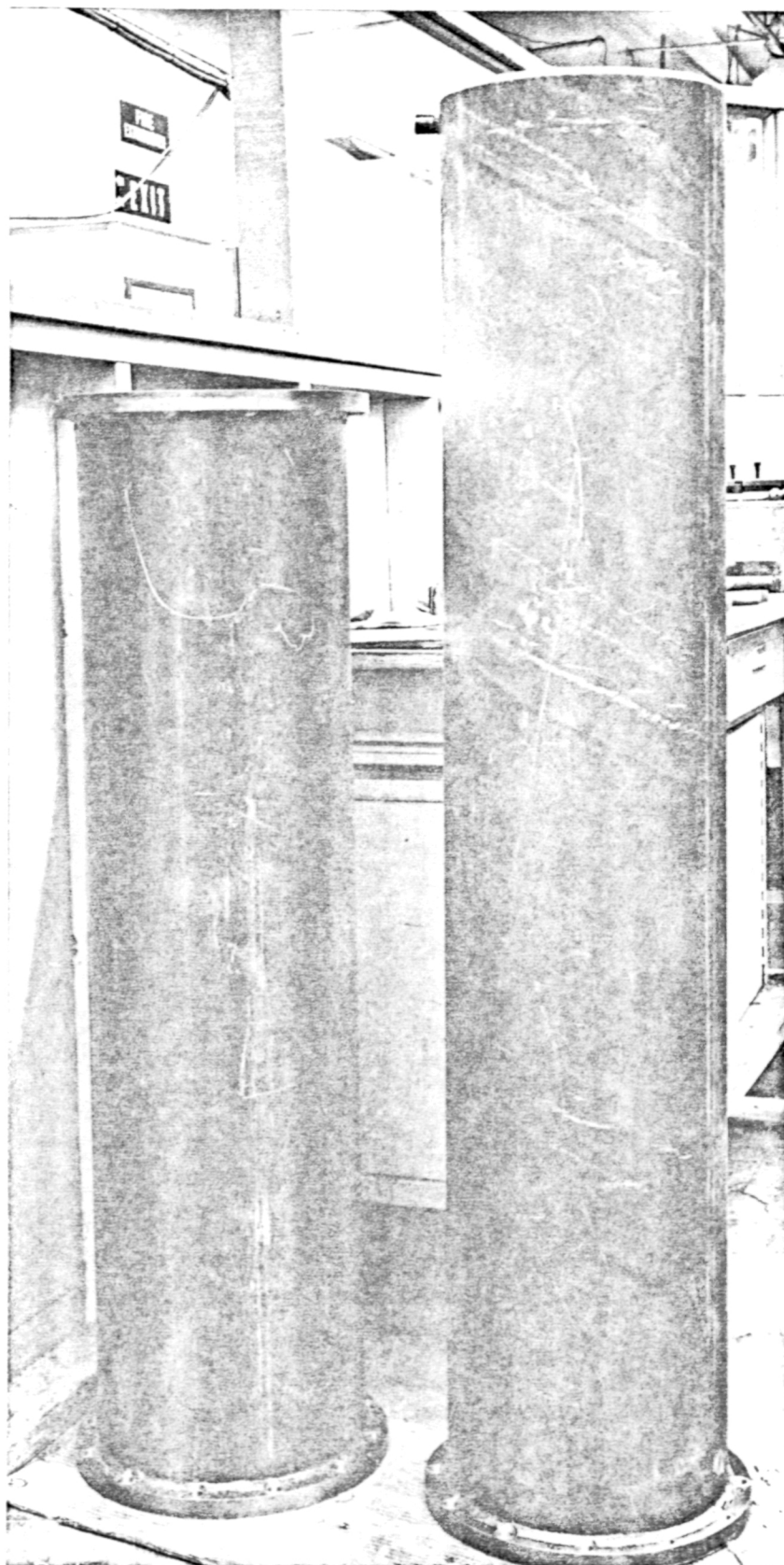


Figure 30. Two-Piece Cylindrical Diffuser for 20:1 Area Ratio Nozzle

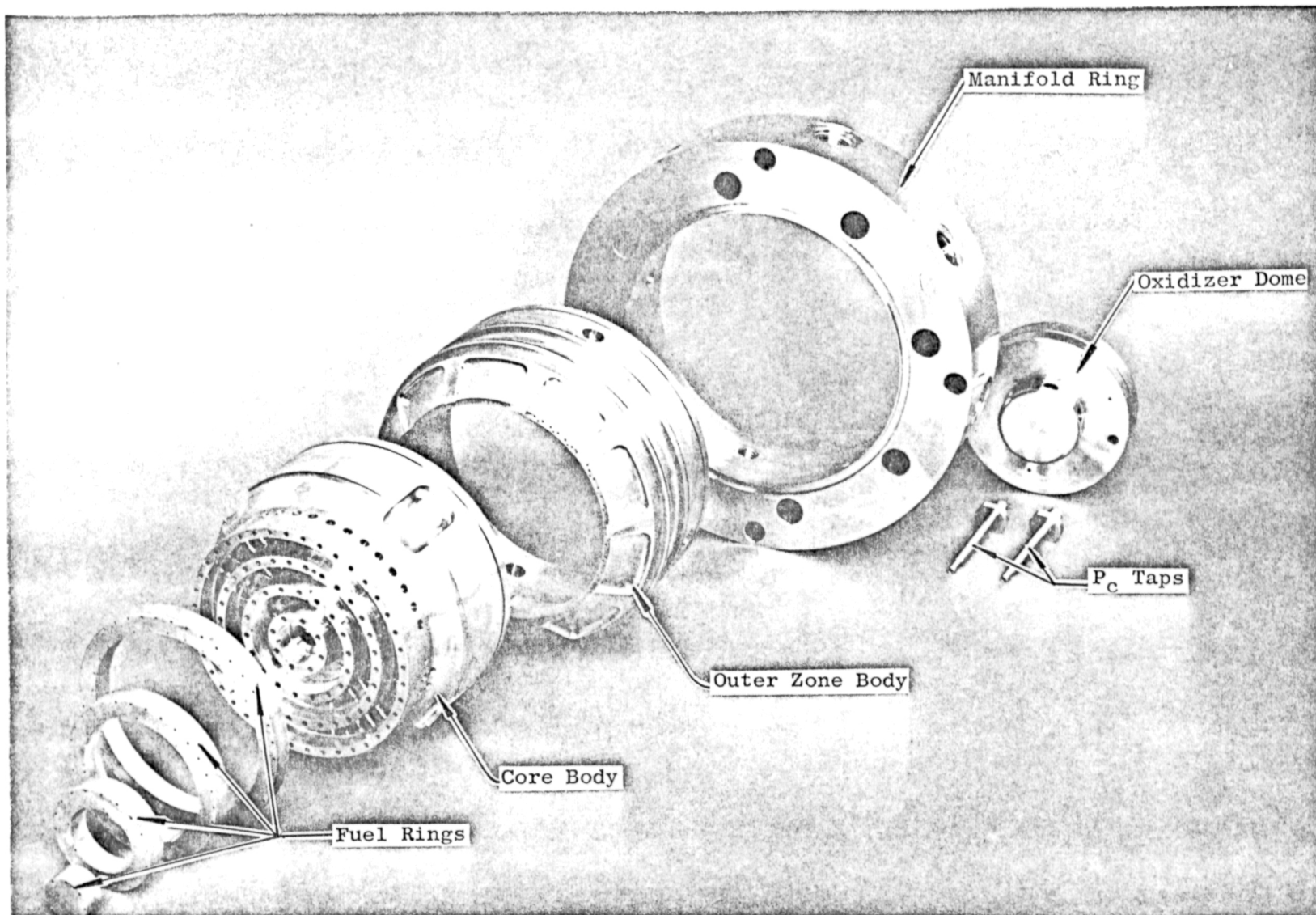


Figure 31. Exploded View of Injector Components

and orifices and the outer fuel orifices of the fourth row of elements. The acoustic cavities and cavity dams are also incorporated. The manifold ring contains eight fuel inlet fittings (4 core and 4 film) and the injector-to-thrust chamber bolt circle. The oxidizer dome (Fig. 32) fits into the back of the core body and contains the oxidizer inlet fitting. The assembled unit is shown with the acoustic cavity in Fig. 33 . The cavity cover was planned for use only in the calorimeter tests. A detailed injector design may be seen in Ref. 3.

The triplet No. 1 unit was brazed and the assembled injector was water flowed to check orifice alignment and joint integrity, and to obtain a preliminary flow calibration. Results of the water flow tests are shown in Fig. 34 and 35 . In these photographs the water used was flowed at a mass flowrate nearly 100 times the gas-gas values used in actual operation. The film coolant is seen flowing alone in Fig. 34 without the acoustic cavity cover. Figure 35 shows the complete triplet element flowing. (The flows were not in proportion to their use with actual propellants.)

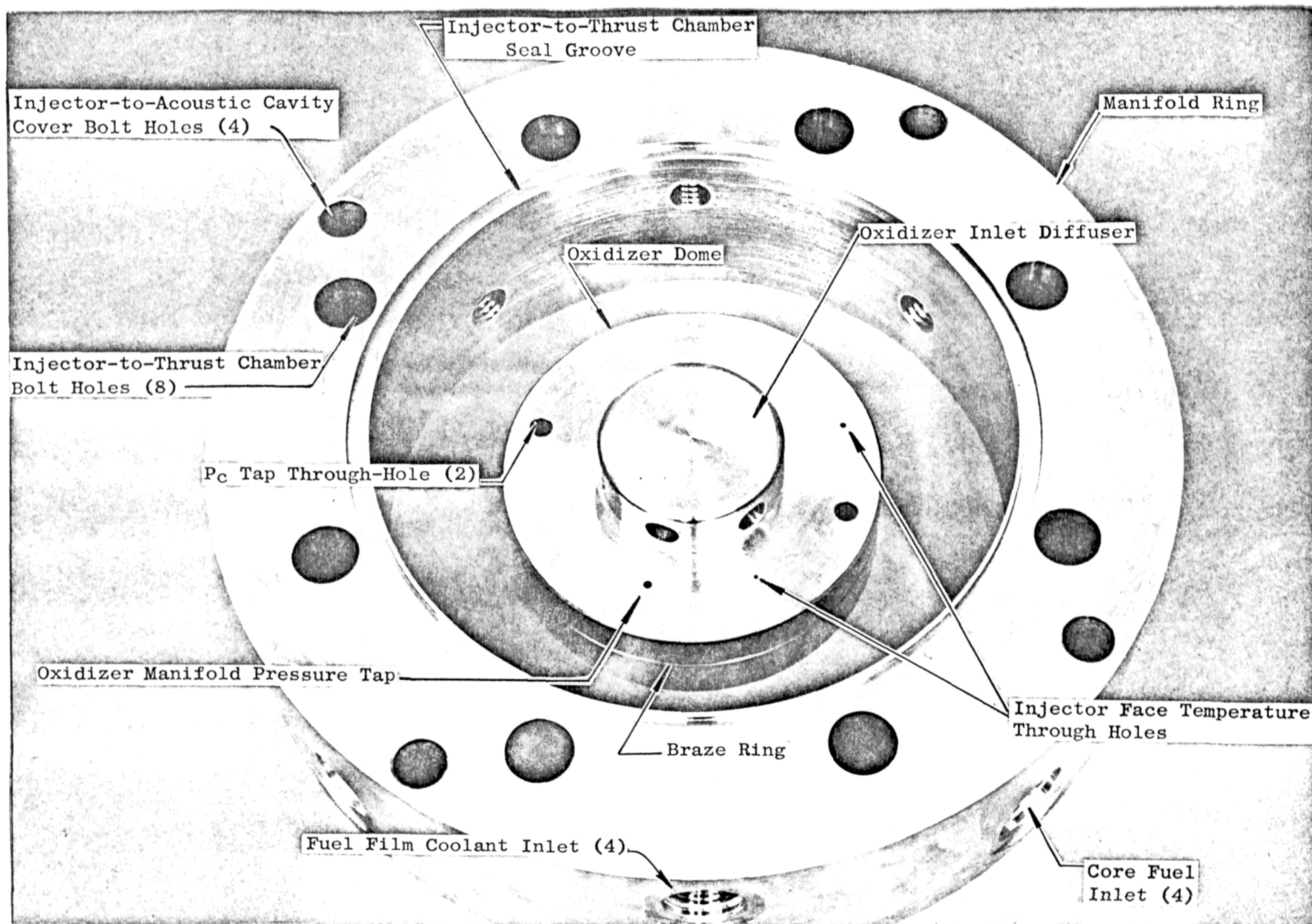


Figure 32. Injector Oxidizer Dome and Manifold Ring

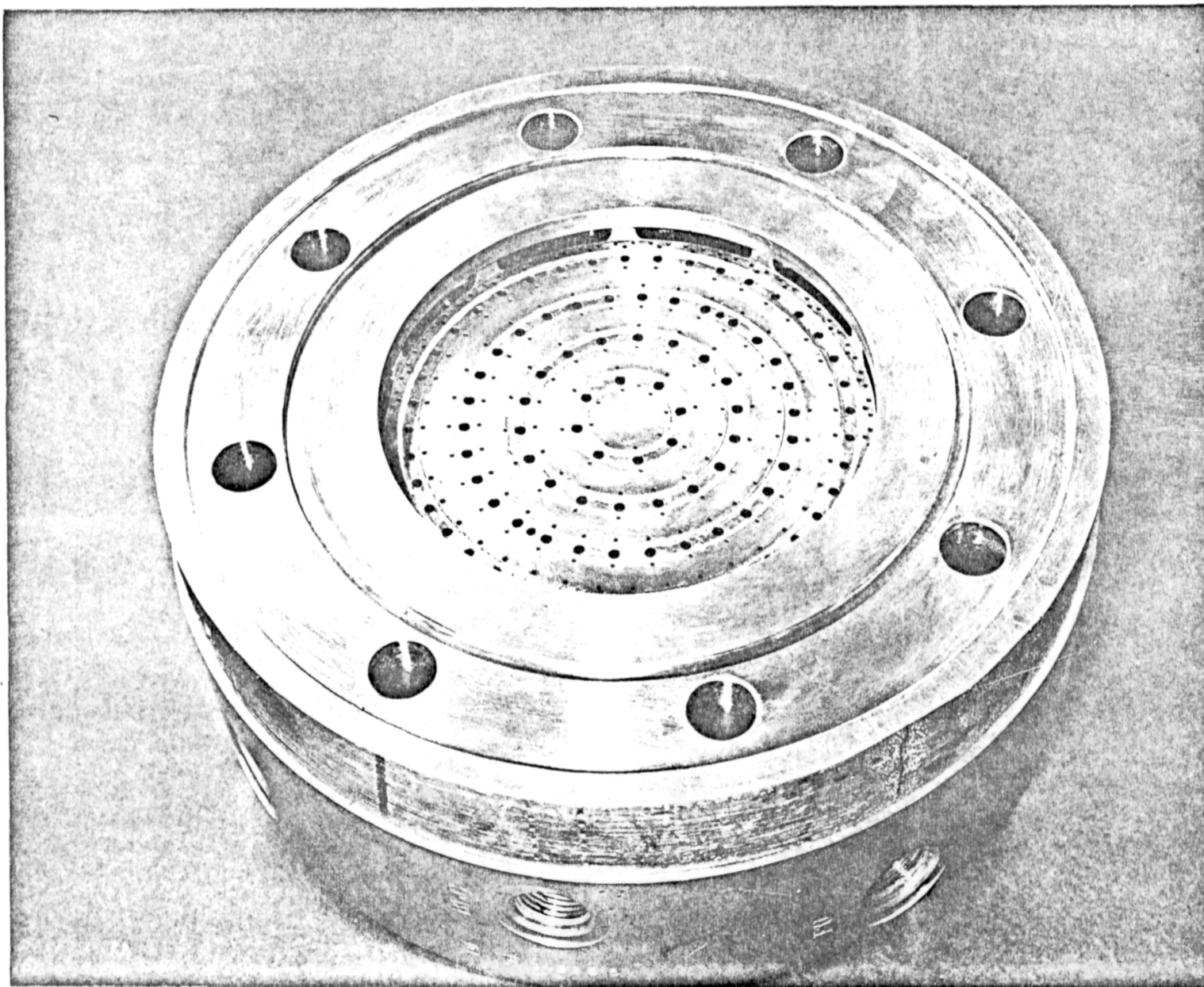


Figure 33. Front View of Injector with Acoustic Cavity Cover in Place

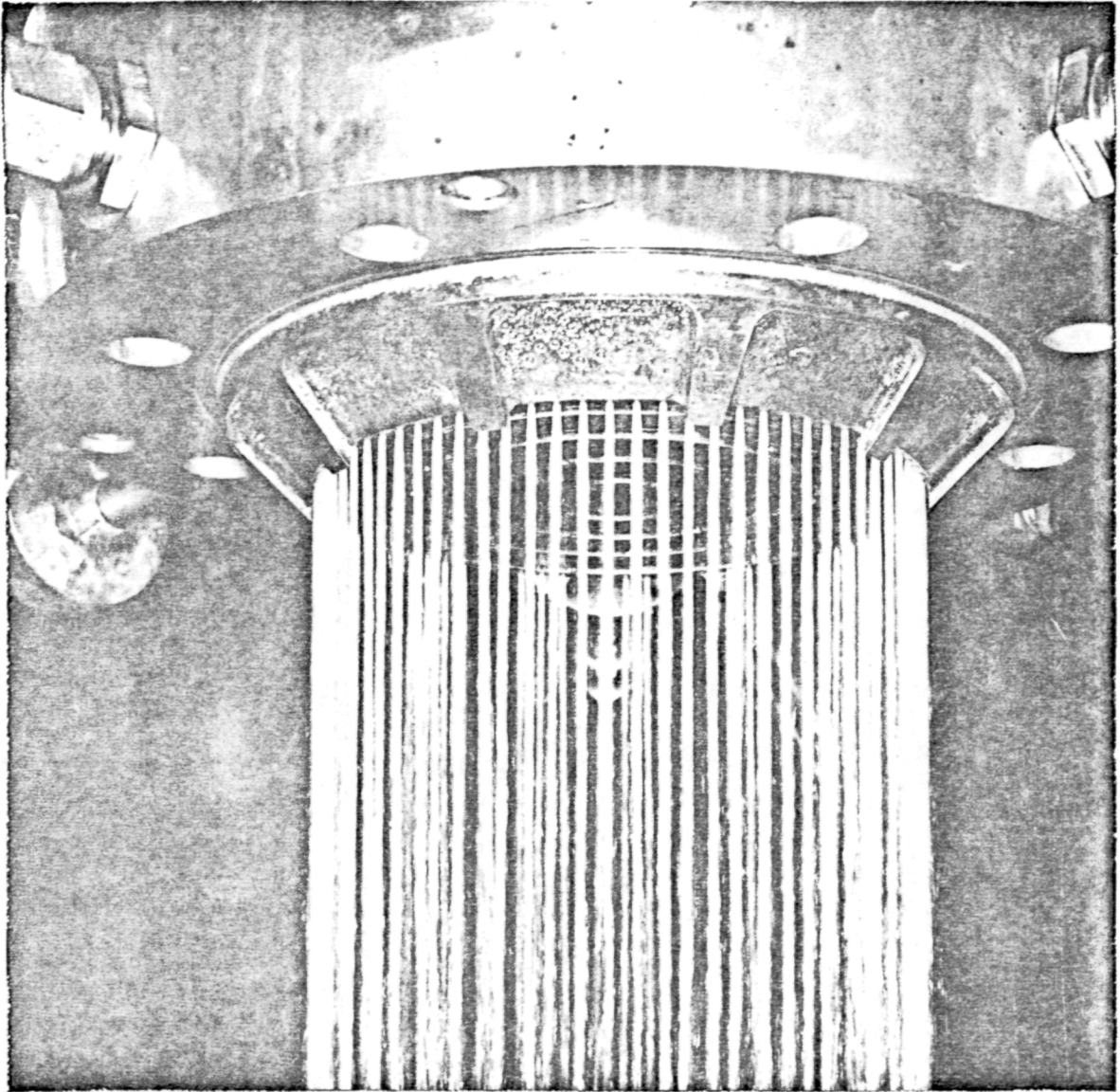


Figure 34. Water Flow of Film Coolant Orifices

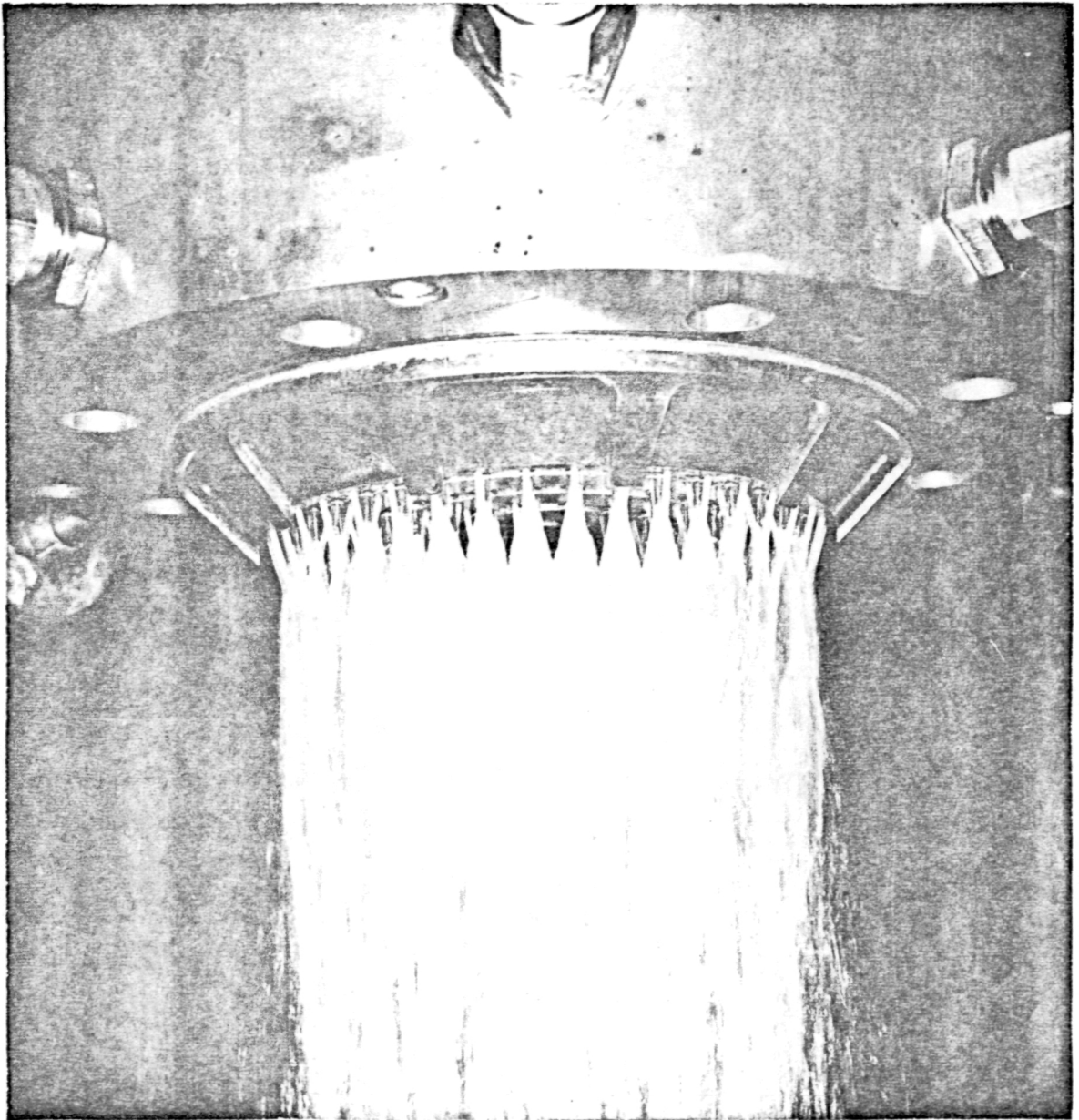


Figure 35. Water Flow of Injector Core Triplet Elements

TASK II - CALORIMETER TEST PROGRAM

The Task II thrust chamber test program using calorimeter hardware was conducted at the Reno facility during a series of 27 tests conducted using the 9.5 and 12-inch combustion chambers. Data were obtained in the areas of performance, thrust chamber heat flux, injector heat flux, and deposition. These results are discussed in the following section.

Calorimeter Test Series

The test program consisted of four test series comprising the total of 27 tests. These series were:

Test 068, 069. System Checkout tests.

Test 070-082. A complete survey of mixture ratio and film coolant flowrates conducted with the 12-inch combustion chamber.

Test 083-085. A series designed specifically to study the sensitivity of injector face deposition to mixture ratio with the 9.5-inch chamber.

Test 086-094. A survey of mixture ratio and film coolant flowrates conducted with the 9.5-inch combustion chamber.

Table 4 contains a list of the tests conducted along with test objectives. (Tests are numbered consecutively through a year for a single test stand.) In the table mixture ratio is defined as the ratio of total oxidizer flowrate to total fuel flowrate. (Mixture ratio is defined in this way throughout the report unless specifically indicated to be otherwise.) Film coolant flowrate in this table is defined as a percentage of total fuel flowrate. Figure 36 depicts the relationships between film coolant flowrate and overall and zone mixture ratios for the injector used in the calorimeter test programs of Task II and IV and the regenerative testing of Task IV.

TABLE 4. TASK II TEST DESCRIPTION

Test Number	Combustion Chamber Length, inches	Mixture Ratio, O/F	Film Coolant, % of Fuel	Objectives
068	12	3.96	0	System Checkout
069	12	--	--	
070	12	2.45	44	Full Mixture Ratio/Film Coolant Test Matrix at nominal $P_c = 100$ psia
071	12	3.01	34	
072	12	3.23	21	
073	12	3.06	35	
074	12	3.00	44	
075	12	2.47	20	
076	12	2.32	34	
077	12	2.74	20	
078	12	2.64	44	
079	12	2.66	34	
080	9.5	2.86	20	Film Coolant Test Matrix at nominal $P_c = 50$ psia
081	9.5	2.80	34	
082	9.5	2.98	43	
083	9.5	2.78	34	Deposit Study at nominal $P_c = 100$ psia
084	9.5	2.48	43	
085	9.5	3.02	43	
086	9.5	3.12	34	Full Mixture Ratio/Film Coolant Test Matrix at nominal $P_c = 100$ psia
087	9.5	3.31	20	
088	9.5	3.25	34	
089	9.5	3.10	43	
090	9.5	2.80	20	
091	9.5	2.72	34	
092	9.5	2.92	20	
093	9.5	2.46	34	
094	9.5	2.65	34	

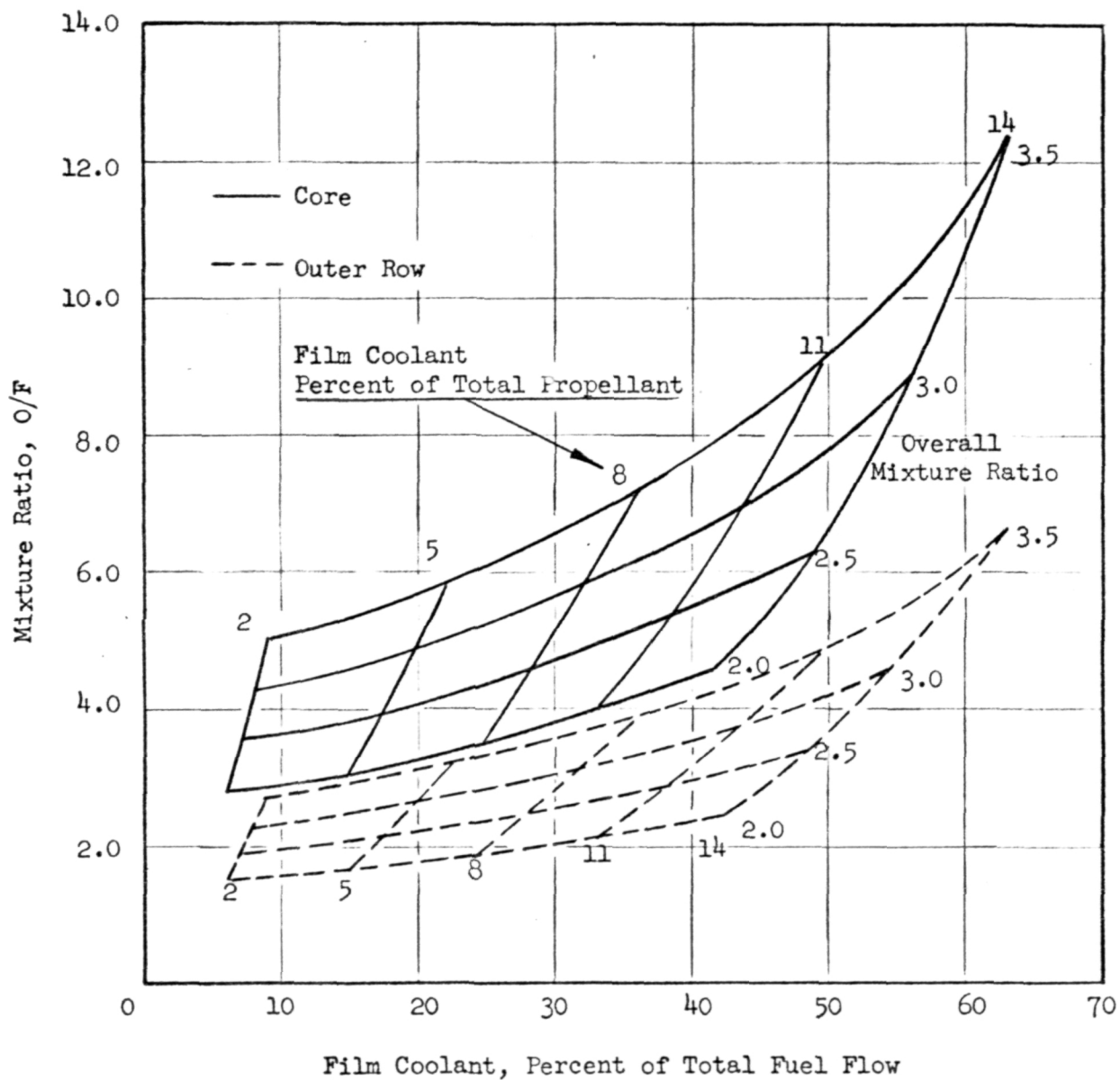


Figure 36. Film Coolant and Mixture Ratio Relationships for Calorimeter Test Program

TASK II CALORIMETER TEST RESULTS

The data derived during the Task II testing of the calorimeter were computer reduced and the basic test data summary may be seen in Table 5. .

Performance

Performance was determined based on both specific impulse and characteristic velocity. Thrust was based on correction for estimated diffuser forces.

Table 6 lists the experimental vacuum specific impulse efficiency for the calorimeter tests conducted at the NFL facility. In addition the operating conditions (chamber pressure and overall propellant mixture ratio), site measured thrust, propellant weight flowrate, cell environmental pressure, and ODE vacuum specific impulse calculated for the individual test conditions are presented.

The corrected experimental vacuum specific impulse efficiencies were approximately 100 percent as shown in Table 6 . The individual reference specific impulse was obtained from an ODE computation tailored to the specified test condition, average chamber propellant mixture ratio, $\epsilon = 10$, and inlet temperature and propellant impurities. The experimental vacuum specific impulse which was computed following the procedure outlined in Appendix B was corrected for the base force which is the product of the ambient environmental differential pressure and the base cross-sectional area. The lip area was negligible.

The injector was found to be generally high performing, delivering efficiencies in the range of 96 to 99 percent with the 12-inch chamber. The results from the 9.5-inch chamber were compromised, however by injector orifice clogging caused during an on-stand deposit removal during the test program. Later results (Task IV testing) verified the high performance in the 9.5 inch length.

TABLE 5. TASK II TEST DATA SUMMARY

1	2	3	4	5	6	7	8	9	10	11	12	13	14	15	16	17	18	19	20	CHARACTERISTIC VELOCITY		
TEST NUMBER	PROPELLANT COMBINATION	CHAMBER LENGTH (IN.)	OXIDIZER VENTURI TEMP °F	OXIDIZER VENTURI PRESS PSIA	OXIDIZER FLOWRATE LBM/SEC	FUEL VENTURI TEMP °F	FUEL VENTURI PRESS PSIA	FUEL FLOWRATE LBM/SEC	FILM COOLANT VENTURI TEMP °F	FILM COOLANT VENTURI PRESS PSIA	FILM COOLANT FLOWRATE LBM/SEC	FILM COOLANT % TOTAL FLOWRATE	TOTAL FLOWRATE LBM/SEC	CORRECTED THROAT AREA IN. ²	AVE CHAMBER PRESS PSIA	NOZZLE STAGNATION PRESS PSIA	MIXTURE RATIO ENGINE	MIXTURE RATIO CORR	MIXTURE RATIO OUTER RING	ACTUAL FT/SEC	THEORETICAL FT/SEC	*** EFFICIENCY
068	FLY 8 ₂ B ₂	12.0	56	461	1.759	74	409	.444	---	---	---	---	2.203	5.31	74.66	75.63	3.96	5.510	2.935	5870	7115	80.5
069			55	502	1.919	44	400	---	78	34	two phase flow in sonic venturi											
070			48	442	1.699	130	399	.398	108	305	.306	12.77	2.393	5.31	93.02	94.23	2.447	5.701	3.043	6723	6964	96.5
071			48	504	1.942	95	410	.424	83	390	.221	8.53	2.587	5.31	102.84	104.18	3.010	5.966	3.184	6878	7094	97.0
072			50	504	1.938	106	462	.476	86	451	.124	4.09	2.539	5.31	101.52	102.84	3.227	5.354	2.831	6919	7120	97.2
073			50	503	1.933	84	395	.412	80	386	.221	8.61	2.566	5.31	101.97	103.29	3.056	6.124	3.269	6860	7100	96.9
074			50	499	1.919	86	349	.360	72	336	.279	10.92	2.559	5.31	100.68	101.99	2.988	6.941	3.705	6816	7090	96.1
075			50	452	1.737	91	513	.558	80	502	.144	5.90	2.439	5.32	97.12	98.30	2.472	4.695	2.164	6699	6974	98.9
076			49	450	1.726	94	460	.486	84	444	.257	10.39	2.472	5.32	95.51	96.79	2.325	4.633	2.473	6609	6931	98.6
077			51	471	1.810	94	490	.524	81	479	.135	5.48	2.470	5.32	98.49	99.77	2.744	4.751	2.403	6914	7040	98.2
078			50	469	1.803	85	367	.302	71	356	.301	12.12	2.486	5.32	98.08	99.35	2.639	6.156	3.286	6842	7016	97.5
079			49	463	1.780	88	417	.439	78	406	.230	9.40	2.451	5.32	97.28	98.54	2.662	5.296	2.656	6854	7020	98.1
080			49	243	.928	75	252	.268	59	246	.066	5.20	1.282	5.32	48.96	49.60	2.865	4.694	2.566	6786	6977	97.0
081			48	236	.903	66	208	.213	55	198	.110	8.98	1.226	5.33	47.50	48.12	2.799	5.540	3.067	6725	6983	96.3
082			48	234	.894	60	167	.170	49	160	.130	10.92	1.195	5.33	45.96	46.56	2.979	6.870	3.667	6679	7011	95.3
083		9.5	61	435	1.650	133	406	.394	134	387	.201	8.94	2.245	5.31	88.01	89.16	2.775	5.460	2.914	6761	7035	96.4
084			66	472	1.782	141	425	.410	144	411	.311	12.41	2.502	5.31	95.30	96.54	2.475	5.675	3.029	6591	6973	94.5
085			67	480	1.808	140	358	.341	145	346	.259	10.74	2.408	5.31	91.92	93.11	3.016	6.915	3.691	6506	7082	93.3
086			67	483	1.821	141	404	.387	142	382	.196	8.14	2.404	5.31	85.91	87.03	3.124	6.131	3.272	6185	7090	87.2
087			64	484	1.833	129	450	.444	135	442	.110	4.63	2.387	5.31	86.00	87.12	3.306	5.384	2.874	6239	7110	87.8
088			62	483	1.832	118	378	.374	115	358	.190	7.93	2.395	5.32	85.18	86.29	3.250	6.394	3.413	6162	7103	86.8
089			61	481	1.827	110	339	.336	113	327	.254	10.50	2.416	5.32	85.05	86.15	3.100	7.100	3.789	6101	7096	86.1
090			61	473	1.800	104	491	.512	106	482	.128	5.26	2.437	5.32	87.58	88.72	2.805	4.572	2.440	6231	7040	86.5
091			59	471	1.790	100	423	.436	96	400	.222	9.05	2.447	5.32	86.08	87.20	2.721	5.351	2.856	6101	7021	86.9
092			60	488	1.858	94	477	.508	93	470	.128	5.14	2.493	5.32	90.95	92.13	2.922	4.772	2.547	6329	7066	89.6
093			59	473	1.800	94	459	.485	89	435	.247	9.77	2.532	5.33	93.01	94.22	2.457	4.828	2.582	6377	6966	91.5
094			59	471	1.791	92	427	.448	89	405	.228	9.23	2.466	5.33	92.30	93.50	2.650	5.212	2.782	6498	7012	92.7

Area ratio = 10, * A_{corrected} = (A_{T geometric} minus throat shrinkage and boundary layer), ** Correction for combustor Mach number,*** $(\eta_{c*})_{kin} (\eta_{c*})_{ER} + (P_7 + P_8 + P_9)/3$

TABLE 6. VACUUM SPECIFIC IMPULSE TEST SUMMARY

	1	2	3	4	5	6	7	8	9	10 *	
	Test Number	Average Chamber Pressure (psia)	Environ- mental Pressure (psia)	Site Thrust lbf	Vacuum Thrust lbf	Total Flowrate (lbm/sec)	Vacuum Experi- mental Impulse (sec)	Engine Mixture Ratio	Vacuum Specific Impulse (ODE) (sec)	Vacuum Specific Impulse Efficien- cy (exp)	
1	068	74.7	12.1	230.7	871.7	2.203	395.6	3.96	395	1.001	
2	070	93.0		297.0	940.4	2.393	392.9	2.45	387	1.015	
3	071	102.8		345.2	988.4	2.587	382.0	3.01	391	0.977	
4	072	101.5		330.6	974.7	2.539	383.8	3.23	393	0.976	
5	073	102.0		332.1	976.3	2.566	380.4	3.06	392	0.970	
6	074	100.7		339.2	981.7	2.559	383.6	3.00	392	0.978	
7	075	97.1		296.5	940.8	2.439	385.7	2.47	386	0.999	
8	076	98.5		291.9	936.7	2.472	378.9	2.32	381	0.994	
9	077	98.5		294.2	937.9	2.470	379.7	2.74	389	0.976	
10	078	98.1		271.9	915.2	2.486	368.1	2.64	388	0.948	
11	079	97.3		269.7	912.5	2.451	372.3	2.66	387	0.962	
12	080	49.0		18.6	662.1	1.236	535.6	2.87	390	--	
13	081	47.5		16.0	659.0	1.249	527.6	2.80	391	--	
14	082	46.0		11.3	654.0	1.195	547.2	2.98	395	--	
15	083	88.0		299.8	942.4	2.282	412.9	2.78	391	1.056	
16	084	95.3		411.0	1053.3	2.550	412.9	2.48	387	1.060	
17	085	91.9		380.8	1022.8	2.446	418.1	3.02	395	1.058	
18	086	85.9		304.0	946.1	2.404	393.5	3.12	393	1.001	
19	087	86.0		325.5	967.7	2.387	405.4	3.31	391	1.036	
20	088	85.2		254.6	896.5	2.395	374.3	3.25	394	0.950	
21	089	85.1		221.7	862.9	2.416	357.1	3.10	395	0.904	
22	090	87.6		294.0	935.6	2.437	383.9	2.81	384	0.999	
23	091	86.1		297.3	939.2	2.447	383.8	2.72	390	0.984	
24	092	91.0		306.5	947.8	2.493	380.0	2.92	387	0.982	
25	093	93.0		324.8	966.9	2.532	381.8	2.46	386	0.989	
26	094	92.3		338.4	979.7	2.466	397.2	2.65	389	1.021	
27											
28											
29											
30											
31	* Efficiency = $\frac{\text{measured (corrected for diffuser thrust) impulse}}{\text{O.D.E. vacuum impulse at } \epsilon = 10}$										
32											
33											
34											
35											

The selected performance indicator was injector efficiency, and this was defined as shown in Appendix A. No corrections except the isentropic pressure ratio from measured to stagnation pressure and the discharge coefficient contributions caused by the boundary layer displacement thickness and flow divergence were employed. The efficiency computed consequently contains all losses due to flow striations and chemical nonequilibrium of the flow.

The performance data are tabulated in Table 5 . The 12-inch chamber results are shown graphically in Fig. 37. At a mixture ratio of 3:1 the values are seen to vary from 96 to 97.5 percent with varying film coolant flowrate. At lower mixture ratios, the efficiency becomes both higher and less sensitive to film coolant flowrate. The 12-inch data are cross plotted versus film coolant flowrate in Fig. 38.

As an indication of the degree to which the flows from the various injector zones mix upstream of the throat, a theoretical mixture ratio maldistribution efficiency was computed with the efficiency defined as the mass weighted average of the theoretical c^* for each zone divided by the theoretical c^* at overall mixture. The delivered efficiency was divided by this value with the result in Fig. 39. Considerable mixing takes place and the mixing increases as the stratification increases.

Thrust Chamber Heat Flux

Thrust chamber heat flux was determined as a function of film coolant flowrate, overall mixture ratio, and chamber length. Data correlations of, directly observed heat flux, film coefficient determination for an assumed value of adiabatic wall temperature, and heat flux distribution correlations using a detailed model of the film-core interactions of $\text{FLOX/B}_2\text{H}_6$, were made.

Heat flux data were obtained using thermal isolation sections machined within the copper uncooled thrust chamber walls. Thermocouples located on the back surface of these segments provide the temperature-time histories which were converted to heat flux by comparison with theoretical predictions. The isolation segments depicted in Fig. 40 were made by cutting circumferential grooves into the copper chamber walls leaving a cylindrical plug which contacts the parent material only along the gas-side surface. This method reduces the three-dimensional heat transfer effects.

To facilitate rapid evaluation of the test data, an analysis was conducted for parametric heat flux levels with a heating profile for a 200-millisecond start transient and then steady state combustion chamber operation. This

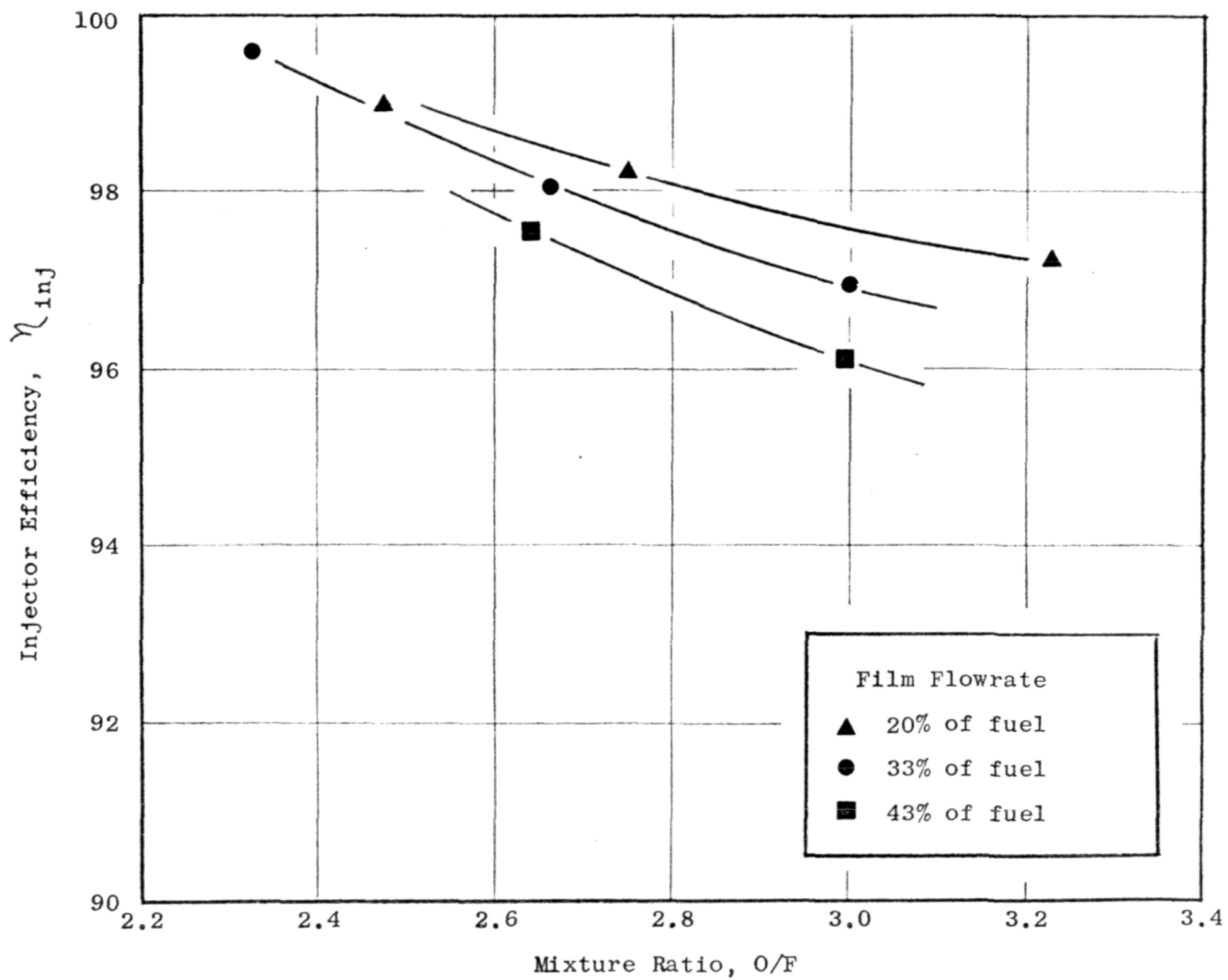


Figure 37. Performance Results for F_2-O_2/B_2H_6 with the 12-inch Combustion Chamber.

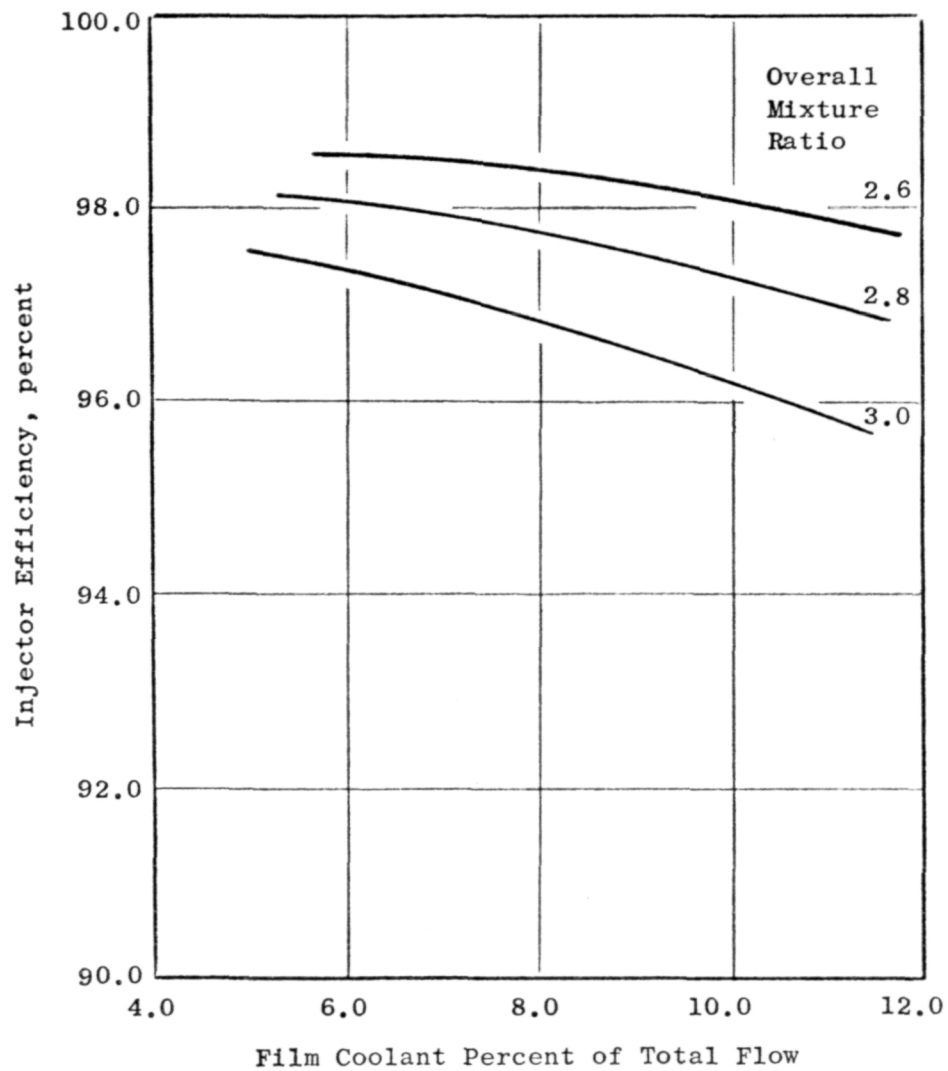


Figure 38. Injector Efficiency as a Function of Film Coolant Flowrate for 12-inch Combustion Chamber.

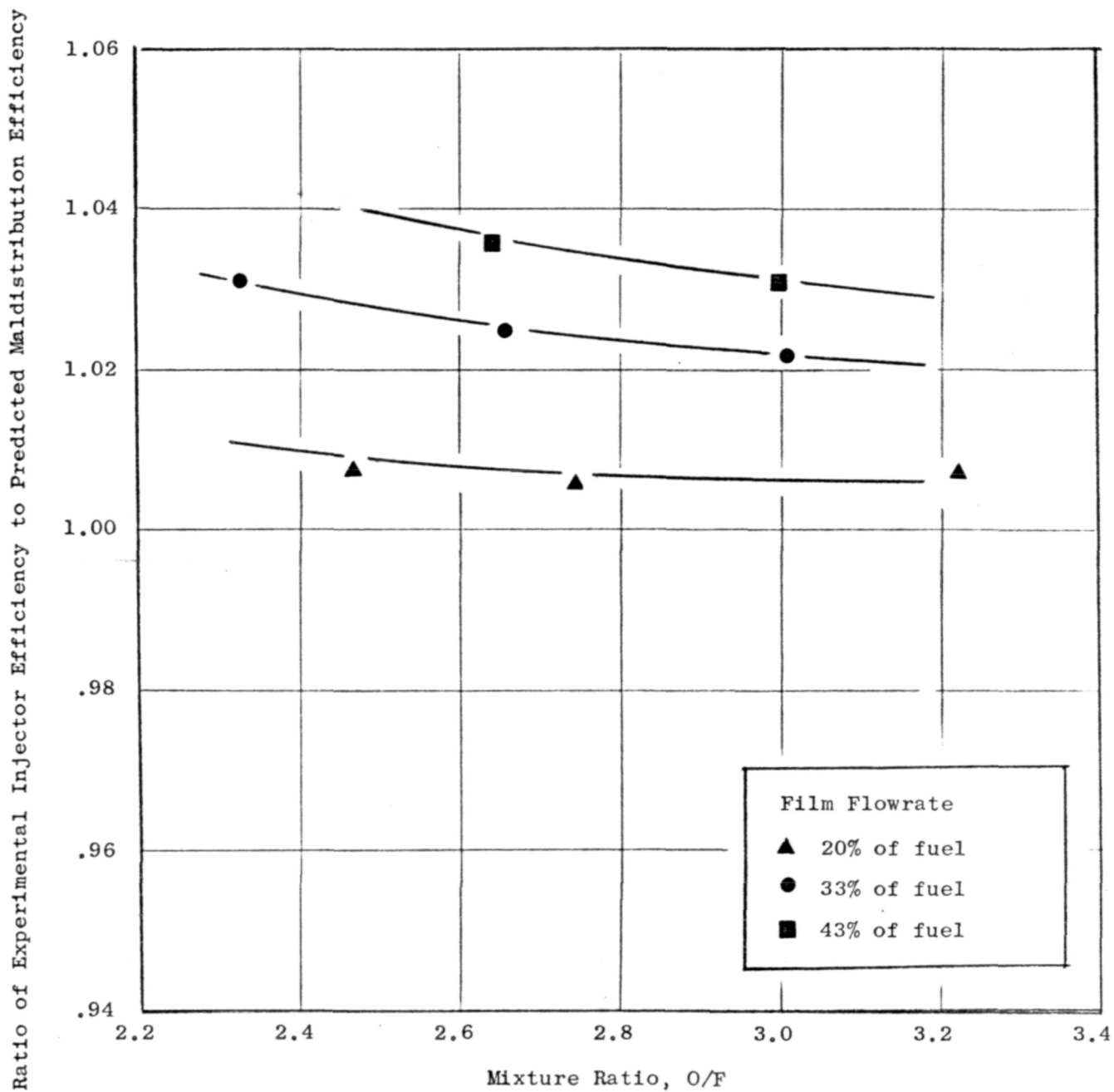


Figure 39. Injector Performance Comparison with Predictions Based on Injected Mixture Ratio Maldistribution.

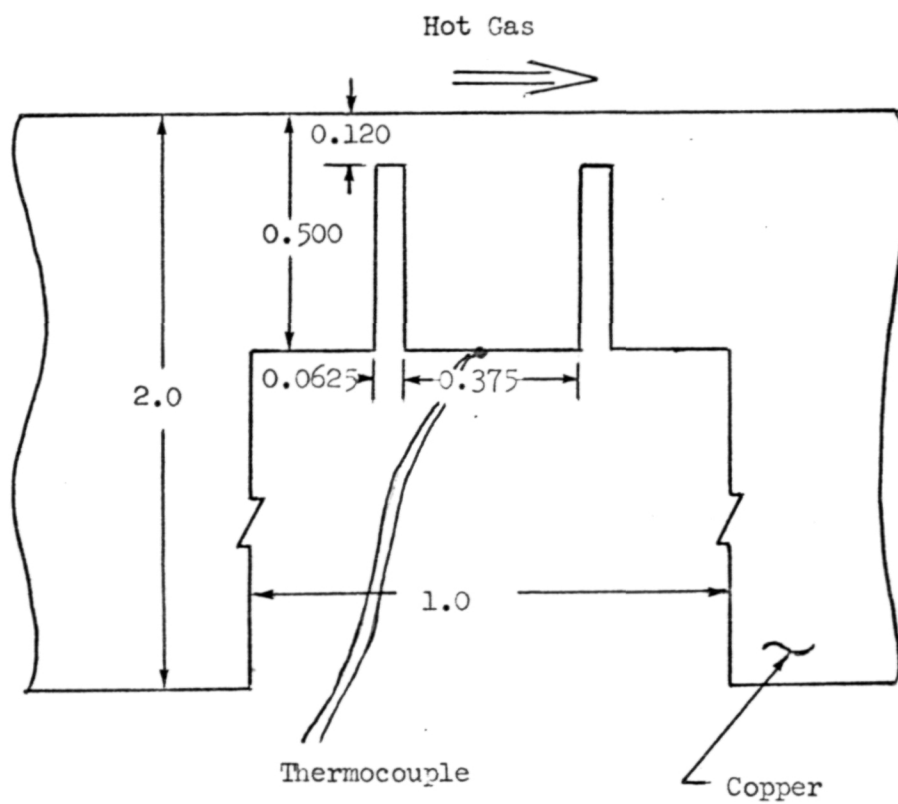


Figure 40 . Cross-section of Combustor Heat Transfer Isolation Segments

start profile was in good agreement with the starts actually recorded. Heat flux during the start was assumed to vary as $(P_c/P_c \text{ (steady state)})^{0.8}$. The resultant normalized temperature-time histories are based on an assumed adiabatic (reference) wall temperature of 7000 F. For the film coefficient correlation, the 7000 F value was arbitrarily selected, however, the values of film coefficient and adiabatic wall temperatures are consistent with the measured heat flux value (Fig. 41).

A heat flux distribution is shown in Fig. 42 for the Test 083 which was made with the 9.5-inch chamber (film coolant flowrate of 8 percent of total flow and overall mixture ratio of 2.78). The data shown were taken in four circumferential locations through the chamber and nozzle. The results were compared with the curve which was used in Task I for concept selection and preliminary design studies and the two are shown in good agreement. The heat flux is shown to be circumferentially uniform. Other test results were generally similar to those shown although data scatter was increased on tests which are known to have injector deposits. Data correlation was concentrated primarily on throat heat flux. Examination of combustion chamber and nozzle heat flux indicates some sensitivity to injection parameters similar to results at the throat.

Cross plots of throat heat flux versus overall mixture ratio for parametric film coolant flowrate are shown in Fig. 43 and 44. Although there is a general trend in each case for the heat flux levels, there is a fair degree of overlap, largely caused by variations in chamber pressure and injector efficiency.

Inconsistencies were corrected out of the data by assuming that adiabatic wall temperature and therefore heat flux would have increased as the square of the injector c^* efficiency. Moreover, it was assumed that film coefficient and therefore heat flux would have increased as the mass velocity to the 0.8 power. Experimental heat flux was corrected to a 95 percent injector efficiency by

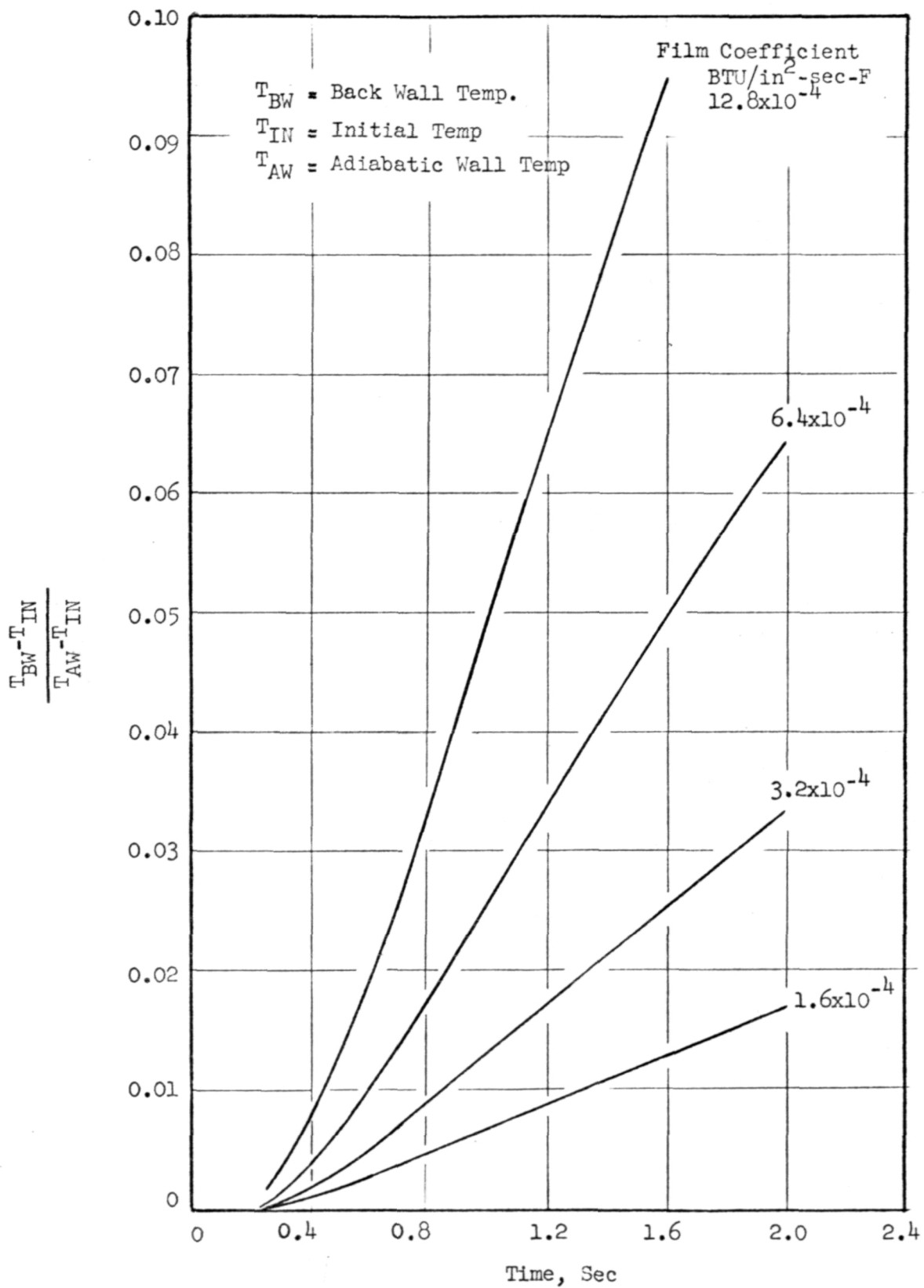


Figure 41. Isolation Segment Normalized Temperature History
(includes start transient)

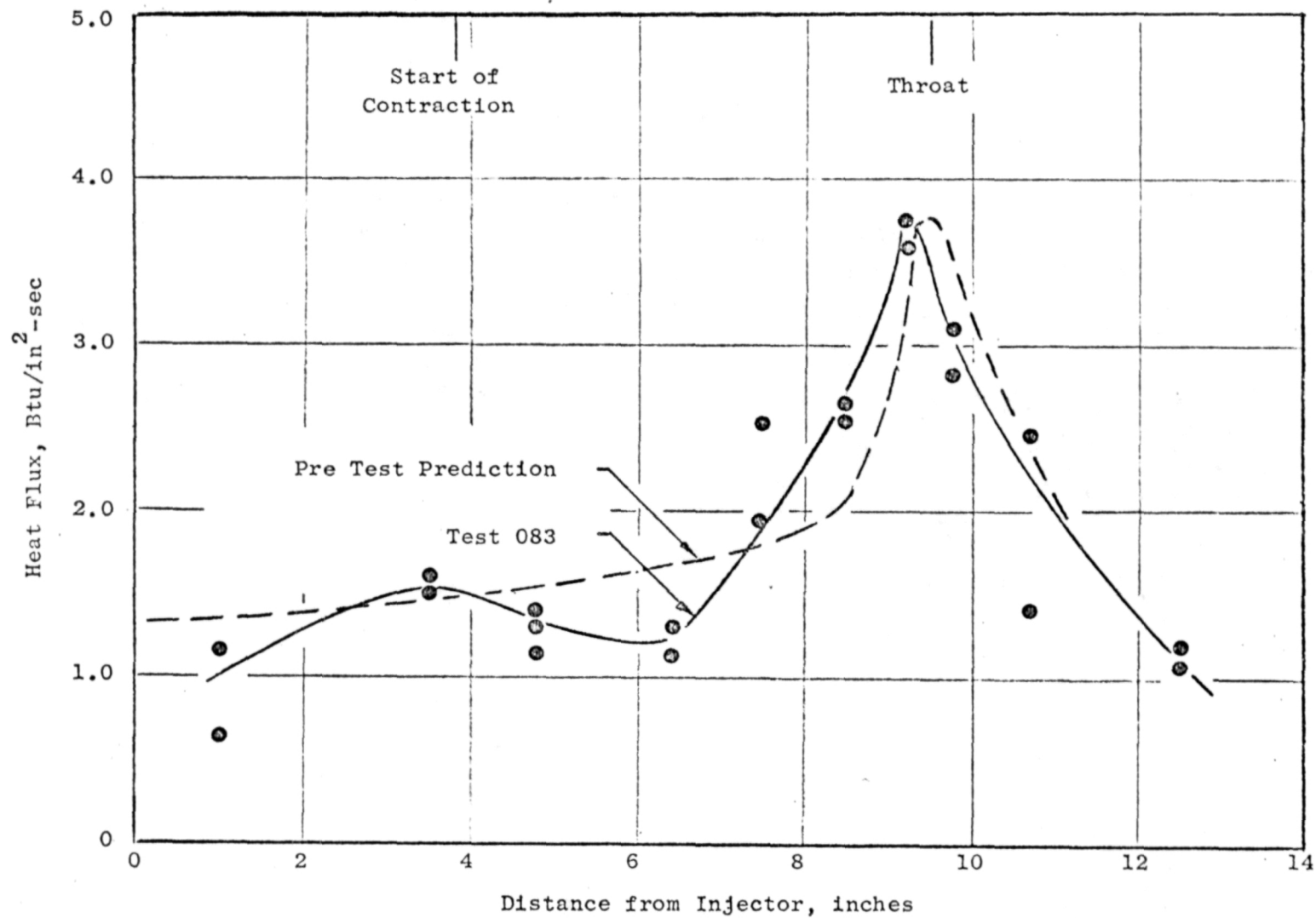


Figure 42. Heat Flux Profile for Nominal Test Conditions With 9.5-inch Combustion Chamber

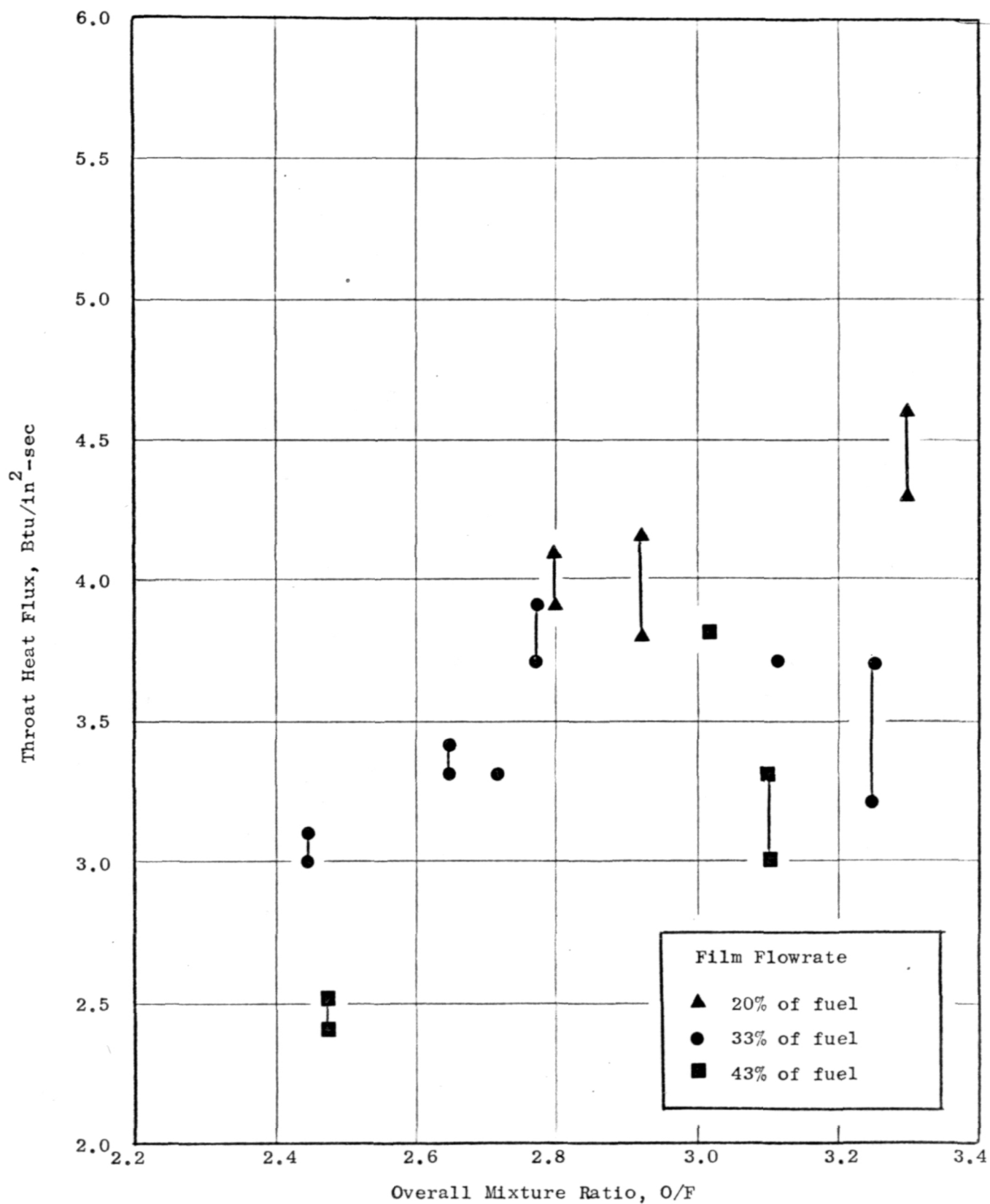


Figure 43. Throat Heat Flux Data for 9.5-inch Combustion Chamber.

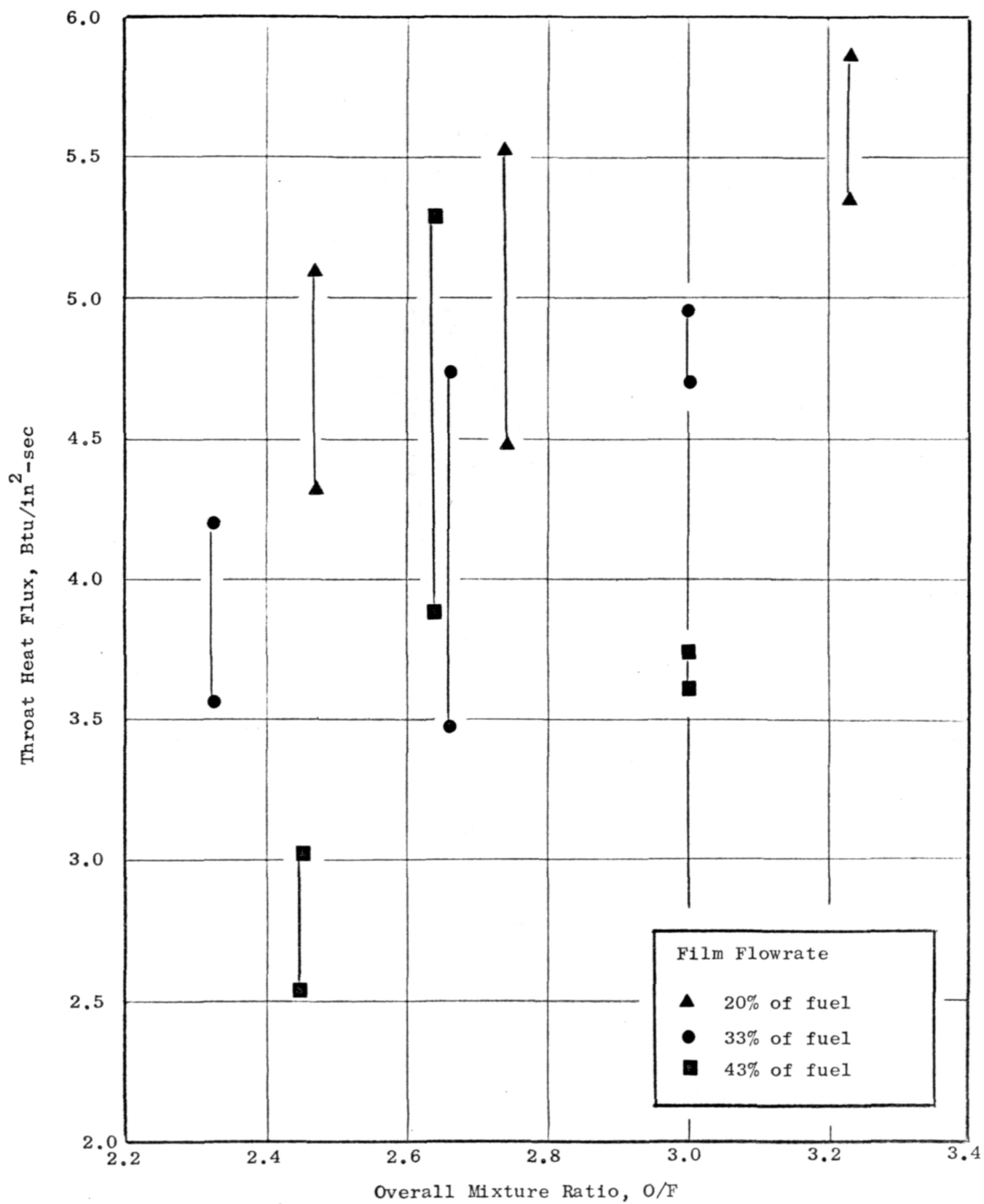


Figure 44. Throat Heat Flux Data for 12-inch Combustion Chamber.

$$(Q/A)_{\text{exp}} \left(\frac{0.95}{\eta_{\text{inj}_{\text{exp}}}} \right)^2$$

At a fixed value of injector efficiency the mass velocity is proportional to chamber pressure, and the experimental pressure was corrected for injector efficiency by

$$P_{c_{\text{exp}}} \left(\frac{0.95}{\eta_{\text{inj}_{\text{exp}}}} \right)$$

These combined simplify to

$$(Q/A)_{\text{normalized}} = (Q/A)_{\text{exp}} \left(\frac{0.95}{\eta_{\text{inj}_{\text{exp}}}} \right)^{1.2} \left(\frac{100}{P_{c_{\text{exp}}}} \right)^{0.8}$$

A normalized film coefficient correlation based on an adiabatic wall temperature of 7000 F is shown in Fig. 45 and 46. The data shown give a good discrimination of the effect of film coolant flowrate and overall mixture ratio.

For each test an effective outer zone mixture ratio was computed by analytically combining the flow from the outer row of elements with the film coolant flow. This is the mixture ratio which would result if the film mixed completely with the flow from the outer row but no mixing took place with the inner core. The normalized film coefficients obtained were then plotted versus outer zone mixture ratio with the results shown in Fig. 47 and 48. The collapse to a single curve indicates that the film is nearly fully mixed by the time it reaches the throat. This result is in good agreement with performance trends discussed above which also indicated considerable mixing between zones.

The variation of throat heat flux with η_{c*} for a mixture ratio of 3:1, is shown in Fig. 49. Here it is seen that at the nominal throat heat flux of 4.5 Btu/in²-sec, the injector efficiency is 97-97.5 percent (L = 12 in.)

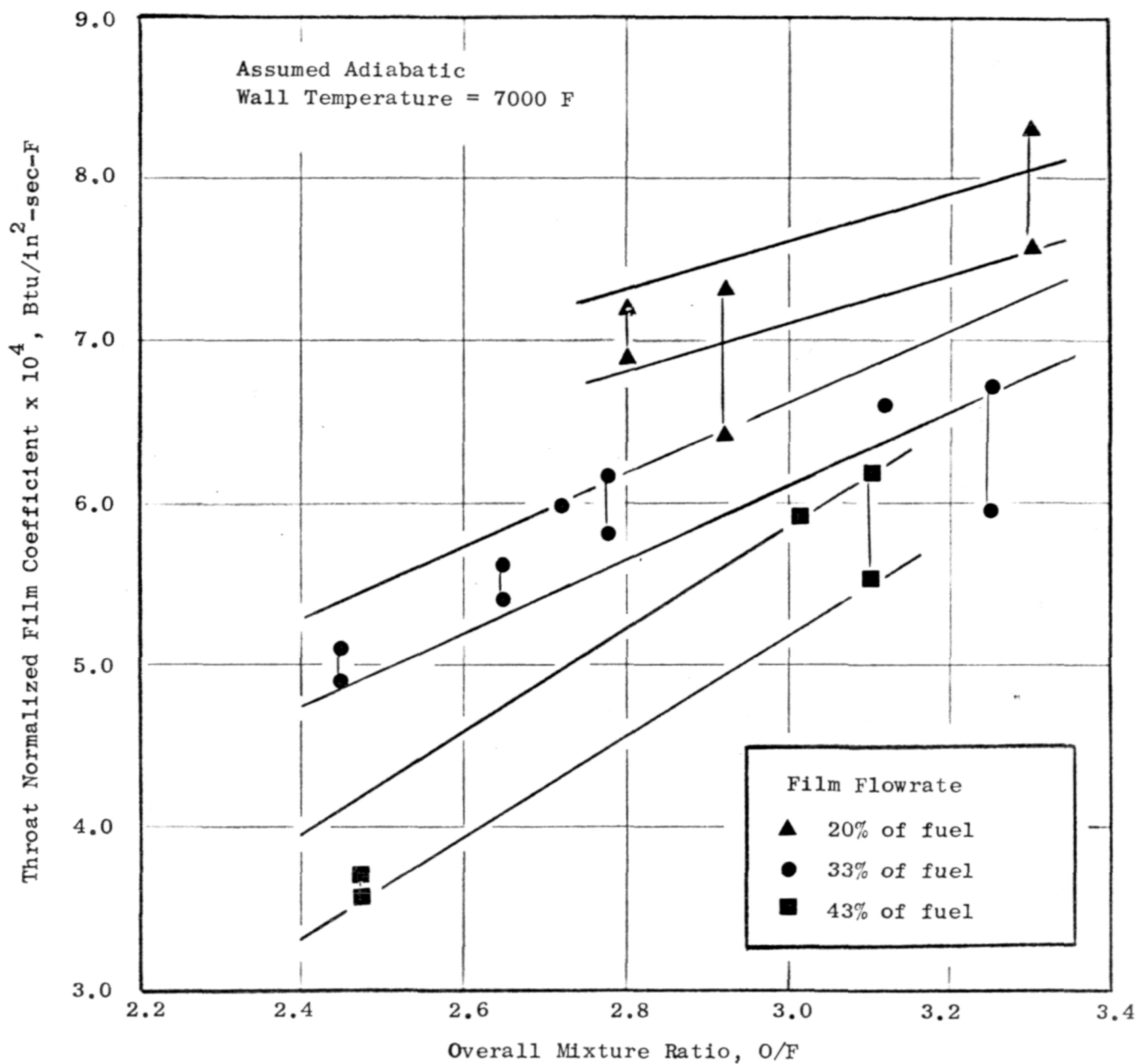


Figure 45. Throat Normalized Film Coefficient Data for 9.5-inch Combustion Chamber.

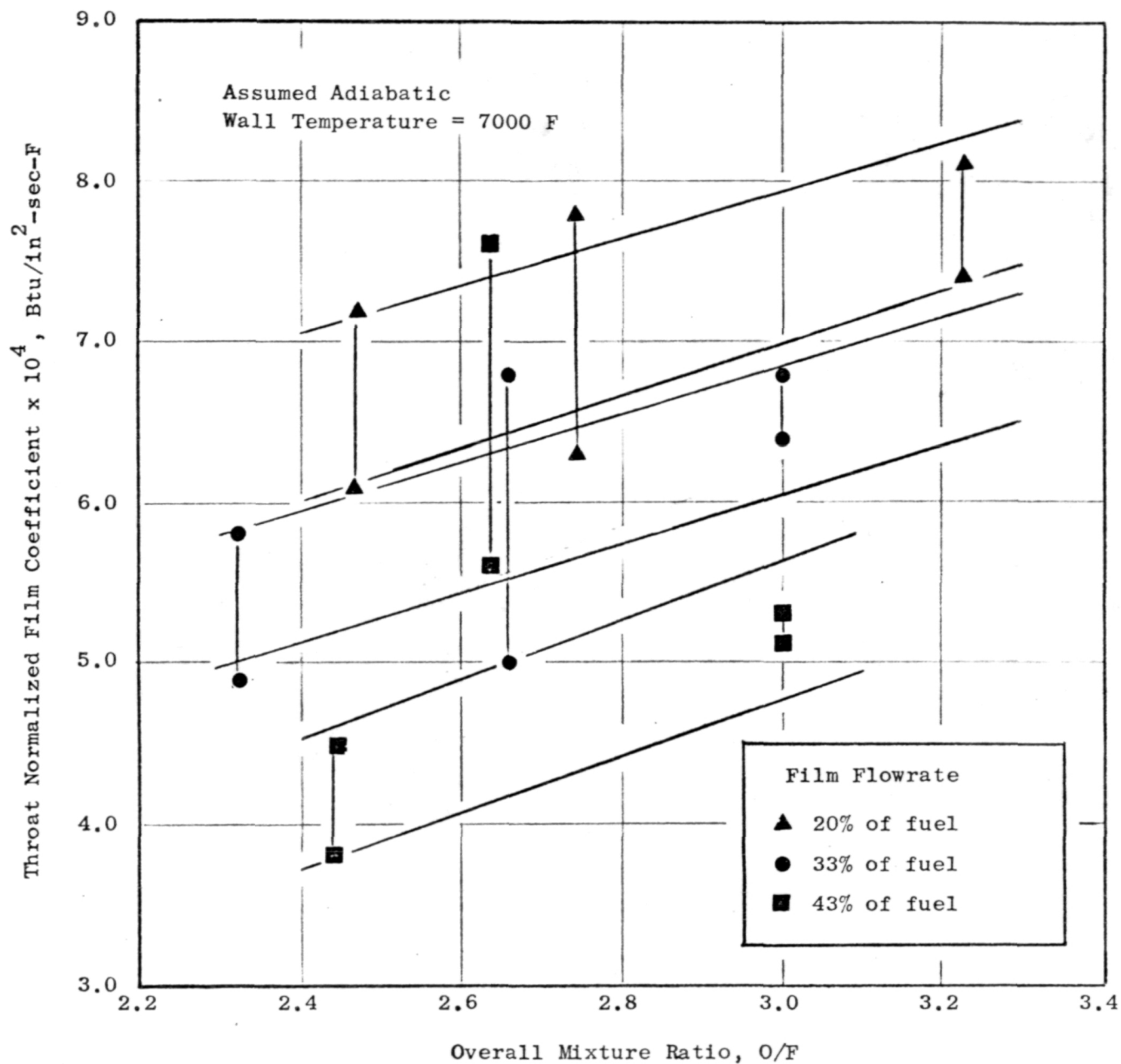


Figure 46 . Throat Normalized Film Coefficient Data for 12-inch Combustion Chamber.

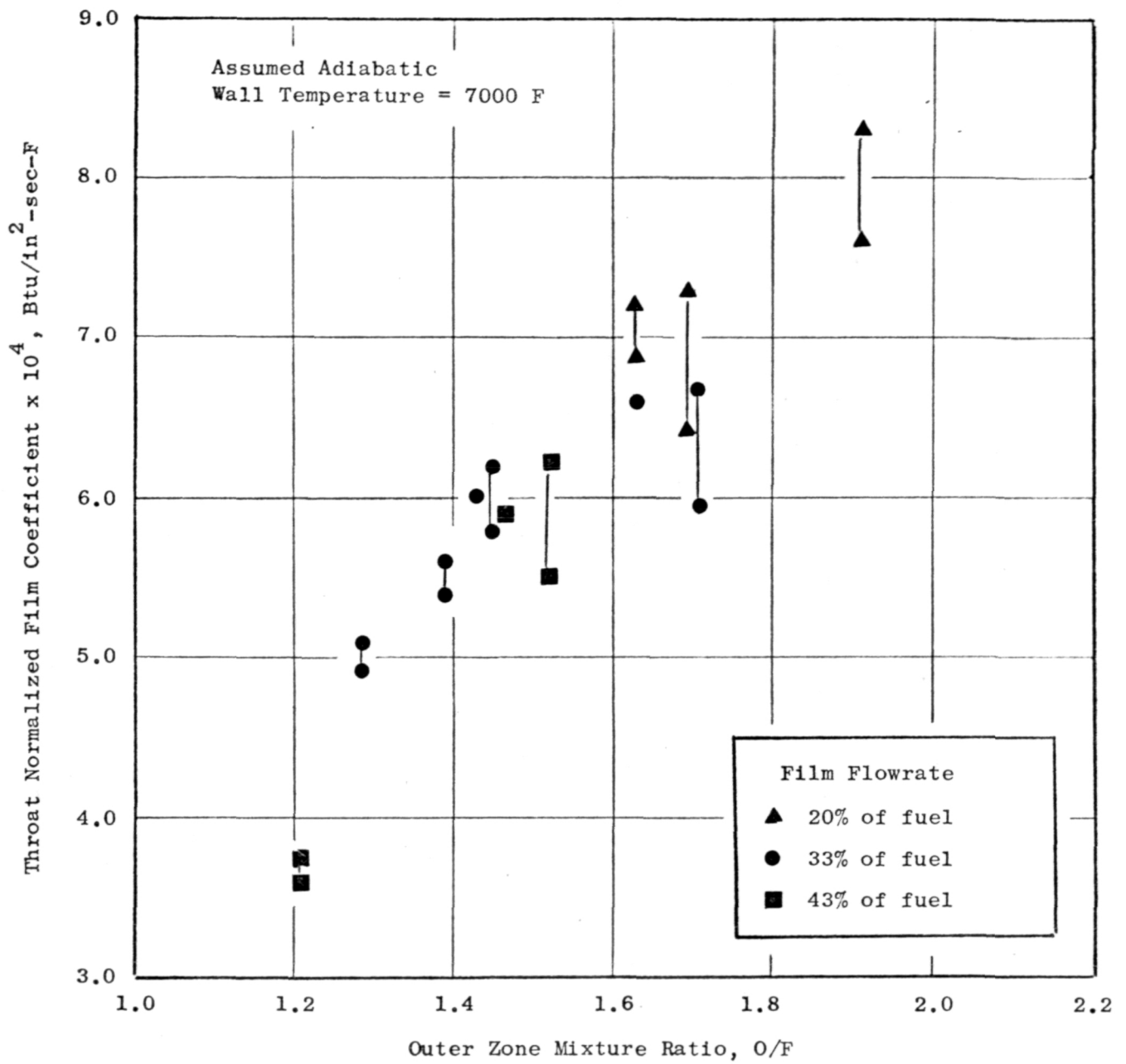


Figure 47. Throat Normalized Film Coefficient Correlation with Outer Zone Mixture Ratio for 9.5-inch Combustion Chamber.

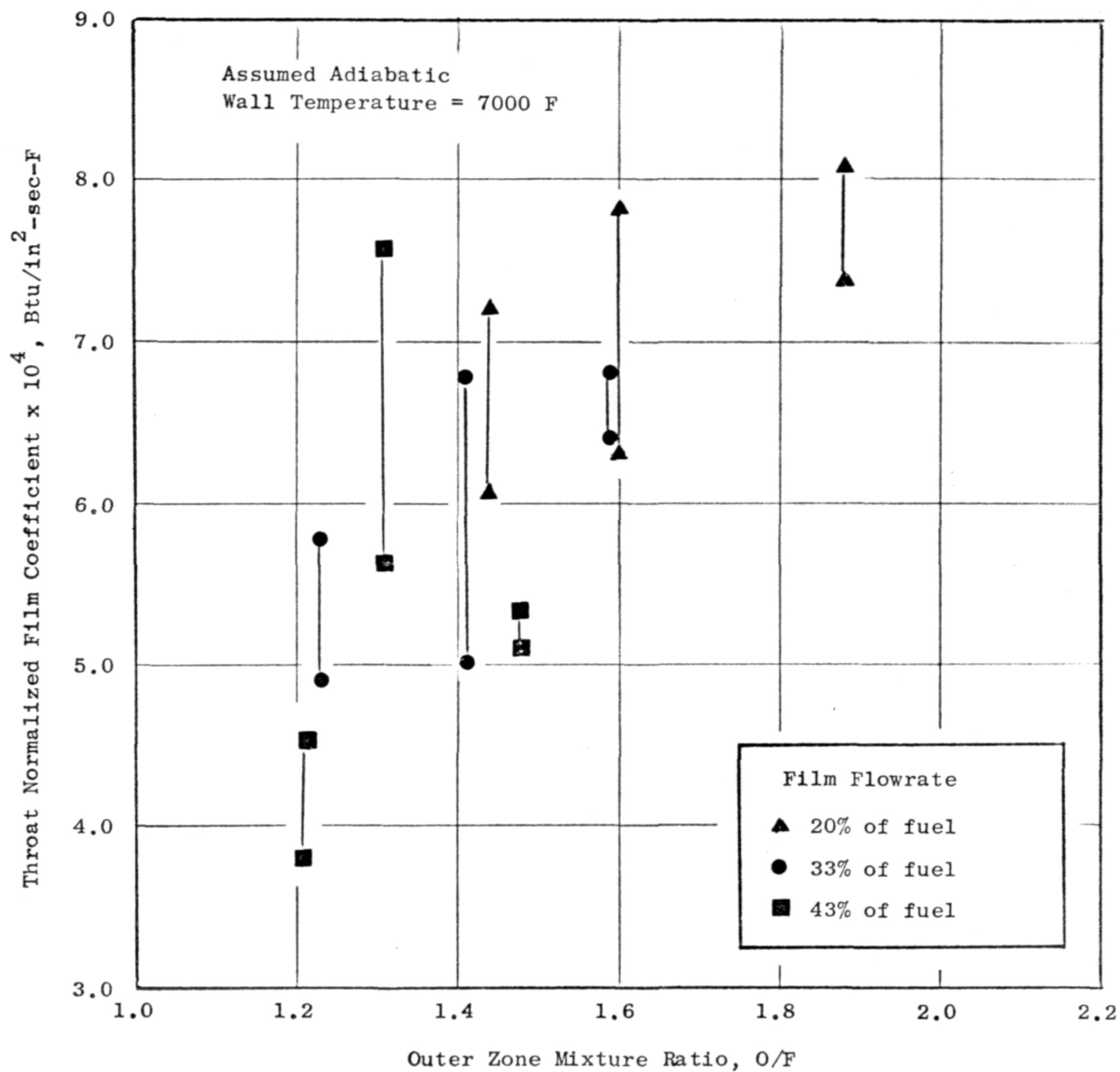


Figure 48. Throat Normalized Film Coefficient Correlation with Outer Zone Mixture Ratio for 12-inch Combustion Chamber.

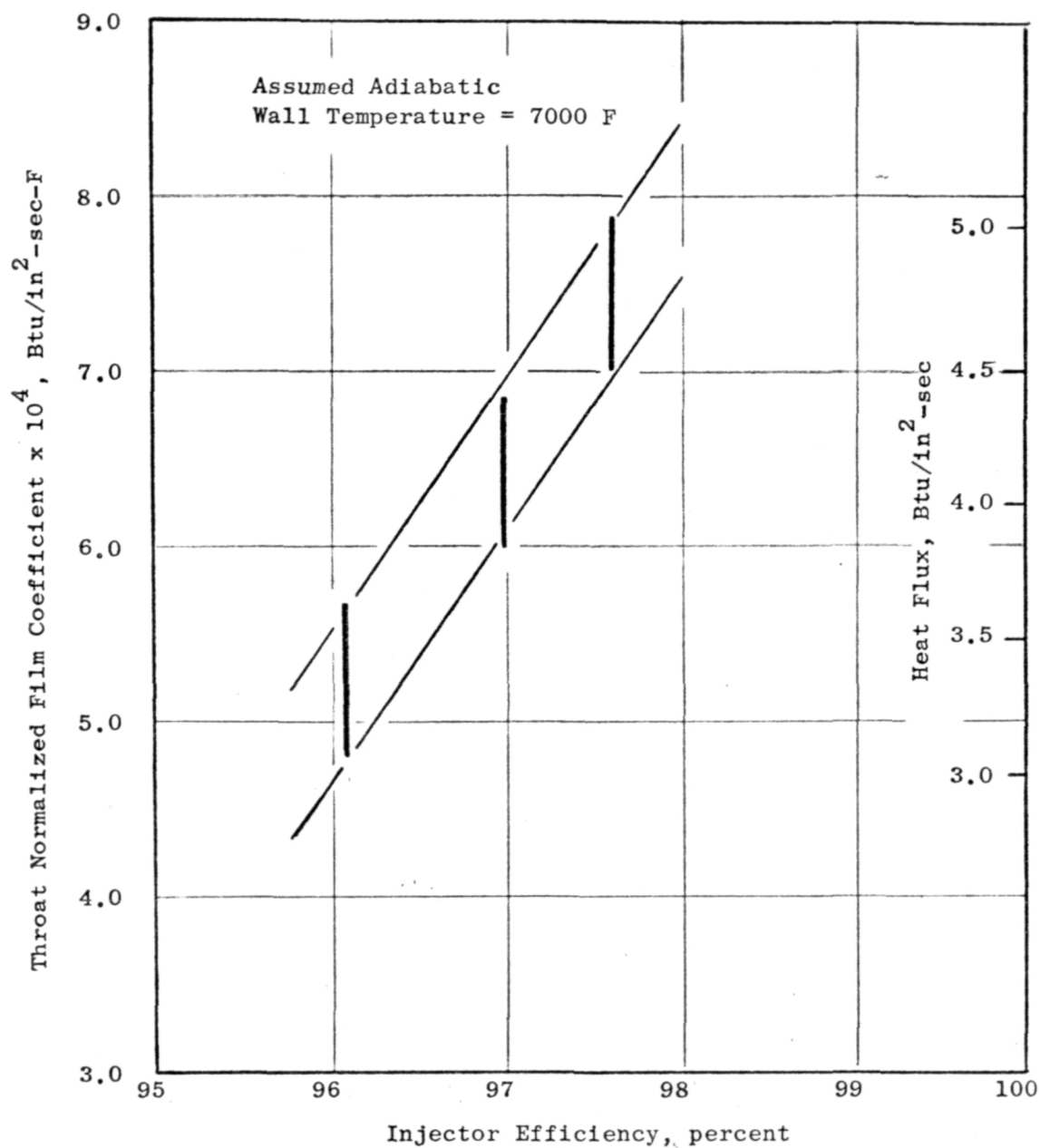


Figure 49. Throat Heat Flux Correlation with Injector Efficiency for 12-inch Combustion Chamber.

and that substantial reductions in heat flux are possible with only a small penalty in performance. For example, a reduction to $3.5 \text{ Btu/in}^2\text{-sec}$ incurs a performance loss of only about 1 percent. Reference 4 reports a specific impulse value of 408 lbf-sec/lbm at an injector efficiency of 97.5 percent in a 60:1 area ratio 15 degree conical nozzle.

Injector Heat Flux

Injector heat flux was determined from the temperature history recorded with three thermocouples located 0.090 inch back from the face of the injector. A three-dimensional analysis was conducted for parametric values of injector face heat flux during Task I.

Injector face heat flux levels were found to be consistent and correlatable (Fig. 50) except when deposits were present. Some results for the core region are shown in Fig. 51 with the data presented in the form of inner core injector face heat flux as a function of inner core mixture ratio. Only tests for which deposits are not believed to have been present at start are shown. The data show a clear trend of decreasing heat flux with increasing mixture ratio. The heat flux observed with the Rocketdyne IR&D injector is also shown in this figure. That injector had an orifice geometry nearly identical to the one used in this program and also had a large percentage of the fuel injected axially.

Deposition

At the nominal mixture ratio of 3:1, injector face deposits were minimal or non-existent. However, there was a strong mixture ratio dependence with deposits increasing as mixture ratio decreased. At $MR \leq 2.4$ deposits became totally unacceptable. The first opportunity to observe the injector was after completion of the 12-inch chamber test series, ending with Test 082. Figure 52 shows the appearance of the injector when the hardware was disassembled. The heaviest deposits were near the edge and clearly grew out from the injector rather than growing on the wall. The deposit seemed to have no effect on performance, but clearly increased the scatter in the chamber heat flux data.

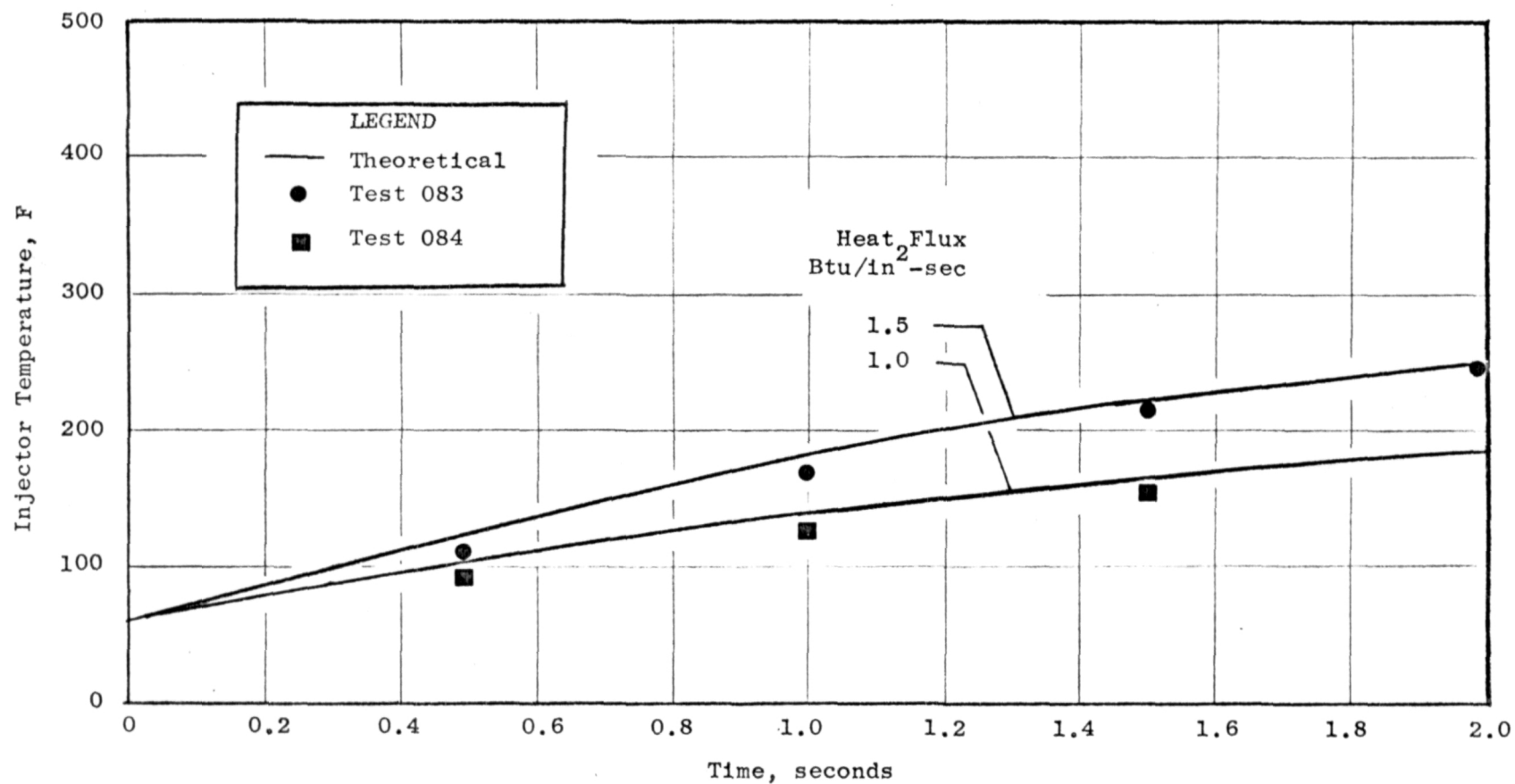


Figure 50. Injector Temperature Histories for Tests 083 and 084.

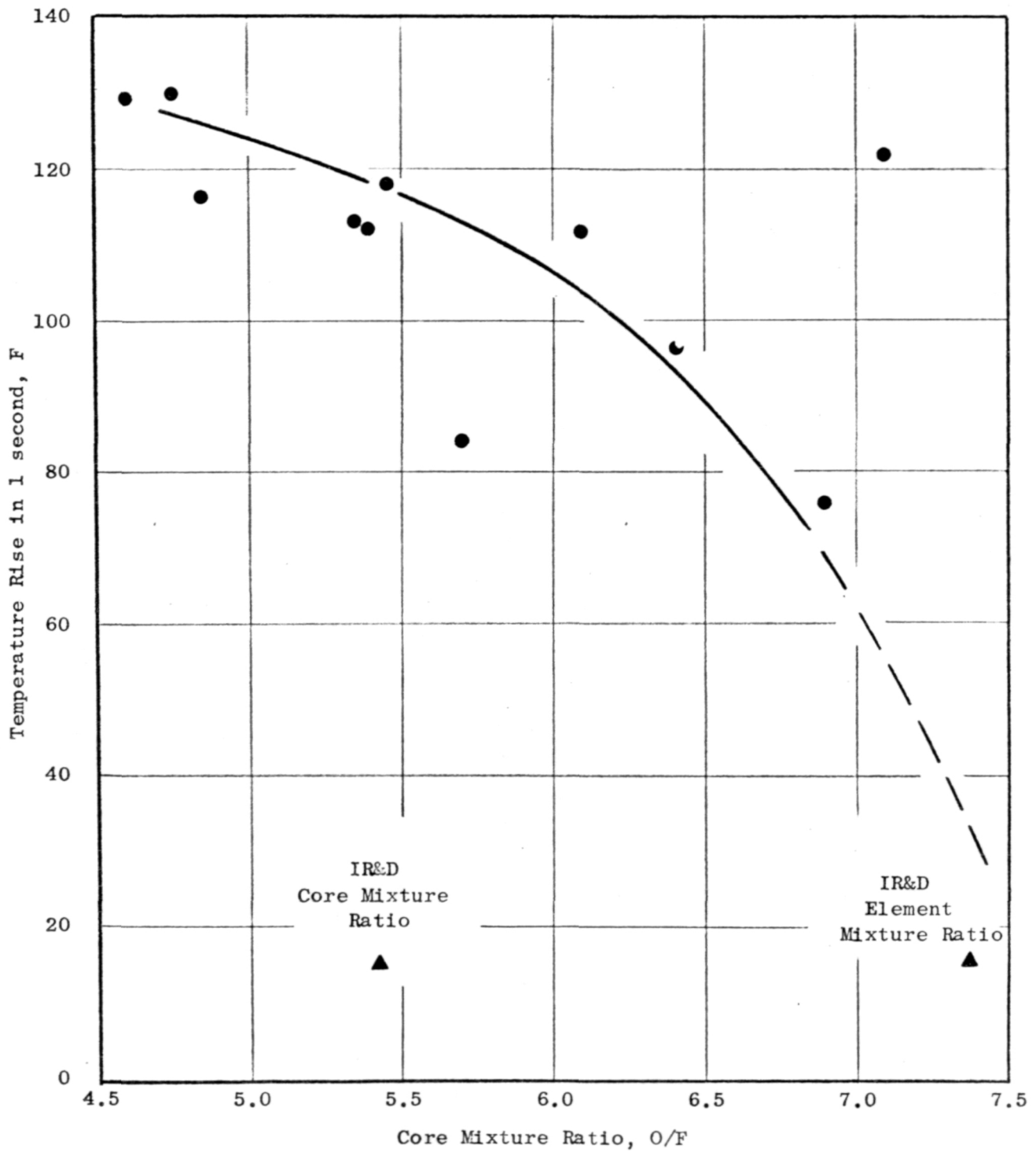


Figure 51. Injector Face Heating Correlation.

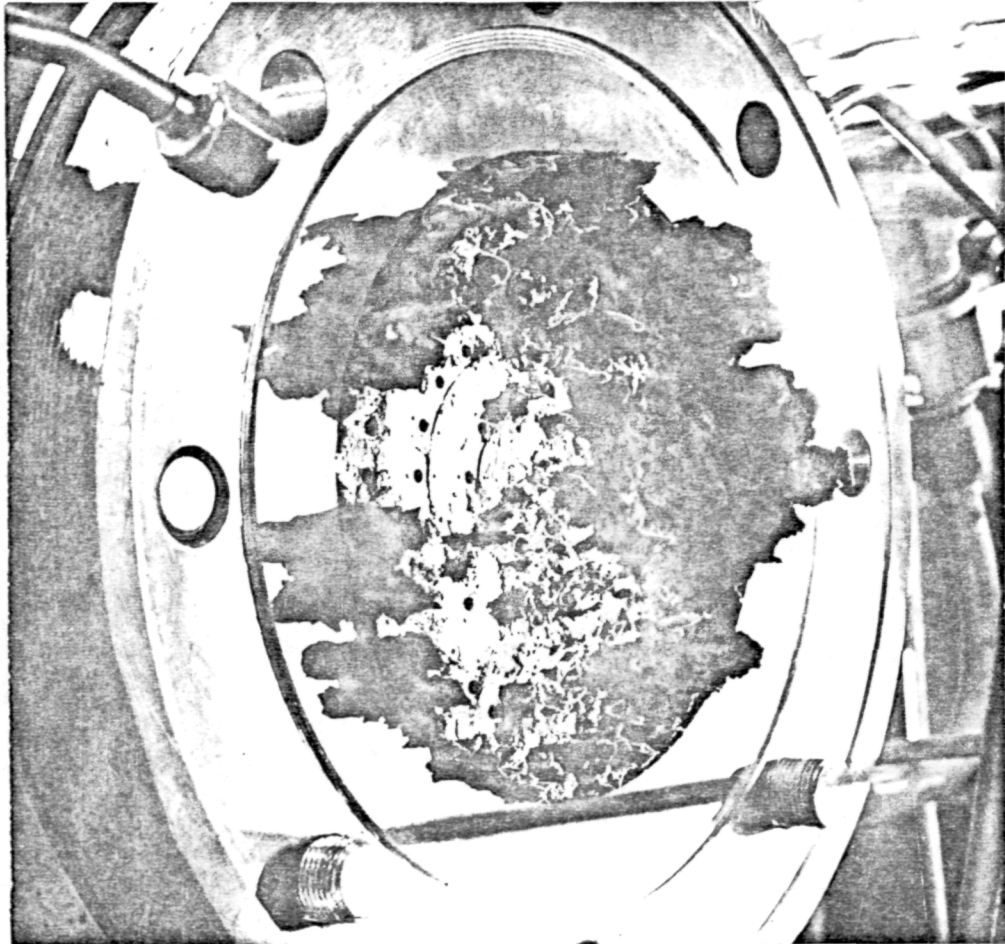


Figure 52. Injector Face Deposits After Tests 070 through 082.

At this point in the program the injector was cleaned, and using the 9.5 inch chamber, a test series was undertaken specifically to study deposition. A series of three 2-second tests was conducted, at differing mixture ratios. After each test the injector was inspected and brushed clean. Photography was not convenient because the injector was viewed through the throat.

Test 083. Nominal conditions were targeted, with a mixture ratio 2.8:1. The injector core face was clean as was most of the periphery, however, in the core area approximately 50 percent of the fuel orifices had begun to develop volcano shaped deposits. The volcanoes were about 0.020 to 0.030 inch high and about 0.005 inch thick. The injector periphery was mostly clean except at two locations 180 degrees apart where cylinders about 1.5 to 2.0 inches long had developed at several film coolant holes in line with two of the core fuel feeder passages. The injector was then brushed clean.

Test 084. This test reduced the mixture ratio to 2.5:1. The injector deposits after two seconds were dramatic with a heavy deposit loosely covering the entire injector face. There was the appearance of considerable turbulence and the film coolant holes in line with the same main fuel feeders were surrounded by long cylindrical growths. The face was brushed clean subsequently.

Test 085. This test was conducted at an overall mixture ratio of 3.0:1. At the end of two seconds the core was clean, with no volcanoes around the fuel holes. Cylinders around the film coolant discussed above were only about 0.5 inch long. There was a very light flaky scale in the vicinity of the outer ring. The injector face was brushed and a series of high pressure purges was conducted.

Tests 086-094. A full test matrix was conducted deliberately avoiding low mixture ratios until Test 093 which was at mixture ratio of 2.5. The hardware was disassembled and photographed after two days of exposure to air. The deposits showing in Fig. 53 were worse than the appearance immediately after the tests.

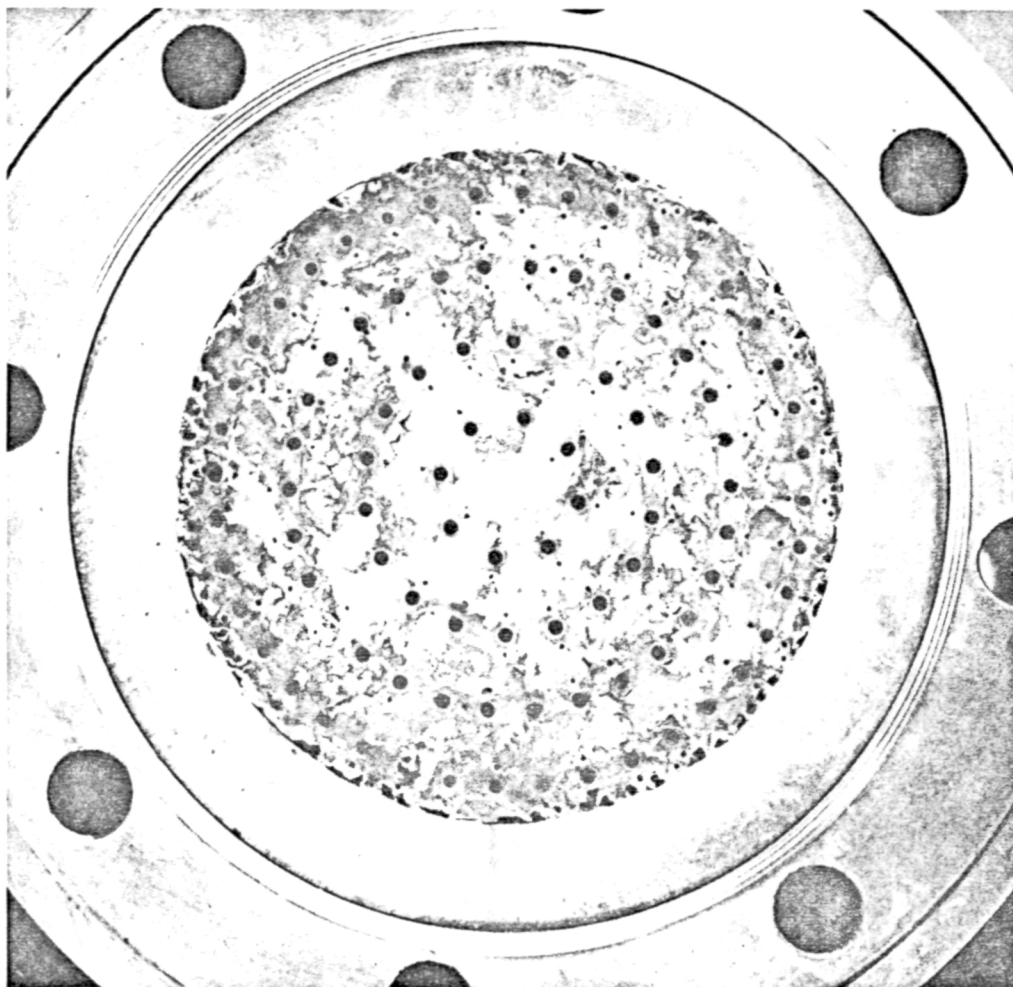


Figure 53. Injector Face Deposits After Tests 086 through 094.

It was clearly established that deposition for this triplet injector was very sensitive to mixture ratio. A potential explanation is the variation with mixture ratio and the chemical composition of the combustion products. It is reasonable that high mixture ratios would be less prone to deposition, containing less boron. Another similar injector tested in a Rocketdyne sponsored program with FLOX/ B_2H_6 did not produce deposits, even at low mixture ratios. The difference appeared to be based on the turbulence level of the flow in the immediate vicinity of the injector face. The Rocketdyne injector had twice the oxidizer pressure drop as this one but the same fuel pressure drop with both low deposition and heat flux conditions.

Acoustic Cavity Conditions

Acoustic cavities were used in this injector primarily to study the influence of the cavity on injector design and function. Design studies leading to selection of the cavity geometry are described in Ref. 3. Significant experimental results relate to the effect of the cavity on the film coolant, gas temperature inside the cavity, and cavity deposits. Since no high speed pressure instrumentation was used during Task II, only indirect evidence regarding stability is available.

Evidence of cavity deposits was available from the occasions on which the injector was disassembled. After the 12-inch and 9.5-inch chamber test series, the cavities were nearly filled with deposit. The deposit had a different form than was present any place else in the chamber, being a densely packed powder.

The unstructured deposit which occurred was theorized to be formed in the chamber and recirculated into the cavity. A likely time for this to occur was on start by a pressure wave from ignition.

The triplet injector film coolant streams were injected directly across the openings of the cavity. Since no cavity with a gas film coolant flow had been fired with this orientation before, it was important to determine if the cavity

would interfere with the film. The excellent effectiveness of the film based on heat flux control indicated no adverse interference. Moreover, as seen in Fig. 54, the film coolant streams seem to jump the cavity opening, attach to the wall and fan out.

An acoustic cavity temperature was determined by a tungsten-rhenium thermocouple located half way down the cavity depth. These data were useful both for determining the correct gas properties for use in cavity design and for studying cooling requirements of the cavity walls. In addition, monitoring of the temperature was instructive as to the formation of cavity deposits.

The temperature-time history of the cavity gas (Tests 083 and 084) shown in Fig. 55 indicates that the peak temperature reached was only 635 F. The cavity apparently receives an initial charge of hot gas during start with the gas fairly stagnant during the remainder of the test. This also gives credence to the possibility that the cavity deposits could be enhanced by repeated starts rather than entirely from mainstage operation. Cavity temperature as a function of test number is shown in Fig. 56. The deposit apparently accumulated gradually, with the tests at the end of the 12 inch combustion chamber test series showing virtually no response (the cavities were probably completely filled).



Figure 54. Cavity Cover Stains After Tests 083 through 094.

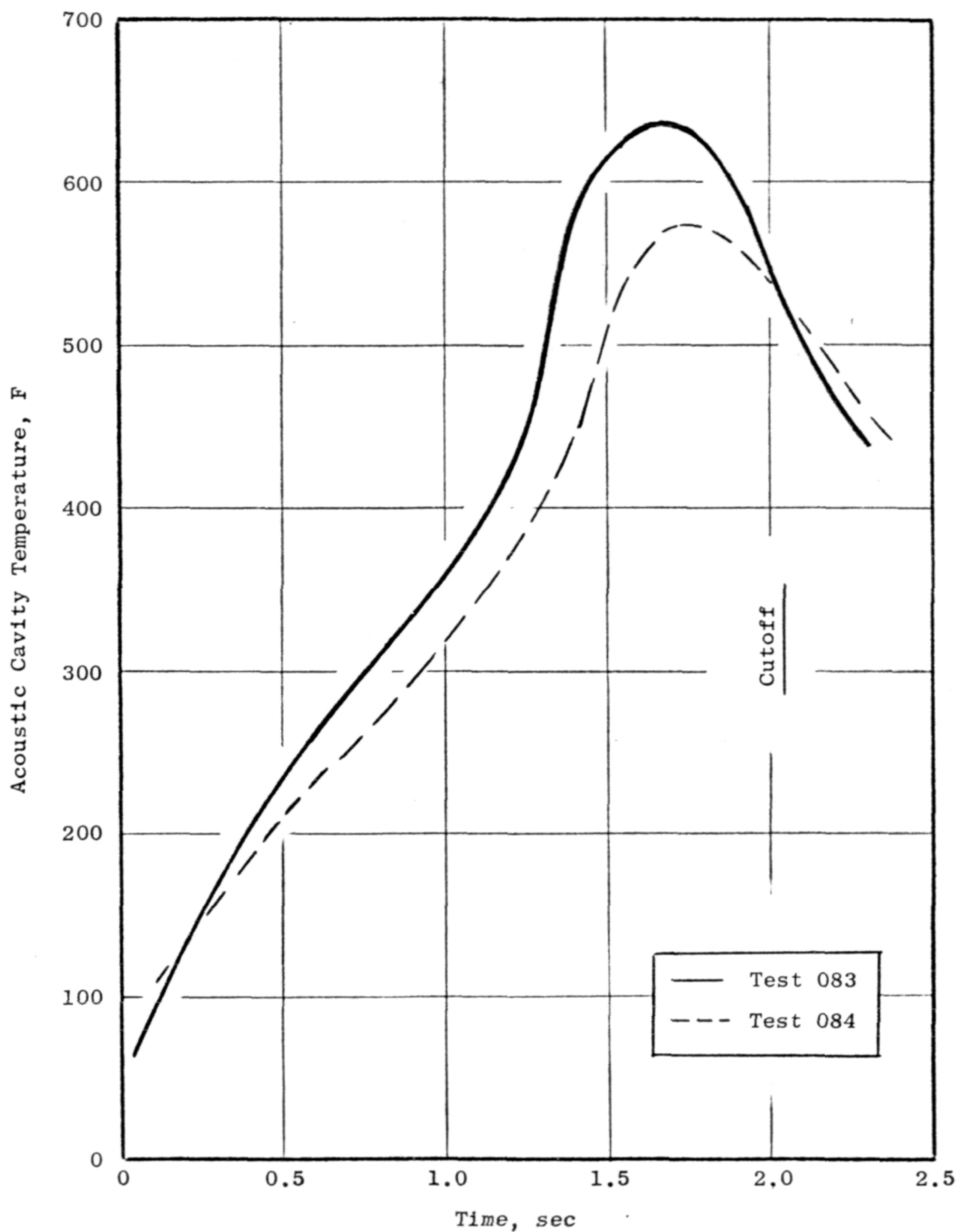


Figure 55. Acoustic Cavity Temperature History for Tests 083 and 084.

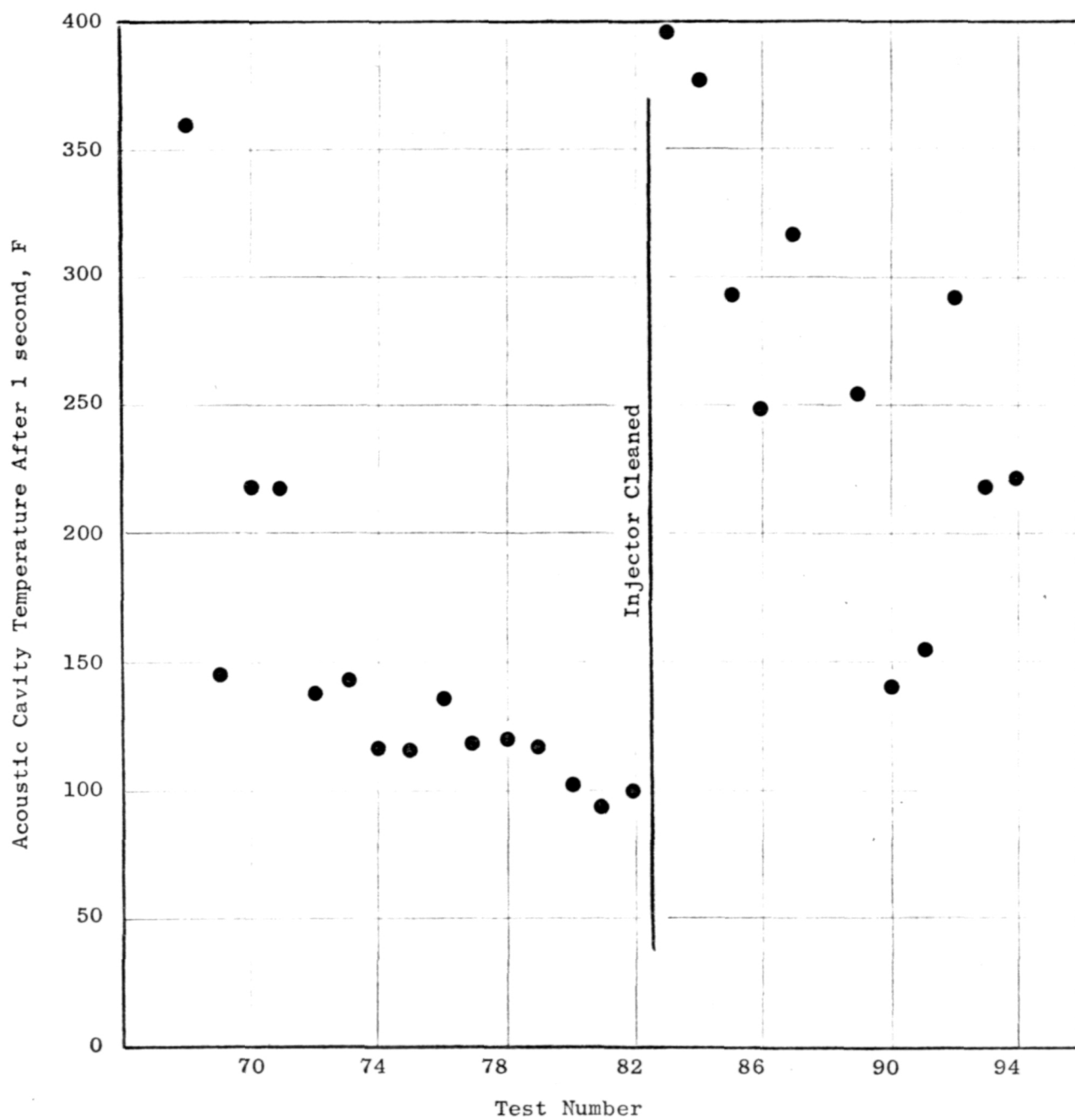


Figure 56. Test Number Dependence of Acoustic Cavity Temperature.

COOLANT HEAT TRANSFER TEST HARDWARE

The coolant heat transfer effort conducted during Task II study had the primary objective of determining the cooling capability of OF_2 and B_2H_6 , and secondary objectives of studying decomposition/deposition for B_2H_6 . The test hardware used was designed to provide a nearly constant wall temperature heat source for a coolant flowing in a small passage. Test variables were wall temperature, coolant mass velocity, coolant pressure, coolant bulk temperature, and passage diameter. The B_2H_6 flow schematic shown in Fig. 57 shows a series of heated metal blocks with coolant passage sizes and lengths representative of conditions anticipated for the engine.

B_2H_6 Block Hardware Design

The unit consisted of a series of three masses with internal passages for B_2H_6 flow. Electric heaters were used to heat the blocks to preselected temperatures and turned off. The insulated masses were large enough to be considered nearly constant temperature heat sources but small enough to produce a measurable temperature decay in 30-60 seconds. Heat transfer data were determined from both coolant temperature rise and block temperature decay.

The three blocks in series were designed to produce data on three aspects of diborane cooling. The first block is designed for liquid, boiling, and two-phase data, the second for gas forced convection, and the third for curvature effects. On most tests, all three types of data were obtained simultaneously. Flowrate was measured both upstream with a cavitating venturi and downstream with gas sonic venturis and controlled by regulating the pressure upstream of the cavitating venturi. Pressure was controlled by valving of the three parallel gas venturis. Detailed designs of these units are shown in Fig. 58, 59, and 60.

The unit shown in Fig. 60 was designed to measure the curvature effect on gas forced convection heat transfer for diborane. It consists of a curved stainless steel tube brazed to two steel fins, one on the inside and one on

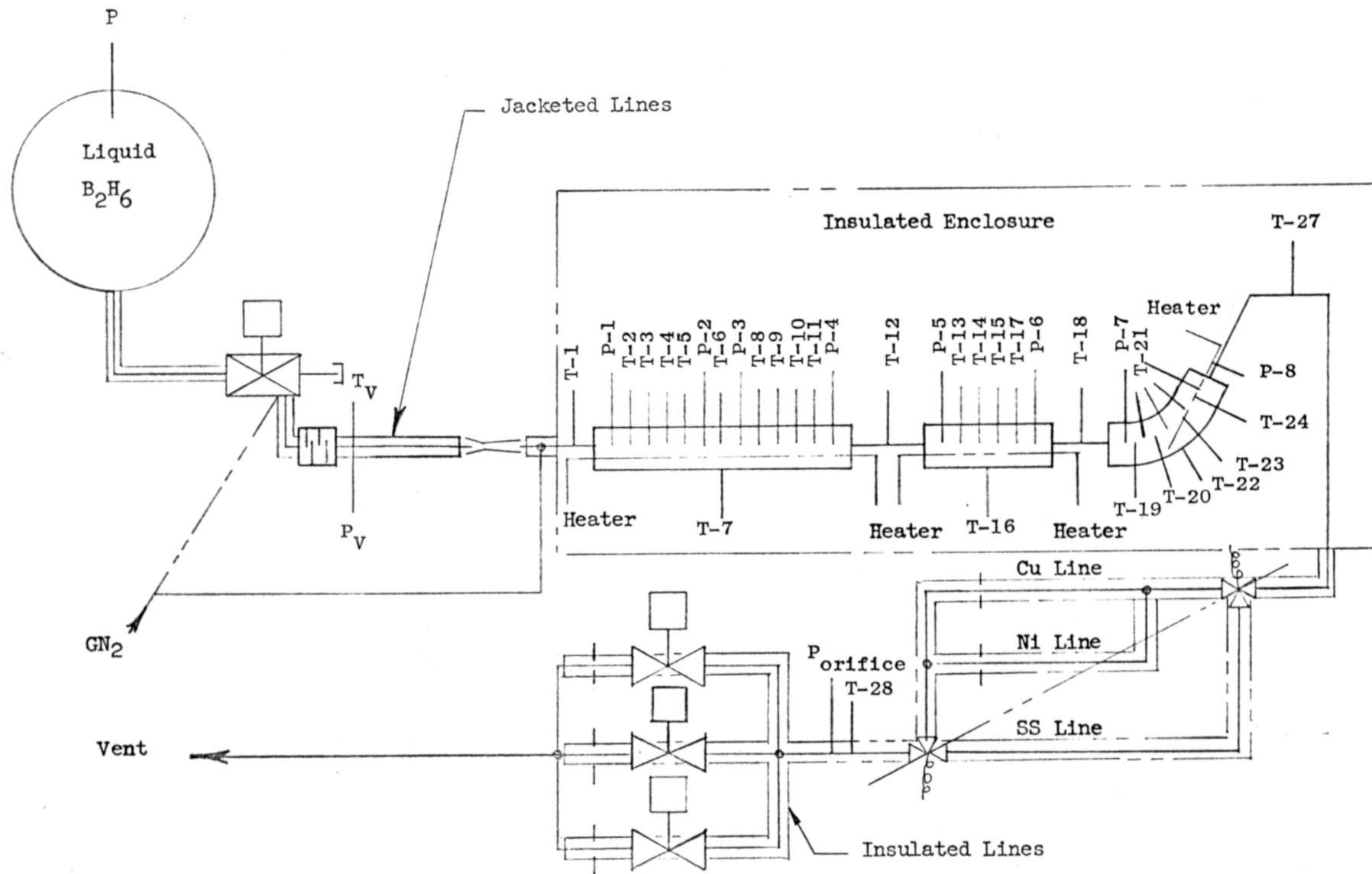


Figure 57. Diborane Heat Transfer Flow Schematic

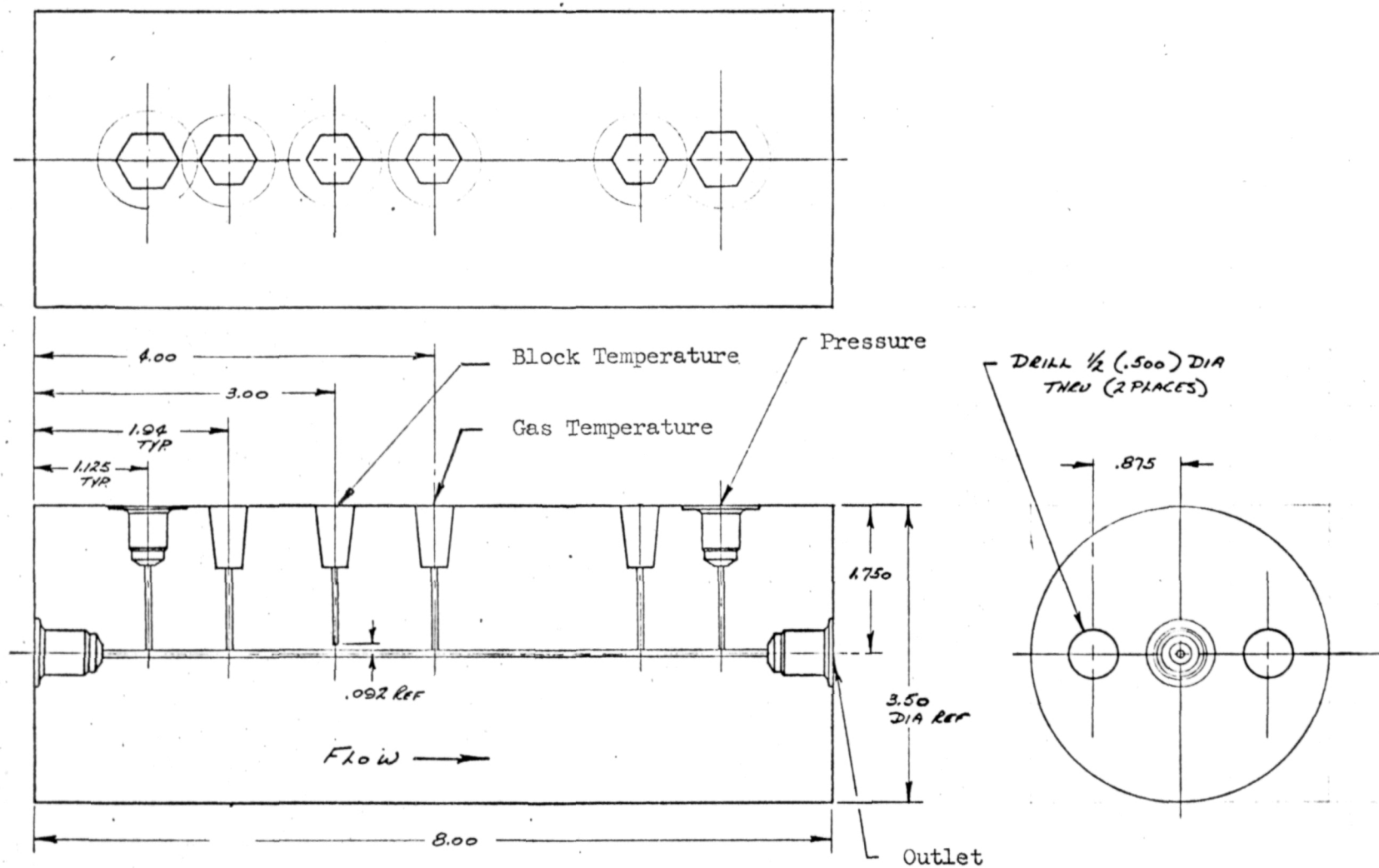


Figure 59. Diborane Heat Transfer Gas Block



Figure 60. Diborane Heat Transfer Curvature Block

the outside of the curve. The steel part containing the fins was then brazed to a copper mass which contains the heaters. Once the two nearly isolated fins are heated and diborane is flowing through the tube, the outer fin will decay in temperature faster than the inner fin. The difference is a measure of the curvature effect. The usefulness of the method was confirmed by a three-dimensional heat transfer analysis.

As a very simple additional experiment, the heated diborane was allowed to flow through two identical lines and orifice plates made of copper and nickel, the two candidate thrust chamber and injector materials. Orifice sizes and pressure drops simulate the injector design. The experiment consisted of observing the pressure drop across these devices. A photograph of the completed hardware is shown in Fig. 61. .

OF₂ Block Hardware Design

The apparatus for the OF₂ was less complex, as shown in Fig. 62 . The system is similar in concept to the B₂H₆ system described above. Block details are shown in Fig. 63 and 64 and a photograph of the completed parts is shown in Fig. 65. .

OF₂ AND B₂H₆ HARDWARE INSTALLATION AND TEST PROCEDURES

The test hardware set up at the Reno facility consisted of heated copper blocks as constant temperature heat sources with enclosed coolant passages. The blocks, as installed in the test facility are shown in Fig. 66 and 67..

The installation of the OF₂ heat transfer apparatus without insulation is shown in Fig. 66. "Vermiculite" was loosely packed around the blocks for insulation with excellent results. The direction of flow was first through the rectangular block located in the metal container, then through the circular block supported inside the helical spring. Two flow measurement systems were built into the OF₂ test apparatus, a cavitating venturi upstream and a sonic venturi downstream. The cavitating venturi was considered the primary

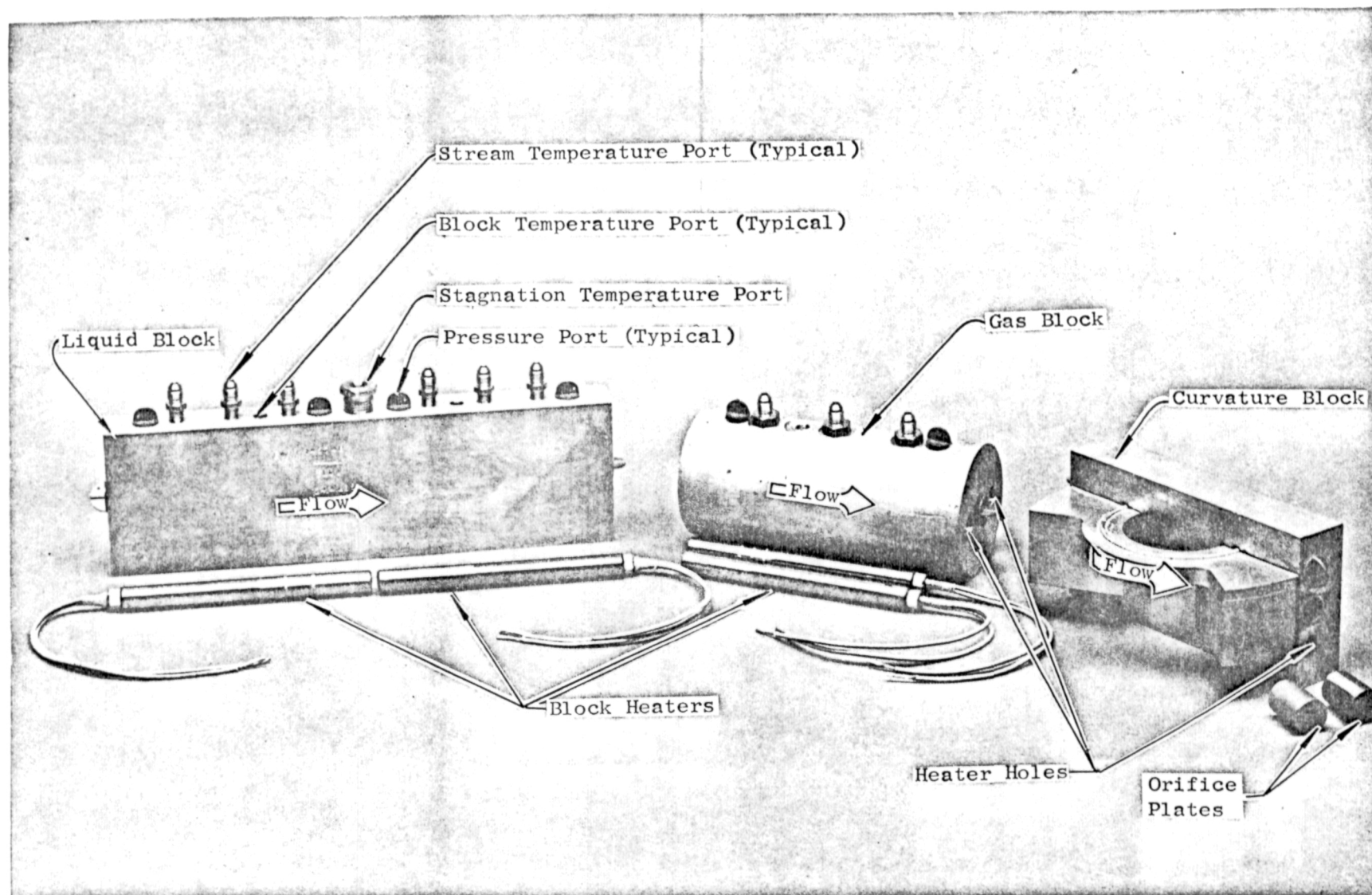


Figure 61. Photograph of Diborane Heat Transfer Test Hardware

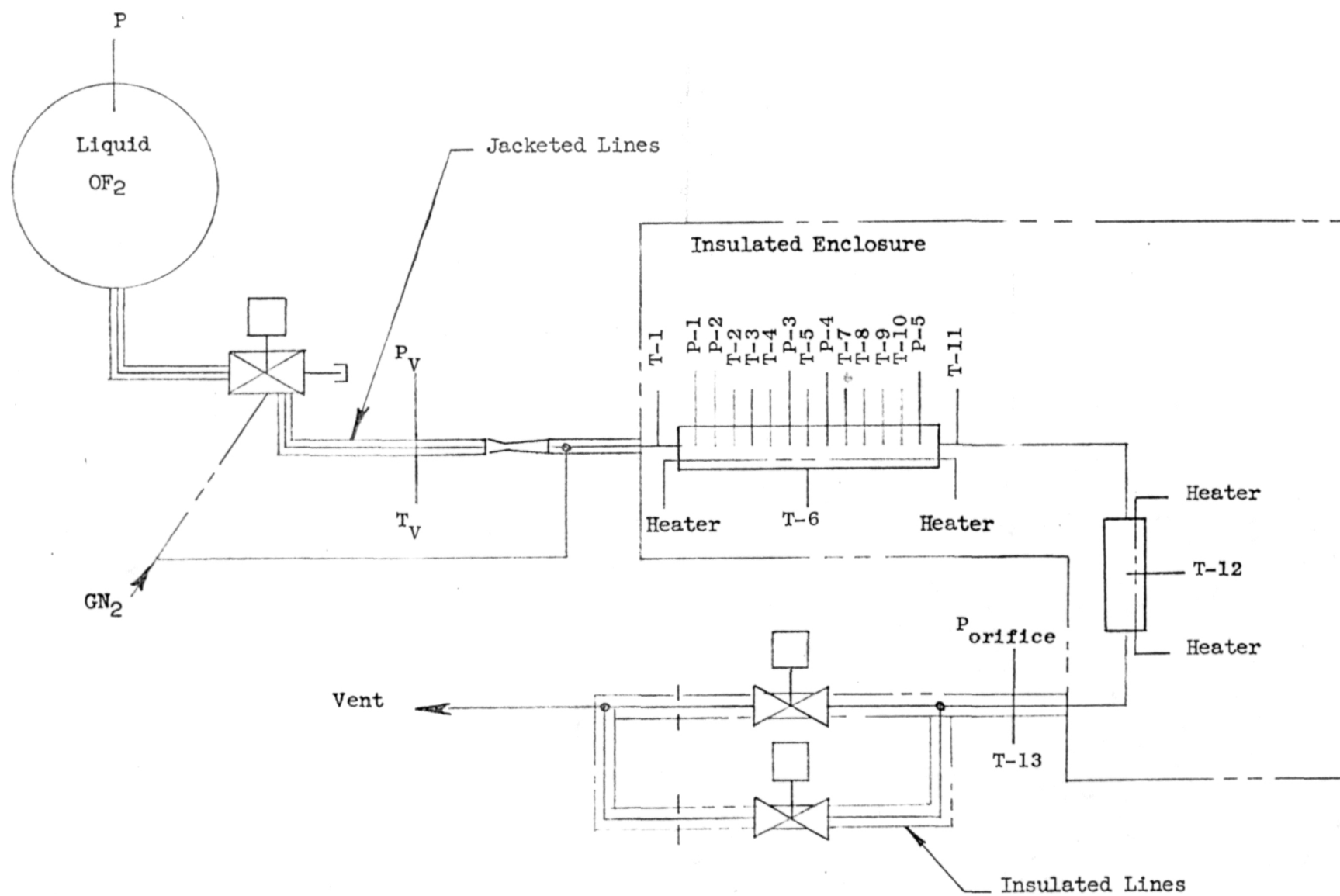


Figure 62. Oxygen Difluoride Heat Transfer Flow Schematic

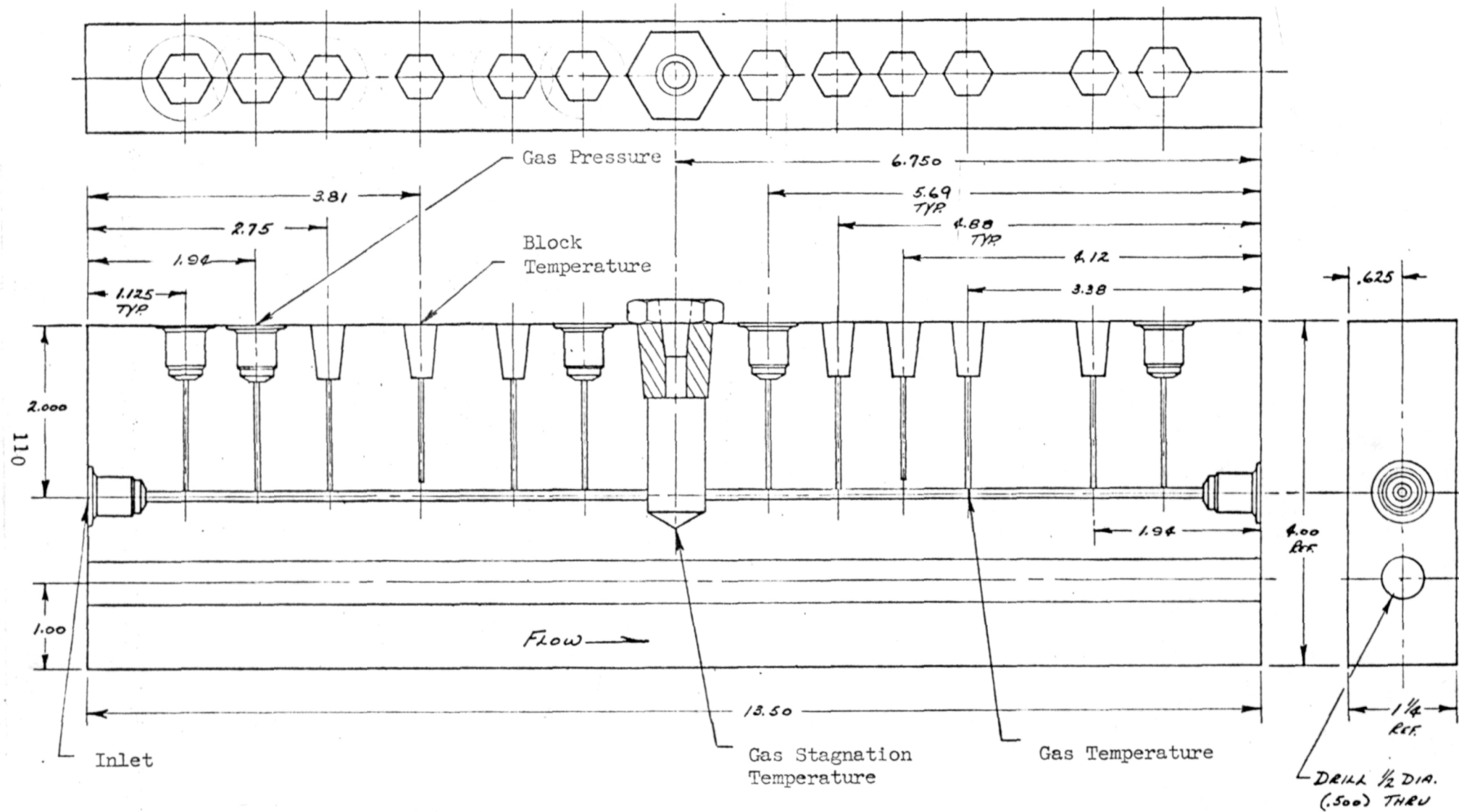


Figure 63. Oxygen Difluoride Heat Transfer Liquid Block

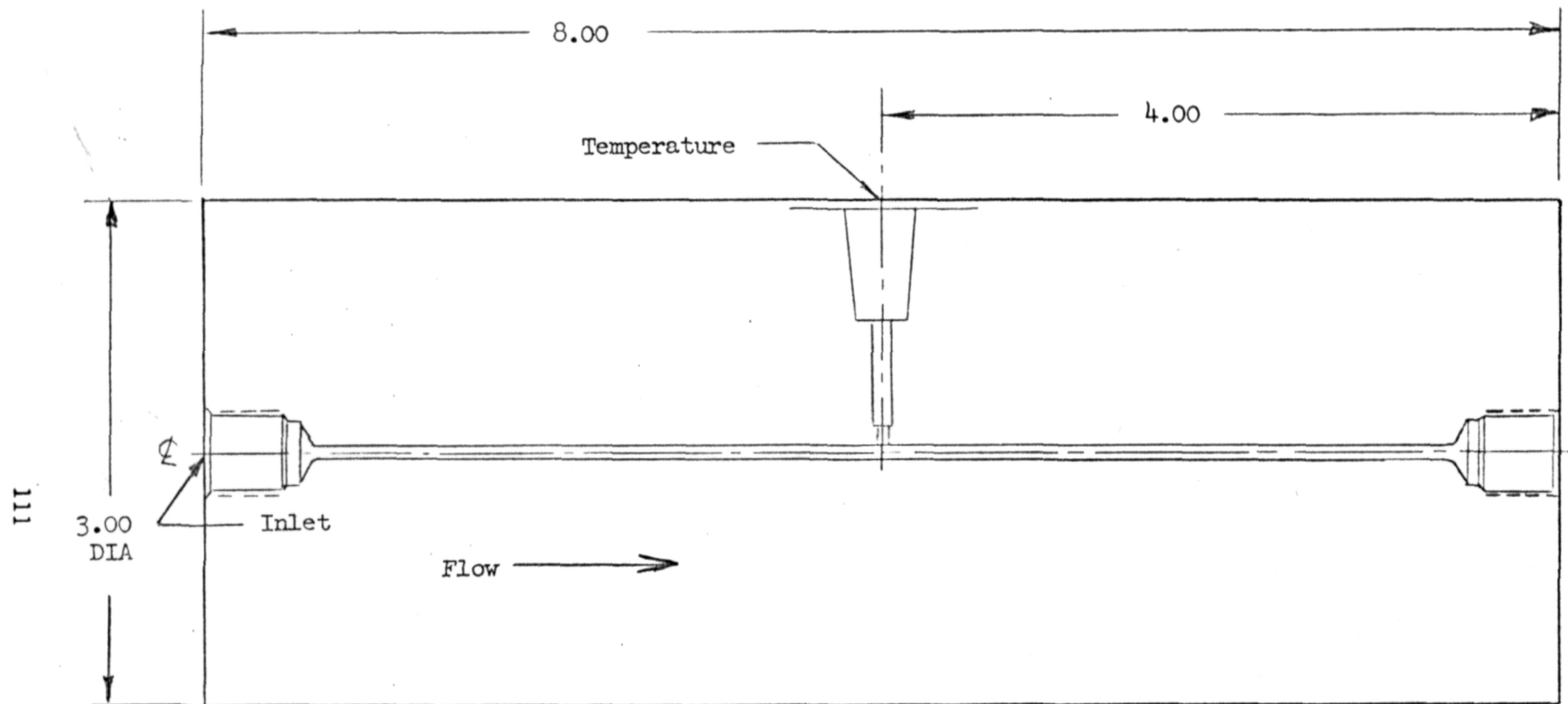


Figure 64. Oxygen Difluoride Heat Transfer Gas Block

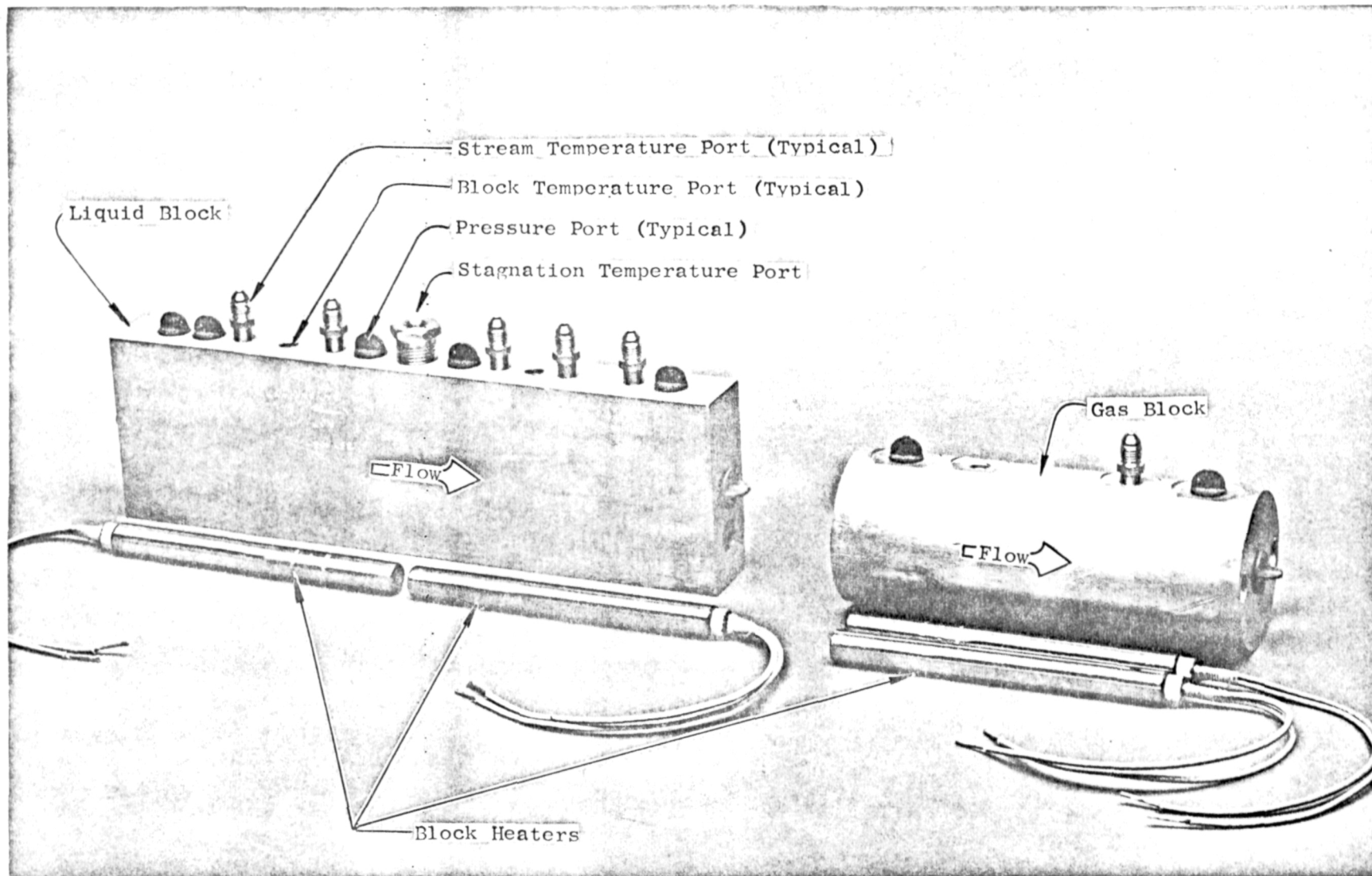


Figure 65. Photograph of Oxygen Difluoride Heat Transfer Test Hardware

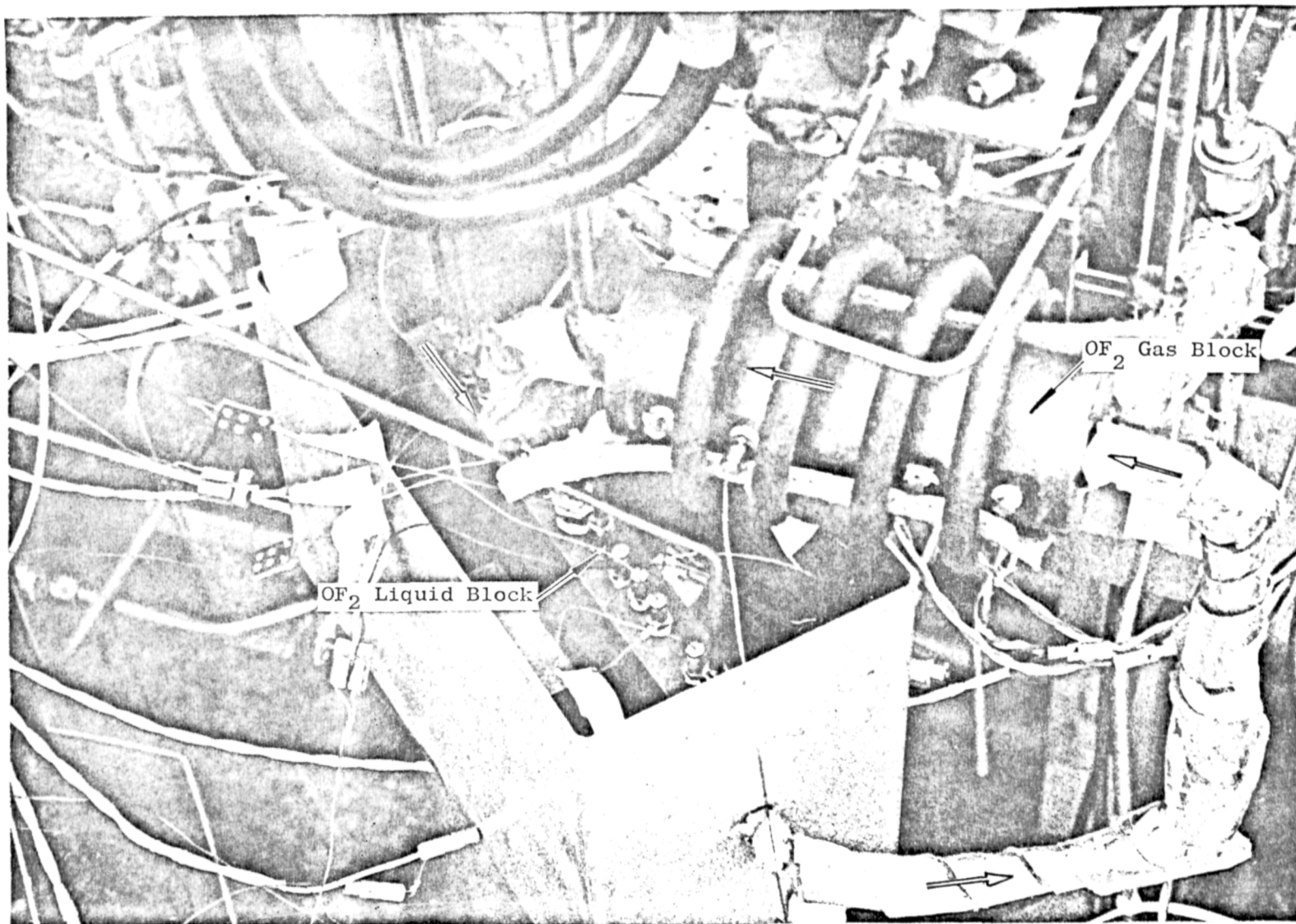


Figure 66. Oxygen Difluoride Heat Transfer Test Setup Before Insulation

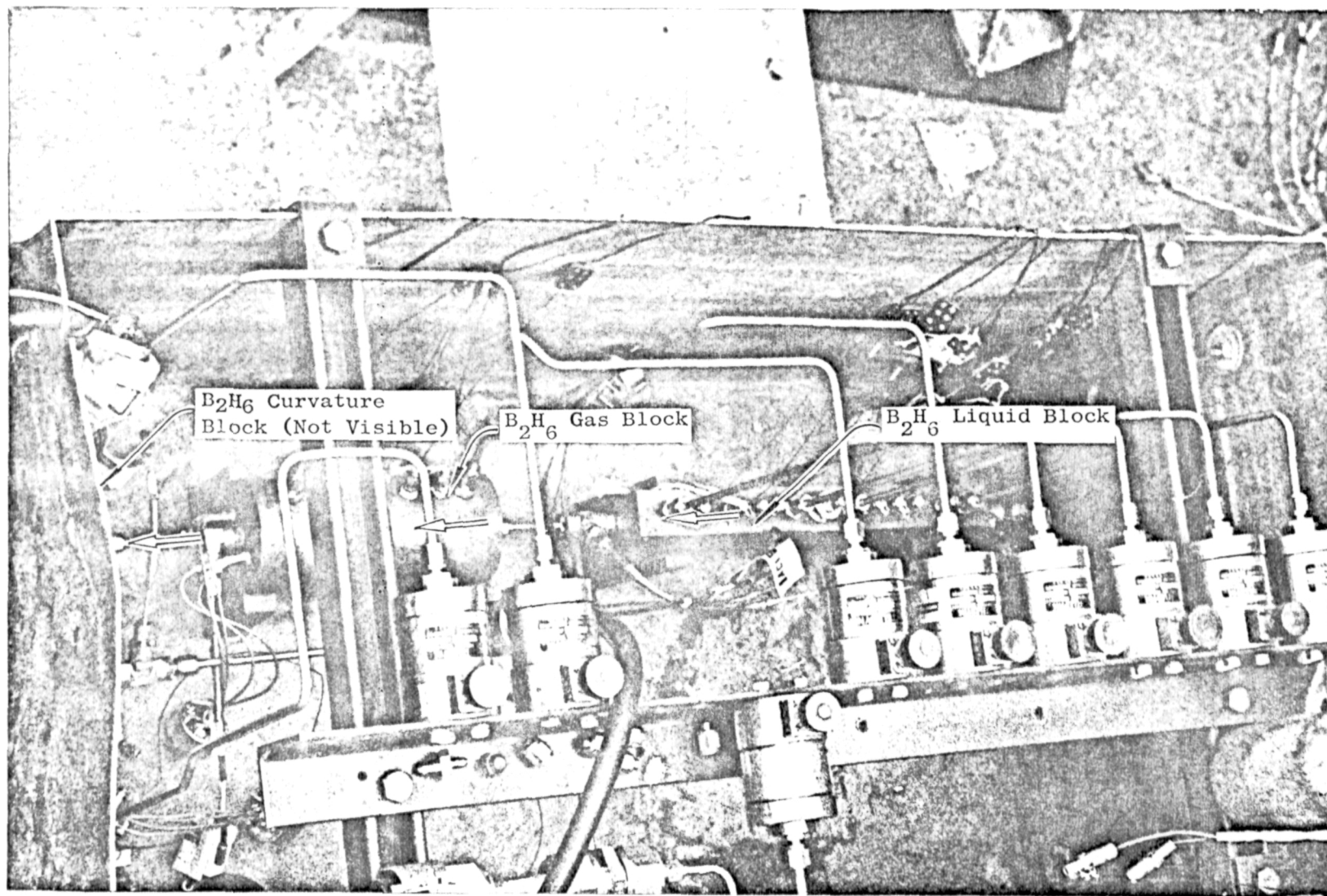


Figure 67. Diborane Heat Transfer Test Setup Before Insulation

system but difficulties encountered during the test program invalidated the liquid measurement. The sonic orifice results were used in the data reduction. As a result tests in which the OF_2 was two-phase at the throat of the downstream sonic venturi were in error.

The diborane heat transfer apparatus shown used insulation the same as the OF_2 tests. The diborane flowed in series through the liquid block (rectangular), the gas block (cylindrical), and finally the curvature block.

In the test series zero flow tests were used to calibrate the apparatus for heat loss to the environment and consist of monitoring block temperatures with the heaters off and no coolant flow. Heat leakage was found to be negligible over the range of block temperatures studied. Helium tests were also conducted to calibrate the system for known He heat transfer coefficients. The propellant tests covered a range of mass velocities, pressures, and block temperatures. Because the block temperature decays with time into each test, the longer tests produced a range of wall temperatures. In addition, during some long tests mass velocity and pressure were varied.

B_2H_6 COOLANT HEAT TRANSFER TEST RESULTS

The experimental coolant heat transfer program outlined was conducted at the Reno test facility. Test conditions were selected to cover the range of wall temperatures, bulk temperatures and mass velocities anticipated in the regeneratively cooled engine. The test range covered for diborane is depicted in Table 7 with a final test (Test 066) covering extreme temperatures for a duration of 1000 seconds without deterioration of flow properties or heat transfer. Total diborane operation time was 2700 seconds with no cleaning of the coolant passages. Hardware installation photographs were shown in the previous section.

The B_2H_6 investigation conducted covered a range of coolant pressures from 100 to 400 psia, coolant temperatures of -200 to +400 F, wall temperatures from 10 to 700 F and coolant mass velocities from 0.9 to 3.0 $\text{lb/in}^2\text{-sec}$ (Fig. 68).

TABLE 7 . B_2H_6 HEATED BLOCK TESTING SUMMARY

Test	Test Type	Fluid	T _{initial} B1/B2	P _{tank} (psig)	Vent Orifice	Cu-Ni	Time (sec)
036	No flow	--	100	--	.0105		60
037		GN ₂	100	250		2	30
038		GN ₂	100	250		1	40
039	No flow	--	200				60
040		GN ₂	200	250		1	40
041	No flow	--	300				60
042		GN ₂	300	250		1	40
043	No flow	--	400				60
044A		GN ₂	400	250		1	40
044B						2	20
045A		GN ₂	400	250		2	30
045B						Sample	10
046	No flow	--	500				60
047		GN ₂	500	250		1	40
048		B ₂ H ₆	230/440	240		1 & 2	No flow
049		B ₂ H ₆	230/440	240		Varied	90+
050		B ₂ H ₆	100/400	Varied		Varied	160+
051		B ₂ H ₆	200/300	Varied			168+
052		B ₂ H ₆	300/250	300-500		2	80+
053		GN ₂	350/450	250		2	10
054		B ₂ H ₆	350/500	300-600		2	
055		GN ₂	350/500	250		2	10
056		B ₂ H ₆	380/600	1400		All	45
057		GN ₂	380/600	250		All	20
058		B ₂ H ₆	270/540	400		1 & 1.5	49
059		GN ₂	180/500	250		2	20

TABLE 7. (Concluded)

Test	Test Type	Fluid	T _{initial} B1/B2	P _{tank} (psig)	Vent Orifice	Cu-Ni	Time (sec)
060		B ₂ H ₆	320/520	1400	.009	2	160
061		B ₂ H ₆	160/460	500		1	200
062		B ₂ H ₆	500/500	1400		1 & 1-1/2	200
063		GN ₂	330/450	250		2	45
064		B ₂ H ₆	500/600	1400		1 & 1-1/2	170
065		GN ₂	340/550	250		2	30
066		B ₂ H ₆	570/700	1400		1 & 2	
067		GN ₂	140/480	750		All	1000

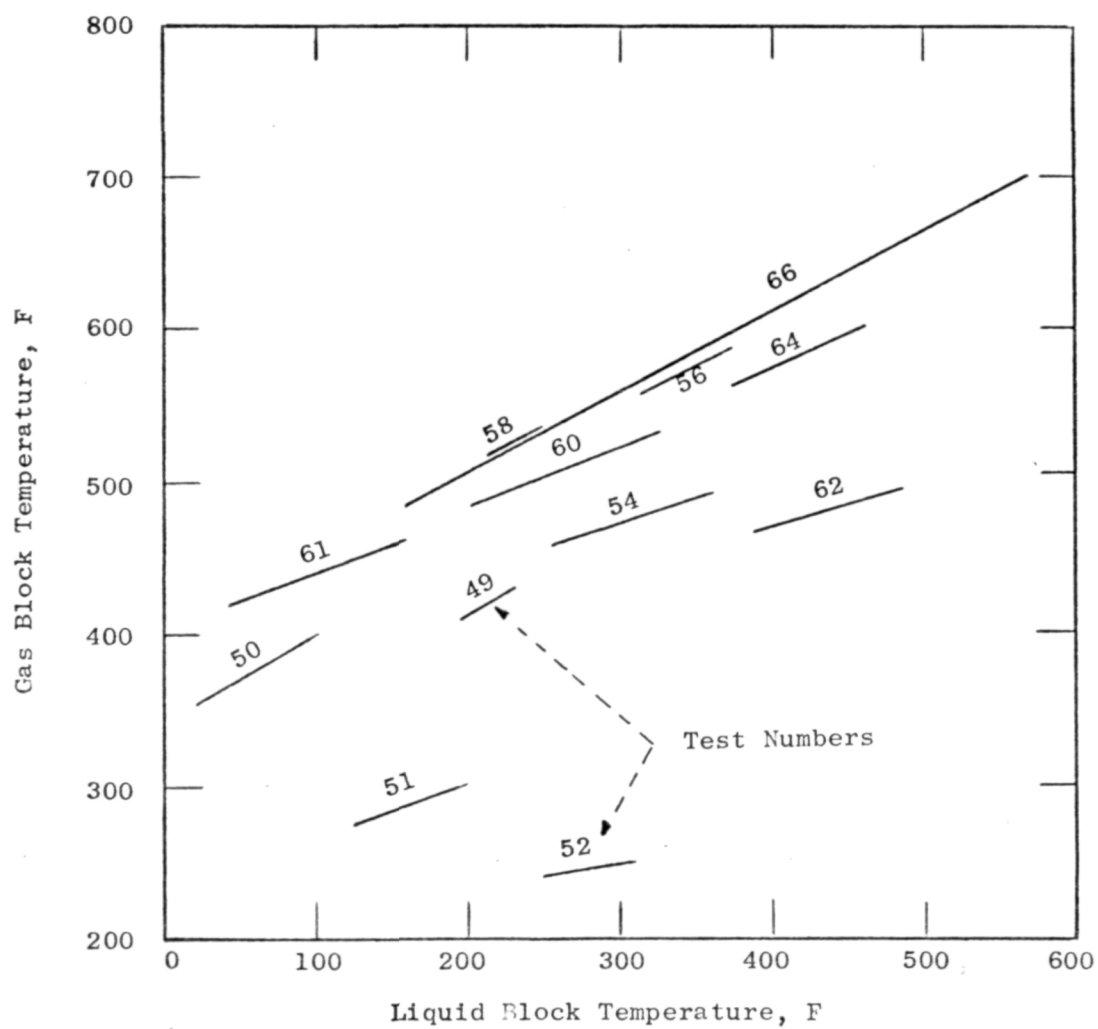


Figure 68. Diborane Coolant Property Test Range.

Although the complete test series imposed extreme diborane bulk and wall temperature conditions on the test apparatus, no apparent heat transfer problems were noted. Heat transfer rates were determined from measurements using thermocouples imbedded in the copper block and thermocouples directly exposed to the diborane fluid. The gas forced convection data were found in excellent agreement with tests conducted earlier by Rocketdyne and confirmed an earlier decision to cool the throat with gaseous diborane. The Stanton numbers obtained for the anticipated range of engine diborane mass velocities showed that gas-side heat fluxes of 5 Btu/in²-sec could be absorbed maintaining low wall temperatures compatible with diborane. The fin effect for a channel design makes it possible for diborane to absorb relatively high gas-side heat fluxes by heat distribution around the coolant passages.

Gas Forced Convection Results

The gaseous diborane forced-convection heat transfer data obtained are shown in Fig. 69 in terms of Stanton number. The Stanton number reflects average heat transfer occurring over a length of coolant passage where the flow is exposed to a uniform wall temperature. In the analytical model used in the data reduction, it was assumed that the wall temperature was constant, (low copper thermal resistance), and the heat transfer coefficient was uniform. The assumption of constant wall temperature was valid since the test time slices were chosen to minimize temperature variations. (The validity of the uniform heat transfer coefficient assumption was substantiated upon data reduction.) The final derived form for average Stanton number is as shown,

$$N_{ST} = \frac{D}{4L} \ln \left(\frac{T_{wc} - T_{B_{in}}}{T_{wc} - T_{B_{out}}} \right)$$

where

- D = diameter (in.)
- L = length (in.)
- T_{wc} = wall temperature (F)
- T_{B_{in}} = inlet bulk temperature (F)
- T_{B_{out}} = outlet bulk temperature (F)

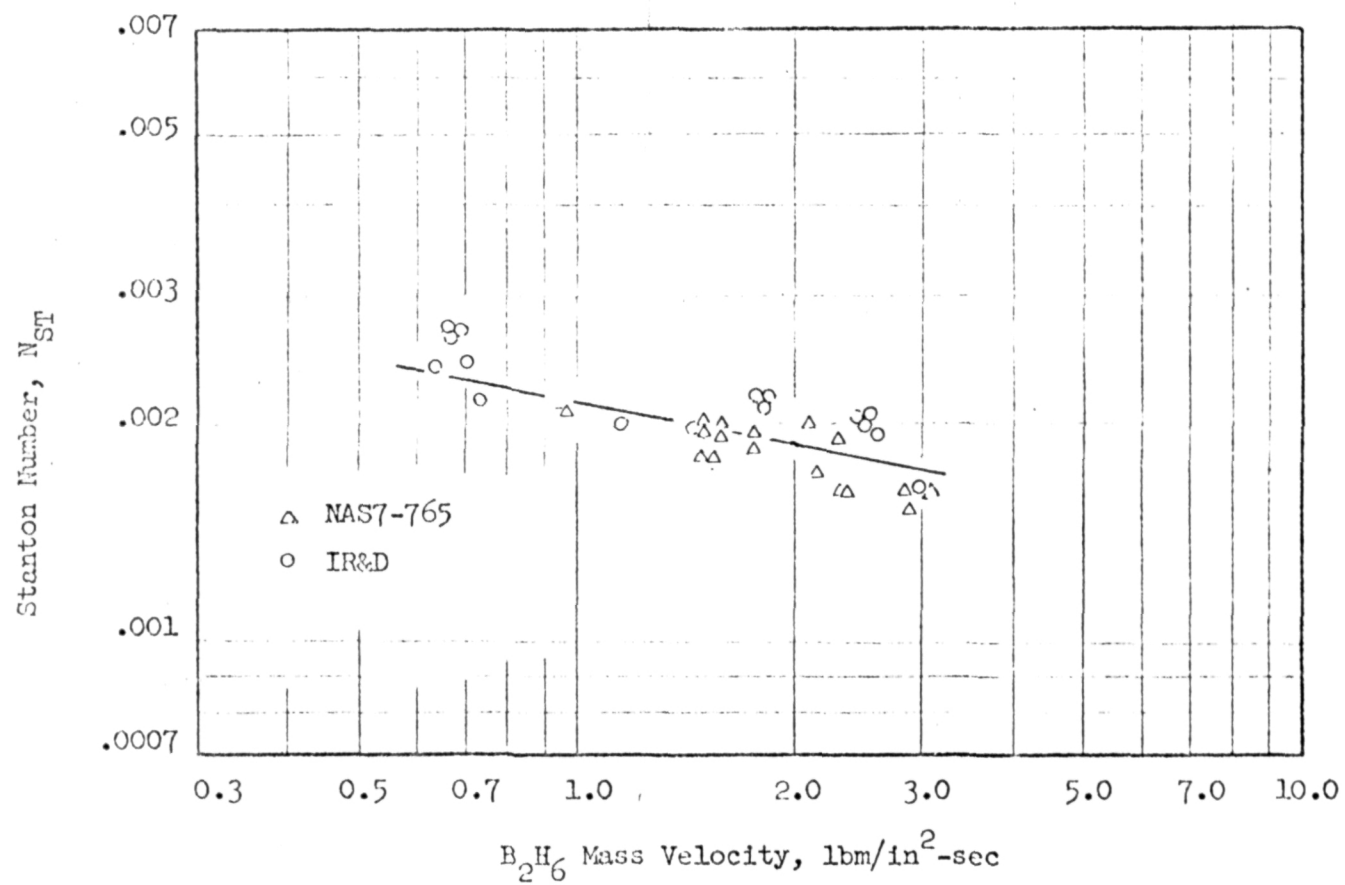


Figure 69. Gaseous Diborane Heat Transfer Data Correlation

Figure 69 shows the Stanton number plotted as a function of mass velocity. The sensitivity of Stanton number to mass velocities follows a normal 0.2 slope for turbulent flow. The level of Stanton number is also in agreement with similar data obtained under a Rocketdyne IR&D heat transfer program. Further detailed review of the data shows, over the range tested, no apparent wall temperature, wall-to-bulk temperature ratio, or coolant pressure effects. The data show only + 10 percent variation over a wall temperature range from 290 F to 580 F, bulk-to-wall temperature ratio between 0.62 to 0.84, and coolant pressure from 100 psia to 400 psia.

Liquid and Two-Phase Results

The liquid data obtained were in general agreement with diborane splash plate results documented in Ref. 6 and showed that the nozzle could be cooled with liquid diborane. The heat transfer data obtained for the anticipated range of engine wall temperature and mass velocity showed that if nucleate boiling occurred, low wall temperatures (~ 70 F) would result. Conversely with film boiling, wall temperatures of 400 F above saturation temperature could result. From the Task IV experimental data, it was observed that the wall temperatures reflected the higher wall temperature levels indicative of film boiling. Higher B_2H_6 liquid and two-phase mass velocity levels can be used in modified hardware to counteract this effect.

Figure 70 illustrates the average heat flux plotted as a function of the difference between surface and saturation temperatures. The variable diborane pressure is reflected in the saturation temperature and the variable mass velocity effect is shown. The reduced heat flux data follow the usual boiling trends, undergoing a transition from nucleate to stable film boiling at relatively low wall temperatures. The average B_2H_6 flux capability increases as the wall temperature is increased for a given diborane pressure until a temperature difference of 100 F is attained. With small increases in wall temperature, the heat flux capability sharply diminishes and then gradually increases as the wall temperature is increased. In the film boiling regime, the mass velocity dependence is shown. There were insufficient data in the nucleate boiling regime to assess mass velocity effects.

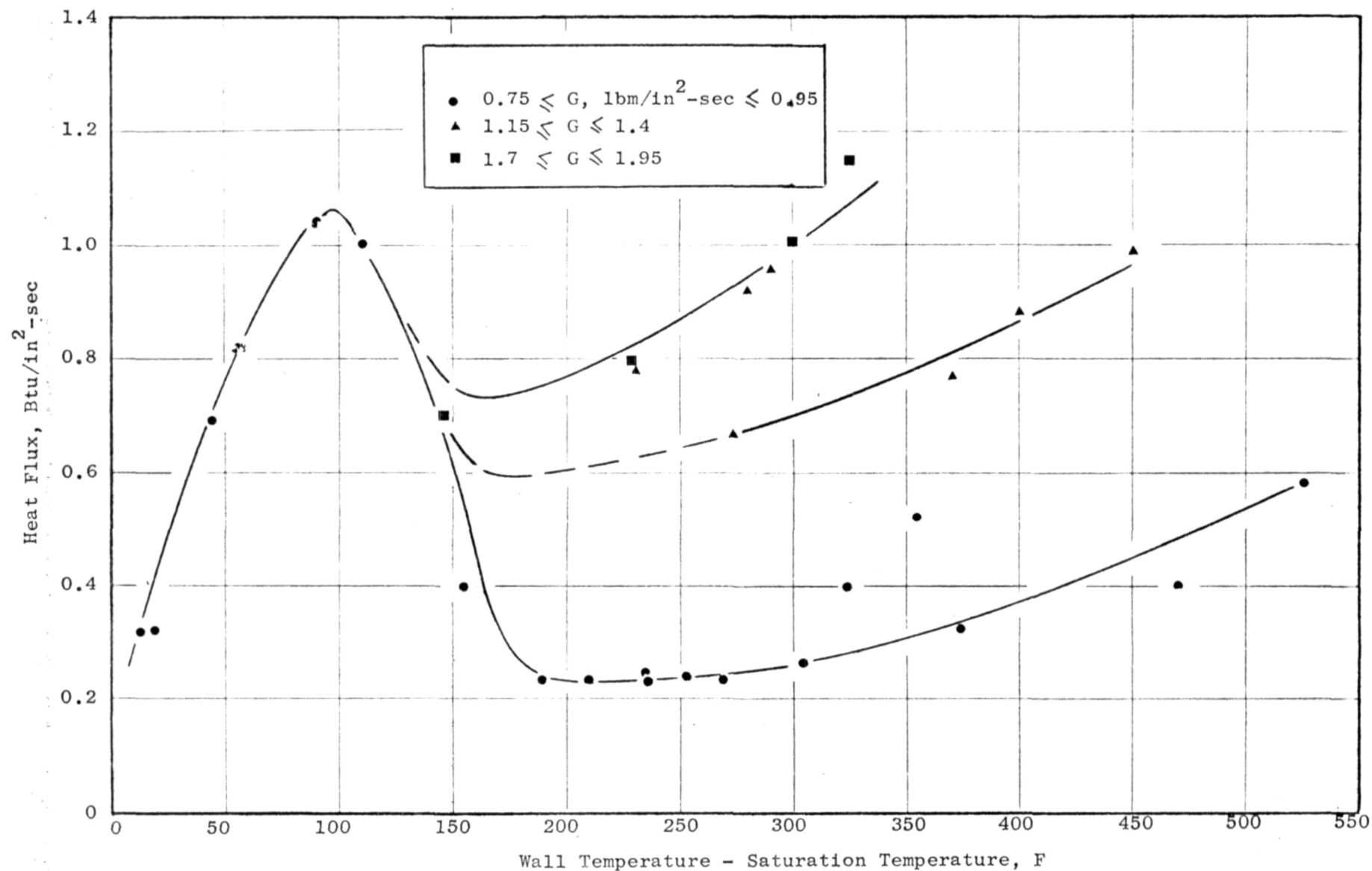


Figure 70. Experimental Boiling Data for Diborane.

For a given mass velocity condition, the distribution of local heat transfer versus liquid temperature and two-phase quality data indicated that the heat flux was at a minimum in the low quality (20-50 percent) two-phase region. At test values of mass velocity this level of heat flux appeared only slightly less (10 percent) than the heat transfer capability at corresponding liquid and higher quality conditions.

B₂H₆ Curvature Results

Evaluation of the B₂H₆ curvature block test data indicated that the specific thermocouple leads were not correctly specified. As a result the test data could not be translated to the locations along the curved section.

OF₂ COOLANT HEAT TRANSFER RESULTS

A series of 35 tests with liquid and gaseous OF₂ and reference gaseous He flow was conducted with the OF₂ heated block setup described previously. Within the 35 test series, multiple tests were conducted for 4 tests with variances in flow and inlet pressure provided.

The test series conducted is shown in Table 8. Initial tests 008-013 were conducted with He for a reference gas blowdown condition. Tests 014-016 were conducted at block temperatures of 260-300 F with tank pressures ranging from 260-300 psia. Tests 017 and 018 were helium check tests at up to 400 F block temperature. This was followed by multiple tests (020-021) with OF₂ at block temperatures of 425 F.

A high temperature block test (024) was conducted at 500 F with multiple flow conditions. Following this test a series of reduced block temperature (100-350 F) and flow conditions were conducted (025-035).

The results of the OF₂ tests in general indicated block cooldown times on the order of that predicted. Due to a venturi bypass bleed line which was inadvertently left open, the flow through the test section was changed to a higher value which could not be well defined.

TABLE 8 . SUMMARY OF OF₂ HEATED BLOCK TESTING

Test	Type	Fluid	T _{initial} (F)	P _{tank} (psia)	Orifice 1 Line Bleed	Orifice 2 Igniter Prevalve	Duration (sec)
008	No Flow	--	120	--	Closed	Open	50
009		He	120-85				
010	No Flow		220				60
011		He	220-160		Closed	Open	
012	No Flow		300				
013		He					
014		OF ₂	300	840		Open	60
015		OF ₂	280	370		Open	
016		OF ₂	290/260	200/140		Open	
017		He	295/265			Open	
018	No Flow	--	400				
019		He	395	115			
020	3 Tests	OF ₂	415	200			
021	3 Tests	OF ₂	425	400			
022	No Flow	--	500				
023		He	480		Open		
024	9 Tests	OF ₂	500	200			
025	Multiple	He					
026		OF ₂	350	200		Open	60
027		OF ₂	300	200		Open	30
028		OF ₂		200		Open	60
029		OF ₂		200		Closed	120
030		OF ₂	150	200		Open	60
031		OF ₂	130	200		Open	30
032		OF ₂	100	200		Open	50
033		He			Open	Open	
034	3 Tests	OF ₂	150	130/75		Open	360
035		OF ₂		500		Closed	66

Examination of the Brush records indicated stable flow conditions except for low weight flow conditions where a small pressure drop existed through the flow section. The boiling oscillations obtained during these tests appeared to reflect into flow and pressure oscillations within the test sections. Stabilization of low flow conditions could be accomplished by smaller flow areas or inlet orifice restriction.

Table 8 illustrates the OF_2 test summary performed for multiple test series 024 over a 100 second period. Block temperature decay from 520 F to 449 F was noted over the test run. Block inlet pressure was approximately 190 psia. Heat flux levels during the test conducted ranged from 0.25 to 0.43 Btu/in²-sec. Total coolant pressure drop varied during the test from 35-36 psi. Comparisons shown in Table 9 illustrate the heat flux conditions on the first test block (liquid to two-phase flow) to be somewhat greater than for the second block (two phase and gas flow). Although no flow quality measurements were made, it is expected that the second block was mostly in the two phase region.

In detail comparison of Reynolds number effects could not be made due to lack of accurate flow values. Flowrate for the test No. 24 shown is estimated at $\approx .048$ lb/sec.

TABLE 9. OF₂ COOLANT HEAT TRANSFER TEST 024 SUMMARY

Test No.	24-1	24-2	24-3	24-4	24-5	24-6	24-7	24-8	24-9	24-10
t (sec)	7.3	14.8	17.8	24.8	26.8	34.8	37.9	47.7	51.9	56.9
T3 (F)	520.3	516.1	514.5	510.4	509.1	502.8	500.0	491.3	487.3	482.1
T6 (F)	518.5	513.2	510.5	504.3	502.6	495.6	492.6	484.2	480.6	476.2
T8 (F)	518.1	506.8	503.4	496.3	493.9	483.9	481.7	474.0	469.6	464.1
\bar{Q} (Btu/sec)		2.05		1.84		2.15				2.17
*Q/A (Btu/ in ² -sec)		.52		.47		.54				.55
T12 (F)	517.2	514.6	513.7	511.6	510.5	506.9	505.9	502.6	500.7	498.4
\bar{Q} (Btu/sec)		.52		.45		.68				.67
**Q/A (Btu/ in ² -sec)		.29		.25		.38				.38
P1 (psia)	192.9	188.0	193.2	191.4	192.6	190.1	190.6	192.8	189.9	188.9
P2 (psia)	192.7	187.6	192.3	190.1	192.3	189.8	190.7	191.5	189.5	187.7
P3 (psia)	195.2	188.8	192.5	191.1	194.2	189.7	191.7	191.4	188.3	187.2
P4 (psia)	179.5	174.9	182.1	181.5	179.5	178.6	178.9	181.7	176.0	177.0
P5 (psia)	156.8	153.8	166.9	169.1	155.7	158.3	161.0	167.0	151.9	153.6

* First OF₂ test block** Second OF₂ test block

$$G_{\text{OF}_2} \approx 9.3 \text{ lb/in}^2\text{-sec}$$

$$\dot{W} \approx .048 \text{ lb/sec}$$

TABLE 9. (Concluded)

Test No.	24-11	24-12	24-13	24-14	24-15	24-16	24-17	24-18	24-19
t (sec)	60.6	66.9	69.9	75.3	77.8	85.2	87.9	97.8	109.5
T3 (F)	479.0	473.7	471.3	467.7	465.1	459.6	457.3	449.2	
T6 (F)	472.8	467.2	464.6	460.7	457.7	451.8	449.8	443.9	
T8 (F)	459.9	453.4	451.0	447.5	445.2	440.2	437.0	428.0	
\overline{Q} (Btu/sec)		2.05		1.51		1.63		1.74	
Q/A (Btu/ in ² -sec)		.52		.38		.41		.44	
T12 (F)	496.6	493.8	492.8	491.3	490.0	487.4	485.6	480.6	
\overline{Q} (Btu/sec)		.67		.42		.53		.77	
Q/A (Btu/ in ² -sec)		.38		.24		.30		.43	
P1 (psia)	190.1	193.0	192.5	191.8	191.4	192.4	192.0	193.6	
P2 (psia)	189.5	192.1	192.3	191.5	190.1	192.1	190.6	191.2	
P3 (psia)	188.9	192.0	193.0	193.5	189.6	194.3	189.3	191.9	
P4 (psia)	177.3	180.0	180.8	179.5	180.8	181.8	180.0	180.8	
P5 (psia)	155.1	157.5	164.5	161.7	168.1	169.7	159.0	157.9	

REGENERATIVE CHAMBER COOLANT CHANNEL GEOMETRY OPTIMIZATION

Based on the Task II heat flux and fluid cooling studies, a detailed optimization of the cooling passage was performed. Optimization of a double panel cooled thrust chamber is a complex procedure with propellant vaporization, balancing of heat loads between the two coolants, and minimizing chamber wall temperatures considered. The first location studied was the chamber throat, primarily because this is the region of maximum heat flux but also because it was relatively simple to predict the conditions of the coolants at the throat plane. The diborane was designed to be a gas slightly above its boiling point due to nozzle cooling. The oxygen difluoride will be a liquid because it enters the coolant jacket only slightly downstream of the throat. After the throat geometry was determined, the single panel nozzle, which vaporizes the diborane, and the double panel combustion chamber which also vaporizes the OF_2 , was designed.

At the throat design variables are number, width, and height of both sets of coolant channels. To avoid a simultaneous multi-parameter optimization with this complex analysis, a step-by-step approach was chosen which will produce a near-optimum design. First, ignoring the presence of the second cooling panel, the width and spacing of the diborane channels were studied. The optimization was based on wall temperature because of diborane decomposition.

It was clear for a fixed mass velocity, a larger number of narrow channels is preferred. This condition minimizes the ratio of gas-side area to total channel surface area and therefore the coolant-side effective heat flux is less, and the wall temperature decreases. Therefore, a preliminary selection for the diborane channel geometry was made at widths and lands of 0.040 inch, giving approximately 90-100 channels. The selected diborane channel width and land width and OF_2 geometry showed maximum surface temperature in contact with diborane as 530 F. It was clear that a good design with a large cooling margin could be achieved.

The basic design concept to be finalized was a primary diborane cooling circuit with a water cooling jacket to simulate the presence of a secondary OF_2 cooling panel behind the diborane. The milled channel design was chosen to allow control of heat flux paths and to take advantage of the cost and schedule benefits of the approach. Additional good developmental features were noted for future reference.

Finalized Coolant Channel Geometry and Heat Transfer Conditions

Studies of the coolant geometry involved several separate steps. The throat, nozzle, chamber, and water jacket all represent distinctly different cooling problems and are discussed in the following sections. Figure 71 and Table 10 summarize the final selections for the coolant channel geometry. Predicted diborane temperature as a function of position in the cooling jacket is shown in Fig. 72. For convenience, the relationship between axial position in the nozzle and area ratio is shown in Fig. 73.

Hot Gas Side Heat Transfer. All of the coolant geometry studies were based on the experimental hot gas side heat transfer results from the Task II calorimeter thrust chamber test program. The results were corrected to the nominal demonstration test conditions and are shown in Fig. 74. Cumulative heat load is shown in Fig. 75 with heat summed for the uppass cooling direction.

Throat Section. Since the throat is the critical heat transfer region, throat cooling studies were used to select the number of coolant channels as well as channel geometry. At the throat the design variables were number, width, and height of both sets of coolant channels. The optimization criterion was selected to be wall temperature because of diborane decomposition. Figure 76 shows maximum surface temperature in contact with diborane as a function of channel width and the ratio of land to width for a selected heat flux and mass velocity. The land/width ratio for a given width determines the chamber of channels. Channel height is a variable on this plot. It is clear that for a fixed mass velocity a larger number of narrow channels is preferred. This

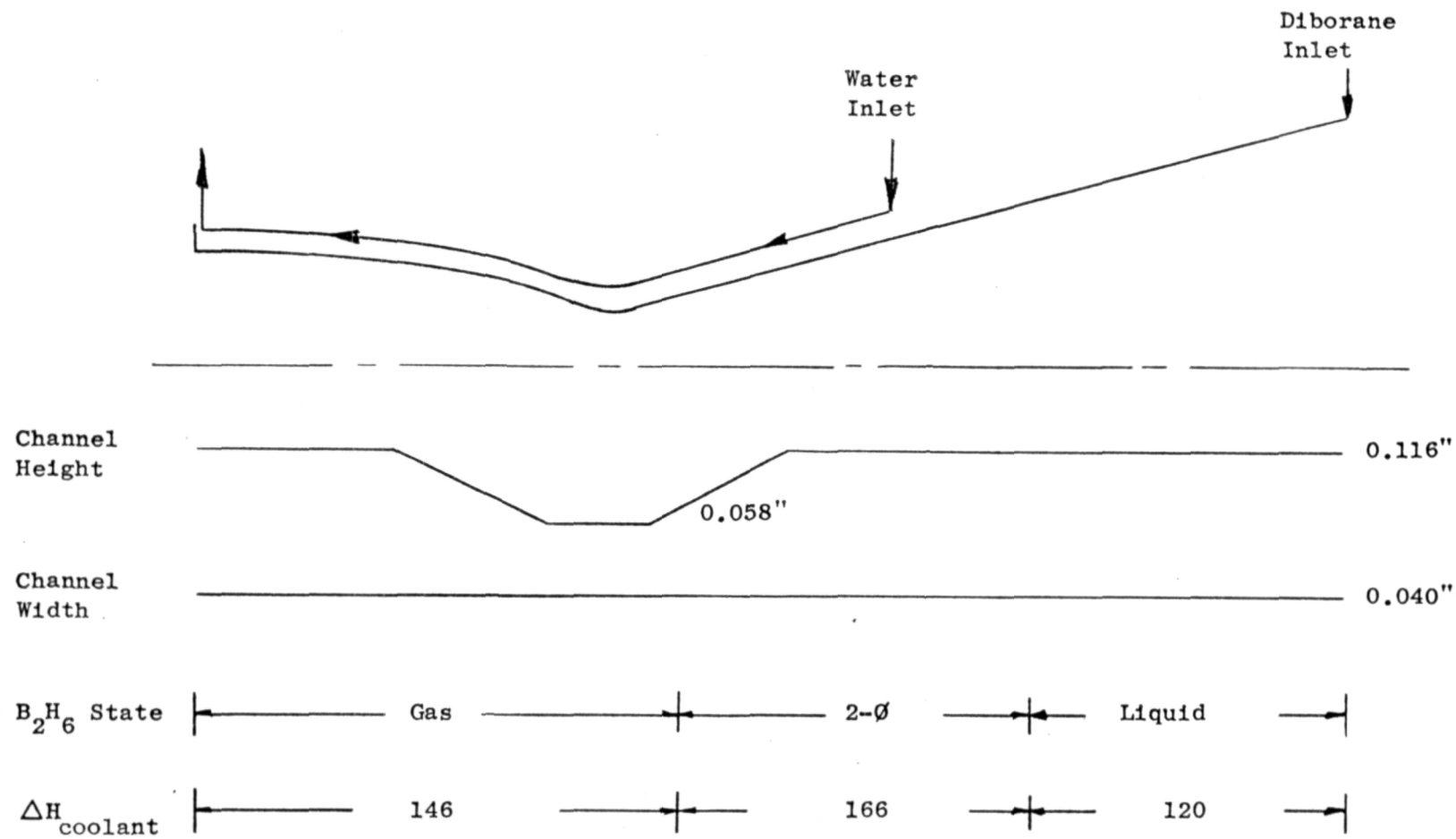


Figure 71. Diborane Coolant Channel Profile.

TABLE 10
CHANNEL GEOMETRY SELECTION

DIBORANE

Number of Channels = 90

Channel Width = 0.040 inch

LOCATION	CHANNEL HEIGHT (inch)	MASS VELOCITY (lb/in ² -sec)
Nozzle Section		
20 $\gg \epsilon \gg 3.3$	0.116	1.5
3.3 $\gg \epsilon \gg 1.5$	0.116 to 0.058	1.5 to 3.0
Throat Region		
x = -1.5 to ϵ = 1.5	0.058	3.0
Combustion Chamber		
-1.5 $\gg x \gg -5$	0.058 to 0.116	3.0 to 1.5
-5 $\gg x \gg -9.5$	0.116	1.5

OXYGEN DIFLUORIDE

Number of Channels = 90

Channel Width = 0.060 inch

Channel Height = 0.115 inch

Mass Velocity = 3.0 lbm/in²-sec

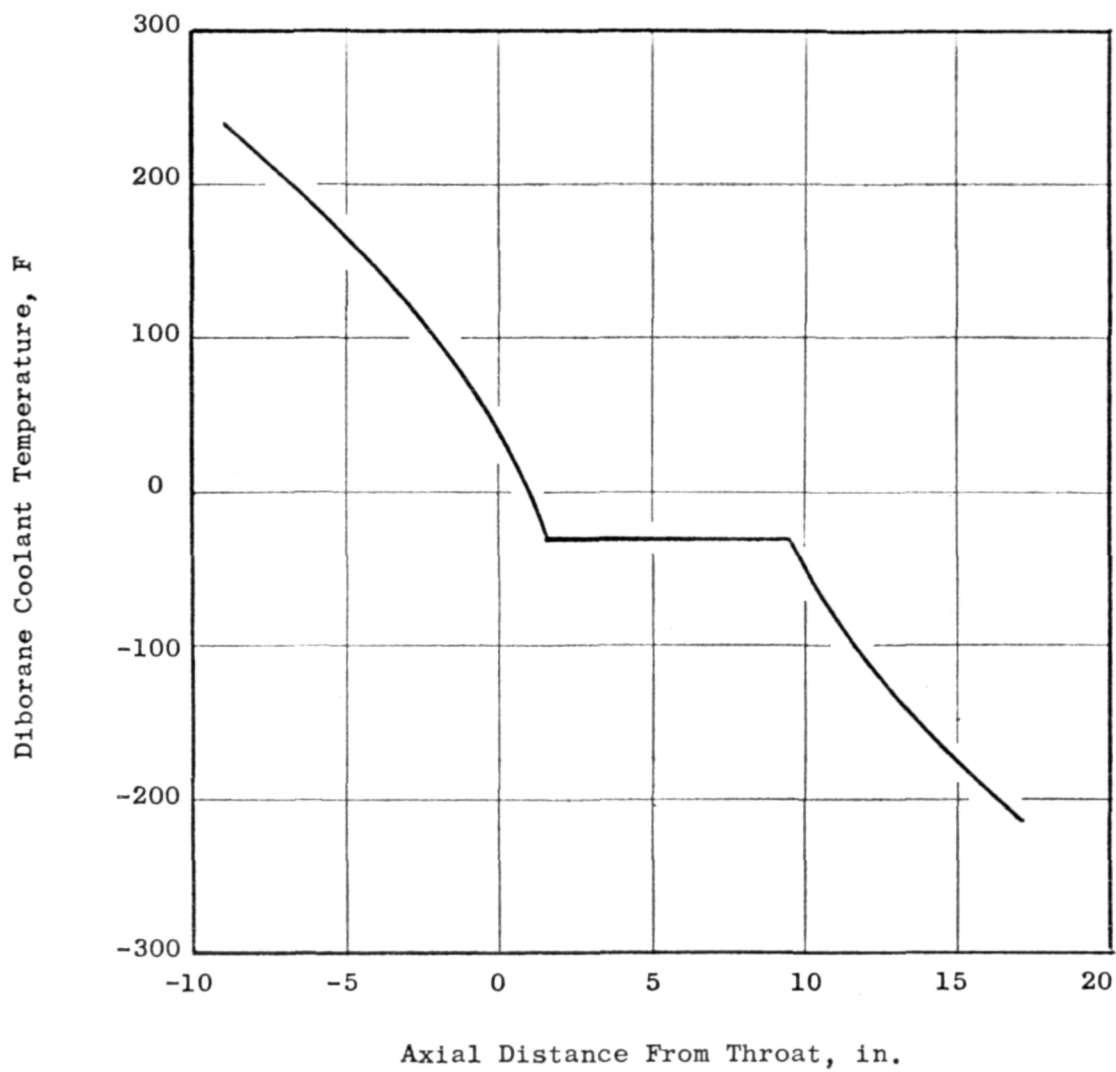


Figure 72. Diborane Coolant Temperature Profile (Predicted)

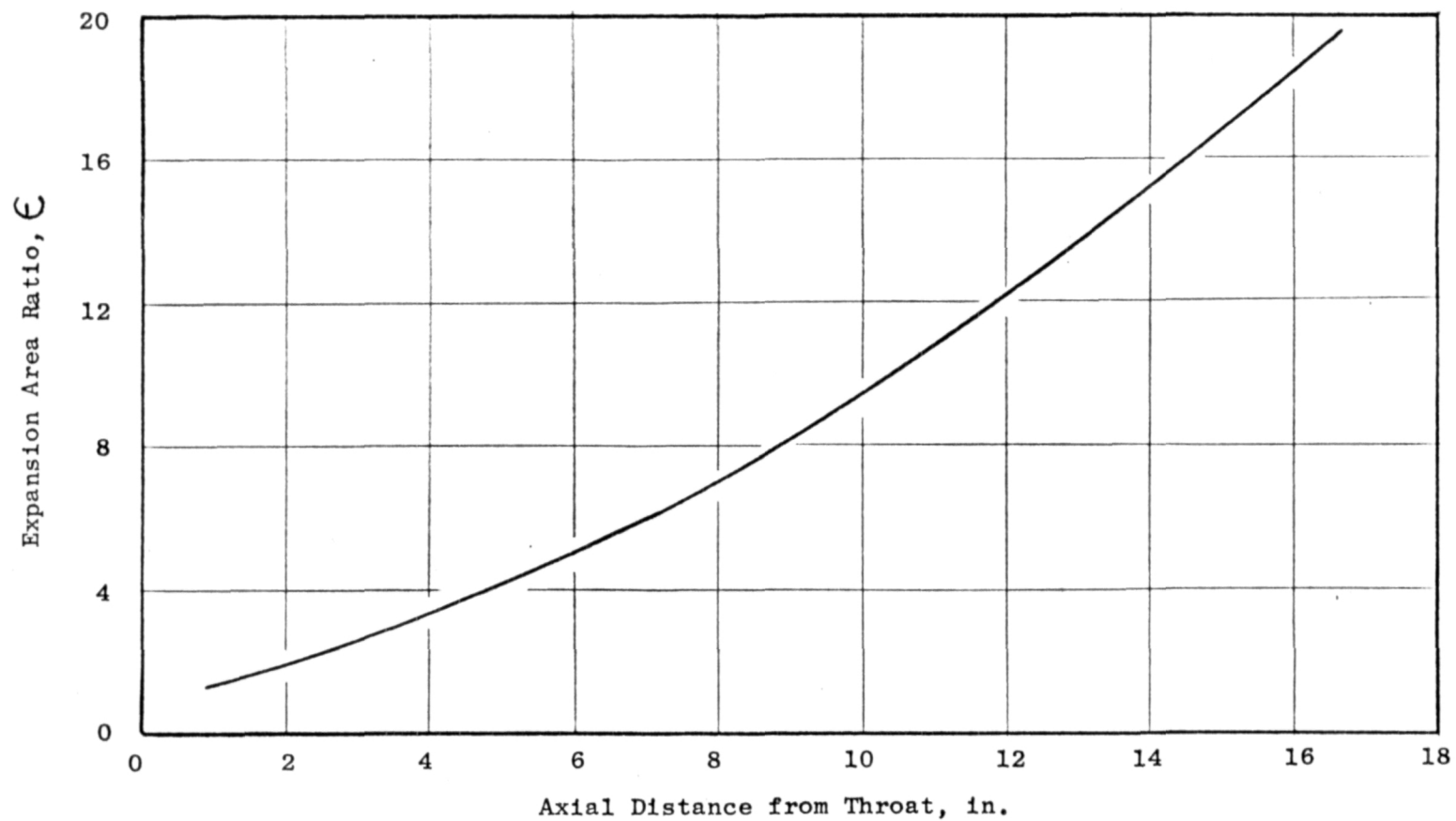


Figure 73. Nozzle Area Ratio vs Length.

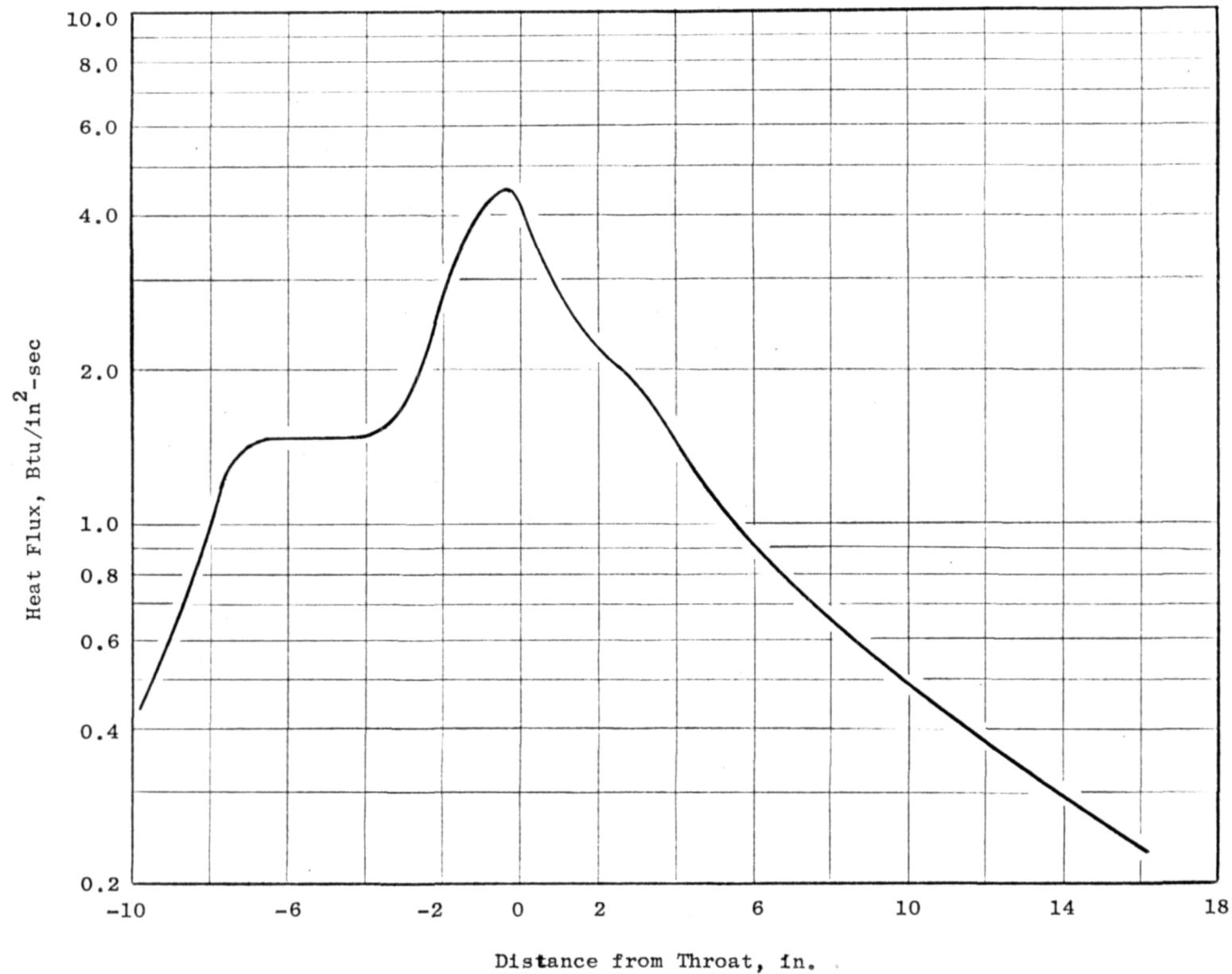


Figure 74. Hot Gas Side Heat Flux Distribution.

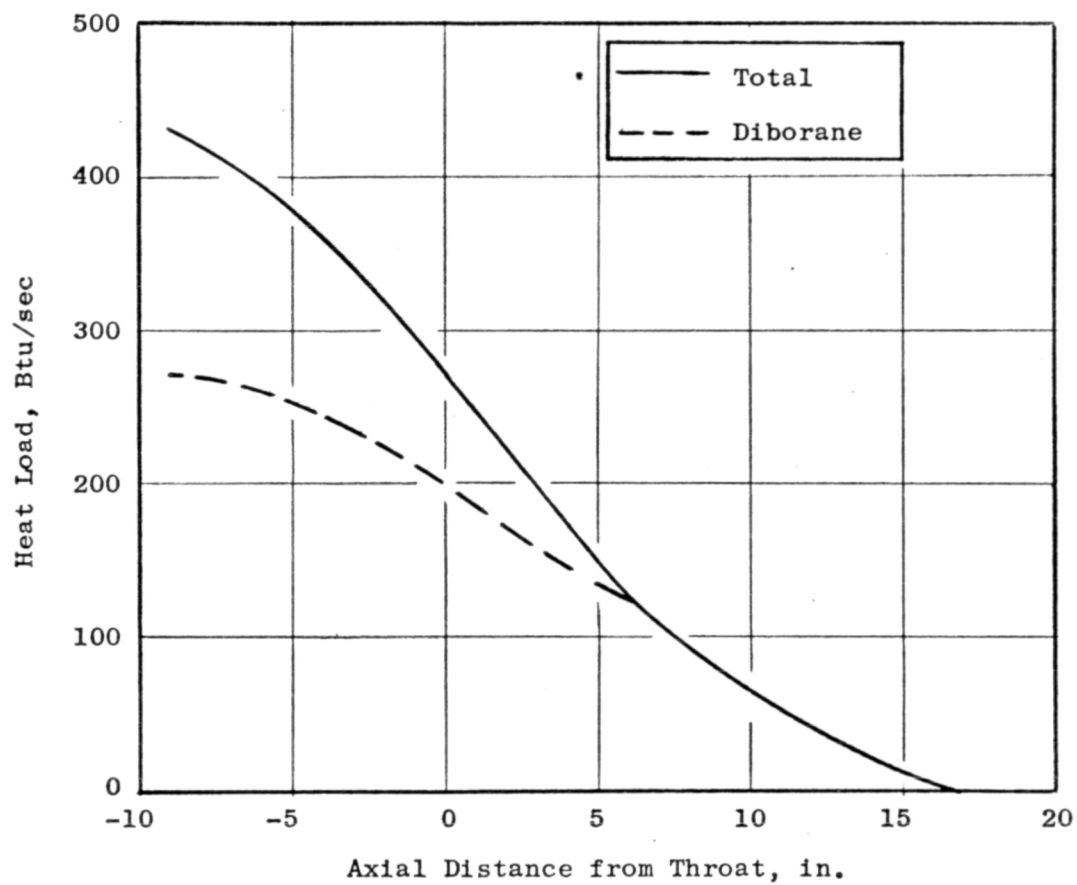


Figure 75. Coolant Heat Load Profile.

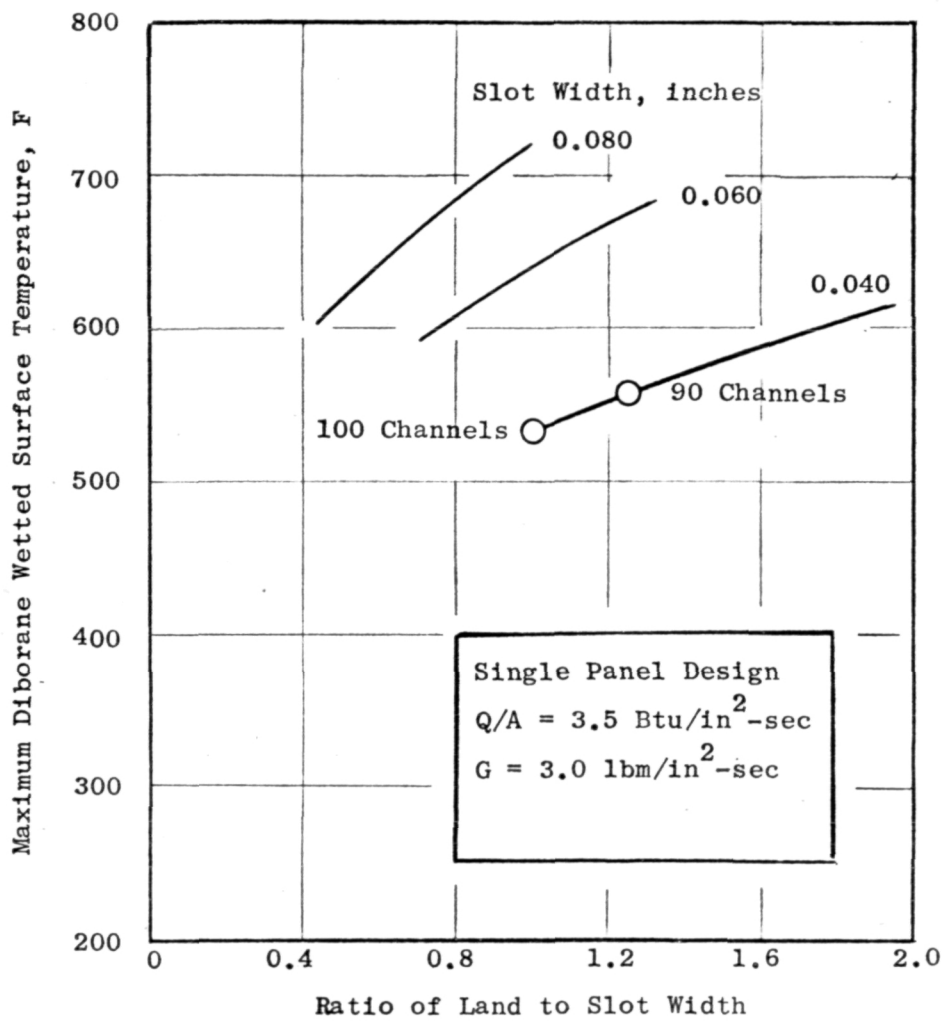


Figure 76. Wall Temperature Predictions for Single Panel Cooling Design.

condition minimizes the ratio of gas-side area to effective channel surface area and therefore the coolant-side effective heat flux is less (with a wall temperature decrease).

Figure 77 shows maximum surface temperature in contact with diborane as functions of heat flux and diborane mass velocity (or channel height) for the selected design. For a heat flux of $5 \text{ Btu/in}^2\text{-sec}$ and a mass velocity of $3 \text{ lbm/in}^2\text{-sec}$, the maximum temperature is 550 F. With 90 channels this temperature is approximately 550 F. The selected throat mass velocity was maintained at a constant value both upstream and downstream of the throat a sufficient distance for the heat flux to become reduced to $3.5 \text{ Btu/in}^2\text{-sec}$. This approach eliminated the need for exact knowledge of the peak heat flux point and provided an extra cooling margin in the throat region.

Nozzle Section. The nozzle, which is cooled only by diborane, has two fluid zones. From the inlet at an area ratio of 20:1 up to 10:1 the diborane is a liquid. From 10:1 to approximately 2:1 the diborane is an increasing quality two-phase flow.

Since the nozzle heat flux levels are low with a copper wall, it was found that all four surfaces of each coolant slot were at approximately the same temperature. The hot gas wall heat flux is related to the coolant heat flux by the ratio of hot gas to coolant surface areas. For the 90 coolant slots at a width of 0.040 inch, Fig. 78 shows this ratio of areas as a function of local area ratio for three different values of mass velocity. For various conditions the coolant heat flux can be greater or less than the hot gas heat flux, with an improved ratio making it easier to handle a higher hot gas heat flux.

Figure 79 shows coolant heat flux versus area ratio for three different mass velocities. Lower mass velocities are associated with reduced coolant heat flux because of the increased coolant surface area. This figure was examined in conjunction with the liquid diborane coolant data shown in Fig. 80. Assuming first, mass velocity has negligible effect on nucleate boiling, it is

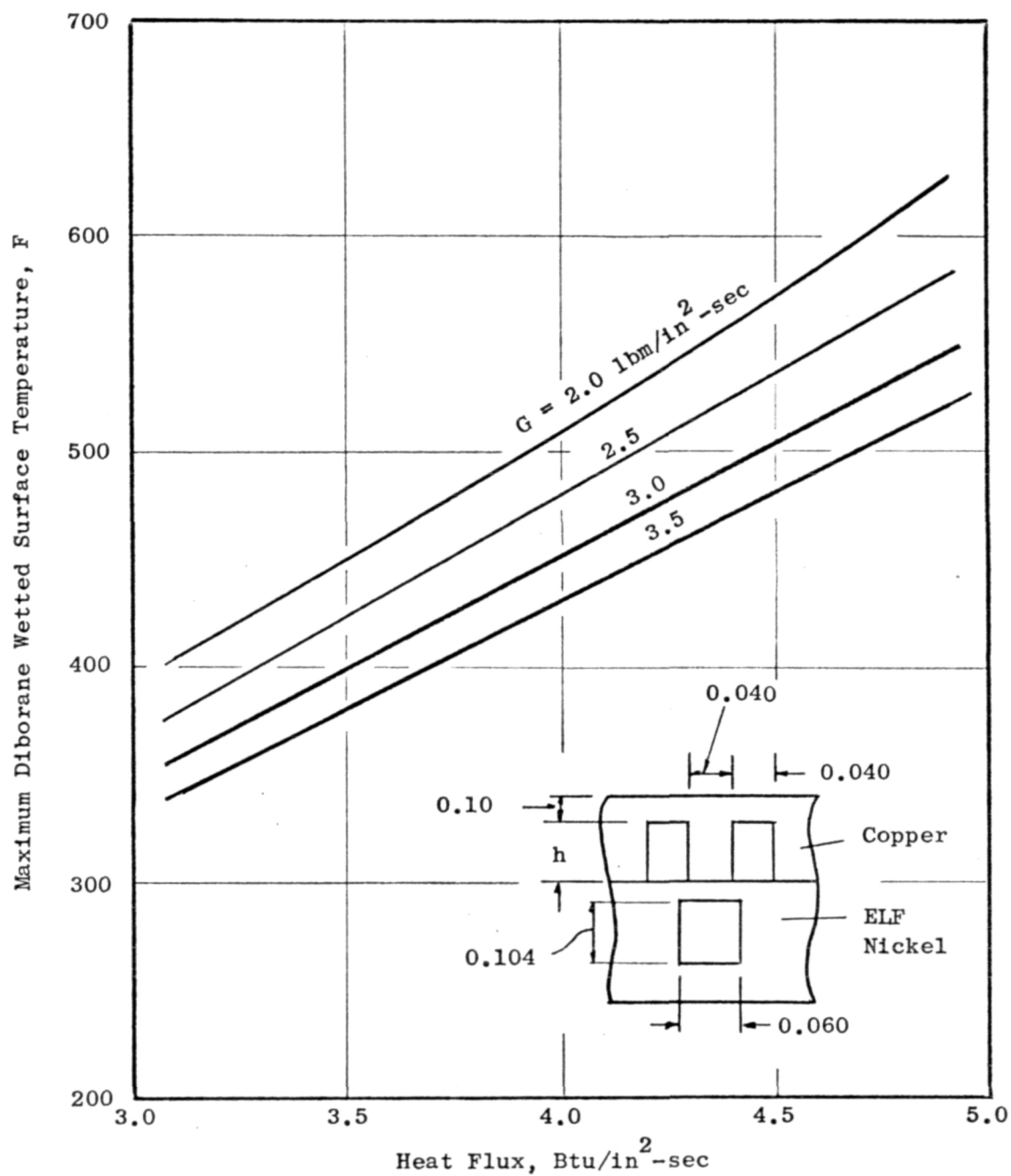


Figure 77. Throat Wall Temperature Predictions for Double Panel Cooling Design.

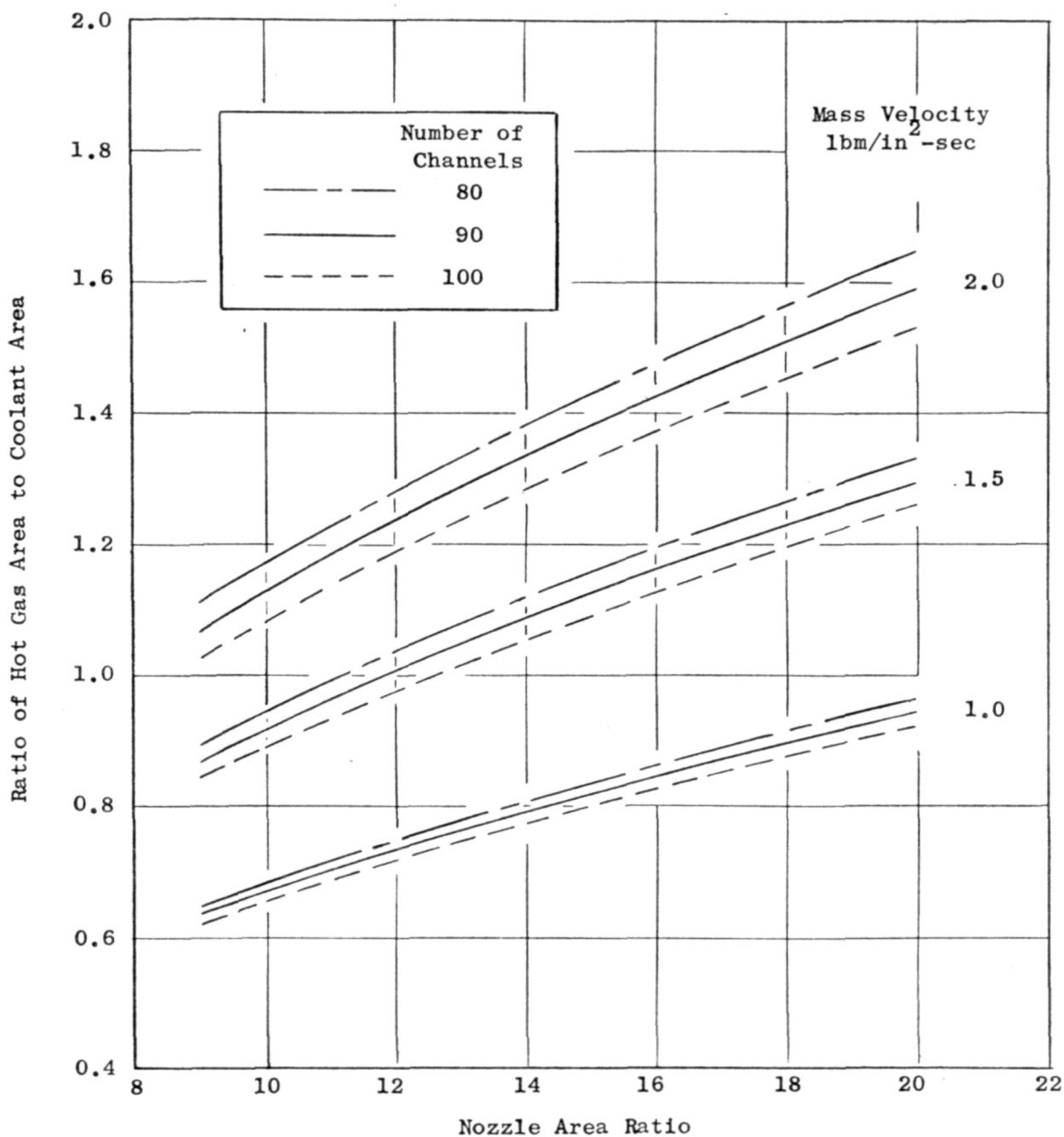


Figure 78. Ratio of Hot Gas Area to Coolant Area in the Thrust Chamber Nozzle.

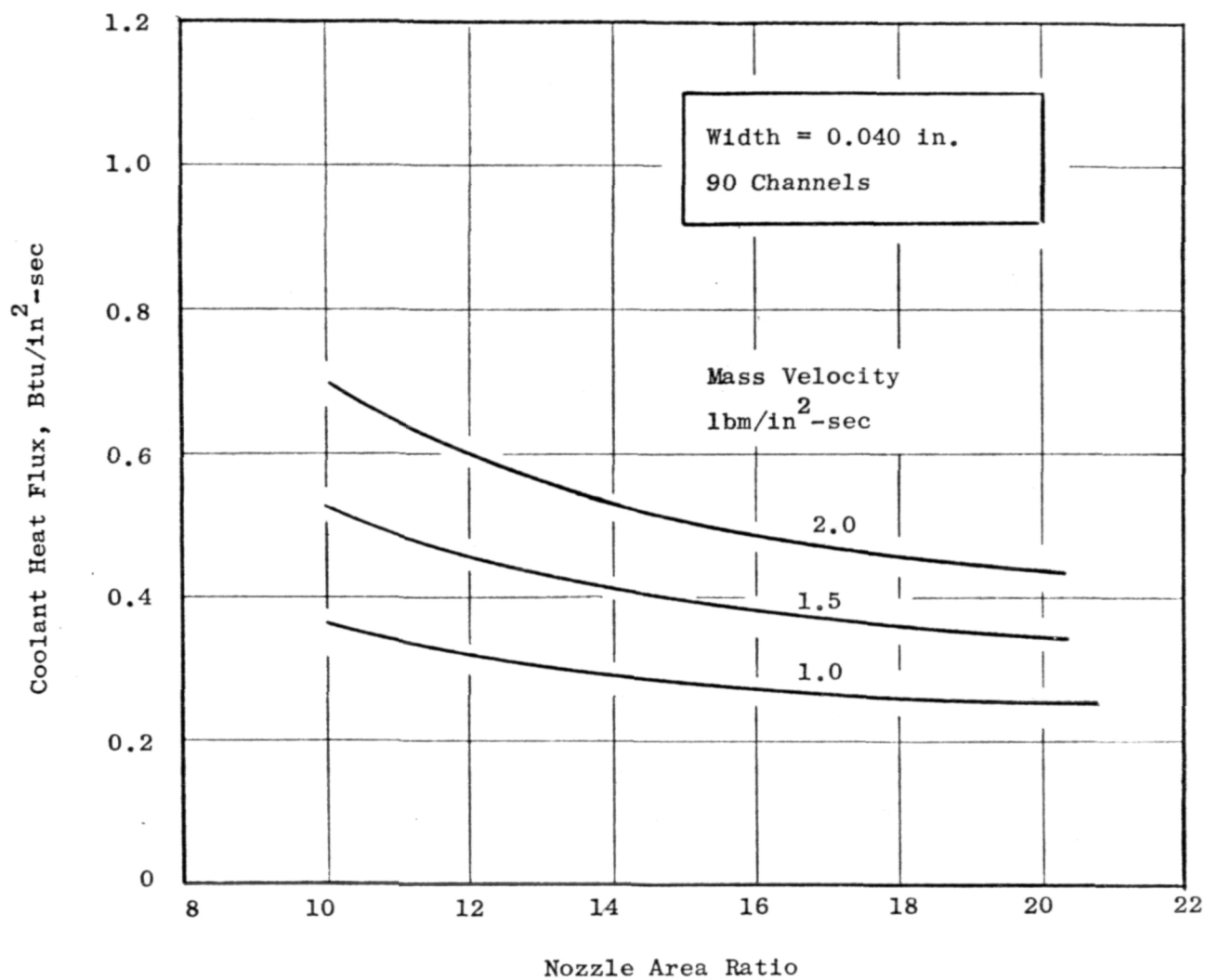


Figure 79. Coolant Heat Flux Distribution for the Nozzle Section Cooled by Liquid Diborane (Based on Two Dimensional Analysis).

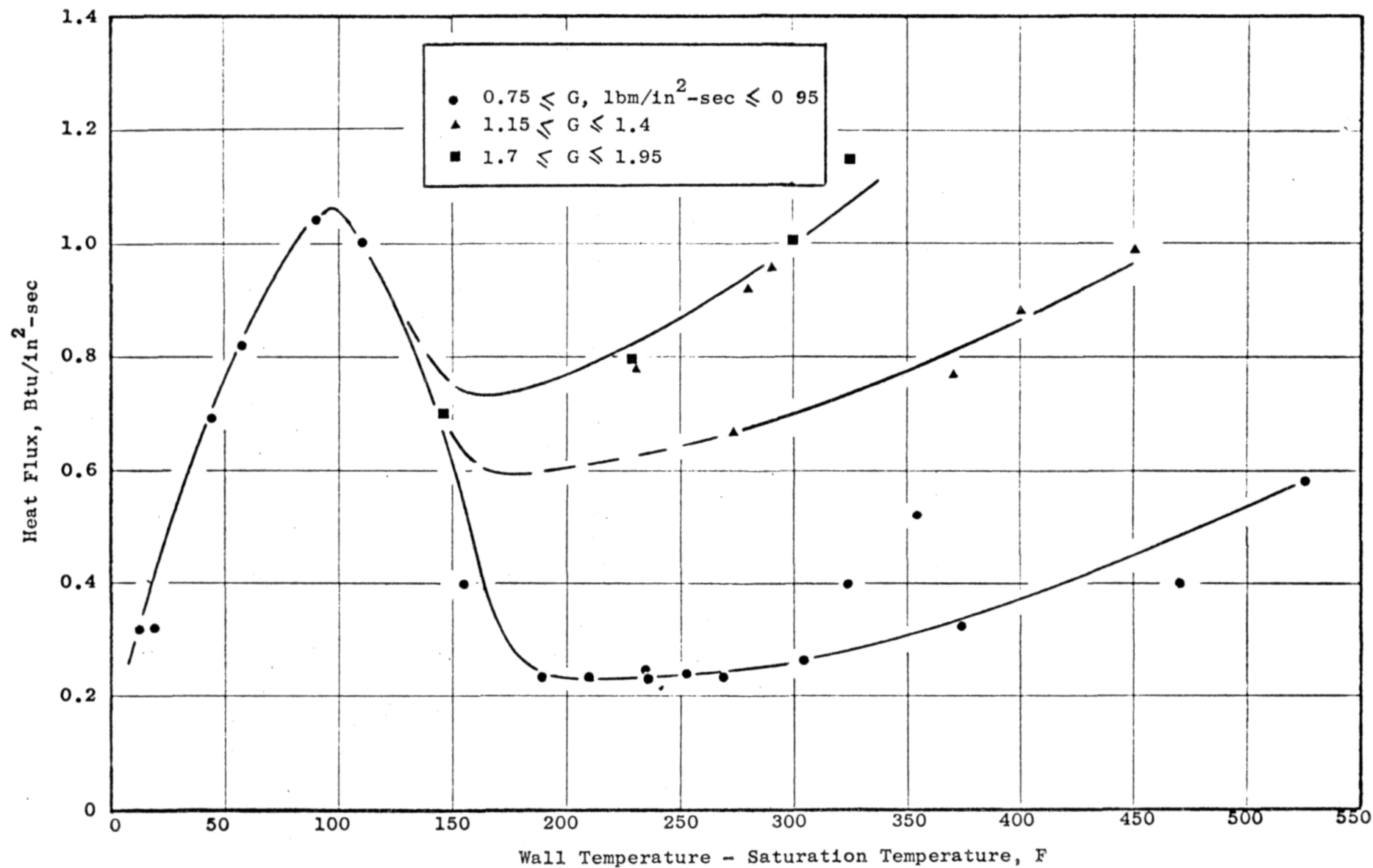


Figure 80 . Experimental Boiling Data for Diborane.

seen that lower mass velocities operate at lower wall temperatures. However, for a mass velocity of $1.0 \text{ lbm/in}^2\text{-sec}$ and coolant heat flux greater than about $0.25 \text{ Btu/in}^2\text{-sec}$, the cooling curve shows two stable points, corresponding to nucleate and film boiling. If the wall were driven above the nucleate boiling heat flux limit, the nozzle will rise from temperatures of about 50 F to values of 300 F to 600 F. At higher mass velocities, the nucleate boiling temperatures are higher but the cooling curve appeared single valued up to a higher heat flux. As mass velocity is increased to $2.0 \text{ lbm/in}^2\text{-sec}$, a decreased wall temperature associated with film boiling is noted. A mass velocity of $1.5 \text{ lbm/in}^2\text{-sec}$ was selected for the design as a reasonable compromise since for this value the heat flux is always less than approximately $0.5 \text{ Btu/in}^2\text{-sec}$. At an area ratio of 10:1 which is the location of onset to two-phase flow, the diborane heat flux was estimated at $0.5 \text{ Btu/in}^2\text{-sec}$. (The wall temperature was found to exceed the value associated with the nucleate boiling during Task IV testing and stabilized at approximately 550-800 F indicating a film boiling condition.) The nozzle region from 20:1 to 10:1 area ratio was designed with the coolant channels at a constant height of 0.116 inch giving the design mass velocity of $1.5 \text{ lbm/in}^2\text{-sec}$.

Continued studies of the two-phase coolant region from area ratio of 10:1 toward the throat concluded that, since coolant heat flux remains low for some distance, continuation of the design G of $1.5 \text{ lbm/in}^2\text{-sec}$ was satisfactory and minimized pressure drop. As seen from Fig. 81 the design heat flux remains below $0.8 \text{ Btu/in}^2\text{-sec}$ and maximum coolant side wall temperature was designed to be below 500 F all the way up to an area ratio of 4.0:1. At this point the hot gas side design heat flux was $1.5 \text{ Btu/in}^2\text{-sec}$ where channel height tapering was begun. A linear taper was selected to keep the wall temperature below 500 F until a hot gas heat flux of $3.5 \text{ Btu/in}^2\text{-sec}$ is reached.

Combustion Chamber Section. In the double panel combustor section, the design variables were the height of the diborane channel and the OF_2 channel geometry. The optimization criterion was selected to be overall OF_2 heat absorption because of the OF_2 minimum vaporization requirement. With the selected

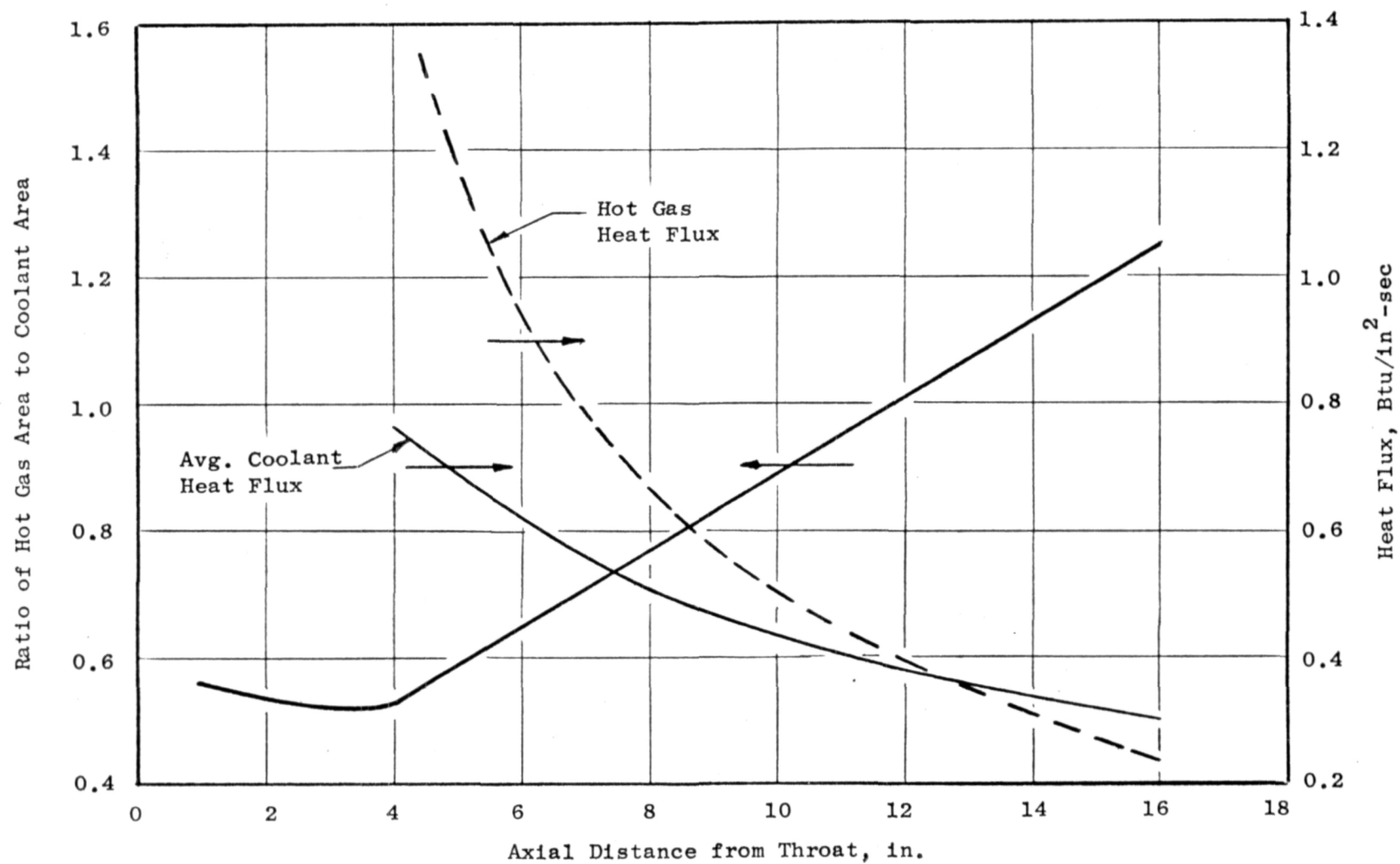


Figure 81. Nozzle Coolant Heat Flux Distribution for Selected Channel Design.

diborane throat channel width and land spacing (defining the combustor diborane channel width and spacing), and a constant OF_2 geometry, Fig. 82 shows the wall temperature distributions for two diborane height selections. It is seen from the wall temperatures that a diborane mass velocity change associated with a height variation does not alter the overall OF_2 heat input with the OF_2 wall temperatures similar. A varying diborane mass velocity condition primarily alters the diborane wall temperatures. The OF_2 absorbs over 55 percent of the total heat input because of a lowered diborane effectiveness at low wall temperature and due to an increased surface area (nearly proportional to the increased flow area in the two cases shown). A design mass velocity of $1.5 \text{ lbm/in}^2\text{-sec}$ was selected as a compromise between the cooling margin of a smaller channel and the lower pressure drop of a larger channel.

Tapering of the channel was similar to the nozzle with the taper beginning where heat flux reached $1.5 \text{ Btu/in}^2\text{-sec}$ and minimized at the throat heat flux point.

Two-Dimensional Analysis. For the selected design and for the nominal heat flux distribution, two-dimensional heat transfer analyses were conducted for a series of locations along the length of the chamber and nozzle. From these analyses the maximum wall temperature distribution were computed and is shown in Fig. 82. Isotherms are shown for a series of stations in Appendix D. A thrust chamber cooling sensitivity analysis was conducted for the throat region. Sensitivity of the nozzle throat to two possible hot-fire problems was studied. These were blockage of one coolant channel and a possible heat flux nonuniformity. As a reference case for the variations studied, Fig. 1 illustrates the throat region isotherms for a heat flux of $4.5 \text{ Btu/in}^2\text{-sec}$ and with the backup water jacket operating in the boiling mode.

Since diborane could under extreme conditions, decompose and potentially block a coolant channel, the effect of a blocked channel was computed and is shown in Fig. 83. Temperatures in the vicinity of the blocked and adjacent channels increased by approximately 50 F except temperatures near the water jacket, which were constant due to the boiling heat transfer. It was clear

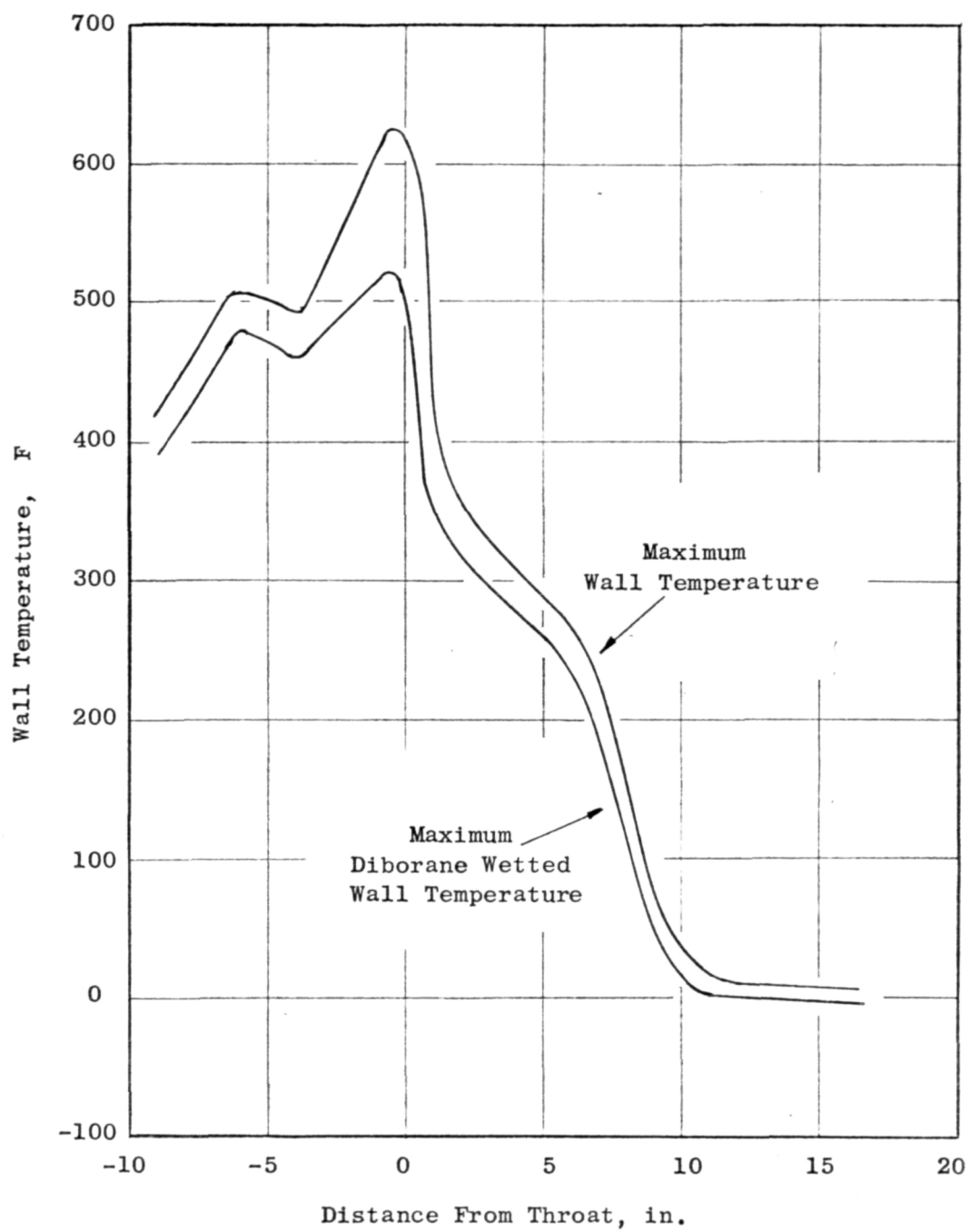


Figure 82. Wall Temperature Distribution

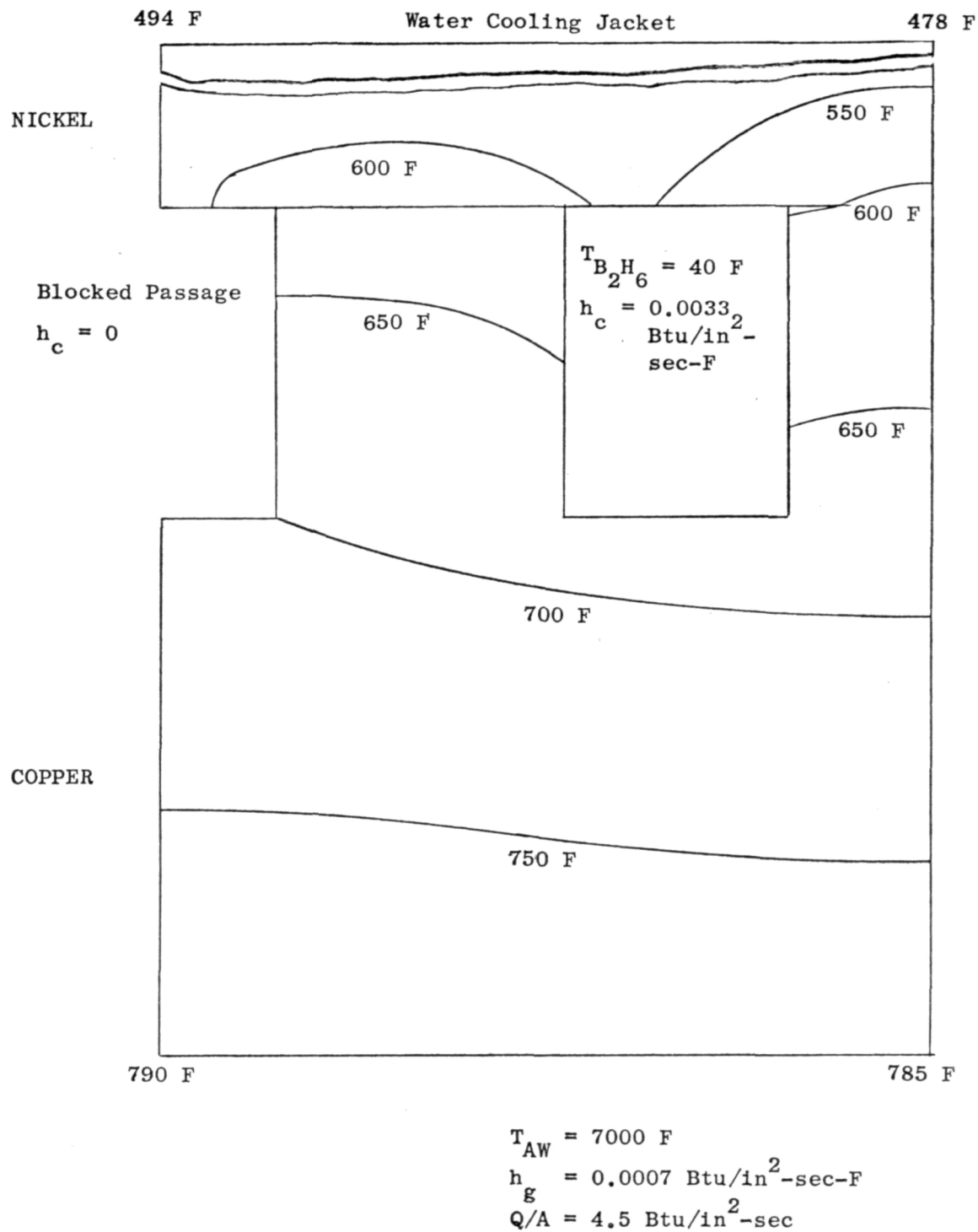


Figure 83 . Throat Isotherms for Non-Boiling Water Heat Transfer and One Blocked Diborane Passage.

that the chamber could tolerate a single blocked coolant passage and could probably survive the loss of every third channel. Loss of two adjacent channels might also be tolerable, but would be marginal. An insensitivity to channel blockage is due partially to a stabilizing effect of the backup panel (water) heat transfer which anchors the back wall temperatures.

A 50-percent increase in heat flux in the area in front of one coolant channel was also studied (Fig. 84). This might correspond to anomalous behavior of a single film coolant hole or an element in the outer row of the injector. For this case the surface temperatures in contact with diborane remained well below 600 F.

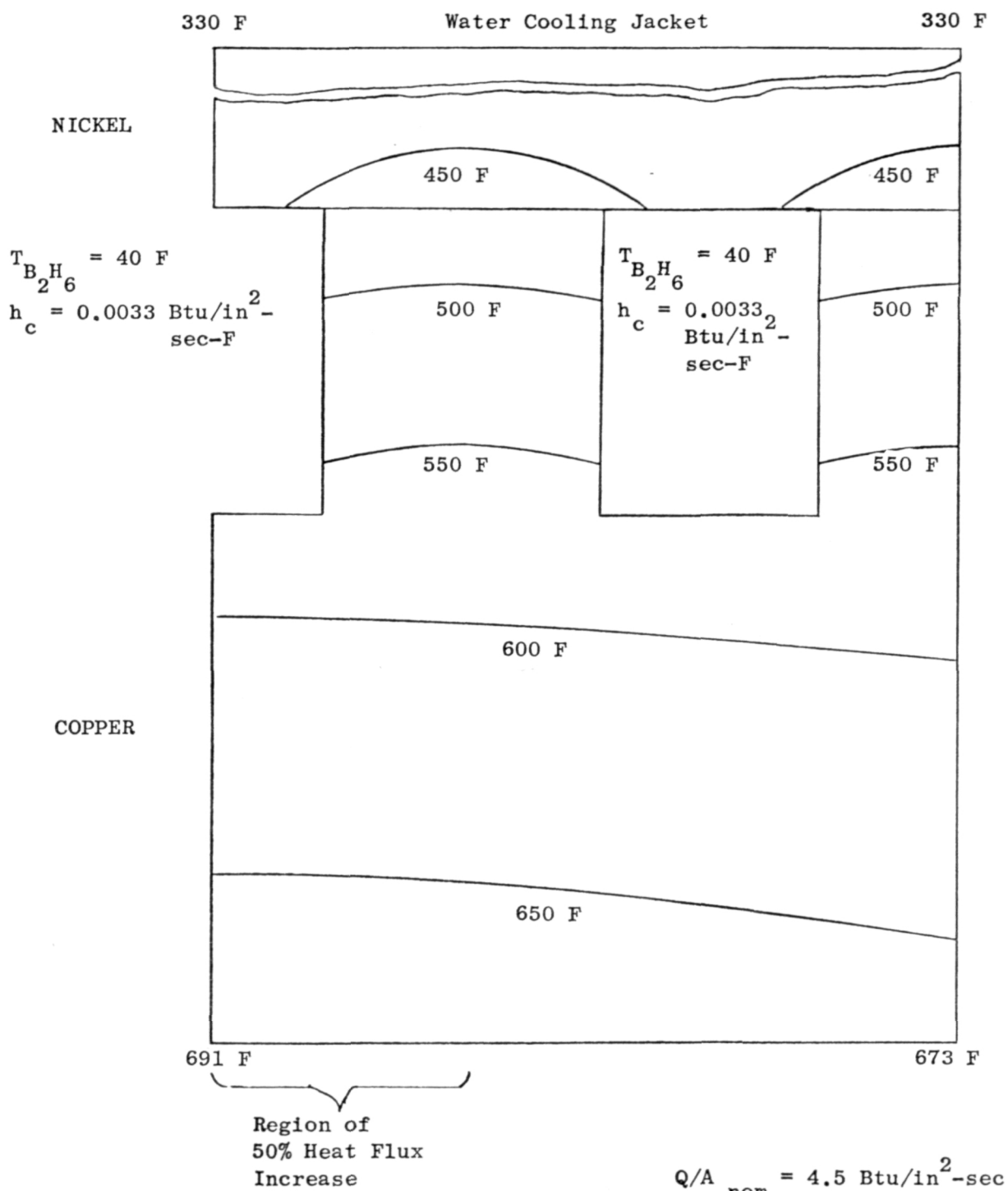


Figure 84. Throat Isotherms for Boiling Water Heat Transfer and a Local Heat Flux Increase.

TASK III - REGENERATIVE CHAMBER AND TRIPLET NO. 2 DESIGN/FABRICATION

Preparatory to the Task IV study of the feasibility of regenerative cooling with B_2H_6 , the hardware necessary was designed and fabricated during Task III study. This fabrication included two B_2H_6 fuel cooled regenerative 20:1 area ratio chambers with OF_2 simulated water jackets. In addition a second impinging element injector, Triplet No. 2, was fabricated of similar design to that tested during Task II but with face deposit factor improvements. Modification of the Task II calorimeter chamber to ensure better sealing and instrumentation was also accomplished.

THRUST CHAMBER DESIGN FEATURES

The demonstration thrust chamber assembly, complete with the injector and the water cooling jacket, was shown in cross section in Fig. 7. The critical design features of the demonstrator were the inlet/distribution manifold, outlet manifold, coolant channel access ports, water cooling jacket, and pressure budget. Initial design study was shown in Task II.

Inlet/Distribution Manifold

The thrust chamber coolant inlet was designed to accept a single liquid diborane inlet line (to be eventually mated with a valve under development in another program). The criteria for design of the inlet manifold were:

1. A low velocity flow feeding the coolant passages.
2. A minimum volume to reduce priming time.
3. Minimum gravitational orientation of the diborane during start in a horizontal test facility.

The combination of these three requirements led to selection of the three-stage manifold shown in Fig. 85.

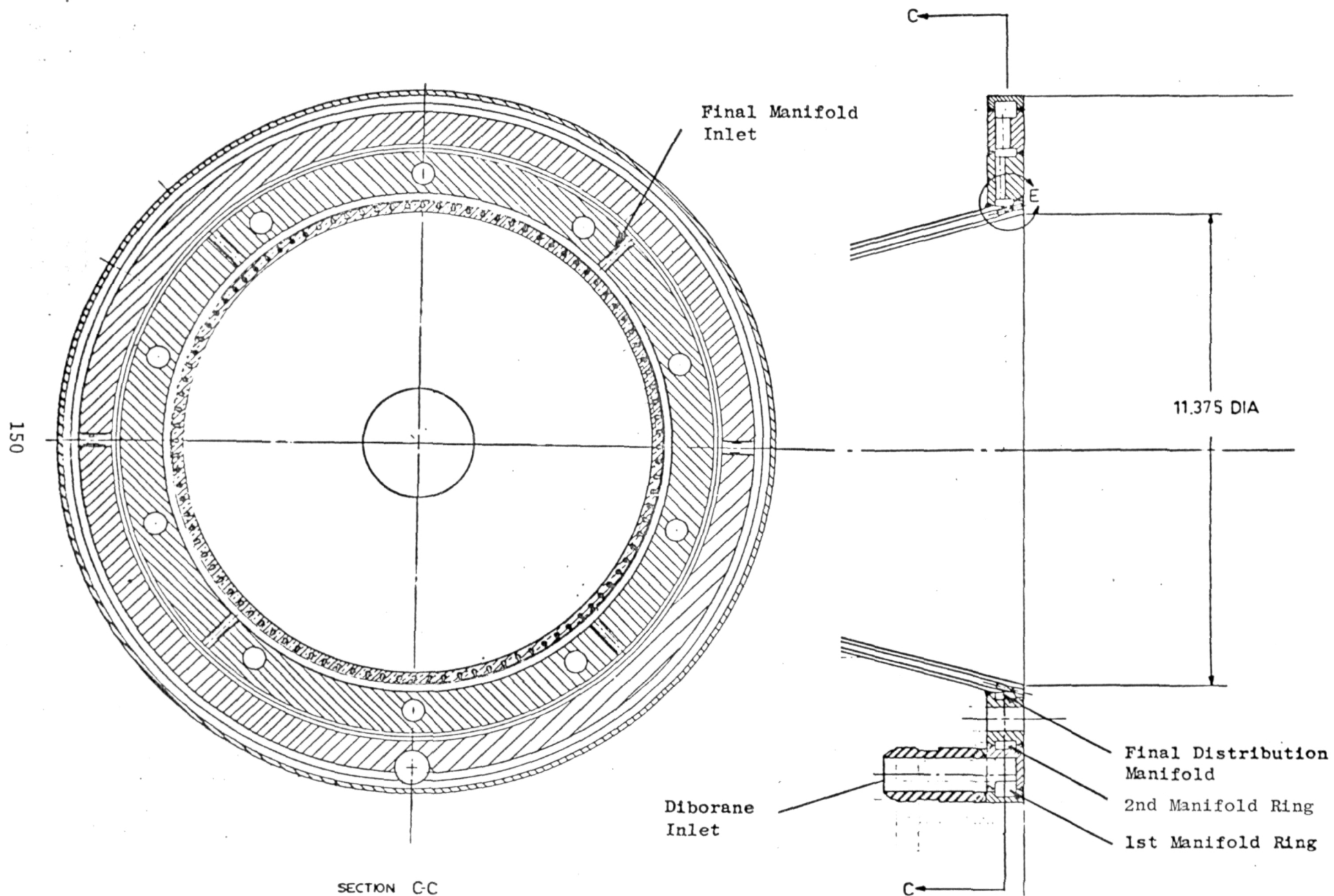


Figure 85 . Inlet/Distribution Manifold.

During mainstage operation the pressure drop through the coolant passages is approximately 70 psi or greater. It was determined that a ± 1 percent variation in flowrate caused by manifold hydraulics would be a reasonable target, achievable if the dynamic pressure in the manifold was 0.7 psi or less. The entrance velocity of the liquid in the coolant passages is about 10 ft/sec, and a dynamic pressure of 0.075 psi occurs. As a result, the manifold contribution to mainstage flow nonuniformity is insignificant.

The engine is required to have a single inlet, and internal manifolding is needed to adapt from the single engine inlet to multiple final manifold inlets for a good inlet flow distribution. This was done in the outer two manifold rings shown in Fig. 85. The passages are arranged to force the flow reaching each of the final inlets to negotiate identical paths, assuring uniform inletting. The design chosen had a total volume of approximately 6 in³, as did a single 10 ft/sec manifold design. The inlet to each coolant channel was also restricted by providing a pressure drop of about 2 psi. In a more extensive program, tests might be conducted to determine if a less conservative inlet manifold design would be adequate, as is believed to be the case. In this limited effort, however, the most conservative approach was considered the best.

Outlet Manifold

The thrust chamber outlet manifold was required to receive the heated gaseous diborane from the coolant passages and distribute it to eight injector inlets. The dynamic pressure of gaseous B₂H₆ at 50 ft/sec is only 0.16 psi compared with an injector pressure drop of 20 psid (0.8 percent). With these manifold outlets a 50 ft/sec maximum velocity manifold required a cross-sectional area of only 0.2 in². Furthermore, the flow was remanifolded within the injector providing uniformity. The manifold was designed to be open at one end as seen in Fig. 86. The open side is closed by the injector mating surface and two seals and was selected to permit access to each cooling channel for inspection and flushing. The manifold was on the same circle as the bolt circle and the injector-to-thrust chamber bolts go directly through

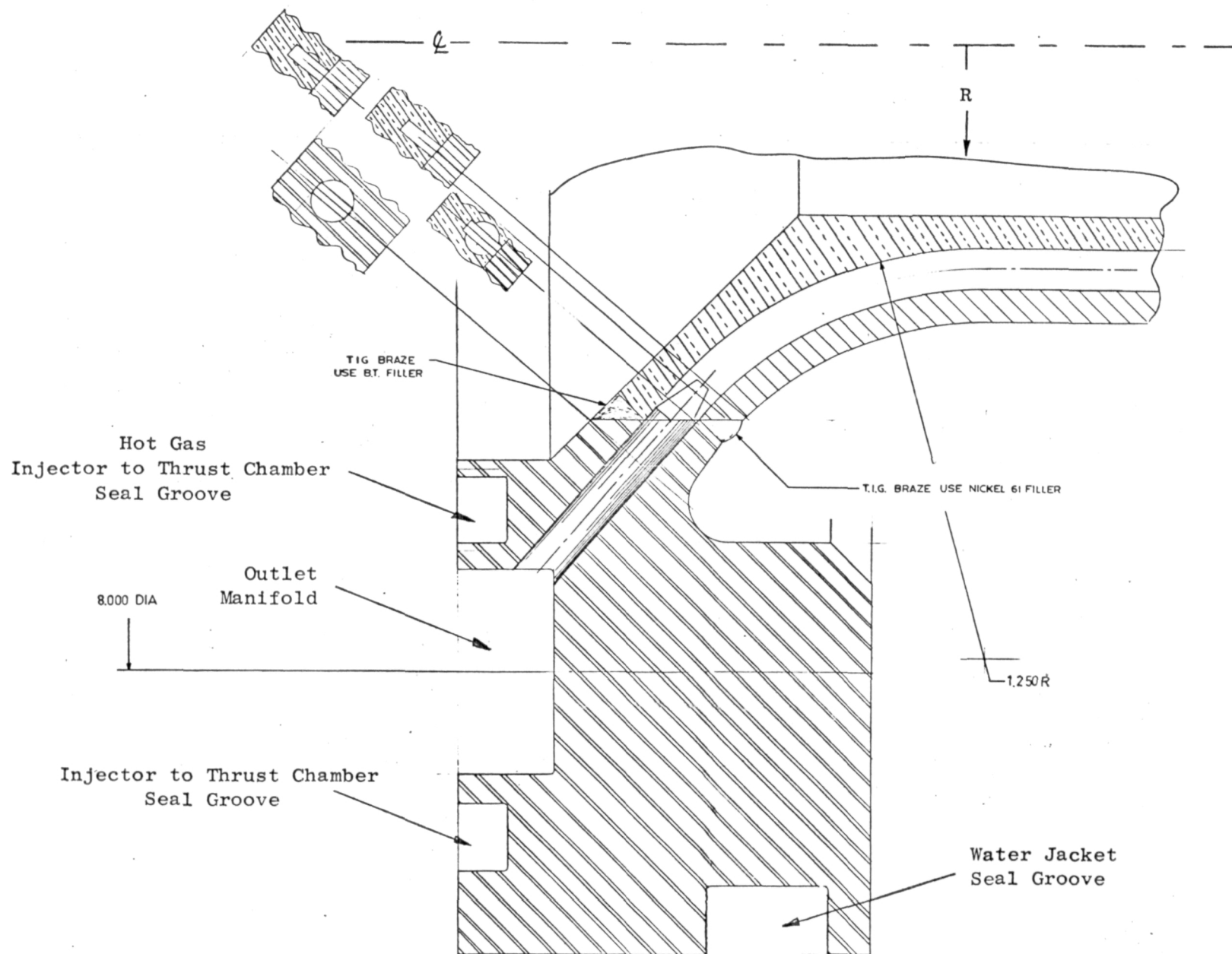


Figure 86. Outlet Manifold.

the manifold into threaded holes in the flange. At the locations where the bolts come through the manifold, the manifold was enlarged to maintain adequate flow area. Seals were used around the heads of the bolts with threaded holes in the flange instead of through-holes to avoid additional isolation seals between the diborane manifold and water jacket. The resulting injector to thrust chamber interface is shown in Fig. 87.

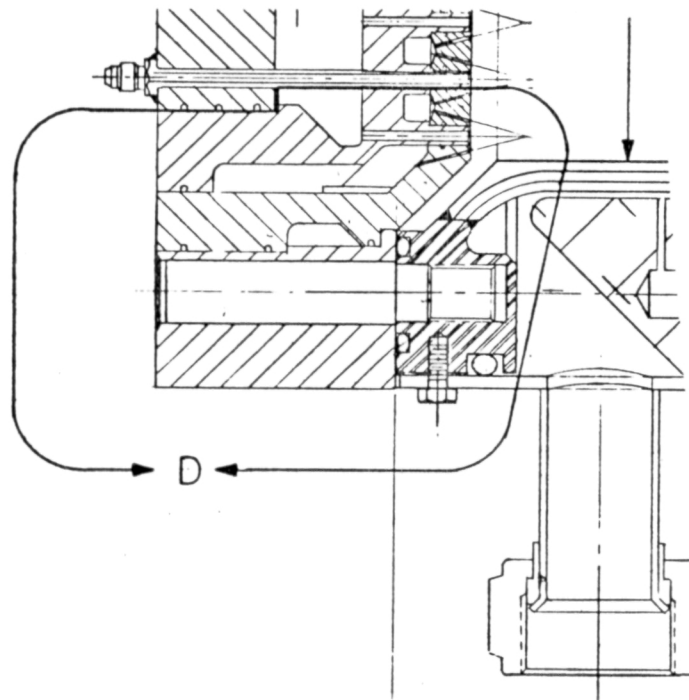
Access Ports

One of the initial Rocketdyne design criteria for this workhorse design was that the coolant passages would be accessible for servicing or inspection from both ends. This was achieved at the injector end manifold by making one side of the manifold open with the coolant channels intersecting the manifold at an angle which provided observation or servicing. The structural tie is necessary to permit adequate compression of the hot gas seal between the injector and chamber. After several approaches were examined, drilled passages were selected as a transition between the coolant passages and the manifold.

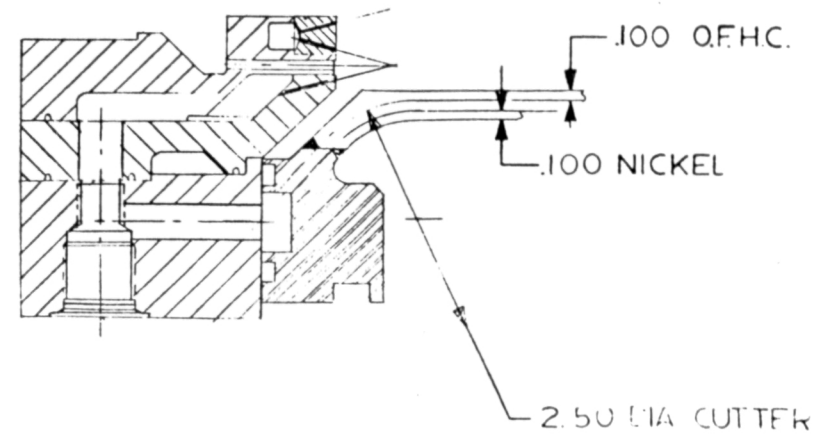
At the inlet manifold (Fig. 88), drilled ports were threaded and plugged with recessed fittings. A sealing device such as a ring around an annular opening would either have had the problem of loading the hot-gas seal or would have had heat transfer problems. During preliminary water flow and pressure check, the leakage observed led to brazing over the plugs after other attempted sealing approaches proved inadequate.

Water Jacket

The demonstration thrust chamber used a water jacket to simulate the secondary OF_2 cooling panel. The water cooling jacket imposed two complications on the thrust chamber design. Because the water passage is annular, around the entire chamber (rather than a slotted flight design), it imposes a compressive load on the thrust chamber. Additionally, the water jacket complicated the procedure for thermal instrumentation of the thrust chamber wall.



View Through Bolt Hole



DETAIL D ROTATED 22.5° C.W.

View Through Core Fuel Feeder Passage

Figure 87. Injector - Thrust Chamber Interface.

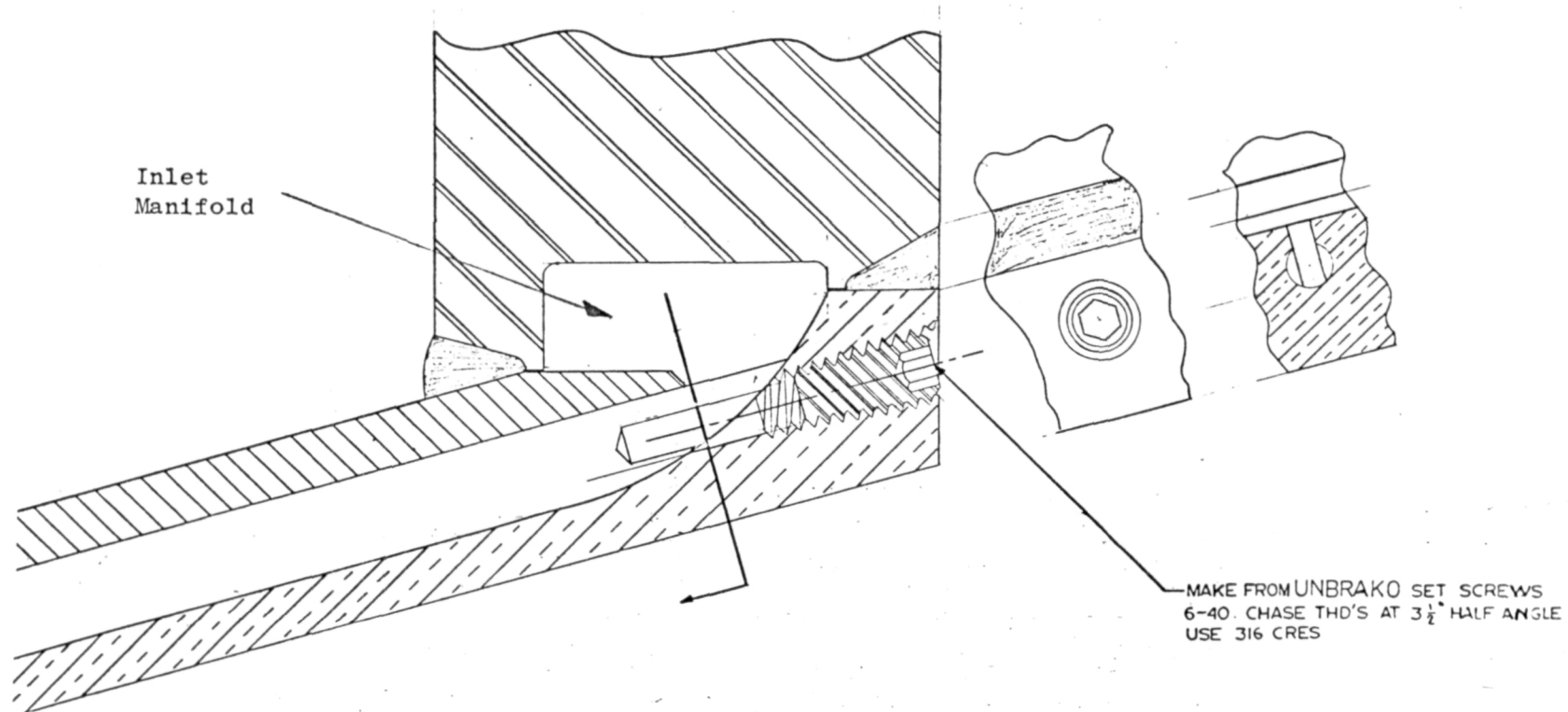


Figure 88 . Nozzle-End Coolant Channel Access Ports.

The selected design is shown in Fig. 89 and the main assembly view, Fig. 7. . A segmented aluminum filler block is secured around the chamber. A cylindrical steel pressure shell is slipped into place and sealed with O-rings. The thermocouple leads were brought out through tunnels located in the parting planes of the filler blocks and through ports in the nozzle-end flange. The additional flange for the water jacket was chosen instead of using the inlet manifold flange in order to improve the stability of the chamber under the water compressive load. The thickness of the electroformed nickel closure was also increased to 0.1 inch above the thickness needed for the flight engine, to assist in carrying this load.

The gap between the filler block and the nickel chamber wall was controlled by pins located in the filler block wall. The pins were designed so that differential expansion between the chamber and the water jacket would cause yielding of the aluminum rather than in the nickel surface.

Pressure Budget

The pressure budget of the demonstration chamber differed in some respects from a flight design. A preliminary comparison of the diborane pressure budgets for the demonstrator and a representative flight engine is shown in Table 11 .

TABLE 11. TYPICAL DIBORANE PRESSURE BUDGET

Location	Pressure Drop, psi	
	Demonstrator Engine	Representative Flight Engine
Inlet/Distribution Manifold	3	1
Coolant Passage	70	40
Outlet Manifold	3	1
Injector Flow Balance Orifice	20	None
Injector Element	20	13
Total	116	55

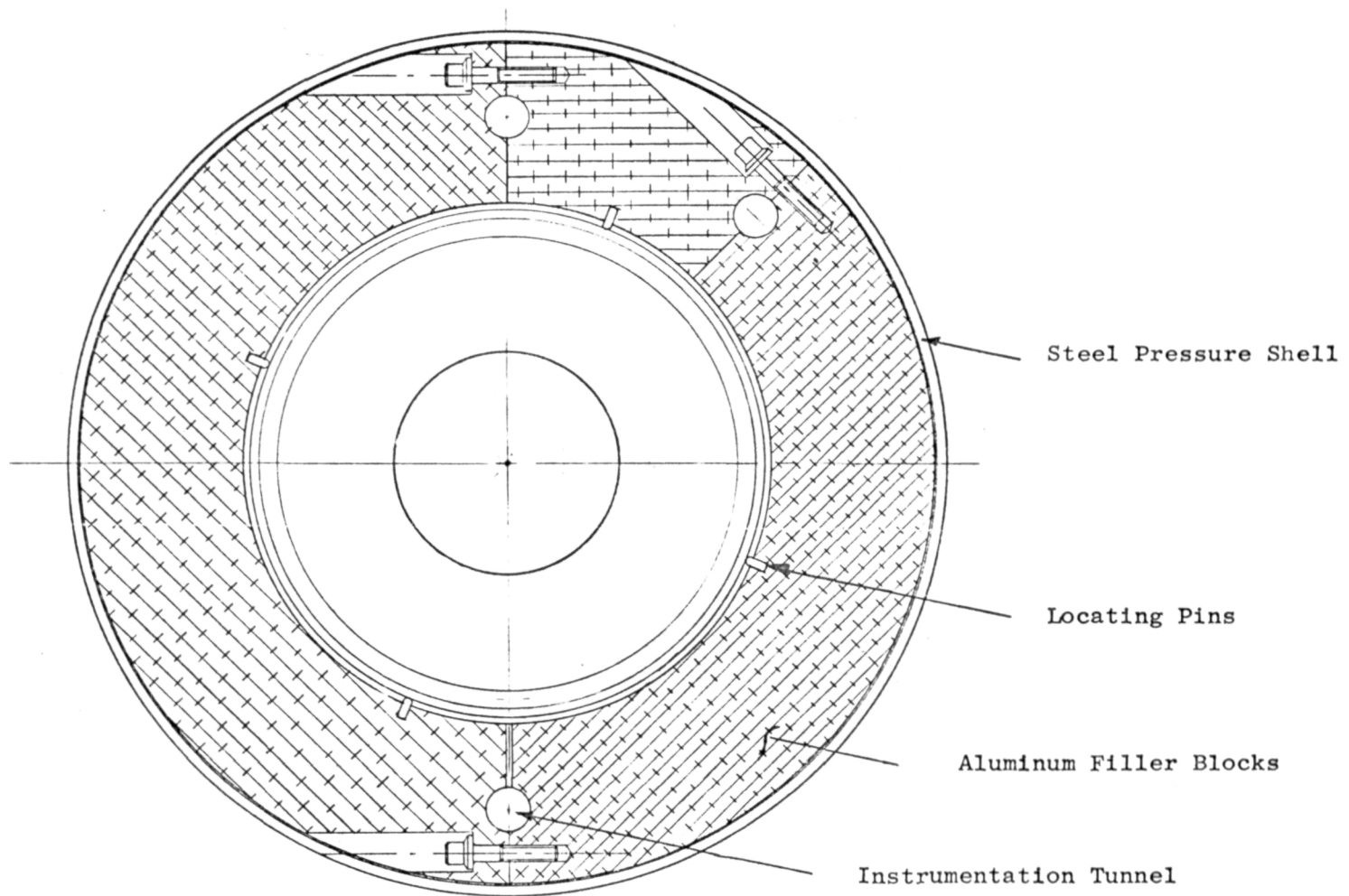


Figure 89. Water Jacket Assembly.

The thrust chamber inlet/distribution manifold was designed for a pressure drop of 6.0 psi, as described, to assure uniform distribution during start. This was considered very conservative and this large pressure drop would probably be eliminated in a flight design.

The approach to coolant channel design was described under Task II. The selected channel geometry dictated a pressure drop of 70 psi as a result of the decision to design the throat for a mass velocity of $3.0 \text{ lbm/in}^2\text{-sec}$ and to use conservative nozzle and chamber designs. A flight engine would decrease this pressure drop. In addition to the drop in total pressure, as the coolant leaves the coolant passage it loses its dynamic pressure. The demonstrator has a higher velocity in the chamber cooling region and loses a larger dynamic pressure.

The injector was designed with orifices to distribute fuel between the core and film coolant zones, creating an additional pressure loss.

Finally, the injector was designed for a fuel pressure drop of 20 psid. It is likely that pressure drop reduction is limited only by feed-system-coupled instability modes and that 5 to 10 psi could be eliminated.

Thrust chamber inlet pressure for a chamber pressure of 100 psia was estimated about 216 psia for the demonstration engine with potential reduction to 155 psia for a final design.

REGENERATIVE CHAMBER HARDWARE FABRICATION AND ASSEMBLY

A demonstrator cooled with both propellants was the primary objective of the initial cooling channel design studies. This engine was studied thermally and structurally but not built in this program due to cost factors. A configuration with a backup water jacket cooling circuit was designed to simulate the OF_2 cooling jacket of the flight design configuration. Initial detailed thermal studies and hardware design studies were directed at the $\text{B}_2\text{H}_6/\text{H}_2\text{O}$ cooled chamber which has been built for test demonstration. The thermal and hardware design studies were described previously under Task II.

Task III of this effort study proposed the fabrication of two regeneratively cooled chambers (No. 1 and No. 2) for the Task IV demonstration firings. The chamber hardware fabrication procedure used is outlined below.

Thrust Chamber Fabrication Sequence

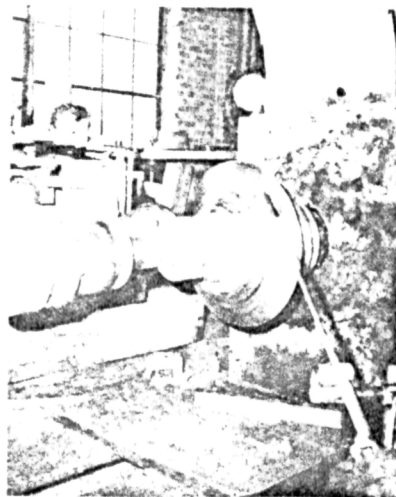
The overall fabrication procedure for the $\text{OF}_2/\text{B}_2\text{H}_6$ regenerative chambers is illustrated in Fig. 90. Upon receipt of the rough forging the internal and external contours were rough machined. This process was followed by inspection of the material for inclusions and oxides in the wall. Following this inspection, the liner was detailed with the final internal/external dimensions and machined coolant channels. The liner was then prepared for electroforming, and an electroformed nickel strike was applied, followed by a buildup to 0.10 inch nickel thickness. In final assembly the coolant manifolds were TIG brazed into place, and the assembly flow checked for channel flow uniformity and to ensure against coolant channel plugging.

Liner Material Selection and Procurement

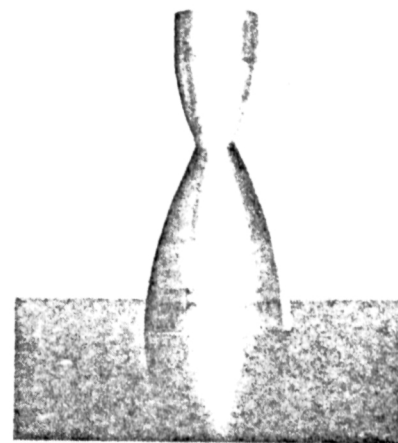
Procurement of the OFHC copper liner for the No. 1 and No. 2 chambers was made by obtaining a rough 1 inch thick wall hollow forging of double conical shape representing the combustor and nozzle regions. Selection of this manufacturing approach for the raw copper stock was made after consideration of



Forged Copper Material



Rough Machining



Contoured Liner



Slotted Liner

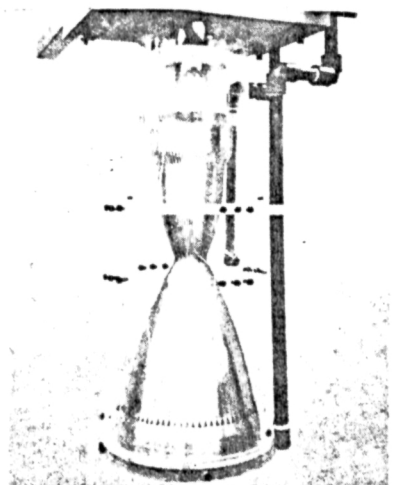
Liner Prepared For
ElectroformingNickel Electroformed
(Initial 24 hr. strike --
Final 7 day plating)

Figure 90. OFHC Copper Liner Fabrication Sequence.

the material cost and wall structural properties required for this low pressure application. Normal processing of higher strength materials is accomplished on chambers of this milled channel type by lathe hot form spinning of the material from a hollow disc shape forging over a center mandrel to the final combustor and nozzle shape.

Selection of the OFHC copper wall material was made considering candidate high conductivity high strength copper alloys of NARloy-Z (copper silver alloy), Beryllium (10) copper alloy, and Zirconium (Amzirc) copper alloy. Alternate non-copper wall materials considered were nickel (200) and stainless steel (347 CRES). Selection of the copper/copper alloys over the nickel and stainless steel alloy was made on the basis of obtaining a very low wall temperature ≈ 600 F maximum (with high thermal conductivity) and the best heat transference to the backside of the B_2H_6 cooling channels to provide the required heat input to the OF_2 simulated coolant (water jacket). The design has a heat input distribution representative of the OF_2 vaporization heat input for a final flight configuration. Moreover, since high strength properties were not necessary for satisfactory low test pressure operation, the choice of the higher conductivity OFHC copper was made.

Upon receipt of the rough thick wall forging, inspection of the material for voids and oxide inclusions was accomplished by detailed ultrasonic inspection of the forgings. Acceptance of the material was based on the Rocketdyne materials specification RB0170-49 for voids and inclusions. Inspection showed the forgings to be void and inclusion free.

Liner Contour and Channel Machining

Outer and inner wall contours (No. 1 and No. 2 chambers) were machined to print dimensions using good conventional lathe equipment to provide the required drawing accuracy (Fig. 91). Internal and external wall contour templates were made and trace machined onto the copper liners. Visual inspection was provided at this point in the fabrication to ensure surfaces free of

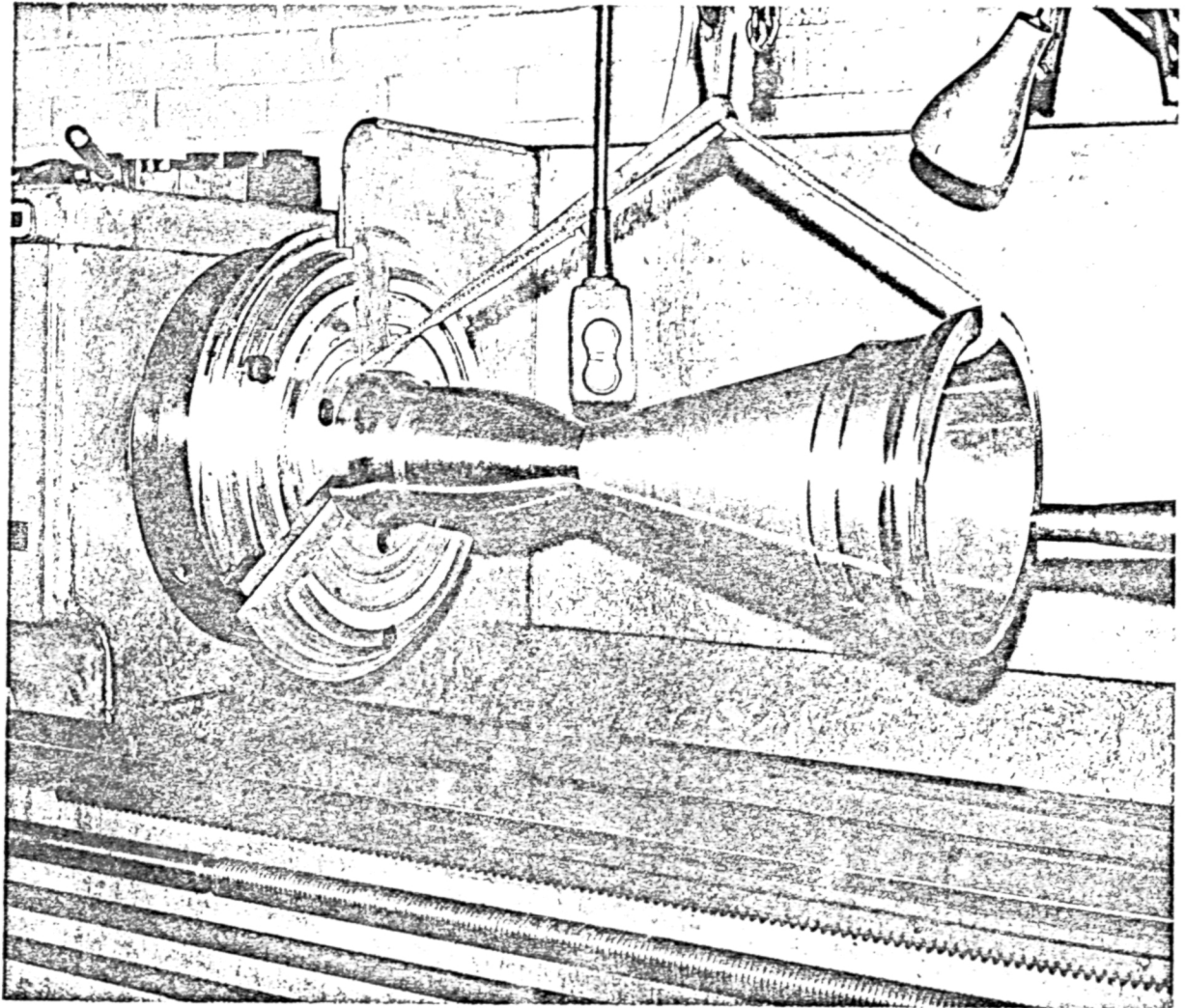


Figure 91. Internally and Externally Contoured Nozzle.

machining blemishes for good electroform nickel buildup on the channel back wall and for good gas side surface heat transfer coefficient characteristics.

Channels were machined into the liners employing .040 inch width slitting saw cutters (Fig. 92) turning at a high speed to ensure proper surface finishes at the base and sides of the channel. Inspection indicated the surface finish to be between 15-40 RMS surface finish. Selection of the 90 cooling channel design was made as a compromise (thermal optimum at 100) on the basis of lathe indexing and division to assure equal land widths. Two pass machining of each channel was employed with the combustor to throat machined first followed by the nozzle section machining (Fig. 93). This approach was employed to assure proper channel dimensions in the throat region where the wall contour radii are small. For flight design configurations single pass cutting operations would be employed unless channel step width changes or branching are employed in the nozzle section. Chamber inside and outside dimensioning and channel dimensions were checked and determined to be at the nominal of the tolerance bands.

Liner Electroform Preparation

The liner was prepared for the nickel electroforming process as shown by the electroforming sequence flow diagram outlined in Fig. 94 . Careful inspection was provided prior to bath immersion to ensure uniform growth of the nickel plating since any small surface discontinuities (mars, scratches, nicks, etc.) would have resulted in non-optimum plating at these discontinuity points. Rigidax filler was applied in the channel passages to provide a base over which the plating occurs. Extreme care was also taken at this process point to ensure that uniform plating bonding occurred over the full land width.

The electroforming portion of the fabrication sequence took approximately a one week period (120 hours) after which final machining and manifold assembly was accomplished. Intermediate machining was not necessary during the plating period since nonuniform growth was not noted in the plating bath on either the No. 1 or No. 2 chamber. Figure 95 illustrates the liner shielding.

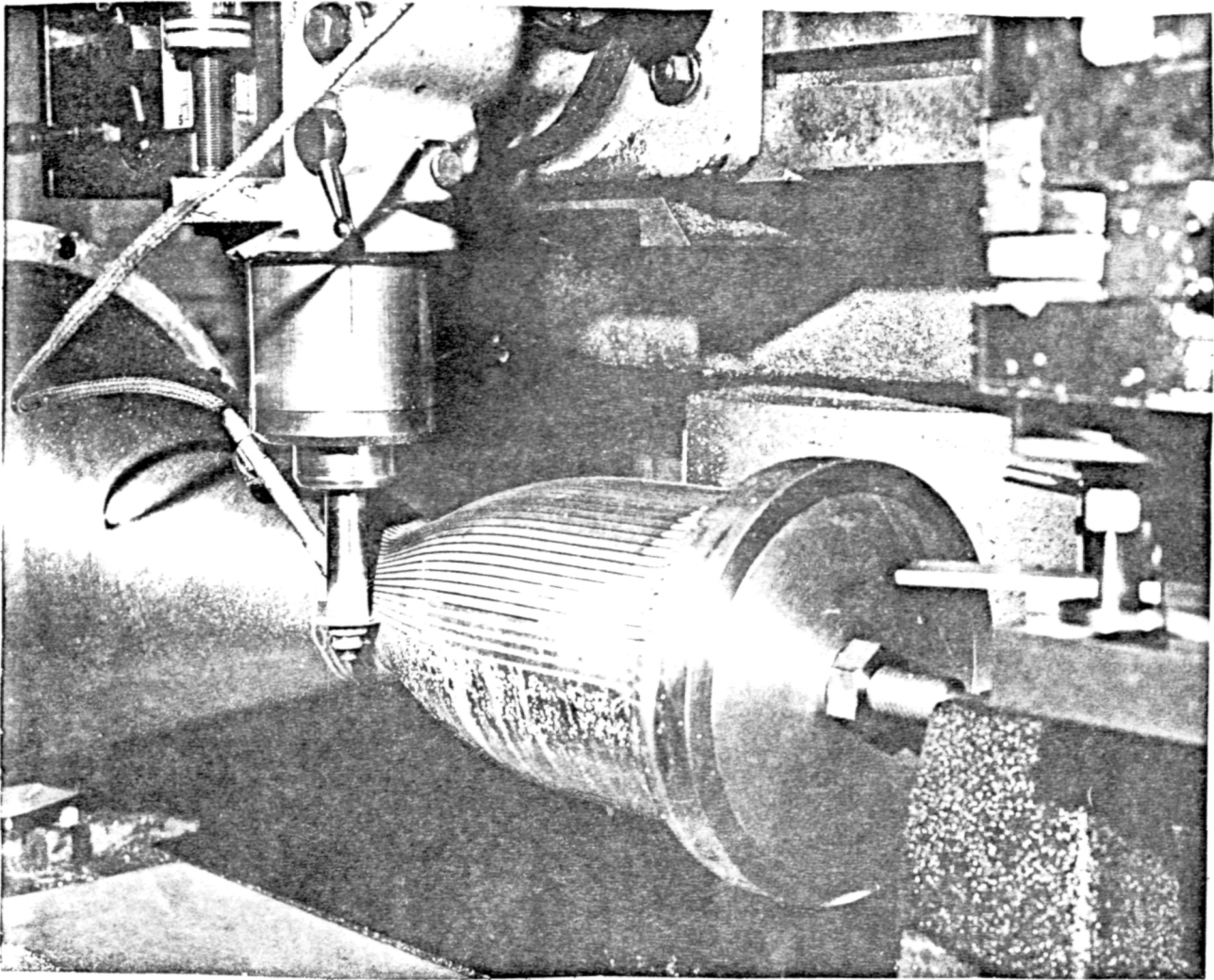


Figure 92 . Combustor Region Channel Passage Machining.

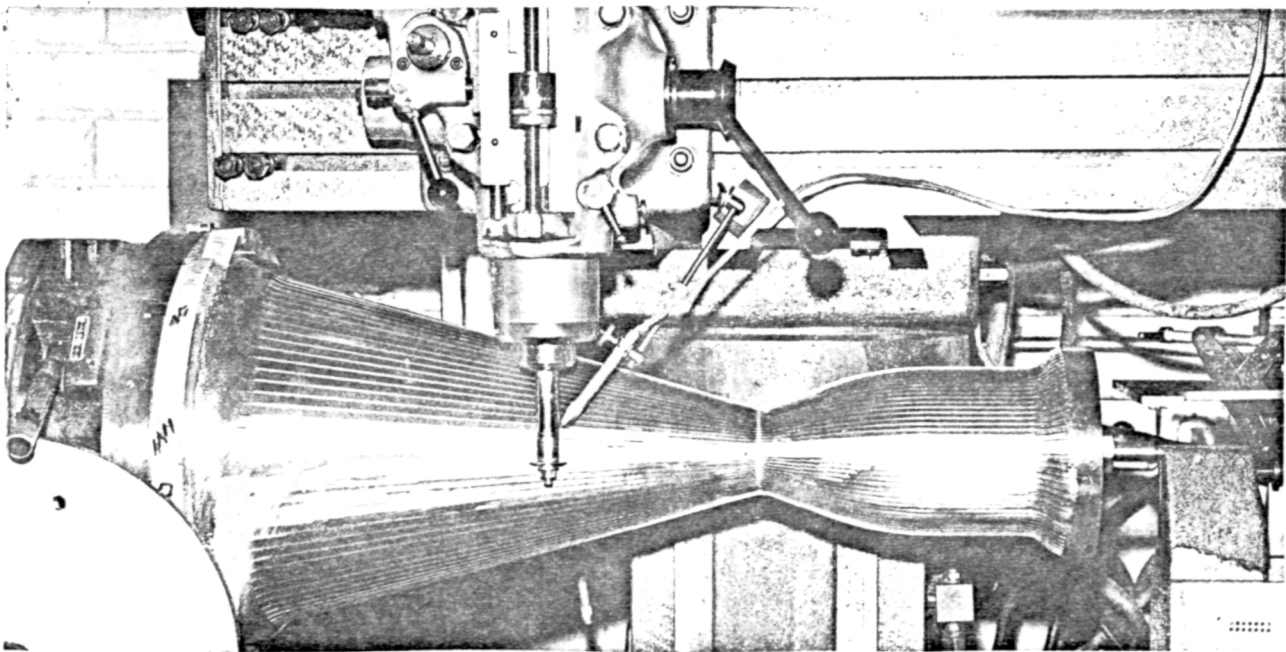


Figure 93 . Nozzle Region Channel Passage Machining.

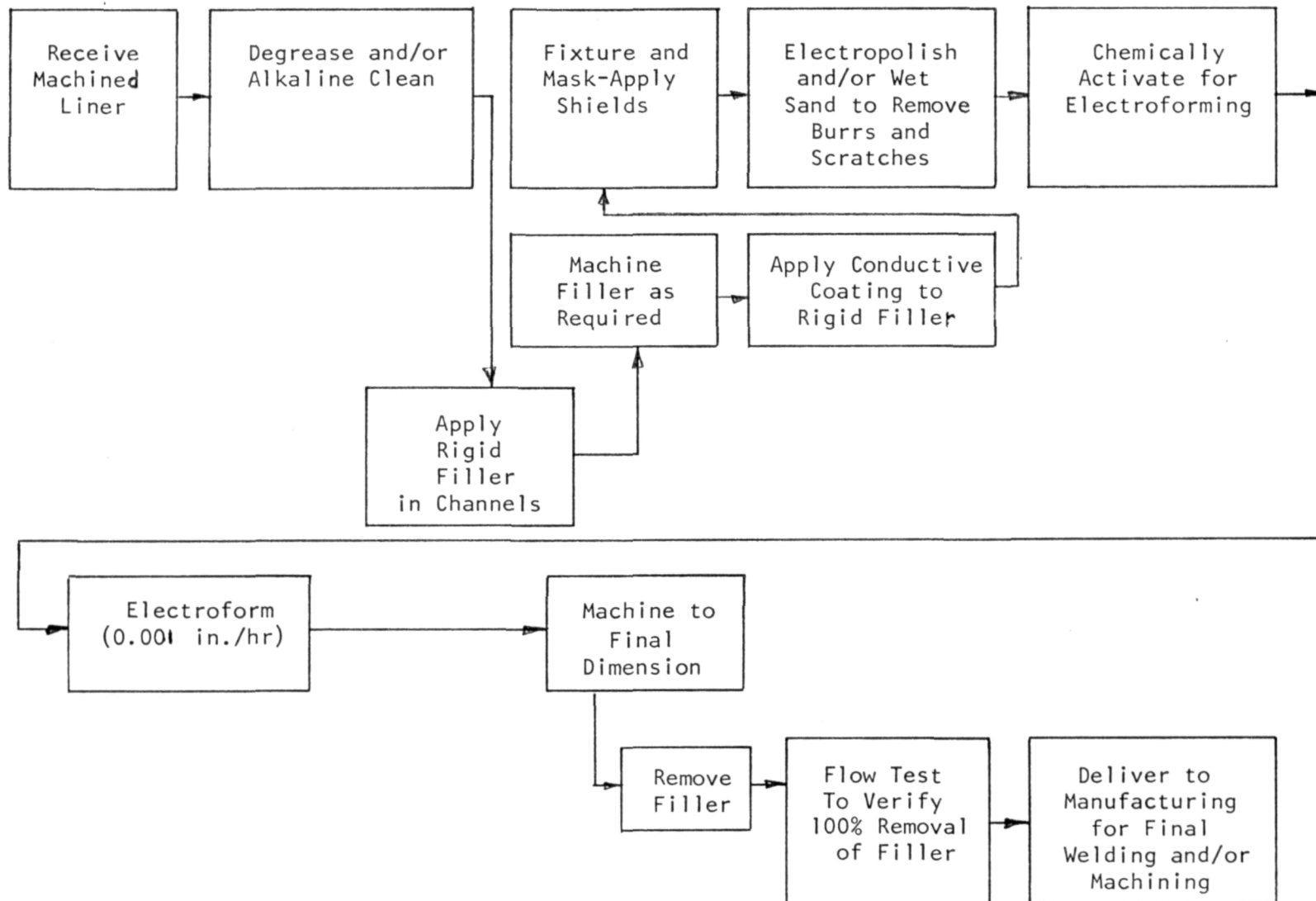
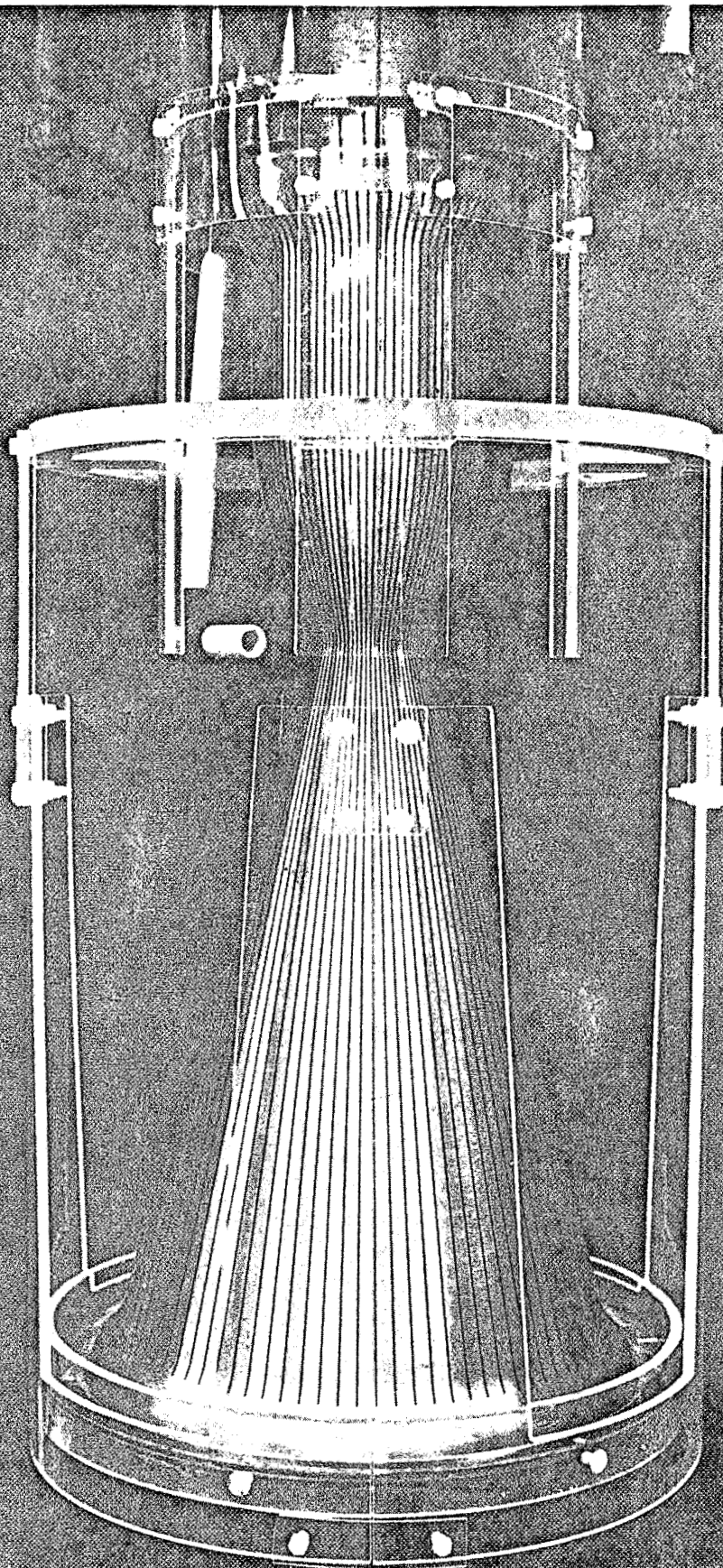


Figure 94. Typical Electroforming Sequence



 **Rocketdyne**
North American Rockwell
6633 Canoga Ave. Canoga Park Calif 91304

1XZ32-5/27/71-C1*

Figure 95. Machined Liner Prepared With Electroform Shielding Prior to Immersion Into the Nickel Bath for Plating.

The liners were provided with an initial 24-hour plating which established a closure (.024 inch) over the cooling channels. Upon removal for intermediate inspection, a satisfactory uniform nickel buildup was noted. The parts were surface prepared and then returned to the plating bath for final nickel buildup to a .100-inch thickness. Analysis of the completed electroformed nickel closure on the No. 1 unit indicated a satisfactory buildup with a greater than required thickness in the large diameter nozzle and combustor regions. Minor readjustment of the electroform shield tooling was accomplished to assure a more nearly equal plating rate for the large and small diameter portions of the No. 2 chamber. Figure 96 illustrates a completed electroformed liner.

Machining the electroformed nickel jackets for attachment of the manifolds and the double panel simulator then followed. The liners were contour machined with a template which matched the water jacket contour. Figure 97 illustrates a completed machined liner. Identical machining of the electroformed nickel jacket (including attachment points of the manifolds and the double panel simulator) allows either chamber to be fitted with the water jacket (.040-inch gap) for providing a sufficient H_2O velocity (30-40 ft/sec) for backup cooling. Provision was made for either chamber to be converted later to OF_2 backup cooling with an electroplated Ni milled channel structure.

The chamber machined assemblies were processed through the Rigidax removal phase. For this step previous experience derived from other programs was utilized. The Rigidax removal from the coolant passages followed the below listed procedure:

1. Bath vapor degrease with perchloroethylene
2. Liquid flush wax removal in perchloroethylene
3. Acetic acid ultrasonic cleaning
4. Distilled water flush
5. Distilled water-methyl alcohol flush

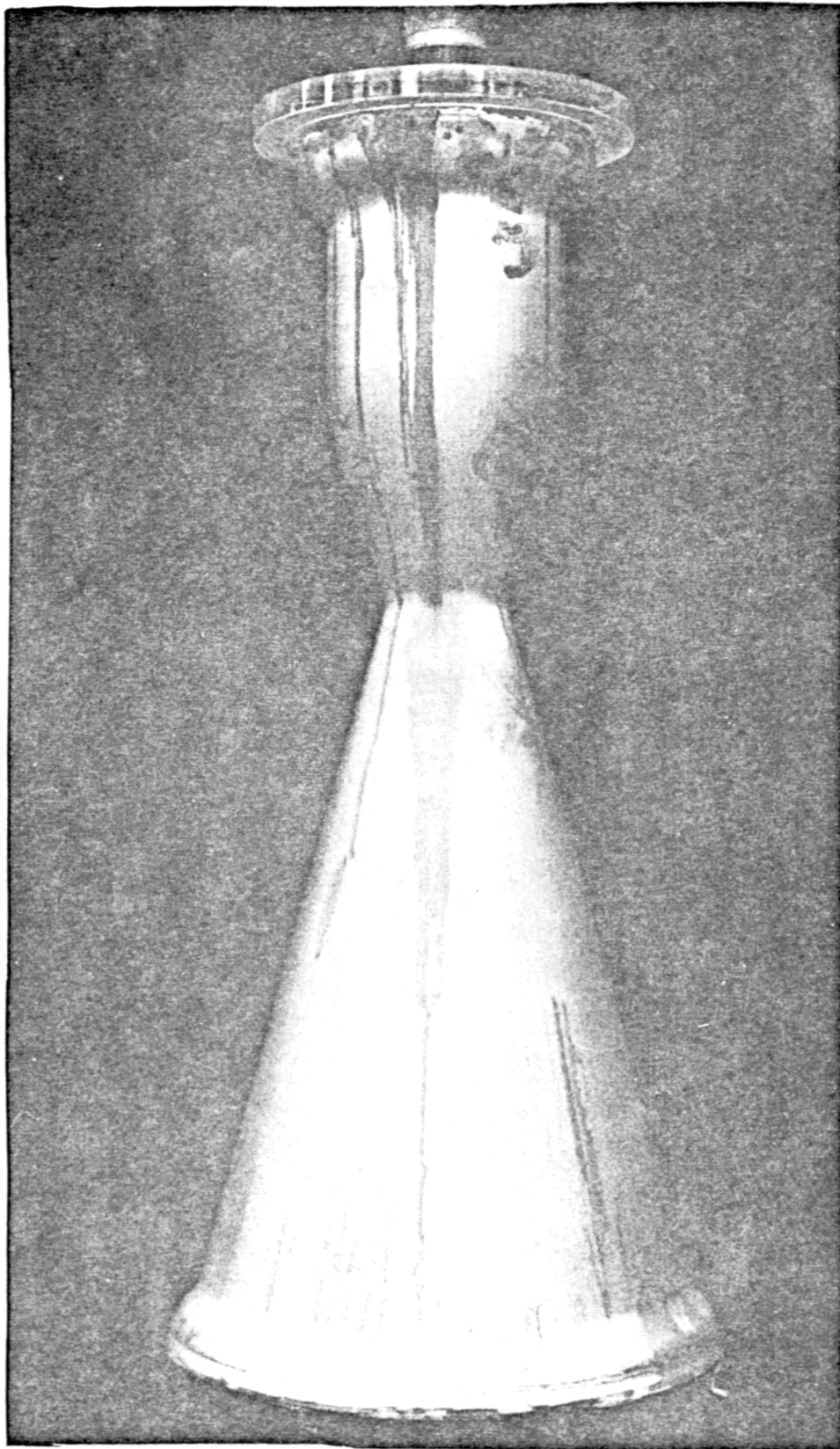


Figure 96. Regenerative Liner No. 1 With Channel
Closeout Nickel Plating.

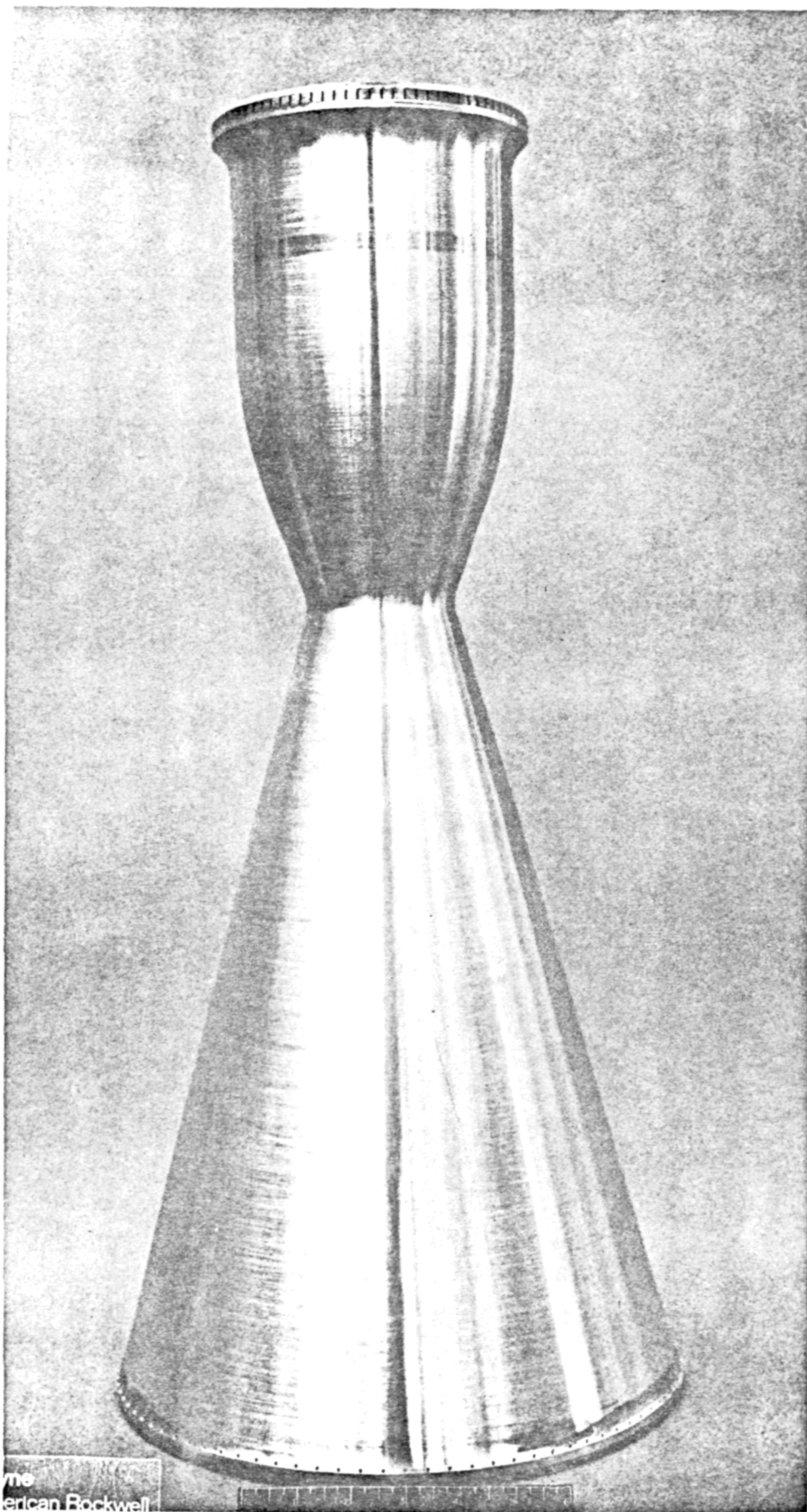


Figure 97, Machined No. 1 Regeneratively Cooled Thrust Chamber Prior to Manifold Attachment.

6. Individual channel passage water flow check for flow uniformity
7. Oven drying at 150 F

Flow checking of each thrust chamber was provided to ensure each passage was open and had an equal flow discharge.

TIG brazing of the lower and intermediate coolant flow manifolds to the thrust chambers with Palniro 7 alloy (palladium-nickel-gold) with a 1900 F melting point was employed to join the CRES manifold sections to the nickel electroformed material. Previous good success had been demonstrated with this joining method. Difficulty however occurred in brazing with this alloy on chamber flanges due to joint braze shrinkage cracks. Rework of these joints by brazing with BT alloy at a lower (1500 F) temperature was accomplished. The No. 2 chamber upper manifold was subsequently brazed using this revised BT procedure without difficulty.

Machining of the water jacket assembly for the combustion chamber was completed with final match machining to the completed electroformed chamber to assure a close fit. Final water jacket assembly with installation of the wall thermocouples was completed at the PRA test facility. Figure 98 illustrates an intermediate machining operation on this assembly.

Entrance/Exit Manifolds

Machining for the split ring nozzle exit manifold and the injector end manifold was accomplished. The manifolds were of 321 CRES alloy for ease of attachment to the electroformed nickel channel closeout. The three piece nozzle exit manifold was TIG welded together with 18-8 weld rod and both manifolds were to be TIG brazed to the electroformed nickel closure with BT (1400 F) braze alloy. A comparatively low temperature braze alloy was selected to ensure the least distortion at the weld affected area and the minimum differential thermal expansion of the nickel and 321 CRES materials during welding. Final brazing of the manifolding was accomplished subsequent to the electroformed nickel final machining operation.

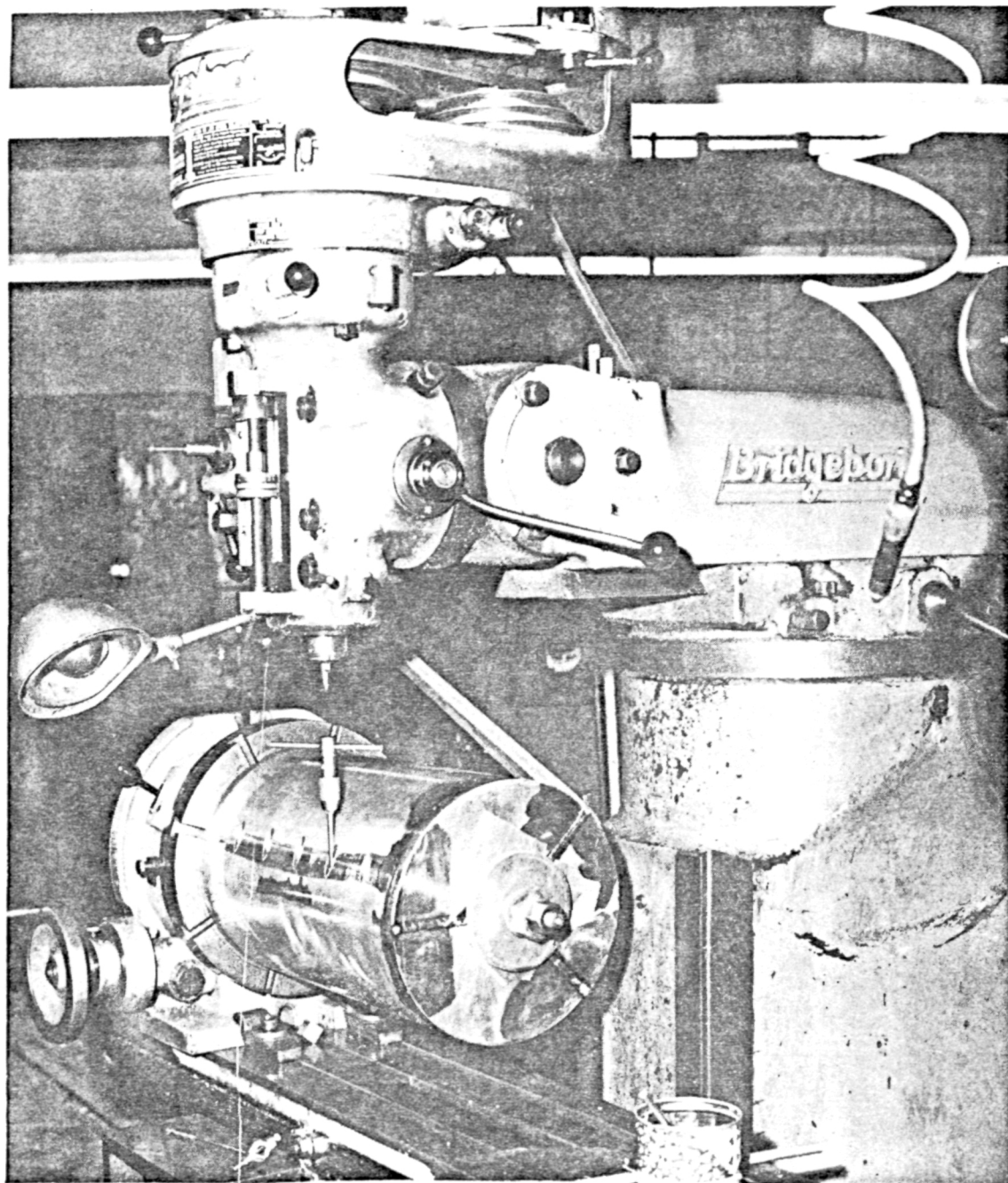


Figure 98, Water Cooled Jacket Assembly Closure
Machining Operation

Water Jacket Assembly Fabrication

Fabrication was completed on the three piece water jacket assembly which is interchangeable between the No. 1 and No. 2 regenerative chambers. Figure 7 illustrates the installed assembly schematic. Removability was accomplished by providing an aluminum two piece clamshell with a concentric tube shell which is slipped into place and bolted to the chamber forward manifold. Sealing against water leakage is provided by rubber O-ring seals at the inlet and exit manifold locations. The internal contour dimension of the aluminum clamshell section was match machined to the electroformed nickel No. 1 chamber. The No. 2 chamber was machined identical to the No. 1 chamber external contour for interchangeability of the water jacket.

The No. 1 chamber was assembled as shown in Fig. 99 and 100 and shipped to the PRA test site for final wall thermocouple installation.

Regenerative Chamber Instrumentation

During test operation of the regeneratively cooled chamber, evaluation of overall coolant flows, inlet and outlet pressures, and coolant temperature rise values was accomplished. Additionally, the unique construction of the water jacketed regenerative chamber allowed for provision of open tip thermocouples to be attached onto the electroformed nickel skin both underneath the water jacket and on the exposed nickel supersonic nozzle surface.

Chromel-Alumel thermocouples were attached with the open tip junctions welded to the nickel surface. With these back wall temperature measurements together with analytical two dimensional conduction thermal analyses, the wall temperatures and heat fluxes were deduced. Table 12 lists the location of the back wall measurements.

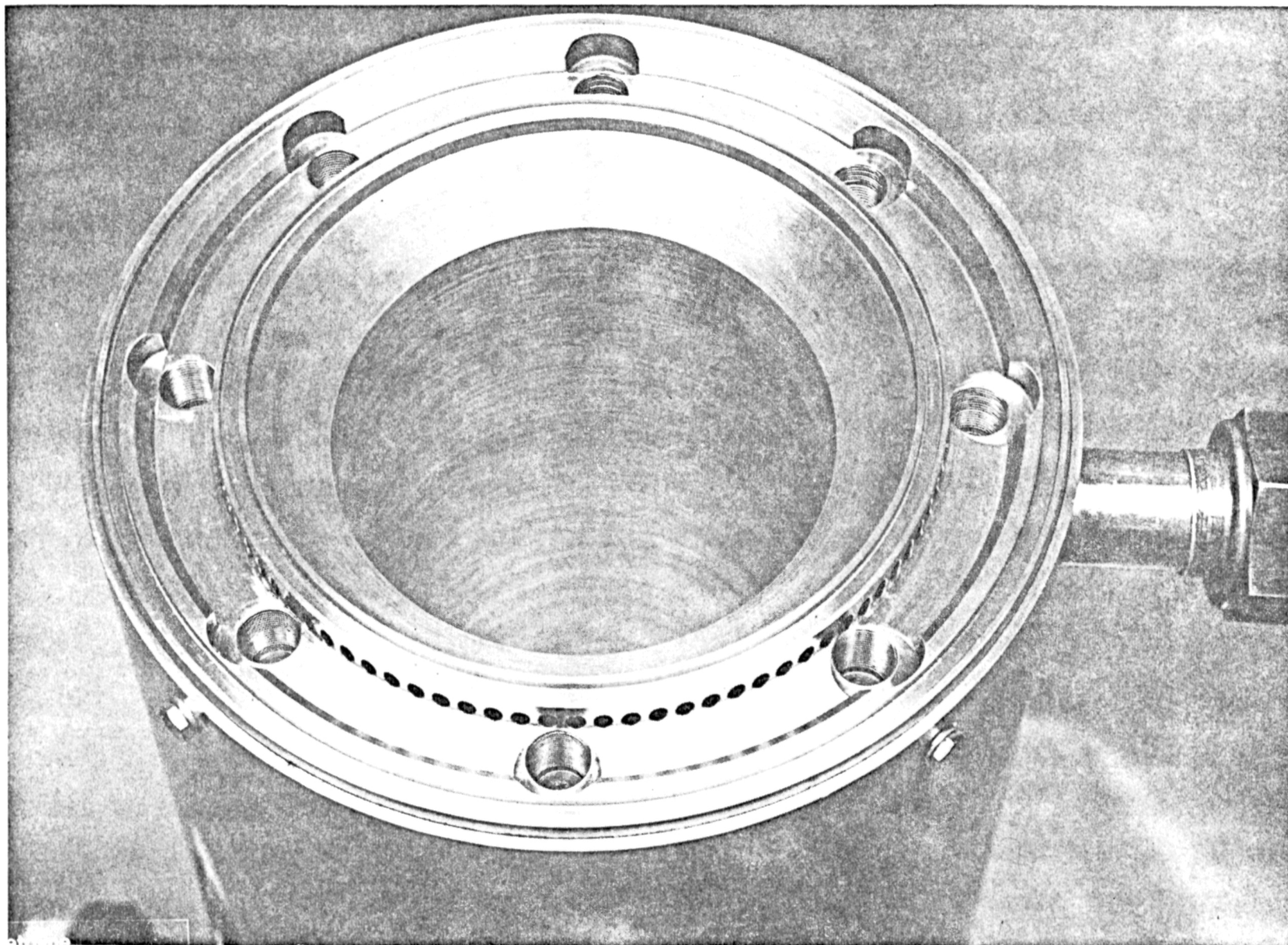


Figure 99. Thrust Chamber Assembly End View Illustrating Coolant Passage Discharge Porting

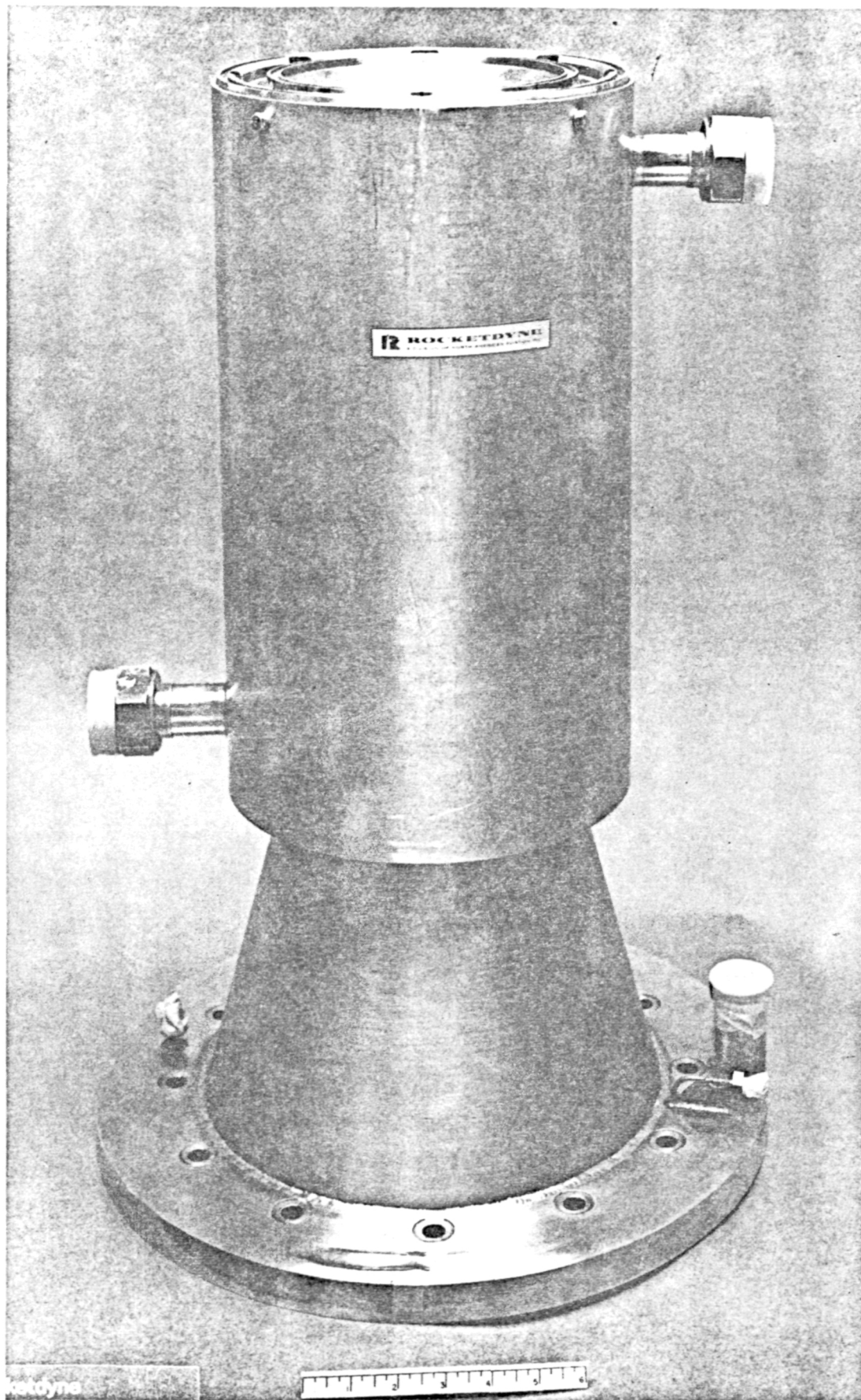


Figure 100. Final Assembly of No. 1 Thrust Chamber with Auxiliary Water Cooling Jacket Installed

TABLE 12. SUMMARY OF BACK WALL THERMOCOUPLE MEASUREMENT
LOCATIONS FOR $F_2/O_2-B_2H_6$ REGENERATIVE CHAMBER

Thermocouple	x Location (in.)	Area Ratio
TN-1	--	6.9
TN-2	--	9.2
TN-3	--	12.4
TN-4	--	14.2
TC-1	-6.0	4.0
TC-2	-3.0	3.0
TC-3	0.0	1.0
TC-4	+3.0	2.5

TRIPLET INJECTOR (NO. 2) FABRICATION AND ASSEMBLY

During Task III study fabrication was initiated on the No. 2 triplet (fuel-oxidizer-fuel) injector as part of the fabrication effort. Triplet injector No. 2 was planned for use in the calorimeter/regenerative chamber testing for Task IV study.

Injector Features

The triplet injector No. 2 designed was a gas-gas triplet design with a 96 element pattern (thrust per element = 10 lb) supplemented by 80 peripheral face boundary layer coolant showerhead orifices. A face pattern detail is shown in Fig. 101. For the control of the wall heat flux and total integrated heat load along the combustor, a nominal 8 percent (of total flow) film coolant was employed.

As for the previous No. 1 triplet design, a copper ring injector brazed with a CRES body was employed for uniform face heating characteristics. Improved face heating characteristics were expected with No. 2 design by an increased oxidizer velocity ($\Delta P_o = 40$ psi compared to 20 psi previously). This is accomplished by a reduction in the oxidizer orifice diameter to .098 inch from the previous .116 inch diameter. It was proposed that the higher oxidizer velocity through the injector face would result in greater face convective cooling. Additionally, it was anticipated that the combustion process would be moved downstream by the higher oxidizer velocity, tending to reduce face heating rates and injector face deposition rates.

For the No. 2 triplet injector, acoustic cavities were not incorporated initially, however the capability for their addition by machining was provided during calorimeter testing on Task IV study. The initial decision to not provide acoustic cavities was based on the lack of any evidence of an acoustic instability to that date (as recorded by chamber mounted accelerometers), coupled with some previous adverse combustion deposit accumulations in this cavity area noted during previous testing on Task II. It was

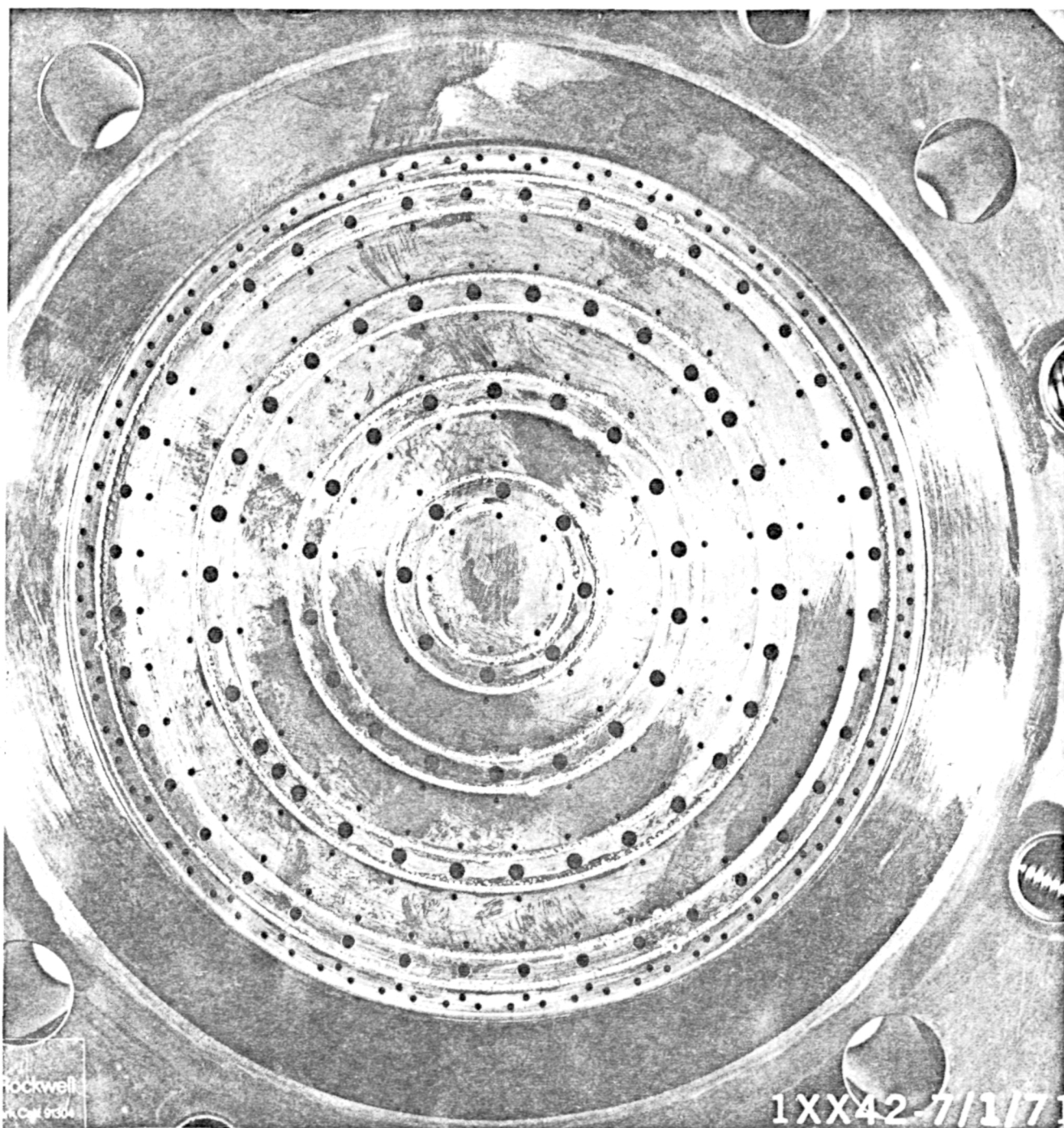


Figure 101. Triplet No. 2 Injector Face Detail of Assembly Post Second Braze Cycle.

7

anticipated that no detrimental effect on the boundary layer coolant streams would be incurred as a result of the lack of the acoustic cavity apertures.

New fuel inlets to the injector from the B_2H_6 regenerative jacket and better uniformity of feed to the injector face were accomplished by reducing fuel velocity conditions in the injector body. For the No. 2 injector, the capability for regenerative cooling was added by incorporation of added feed passages from the regenerative chamber channel passage outlets into the injector. This feature was illustrated in Fig. 87. Checkout of this No. 2 triplet injector was accomplished in the calorimeter heat sink chamber prior to regenerative testing during Task IV to be described later.

Review of the JPL combustion stability test results with oxygen/ethylene propellants on an injector identical to the No. 2 unit, which indicated stabilizing effects of the acoustic cavities, was made. Based on these JPL test results chamber photocon pressure instrumentation was employed on the No. 2 triplet checkout test phase in the calorimeter chamber to reveal any combustion instability. Stability problems encountered during Task IV test study led to subsequent machining of the cavities in the injector body.

Triplet No. 2 Fabrication

Fabrication improvement for the injector was provided to assure accurate ring and body alignment through multiple alignment pins. This approach was used to assure accurate orifice impingement on the finished injector assembly. The unit was brazed in a face-up position with slightly excess braze alloy to assure a single braze operation success. Some difficulty in initial brazing of the assembly with Nicoro alloy necessitated a second braze cycle on the No. 2 injector with a Nicro braze alloy at reduced melting temperature (1742 F). Two locations appeared to have insufficient braze fill; one located on the oxidizer dome portion as shown in Fig. 102 and the second in a ring-to-land joint on the injector face side. The second braze cycle, however, eliminated these bond voids and subsequent pressure check showed no joint leakage.

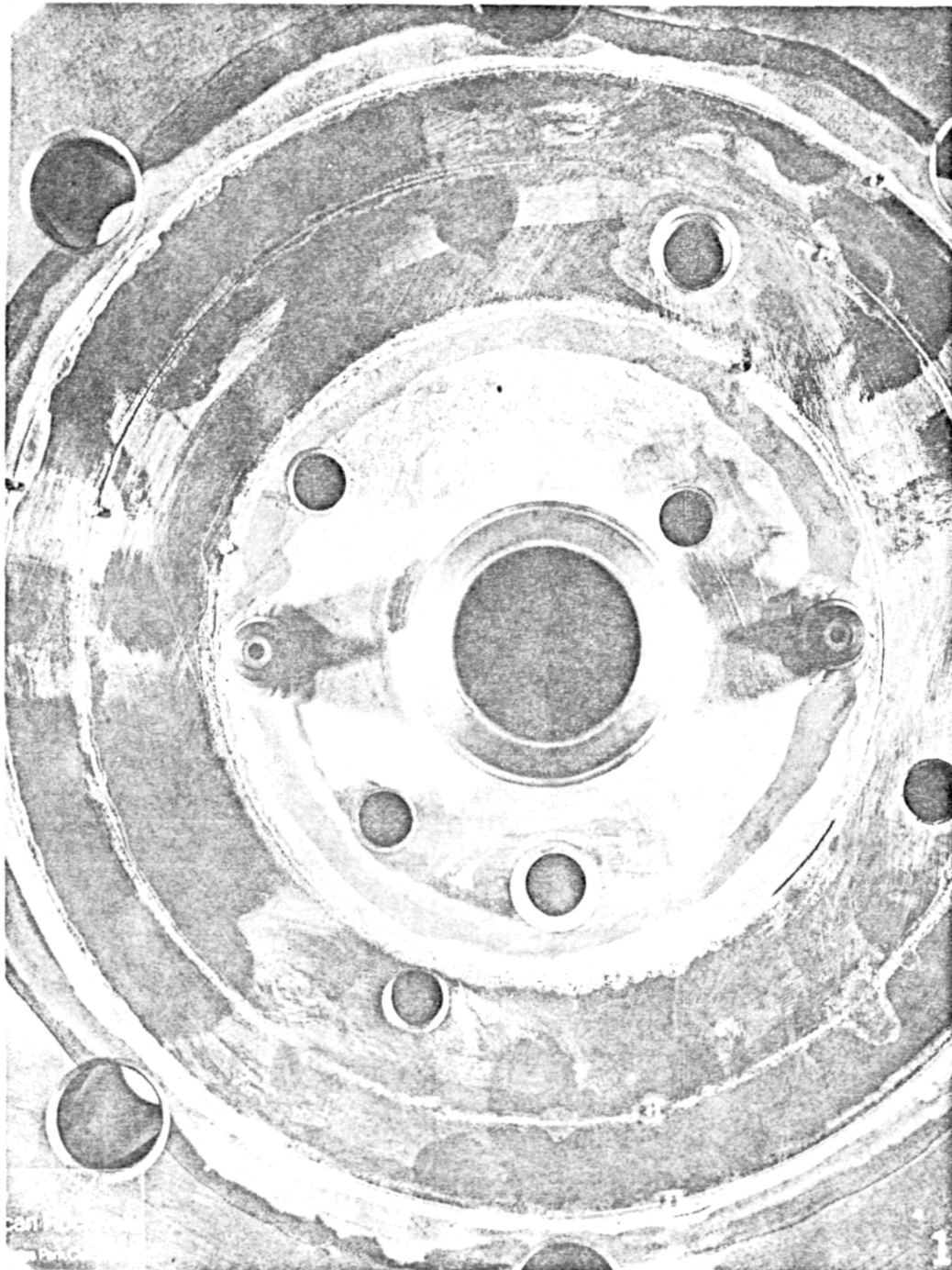


Figure 102. No. 2 Injector Illustrating Braze Void on Oxidizer Dome Closure Prior to Successful Second Braze Effort.

7

Plugging with excess braze in two fuel film coolant passages in the outer row and one oxidizer passage, which occurred during the second braze cycle, was removed by drilling and cleanup from the face side. Care was taken to ensure no residual drill chips within the ring feed passages. Final flow check of the assembly was accomplished prior to shipping to the test facility. Fuel side (Fig. 103) and oxidizer side (Fig. 104) discharges during water flow indicated good orifice alignment and stream flow.

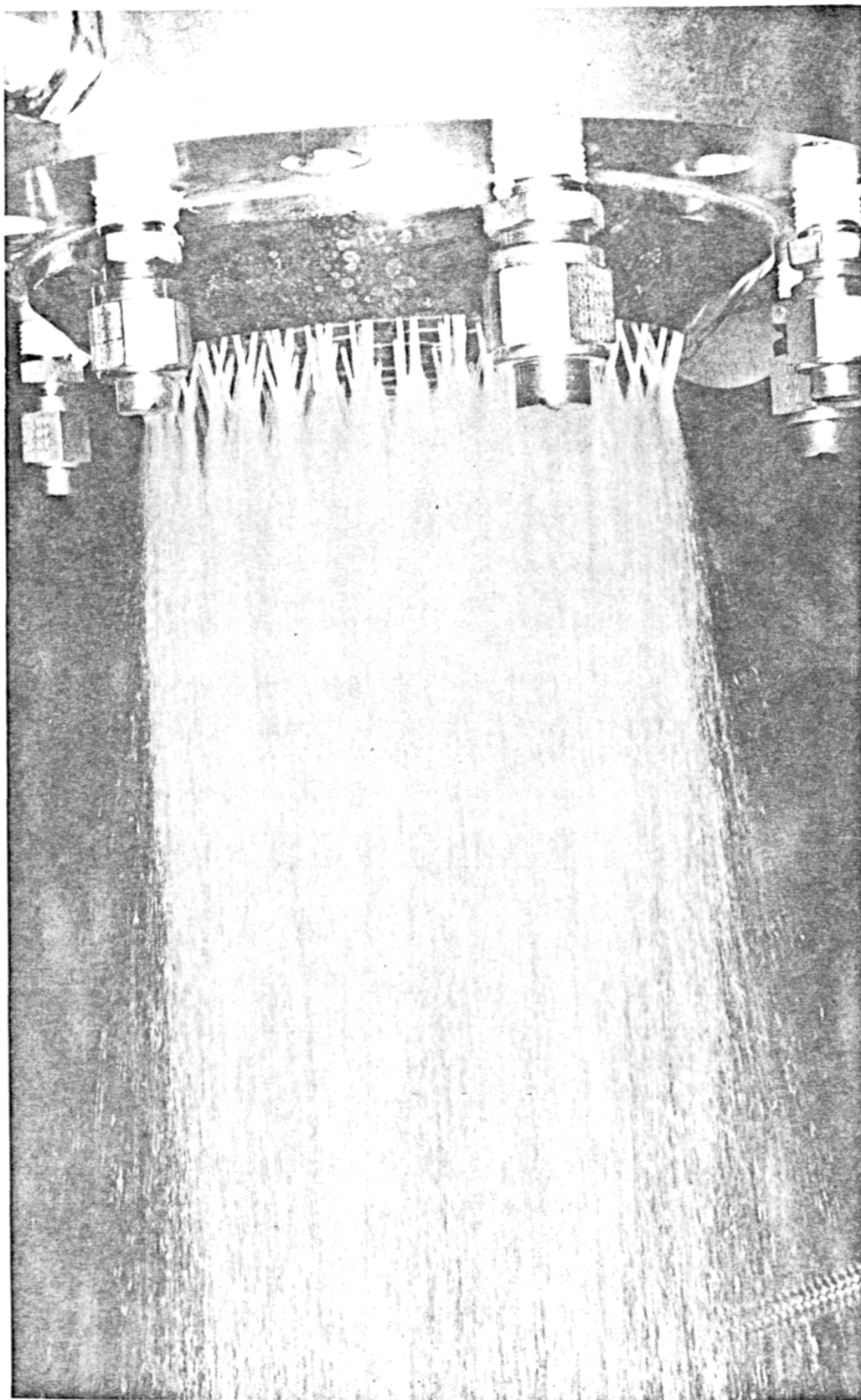


Figure 103, Water Flow Testing on No. 2 Triplet
Injector-Fuel Side.

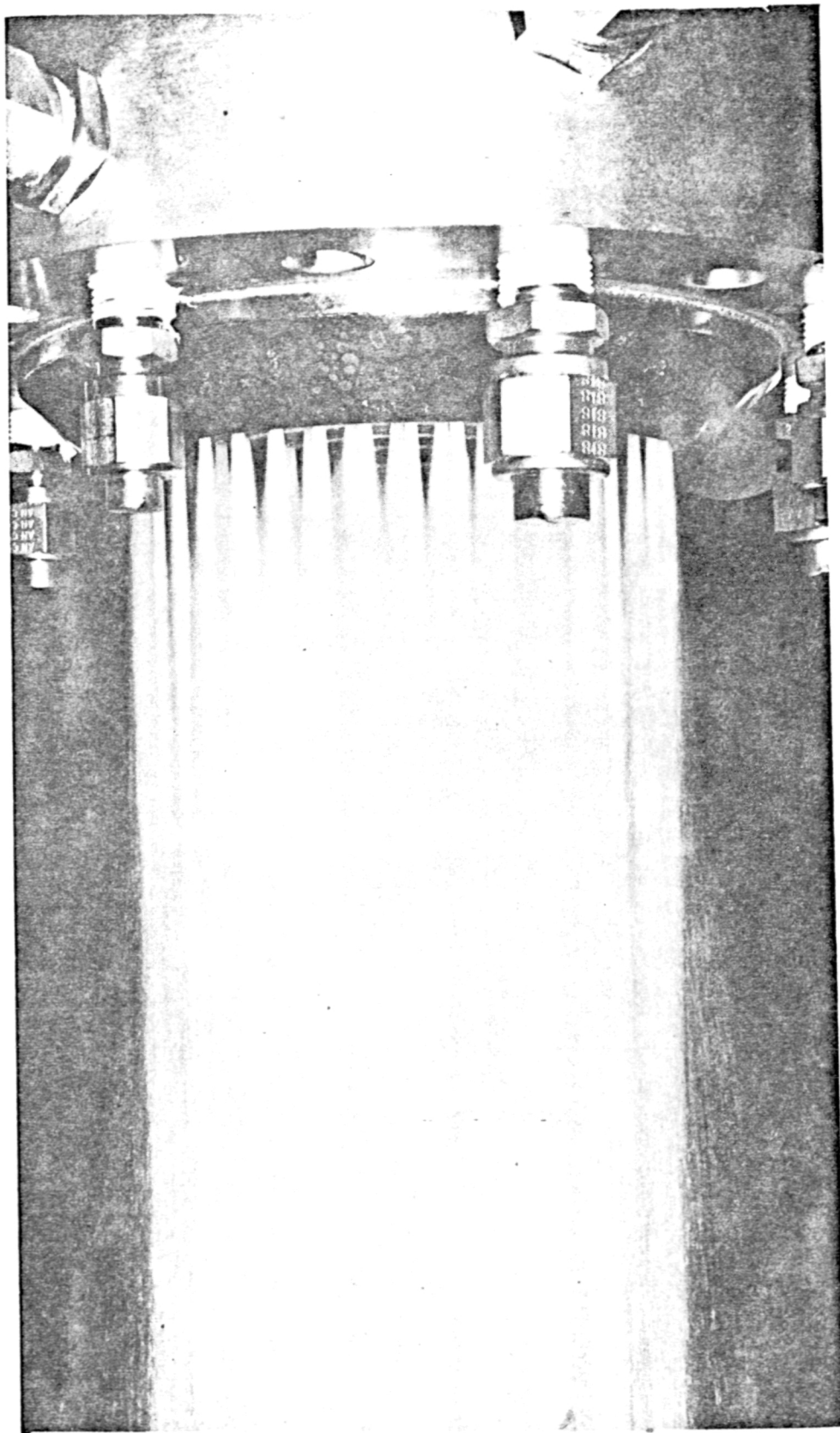


Figure 104, Water Flow Testing on No. 2 Triplet, Injector-Oxidizer Side.

CALORIMETER CHAMBER MODIFICATION

The copper heat sink calorimeter chamber (Fig. 105) which was previously used during Task II testing on this program to develop axial and circumferential heat flux profile data for chamber length, mixture ratio and boundary layer bias conditions, was reactivated preparatory to Task IV testing. To develop better capability for monitoring instability and high frequency chamber pressure behavior, the decision to install a high frequency chamber pressure transducer was made.

Modification of the uncooled instrumented heat sink copper calorimeter chamber to incorporate a high response photocon was completed with a 7/16-inch-diameter Model 306 high pressure water cooled photocon pickup located 1-1/2 inches downstream of the injector face. Additionally, three accelerometer pickups, with data to be recorded on the high response oscillograph, were installed.

The 20:1 area ratio uncooled calorimeter nozzle (Fig. 106) which was fabricated previously for hot fire testing was used with heat plug and nozzle pressure instrumentation, together with the copper chamber section and the injector assembly. Figure 105 illustrated the heat plug and pressure locations in the combustor, and Fig. 107 the nozzle instrumentation locations. Initial testing was to be conducted with the copper calorimeter chamber only without the altitude diffuser to establish face deposition characteristics and heating rates in the combustion zone. Visual inspections performed indicated multiple tests could be accomplished (minor face or chamber deposits).

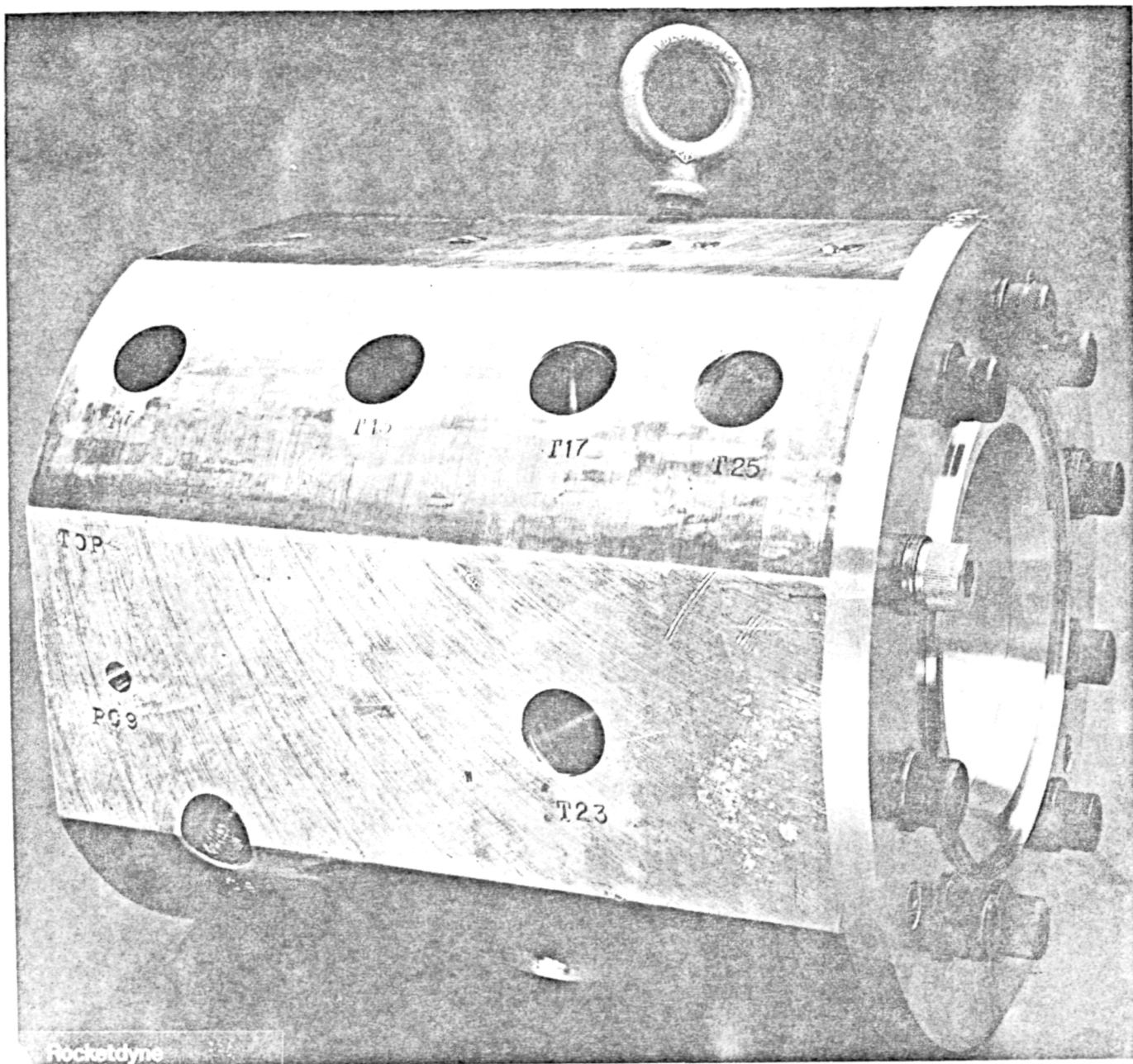


Figure 105. $F_2/O_2-B_2H_6$ Copper Calorimeter Chamber With
Recessed Temperature Plug Porting

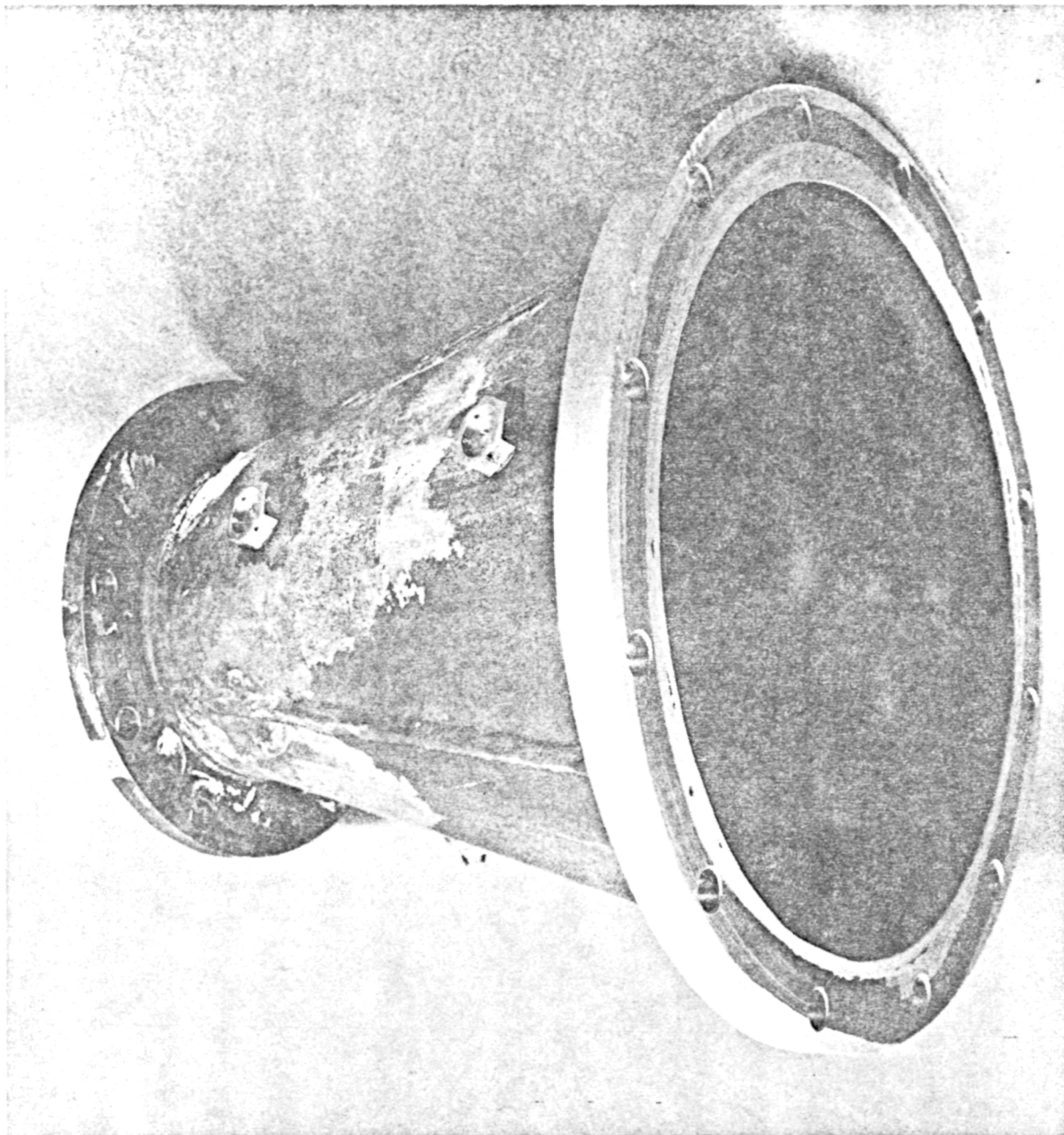


Figure 106, 20:1 Area Ratio $F_2/O_2-B_2H_6$ Nozzle Extension
with Temperature and Pressure Instrumentation
Ports

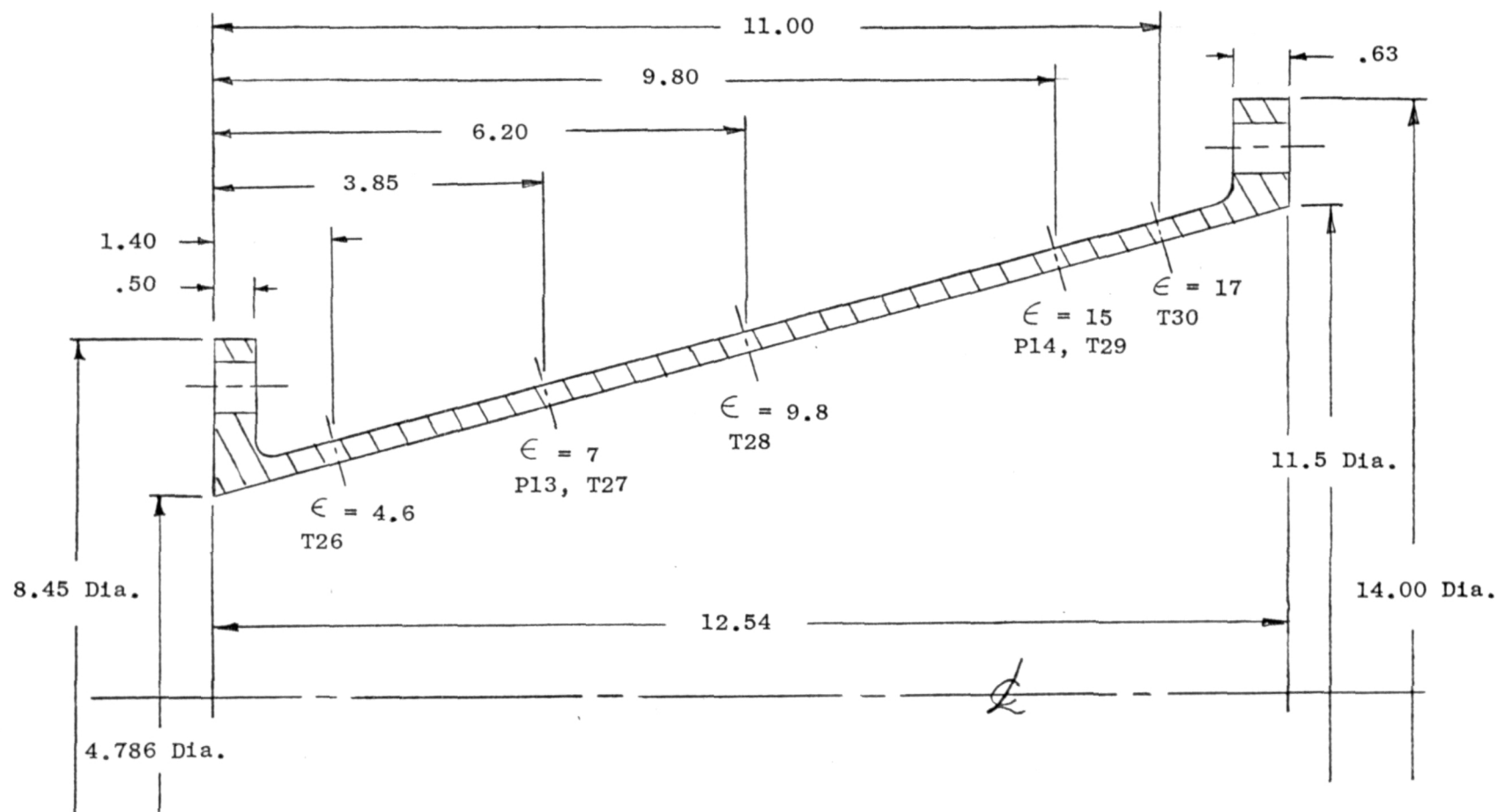


Figure 107. 20:1 Calorimeter Nozzle Extension Temperature and Pressure Location Summary

TASK IV - CALORIMETER/REGENERATIVE CHAMBER TESTING

Activity for the Task IV final demonstration test phase included the test stand preparation (Yoke Stand - Propulsion Research Area) of the feed system plumbing, the installation of the altitude diffuser together with its ejector pumping and water cooling system.

A series of system flow checks and sequencing for both the F_2/O_2 and B_2H_6 propellants were provided to establish propellant flow and timing. The specially built altitude diffuser was made operational during this task.

Blowdown testing of the No. 2 triplet injector with the modified feed system was satisfactorily accomplished with an inline H_2O heat exchanger to provide gaseous B_2H_6 propellant. This series was followed by Tests 004-008 on the uncooled calorimeter chamber to verify stability, performance and thrust chamber heat transfer.

Tests 009-017 were conducted on the regenerative chamber at a nominal mixture ratio of 3.0 and chamber pressure of 100 psia, culminating in a final 45 second test limited only by B_2H_6 propellant supply.

All primary planned objectives were met during this series.

TEST FACILITY PREPARATION - YOKE STAND (PROPULSION RESEARCH AREA)

Activity preparatory to Task IV testing included the installation of a high-pressure GN_2 hyperflow system, fabrication of a water cooled diffuser duct, design of the water coolant jacketing for the diffuser ejector system, design of the gaseous FLOX delivery system, and preliminary evaluation and design of the F_2/O_2 servo control system and the B_2H_6 liquid/gaseous feed system with inline heat exchanger.

Completion of the diffuser-ejector system, installation of the gaseous servo-controlled FLOX system, and B_2H_6 system installation and checkout of the two servo systems were accomplished upon completion of hot-fire testing a previous

(NAS7-767) contract effort on Yoke Stand at PRA. Modification to the B_2H_6 flow system for delivery of 100 F B_2H_6 gas, diffuser installation and check-out, and instrumentation setup and calibration was proposed.

Facility plumbing modifications for Task IV consisted of plumbing effort on the gaseous FLOX lines and servo system and plumbing of the liquid B_2H_6 line and liquid to gas heat exchanger. Chamber installation on the thrust mount (without the altitude diffuser) was accomplished upon completion of the feed system.

FLOX Feed System

Figure 108 illustrates the gaseous FLOX flow system utilized. A servo-control regulating the inlet pressure to the venturi allowed a tight control over the flow to avoid any decay due to tank pressure decay. A GN_2 purge system was provided downstream of the FLOX main valve to allow pretest and shutdown purging through the injector. This system was employed for both the calorimeter and regenerative operation during Task IV testing.

B_2H_6 Feed System

Figure 109 illustrates the feed system for the B_2H_6 flow. Liquid B_2H_6 was stored in 40 pound cylinders packed in dry ice. Prior to run operation, transfer from one of these cylinders to a 25 gallon run tank was accomplished through a fill valve with two in-line turbine flow meters to monitor the weight of B_2H_6 transferred to the run tank.

A methyl cyclohexane (MCH) jacketed recirculation line chill system was employed to maintain tank and line temperatures upstream of the turbine flowmeters. The MCH system is set to establish heat exchanger inlet conditions at -30 to -10 F with line pressure of about 450 psia. (Lower temperature levels were employed for the regenerative chamber inlet conditions.)

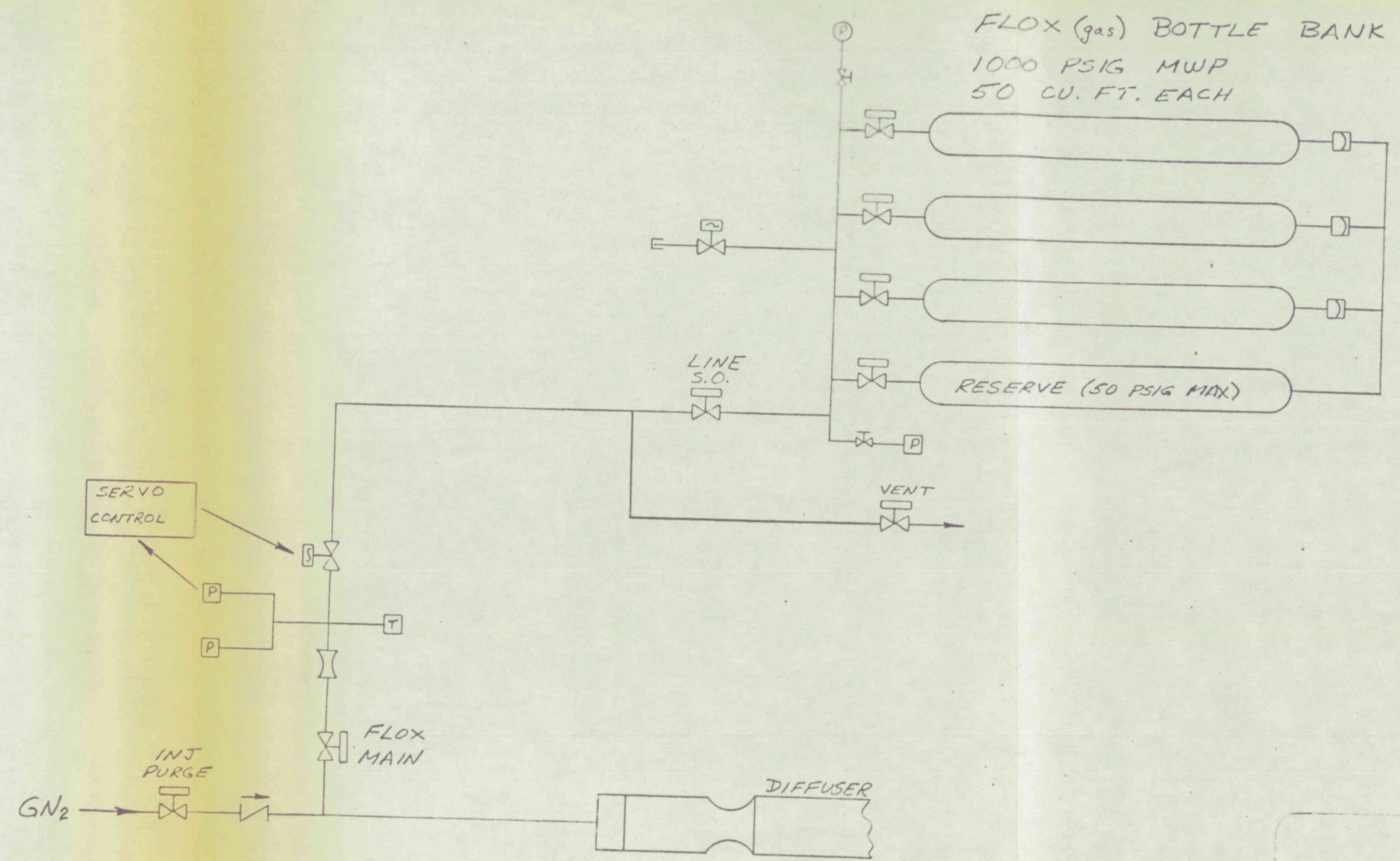


Figure 108, FLOX System Yoke Stand - PRA

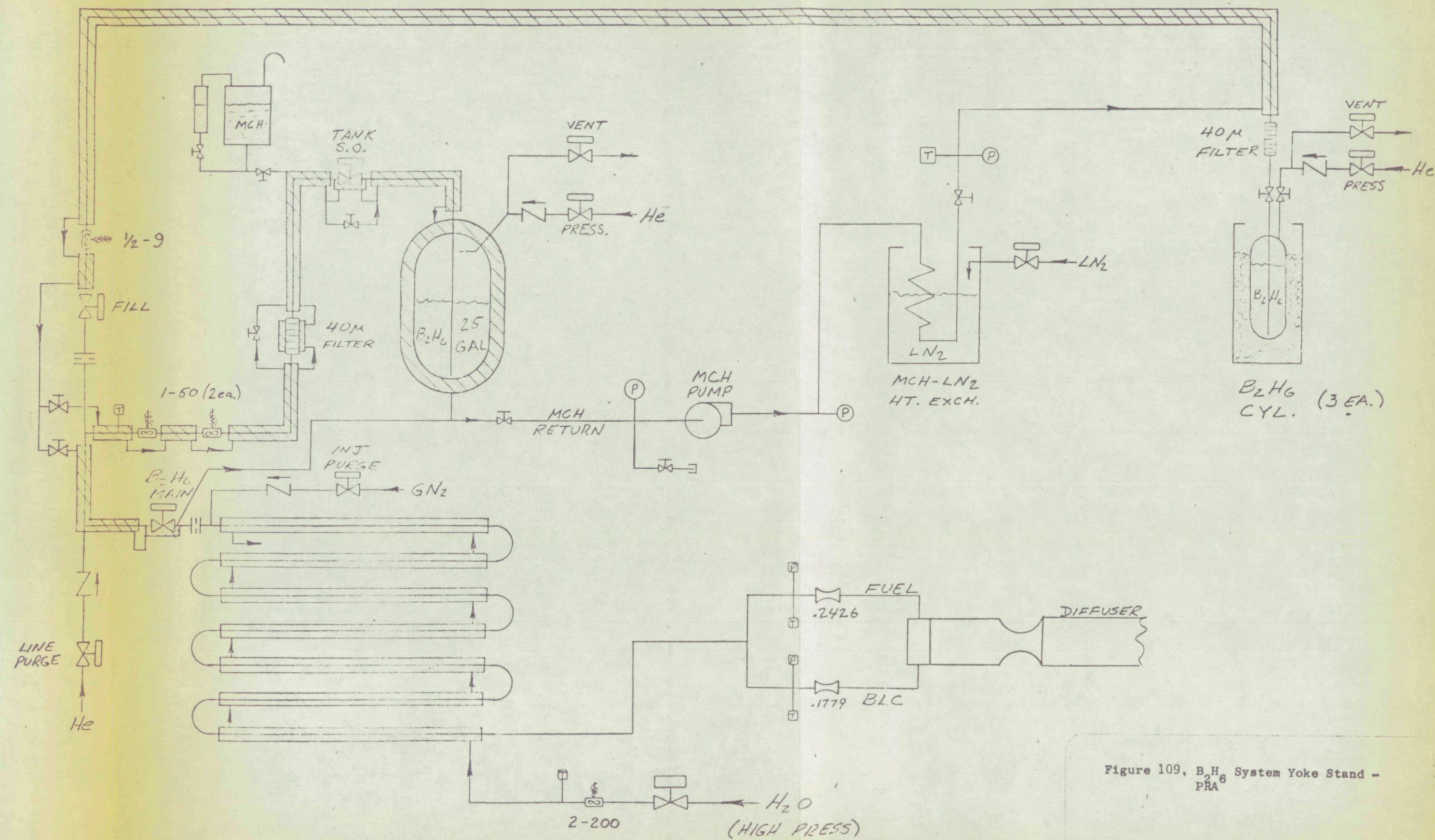


Figure 109, B₂H₆ System Yoke Stand - PRA

Two gas flow choked sonic venturis were provided at the heat exchanger exit for division of the boundary film coolant and main fuel flow. Interchangeable BLC venturis are available for varying the BLC to main flow ratio.

A GN_2 purging system was supplied through the heat exchanger and feed system for pretest and post-test B_2H_6 purging.

B_2H_6 In-line Heat Exchangers

A liquid B_2H_6 to H_2O heat exchanger provided, to elevate the B_2H_6 temperature to 65 F (with a phase change to gas from an inlet of -25 F), was constructed from 2 inch and 1 inch (.065 wall) concentric stainless steel tubing. Six 7 ft length sections were placed in series to provide an $L/D_1 = 604$ (inside surface area of 1370 in^2). A 40 lb/sec water flow at 90 F and 2350 psi tank pressure provided a low H_2O film drop on the water side. The estimated stainless steel wall ΔT was 18 F and 5 F (inlet/outlet) resulting in an available inlet B_2H_6 film ΔT of 97 F and at an outlet film ΔT of 10 F for an assumed 65 F B_2H_6 discharge temperature. Based on the previously derived film/nucleate boiling B_2H_6 data, the capability of the B_2H_6 was predicted to range between 0.3 to 1.0 $\text{Btu/in}^2\text{-sec}$. The heat transfer requirement for a 185 Btu/lb enthalpy increase (.61 lb/sec B_2H_6 flow) was .082 $\text{Btu/in}^2\text{-sec}$.

Initial blowdowns of B_2H_6 in this system indicated that the time response of the system was due to a large heat exchanger plus feed system volume. Additionally, it appeared that the predicted B_2H_6 film coefficient for the 1 inch diameter tubing was greater than experimentally achieved, since only a 16-20 F B_2H_6 outlet temperature could be attained.

A second in-line series heat exchanger was provided from two parallel 50 ft 1/2 inch (.049 wall) coils of copper tubing submerged in an electrically heated boiling (209 F) water bath. This was plumbed in series with the steel in-line heat exchanger and provided a 90-110 F outlet temperature. Blowdown tests indicated an excessive 7-9 second flow stabilization time. As a consequence to reduce the start sequence time, the steel in-line heat

exchanger was removed and the copper coil heat exchanger was changed from a parallel to a series arrangement. The resulting outlet temperature (80-100 F) and transient time (5 seconds) was satisfactory and this heat exchanger arrangement was employed for the uncooled calorimeter testing.

The in-line copper coil heat exchanger was removed for the regenerative chamber testing.

DIFFUSER INITIAL INSTALLATION

During the initial Task IV preparation time period, the altitude diffuser fabrication and installation including the water jacketing and installation of the ablative on the ejector driver section were completed. This was necessary to ensure diffuser capability for 75 seconds duration. Mounting of the diffuser to the chamber and supports was accomplished in such a manner as to allow diffuser support flexibility.

Diffuser Predicted Altitude Capability

Figure 110 illustrates the altitude diffuser provided to accommodate either the 20:1 area ratio calorimeter nozzle or the 20:1 regenerative nozzle. Analysis check of diffuser start and operation predicted successful operation should be attained with 58 lb/sec of ambient GN_2 secondary flow at a secondary chamber pressure of 575 psia. Reduction in the GN_2 flow and chamber pressure requirement with the augmenting effect of the combustor hot primary gases was expected to reduce the requirement of the ejector driver pressure to in the vicinity of 500 psia. The hysteresis effects of minimum start and minimum run ejector chamber pressure were to be established during the calorimeter test series to determine any GN_2 flow supply marginality for long duration operation.

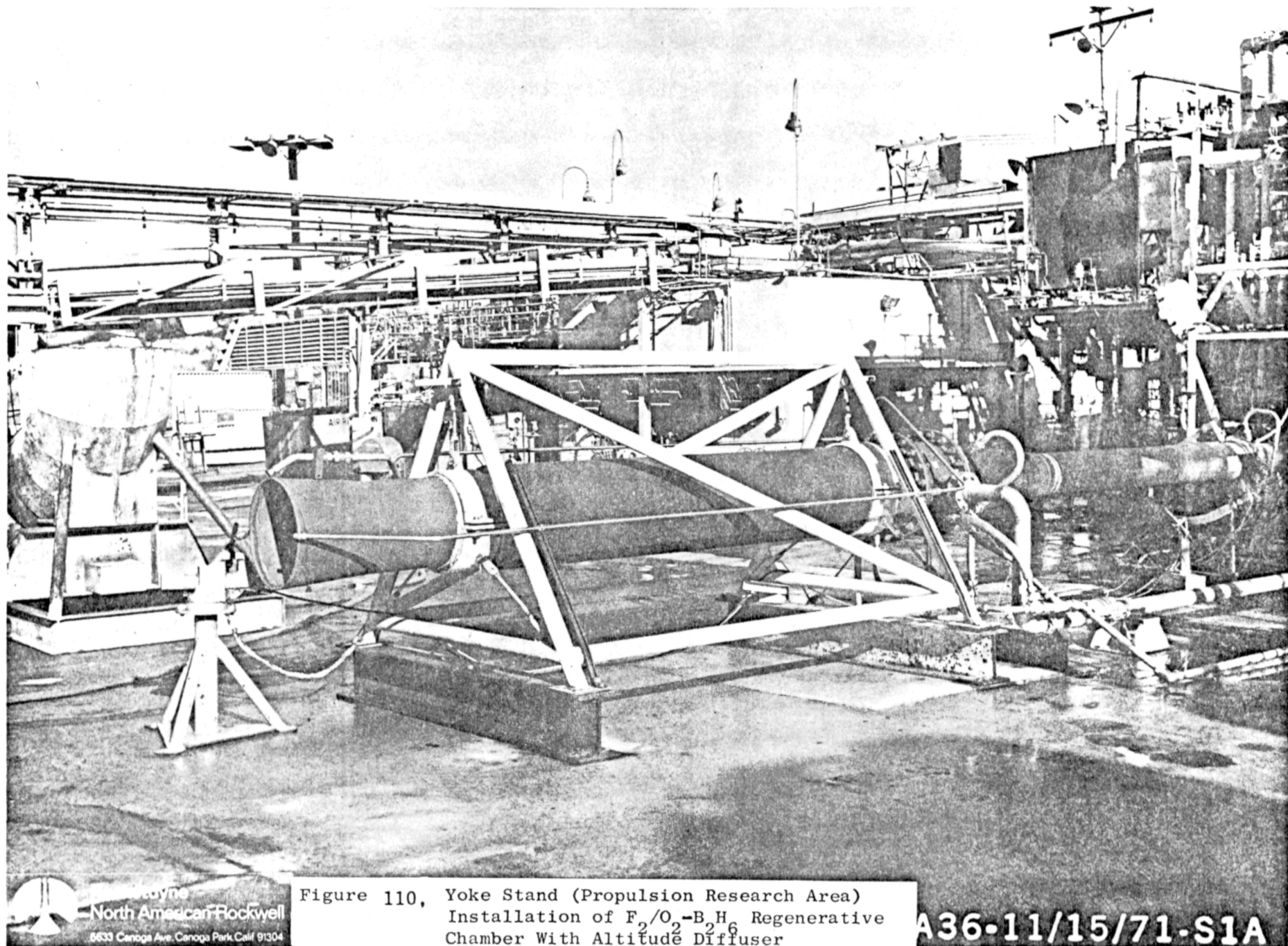


Figure 110, Yoke Stand (Propulsion Research Area)
Installation of $F_2/O_2-B_2H_6$ Regenerative
Chamber With Altitude Diffuser

A36-11/15/71-S1A



North American Rockwell
8633 Canoga Ave. Canoga Park, Calif. 91304

Diffuser Predicted Heat Transfer

Water jacketing of the entire diffuser length was completed. A concentric external pipe with a 12-inch pitch, 1/4 inch diameter, spiral wire spacer was provided. Diffuser section coolant was plumbed in series, with the exception of the driver coolant, to minimize water flow and provide a maximum water velocity. Water velocity values initially used were 20-30 ft/sec to ensure an adequate nucleate boiling burnout margin with a 24 lb/sec water flow available. Modification of the secondary gas injector feed line (located in the center of the diffuser), to ensure 75-second duration with hot exhaust gas impingement heat flux conditions, was accomplished with refrasil ablative protection wrapped over the surfaces.

Diffuser Mounting

Figure 111 illustrates the diffuser tie down to the concrete pad. A triangular adjustable rod support was provided near the chamber section (A) to allow alignment to the chamber exit flange. The rearward supports were triangular frames allowing for axial but not radial deflection. The GN_2 ejector driver section was plumbed with a bellows to allow axial flexibility for thrust measurement purposes. Thrust measurement was to be made with and without ejector operation, with correction for the pressurized water line effects. Preliminary loading measurements indicated the system to be capable of measurement in the 1000 pound thrust range. Corrections applied were to be dependent upon the thrust and diffuser pressures measured.

The diffuser to thrust chamber exit attachment with a flexible bellows unit to allow a better thrust measurement was reviewed. Study of previous test data with burnout of this type of joint as a result of convective back-flow during low pressure starts were made. Moreover, approaches for internally or externally cooling the bellows joint were considered, internal film cooling was projected to interfere with the altitude pumping capability of the diffuser (possibility of not attaining sufficient altitude conditions). Efficient external convective cooling appeared to severely interfere with an

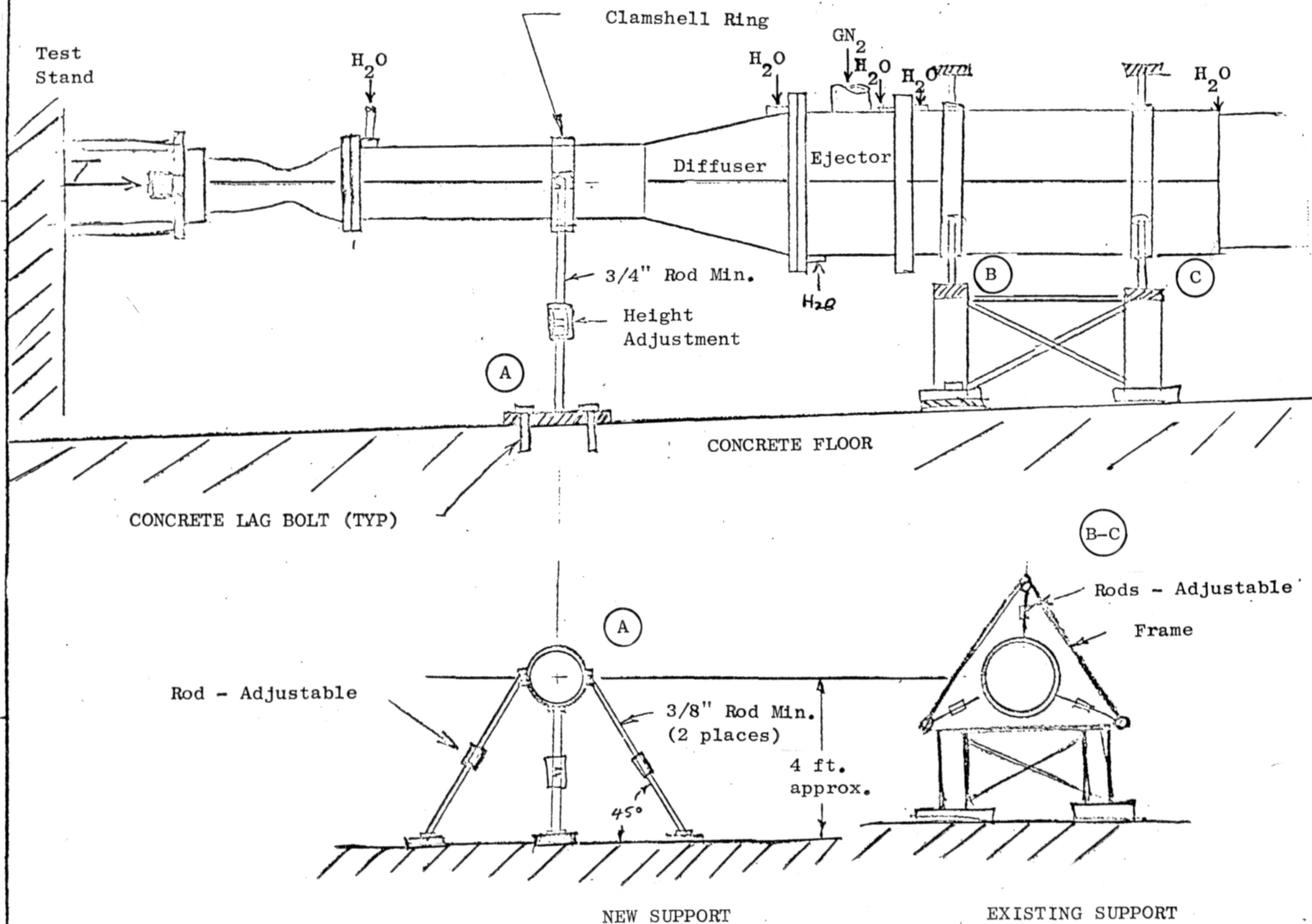


Figure 111. Diffuser Support and Mounting Detail

accurate thrust measurement. Based on the results of this study the least risk approach of a hard mount to the chamber exit was selected to assure the best potential for successful demonstration of long duration regenerative cooling. This was found to compromise the thrust measuring capability as shown by data obtained during the Task IV test series.

DIFFUSER TEST OPERATION

The altitude diffuser was verified for the attainment of vacuum during engine off and engine on test study.

Diffuser-Ejector Vacuum Test Operation

A series of ambient GN_2 blowdowns was made from the 3000 psia large bottle bank through the driver of the diffuser (Fig. 112) to determine the altitude pumping capability without engine operation. Several tests were performed on 2 August 1971 for 5 and 20-75 seconds duration. Based on analytical study the required cell pressure level would be attained with 575 psia ejector chamber pressure without engine operation.

The results of this study determined that the GN_2 supply flow to the diffuser could only be maintained at a 50 lb/sec (500 psia) peak level and then would be diminished (due to some tank pressure decay) to 380 psia (38 lb/sec) for long durations. From this test series it was determined that the pressure required (without the augmenting effect of the engine on) would not allow long duration (75 seconds) at a nozzle pressure low enough to prevent separation at the 20:1 area ratio point. The minimum driver pressure to provide a nonseparating nozzle was shown to be about 485 psia ($P_{\text{nozzle}} = 1.5$ psia, Fig. 113).

Study with pressure transducers in one of the two 2-inch feed lines halfway between the tank and the diffuser driver (upstream of a "T" section where the two feed lines were supplied to a 3-inch Grove regulator) was made. This study indicated that restriction existed in the feed lines due to insufficient

OPERATIONAL PRESSURES (PSIA)

(0)	0.8
(1)	3.8
(2)	7.5
(3)	13.8

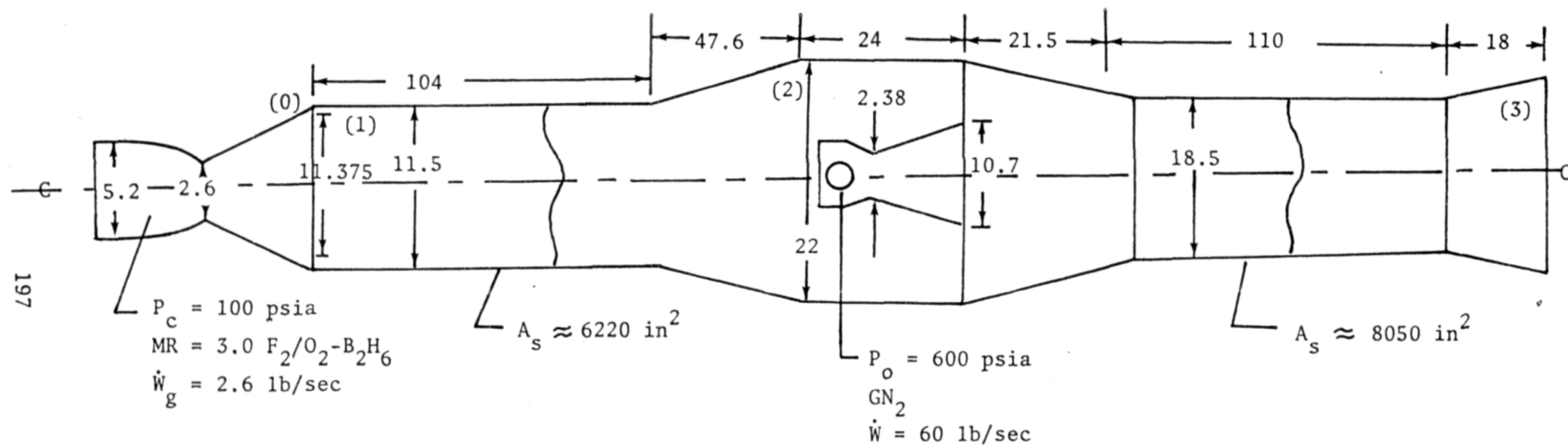


Figure 112. Altitude Diffuser Section Internal Geometry and Operating Conditions

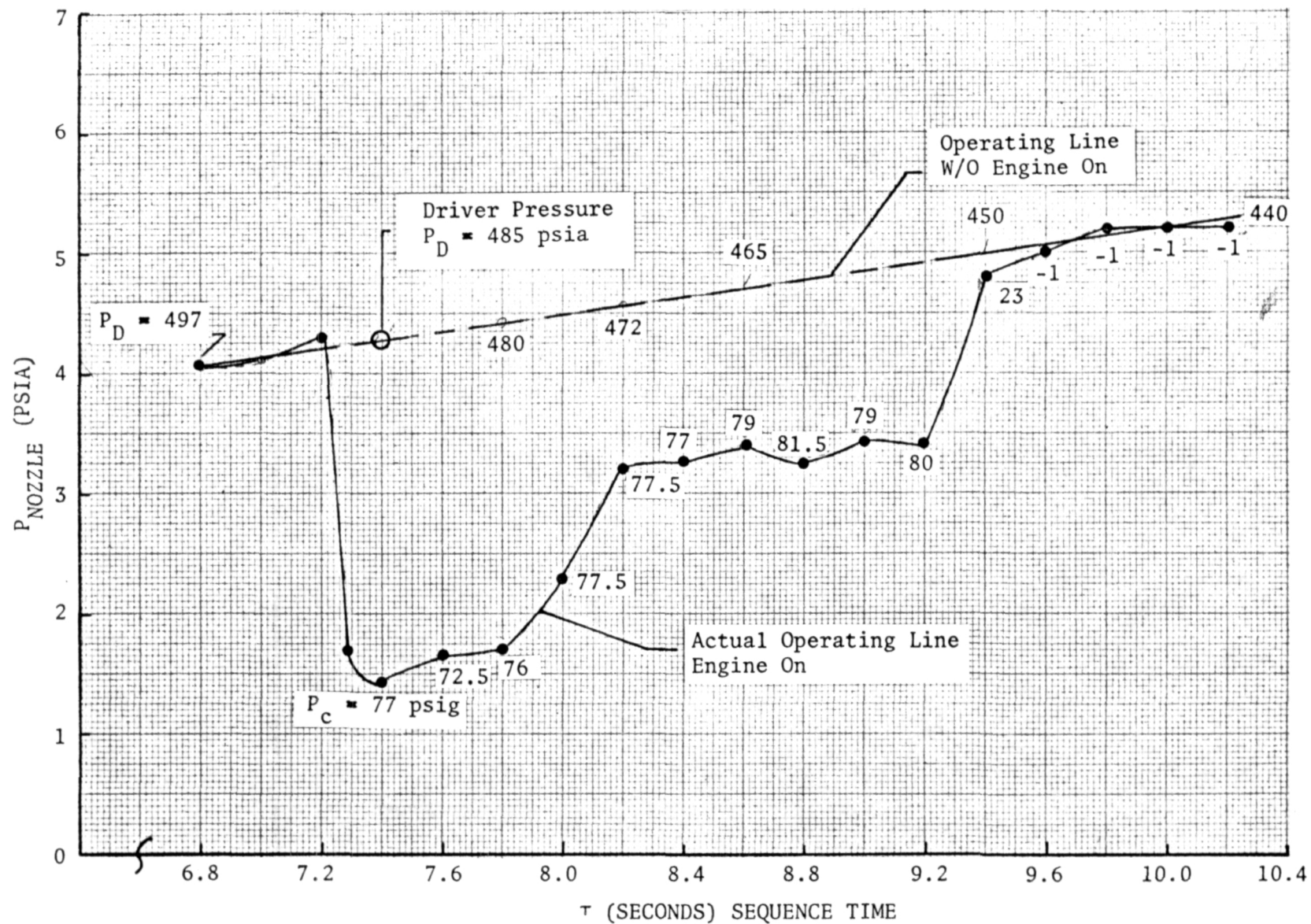


Figure 113 . 20:1 Exit Nozzle Wall Pressure Tap vs Time (Run 006)

flow area (due to accumulated effects of angle bends). Additionally, it was determined that the "T" section into the regulator provided a sizable restriction since the two 2-inch lines were reduced into a single 2-inch line at this point.

Steps were taken to improve the diffuser flow capability by increasing the "T" section capacity by provision for a third flow leg, increasing its diameter to 3 inches, and by implementing installation of a 3-inch third flow line back to the GN_2 tank supply. It was then planned to operate the calorimeter tests initially without the 20:1 nozzle and diffuser and then with the nozzle and diffuser installed (with the improved "T" section). Duration testing was planned with both of the improved capability features described. Testing on 13 August indicated improved flow capability (Fig. 114) but a flow insufficient for full duration operation for the modified section. The additional 3-inch flow leg back to the GN_2 supply was plumbed in prior to Test 011 on the regenerative chamber.

A second series of ambient GN_2 blowdowns was made from the 3000-psia large bottle bank through the modified feed system with three parallel feed lines (one 3- and two 2-inch lines) to the driver of the diffuser to determine the altitude pumping capability without engine operation. Tests were performed on 17 September 1971 for 15 and 75 seconds duration. Based on analytical study, the anticipated cell pressure level would be accomplished with ≥ 575 psia ejector chamber pressure. The results of this study are illustrated by the points in Fig. 115. It was determined that the supply flow to the diffuser could be maintained at a ≥ 60 lb/sec (600 psia) level without diminishing for long durations. From this test series it was determined that the pressure required (even without the augmenting effect of the engine on) would satisfactorily allow long duration (75 seconds) at a nozzle pressure low enough (≤ 1.5 psia) to prevent separation at the 20:1 area ratio point. No further operational checks were provided for the vacuum operation except to monitor the internal time/pressure behavior at points 0, 1, and 2 (Fig. 112).

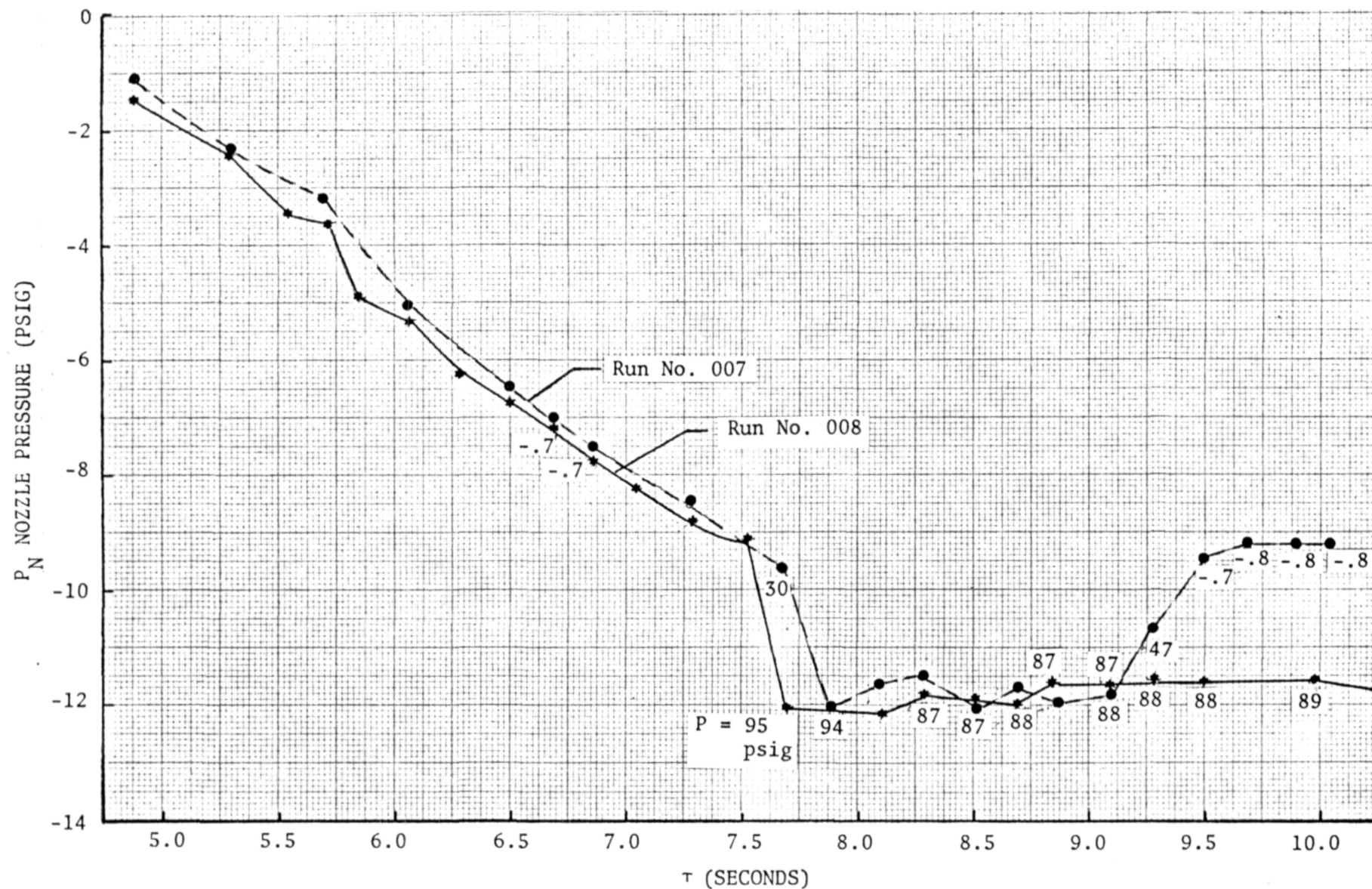


Figure 114 . Exit Nozzle Wall Pressure vs Modified "T" Section (Runs 007 and 008)

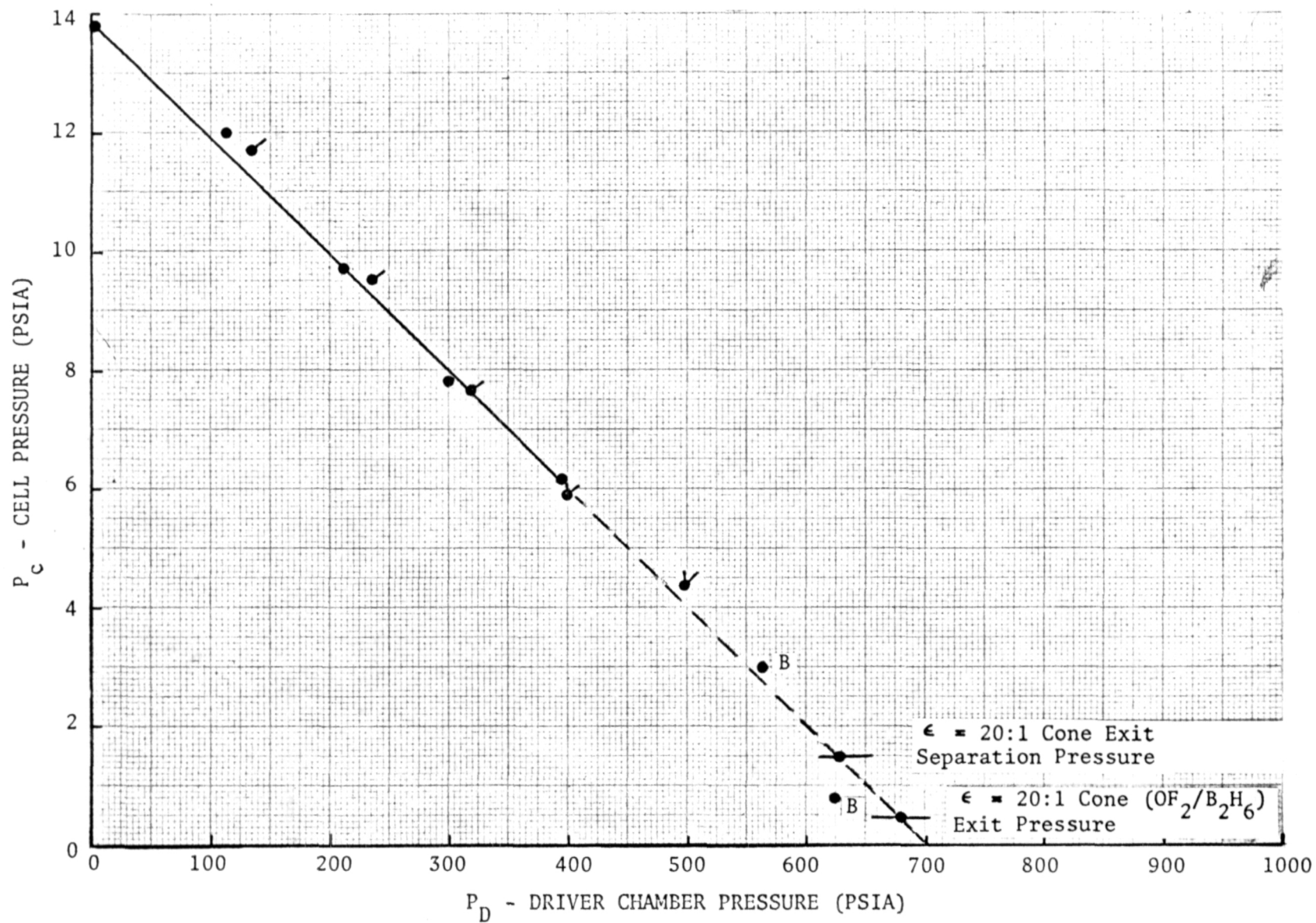


Figure 115. Yoke Stand $F_2/O_2-B_2H_6$ Diffuser Pressure Without Engine Operation (Location 1)

Diffuser Cooling Test Operation

Facility diffuser H_2O cooling (Tests 010 to 015) was provided from a 140-psig line source determined to provide 24 lb/sec through the spiral annular passages between the diffuser inner wall and outer shell. Satisfactory operation was obtained (Tests 010-014) with the section upstream of the ejector driver and the nozzle aft section cooled in series were conducted for a maximum duration of 10 seconds. The ejector driver H_2O coolant was plumbed in parallel with the feed system and presented no anomalous operational behavior during any of the tests.

A scheduled duration test (015), indicated abnormal operation of the engine by a premature shutdown. Post test visual inspection of the altitude diffuser indicated a diffuser failure in the forward section with an 85-percent buckling collapse of the inner wall. This was shown to initiate at about 10 seconds into the test where the diffuser pressure rose (Fig. 116). Collapse appeared to occur at ≥ 12 seconds mainstage time as evidenced by the pegging of the diffuser pressure. Extensive post test analysis indicated that for the 24 lb/sec diffuser H_2O coolant flow, the total heat load imposed onto the diffuser led to flow bulk boiling and a consequent accelerated reduction of the water coolant flow, leading to film boiling, overheating, and collapse of the diffuser forward section inner wall. This was also verified by motion pictures of the test which indicated steam issuing from the coolant discharge port. Figure 117 indicates the thrust change due to internal water leakage addition to the ejector and thrust chamber flows. A thorough post test analysis indicated the overall diffuser design to be satisfactory providing a sufficient H_2O flow was used to ensure against bulk boiling of the water coolant. A redesign of the diffuser to provide a minimum 40 lb/sec H_2O flow was accomplished.

Modification of the diffuser feed system was accomplished by providing a straight rather than spiral flow passage through the forward high heat load with an annulus gap of 3/16 inch maintained by 24 wire spacers. A separate water feed system from the fire-supply system was provided to allow the

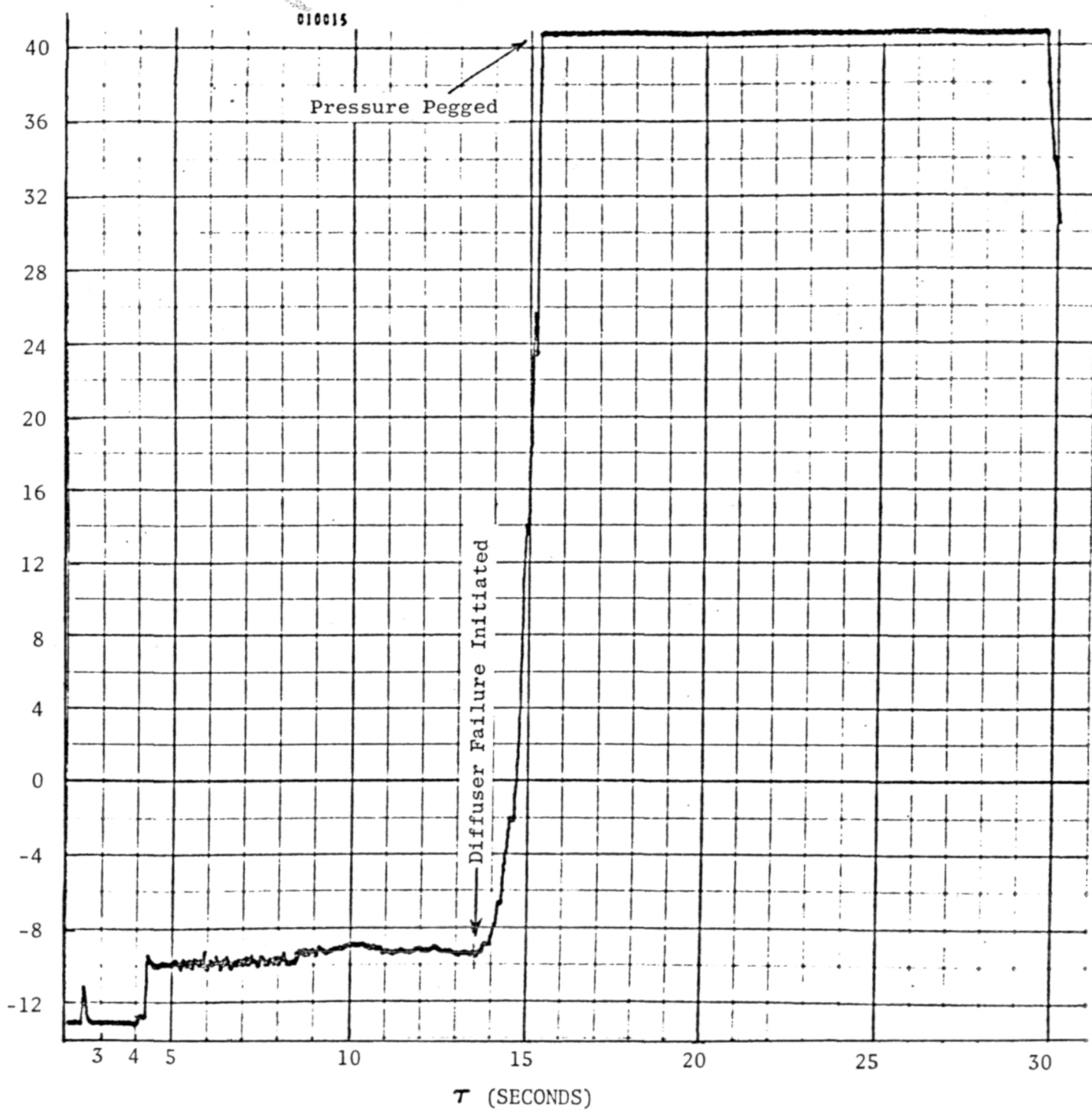


Figure 116 Upstream Diffuser Pressure vs Time (Test 015)

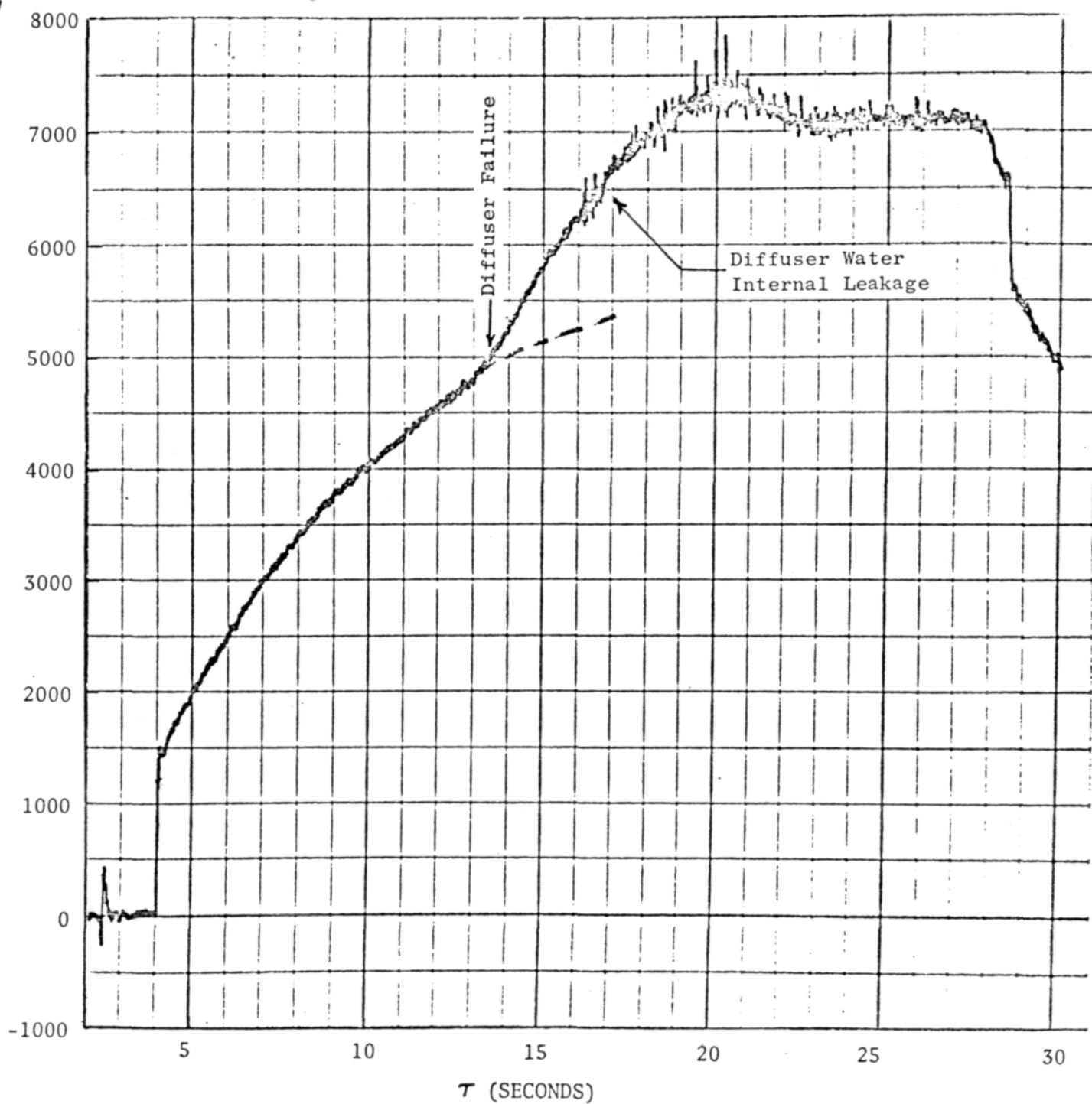


Figure 117. Ejector and Thrust Chamber Thrust vs Time (Test 015)

forward, aft and driver sections to be flowed in parallel for maximum flow capacity. Additionally, two 180-degree 2-inch inlet and outlet lines were provided for minimum pressure head losses (Fig. 118).

Subsequent tests were conducted without incident for a maximum duration to 45 seconds. Outlet water temperature was 160 F indicating 4000 Btu/sec to the water coolant in the forward end. This is comparable to the predicted level 4640 Btu/sec ($\bar{Q}/A = .747 \text{ Btu/in}^2\text{-sec}$). The aft (GN_2 mixing) diffuser section encountered no problems and was not changed throughout the test series except for separate H_2O coolant flow circuiting provided during the following testing.

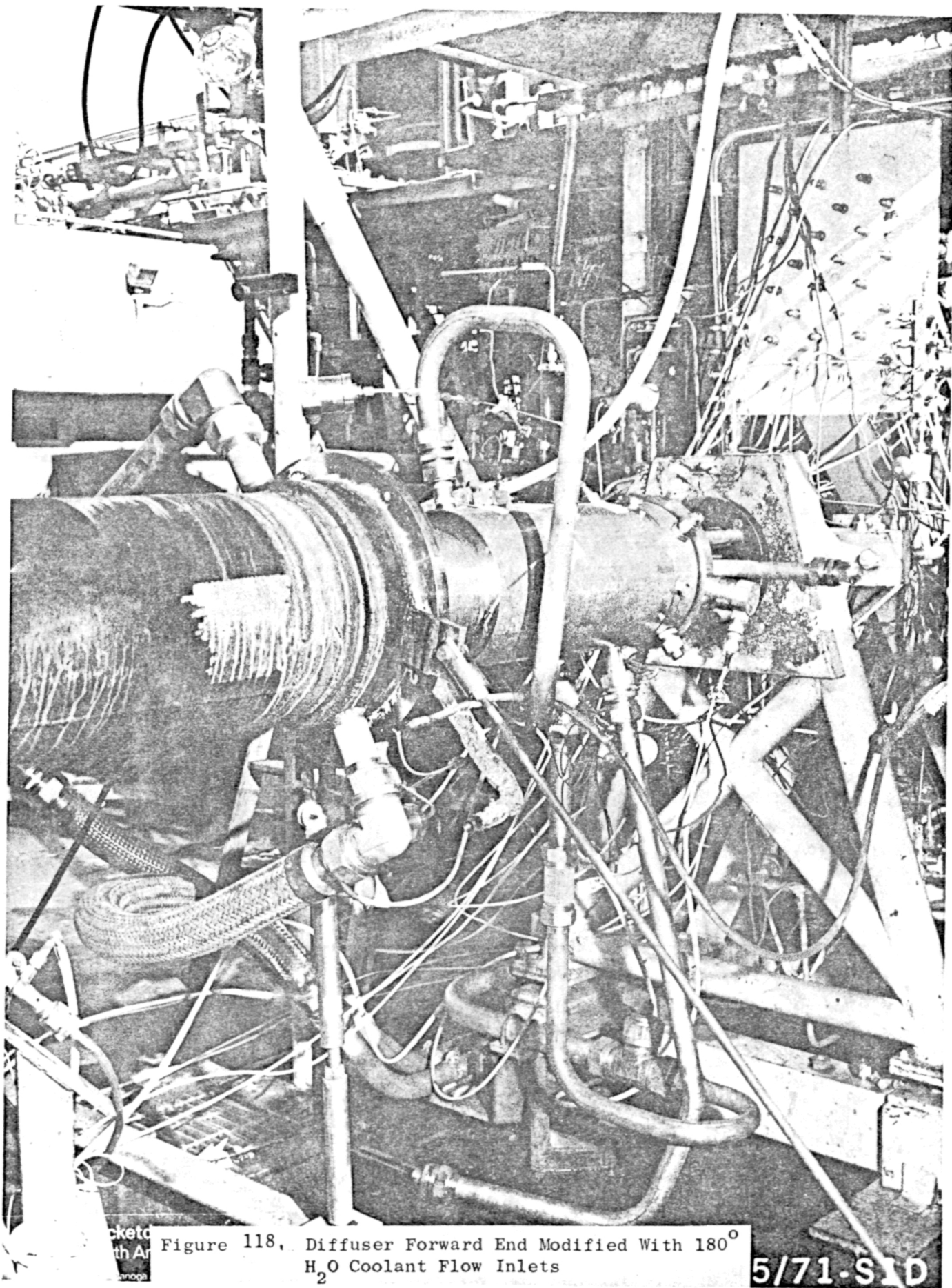


Figure 118. Diffuser Forward End Modified With 180°
H₂O Coolant Flow Inlets

5/71-SID

$F_2/O_2-B_2H_6$ TEST PROGRAM

The planned testing series was to provide initial calorimeter checkout and finally B_2H_6 regenerative cooling demonstrations. As a result of discussion with JPL personnel, increased scope to the preliminary checkout testing, as well as to the regenerative testing, was added to ensure the maximum test success and acquisition of data for the regenerative chamber.

Added diffuser and B_2H_6 blowdown checkout tests preparatory to calorimeter testing were also provided. Calorimeter testing with varying boundary layer bias and duration were planned to establish the combustion stability and heat transfer. Regenerative cooling tests of increasing duration were to be scheduled to assess chamber wall temperature heat load and coolant bulk temperature rise as a function of time with successively increasing time durations. An overall test summary may be inspected in Table 13.

BLOWDOWN TEST SERIES FOR CALORIMETER OPERATION

A preliminary series of oxidizer and fuel blowdowns was provided to establish feed system gaseous flows, pressures, temperatures and stabilization times prior to calorimeter chamber operation.

F_2/O_2 Blowdowns

A gaseous F_2/O_2 blowdown series was conducted on 3 August 1971 with the gas servo-system installed. Satisfactory bracketing the 1.9 lb/sec flowrate required for mainstage operation was achieved without any difficulty. The schematic of this system was shown in Fig. 108. A sonic venturi was employed for flow control.

B_2H_6 Blowdowns

A first series of B_2H_6 blowdowns was conducted (4 August 1971) to assess the capability of the inline water to B_2H_6 steel heat exchanger. Water temperature conditions were approximately 85 F with the anticipated B_2H_6 outlet

TABLE 13. $F_2/O_2-B_2H_6$ TASK IV EXPERIMENTAL TEST PROGRAM SUMMARY

Date	Test Hardware	Test Duration, (sec)	Objective
8-2	Diffuser	5	Diffuser Start Characteristics
8-2	Diffuser	20-75	Diffuser Duration
8-3	Injector	5	FLOX Blowdown
8-4,6,11	Injector	5	Diborane Blowdowns
8-11	Calorimeter, No Diffuser	1.5	Ignition Checkout (Test 004)
8-11	Calorimeter, No Diffuser	2	Mainstage Stability, Heat Transfer Rates at BLC #1 (Test 005)
8-13	Diffuser	60	Diffuser Maximum Flow and Vacuum
△	JPL Check Point		
8-17	Calorimeter/Diffuser	10	Blowdown, Valve Sequencing, Diffuser
8-17	Calorimeter/Diffuser	2.0	Mainstage Stability, Heat Transfer (Test 006)
8-25	Calorimeter/Diffuser	1.5	Mainstage, Heat Transfer, and Stability with Cavities (Test 007)
8-25	Calorimeter	3.0	Heat Transfer (Test 008)
△	JPL Check Point		
9-17	Regen. Chamber	5	Chamber Chill and System Checks
9-17	Regen. Chamber	0.5	Ignition Checkout (Test 009)
9-24	Regen. Chamber	1.5 - 4.0	Mainstage (Test 010-011)
9-28	Regen. Chamber	2.0 - 10	Mainstage (Test 012-013)
△	JPL Check Point		
9-30	Regen. Chamber	2.0 - 25	Ignition Check, Partial Duration Test (Test 014-015)
11-13	Regen. Chamber	3.0 - 45	Check and Final Regenerative Duration Demonstration (Test 016-017)

temperature of 60-70 F. Test data results yielded B_2H_6 outlet temperatures in the 16-20 F temperature range indicating an inability of the B_2H_6 to pull through the two-phase operating range (with the one-inch-diameter tubing and the comparatively low driving temperature difference available).

A second series of B_2H_6 blowdowns was then conducted on 6 August 1971 to assess the added effect of two parallel 1/2-inch (.049 wall) 50-ft copper tubing coiled elements, submerged in an electrically heated (Calrod) boiling water bath, and plumbed in series with the upstream steel heat exchanger. These tests indicated an improved B_2H_6 temperature outlet of 80-100 F which was satisfactory from an injection temperature standpoint. However, it was determined from the first and second B_2H_6 blowdown test series that the sum of the volumes of the run line plus both heat exchangers resulted in a 7-9 second flow stabilization time for a .62 lb/sec fuel flowrate.

The decision was made to reduce the flow system volume by removing the one-inch steel heat exchanger (and its volume) from the flow system and to plumb the 1/2-inch copper coils in series for a total heat exchanger length of 100 ft. Additionally, three valves were provided in the heat exchanger line to provide a purge through the heat exchanger on start and shutdown and to provide bypass operation for the heat exchanger fill time period.

A third blowdown series, with the improved system valving described and reduced B_2H_6 feed system volume (Fig. 119), was conducted (11 August 1971). A satisfactory B_2H_6 outlet temperature (80-100 F) and valve sequencing were accomplished for the required fuel flowrate range. The B_2H_6 system response was lowered to 5 seconds which was satisfactory for the start sequence planned.

The sequence planned was to allow for stabilized gaseous B_2H_6 flow through the injector followed by opening of the main oxidizer valve. Bypass GN_2 purges were to be provided on start and shutdown to prevent B_2H_6 deposit formation with a fuel override. Fuel venturis were provided for both the main fuel and BLC for flow control and measurement. These were backed up by two liquid turbine flowmeters upstream of the heat exchanger section.

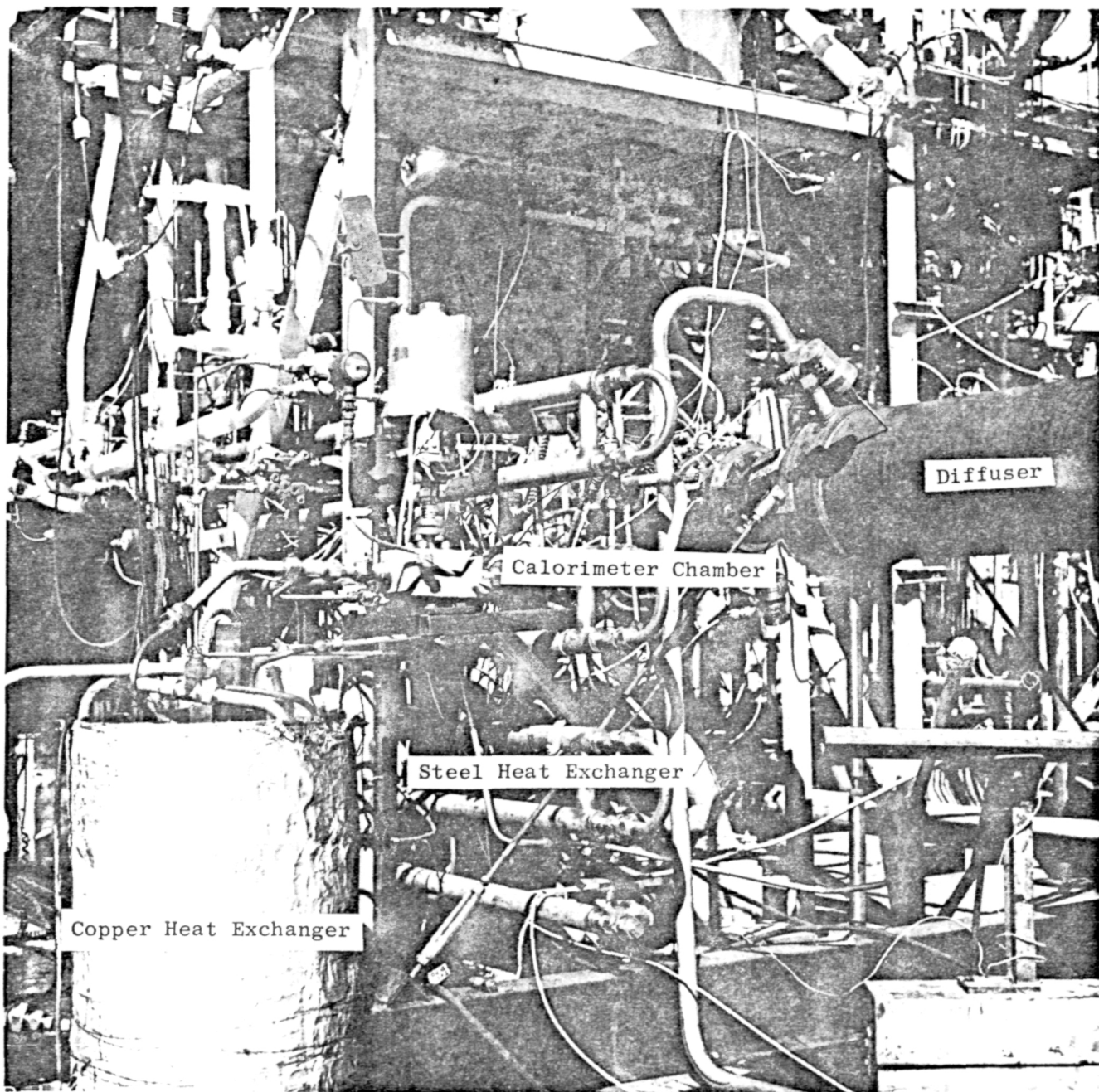


Figure 119. Calorimeter Chamber Test Setup With Steel Inline and Copper Coil Bath Heat Exchangers

CALORIMETER TEST SERIES

The calorimeter test series (004-008) were conducted to evaluate stability, performance, heat transfer, combustion deposit effects, and overall test stand and calorimeter chamber operational factors.

Tests No. 004 and 005

Two hot fire calorimeter tests were conducted (17 August 1971) with the nominal BLC flow of 33 percent (of fuel flow) with run durations of 1.5 and 2.0 seconds. Satisfactory ignition and mainstage pressure buildup were achieved and a nominal shutdown was observed. These tests were conducted with the 20:1 nozzle detached and the diffuser removed to allow inspection for B_2H_6 deposits between tests.

Heat transfer profiles were obtained for Tests 004 and 005 based upon the reduction of the heat plug transient data along the chamber length. It was noted that the peak throat heat flux level was reduced from $5.25 \text{ Btu/in}^2\text{-sec}$ to $4.0 \text{ Btu/in}^2\text{-sec}$ between Tests 004 and 005 as a result of some thin B_2H_6 insulating deposits formed along the thrust chamber convergence ramp. It was theorized that deposit buildups are partly due to run duration and partly due to formation during the shutdown sequence.

No evidence of any combustion instability was observed on photocon or accelerometer pickup measurements. Only minor face deposits were observed as shown in Fig. 120 for this No. 2 unit triplet injector.

Test No. 006

For the calorimeter Test No. 006, the BLC flowrate was increased by providing an additional flow venturi in parallel with the previously used BLC fuel venturi (in parallel with the previously used main fuel venturi). This was projected to increase the BLC flow to 43 percent. Testing was conducted

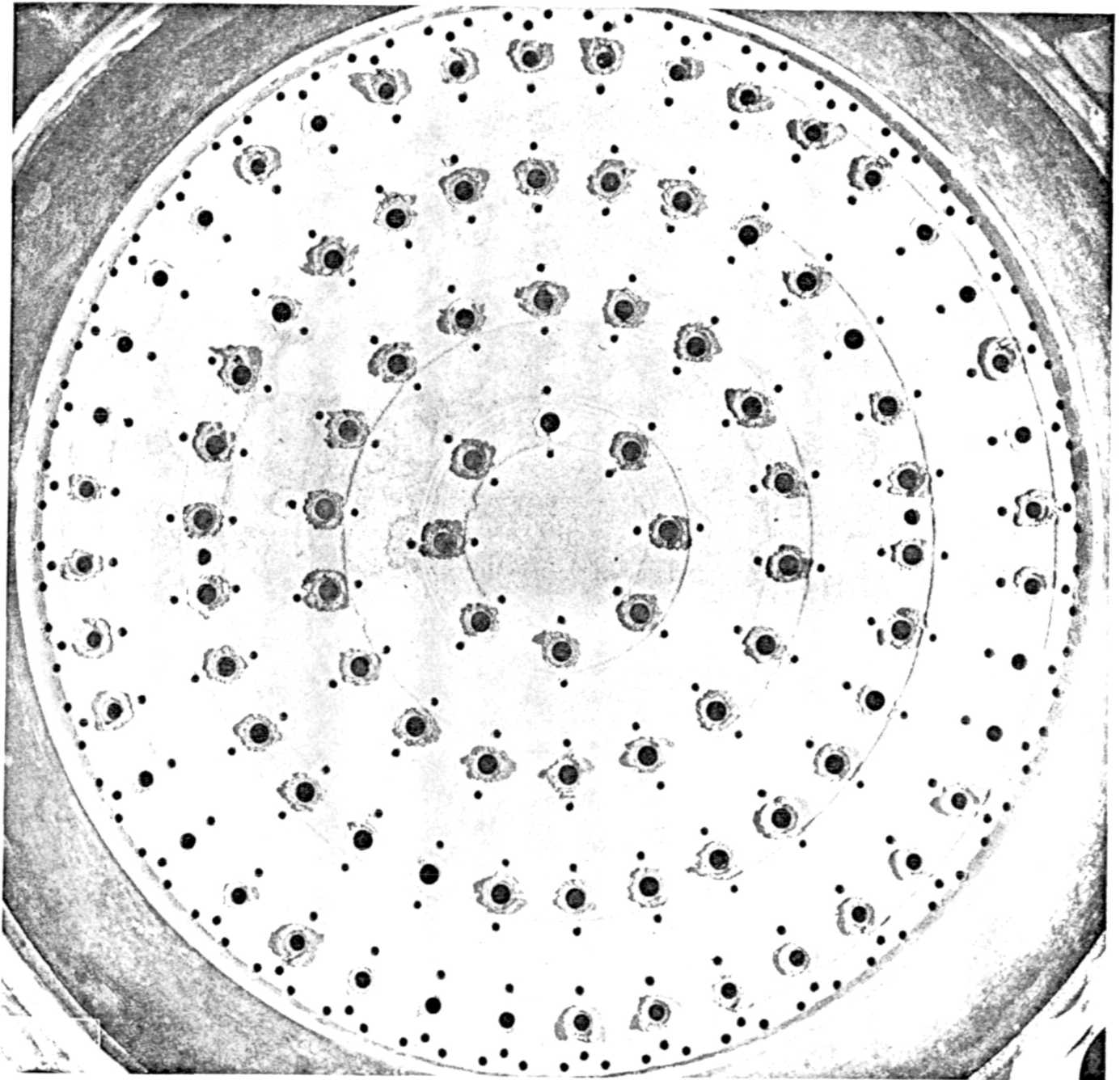


Figure 120, Triplet Injector Post Test 004-005 Showing Lack of Face Deposits

with the diffuser in place to establish the additional pumping augmentation provided by the engine, together with the driver, and to establish the 20:1 nozzle heat flux profile with a full flowing nozzle.

Spontaneously triggered instability was observed at the onset of chamber pressure rise to the cutoff signal. Post test inspection indicated some erosion over the oxidizer lands as a result of the circumferential acoustic instability wave travel. Figure 121 illustrates the injector post test prior to rework. This injector was reworked by incorporating acoustic cavities at the injector periphery and by surface machining of the face to clean up the erosion. The fuel side orifices which experienced some deposit plugging due to the instability pressure fluctuation, were cleaned and the entire assembly satisfactorily flow checked. The calorimeter chamber sustained no damage as a result of this abnormal operation other than nozzle heat plug failures due to vibration.

Figure 122 illustrates the $4.0 \text{ Btu/in}^2\text{-sec}$ heat flux rates observed at the injector face during the instability period. It is theorized that the overloading of the outer periphery of the injector with excess fuel was the causative effect of the instability. Further investigation of this instability point was verified by JPL in-house testing on a duplicate triplet injector.

Since the $4.0 \text{ Btu/in}^2\text{-sec}$ throat region peak heat flux rate previously observed in Test 005 represented the near-design heat transfer rate, it was decided to recheck the nominal 33 percent BLC flowrate (rather than to further jeopardize the injector hardware at the 43 percent flow point).

Satisfactory diffuser operation was noted during the mainstage time period of 7.3 to 7.8 seconds for Test 006 where the diffuser driver pressure was near maximum at 485 psia. However, without engine operation or with reduced driver pressure ($< 485 \text{ psia}$) a satisfactory ($< 1.5 \text{ psia}$) nozzle pressure was not obtained for the diffuser as shown by loss in vacuum as the driver pressure decreased to 440 psia at the end of the run.

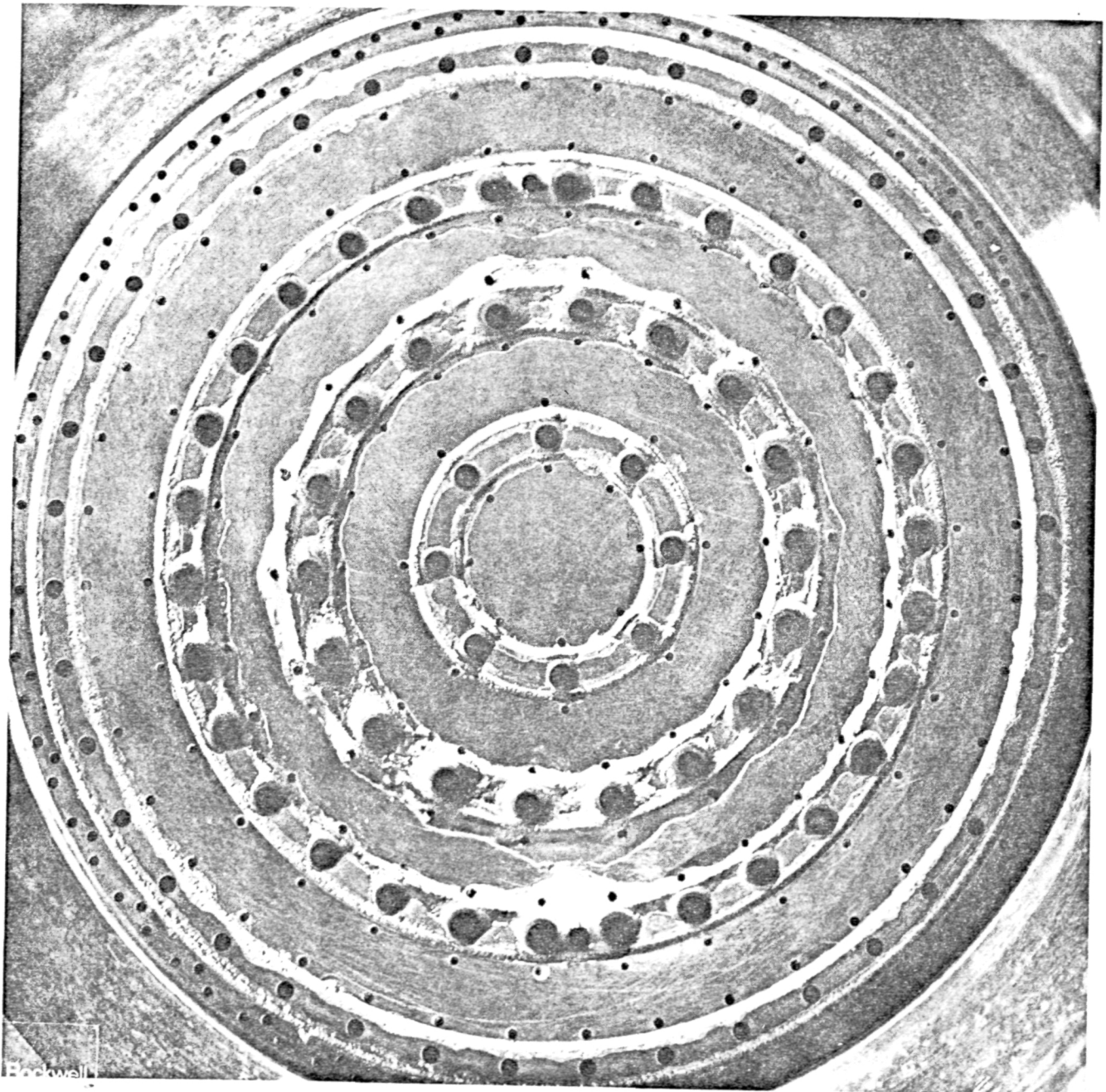


Figure 121, Triplet No. 2 Injector Post Test 006 Showing Oxidizer Ring Erosion Resulting From Acoustic Instability

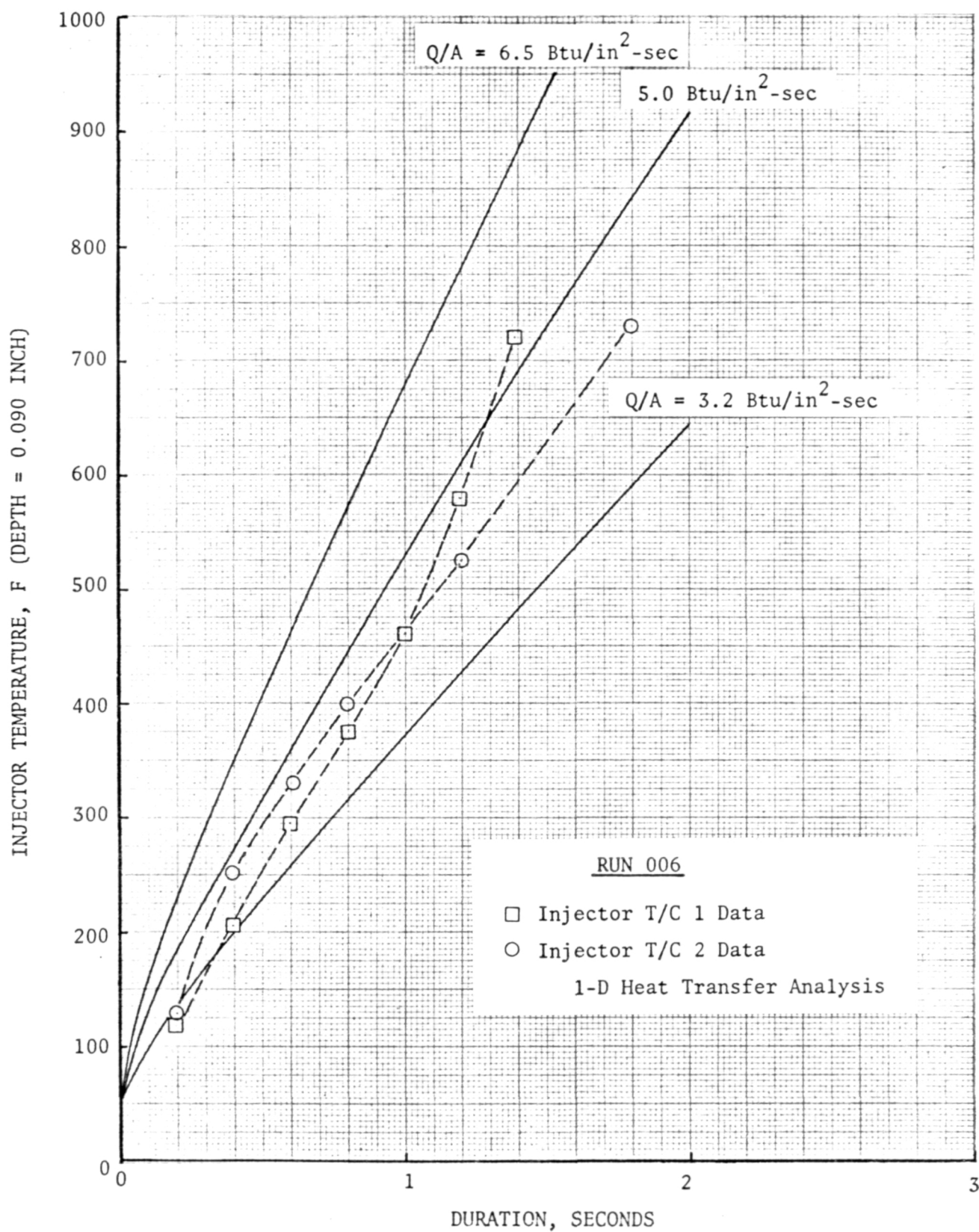


Figure 122 . FLOX/B₂H₆ Injector Temperature History

Tests No. 007 and 008

Tests 007 and 008 of 1.5 and 3.0 seconds, respectively, were conducted (25 August 1971) with the calorimeter chamber to establish stability and cavity deposits with the installed acoustic cavities. Satisfactory and stable operation was achieved on both runs with no accelerometer or chamber pressure photocon disturbances. These tests were made with the diffuser with the modified feed line "T" section. Heat flux data were obtained on the copper calorimeter section but not on the steel 20:1 nozzle extension due to the heat plug vibrational failure which occurred during Test 006. It was theorized that the nozzle data were acceptably close to previously taken data with a triplet injector. The test heat transfer data taken in Tests 007 and 008 indicated that the heat flux rates were nearly identical to those of Tests 004 and 005 with evidence of a further heat flux reduction to be expected for longer than 3.0-second run durations. Figure 123 illustrates the injector post test 008 after cleaning.

It was indicated that the vacuum held to a good level for duration for these tests with the improved "T" section and slightly higher chamber pressure compared to Test 006.

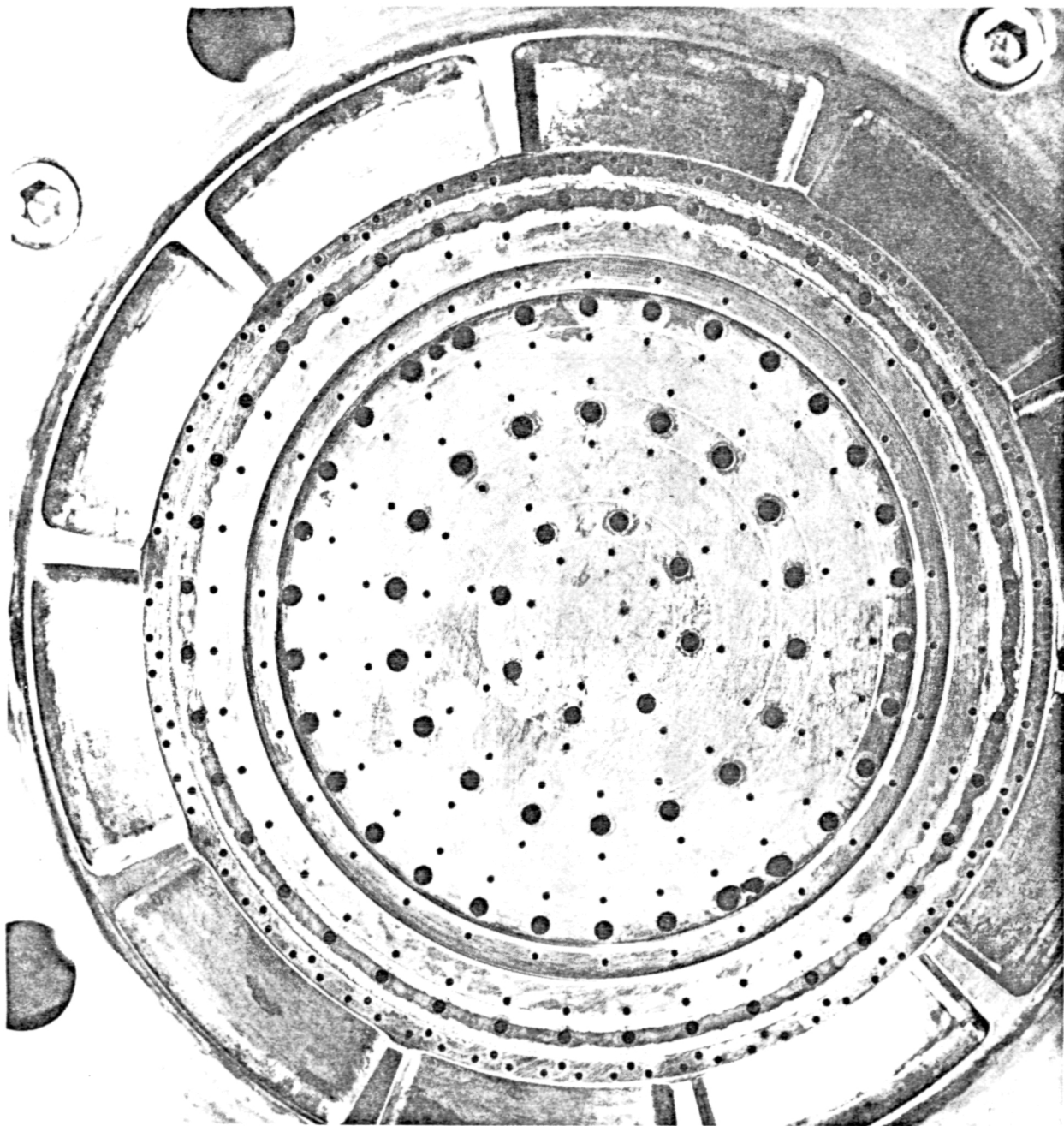


Figure 123, Triplet Injector With Acoustic Cavities - Post Test 007-008

BLOWDOWN TESTING FOR REGENERATIVE OPERATION

A series of B_2H_6 blowdowns through the regenerative chamber was accomplished subsequent to stand modification and installation of the regenerative hardware, to establish feed system flows, pressures, and temperatures throughout the fuel feed system. No further F_2/O_2 feed system blowdowns were provided since the oxidizer gas servo-controlled feed system was unchanged from the previous calorimeter testing.

B_2H_6 Blowdown Testing

Setup of the B_2H_6 feed system to include a cavitating venturi for flow control was accomplished. At nominal fuel flow conditions the venturi inlet total pressure (440 psia) was sized large enough to potentially allow the downstream fuel jacket inlet pressure to rise to a high level (385 psia) before flow control was lost. On 17 August 1971, a blowdown of 6 seconds maximum duration was performed which accomplished the planned objectives. The fuel venturi inlet pressure was set for the nominal 0.63 lb/sec flow value and main fuel valve opened for the specified period. B_2H_6 burnoff was accomplished by an open flame afterburner.

The results of this testing indicated that a 2-second lead was more than adequate to assure a sufficient chill and stabilized flow. Figure 124 illustrates that at a time of approximately 0.5 seconds the flow was established and at the end of a 1.7-second time, the jacket discharge temperature reached a steady state value. During the 1- to 2-second period the thermal mass of the chamber moderates the coolant temperature to prevent an immediate chilldown.

For the first ignition test (009) the fuel lead was held to a 2-second lead. Subsequent tests were with a 1-second lead for ignition with a coolant injection temperature of ≈ 50 F instead of -60 F. Detailed further reduction of the fuel lead was not undertaken due to the limited extent of the planned test program.

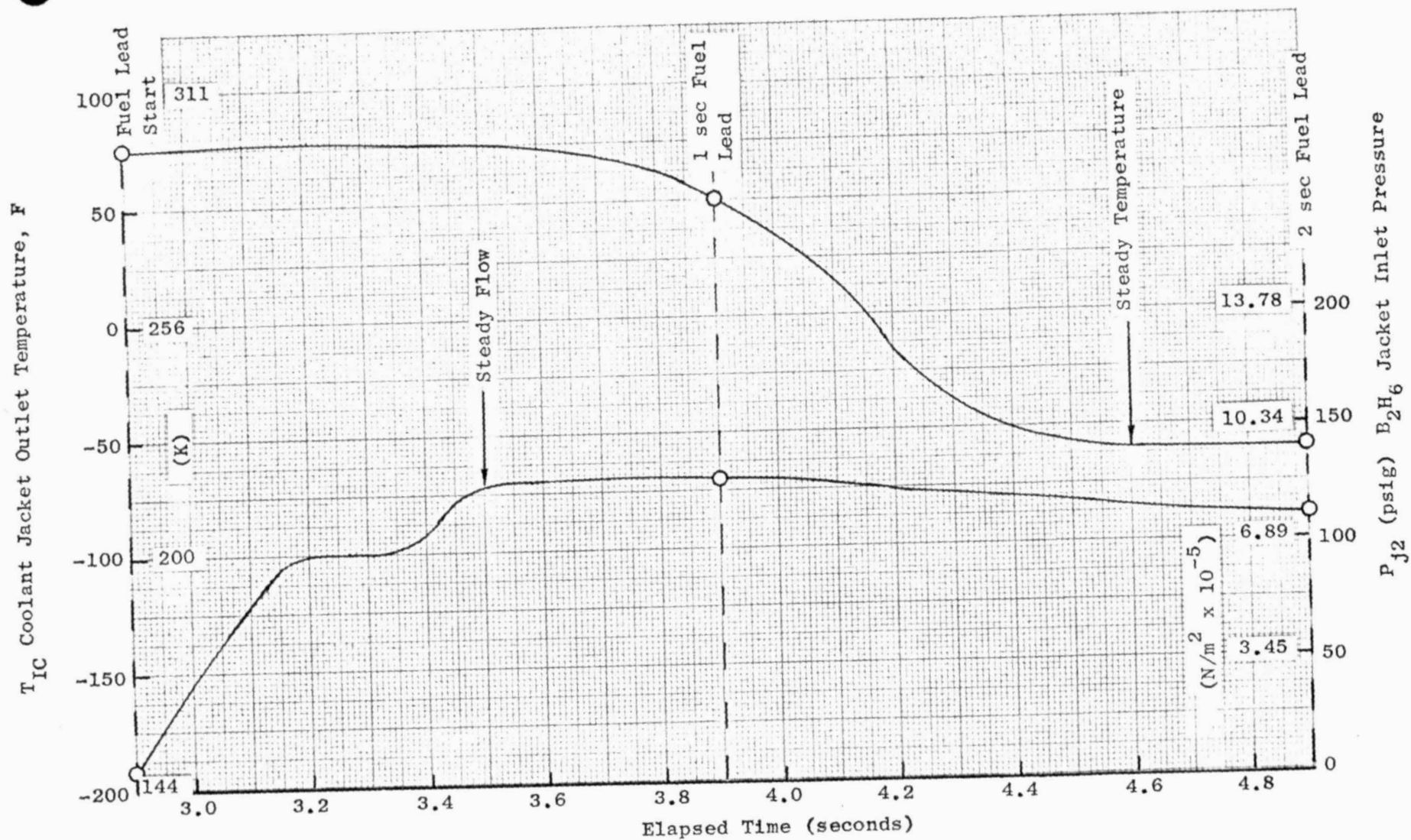


Figure 124, $F_2/O_2-B_2H_6$ Thrust Chamber Jacket Inlet Pressure and Discharge Temperature During Fuel Lead Sequence ($\dot{W}_f = 0.63 \text{ lb/sec}, .29 \text{ kg/sec}$)

REGENERATIVE TEST SERIES

Nominal targeted mixture ratio and chamber pressure conditions were 3.0 and 100 psia, respectively, for the test series (Tests 009-017). These tests were of successively increasing duration from 0.5 to 45 seconds. An outline summary of the completed tests is indicated below.

Ignition Test 009 (0.5 Second)

Test 009 was provided with a 2-second fuel lead to ensure stabilized flow with satisfactory ignition achieved for a stable 0.5-second mainstage duration. Fuel discharge temperature reached was 4 F with the jacket inlet pressure rising to 150 psig during this short mainstage period.

Mixture ratio achieved was 2.5, lower than targeted due to a F_2/O_2 low bottle bank pressure. Remedial action was taken by using a larger sonic venturi to allow servo-system control with the available gas supply pressure for future tests. Figure 125 illustrates the chamber pressure vs time for Test 009. Figures 126 and 127 are post test photos of the injector and chamber, showing a lack of deposits.

Mainstage Test 010 (1.5 Seconds)

Test 010 was directed toward increasing the total heat load to the jacket. A good ignition and steady state chamber pressure were achieved and the mixture ratio was 3.0. Heat load increased to the B_2H_6 and water coolant with discharge temperatures of 142 F and 100 F, respectively. Figure 128 illustrates a post test injector photo for Tests 010-011 with minimal deposits observed.

Mainstage Test 011 (4.0 Seconds)

Test 011 was a 4.0 second test at a mixture ratio of 3.1 and chamber pressure of 93 psia aimed at nearly stabilized throat wall temperatures with a longer duration. Fuel jacket discharge temperature achieved was 192 F and

302906
092071 0025

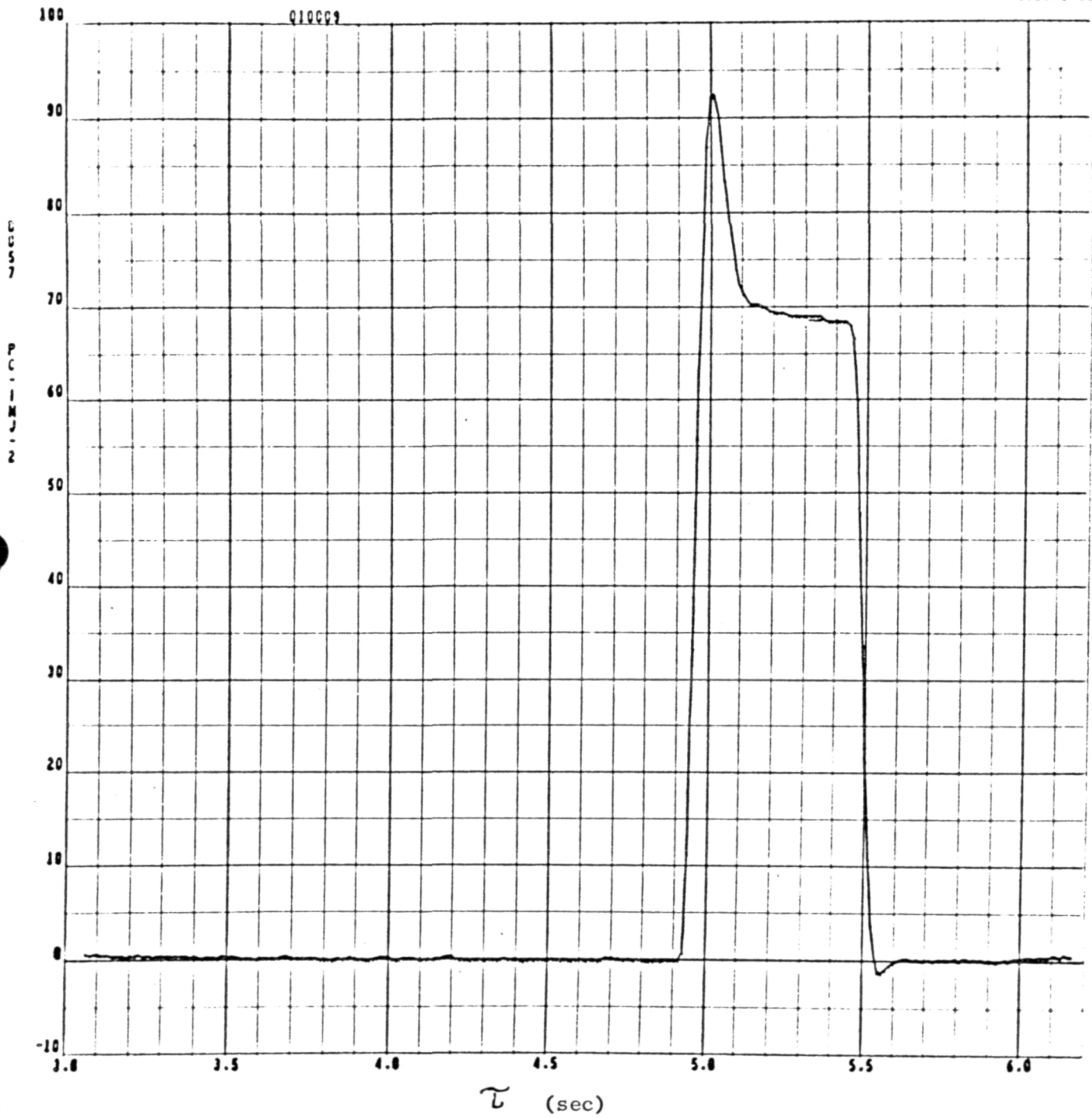


Figure 125. Chamber Pressure vs Time (Test 009)

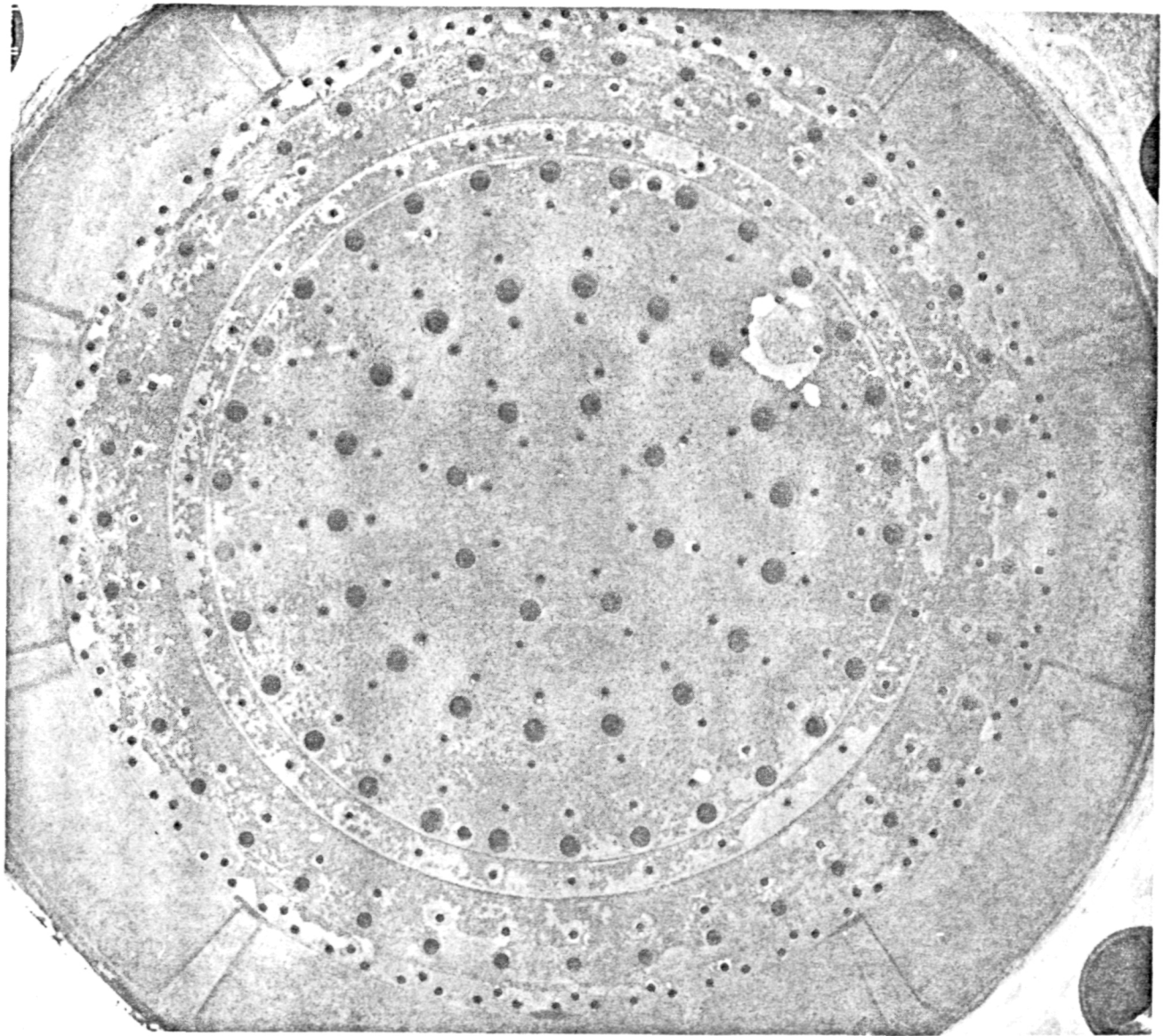


Figure 126, $F_2/O_2-B_2H_6$ Triplet Injector Face Photo Post Test 009
(1/2 sec test)

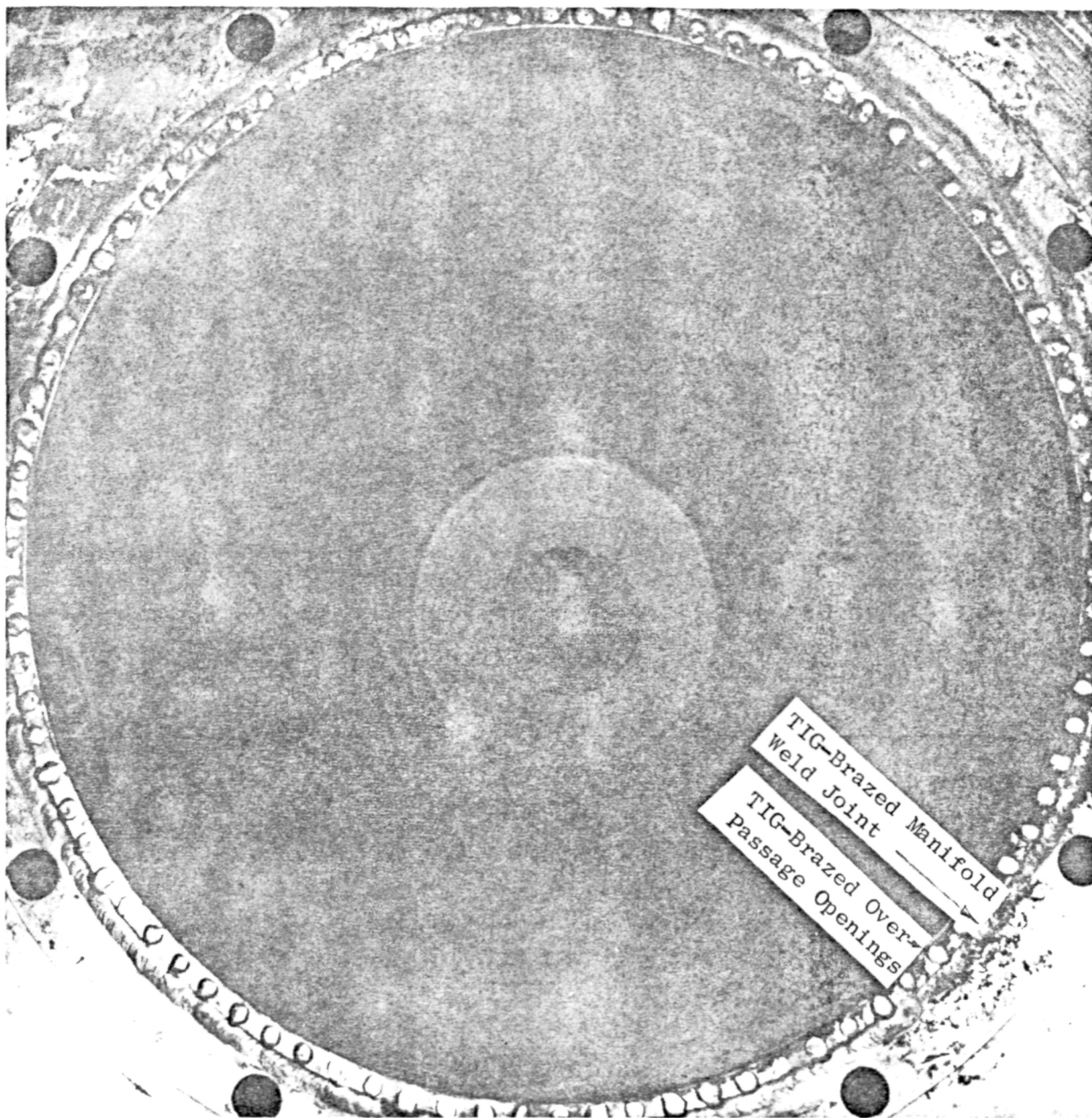


Figure 127, No. 1 Regenerative Chamber Viewed From Nozzle End Post
Test 009 (1/2 sec duration)

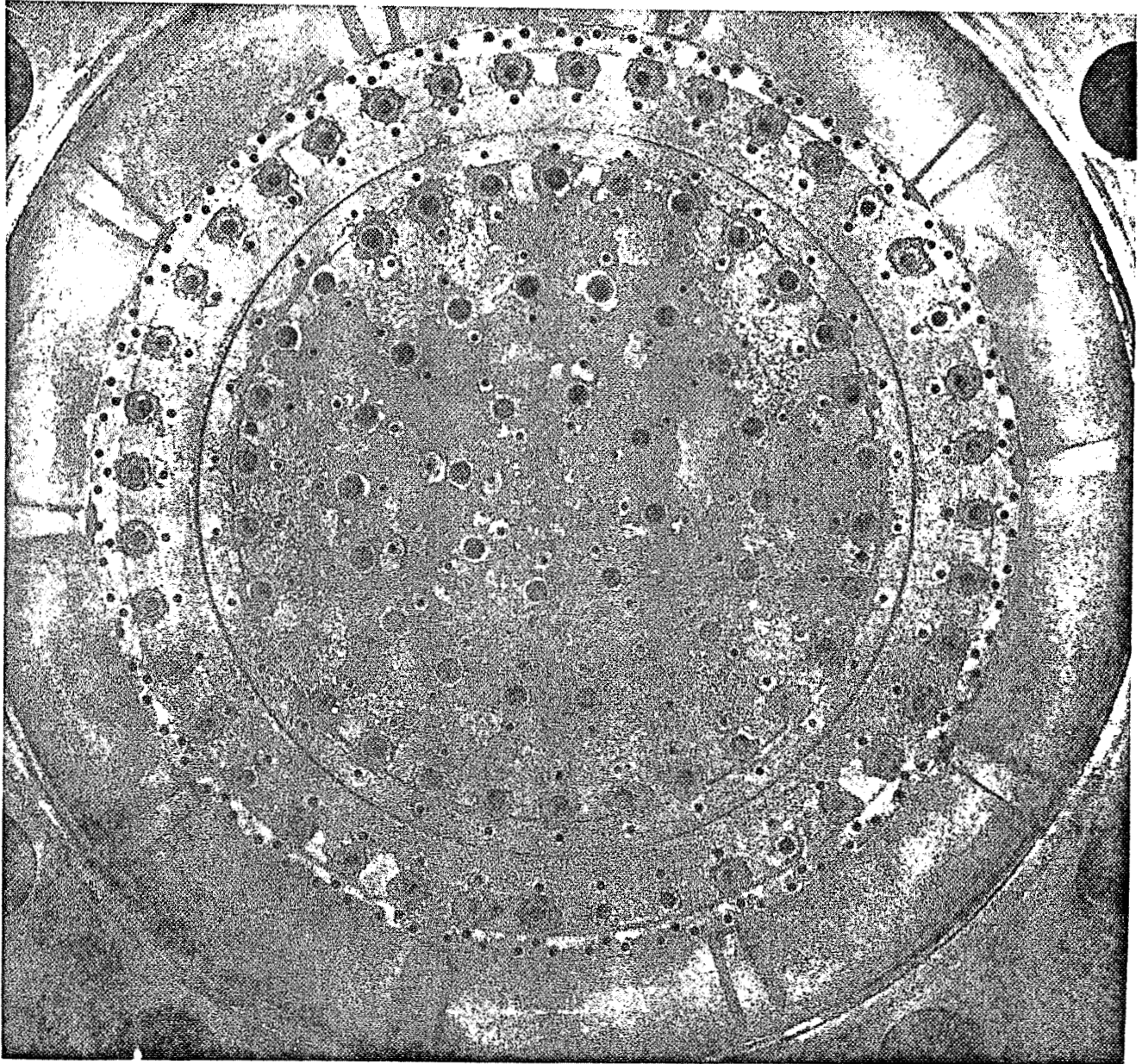


Figure 128, $\text{F}_2\text{O}_2\text{-B}_2\text{H}_6$ Triplet Injector Face Post Test 010-011
(1.5 and 3.5 sec duration)

a B_2H_6 jacket inlet pressure of 211 psig was attained. Water jacket discharge temperature was 105 F. Chamber and injector hardware was in excellent condition as shown in Fig. 127,

Mainstage Test 012 (2.0 Seconds)

Test 012 was a 2.0-second duration test aimed at checkout prior to a 10-second duration run. B_2H_6 and water discharge temperatures based heat loads achieved agreed well with Test 010 with a B_2H_6 jacket inlet pressure of 182 psig achieved.

Mainstage Test 013 (10 Seconds Duration)

Test 013 was a 10-second test at 95.9 psia and $MR = 2.97$ to evaluate stabilized throat and combustor conditions and higher cooling jacket discharge temperature and heat load conditions. Satisfactory ignition, mainstage, and normal shutdown were achieved. A jacket inlet pressure of 218 psig was reached with B_2H_6 and H_2O discharge temperatures of 228 F and 125.5 F, respectively. As shown in Fig. 129 the stabilization of the jacket temperature appeared to occur near the 10-second time point. Heat load to the water and B_2H_6 fuel were 271 Btu/sec and 231 Btu/sec, respectively. Figure 130 illustrates the hardware condition post test 012-013. Light, loose combustion deposits were indicated on the injector with similar deposits along the convergence ramp to the chamber throat. All hardware was cleaned, inspected, and reinstalled in the facility. During water flow testing of the chamber and injector, no evidence of flow impairment or plugging was noted.

Mainstage Test 014 (2 Seconds)

Test 014 was a short checkout test to be conducted prior to the planned final duration test run. A nominal chamber pressure of 94.2 psia at a $MR = 2.97$ was achieved. Data agreed closely with the previous 2-second duration tests.

55903910
092971 0015

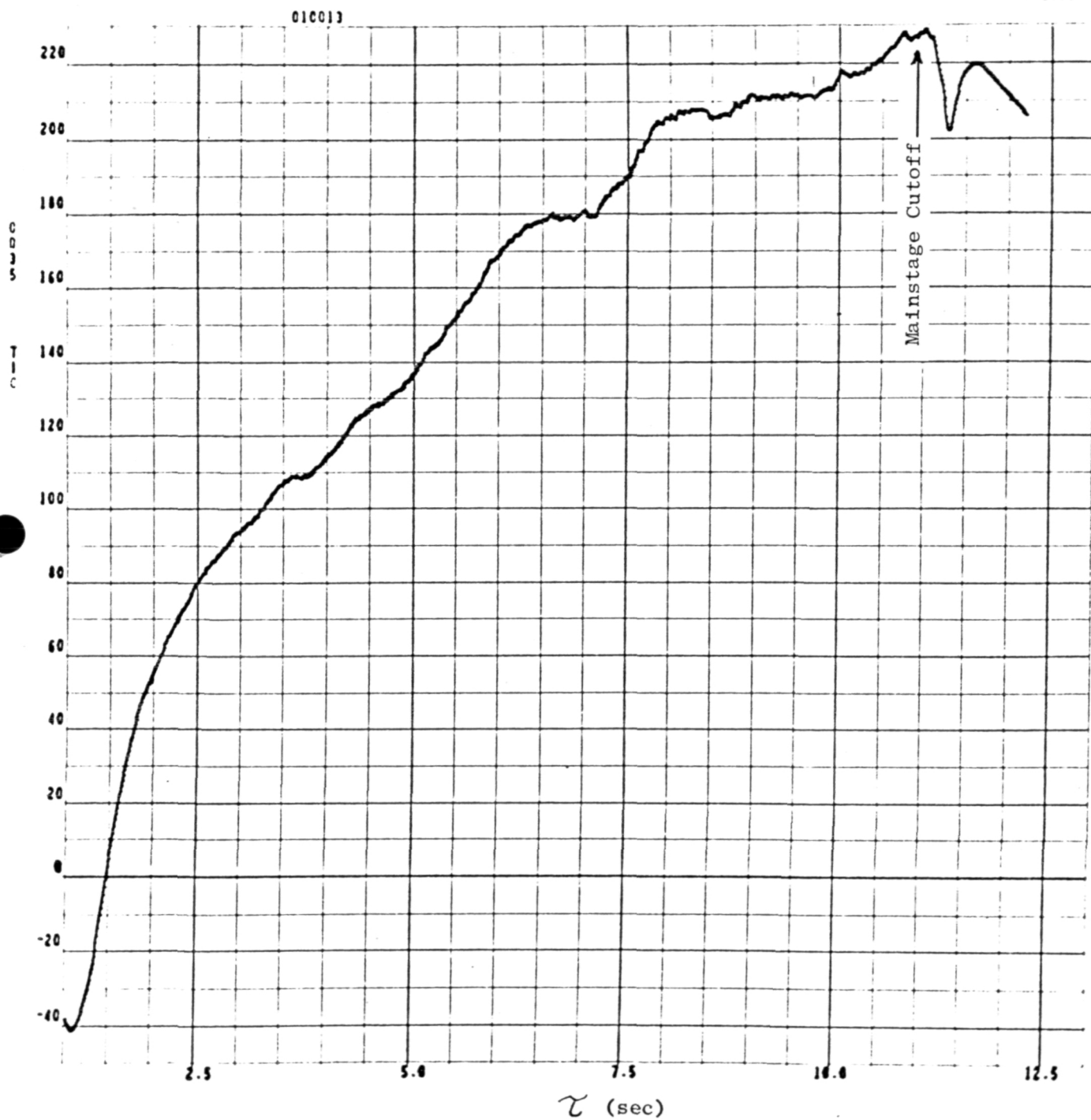


Figure 129. B_2H_6 Regenerative Coolant Discharge Temperature vs Time During Test 013

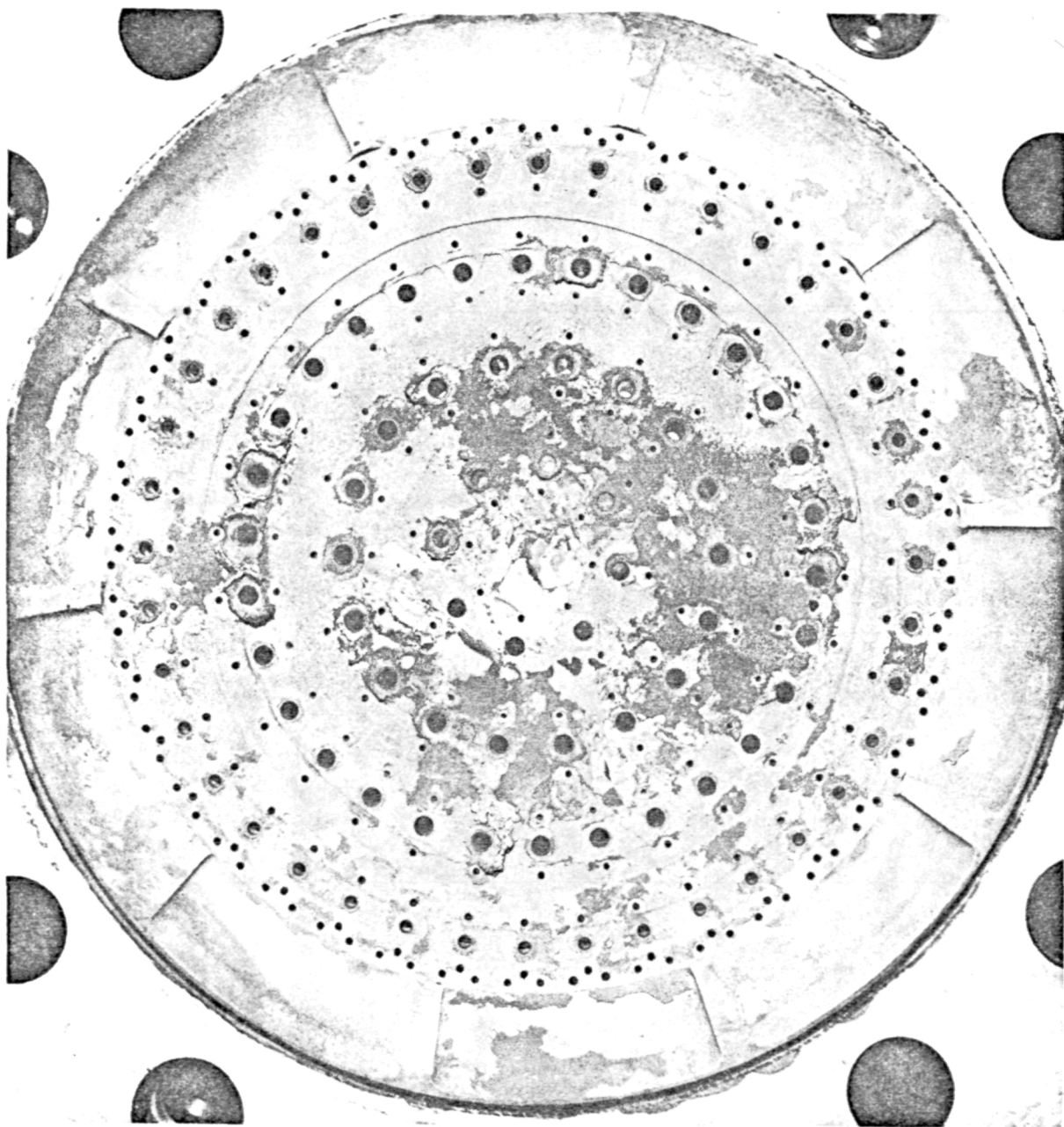


Figure 130, $F_2/O_2-B_2H_6$ Triplet No. 2 Injector Face Post Test 012-013
(2 and 10 sec duration)

Mainstage Test 015 (25 Seconds)

Test 015 was initially scheduled as final test of 75 seconds at a mixture ratio of 3.0. Pretest objectives were to establish duration, stability, hardware, integrity, performance, and heat load to the cooling systems. A mixture ratio of 2.9 and chamber pressure of 98.3 psia were attained for 25 seconds of mainstage. Premature shutdown was initiated by a set redline cut at a B_2H_6 coolant jacket discharge temperature of 425 F as a result of the altitude diffuser collapse described previously. Post test inspection indicated the thrust chamber and injector hardware to be in satisfactory condition with somewhat heavier surface deposits on the injector face and chamber nozzle (Fig. 131) than previously noted. Cleanup of the hardware was accomplished, however, without difficulty. The chamber and injector hardware was in excellent condition and was reassembled for a final duration test. Chamber pressure as shown in Fig. 132 held steady throughout the test period.

Mainstage Test 016 (3 Seconds)

Test 016 was conducted on 13 November 1971 upon completion of the altitude diffuser rework to provide added water flow to all sections and to replace the forward collapsed diffuser section which failed during Test 015. Test 016 was a planned checkout test to establish preliminary chamber pressure, mixture ratio, and diffuser operation points prior to the final test duration run. Test 016 achieved a mixture ratio of 2.8 and a chamber pressure of 96 psia with maximum B_2H_6 fuel and H_2O outlet temperatures of 143 F and 94 F, respectively. Diffuser vacuum and H_2O coolant flow was indicated to be satisfactory to commit to the final duration test.

Mainstage Test 017 (45 Seconds)

Prior to Test 016, the remaining B_2H_6 propellant supply on hand was assessed at approximately 44 lb of which 2.5 lb were used during Test 016. On concurrence of Rocketdyne and JPL representatives prior to Test 017, it was

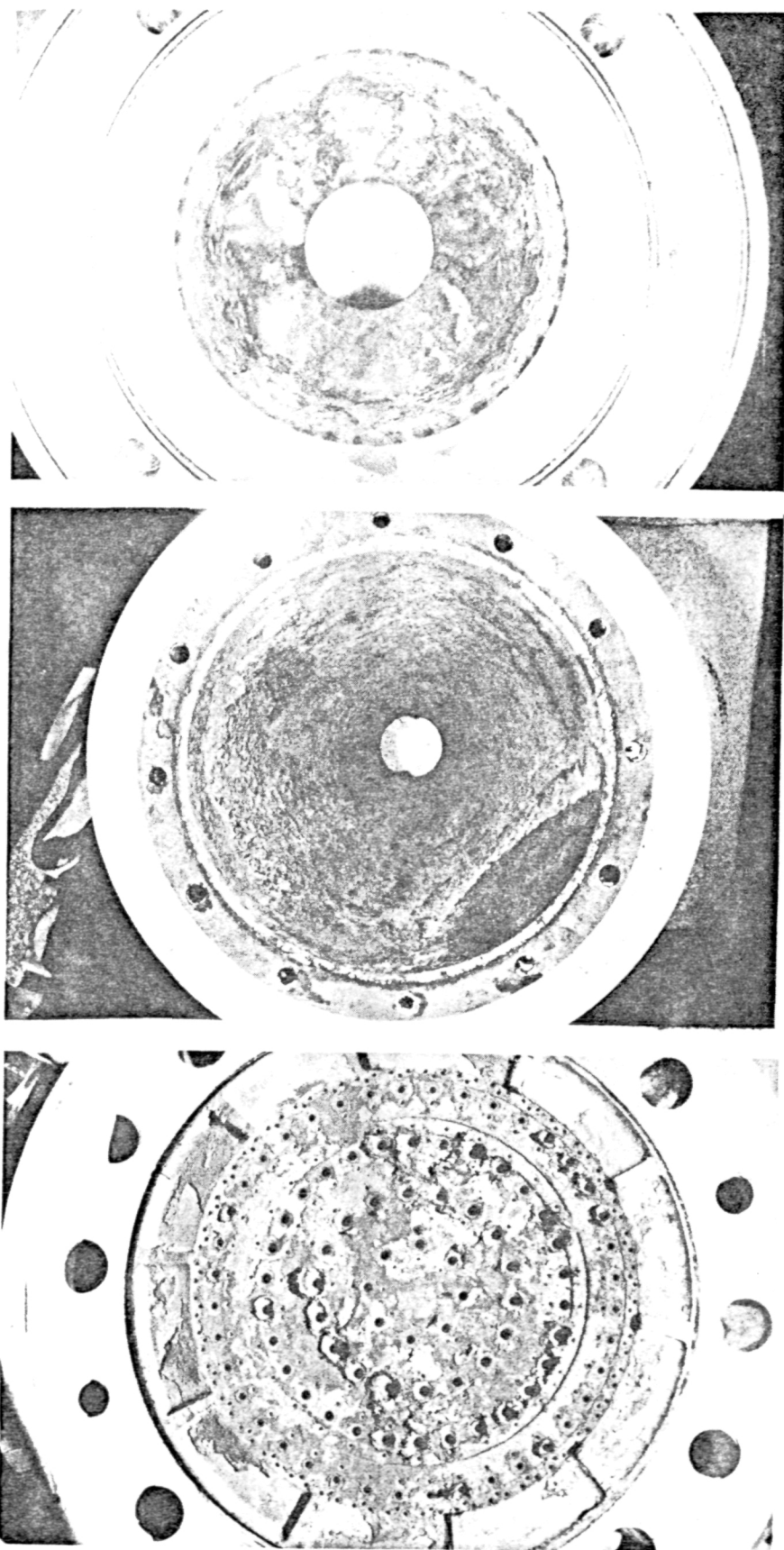


Figure 131, $F_2O_2-B_2H_6$ Regenerative Chamber Viewed From Injector and Chamber End; and Triplet Injector Face View Post Test 014 and 015 (2 and 25 sec duration)

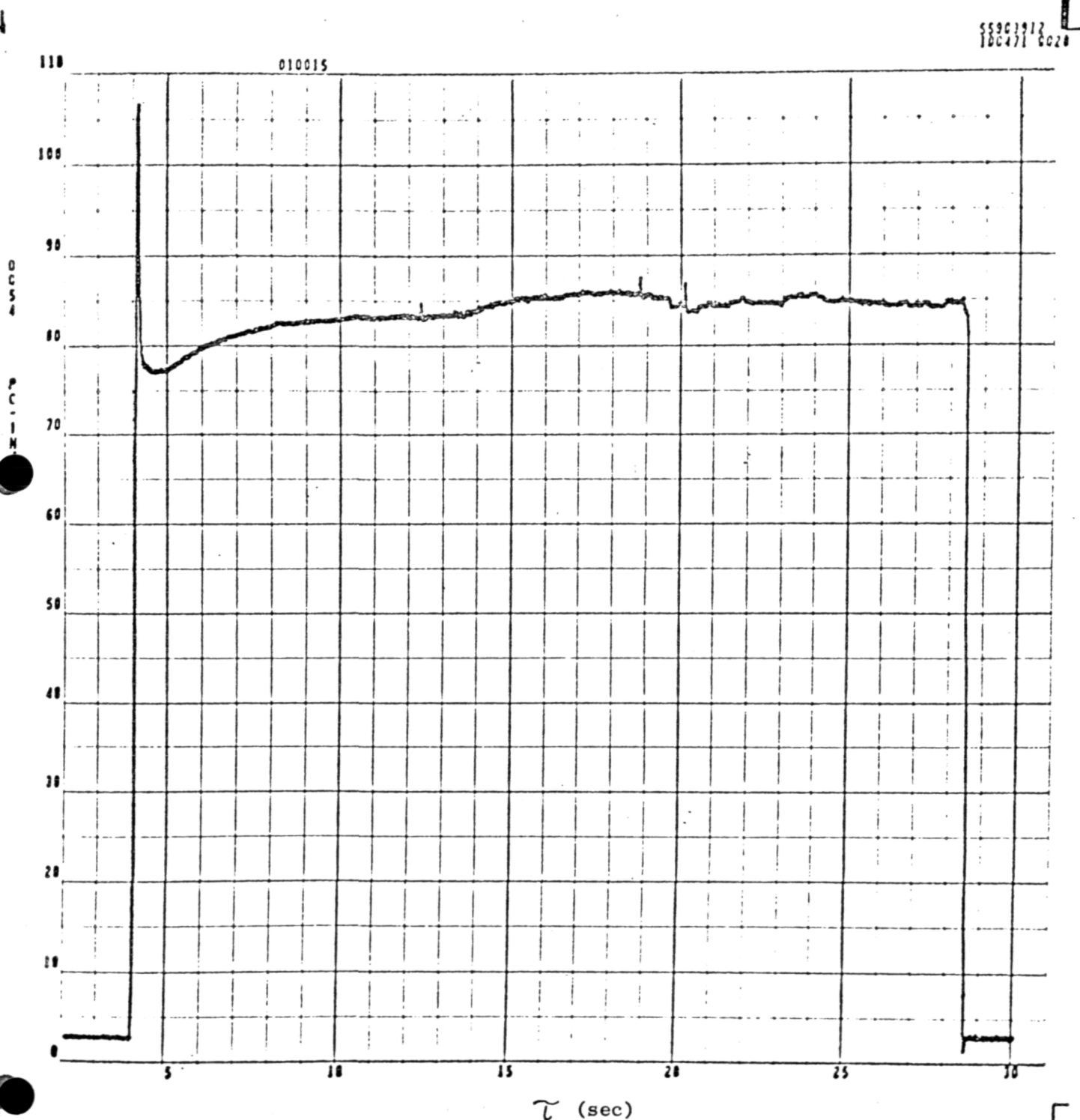


Figure 132. Chamber Pressure vs Time (Test 015)

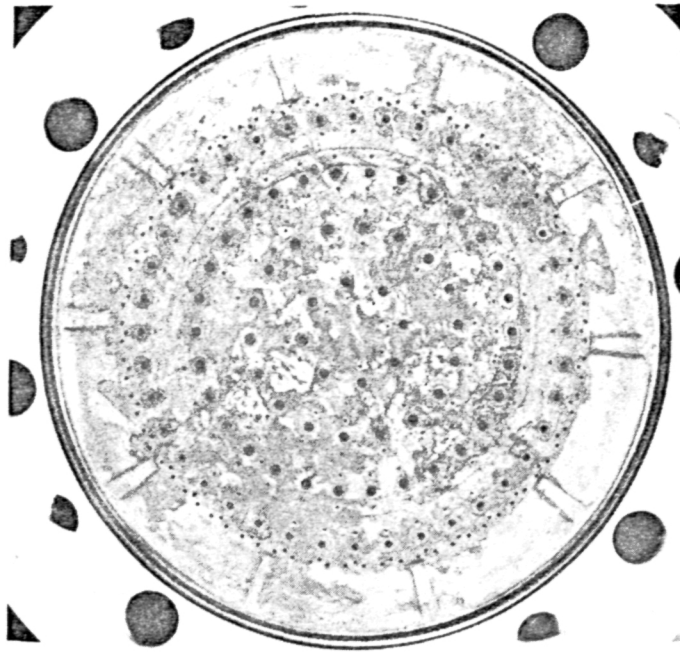
determined that a test duration of 45 seconds would ensure approximately 12.5 lb of B_2H_6 propellant in the run tank to avoid any potential tank liquid fuel depletion. It was also determined that a 45-second test would demonstrate the original objectives of the program without compromise. The test was programmed for 45 seconds duration with a targeted MR = 3.0 at 100 psia.

Test 017 achieved a programmed cutoff at 45 seconds with a nominal peak chamber pressure of 102 psia and 2.98 mixture ratio. Main fuel temperature and H_2O coolant outlet temperatures reached were 290 F and 98 F, respectively. Post test inspection indicated the hardware condition to be excellent (Fig. 133) with injector and chamber deposit conditions similar to Test 013 (10 seconds) and 015 (24 seconds). Figures 134 and 135 illustrate the regenerative chamber/diffuser installation.

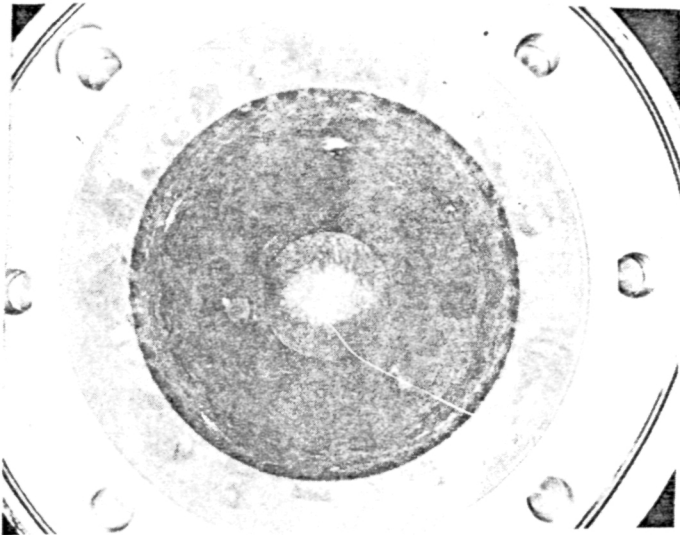
Figure 136 shows the chamber pressure (psig) trace for Test 017. A slight reduction in chamber pressure noted post 22 seconds (run time) is as a result of an oxidizer flow decay reflection into chamber pressure due to some F_2/O_2 tank pressure decay.

Test 017, as the final test, concluded the calorimeter/regenerative test series to be conducted under this feasibility contract (NAS7-765) with all principal objectives achieved. Further in-depth future testing can better detail and characterize the overall $OF_2-B_2H_6$ engine operation and sequencing for flight operational usage.

Injector Face View



Chamber Injector End View



Chamber Nozzle End View

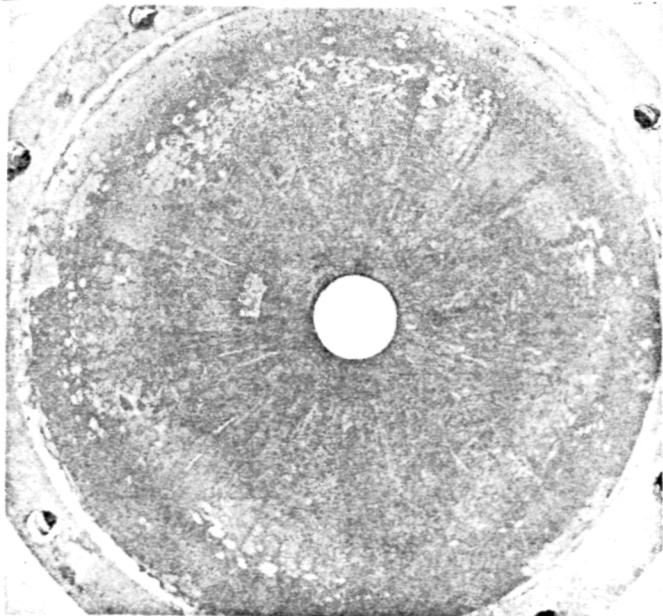


Figure 133, Triplet Injector and Regenerative Chamber Post
Test 016-017

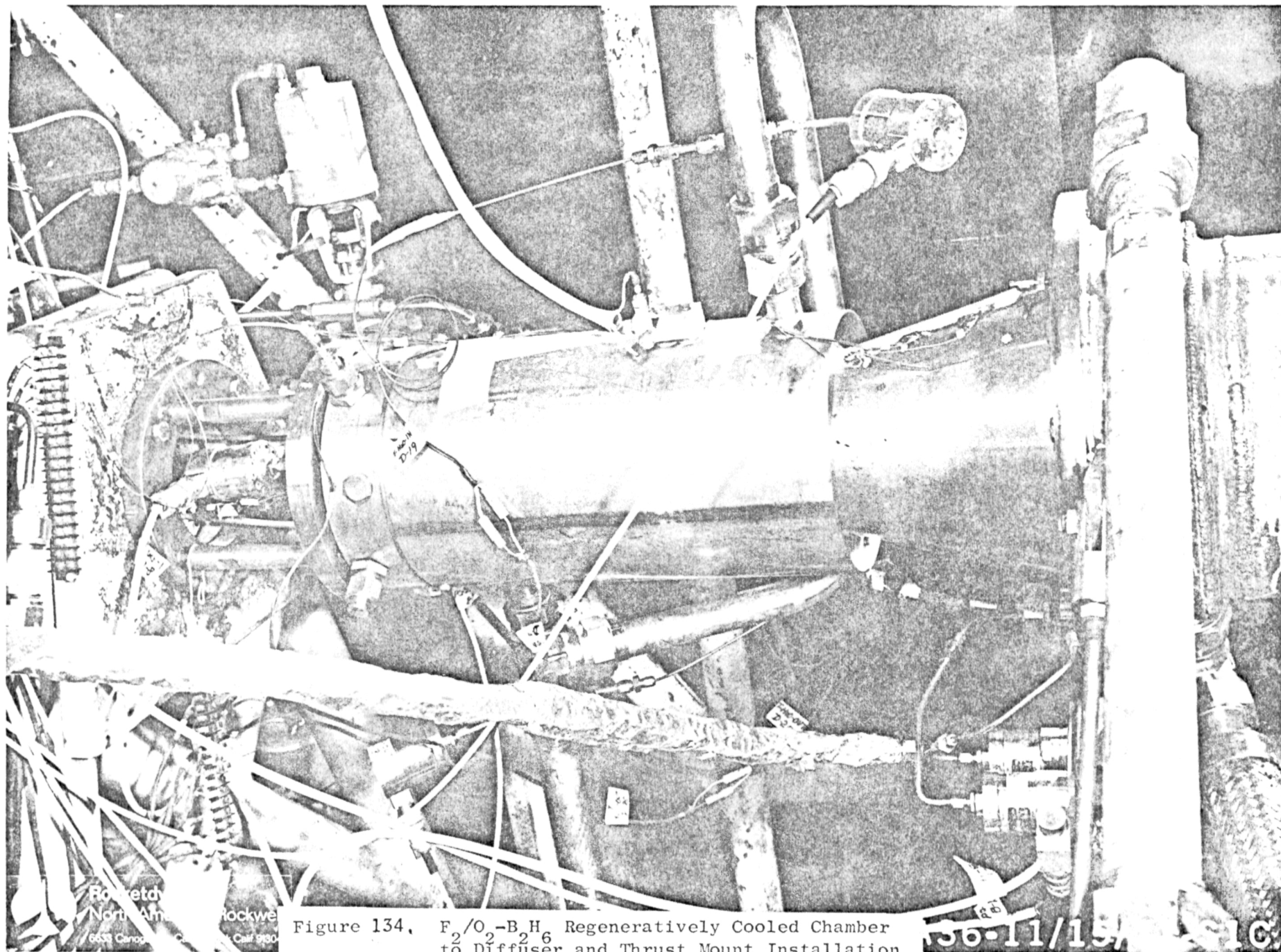
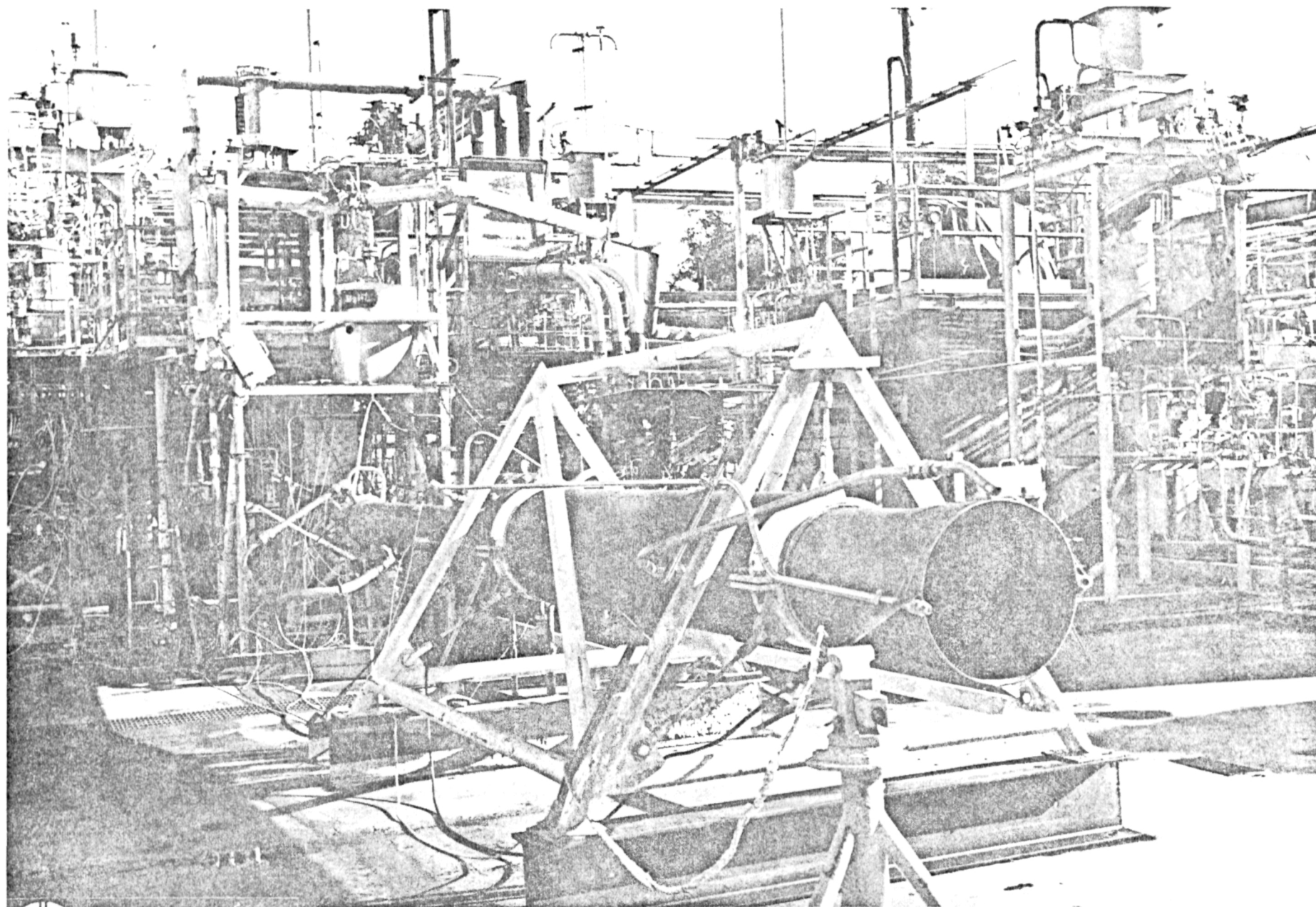


Figure 134, $F_2/O_2-B_2H_6$ Regeneratively Cooled Chamber to Diffuser and Thrust Mount Installation (Tests 016-017)

56-11/15-1C



Rocketdyne
North American Rockwell
8633 Canoga Ave. Canoga Park, Calif. 91304

Figure 135. Regenerative Chamber -- Diffuser Installation
Illustrating Modified Diffuser Cooling
System (Tests 016-017)

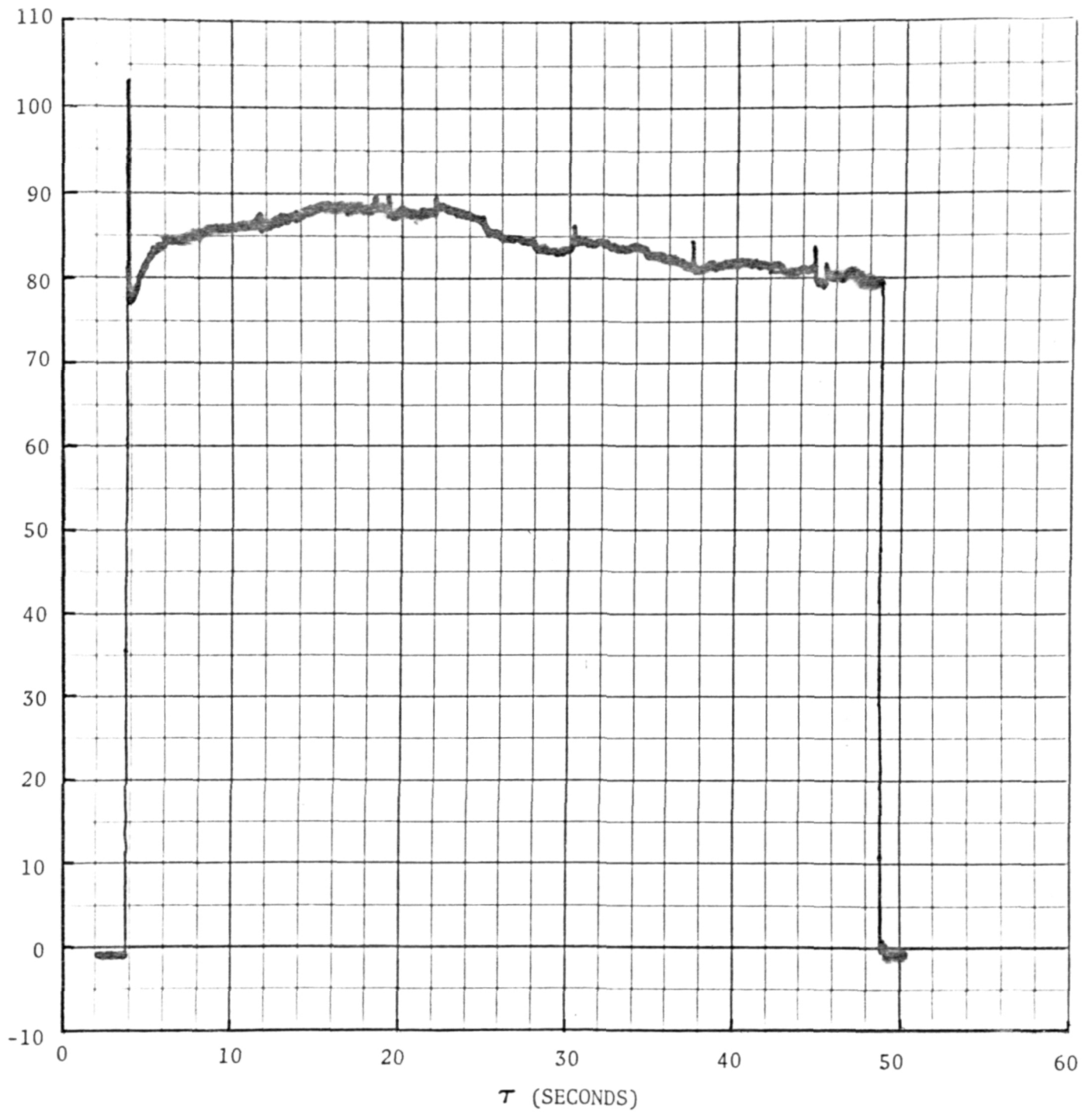


Figure 136. Chamber Pressure (psig) vs Test Run Duration (Test 017)

TASK IV - CALORIMETER-REGENERATIVE TEST SERIES DATA ANALYSIS

Raw test data acquired during the calorimeter-regenerative test series were reduced by the Beckman data system fed into the digital computer. Convenient graphical CRT and printout forms were provided. A summary of the reduced data is shown in Table 14. Appendix A and B outline the methods used to compare the data with the theoretical values.

CALORIMETER SERIES TEST DATA ANALYSIS

Engine test data for the calorimeter series developed characteristic velocity performance, wall temperature and heat load, and injector pressure drop characteristics. The following is a summary of these pertinent test data.

Characteristic Velocity Performance and Corrections

Characteristic velocity performance for the calorimeter series, Tests 004-008, was developed from the chamber pressure, measured throat area and total flow conditions. The reduced calorimeter performance conditions are shown in Table 15. Energy release efficiencies ($\eta_{c^*}^{ER,K}$) from 94.4 percent on short duration tests to 98.5 percent maximum were measured. Detailed repeatability and accuracy were not assessed due to the limited number of test runs, however, values ($\eta_{c^*}^{ER,K}$) in the vicinity of 95-96 percent can be projected for long durations.

Calorimeter Chamber Heat Transfer Measurements

Heat transfer measurements taken during the calorimeter series consisted of two injector face thermocouples, 10 combustion chamber wall thermocouples, and 5 nozzle heat plug measurements.

The injector face thermocouple transient measurements taken as a function of time showed the maximum transient face temperature achieved was 150 F with close agreement shown between the face thermocouples.

TABLE 14. TASK IV CALORIMETER/REGENERATIVE DATA SUMMARY ($F_2/O_2-B_2H_6$)

	1	2	3	4	5	6	7	8	9	10	11	12	13	14	15	16	17	18	19	20
	Test Number	Duration (sec)	Chamber Type	Oxidizer Venturi Temp. (F)	Oxidizer Venturi Pressure (psia)	Oxidizer Flowrate (#/sec)	Fuel Venturi Temp. (F)	Fuel Venturi Pressure (psia)	Fuel Flowrate (#/sec)	Film Coolant (%)	Total Flowrate (#/sec)	Mixture Ratio	Throat Area A_T (cold) (in ²)	Nozzle Stagnation Pressure (psia)	Jacket Inlet/Outlet Pressure (psia)	Jacket Outlet Temp. (F)	H ₂ O ΔT (F)	Water Flow (#/sec)	Q _{H₂H₆} (Btu/sec)	Q _{H₂O} (Btu/sec)
1	004	1.5	Calor.*			1.933			.590	33	2.523	3.27	5.301	102.4	--	--	--	--	--	--
2	005	2.0	Calor.*			1.911			.600	33	2.510	3.19	5.301	103.4	--	--	--	--	--	--
3	006	2.0	Calor.	--	522.8	--	112.7	322.8	--	43	Unstable		5.301	93.3	--	--	--	--	--	--
4	007	1.5	Calor.	78.0	509.1	1.882	75.0	406.5	.673	33	2.555	2.79	5.301	103.5	--	--	--	--	--	--
5	008	3.0	Calor.	74.4	507.7	1.882	85.2	397.8	.649	33	2.531	2.90	5.301	102.2	--	--	--	--	--	--
6	009	0.4	Reg.	67.7	421.7	1.575	-104.0	431.6	.624	30	2.199	2.52	5.305	82.7	143/91	-42	7.0	3.81	27	27
7	010	1.4	Reg.	68.1	320.9	1.842	-106.0	416.1	.615	30	2.457	3.00	5.305	91.1	191/104	125	20.5	1.126	186	23
8	011	3.5	Reg.	64.6	333.4	1.920	-102.4	420.0	.612	30	2.532	3.13	5.305	95.6	214/111	187	30.0	3.56	208	107
9	012	2.0	Reg.	61.2	320.6	1.852	-100.6	433.9	.619	30	2.471	2.99	5.305	93.0	184/104	84	17.0	6.41	169	109
10	013	10.0	Reg.	58.4	325.0	1.882	-105.5	441.6	.633	30	2.515	2.97	5.305	97.3	222/114	226	54.0	5.02	235	271
11	014	2.0	Reg.	59.9	325.2	1.881	-101.0	468.1	.649	30	2.530	2.89	5.305	95.6	181/108	62	36.0	3.38	174	122
12	015	24.0	Reg.	56.6	332.3	1.929	-111.1	481.3	.670	30	2.600	2.87	5.305	100.8	232/121	190	94.5	3.82	300	361
13	016	3.0	Reg.	55.5	333.7	1.938	-100.5	435.2	.622	30	2.560	3.12	5.305	96.5	196/102	143	31.7	8.82	194	270
14	017b	10.0	Reg.	47.8	339.0	1.984	-109.2	476.5	.665	30	2.649	2.98	5.305	103.6	215/111	181	31.7	8.89	220	282
	017c	45.0	Reg.	45.1	304.2	1.785	-111.5	475.4	.667	30	2.452	2.68	5.305	94.1	295/118	302	34.7	9.13	265	317
16																				
17																				
18																				
19	* $\epsilon = 4.0$ (other tests at $\epsilon = 20$)																			
20																				
21																				
22																				
23																				
24																				
25																				
26																				
27																				
28																				
29																				
30																				
31																				
32																				
33																				
34																				
35																				

"Page missing from available version"

Figure 137 and 138 illustrate the combustion chamber wall heat flux condition vs axial length for the 33 percent BLC flow condition. As shown the initial test in a series has a higher wall heat flux. Subsequent tests show reduction in wall heat fluxes as a result of deposit formation. This process is analogous to that seen in F_2/O_2-CH_4 and $O_2/RP1$ test chambers. High heat flux data taken during the unstable Test 006 with the high BLC flow (43 percent) were not considered usable for BLC flow effects upon wall heat transfer rates. The measured chamber wall heat flux rates agreed closely with previous test data for the 33 percent BLC condition. This heat flux level was indicated to be satisfactory for the regenerative chamber and the calorimeter test series was terminated at Test 008.

The nozzle plug heat flux measurements taken on Tests 006-008, with the 20:1 steel nozzle and diffuser attached, were unsatisfactory due to vibrational damage caused during the unstable test run (006). Back wall thermocouple data taken during the later regenerative series were used for nozzle heat fluxes. This was shown to be in good agreement with previous experimental nozzle heat flux levels.

Injector Pressure Drops

Analysis of injector pressure drop data taken during the calorimeter test series is shown in Fig. 139 for the fuel and oxidizer flows. Both pressure drops were near predicted levels at the near design flow test conditions. For Test 006, where instability occurred with attendant orifice plugging, it is shown that high pressure drops were obtained.

Calorimeter Test Summary

In summary, the targeted heat flux, mixture ratio range, chamber pressure, and high characteristic velocity efficiency were established for the No. 2 triplet injector with the calorimeter chamber in the test series. Only minor face deposits were observed for these short tests attesting to the improved oxidizer injection velocity effect for the No. 2 triplet injector over previous triplet

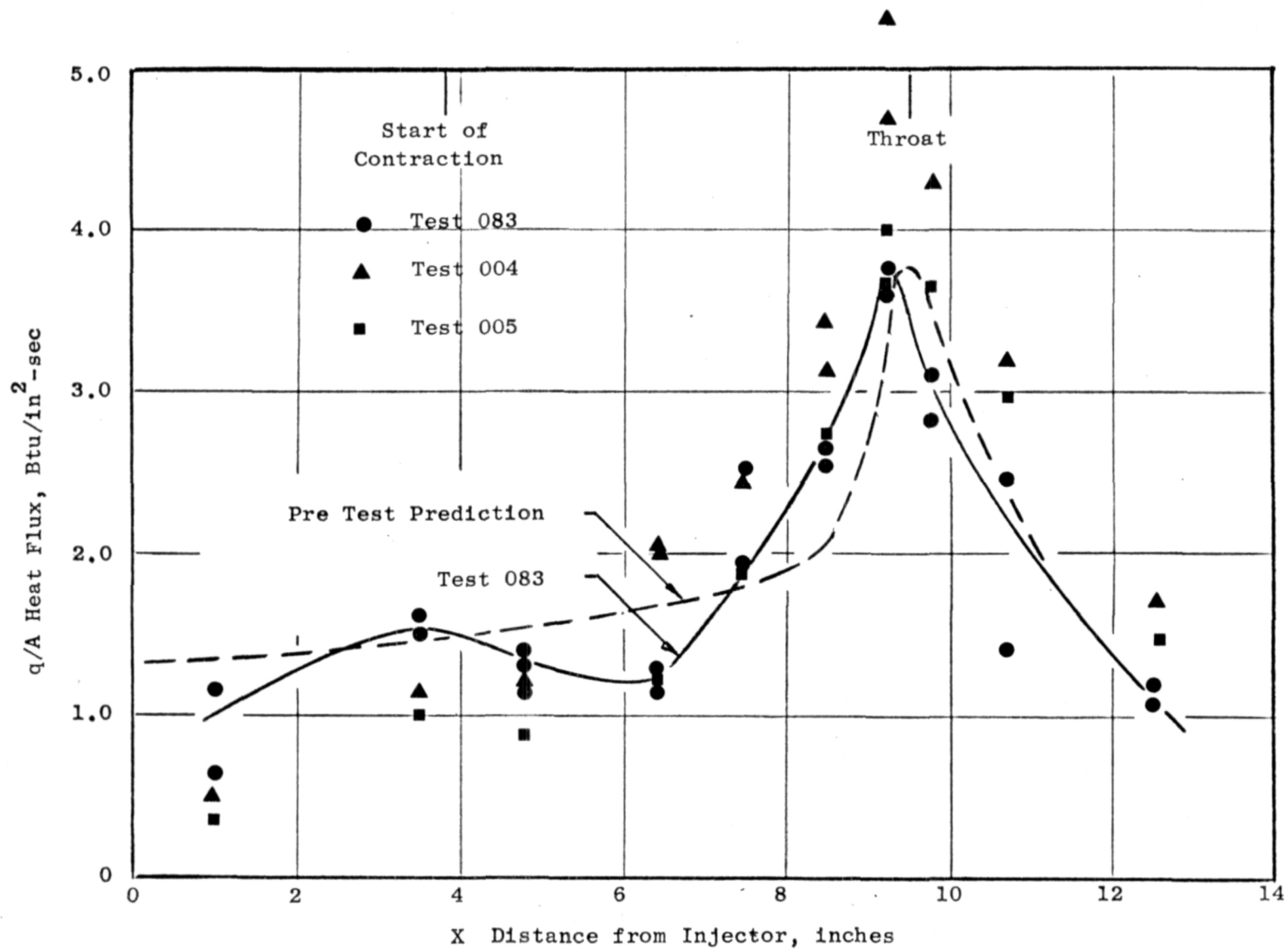


Figure 137. Heat Flux Profile for Nominal Test Conditions with 9.5-inch Combustion Chamber (Tests 004, 005, 083)

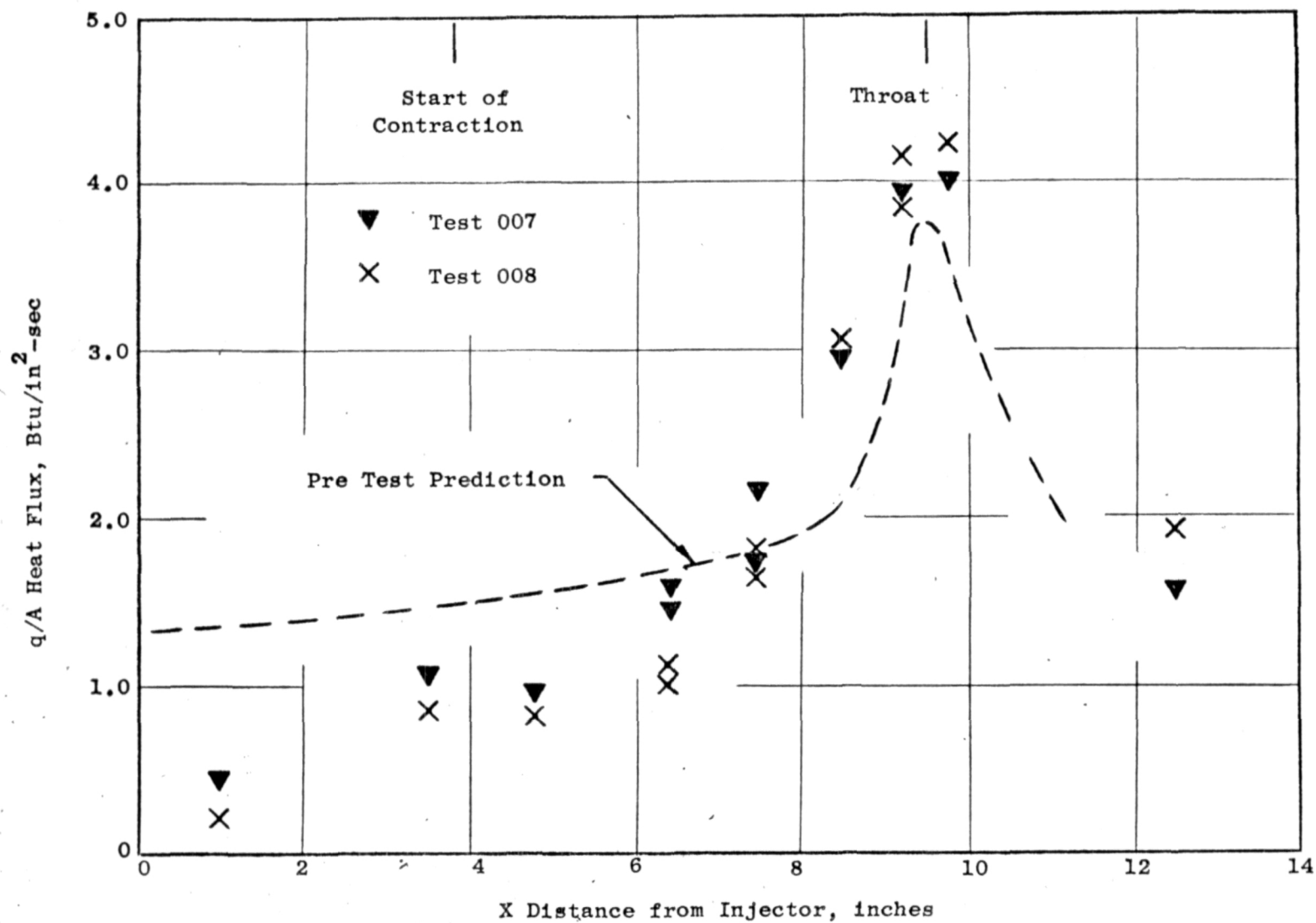


Figure 138. Heat Flux Profile for Nominal Test Conditions with 9.5-inch Combustion Chamber (Tests 007-008)

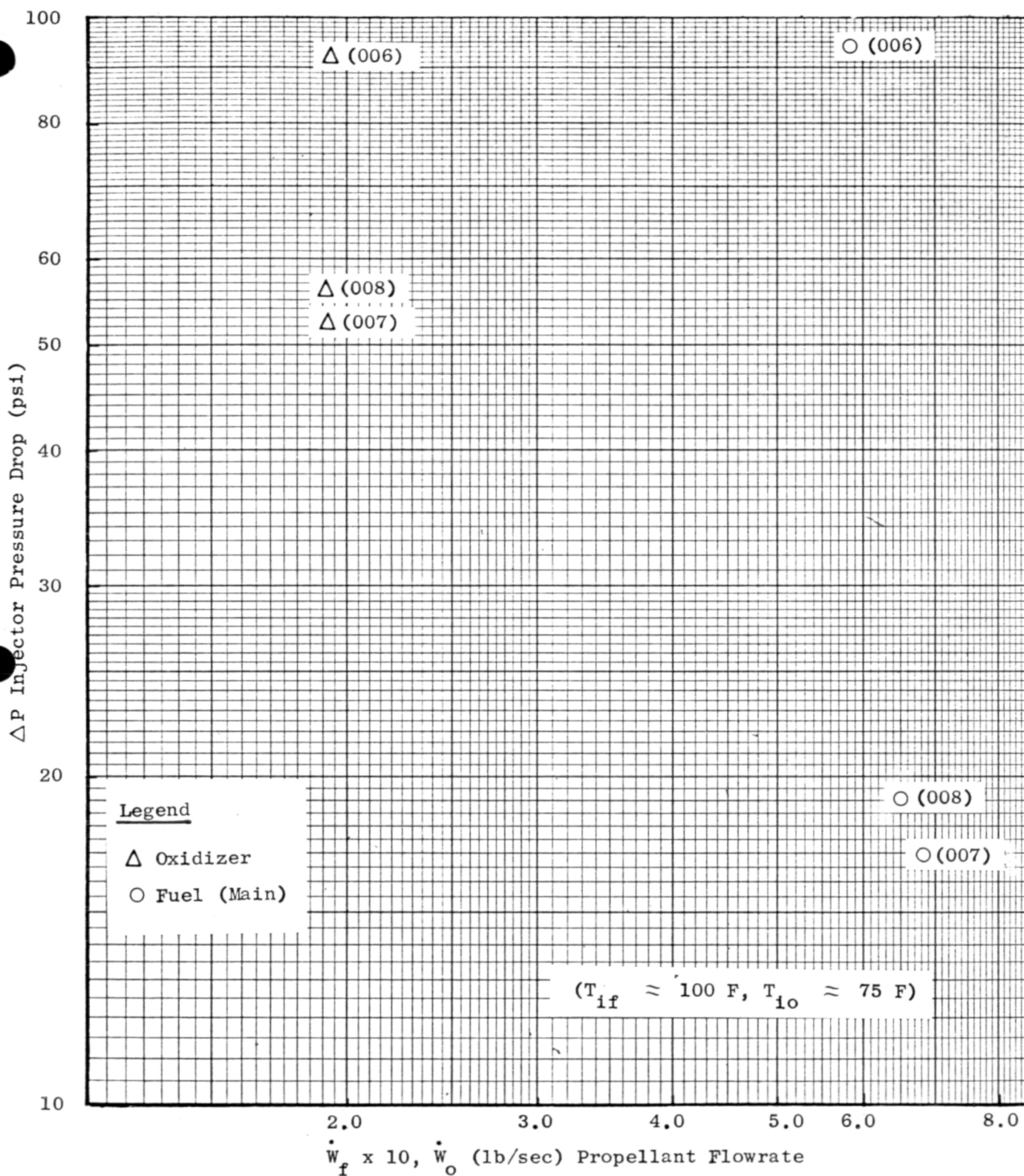


Figure 139. Calorimeter Test Series No. 2 Triplet Injector Experimental Fuel and Oxidizer Side Pressure Drop vs Flow

designs. During Tests 007 and 008 only minor deposits were observed post test in the acoustic cavity region, although no projection could be made for long regenerative durations. Chamber wall heat flux data appeared to be close to that previously taken with some timewise reduction along the throat contour ramp and also as a function of successive test runs (apparent insulating deposit buildup).

REGENERATIVE SERIES -- TEST DATA ANALYSIS

The principal variables developed during the regenerative test series were the injector/chamber characteristic velocity performance, nozzle and combustor heat transfer loads, chamber coolant pressure drop, injector face temperature, and chamber and nozzle wall temperatures. The data reductions of the pertinent parameters measured are described below.

Characteristic Velocity Performance

Data reduction for the c^* efficiency for the regenerative chamber was accomplished in a manner similar to that described for the calorimeter series. Transducer calibration and venturi checks were conducted to compare time changes in calibration on the measurements. Based on data analysis checks some differences between the calorimeter and regenerative testing performance were noted (Appendix).

Performance Results. The nozzle stagnation c^* efficiency performance shown in Table 16 indicates good combustion efficiency was obtained with the No. 2 injector in the regenerative chamber. For the long duration tests, c^* performance was in the 95.8 to 96.8 percent range. Exact and detailed c^* performance repeatability and tolerance of uncertainty would have to be based on a large number of test runs with tolerance and bias levels on all measurements accurately traced. Further refinement of the performance measurements was considered outside of the scope of effort for the current program.

TABLE 16. REGENERATIVE TESTING PERFORMANCE EVALUATION

Run No.	Mainstage Time (sec)	\dot{W}_o (lb/sec)	\dot{W}_f (lb/sec)	\dot{W}_T (lb/sec)	MR	$p_{c\text{inj}}$ (psia)	\bar{p}_o^* (psia)	$c_{TC\text{exp}}^*$ (ft/sec)	c_{ODE}^* (ft/sec)	$\eta_{c_{TC}}^*$ (%)	$\eta_{c_{ER,K}}^*$ (%)
9	0.4	1.575	.624	2.199	2.52	81.5	83.9	6528	6918	94.0	93.7
10	1.4	1.842	.615	2.457	3.00	89.8	92.4	6435	7003	91.6	91.2
11a	2.0	1.899	.606	2.505	3.13	93.1	95.8	6544	7025	92.9	92.5
11b	3.5	1.920	.612	2.532	3.13	94.2	96.9	6549	7026	92.4	92.6
12	2.0	1.852	.619	2.471	2.99	91.6	94.3	6530	7003	92.9	92.6
13a	6.0	1.880	.633	2.513	2.97	94.3	97.0	6605	7004	94.0	93.7
13b	10.0	1.882	.633	2.515	2.97	95.9	98.7	6715	7006	95.5	95.2
14	2.0	1.881	.649	2.530	2.89	94.2	96.9	6554	6990	93.4	93.1
15a	6.0	1.932	.666	2.598	2.90	96.9	99.7	6568	6995	93.6	93.2
15b	10.0	1.926	.670	2.596	2.87	99.3	102.2	6737	6993	96.0	95.7
15c	25.0	1.929	.671	2.600	2.87	98.3	101.1	6653	6993	94.8	94.5
16	3.0	1.938	.622	2.560	3.12	95.1	97.9	6544	7027	92.8	92.5
17b	12.0	1.984	.665	2.649	2.98	102.1	105.1	6789	7014	96.4	96.1
17c	45.0	1.785	.667	2.452	2.68	92.7	95.4	6658	6952	95.4	95.1

$$A_T = 5.305 \text{ in}^2 \text{ (cold)}$$

$$A_T = 5.294 \text{ in}^2 \text{ (hot)}$$

$$c_{\text{exp}}^* = \frac{\bar{p}_o^* A_{T(\text{hot})}}{\dot{m}_T}, \quad \eta_{c_{TC\text{exp}}^*} = \frac{c_{\text{exp}}^*}{c_{ODE}^*}$$

$$\eta_{c_{ER,K}^*} = \frac{C_{D2D} \left(1 - \frac{2 \delta^*}{R_T}\right)}{\eta_{c_{HL}^*}} (\eta_{c_{TC}^*})$$

Combustor and Nozzle Heat Transfer

The heat transfer measurements taken during the regenerative test series included combustor, throat, injector and nozzle back wall thermocouples, H_2O and B_2H_6 fluid temperatures and coolant flowrates. Data were evaluated both on a transient and steady state basis to develop heat fluxes temperature responses and final wall and fluid temperatures.

B_2H_6 and H_2O Coolant Heat Transfer. B_2H_6 coolant transient injection temperature conditions during 0-6.0 second time period are shown in Fig. 140 for Tests 009-017. The start transients are shown to be similar with a dependence of rise time upon the ignition time point temperature (fuel time lead and hardware temperature effects) and the fuel flowrate. As expected larger fuel flowrates resulted in a lowered injection temperature at any time point in the transient rise.

Main B_2H_6 fuel injection temperature vs time for Test 017 is shown in Fig. 141. Maximum temperature reached is shown to be 265 F near the cutoff time. Fluctuations observed in coolant outlet temperature during the testing are believed due to some buildup and decay of the wall insulating deposits. Further investigation and provision of stabilizing influences for these fluctuations can be made in detail during future BLC and mixture ratio survey testing.

B_2H_6 coolant heat load conditions are shown in Fig. 142 for Tests 015 and 017. Nearly stabilized levels of heat load are shown for periods past 15 seconds. H_2O heat load conditions are shown in Fig. 143.

Thrust Chamber Nozzle Heat Transfer. Nozzle wall temperature vs time for the back wall nozzle thermocouples are shown in Fig. 144. Stabilization is achieved at a 15 second time period except for TN4. Future design improvement in the lower nozzle area would reduce the measured temperature to the 400-500 F range to ensure no long term B_2H_6 decomposition deposit formation

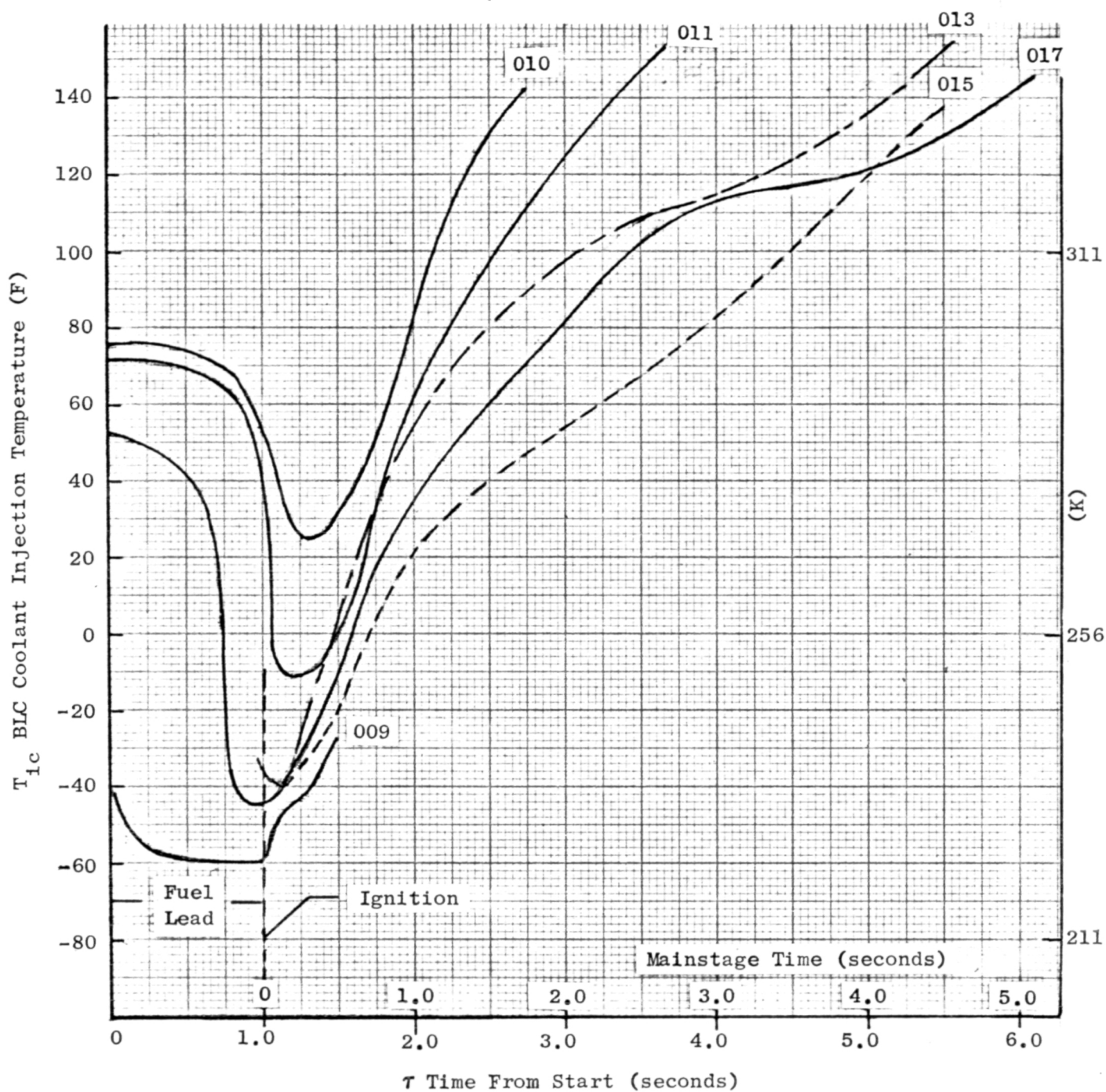


Figure 140. Comparison of Regenerative Chamber BLC Injection Temperature Transients During Ignition and Early Mainstage (Tests 009-017)

55903915
111771 0014

010017

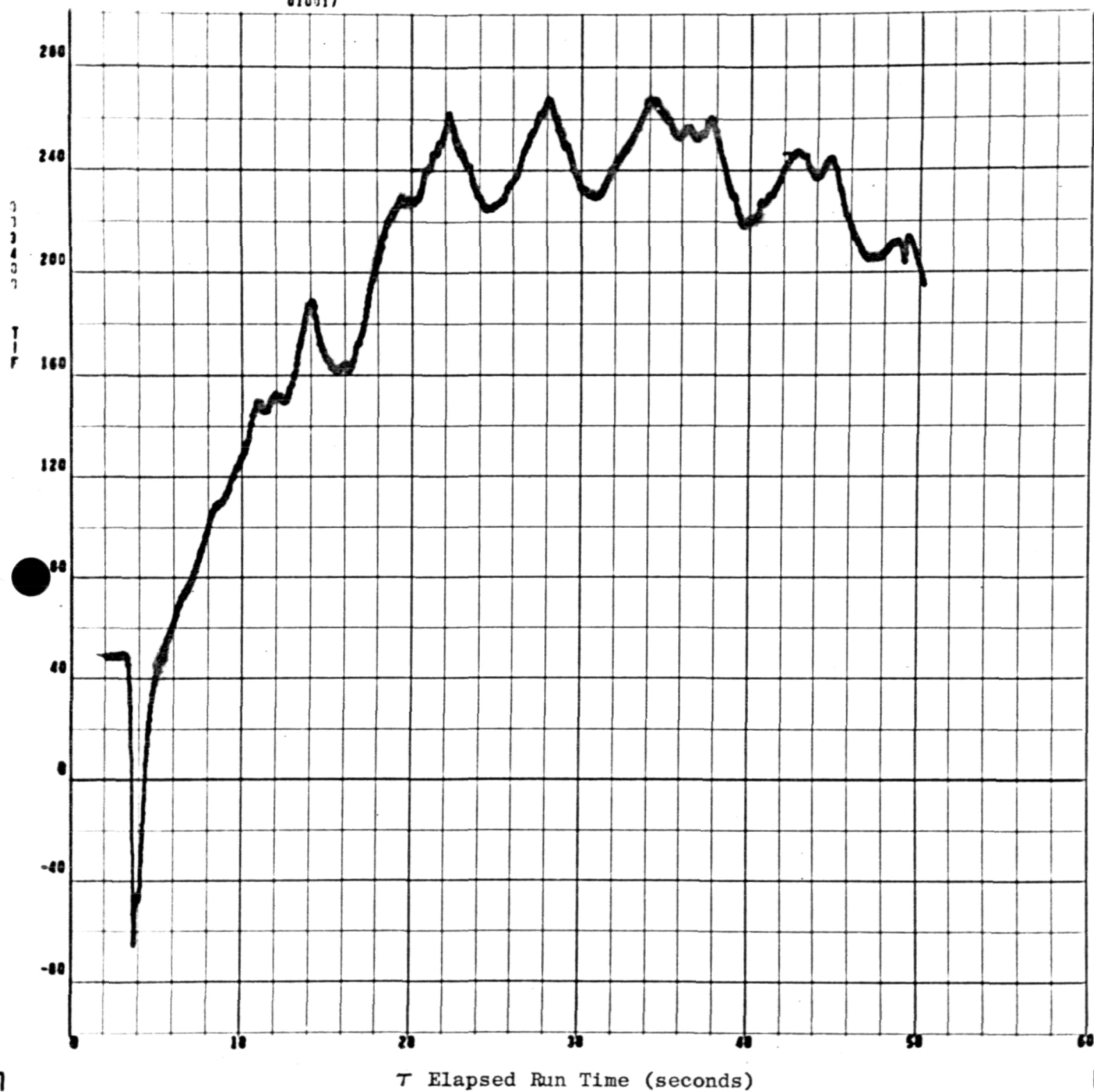


Figure 141. Main Fuel Injection Temperature vs Time (Test 017)

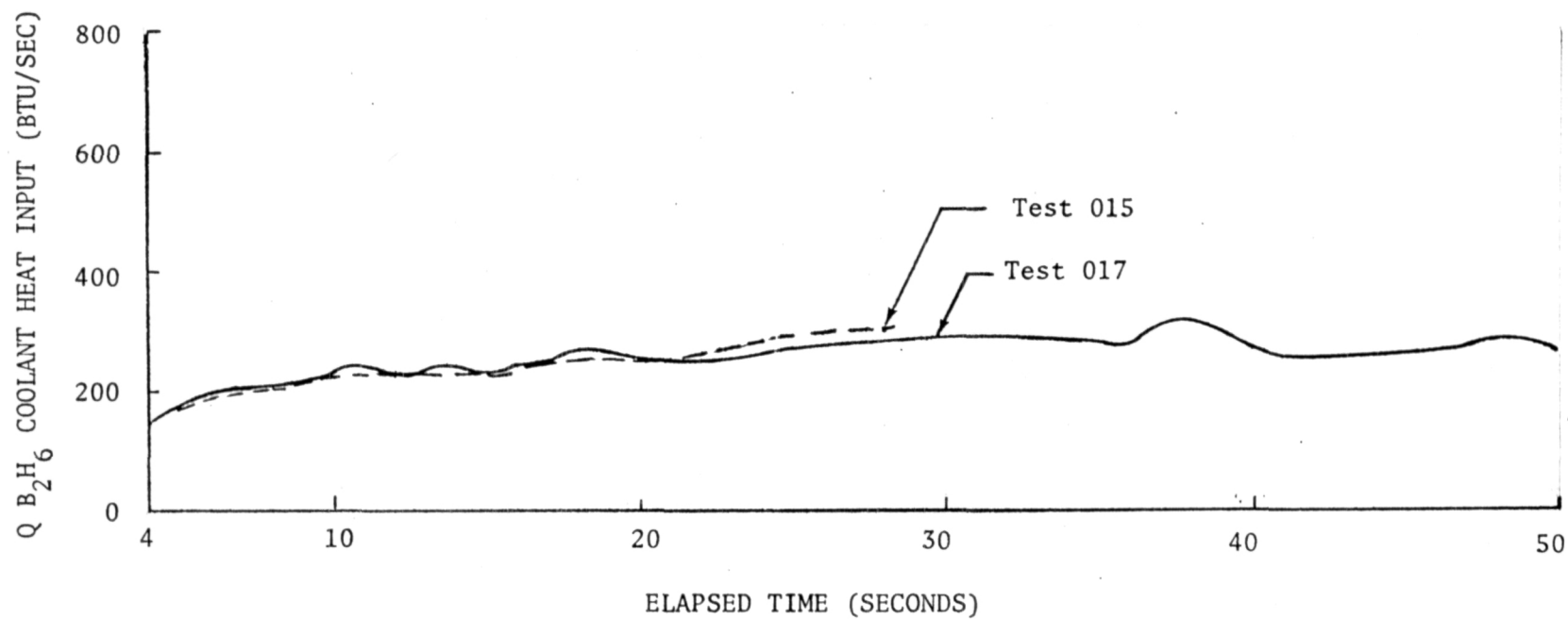


Figure 142. B_2H_6 Coolant Heat Input vs Time (Tests 015 and 017)

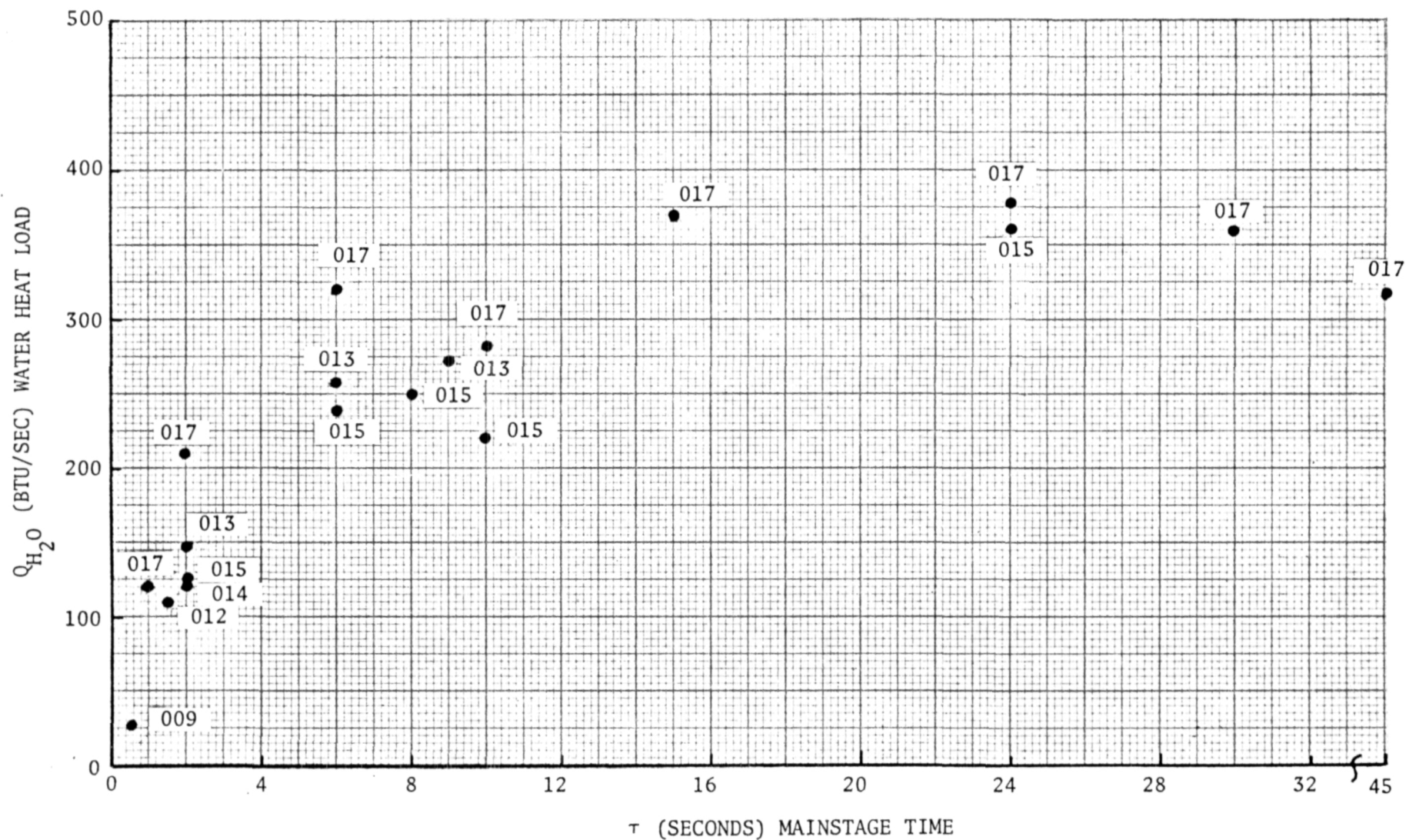


Figure 143. $F_2/O_2-B_2H_6$ Regenerative Chamber - H_2O Jacket Heat Load vs Time
(Tests 009 to 017)

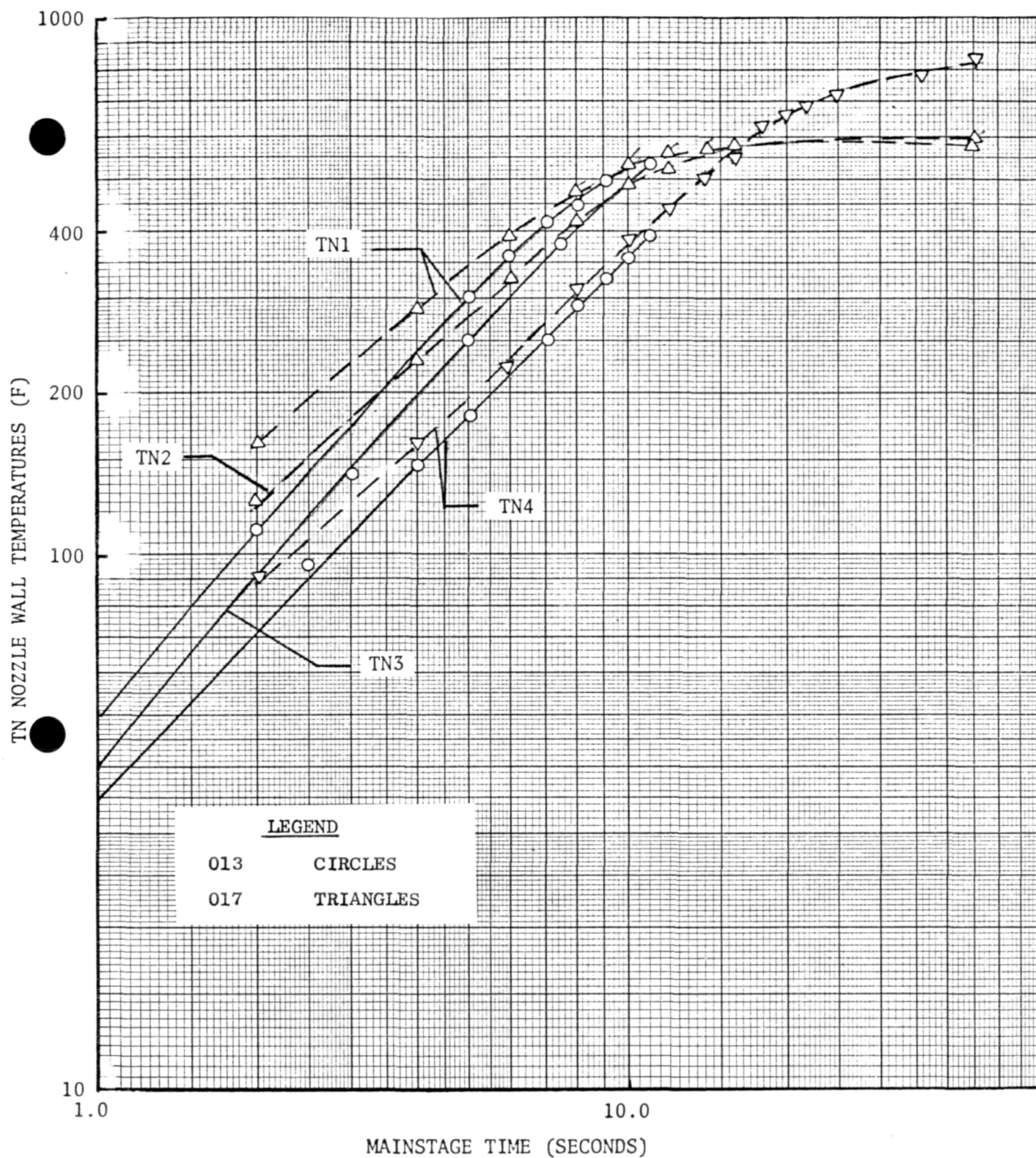


Figure 144. $F_2/O_2-B_2H_6$ Regenerative Nozzle Back Wall Temperature vs Time
(Tests 013 and 017)

in the coolant passages. Flight design inlet temperature conditions (-200 to -250 F) versus -110 F test conditions will also tend to reduce wall temperatures to lower values.

Regenerative nozzle wall heat flux conditions derived from the early (0+) time slope of the nozzle wall temperature are shown in Fig. 145. Higher steady state wall temperature levels will reduce the wall heat flux levels.

Combustor Wall Temperature Conditions. Combustor and throat region back wall temperature conditions were monitored during Tests 009-017. Initial data reduction indicates back wall temperature levels to be between the H_2O bulk and nucleate boiling temperatures, indicating H_2O film boiling did not occur during these tests. Small projections of the back wall thermocouple junctions and leads into the water film boundary layer precludes exact assessment of the water jacket region back wall temperatures.

Injector Face Temperature Conditions. During the regenerative series the injector face temperature was monitored by an injector face temperature thermocouple placed .040 inch from the surface. Figure 146 illustrates the face transient temperature as a function of time. Face temperature levels were seen to be following the coolant jacket exit temperature value. During the calorimeter series, the face thermocouples showed good uniformity of values as expected with the high thermal conductivity copper injector face design used.

Regenerative Chamber Operating Pressure and Stabilization

Coolant jacket inlet pressure vs time in Fig. 147 (Test 017) shows inlet pressure stabilization achieved at 20 seconds mainstage. Coolant jacket exit pressure (fuel injection pressure) shown in Fig. 148 (Test 017), typically stabilizes at 14 seconds into the run. Fuel and oxidizer injector pressure drop for the regenerative series is shown in Fig. 149.

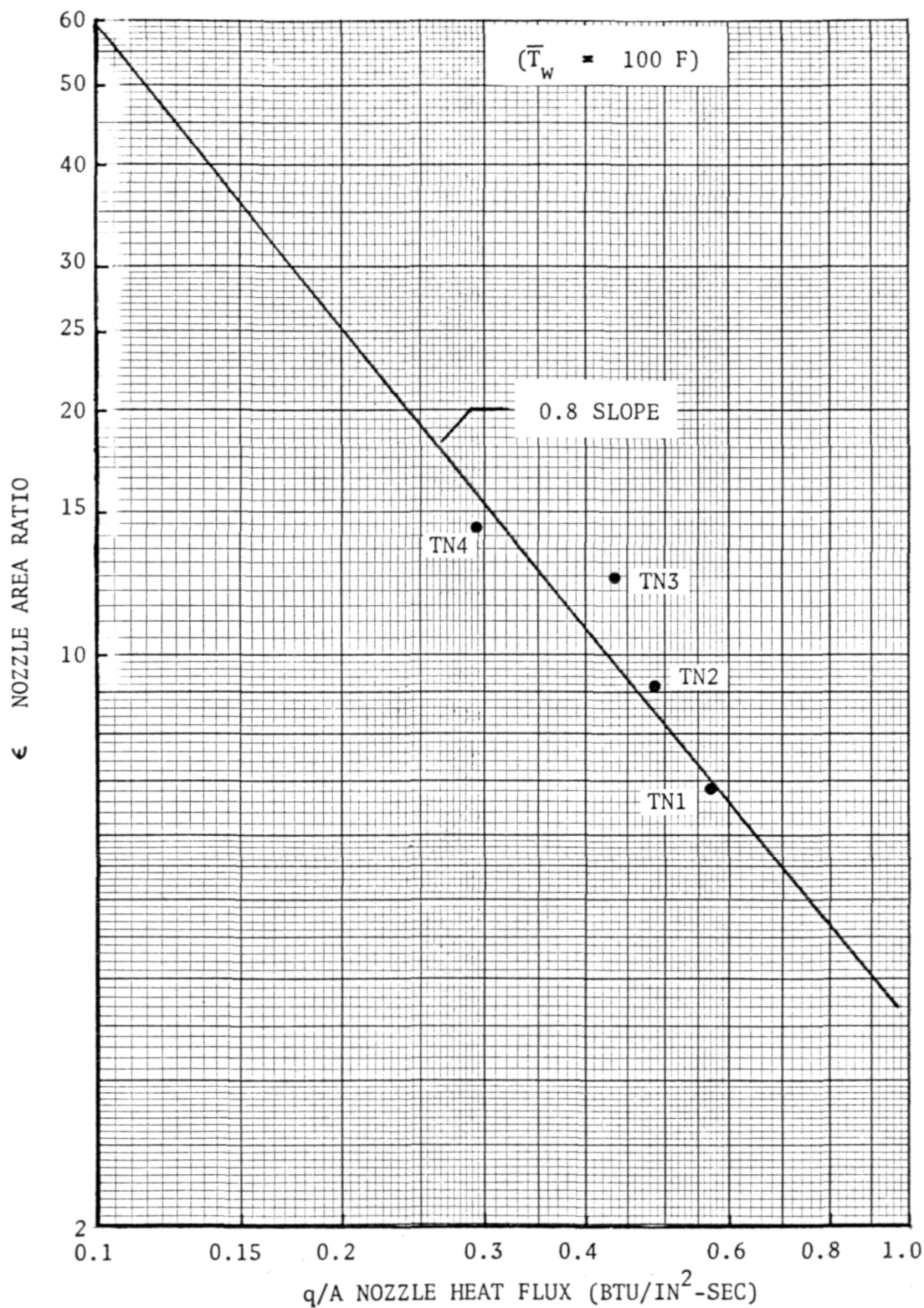


Figure 145. $F_2/O_2-B_2H_6$ Regenerative Nozzle Cold Wall Heat Flux vs Area Ratio

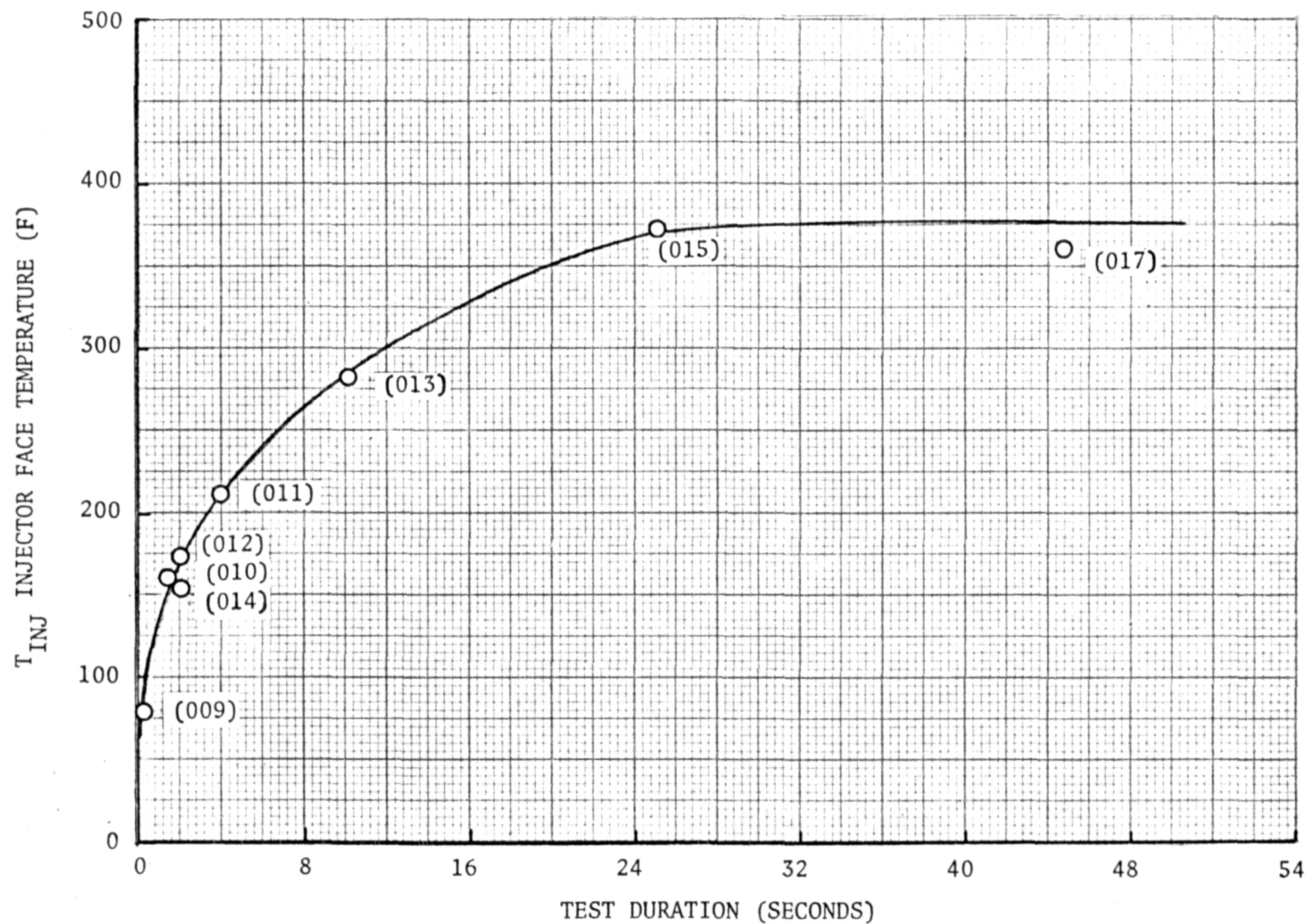


Figure 146. Summary of $\text{F}_2/\text{O}_2\text{-B}_2\text{H}_6$ Experimental Injector Face Temperatures vs Run Time

55903915
111771 0024

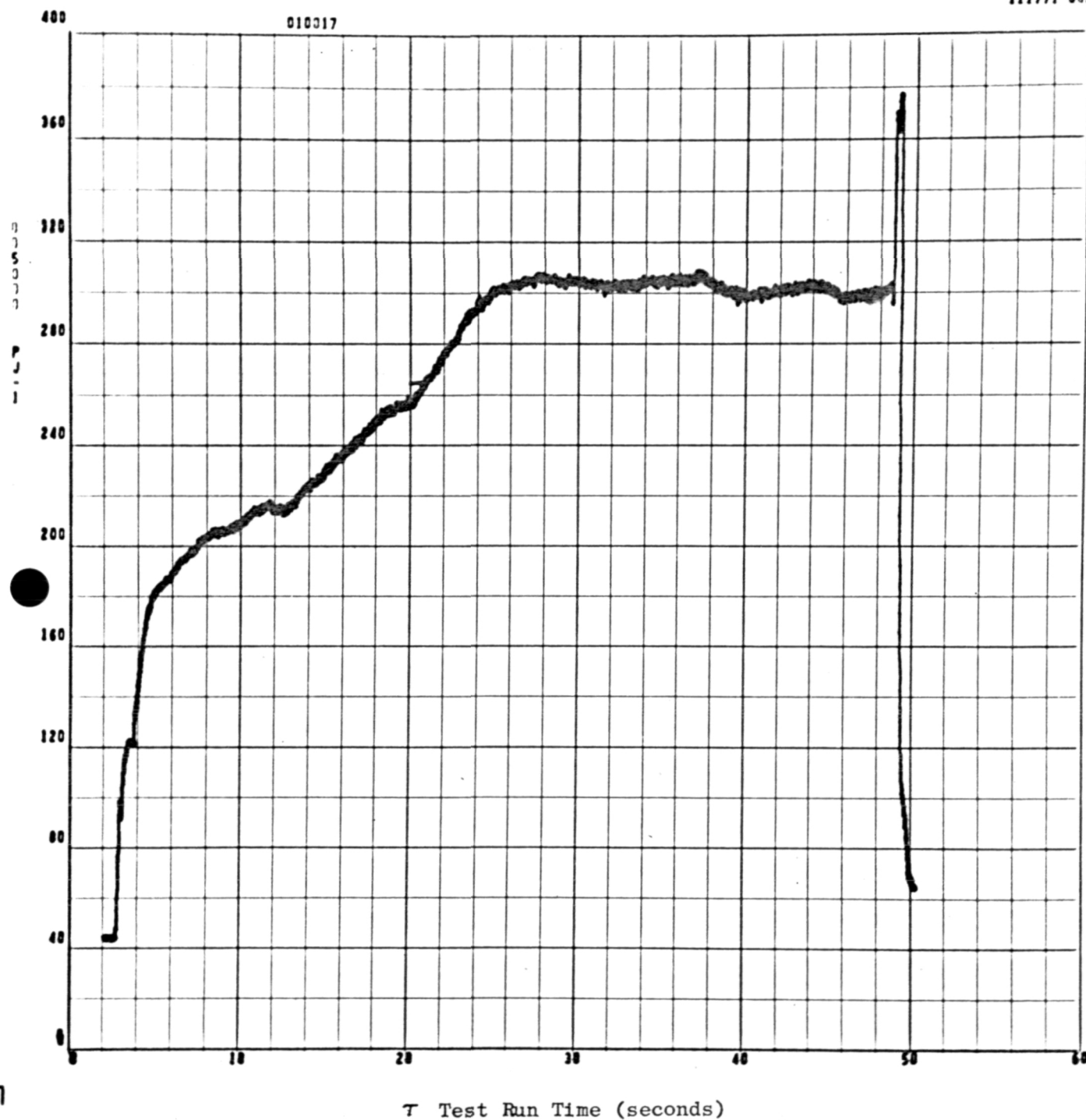


Figure 147, Coolant Jacket Inlet Pressure vs Time (Test 017)

55903915
111771 0026

010317

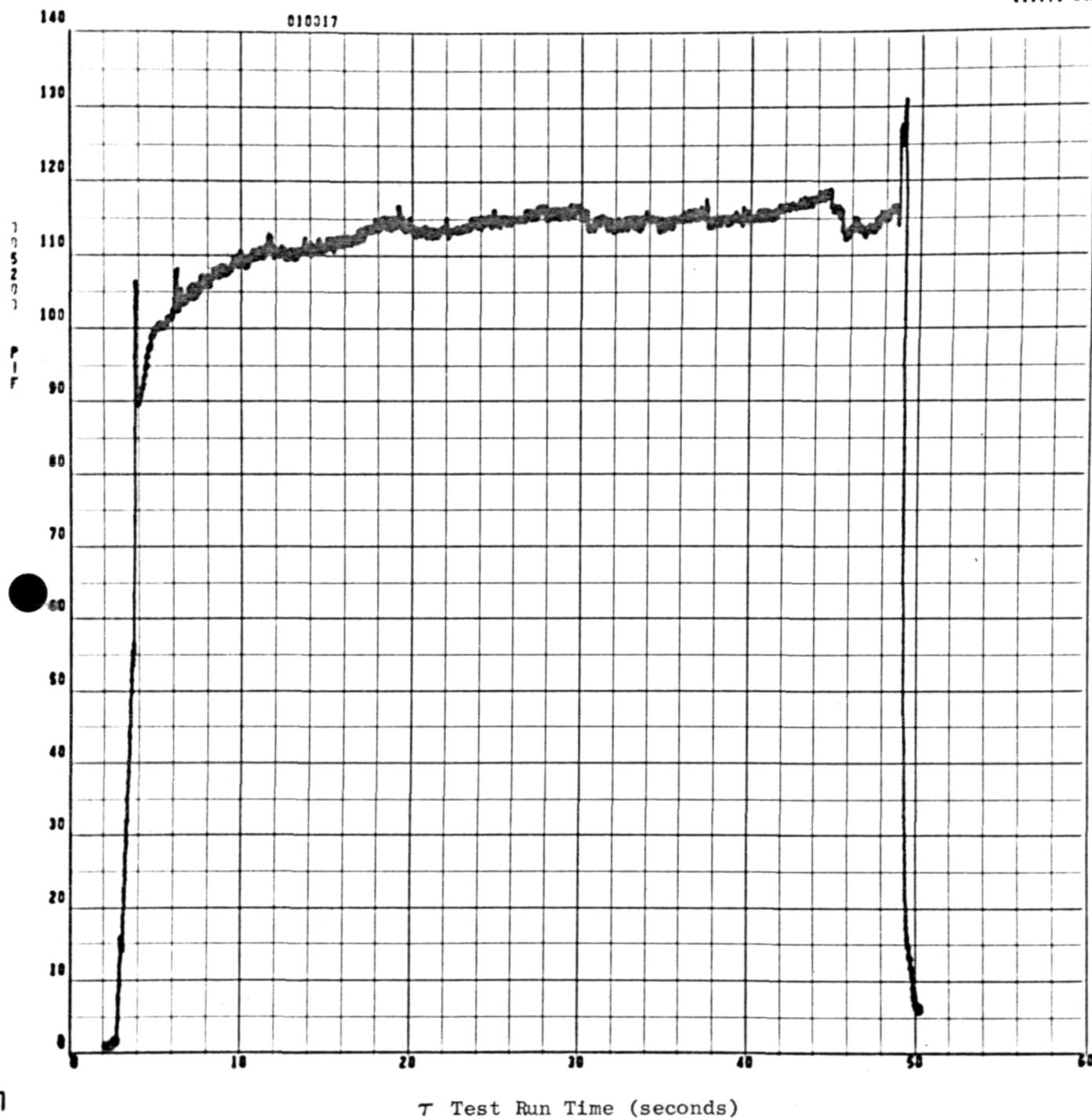


Figure 148. B₂H₆ Coolant Jacket Discharge Pressure vs Time (Test 017)

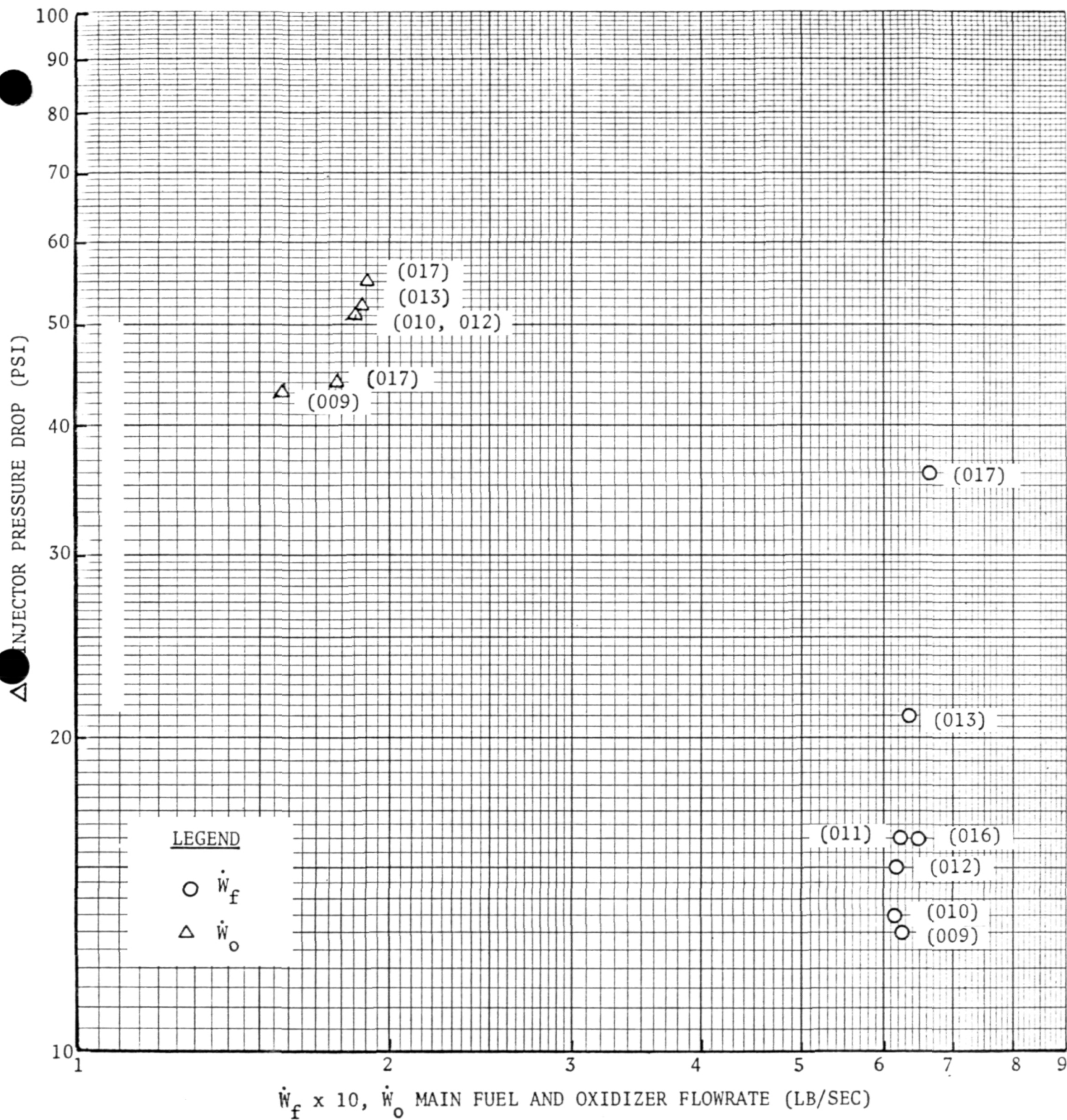


Figure 149. Regenerative Chamber Testing-Injector Pressure Drop vs Flowrate Summary

Chamber pressure stabilization is illustrated typically in Fig. 150 for Test 010. The 90 percent P_c point of mainstage is achieved at 200 ms from pressure rise initiation. Chamber pressure overshoot on ignition is a controllable parameter based on fuel and oxidizer flow ramp rates, fluid passage volumes and injection temperatures and this needs to be developed in detail with further experimental study. Close control of injector, coolant jacket and line fluid volumes between the control valves and the injector face plane, as well as closer coupled chamber pressure instrumentation, is necessary to ensure faster chamber pressure response times. Projected flight design hardware 90 percent P_c can be substantially reduced (≤ 50 ms) with these typical changes.

Regenerative Test Series Conclusions

The results of the regenerative testing verified the cooling concepts predicted at the onset of the contract study. In general, the total wall heat load for long durations was somewhat higher (640 Btu/sec) compared to predicted levels (470 Btu/sec), indicating some modification towards a reduced combustor wall surface area and modified BLC flow may be required for flight design conditions in order to meet flight pressure drop budgets.

Performance as indicated by corrected c^* measurements appeared good (94-96 percent) and in line with previous calorimeter measurements. Thrust measurement verification impulse values were not obtained, however, due to diffuser water and GN_2 feed line thermal expansion effects on thrust calibration values. No adverse stability, start or cutoff transient effects were noted.

Some cyclic variation in heat load was noted on the longer tests, theorized as due to insulating deposit "scaling" as a function of time. Further investigation into this area is recommended during any future experimental study.

In summary the principal objectives outlined initially for the study were met. Some detailed engine refinement will be necessary during future developmental type testing.

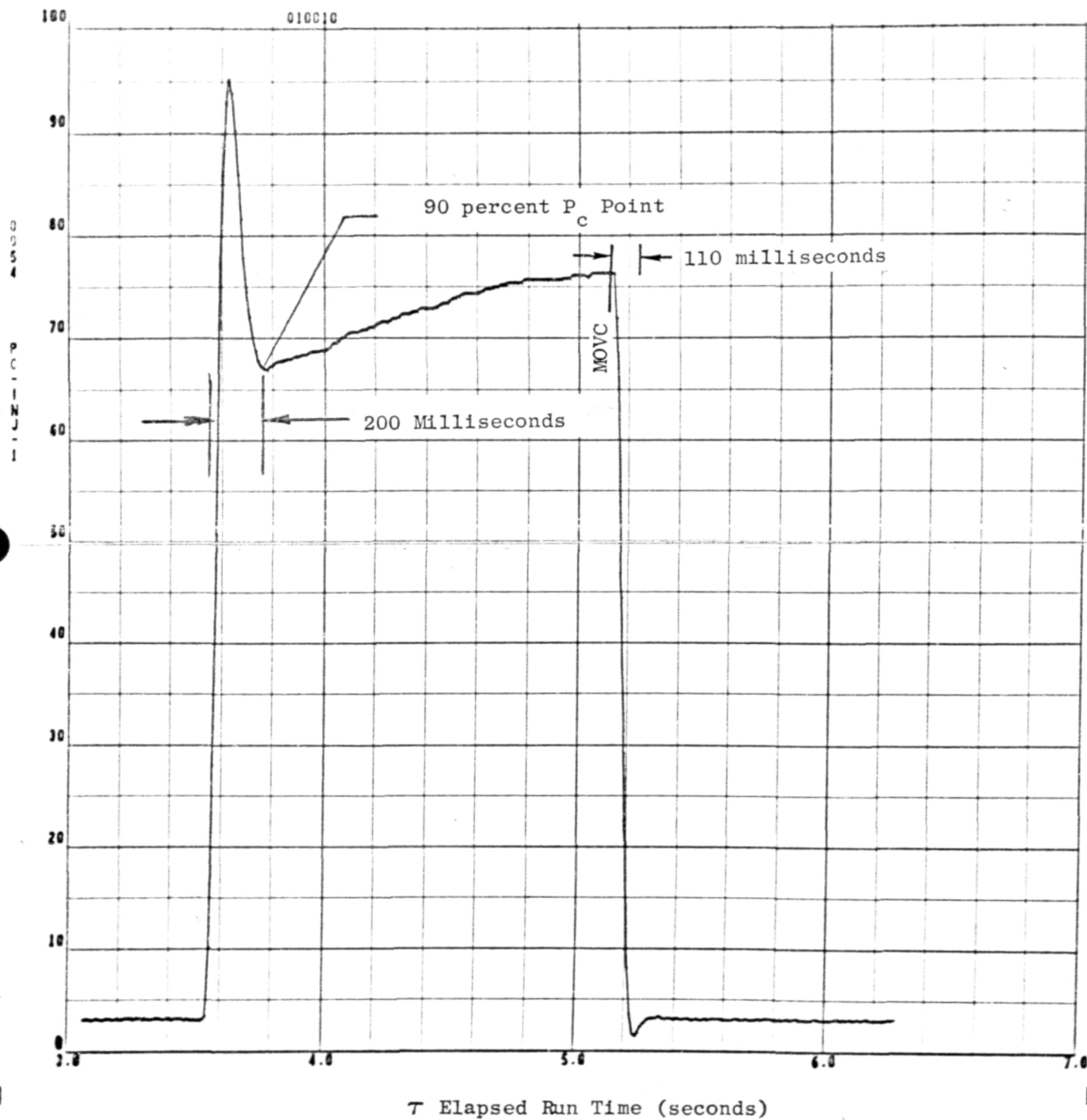


Figure 150. Chamber Pressure Rise vs Elapsed Time (Test 010)

REFERENCES

1. Gambill, W. R., "Heat Transfer-Houston Chem. Eng. Prog. Symposium Series", 59, 41, 71 (1963).
2. AFRPL TR-68-112, "Investigation of Non-Tubular Wall Regeneratively Cooled Concepts, Phase I Report", Rocketdyne, a Division of North American Rockwell Corporation, Canoga Park, California, June 1968.
3. PR 9268-3, "Regeneratively Cooled Rocket Engine for Space Storable Propellants, Quarterly Report for the Period Ending 1 August 1970", Contract NAS7-765, Rocketdyne, a Division of North American Rockwell Corporation, Canoga Park, California, August 1970.
4. PR 9264-3, "Boundary Cooled Rocket Engines for Space Storable Propellants Quarterly Report for the Period 1 April 1970 to 1 July 1970, Contract NAS7-767", Rocketdyne, a Division of North American Rockwell Corporation, Canoga Park, California, July 1970.
5. PR 9268-6, "Regeneratively Cooled Rocket Engine for Space Storable Propellants, Quarterly Report for the Period Ending 1 November 1970", Contract NAS7-765, Rocketdyne, a Division of North American Rockwell Corporation, Canoga Park, California, 30 November 1970.
6. Report 659-F, "FLOX-Diborane Technology - Boundary Reactions", Aerojet General Corporation, Sacramento, California, September 1968.
7. Waldman, B. J., "Fluorine-Hydrogen Performance Evaluation Phase II: Space Storable Propellant Performance Investigation", NASA CR-72542, Report No. R-6636-3, Rocketdyne, a Division of North American Rockwell Corporation, Canoga Park, California, April 1969.
8. Personal Communication with W. B. Powell, NASA Jet Propulsion Laboratory.
9. NASA CR-72542, R-6636-3, "Fluorine-Hydrogen Performance Evaluation, Phase III Space Storable Propellant Performance Demonstration", Rocketdyne, a Division of North American Rockwell Corporation, Canoga Park, California, May 1970.

10. AFRPL TR-68-147, "Correlation of Spray Injector Parameters With Rocket Engine Performance", Rocketdyne, a Division of North American Rockwell Corporation, Canoga Park, California, June 1968.
11. JPL PR20-165, "The Liquid Phase Mixing of a Pair of Impinging Streams", Rupe, J. H., JPL, Pasadena, California, August 1953.
12. JPL TM33-548, "Simplified Procedures for Correlation of Experimentally Measured and Predicted Thrust Chamber Performance", Powell, W. B., JPL, Pasadena, California, to be published.
13. ICRPG Liquid Propellant Thrust Chamber Performance Evaluation Manual.

BIBLIOGRAPHY

1. Diborane Space Storable Handbook, Rocketdyne Report R-8248, by M. T. Constantine, et. al, NASA Contract NAS7-769.

NOMENCLATURE

A	area
BLC	boundary layer
C_D	discharge coefficient
C^*	characteristic velocity
C_P	heat capacity
COS	cosine
D	diameter
F	thrust
G	mass velocity
g	earth gravity constant
h	film coefficient
I_{sp}	specific impulse
L	length
n	logarithm
MR	mixture ratio
m	mass
N	ratio
N_{ST}	Stanton number
ODE	one dimensional equilibrium
P_c	chamber pressure
Q/A	heat flux rate
R	radius
T	temperature
V	velocity
\dot{W}	weight flowrate
α	angle
δ^*	boundary layer displacement
ϵ	contraction ratio
η	efficiency
ρ	density
τ	time
ϕ_T	throat area correction

SUBSCRIPTS

AW	adiabatic wall
avg	average
B	bulk
BL	boundary layer
C	coolant
drop	droplet
ER	energy release
exp	experimental
f	fuel
g	gas
HL	heat loss
i, I	initial
inj	injector
O	total
O	oxidizer
S	surface
T	throat
TC	thrust chamber
t	total
V	venturi
w	wall
K	kinetic
c*	characteristic velocity

APPENDIX A

JANNAF THRUST CHAMBER PERFORMANCE PROCEDURE

INTRODUCTION

Thrust chamber performance can be evaluated in terms of an analytical model incorporating all the loss processes that occur in the rocket motor. The Performance Standardization Working Group of JANNAF has identified the important loss processes in the thrust chamber, and has developed a methodology and a recommended procedure for predicting real thrust chamber vacuum specific impulse

$$I_{sp_{vac}}$$

Simplified equations, based on the JANNAF reference procedure for calculating vacuum specific impulse, have been developed (Ref.) to relate the delivered performance (both vacuum specific impulse and characteristic velocity) to the ideal performance as degraded by the losses corresponding to a specified list of loss processes. These simplified equations enable the various performance loss components, and the corresponding efficiencies, to be quantified separately.

Two rocket motor performance parameters are considered. The vacuum specific impulse ($I_{sp_{vac}}$) is the thrust per unit mass flow of propellant. This parameter directly determines the performance and payload of a rocket-propelled vehicle. The vacuum specific impulse must be measured or predicted with the highest possible accuracy; the current goal is ± 1 percent for new propellants and conditions with even closer prediction for well characterized systems. Both the experimental measurements and the analytical techniques used in evaluating the vacuum specific impulse are capable of achieving this accuracy goal in most instances.

The characteristic velocity c^* is a mass flow parameter. It is used both to predict mass flow (which, in conjunction with the vacuum specific impulse, determines thrust level) and for the preliminary estimation of the effect of the various loss processes on performance. The characteristic velocity can

be determined experimentally by measuring static chamber pressure and flowrate only (thrust measurement is not required). An experimental determination of c^* is generally less accurate than I_{sp} (about ± 2 or 3 percent uncertainty) because of measurement and data correction problems and assumptions involved in the definition of this parameter. An accuracy of ± 2 or 3 percent is considered satisfactory for most design purposes. Both the vacuum specific impulse and characteristic velocity are relatively insensitive to small changes in the level of the chamber pressure at which they are evaluated.

Vacuum specific impulse is the preferred parameter for final performance evaluation and correlation, because specific impulse is more meaningful and can be, with extensive testing of preflight hardware, determined with better accuracy than the characteristic velocity. C^* evaluation serves as a preliminary tool for rating various injectors and combustion chamber geometries.

JANNAF SPECIFIC IMPULSE PERFORMANCE PREDICTION GENERAL APPROACH

The JANNAF performance prediction methodology currently enables calculation of steady-state vacuum specific impulse ($I_{sp \text{ vac pred}}$) of liquid-liquid propellant injection thrust chambers which (1) have only gaseous combustion products, (2) have conventional de-Laval nozzles, and (3) are large enough that the boundary layer affects only a small part of the total flow. The methodology takes into account the following interacting losses, with reference to one-dimensional isentropic equilibrium flow performance as ideal:

1. Energy release loss, consisting of two parts:
 - a. Vaporization loss -- due to incomplete liquid droplet vaporization at the nozzle throat, including thrust effects due to both reacted gas and remaining liquid droplet components.
 - b. Mixture-ratio distribution loss -- due to macroscopic nonuniform lateral distribution of the local time-averaged mixture ratio of vaporized propellant at the nozzle throat.

2. Kinetic loss -- due to rate-limited equilibrium shift during expansion.
3. Two-dimensional loss -- due to upstream nozzle throat curvature (which affects only mass flow and, hence, c^*), and to nozzle divergence shape and exit angle (affects only the vacuum specific impulse).

The analytical model employed for predicting thrust chamber performance can be used to show the effect on the potentially achievable performance of each of the included loss processes. This capability is useful during rocket engine development, as it enables the magnitude and acceptability of individual loss components to be evaluated and thus shows where further development work would be profitable. Experimental performance can be stated for measured conditions and reference ideal performance calculated to correspond to the specified test conditions before comparison with the actual test data.

THRUST CHAMBER SPECIFIC IMPULSE PERFORMANCE METHOD (JANNAF SIMPLIFIED PROCEDURE)

The specific impulse (I_{sp}) for the thrust chamber can be calculated using the JANNAF Simplified Performance Evaluation Procedure (Ref. 13). This procedure is based upon the basic specific impulse definition:

$$I_{SP_{TC}} = \frac{F_{INVISCID\ GAS} + F_{PARTICLES} - \Delta F_{BL}}{\dot{W}_{TC}}$$

The simplified procedure reduces this expression to a set of efficiencies related to the basic physical processes (loss mechanisms) occurring in the thrust chamber. The thrust of the flow particles is assumed to cancel with the loss in thrust in the gas from accelerating the particles.

The specific impulse can be written as:

$$I_{SP_{TC}} \equiv I_{SP_{ODE}} \left[\eta_{I_{SP_{TD}}} \eta_{I_{SP_{KIN}}} \eta_{I_{SP_{VAP}}} \eta_{I_{SP_{MIX}}} \eta_{I_{SP_{HL}}} - \Delta \eta_{BL} \right]$$

AVG MR

The loss mechanisms which are included are;

Two-dimensional flow effects $\left(\eta_{I_{SP_{TD}}} \right)$

$$\eta_{I_{SP_{TD}}} \equiv \frac{I_{SP_{TWO DIMENSIONAL FLOW}}}{I_{SP_{ONE DIMENSIONAL FLOW}}}$$

Reaction kinetic effects $\left(\eta_{I_{SP_{KIN}}} \right)$

$$\eta_{I_{SP_{KIN}}} \equiv \frac{I_{SP_{RATE LIMITED REACTIONS}}}{I_{SP_{EQUILIBRIUM FLOW}}}$$

Vaporization losses $\left(\eta_{I_{SP_{VAP}}} \right)$

$$\eta_{I_{SP_{VAP}}} \equiv \frac{I_{SP_{ACTUAL VAPORIZATION}}}{I_{SP_{COMPLETE VAPORIZATION}}}$$

Mixing losses $\left(\eta_{I_{SP_{MIX}}} \right)$

$$\eta_{I_{SP_{MIX}}} \equiv \frac{I_{SP_{ACTUAL MIXTURE RATIO DISTRIBUTION}}}{I_{SP_{UNIFORMLY MIXED GASES}}}$$

Heat loss not included in boundary layer model $\left(\eta_{I_{SP_{HL}}} \right)$

$$\eta_{I_{SP_{HL}}} \equiv \frac{I_{SP_{ACTUAL \ HEAT \ LOSS}}}{I_{SP_{NO \ HEAT \ LOSS}}}$$

Boundary layer mass, momentum and heat transfer $\left(\Delta \eta_{I_{SP_{BL}}} \right)$

$$\Delta \eta_{I_{SP_{BL}}} \equiv \left[\frac{\Delta F_{BL} \dot{m}_{TC}}{I_{SO_{ODE}} \dot{m}_{TC}} \right]_{AVG \ MR}$$

The efficiencies are multiplicative except for the boundary layer term and the order in which losses are to be considered has been established. This will be published in the near future in JANNAF and JPL reports. An energy release efficiency $\left(\eta_{I_{SP_{ER}}} \right)^*$ can be defined for specific impulse. In general, the simplified procedure is less accurate than the rigorous JANNAF procedures although for certain propellants and conditions the accuracy can be quite high. The current goal of the uncertainty of the simplified procedure for new propellants and conditions is ± 1 percent with less uncertainty for well known propellants.

THRUST CHAMBER CHARACTERISTIC VELOCITY PERFORMANCE (JANNAF SIMPLIFIED METHOD)

According to the proposed JANNAF Liquid Rocket Engine Performance Methodology (Ref. 13), the performance of an injector is to be measured relative to the performance of a perfect injector (defined as an infinite reservoir of perfectly mixed gases reacted to chemical equilibrium). A real injector will usually deliver lower characteristic velocity (c^* and consequently lower specific impulse (I_{SP})) than the perfect injector because of vaporization and (o/f) distribution losses. Cases can be envisioned which (with certain types of stratification or combustion) could yield higher performance. The basic

$$* \left(\eta_{I_{SP_{ER}}} = \eta_{I_{SP_{VAP}}} \eta_{I_{SP_{MIX}}} \right)$$

definition of c^* in terms of mass flowrate, chamber stagnation pressure and nozzle throat area may be expressed as

$$c^* = \frac{\bar{p}_o^* A_{T(HOT)}}{\dot{m}_T}$$

with the various corrections delineated below applied to allow comparison to the theoretical levels. To derive the chamber pressure from measured static pressure, the one dimensional isentropic perfect gas correction is used from start of contraction to effective reservoir pressure. Injector end static pressure can be corrected to start of contraction static pressure using the conservation of momentum (Rayleigh) procedure including the effects of propellant injection momentum. The throat area is corrected for throat dimensional changes due to wall temperature and pressure effects.

For ease of calculation and to aid in achieving a better understanding of the physical processes (loss mechanisms) occurring, the JANNAF Simplified Performance Evaluation Procedure can be used. In this procedure, the c^* is separated into a set of efficiency factors related to the physical processes. Thus c^* is given by the product of the following efficiencies

$$C^*_{\text{PRED}} = C^*_{\text{ODE AVG MR}} \left(\eta_{C^*_{\text{TD}}} \eta_{C^*_{\text{KIN}}} \eta_{C^*_{\text{BL}}} \eta_{C^*_{\text{VAP}}} \eta_{C^*_{\text{MIX}}} \eta_{C^*_{\text{HL}}} \right) = C^*_{\text{ODE AVG MR}} \times \eta_{C^*_{\text{TC}}}$$

Two Dimensional Throat Flow Correction $(\eta_{C^*_{\text{TD}}})$

$$\eta_{C^*_{\text{TD}}} \equiv \frac{C^*_{\text{TWO DIMENSIONAL FLOW}}}{C^*_{\text{ONE DIMENSIONAL FLOW}}}$$

Kinetic Loss Flow Correction $(\eta_{C^*_{\text{KIN}}})$

$$\eta_{C^*_{\text{KIN}}} \equiv \frac{C^*_{\text{KINETIC FLOW}}}{C^*_{\text{EQUILIBRIUM FLOW}}}$$

Boundary Layer Loss Correction ($\eta_{C^*_{BL}}$)

$$\eta_{C^*_{BL}} \equiv \frac{C^*_{\text{WITH HEAT AND MOMENTUM TRANSFER TO WALL}}}{C^*_{\text{INVISCID FLOW}}}$$

Vaporization Loss Correction ($\eta_{C^*_{VAP}}$)

$$\eta_{C^*_{VAP}} \equiv \frac{C^*_{\text{ACTUAL VAPORIZATION}}}{C^*_{\text{PERFECT VAPORIZATION}}}$$

Mixing Loss Correction ($\eta_{C^*_{MIX}}$)

$$\eta_{C^*_{MIX}} \equiv \frac{C^*_{\text{ACTUAL MIXTURE RATIO PROFILE}}}{C^*_{\text{UNIFORM MIXTURE RATIO}}}$$

Heat Loss Correction ($\eta_{C^*_{HL}}$)

$$\eta_{C^*_{HL}} \equiv \frac{C^*_{\text{HEAT LOSS FROM MAINSTREAM (OTHER THAN IN BOUNDARY LAYER)}}}{C^*_{\text{NO HEAT LOSS}}}$$

Comparison of Ideal and Real Injector C^* Efficiencies

For a perfect injector $\eta_{C^*_{VAP}}$ and $\eta_{C^*_{MIX}}$ are equal to 1. Deviation of $\eta_{C^*_{HL}}$ from 1 can be caused by radiation or by large scale turbulence. The perfect injector C^* is then

$$C^*_{\text{PERF INJ}} = C^*_{\text{ODE AVG MR}} \left(\eta_{C^*_{TD}} \eta_{C^*_{KIN}} \eta_{C^*_{BL}} \eta_{C^*_{HL}} \right)$$

In the simplified procedure the various C^* efficiencies are evaluated as follows:

$$\eta_{C^*_{TD}} \approx \frac{C^*_{\text{TDK}}}{C^*_{\text{ODK}}} \approx \frac{1}{C_{D_{\text{INVISCID}}}}$$

$$\eta_{C^*_{BL}} \approx \frac{1}{1 - \left(\frac{2 \delta^*_T}{R_T} \right)}$$

$$\eta_{C^*_{KIN}} \approx \frac{C^*_{ODK} \text{ AVG MR}}{C^*_{ODE} \text{ AVG MR}}$$

$$\eta_{C^*_{HL}} \approx \frac{C^*_{ODE} \text{ AVG MR}}{C^*_{ODE} \text{ HL}} \approx \left[1 - \left(\frac{1}{C^*} \frac{\Delta C^*}{\Delta H} \right) \Delta H_{HL} \right]$$

The characteristic velocity energy release efficiency ($\eta_{C^*_{ER}}$) is used to give a measure of the excellence of the injector. Although less well defined than the specific impulse energy release efficiency ($\eta_{I_{SP_{ER}}}$) because of the correction from static pressure to chamber pressure, $\eta_{C^*_{ER}}$ should be accurate within about 2-percent and within 1-percent of $\eta_{I_{SP_{ER}}}$ for most propellants and area ratios of interest ($\eta_{I_{SP_{ER}}}$ can be either higher or lower than $\eta_{C^*_{ER}}$).

The basic definition of $\eta_{C^*_{ER}}$ is

$$\eta_{C^*_{ER \text{ EXP}}} \equiv \frac{\bar{p}^*_o A_T}{C^*_{PERF \text{ INJ}} \dot{m}_t} = \eta_{I_{SP_{VAP}}} \eta_{I_{SP_{MIX}}}$$

where \bar{p}^*_o is the throat stagnation pressure average value. The throat area (A_T) is corrected only for thermal expansion effects. The $C^*_{PERF \text{ INJ}}$ is based upon equal throat flowrate and throat area for the real injector and perfect injector.

The overall thrust chamber C* efficiency ($\eta_{C^*_{TC}}$) is defined and computed according to the following relationship

$$\eta_{C^*_{TC}} = \frac{\frac{\bar{P}_o A_T}{\dot{m}_t}}{\frac{C^*_{ODE}}{AVG MR}} \quad (A_T \equiv \text{geometric operating throat area})$$

$\eta_{C^*_{TC}}$ is somewhat less informative than $\eta_{C^*_{ER}}$ since it includes the effects of the thrust chamber as well as the injector. However, for virtually identical thrust chambers, this efficiency gives an overall measure of excellence of the injector/thrust chamber combination.

APPENDIX B

THEORETICAL PERFORMANCE CURVES

Theoretical performance curves for F_2/O_2 (70/30) B_2H_6 were developed for both c^* and I_{sp} related parameters and are included in this appendix. They are briefly described below.

CHARACTERISTIC VELOCITY (c^*)

Figure B-1 illustrates equilibrium c^* vs mixture ratio at the 80 F temperature level. The effect of chamber pressure is also shown. A peak c^* is noted at a MR = 3.8. Detailed effects of temperature is shown in Fig. B-2.

COMBUSTION TEMPERATURE (T_c)

Figure B-3 illustrates the combustion temperature vs mixture ratio. A monotonically increasing flame stagnation temperature is noted vs increased mixture ratio.

COMBUSTION ENTHALPY (H_c)

Figure B-3 also illustrates the behavior of the combustion enthalpy for $F_2/O_2-B_2H_6$ with mixture ratio. A decreasing composition enthalpy with increased mixture ratio is shown.

SPECIFIC IMPULSE PERFORMANCE ($I_{sp_{vac}}$)

Figure B-4 - B-7 illustrate the influence of mixture ratio and area ratio on vacuum specific impulse. For an area ratio of 60 nozzle, a peak ODE value of 445 $lb_f\text{-sec}/lb_m$ is shown at a mixture ratio of 3.6.

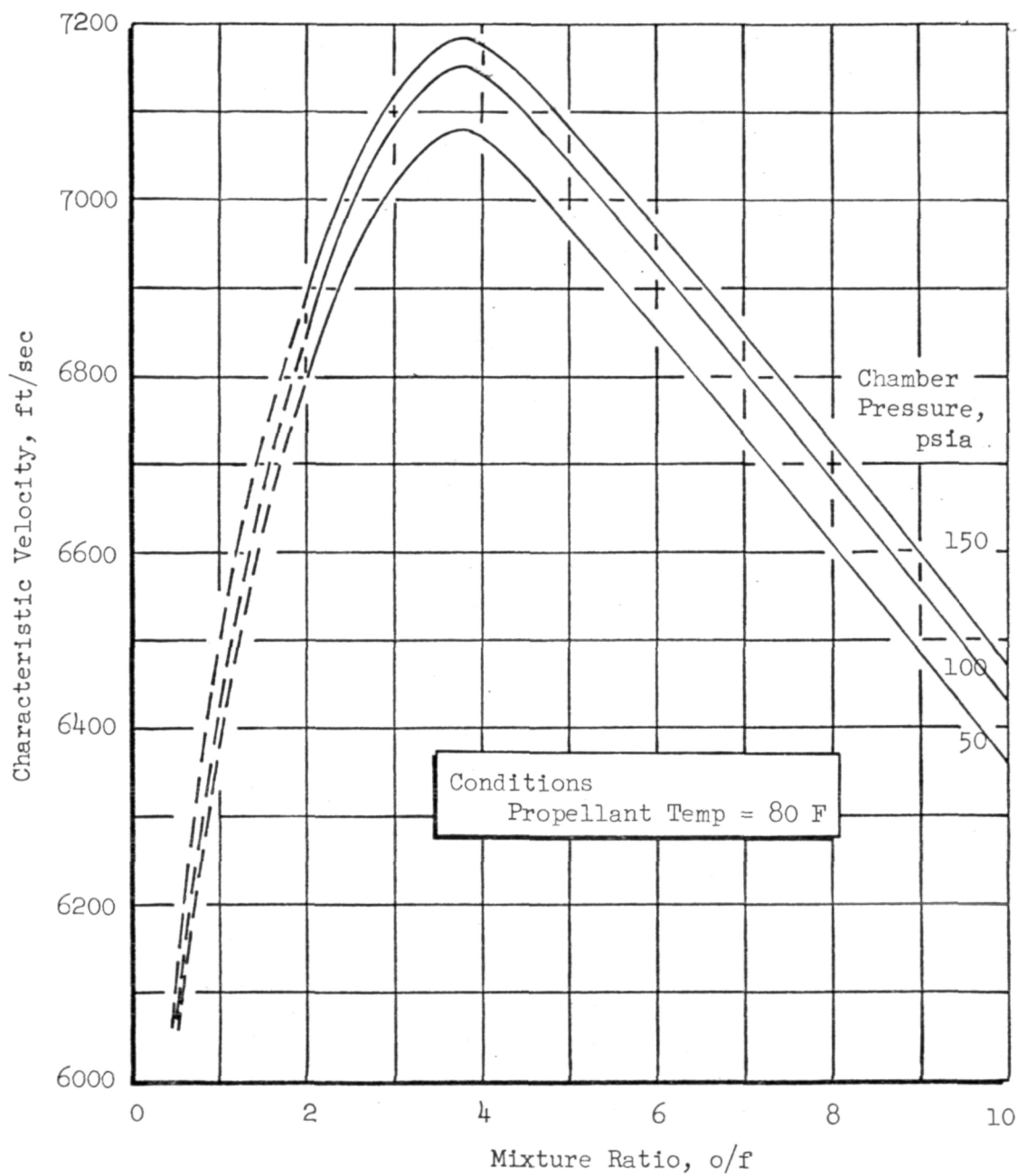


Figure B-1. Effect of Mixture Ratio on Equilibrium Characteristic Velocity for F_2-O_2 (70-30)/ B_2H_6

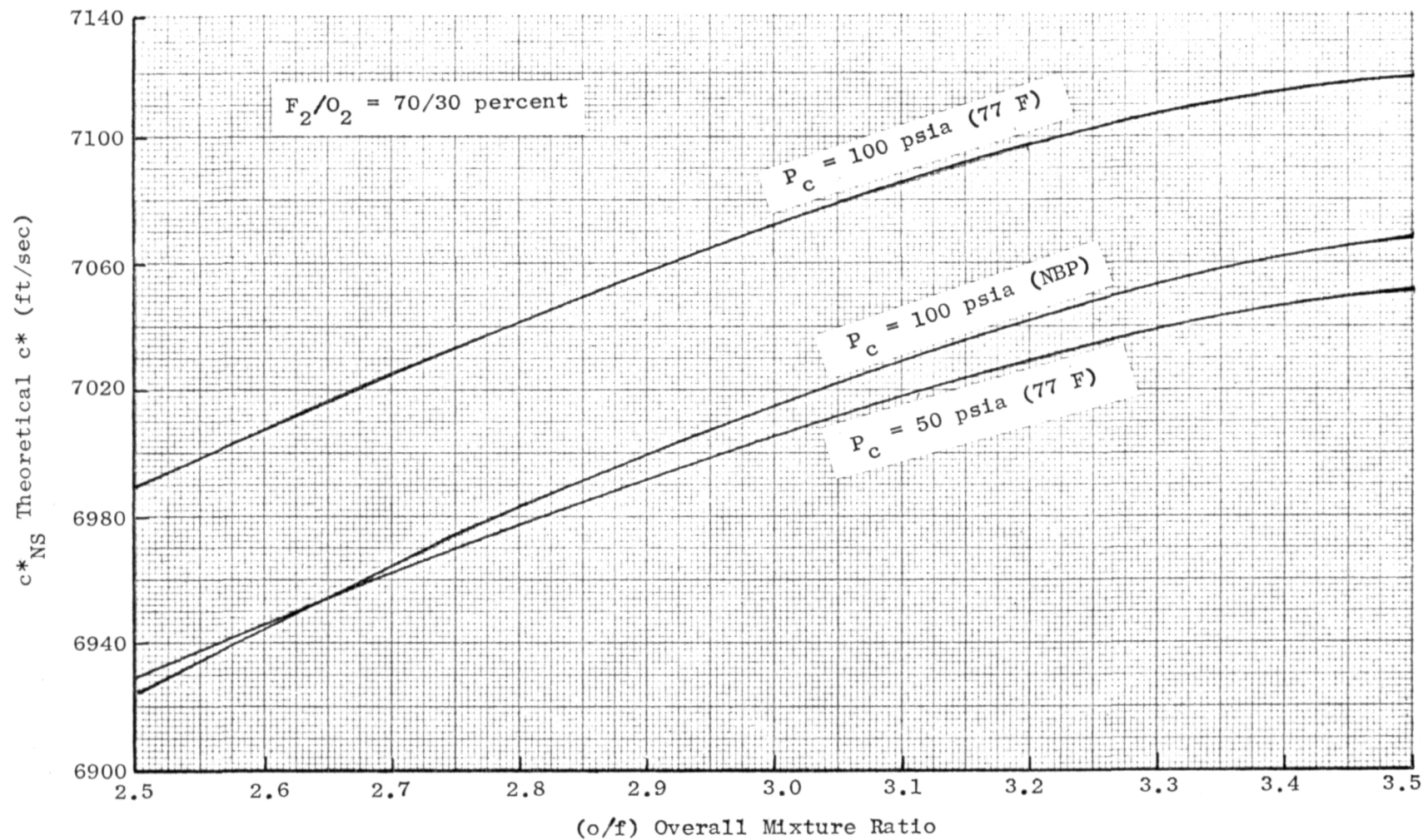


Figure B-2. $F_2/O_2-B_2H_6$ Theoretical c^* vs Mixture Ratio Full Shifting Composition

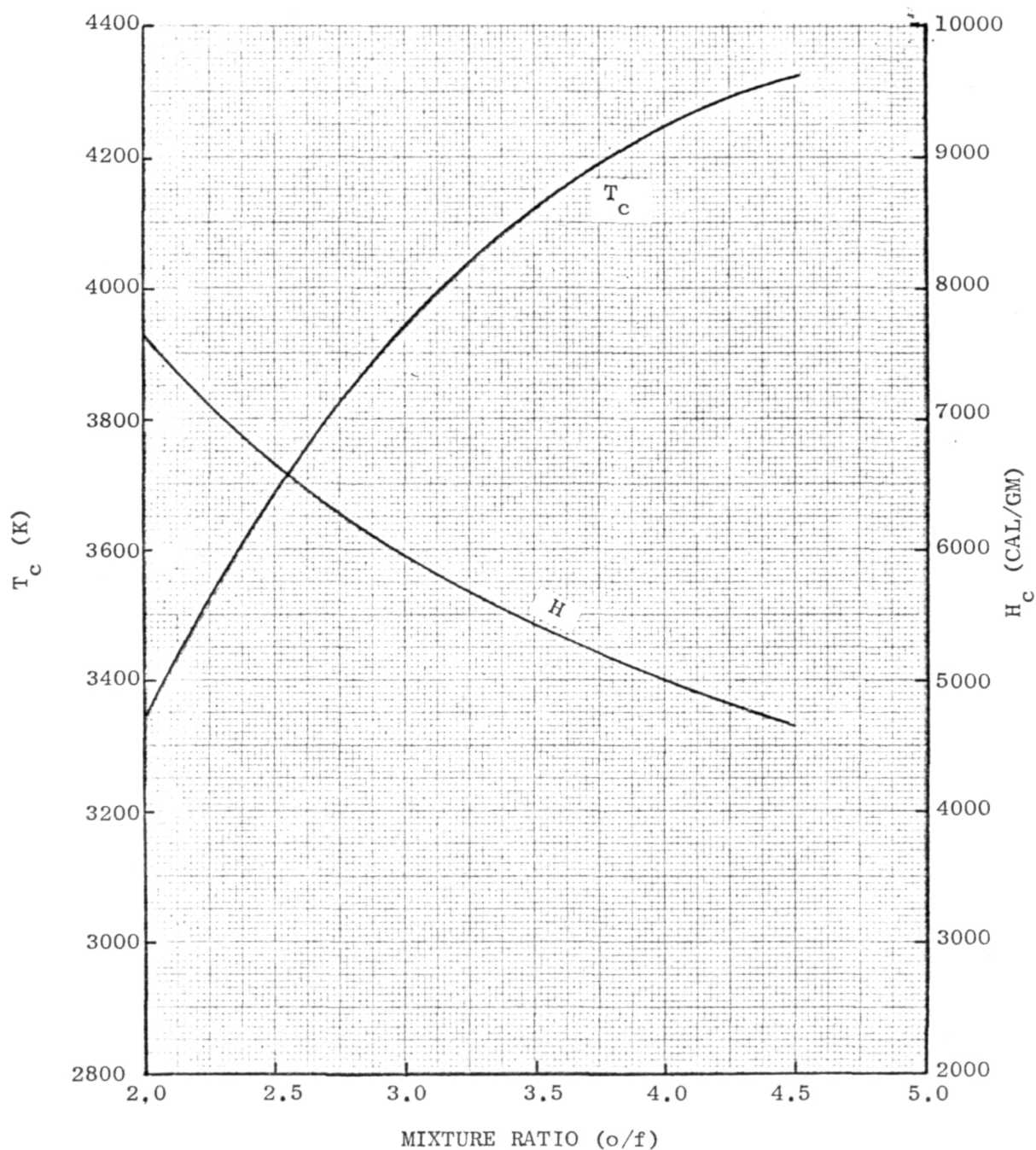


Figure B-3. Equilibrium 70/30 $F_2/O_2-B_2H_6$ Flame Temperature and Enthalpy vs Mixture Ratio (77 F)

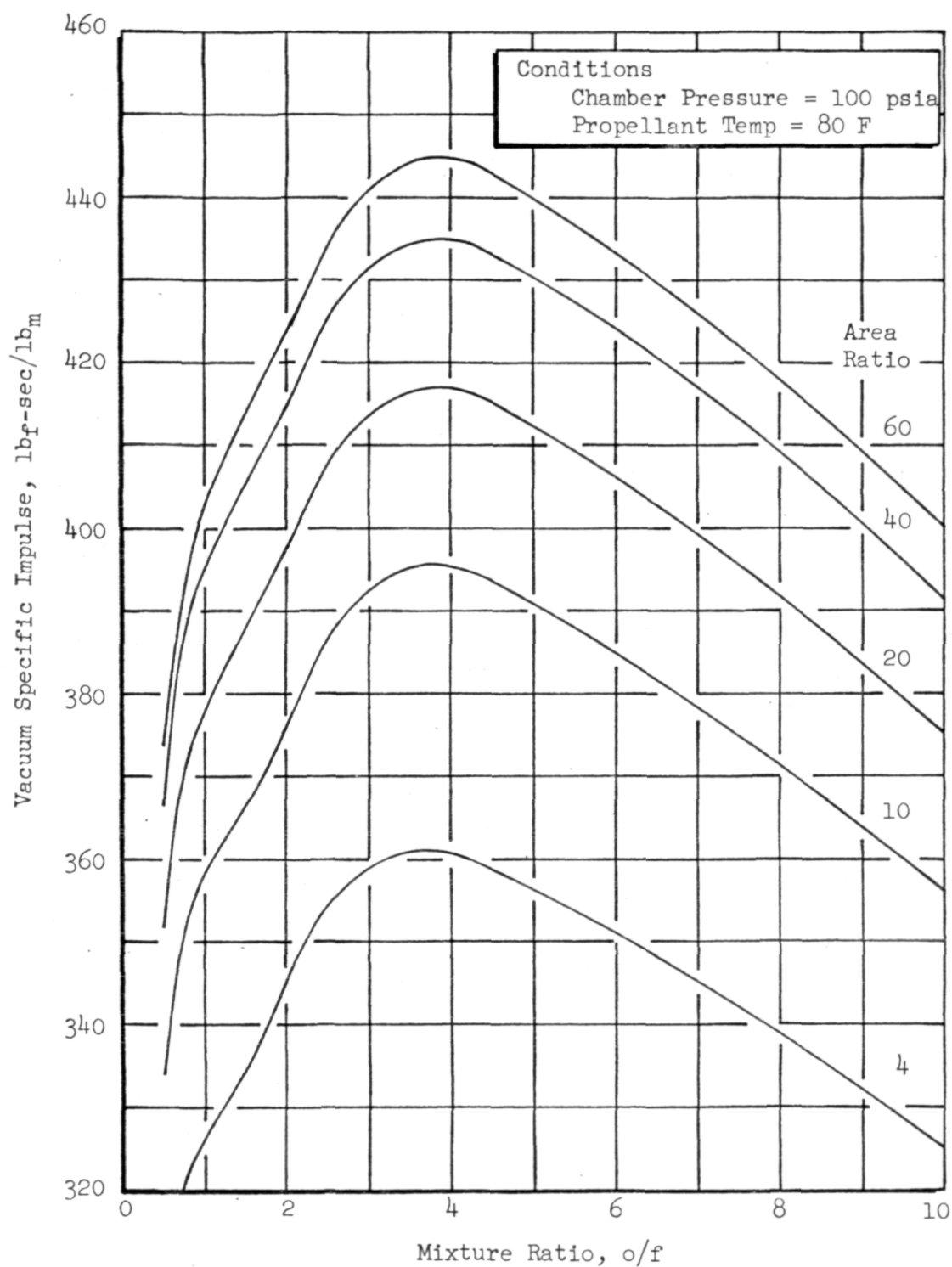


Figure B-4. Effect of Mixture Ratio on Equilibrium Specific Impulse for F_2-O_2 (70-30)/ B_2H_6

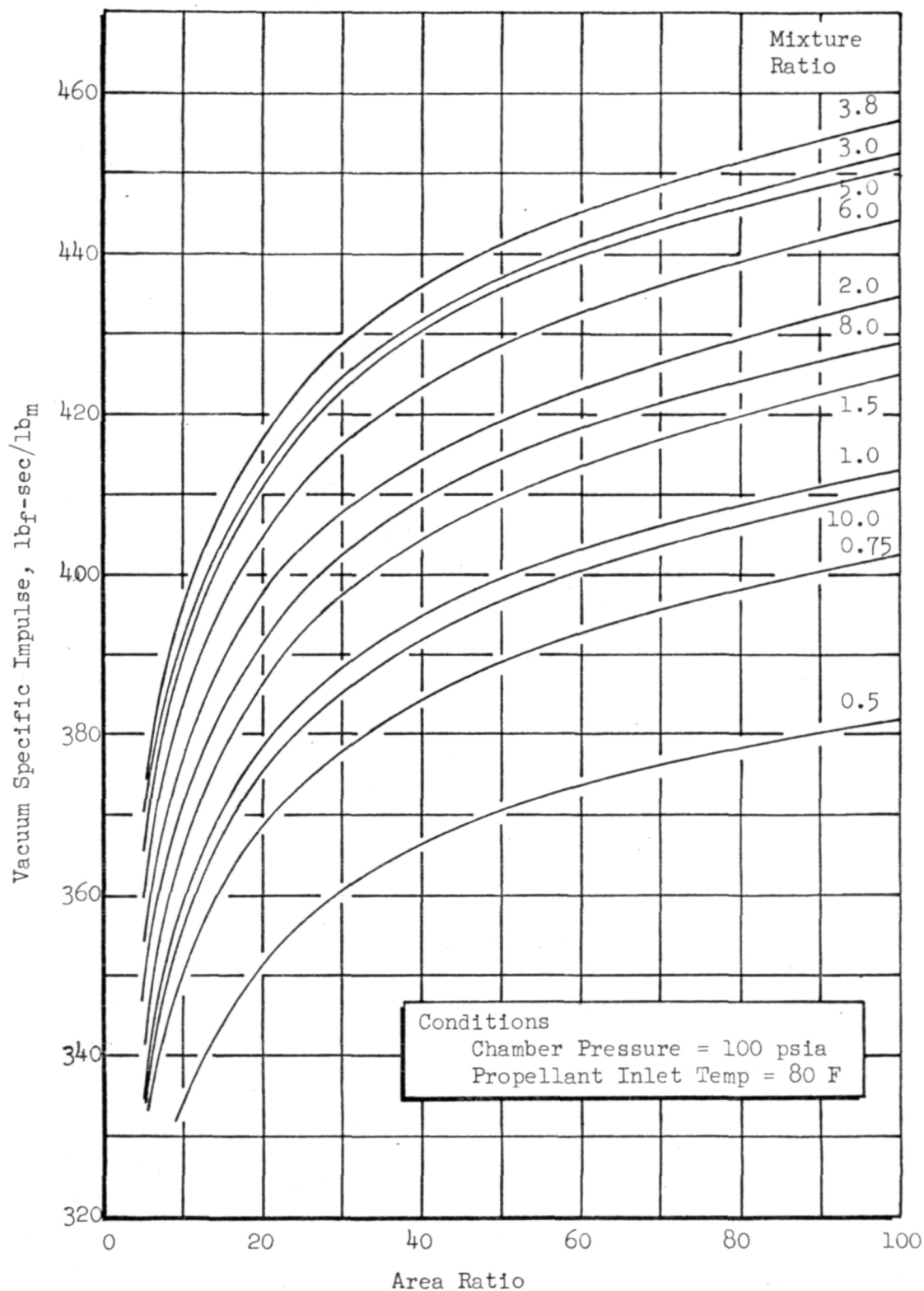


Figure B-5. Effect of Area Ratio on Equilibrium Specific Impulse for F_2-O_2 (70-30)/ B_2H_6

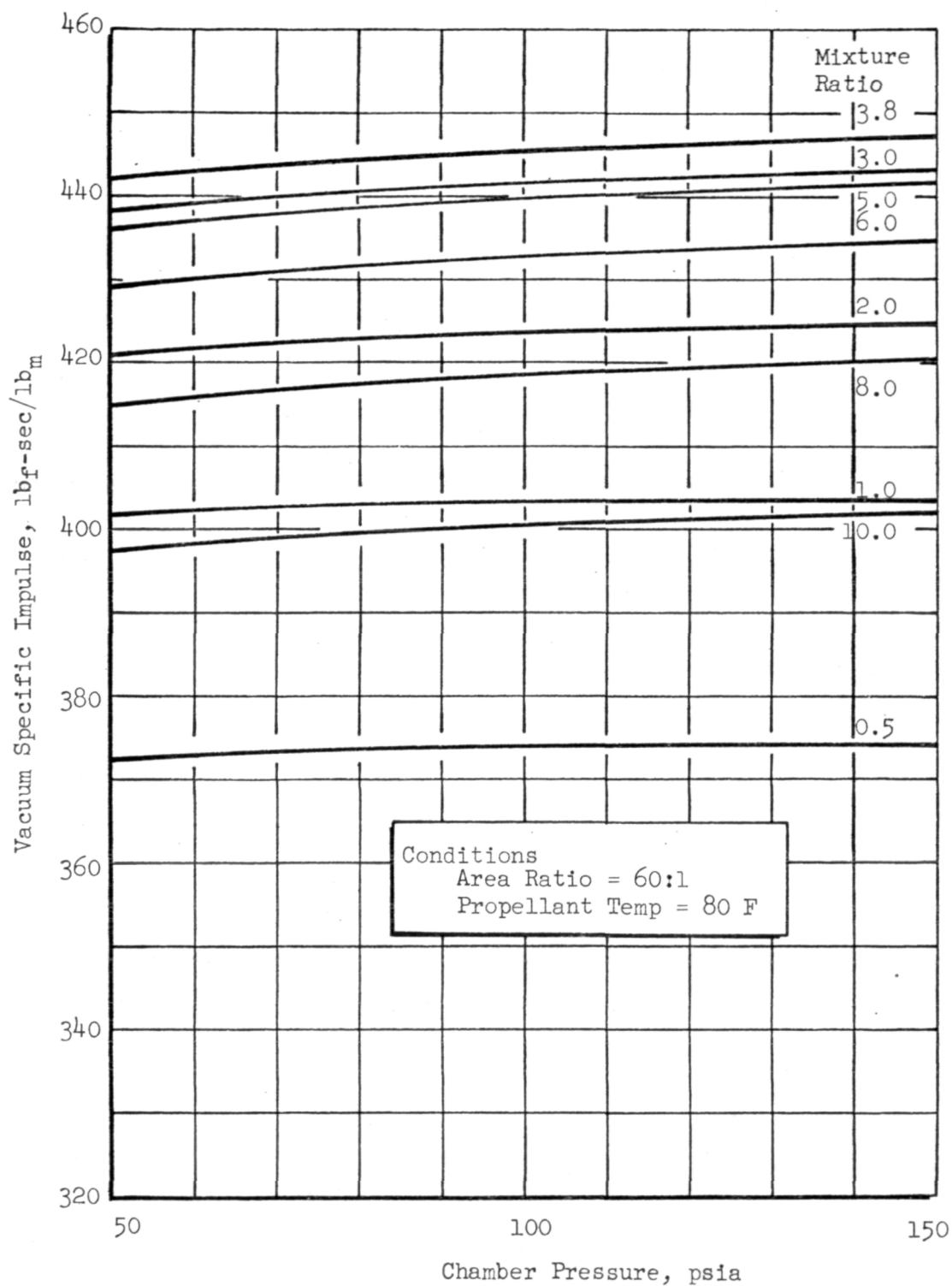


Figure B-6. Effect of Chamber Pressure on Equilibrium Specific Impulse for F_2-O_2 (70-30)/ B_2H_6

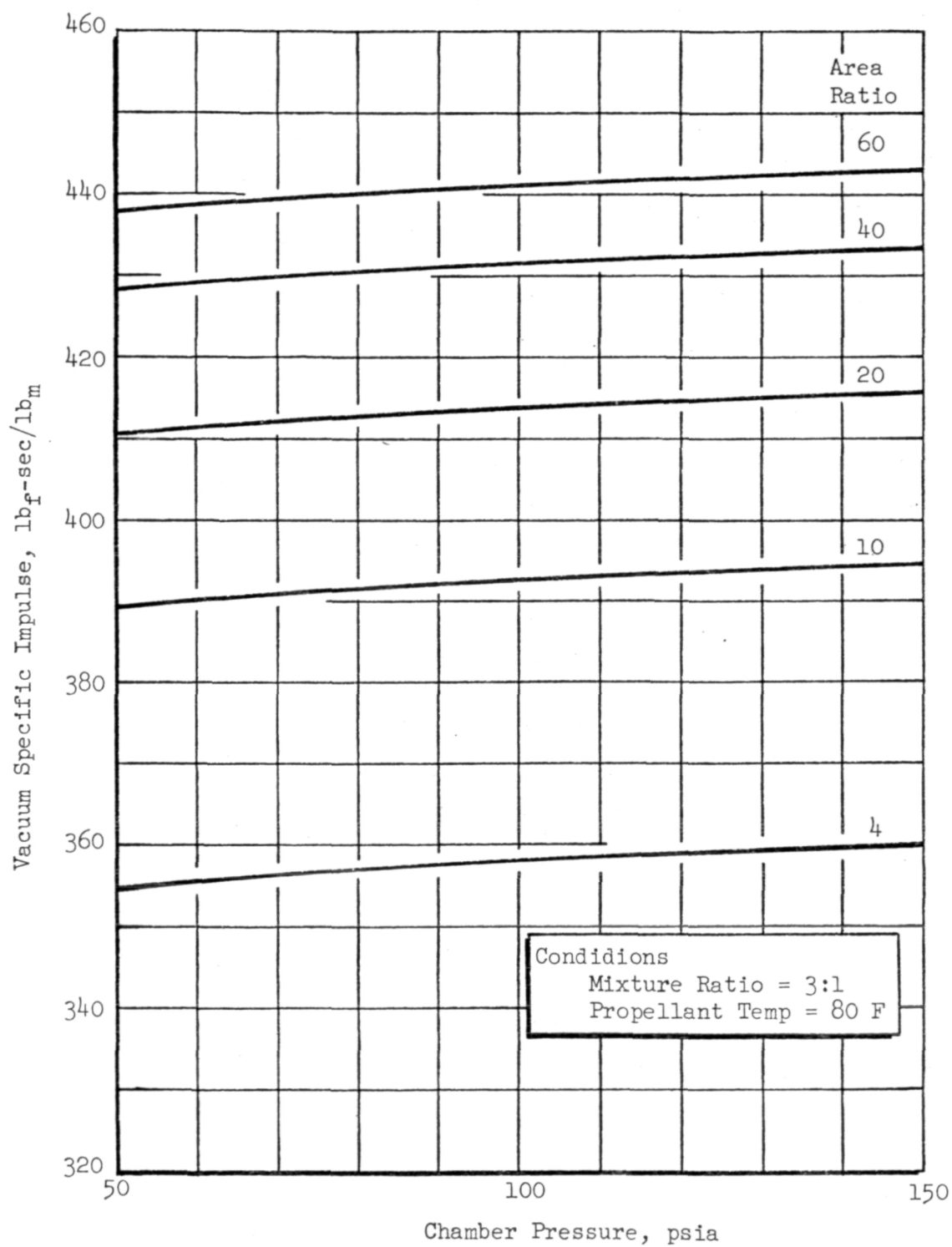


Figure B-7. Effect of Chamber Pressure on Equilibrium Specific Impulse for $\text{F}_2\text{-O}_2$ (70-30)/ B_2H_6

CHARACTERISTIC VELOCITY KINETIC EFFICIENCY ($\eta_{c^*_{kin}}$)

A value of the characteristic velocity kinetic efficiency vs mixture ratio was not determined and was considered outside of the scope of the current program. This value should be high 0.99-1.0.

SPECIFIC IMPULSE KINETIC EFFICIENCY ($\eta_{I_{sp_{kin}}}$)

Effects of mixture ratio on reaction kinetic efficiency is illustrated in Fig. B-8 for a chamber pressure of 100 psia. A 96.9 percent value at a mixture ratio of 3.0 is indicated (Ref. 7).

CHARACTERISTIC VELOCITY -- ENTHALPY INFLUENCE COEFFICIENT $\left(\frac{\Delta c^*}{c^*} \frac{1}{\Delta H_c} \right)$

The effect of propellant enthalpy changes on the c^* value may be developed from Fig. B-9 to B-11 for propellant mixture ratio values over the range from the relationship (Ref. 7).

$$\eta_{c^*_{HL}} = \left[1 - \left(\frac{1}{\Delta H_c} \frac{\Delta c^*}{c^*} \right) \Delta H_{HL} \right]$$

ΔH_c is shown in these figures for the 100 and 200 Btu/lb wall heat rejection (propellant enthalpy loss) conditions. The loss can be directly read from Fig. B-9.

SPECIFIC IMPULSE -- ENTHALPY INFLUENCE COEFFICIENTS $\left(\frac{\Delta I_{sp}}{I_{sp}} \frac{1}{\Delta H_c} \right)$

The effect of propellant enthalpy changes in the I_{sp} level were not developed during this study.

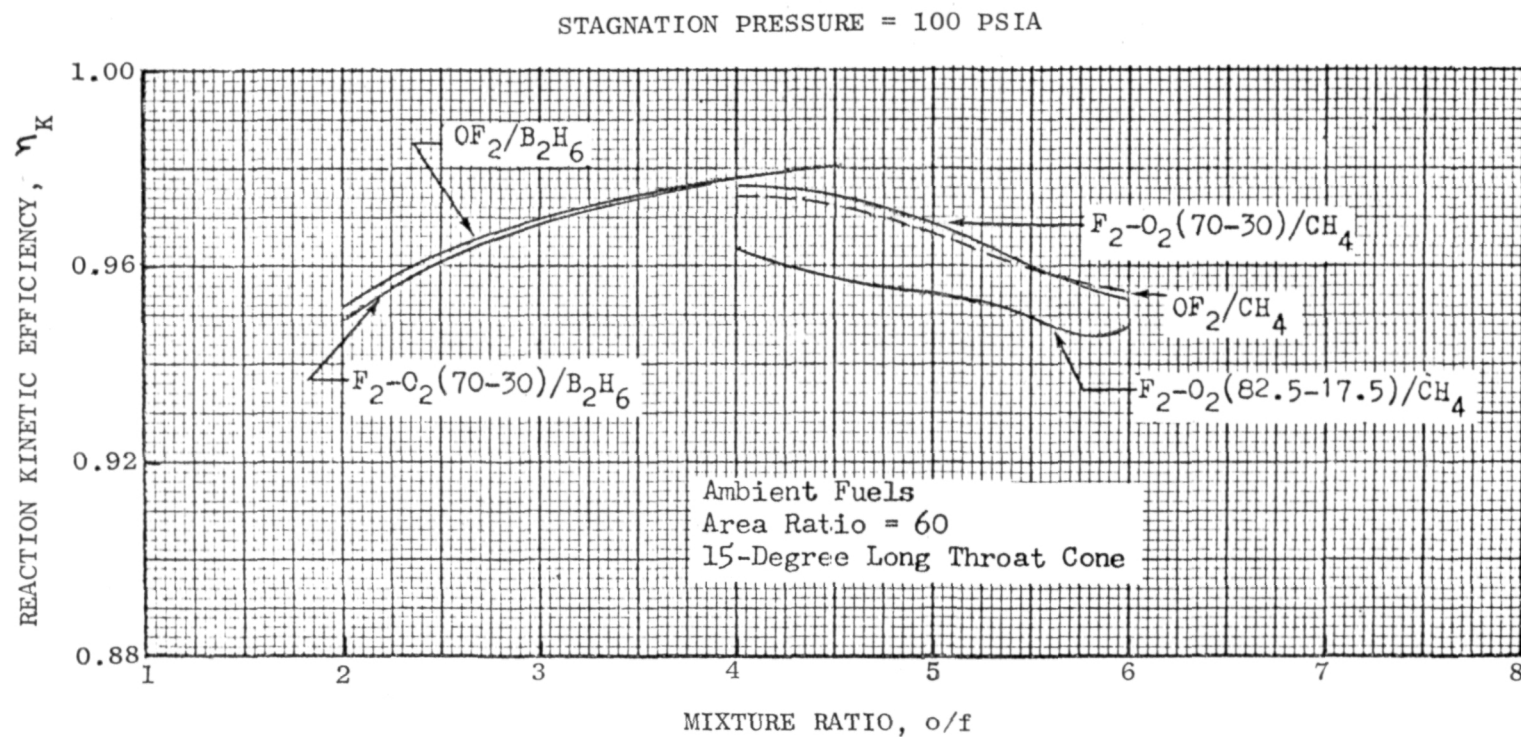


Figure B-8. Effect of Mixture Ratio on Nozzle Reaction Kinetic Efficiency for 15-Degree Long Throat Cone for 100 psia Chamber Pressure (Sudden Freezing Assumed)

STAGNATION PRESSURE = 50 PSIA

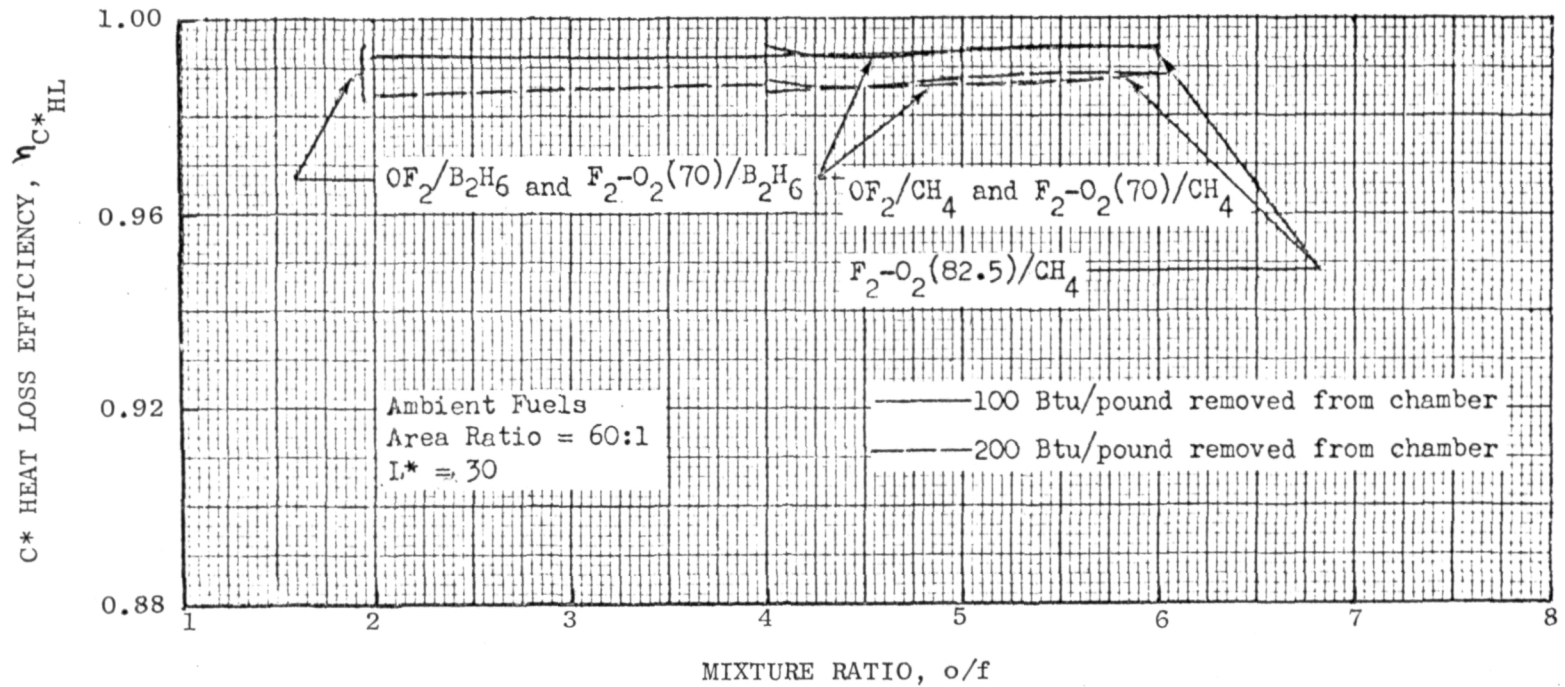


Figure B-9. Characteristic Velocity Heat Loss Efficiency vs Mixture Ratio for 50 psia Chamber Pressure

STAGNATION PRESSURE = 100 PSIA

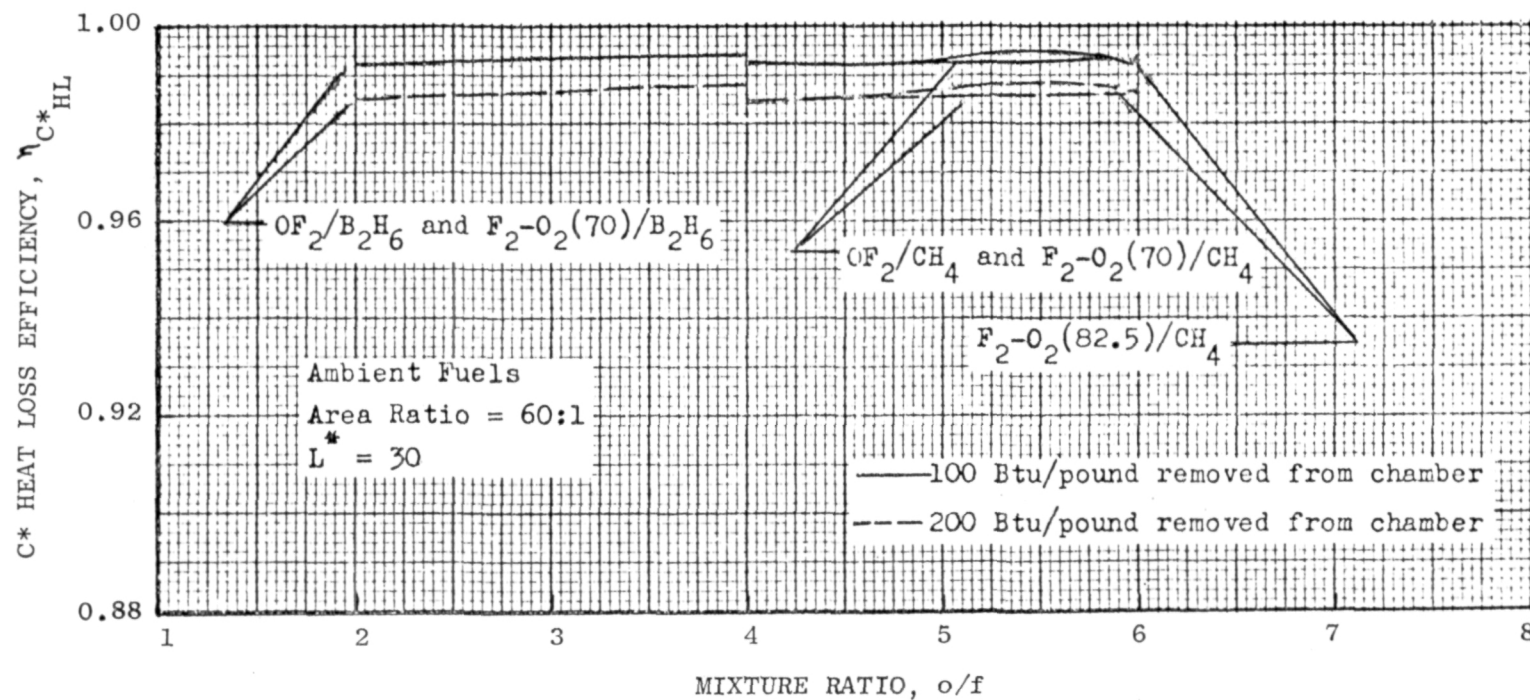


Figure B-10. Characteristic Velocity Heat Loss Efficiency vs Mixture Ratio for 100 psia Chamber Pressure

STAGNATION PRESSURE = 200 PSIA

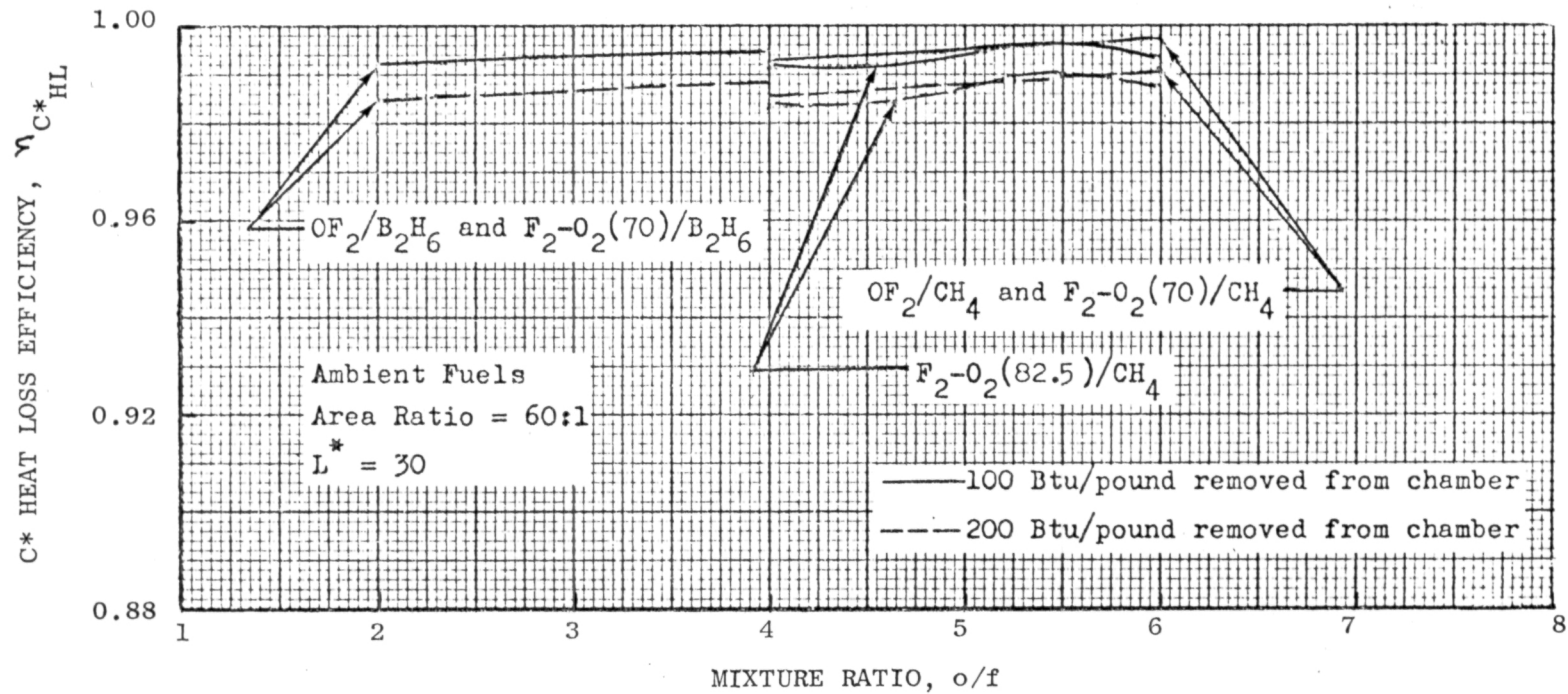


Figure B-11. Characteristic Velocity Heat Loss Efficiency vs Mixture Ratio for 200 psia Chamber Pressure

APPENDIX C

PERFORMANCE DATA REDUCTION AND INJECTOR CALCULATIONS

Transducer electrical signals were converted from analog to digital utilizing a Beckman 210 digital acquisition system. The digital data from the Beckman were recorded on IBM 729 tape. Selected digitized data were converted to analog signals, and a Brush recording was simultaneously made. Upon completion of each test firing, the Brush recording and magnetic tape were further processed with the IBM computer converting the raw data to a graphical CRT output. In addition to the Beckman Digital Acquisition System, oscillographs and direct inking graphic recorders (DIGR) were used to record thrust facility data, temperatures, pressures and flowmeter frequency. The oscillograph served as backup to the Beckman recording system in addition to flowmeter frequency count. Higher response transducer output, such as Photocon pressure measurements and accelerometer outputs, was recorded directly on magnetic tape. Particular time slices of the raw digitized Beckman data were selected during steady-state operation for calculating on-site characteristic velocity.

The oxidizer flowrate was based upon the cavitating venturi. Venturi calibrations were obtained with corrections applied to account for calibration and actual gas property differences. Additional correction was made to adjust the flow for oxidizer impurities as determined by the chemical analysis of the propellant. A cavitating venturi was similarly used to determine the liquid B_2H_6 flowrates. The gaseous B_2H_6 flowrate was obtained from venturi meters installed in series between the heat exchanger and the thrust chamber. The size and number of venturis selected for test was based upon the available bottle bank supply and predicted chamber injection pressures to provide sonic flow at the venturi throats. For the determination of B_2H_6 sonic flow, the real gas properties were programmed into a G.E. terminal computer and flows calculated for a known venturi discharge coefficient and flow area.

Static chamber pressure measurements were taken at chamber locations near the start of convergence (calorimeter) and at the face of the injector (both chambers). The value of throat stagnation pressure was calculated from nozzle inlet static pressure measurements with the injector face static measurement as

a backup (regenerative only). Throat stagnation pressure was calculated from the nozzle inlet static value using the assumption of isentropic flow in the nozzle. The static value was converted to stagnation based upon the Mach number corresponding to the chamber contraction ratio for isentropic flow. The characteristic velocity was based upon the chamber pressure as defined below.

The measured throat areas were corrected for pressure and thermal-induced strains and corrected to the true sonic area. The axisymmetric flow analysis in the region of the nozzle throat considers the sonic surface at the minimum physical area actually is a curved surface (rather than being a plane) starting in the nozzle contraction zone and extending out into the expansion region. (The sonic point occurs actually at different local regions of the flow because the expansion of the exhaust flow is not one-dimensional but occurs at different rates throughout the flow.) The throat area was corrected for the existence of the displacement thickness boundary layer near the wall in which velocities and densities differ from those in the mainstream flow.

CALORIMETER SERIES C* PARAMETERS

Methods for correction of flows, chamber pressure, and throat area measurements are described below for the calorimeter series.

Flows

Flows were determined from the sonic venturi computer programs which allow for the variable properties of the flows during sonic choking conditions. Discharge coefficients were 0.980 for the B_2H_6 cavitating venturis and 0.990 for the F_2/O_2 sonic venturi. Venturi throat areas for the fuel and oxidizer sides were 0.0367 in² and 0.144 in², respectively.

Throat Stagnation Chamber Pressure

The chamber pressure for this series was based on the combustion chamber static wall pressure measurement taken upstream of the convergent section and corrected for the local gas Mach number to a total pressure condition, i.e.,

$$\frac{\bar{p}^*_o}{(p_{cw})_{\text{static}}} = f(\bar{Y}, \epsilon_c) = 1.014$$

It was assumed that at the point of measurement the burning was largely completed resulting in a small further Rayleigh loss to the throat plane. From previous experience on injectors of this type, it has been determined that injector face pressure values are inaccurate due to injection jet aspiration effects. A 1.5-percent lower face pressure compared to wall pressure tap values was noted during the calorimeter series.

Throat Shrinkage Correction

Calorimeter thrust chamber throat diameter deviation from the 2.598 inch measured value was based on the contributions of the chamber throat static pressure tending to enlarge the throat and the externally restrained thermal growth contribution to reduce the throat diameter, i.e.,

$$\frac{(A_T)_{\text{hot}}}{(A_T)_{\text{cold}}} \approx f(p_{\text{throat}}, \bar{T}_W(\bar{\tau})) = 0.996$$

Throat shrinkage was based on previous pressure and thermal analyses and corrections were assumed constant for the calorimeter test series.

Throat Boundary Layer and Potential Deficit Corrections

The calorimeter throat discharge coefficient correction used can be based on the correction for the sonic line warpage ($C_{D_{2-D}} = 0.996$) (potential flow deviation) and the correction based on the boundary layer flow deficit

$C_{D_{BL}} = \left(1 - \frac{2 \delta^*_t}{R_t}\right)$. For the calorimeter tests the total correction was determined as

$$C_D = C_{D_{2-D}} \times C_{D_{BL}} = 0.996 \times 0.997 = 0.993$$

For the $C_{D_{BL}}$ value it was assumed that 60 percent of the injector face to throat heat load was included.

Heat Loss Correction

The calorimeter combustion chamber heat loss was calculated according to Appendix A and determined to be

$$\eta_{c^*_{HL}} = 0.995$$

Theoretical c^* Attainable

The test condition theoretical calorimeter c^* value assuming perfect combustion and mixing was used as the denominator for the c^* performance comparison. The basic values were shown in Fig. B-1 and B-2. The corrections applied are a function of propellant composition and impurities, injection temperature, and chamber pressure. Full shifting composition was assumed as a reference theoretical condition. The experimentally measured exact composition of F_2/O_2 (70.2/29.8) used during the test series was assumed close enough to the available 70/30 performance data so as to not require correction.

REGENERATIVE SERIES C^* PARAMETERS

Parameters for correction of flows, chamber pressure, and throat area measurements are described below for the regenerative series.

Flows

Flows were calculated as described in the previous calorimeter section.

Throat Stagnation Chamber Pressure

The chamber pressure static measurement at the injector face was increased by the difference indicated in previous calorimeter testing and corrected for chamber wall to throat stagnation pressure.

$$\bar{p}_o^* / (p_{c_{inj}})_{static} = (1.015) (1.014) = 1.029$$

Throat Shrinkage Correction

The throat shrinkage area correction was based on a less restrained thermal expansion for the thin wall regenerative chamber and considering a counter balancing effect of the pressure in the water cooling jacket.

$$\frac{(A_T)_{hot}}{(A_T)_{cold}} = 0.998$$

Throat Boundary Layer and Potential Deficit Corrections

The throat discharge coefficient corrections were based on the correction for the sonic line warpage and on the boundary layer displacement thickness (δ^*). The correction (0.993) used was identical to the calorimeter chamber due to a similarity in gas wall to adiabatic wall temperature ratio and identical combustor geometry.

Heat Loss Correction

Correction was made to the c^* efficiency due to the rejection of cooling water heat overboard. Propellant reference temperatures were based on jacket inlet conditions and corrections were based on the water energy lost from the combustion process. The correction resulted in 0.5 percent change and was used as a constant heat loss for all regenerative test runs.

$$\eta_{c^*_{HL}} = 0.995$$

SUMMARY OF CALCULABLE LOSSES AND PERFORMANCE EVALUATION FACTORS

Determination was made for both the calorimeter and regenerative chamber testing of the performance parameters and corrections related to the characteristic velocity efficiency. The following table delineates the corrections applied.

<u>Parameter</u>	<u>Calorimeter</u>	<u>Regenerative</u>
$A_T(\text{hot})/A_T(\text{cold})$.996	.998
$C_{D_{2D}}$.996	.996
$\left(1 - \frac{2 \delta_T^*}{R_T}\right) \equiv C_{D_{BL}}$.997	.997
$\frac{\bar{p}_O^*}{p_s}$	1.014	1.029
$\eta_{c_{HL}}^*$.995	.995

APPENDIX D

TWO-DIMENSIONAL ISOTHERMS OF FLOX-B₂H₆ REGENERATIVELY COOLED CHAMBER

A series of two-dimensional thermal analysis cases were conducted, performed with aid of the Lockheed heating analysis program on the IBM 360 computer. This was done to determine axial wall temperature distributions for various locations in the regenerative chamber.

This series is shown in Fig. D-1 to D-14. Effects of nominal cooling blocked passage effects throat heat flux increases are illustrated. Acceptable chamber wall temperature conditions were shown for the range of conditions investigated.

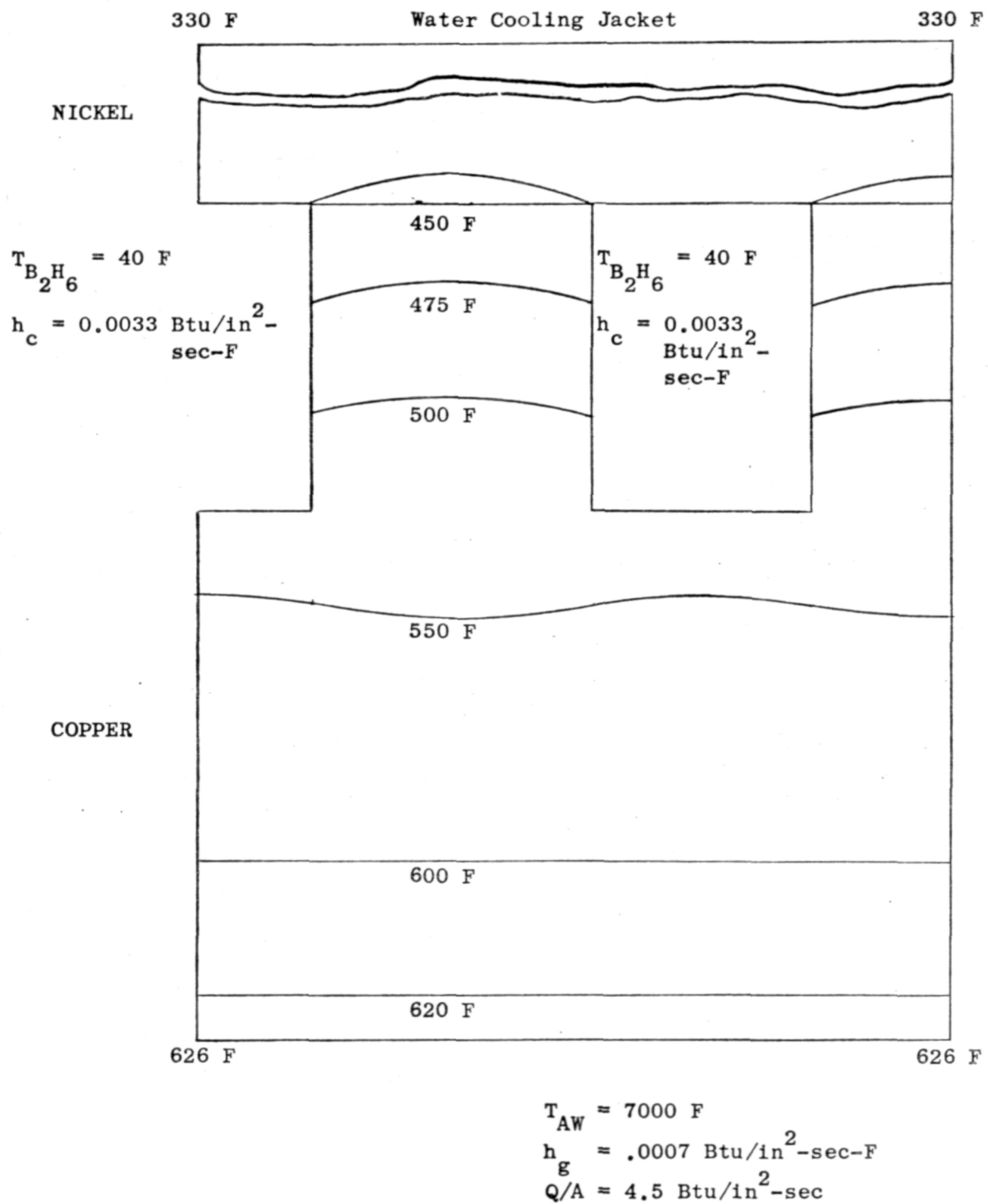


Figure D-1. Reference Case Throat Isotherms for Boiling Water Heat Transfer.

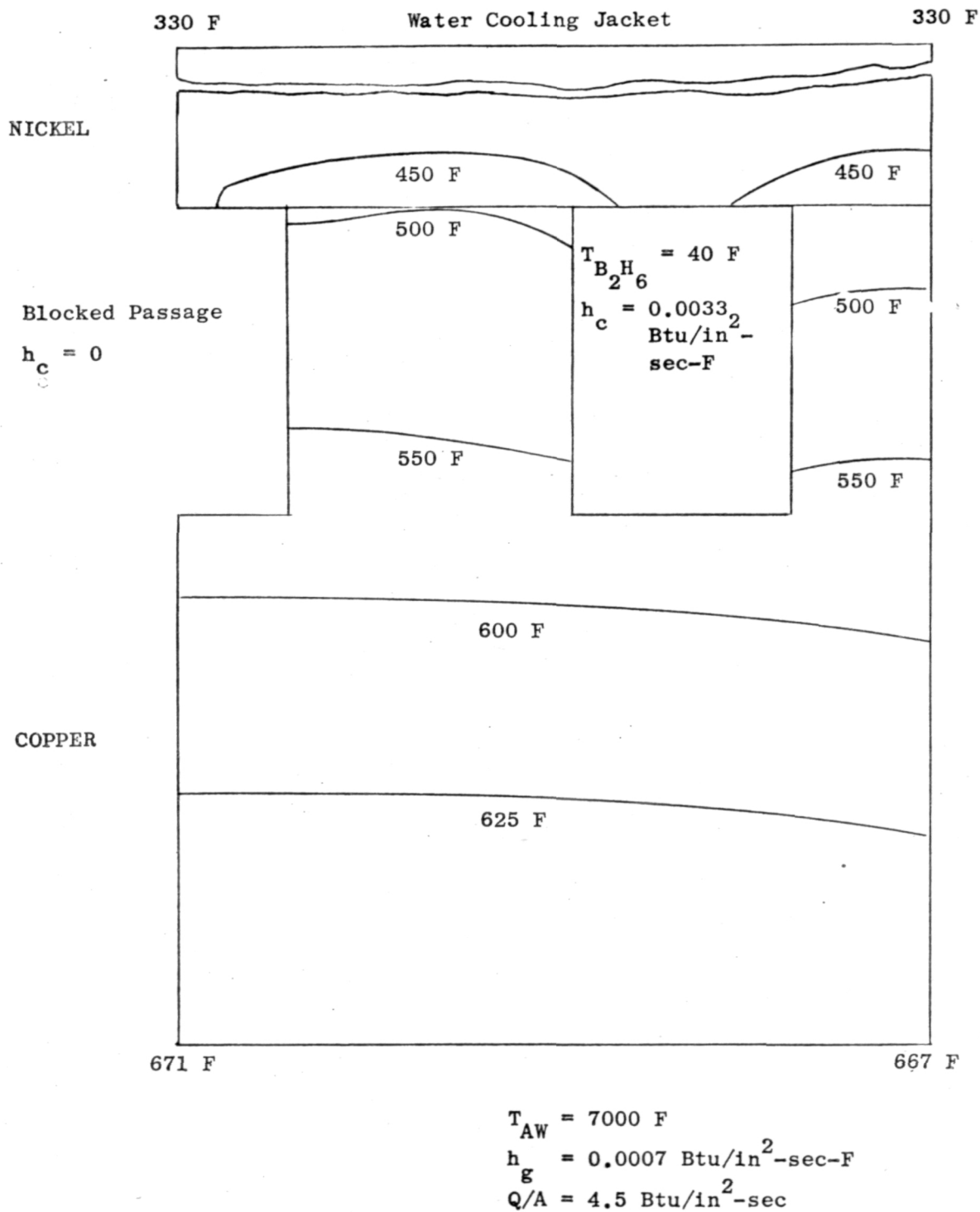


Figure D-2. Throat Isotherms for Boiling Water Heat Transfer and One Blocked Diborane Passage.

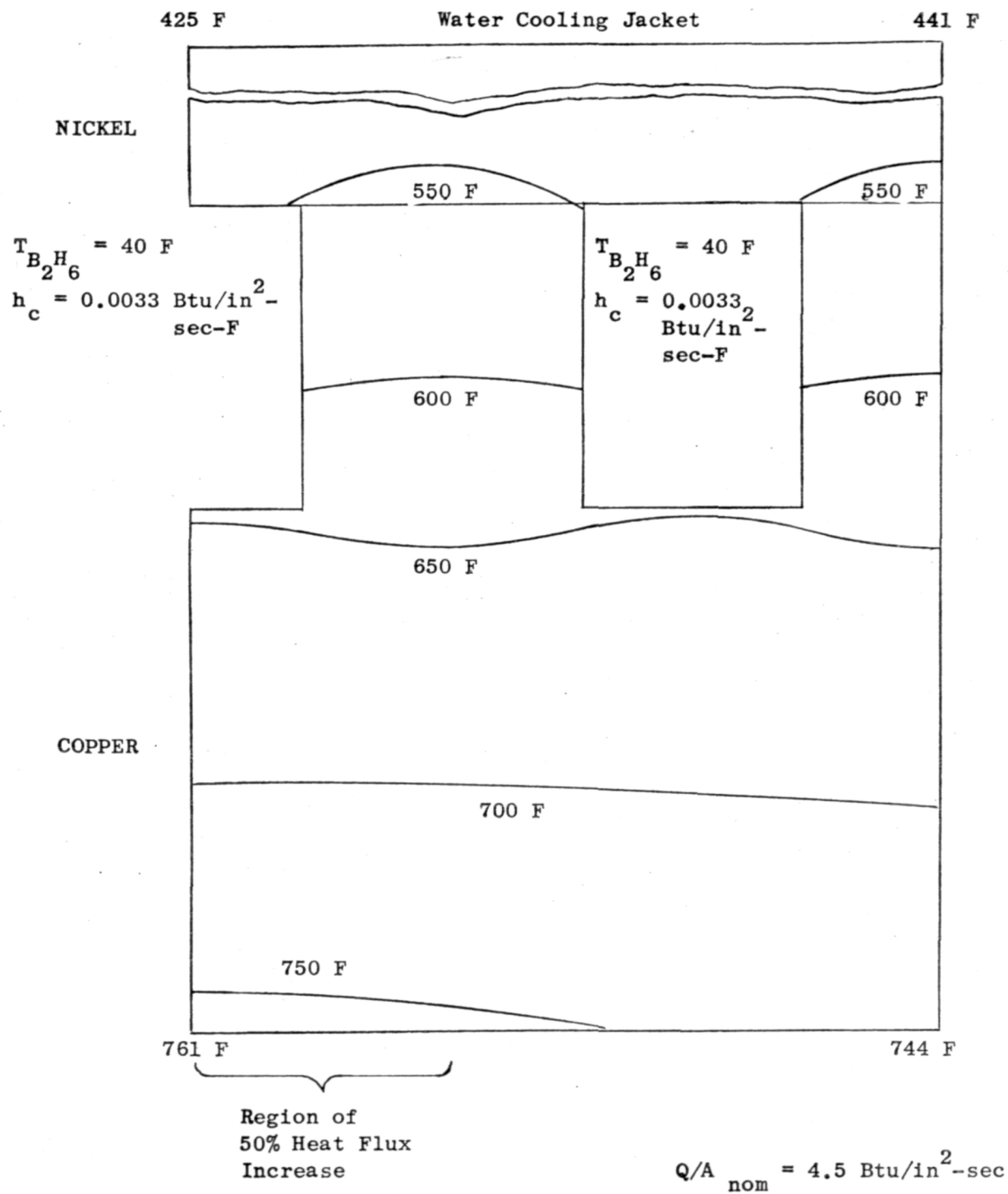


Figure D-4. Throat Isotherms for Non-Boiling Water Heat Transfer and a Local Heat Flux Increase.

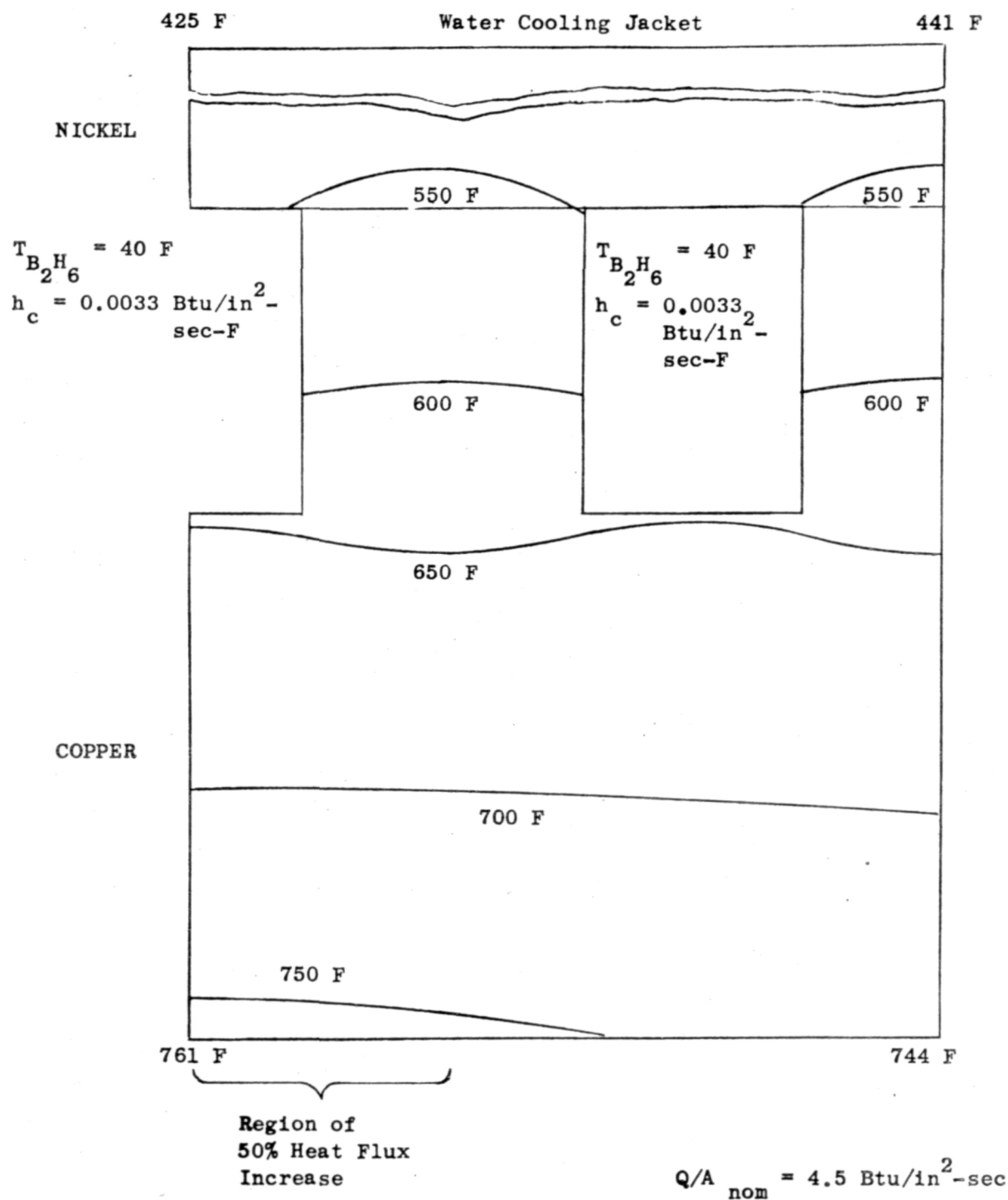


Figure D-5. Throat Isotherms for Non-Boiling Water Heat Transfer and a Local Heat Flux Increase.

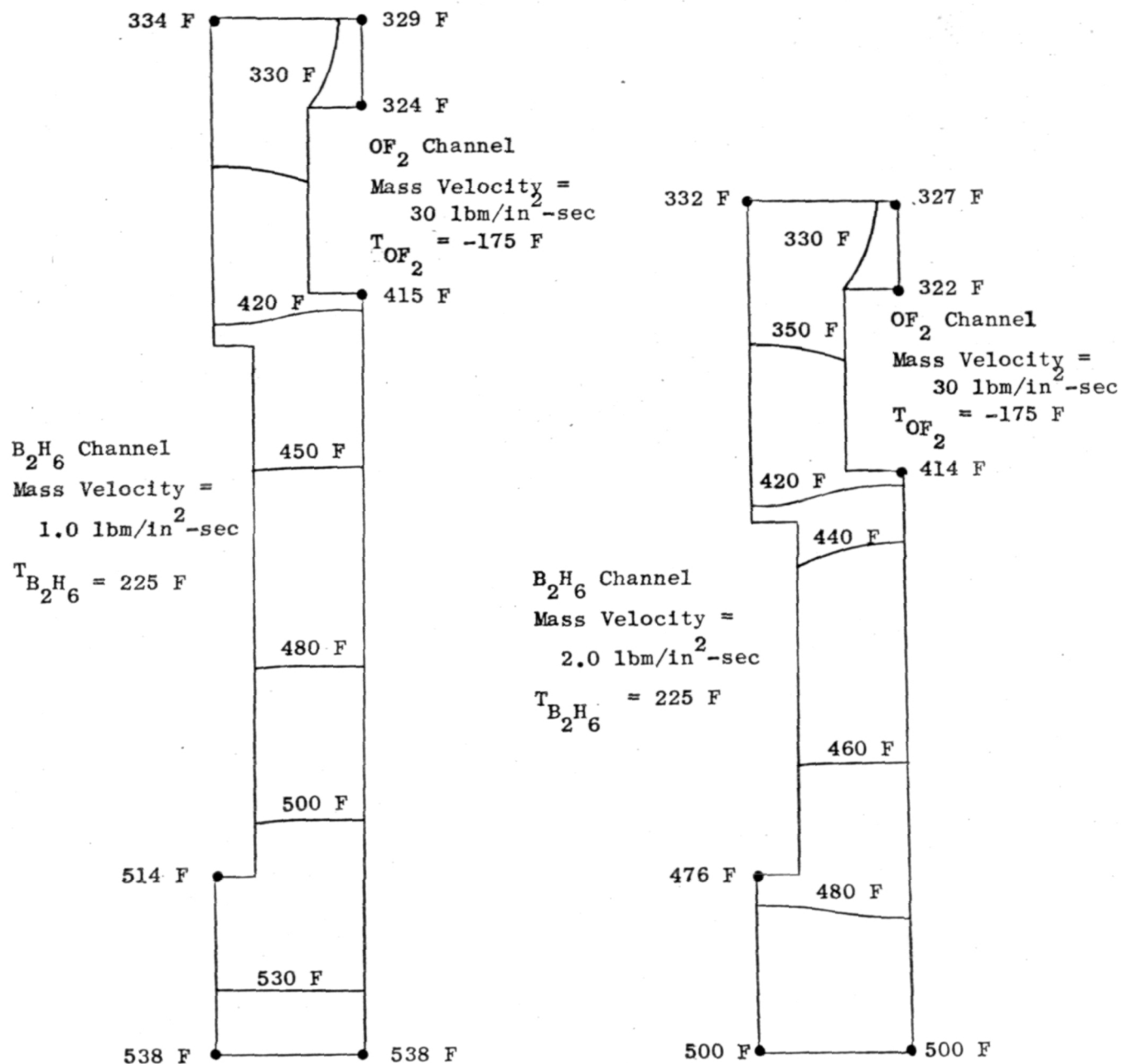


Figure D-6. Comparison of Wall Isotherms for the Combustion Chamber at a Heat Flux of 1.5 Btu/in²-sec.

WATER JACKET

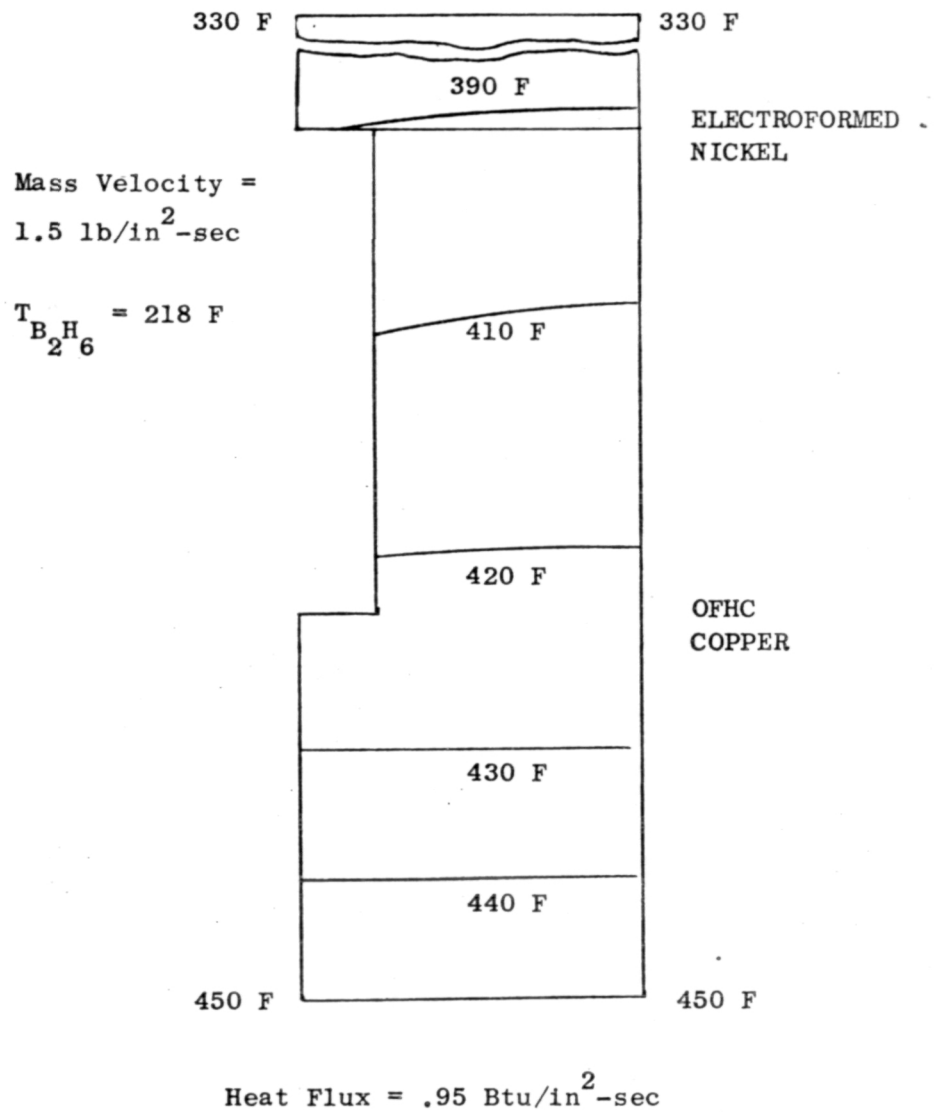


Figure D-7. Isotherms at $x = -8.0$ inches for Selected Design.

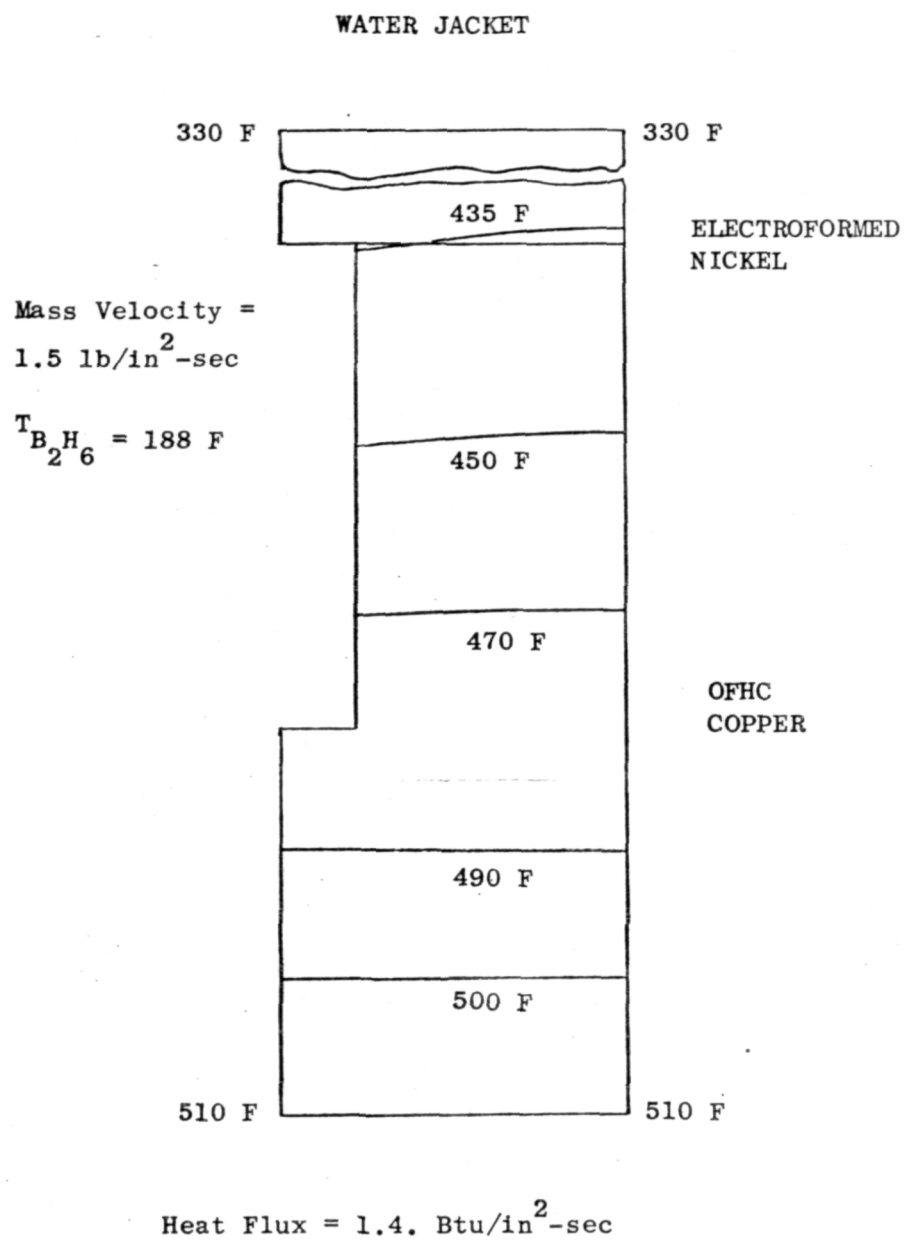


Figure D-8. Isotherms at $x = -6.0$ inches for Selected Design.

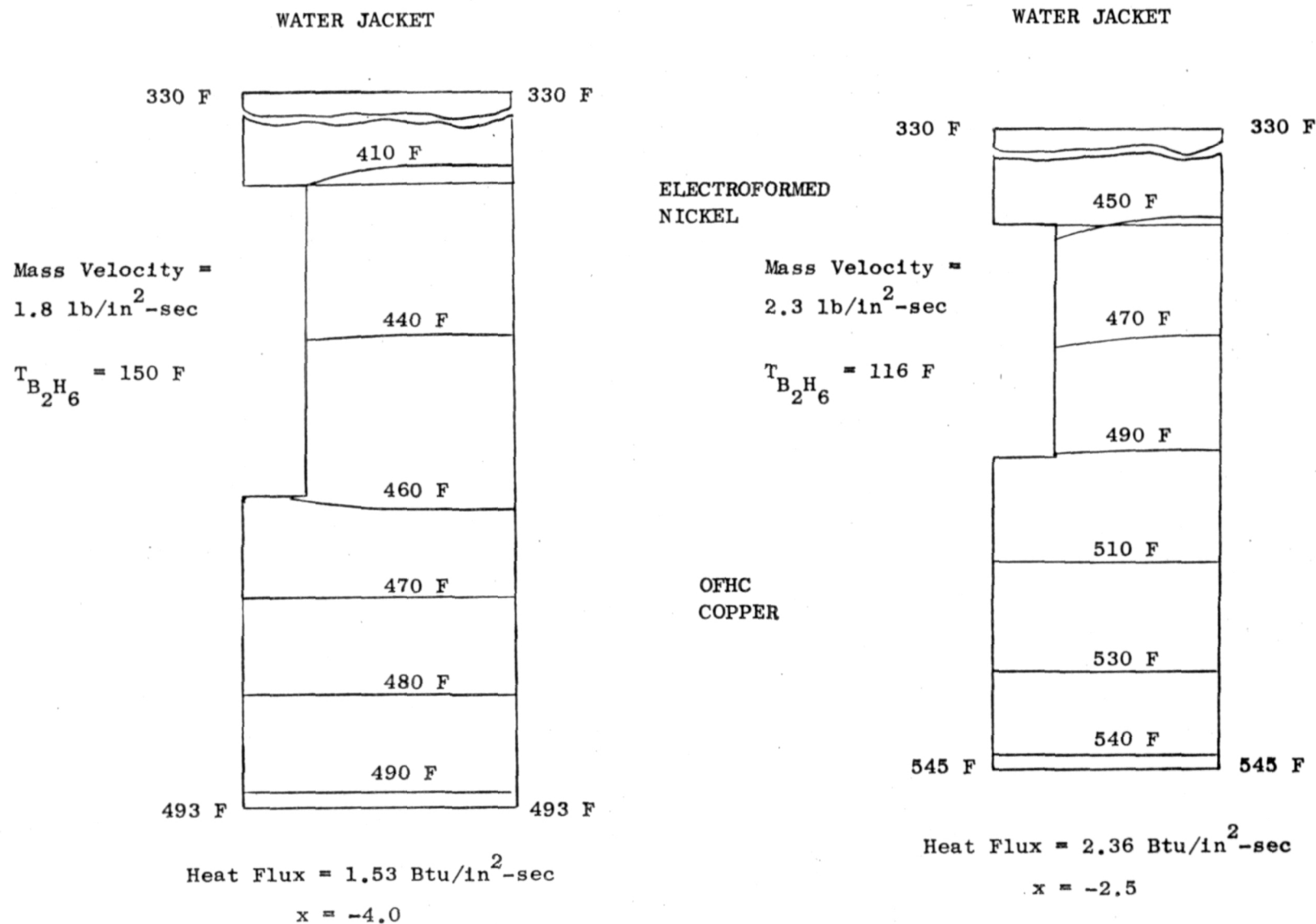
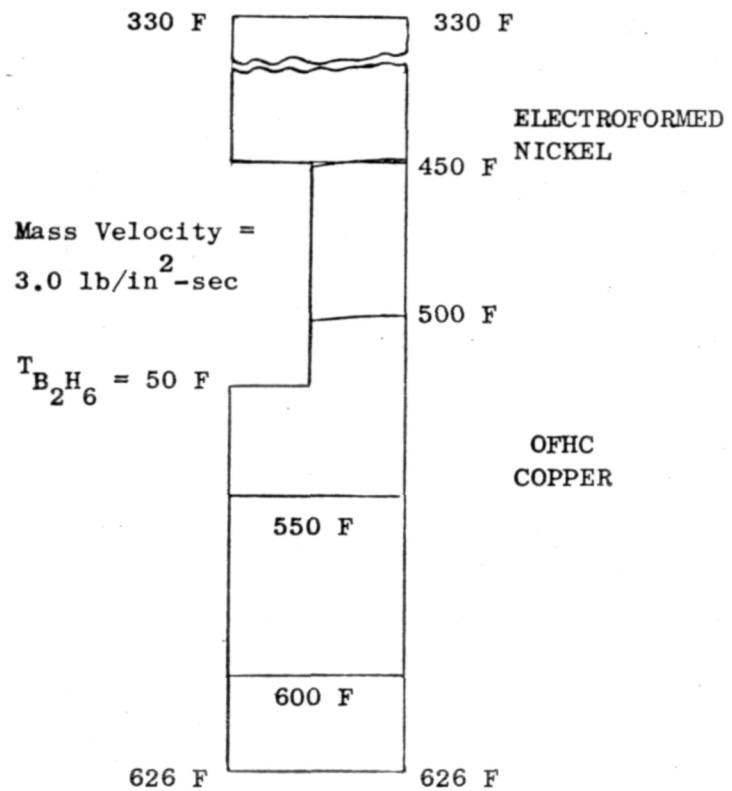


Figure D-9. Isotherms at $x = -4.0$ inches and $x = -2.5$ inches for Selected Design.

WATER JACKET



Heat Flux = 4.5 Btu/in²-sec

Figure D-10. Isotherms at Sonic Point for Selected Design.

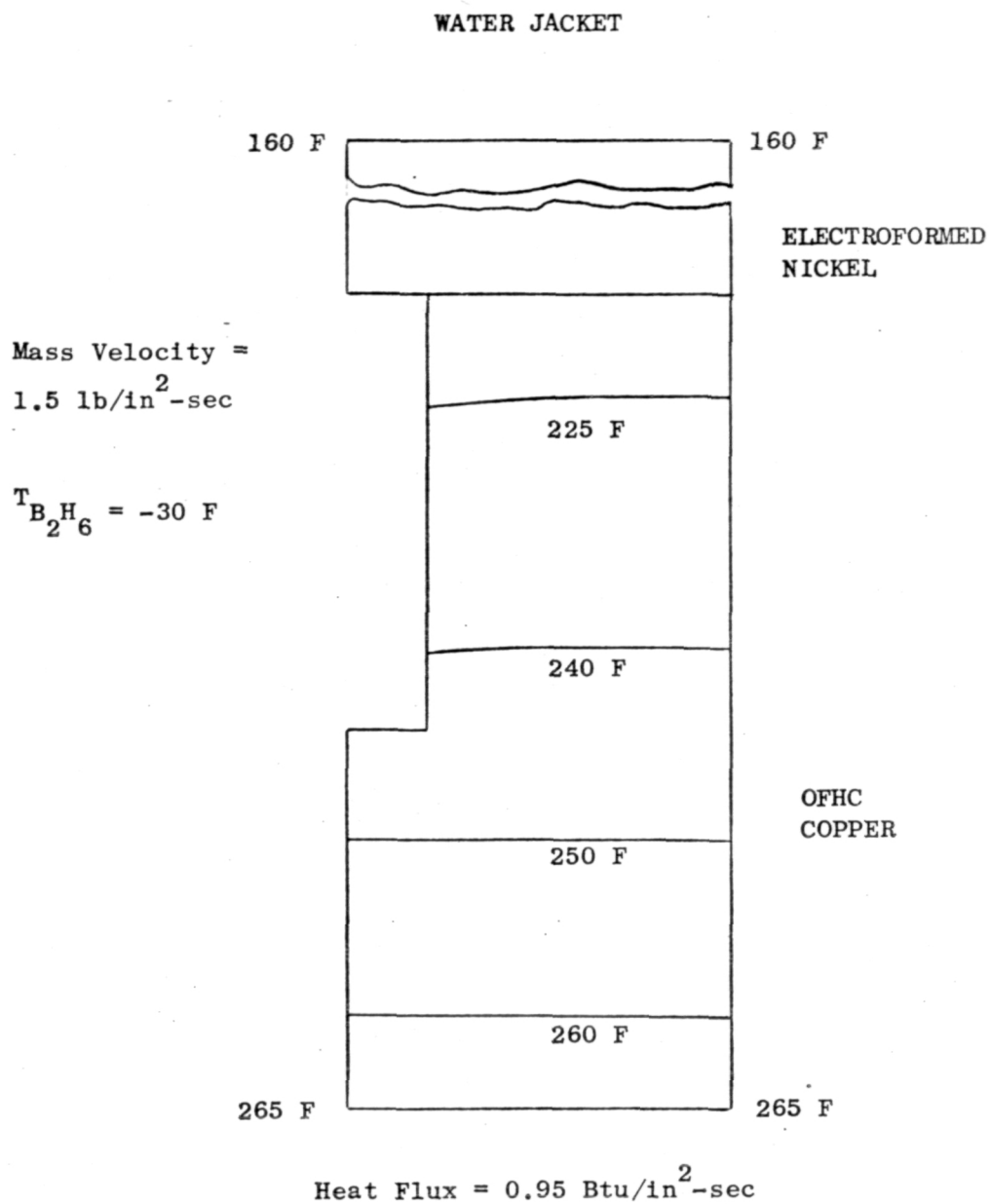


Figure D-11. Isotherms at $\epsilon = 6.0$ for Selected Design.

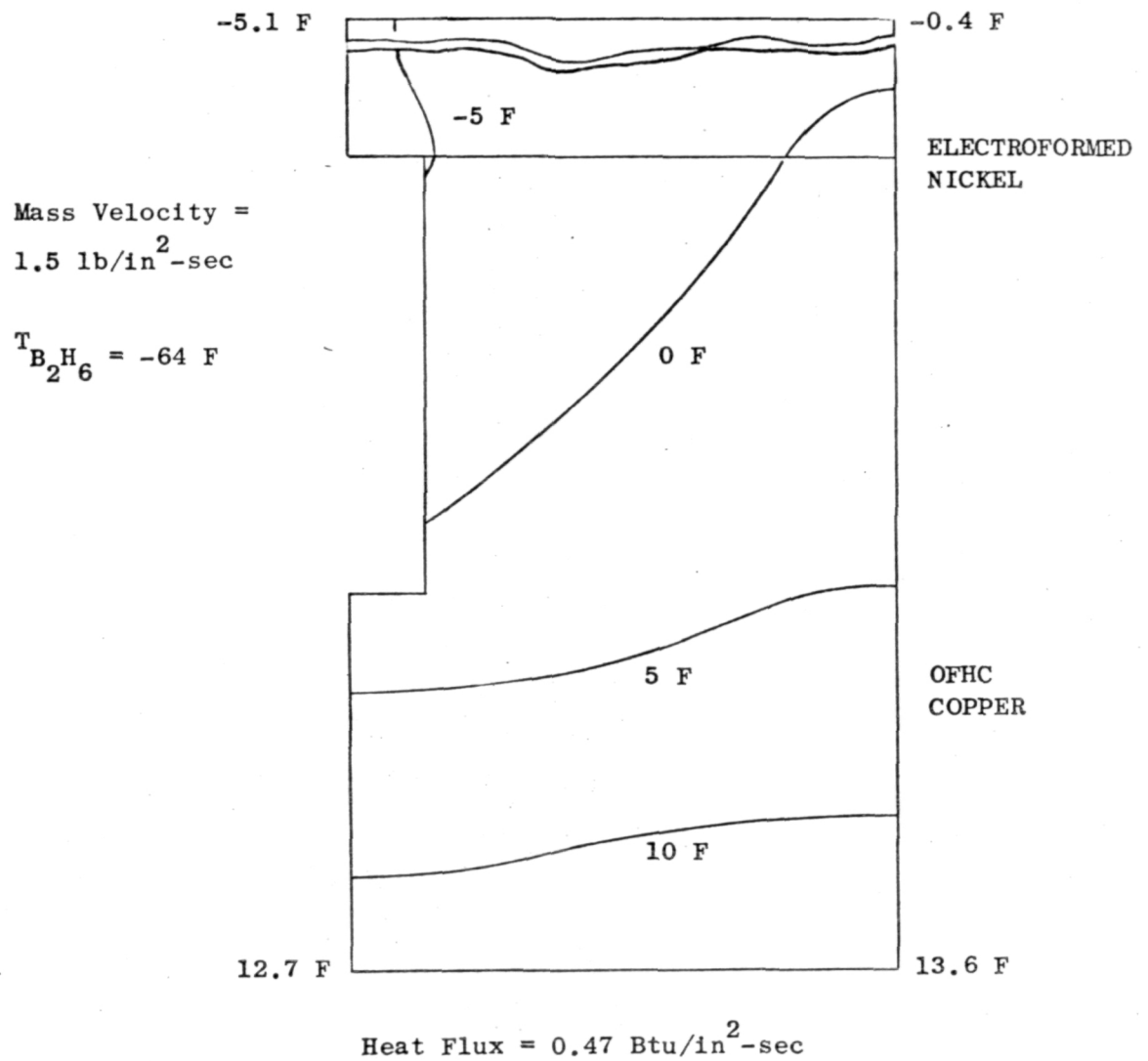


Figure D-12. Isotherms at $\epsilon = 10$ for Selected Design.

ELECTROFORMED NICKEL

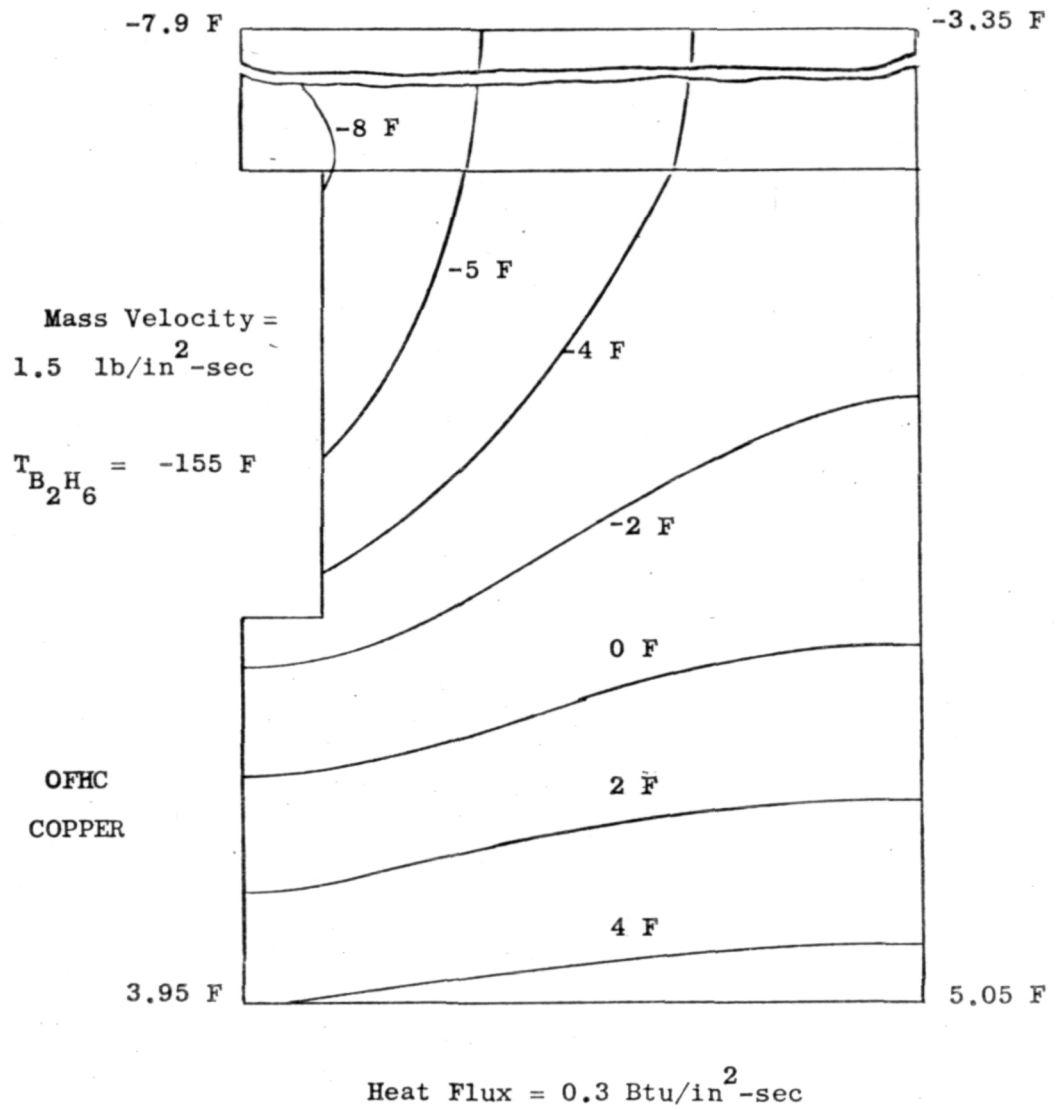


Figure D-13. Isotherms at $\epsilon = 15$ for Selected Design

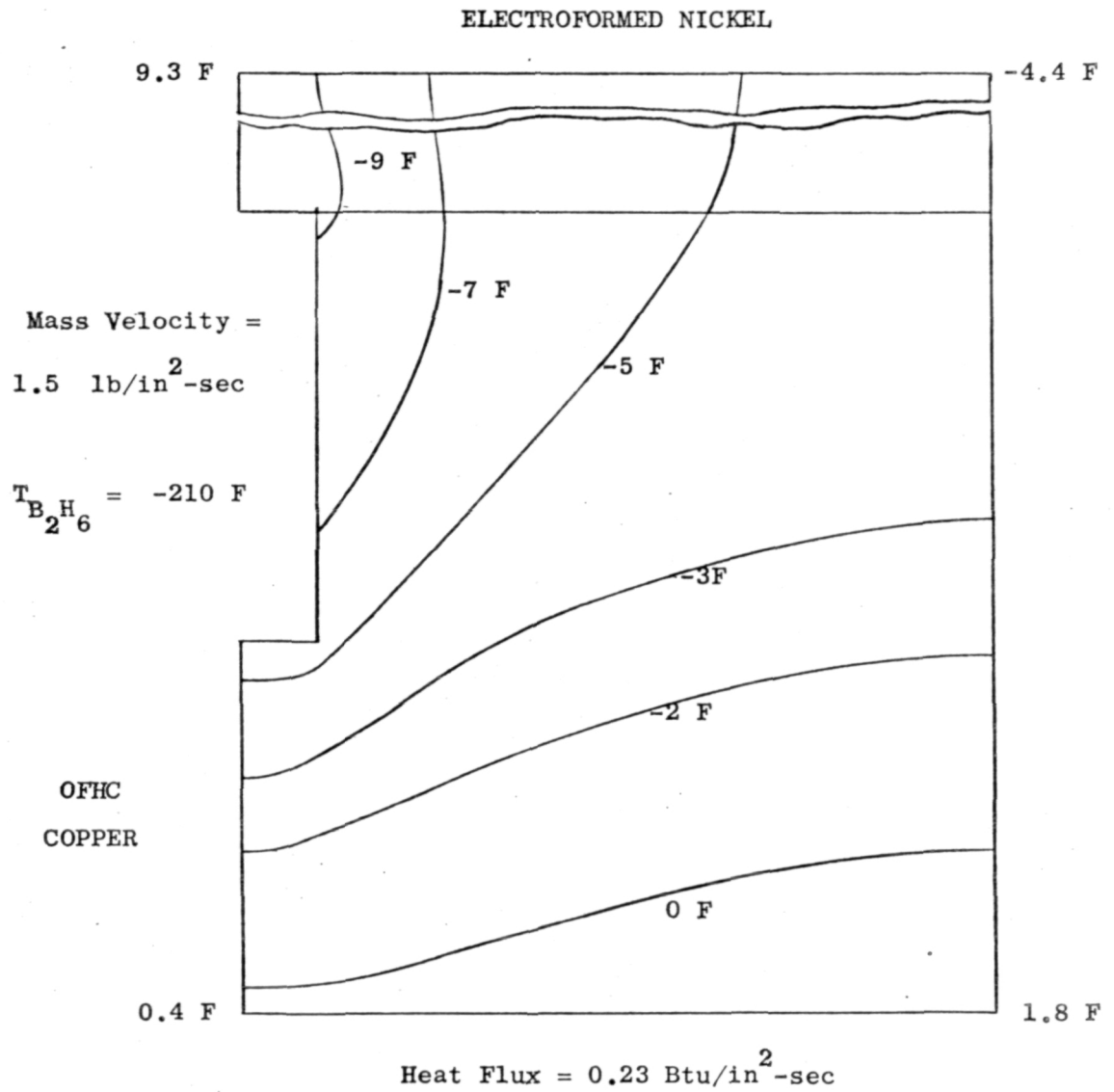


Figure D-14. Isotherms at $\epsilon = 19$ for Selected Design

APPENDIX E

PRA TEST FACILITY AND DATA ACQUISITION

The test facilities are located in the Propulsion Research Area (PRA) (Fig. E-1). The PRA is comprised of five multi-position firing pits with a centrally located blockhouse which permits direct observation of the engine firings. Test Stand Yoke was employed for the Task IV hot-firing calorimeter/regenerative tests.

FLOX (OXIDIZER) SYSTEM ASSEMBLY

The system schematic was previously shown in Fig. 108. Annin valves were used for the tank "pre" valve and the oxidizer main valve. Prior to assembly, FLOX feed system components were carefully and thoroughly cleaned in accordance with prescribed procedures.

Passivation of the assembled system (to the main oxidizer valve), by provision of protective fluoride films on exposed surfaces, is carried out as follows: low-pressure gaseous fluorine was introduced into the system and maintained for successive 15-minute periods at 5, 10, and 15 psig; finally, 20 psig is maintained for several hours. The feed line and thrust chamber system downstream of the main valve was passivated immediately before each set of firings by flowing gaseous low pressure through the system for short intervals of time.

B_2H_6 (FUEL) SYSTEM

High purity B_2H_6 was stored as a liquid in 40-pound cylinders immersed in dry ice packing. These cylinders were manifolded to a 25-gallon run tank. B_2H_6 was supplied to the engine through temperature controlled jacketed 1-inch line to a cavitating venturi. Two turbine flow meters were also used to measure the fuel flowrate. A B_2H_6 heat exchanger previously described was used for the calorimeter testing.

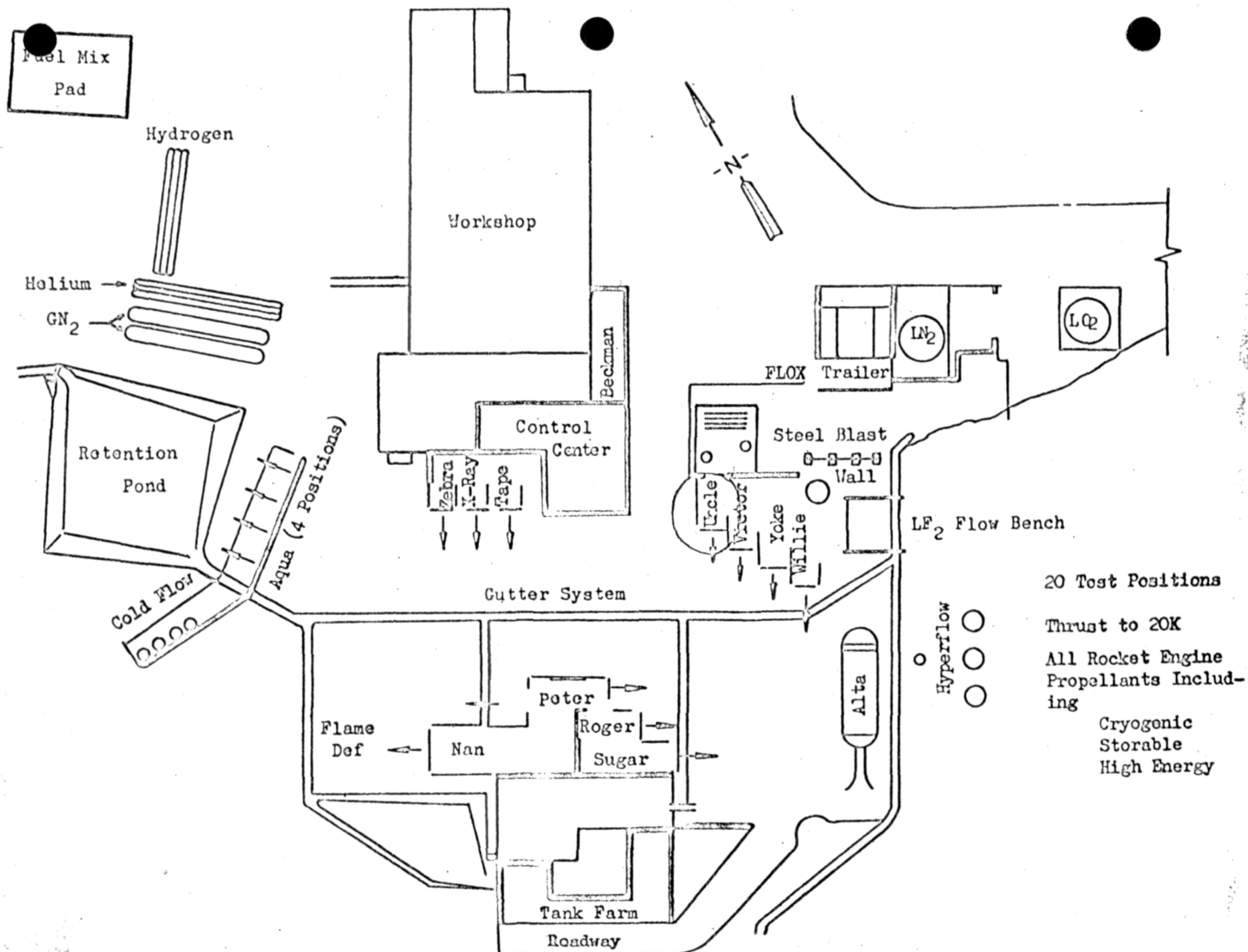


Figure E-1. PRA Test Facility Overall Arrangement

PROPELLANT VENT SYSTEMS

A vent system was provided which allowed safe venting of the fuel system. The B_2H_6 manifold was vented through the facility stack. The gaseous oxidizer storage tank was not vented.

COOLANT WATER SYSTEM

Water for the water cooled diffuser and regenerative chamber OF_2 jacket simulator was supplied to the engine from the main water 140 psia feed system. The water was distributed by a manifold upstream of the engine. A turbine flowmeter upstream of the engine was used to measure the engine H_2O flowrate.

PURGE SYSTEMS

GN_2 purges were provided to purge the transfer line, injector, and run lines. The GN_2 purge systems were supplied from a 3000 psi (2000 N/cm^2) bottle bank. Individual purge pressures were set by hand loaders in the stand area. The oxidizer purge system had both a check valve and a positive closing valve to prevent contamination of the GN_2 system by the high pressure oxidizer during engine operation. The fuel purge system was protected by a check valve.

PROPELLANT SAMPLING

The FLOX composition was determined at the onset of the test program. B_2H_6 supply was sampled by the vendor.

ALTITUDE DIFFUSER

An ejector-diffuser with the dimensions previously described was fabricated from mild steel for the altitude simulation tests. The diffuser was designed to operate water cooled for durations consistent with regenerative wall nozzle operation. The exit of the nozzle was solidly connected to the diffuser. Inspection of the injector and forward end of the thrust chamber with disassembly of the diffuser was accomplished between tests.

START SEQUENCE

Before each firing, liquid methyl cyclohexane was run in a jacket concentric to the main fuel line to chill the B_2H_6 line to the desired run temperature. The firings were sequenced through an automatic timer which controls operation of propellant main valves, chart drives, and cameras. Coolant water and injector purges were initiated prior to test start. The purge pressures were lower than the corresponding injection pressures and were, therefore, suppressed as the injection pressures built up in addition to the positive shutoff valve on the FLOX purge system. A fuel lead was utilized during the test program with an optimum start sequence determined.

INSTRUMENTATION

Facility and engine instrumentation parameters are shown in Table E-1. Redundant measurements were made on the important experimental parameters to increase data reliability. The particular transducers used for the various types of measurements are described below.

The thrust chamber mount was supported on flexure rods, which allowed free movement parallel to the engine axis (horizontally), restrained in the thrust direction by a load cell.

Pressures were measured with Taber "Teledyne" Series 206 or equivalent transducers for low frequency response and with Photocon and Kistler transducers (propellant injection and chamber pressures) for high frequency response. Chamber pressures were measured on the injector face and near the start of nozzle convergence (calorimeter). Pressures were measured at the exit of the 20:1 area ratio calorimeter nozzle to verify full flow in the nozzle for the altitude simulation tests.

The oxidizer flowrates were measured by means of a sonic venturi passivated for service in FLOX. The B_2H_6 line had two flowmeters in series to measure the volumetric flowrate and calibrated sonic venturi (gas) or cavitating venturi (liquid) for redundancy.

TABLE E-1. INSTRUMENTATION LIST FOR TASK IV TESTS

Nomenclature	Parameter Measured	Measurement and Range	Recorder		
			Beckman	Oscillograph	Digital
P_{TO}	Oxidizer Tank Pressure, psig (N/cm^2)	Taber 0-2000 (0-1379)			
P_F	Fuel Tank Pressure	Taber 0-3000 (0-2068)			X
P_{WT}	Water Tank Pressure	Taber 0-3000 (0-2068)			X
P_{IO}	Oxidizer Injection Pressure	Taber 0-2000 (0-1379) Photocon 0-2000 (0-1379)	X	X X	X
P_{IF}	Fuel Injection Pressure	Taber 0-2000 (0-1379) Photocon 0-2000 (0-1379)	X	X X	X
P_{C-1}	Chamber Pressure	Taber 0-1000 (0-689)	X		X
P_{C-2}	Chamber Pressure	Taber 0-1000	X		X
P_{C-3}	Chamber Pressure	Photocon 0-1000 (0-689)		X	
P_{NE}	Nozzle Exit Pressure	Taber 0-50 (0-34)	X	X	X
P_{D1}, P_{D2}	Diffuser Pressure	Taber 0-50 (0-34)	X		
P_{VF}	Fuel Venturi Upstream Pressure	Taber 0-3000 (0-2068)	X		X
P_{TF}	Fuel Venturi Throat Pressure	Taber 0-3000 (0-2068)	X		X
P_{IO}	Oxidizer Injection Pressure	Taber 0-2000 (0-1379)	X		
P_O	Oxidizer Flowmeter Pressure	Taber 0-2000 (0-1379)	X		
P_{IC}, P_{IF}	Fuel Injection Pressure	Taber 0-2000 (0-1379)	X		
P_{W2}	Water Manifold Pressure	Taber 0-2500 (0-1723)			X

TABLE E-1. (Concluded)

Nomenclature	Parameter Measured	Measurement and Range	Recorder		
			Beckman	Oscillograph	Digital
P_{NF}	Fuel-GN ₂ Purge Pressure	Gage 0-2000 (0-1379)			
P_{NO}	Oxidizer GN ₂ Purge Pressure	Gage 0-2000 (0-1379)			
F	Thrust, pounds (Newtons)	Baldwin 0-10,000 (0-44,500)	X	X	X
T_{IO}	Oxidizer Injection Temperature, F (K)	I/C, 60 to 1000 (289 to 812)	X		X
TO-1	Oxidizer Temperature at Venturi	I/C, 60 to 1000 (289 to 812)	X		X
T_{IF}	Fuel Injection Temperature, F (K)	I/C 60 to 1000 (289 to 812)	X		X
T_{UF}	Fuel Upstream Venturi Temperature, F (K)	I/C 60 to 1000 (289 to 812)	X		
T_{WL}	Water Manifold Temperature, F (K)	I/C 60 to 1000 (289 to 812)	X		
TW-1, TW-2	Water Temperature Rise through Chamber, F (K)	I/C 60 to 1000 (289 to 812)	X		X
TC-1 to TC-9	Chamber Wall Temperature, F (K)	C.A. 60 to 1500 (289 to 1090)	X		
TN-1 to TN-4	Nozzle Wall Temperature, F (K)	C.A. 60 to 1500 (289 to 1090)	X		
WW-1	Water Flowrate, gpm (l/sec)	F.P. 5 to 20 (0.32 to 1.26)	X	X	

The temperature rise of the water and B_2H_6 in the coolant was measured with iron-constantan thermocouples to provide a heat flux rate. Temperature measurements at two locations in lands on the injector were made to provide face heat flux data. Temperature measurements were made with copper plugs and from nozzle back wall locations in the solid and regenerative wall nozzles to obtain data for determining the axial heat flux profiles.

DATA RECORDING

All pressure, temperature, and flow measurements were recorded on tape during each firing by means of a Beckman Model 210 Data Acquisition and Recording System. This system acquired analog data from the transducers, which it converted to digital form in binary-coded decimal format. The latter were recorded on tapes which are then used for computer processing.

The Beckman Data Acquisition Unit sequentially sampled the input channel at a rate of 5625 samples per second. Programmed computer output consists of tables of time versus the average parameter value (in engineering units), over an approximately 200 ms time slice printed out at approximately 200-millisecond intervals during the firing, together with calibration factors, prerun and postrun zero readings, and related data. The instantaneous parameter values were machine-plotted and displayed on appropriately scaled and labeled CRT grids for simple determination of gradients, establishment of steady state, etc.

Primary data recording for these firings used the Beckman 210 System. In addition, the following auxiliary recording systems were employed:

1. An 8-channel, Brush, Mark 200 recorder was employed in conjunction with the Beckman unit, primarily to establish time intervals for computer data reduction and, additionally, for "quick look" information on the most important parameters. This is a direct-inking system, with display on high-gloss, graduated paper moving at 20 mm/sec.

2. A CEC, 36-channel, direct reading oscillograph was used as backup for the Beckman 210 System and for indication of any oscillatory combustion.
3. Direct-inking graphic recorders (DIGR's), either Dynalog rotary chart or Esterline-Angus strip chart, were used to set prerun propellant supply pressures, for recording of propellant manifold pressures, to provide quick-look information, and as secondary backup to the Beckman and oscillograph recorders.
4. An Esterline-Angus, 20-channel event recorder was used for direct-inking recording of main propellant valve signal and travel, as well as for chart drive and camera actuations.
5. An Ampex, Model FR-100, 54 khz tape recorder was used to record the output from the high frequency transducers.

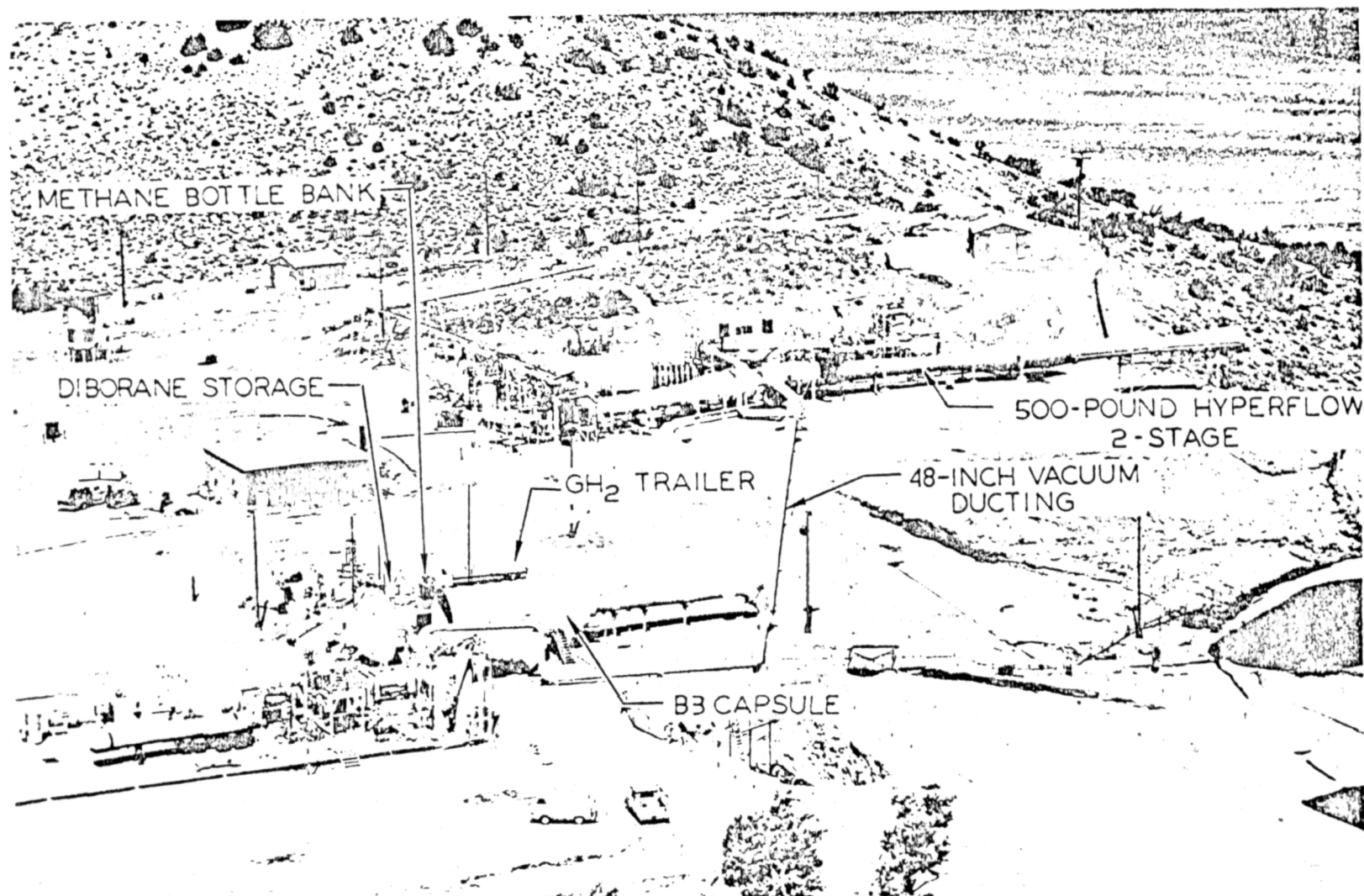
APPENDIX F

RENO TEST FACILITY AND DATA ACQUISITION

The Task II calorimeter and block cooling test programs were conducted in the Rocketdyne NFL B area on the B-3 position (Fig. F-1). This was a highly specialized and flexible, vacuum or ambient high-energy propellant facility, and was unique in its ability to provide all test conditions required in this program. The oxidizer feed system could deliver either liquid or gaseous propellant to the engine. The fuel system could deliver liquid and gas with both systems temperature controlled to any temperature of interest for $\text{OF}_2/\text{B}_2\text{H}_6$, using a specially designed, closed-loop circulating freon system. At the choice of the test engineer, the tests could be at ambient pressure, short vacuum tests could be conducted using the 10,000 cu ft of evacuated volume as a sump (evacuated by the auxiliary vacuum system), or 150-second vacuum tests conducted using the hyperflow system. Data acquisition systems included an Astrodata digital unit coupled to an on-site computer. This facility was used on two previous $\text{OF}_2/\text{B}_2\text{H}_6$ contracted programs and a company-sponsored B_2H_6 Heat Transfer program.

OXIDIZER SYSTEM

The oxidizer liquid feed and 500-gallon storage system was designed for compatibility with F_2 , FLOX, or OF_2 . The entire system was jacketed from the run tank to the main valve just upstream of the engine, and could use LN_2 or Freon for temperature conditioning. The gaseous oxidizer system consisted of a large reservoir that was charged remotely by liquid from the storage tank. The liquid was permitted to vaporize in the reservoir, generating its own pressure. The feed system inside the capsule was common for liquid and gas oxidizers; with only the flow measurement section changed.



6RE11-3/21/68-RLA

Figure F-1. Nevada Field Laboratory Small Engines Area

FUEL SYSTEM

The B_2H_6 feed system was an elaborate liquid and gas feed system. The fuel systems were completely separate for plumbing gas and liquid up to the engine. The facility had a 100-pound liquid storage capability and a 3 cu ft, high-pressure gas run tank. In addition to the liquid storage tank, there was a liquid run tank where B_2H_6 was stored in the liquid state in an LN_2 -regulated environment to preclude propellant decomposition and contamination. With this system, emergencies or propellant recovery could be readily handled by overriding the control circuit and flooding the outer vessel with LN_2 , freezing the B_2H_6 . This extra cooling capacity was essential to B_2H_6 recovery. The B_2H_6 unused after a gaseous diborane test was recondensed in the storage tank. The liquid B_2H_6 run tank was jacketed and insulated for propellant conditioning. The system flexibility permitted introducing various conditioning media to the reservoir for closed-loop circulation.

The gaseous B_2H_6 feed system was designed to permit short, steady tests while avoiding holding temperatures that were too high (from the standpoint of decomposition) or too low (to avoid condensation at the throat of sonic venturis). A two-stage system was designed to meet this unusual requirement. The gas run and holding tank used a circulating, closed-loop, heated-water bath at approximately 90 F for a maximum hold time with minimal decomposition. In addition to the gas run tank, a second-stage heat exchanger was located inside the test capsule. This system was used immediately before a test series and elevated the gaseous B_2H_6 from the run tank environment to temperatures up to 200 F. (B_2H_6 cannot be maintained at elevated temperatures due to the high decomposition rate. The optimum temperature for the heat exchanger is 140 F.) The special features of this system were required in Task II where warm gaseous B_2H_6 was provided by the facility.

ALTITUDE FACILITY

The altitude-simulation system had a main steam ejector and a small auxiliary steam ejector. The main system, consisting of three diffuser stages, was capable of maintaining an altitude in excess of 100,000 feet for 150 seconds of test operation.

The auxiliary ejector unit was supplied by steam from the main steam plant. Although it was not capable of maintaining altitude during engine operation, the 10,000 ft³ volume was large enough that once the system is evacuated, short tests could be conducted without major loss of vacuum, and then recover 120,000 feet in approximately 10 to 20 minutes. This feature was used to get nozzle data in Task II.

INSTRUMENTATION SYSTEMS

The facility instrumentation had demonstrated the capability of measuring small differences in performance between similar engines and propellants. Differences in performance between OF₂ and FLOX (F₂-O₂, 70-30) with B₂H₆ were measured quite accurately. Data reproducibility was consistently within 0.5 percent. Measurement practices were in accordance with CPIA publication No. 179, which was prepared by Rocketdyne under contract to the ICRPG.

ENGINE INSTALLATION AND MEASUREMENTS

The engine was installed in the Reno test stand in such a way that it was free of external interference. No corrections were needed to be made for thrusts caused by supports or propellant lines. The diffuser inlet was adjusted to ensure that there is no effect of the engine plume within the capsule.

The injector was mounted to a thrust plate by three longitudinal standoffs. This plate was supported by one horizontal and two vertical tie rods. Mounted to the thrust plate was a flexure and spacer followed by a dual-element load cell. Two alignment plates separated the two load cells and flexures. This assembly was mounted to a rigid I-beam. Also mounted to this I-beam was a hydraulic ram and the calibration load cell. At the end of the calibration cell was a ball joint in a yoke that was tied to the thrust plate by two tension rods. To minimize the cantilevered engine weight, a vertical rod and a horizontal rod were attached to the nozzle skirt. These rod supports were mounted in clevis fittings through swivel tie rod ends.

The engine thrust was simulated by pressurizing the hydraulic ram which moved the calibration cell putting the two tie rods in tension. In this manner, the simulated engine thrust was transmitted through the centerline of the thrust system putting the dual-bridge load cells in compression in the same way the engine puts them into compression. During test operation the tie rods were loosened and did not interfere with engine movement.

Propellant Lines and Electrical Connections

The engine plumbing consists of instrumentation lines and propellant feed lines. To minimize test stand effect, all the propellant plumbing was introduced to the injector radially, with relatively long straight actions to allow unrestrained movement of the chamber assembly. The engine instrumentation also had the same feature. The lines were "S" shaped with long leg sections and were fabricated from 1/4-inch light wall tubing. There was no insulation or jacketing on any lines downstream of the rigidly mounted valves or transducers.

The engine electrical connections consisted of numerous thermocouple wiring and electrical connections which are attached to the temperature probes. These wires were connected to a "Jones" strip physically mounted to the hardware. From the terminal strip, the wires were bundled and wrapped in aluminum foil, terminating at a master strip mounted to the stand support.

Thrust Measurement

Thrust measurement was made by two-series Baldwin-Lima-Hamilton double-bridge load cells. Each cell (2000 pounds) provided a redundant measurement by the double-bridge network, resulting in four separate thrust measurements. Calibration of the load cells was conducted before and after each test series by means of the calibration load cell and a hydraulic loader. The calibration load cell was calibrated against a proving ring traceable to the National Bureau of Standards.

Pressure Measurement

Pressure transducers were of the bonded strain gage, d-c type. The calibration and verifications of the pressure transducers are accomplished with a dead weight tester or similarly precise calibration device traceable to the National Bureau of Standards. For LOX clean certified pressure transducers, the calibration and verifications were accomplished by introducing GN_2 and measuring the pressure on a Heise gage.

Flow Measurement

Gaseous flowrates were measured by a specially fabricated flow section containing sonic venturis. These sections, having upstream pressure and temperature and downstream pressure measurement, were calibrated and were the same units as previously used during a previous program.

Fluorine liquid flowrate is measured using a 1-inch Foxboro turbine-type volumetric flowmeter. This meter was calibrated using liquid freon which resulted in a more accurate flow measurement than achieved in previous work for which water calibrated meters were used. Flowmeter disagreement throughout the program was normally approximately 0.1 percent.

Temperature Measurement

Iron-constantan thermocouples are used for the B_2H_6 fuel temperature measurements and for the major portion of the thrust chamber temperatures used in the heat transfer calculations. Chromel-Alumel thermocouples were used in the remaining measurements.

Visual Recording

Hot-fire test coverage was made by two Gazap 16-64 frps, 16 mm color cameras. These cameras were located high in the capsule, one on each side, and view the engine and associated plumbing immediately behind the engine. In addition, all tests were monitored with a closed circuit television camera.

DATA ACQUISITION

Data-acquisition capabilities of NFL included a digital recorder, conventional direct-inking graphic recorders (DIGR), oscillographs, and time and sequence recorders. The digital recorder provided high accuracy with immediate response and was used for precise performance characterization. This digital unit was an Astrodata Model 4024 system capable of recording 88 active channels, 12 FM-DC flow channels and 64 event channels. It has a sampling rate of 20,000 samples/sec with 40, 10, and 5 KC options. The sampling time was approximately 5 milliseconds. The Astrodata unit was coupled to an on-site DDP 116 computer with an 8K memory. This computer yielded on-site scaled engineering data and limited on-site data reduction, providing final data calculations shortly after each test. Decisions requiring data review were greatly accelerated by this capability. This computer also has parameter redline capabilities for cutoff and engine control.